LIFT FORCES ON CYLINDRICAL BODIES IN UNSTEADY FLOWS

by

Herricos Stapountzis

November, 1978

A Thesis submitted for the Degree of
Doctor of Philosophy of the
University of London and for the
Diploma of Membership of the
Imperial College

Department of Aeronautics
Imperial College of Science and Technology
London, S.W.7

ACKNOWLEDGEMENTS

The author is grateful to his supervisor Dr. J. M. R. Graham for his guidance and helpful criticism during this work. He also wishes to thank Dr. A. D. Weir for his help in computing problems, Mr. J. Coles for his assistance in the wind tunnel and Mrs. H. Bastin for the typing.

Lastly, the author wishes to express his gratitude to his parents, Georgio and Anastasia, and his wife, Moshanthi, without the help and encouragement of which this work would not have appeared.

ABSTRACT

H. STAPOUNTZIS: LIFT FORCES ON CYLINDRICAL BODIES IN UNSTEADY FLOWS

The unsteady lift behaviour of a NACA 0015 aerofoil, a D cylinder (flat face downstream) and an elliptic cylinder was studied, when they were exposed to a two-dimensional sinusoidal upwash and to grid turbulence. The sinusoidal upwash was generated between the vortex wakes of two oscillating aerofoils. Experiments were undertaken at Reynolds numbers 1.2×10^5 to 3×10^5, sinusoidal flow reduced frequencies between 0.05 and 0.8 approximately, turbulence length scales of the order of the body chord and upwash intensities of the order 5% of the mean free stream speed.

Existing thin aerofoil theories were employed in order to predict the unsteady lift on the bluff bodies, for frequencies not close to those of vortex shedding. The bluff bodies were assumed to behave like flat plates, but of mean lift curve slope equal to the experimentally determined. This assumption further implied the application of an equivalent Kutta-Joukowski condition at the trailing edge of the flat plate.

There was found to be a generally good agreement between the theoretical and experimental aerodynamic admittances of lift for the aerofoil (a result indicating the adequacy of the flows employed) and the D cylinder. The aerodynamic admittance of the elliptic cylinder could not be reasonably predicted for all Reynolds numbers, especially at high frequencies but a better agreement with the theory was observed, when the Reynolds number was the highest, or the boundary layer was supplied with trip wires. This characteristic behaviour was associated with an unsteady movement of the separation points and the existence of separated flow upstream of the assumed "equivalent" trailing edge.

The application of unsteady flows, and especially of turbulence, was found to decrease the peak spectral power of vortex shedding from its smooth flow level.

LIST OF CONTENTS

LIST OF NOTATION

$\|A(k)\|, \|A(k_1)\|$	Magnitude of aerodynamic admittance, see Eqns. (2.19), (5.4) and (6.1).
AR	Aspect ratio (= span/chord).
arg	Argument of complex function.
b, b´	Test model and oscillating aerofoil thickness respectively.
b_t	Bar size of grid.
C_D	Drag coefficient based on chord length.
$\overline{C}_{Df}$	Form drag coefficient.
C(k)	Theodorsen's function, see Eqn. (2.8).
C_L	Filtered root mean square lift coefficient, based on chord length (see Appendix B).
$C_L(t)$	Fluctuating lift coefficient.
C_m	Virtual mass coefficient, see Eqn. (2.16).
$\overline{C}_p$	Mean pressure coefficient (Section 4.3b).
$\overline{C}_{pb}$	Mean base pressure coefficient, see Eqn. (2.3).
c, c´	Test model and oscillating aerofoil chords respectively.
d, D	Body diameter (see also sketch p.63).
$\overline{\partial C_L}/\partial\alpha$	Mean lift curve slope at zero mean incidence.
Eccentricity	See Section 3.3.1 and Table 2.
e	Fluctuating voltage (Appendix A).
$\|F\|$, F(k´)	See Fig. 3.6 and Eqn. (3.30) respectively.
$G(k_1, k_2)$	Graham's function, see Eqn. (2.11).
h	Wind tunnel height.
$H_n^{(2)}$	Hänkel function of the second kind of order n.
i	$= \sqrt{-1}$
j	Component of vorticity in the spanwise direction.
J_n	Bessel function of the first kind, order n.
$K(s_1)$	Küssner's function, see Eqn. (5.6).
k_1, k, k´	Reduced frequency in the streamwise direction, see Eqns. (2.5), (2.9), (3.22) and Fig. 6.1.
k_2	Reduced frequency in the spanwise direction.
k_3	Reduced frequency in the upwash direction.
k_g	$= \sqrt{k_1^2 + k_2^2}$
$\overline{L}$	Mean lift.

ℓ'	Distance between pivot shaft and mid-chord of oscillating aerofoil (see sketch p. 56).
L_x	Longitudinal turbulence length scale, see Eqn. (2.18).
L_A, L_B, L_C	See Eqns. (D-1), (D-2), (D-3).
ℓ_c, ℓ_c'	Spanwise u velocity correlation length and length of long connecting rod respectively.
ℓ_w	Wind tunnel width.
M	Mesh size of grid.
n	Frequency (Hz).
n, n_g	Oscillating aerofoil frequency (Hz).
n_b, n_t	Structural frequencies in torsion and bending, see Eqns. (3.15) and (3.16).
n_N	Nyquist frequency (Hz).
O(x)	Of Order x.
P, p	Pressure.
R	Real part of.
Re	Reynolds number based on model chord length (= U_∞ . c/ν).
$R_{xx}(n, y)$	Spanwise normalized coincident cross spectrum of x at frequency n.
$R_{xx}(y)$	Spanwise correlation coefficient of x.
r	Displacement (eccentricity) of long connecting rod, see sketch p. 63 .
S	Strouhal number, see Section 2.2.3.
s	Test model span.
s'	Span between end plates or span of oscillating aerofoil.
S_a	Reference area.
S_A, S_B, S_C	See Appendix D.
S_{C_L}, L_x	Normalized lift spectrum, see Fig. 6.1.
$S(\bar{k})$	Sears's function, see Eqn. (2.7).
$S(k, k')$	Kemp's function, see Eqn. (2.10).
$S_m(k)$	Modified Sears's function, see Eqn. (5.11).
SR	Sampling rate (Hz).
S_w, L_x	Normalized upwash spectrum, see Fig. 3.26.
$S_{ww}(k_1, k_2)$	Spectrum of the w velocity, see Eqn. (2.21).
S_x, S_{C_L}, S_{α_g}	One-dimensional power spectral densities of x, lift coefficient and upwash respectively.
T	Averaging time.

t	Time.
$T(k)$	Horlock's function, see Eqn. (2.14).
$T(k, k')$	See Eqn. (2.15).
$T(n, n_o)$	Response function of filter (Appendix B).
U	Mean velocity in the streamwise direction, or along the wall.
U'_e, U_1	Unsteady velocity along the wall just outside the boundary layer, unsteady velocity far upstream.
U_∞	Mean free stream speed.
u	Velocity component in the streamwise direction, see Fig. 3.8, or along the wall, see Eqn. (2.2).
v	Velocity of the gust in the spanwise direction.
w	Velocity of the gust in the z direction (upwash), (Fig. 3.8).
x	Distance in the streamwise direction, (Fig. 3.8).
x_g	Streamwise distance between oscillating aerofoil and test model mid-chord points (see sketch p. 56).
$\|X(n)\|^2$	Aerodynamic admittance of drag, see Eqn. (2.28).
x_{cp}	Chordwise position of the centre of pressure.
x_t	Distance between grid and test model mid-chord point.
y	Distance in the spanwise direction, see Fig. 3.8, or normal to the wall, see Eqn. (2.2).
y'	$= 2y/s$.
z	Distance in the upwash direction, see Fig. 3.8.
z_o	Vertical distance between oscillating aerofoils (see sketch p. 56).
α	Geometric incidence.
$\bar{\alpha}$	Mean incidence.
α_g	Filtered RMS gust amplitude ($= \sqrt{\overline{w^2}}/U_\infty$) usually at the point (0, 0, 0).
$\alpha_g(x, y, z)$	Value of α_g at the point (x, y, z).
$\alpha_g(t)$	Fluctuating dimensionless gust amplitude, see Eqn. (2.6) at (0, 0, 0).
β	See Fig. 2.6.
$\bar{\Gamma}$, $\Gamma(t)$	Mean and instantaneous circulation respectively.
γ_a, γ_w	Aerofoil and wake vorticity respectively (Section 3.4.3).

Γ_o, γ_o	Quasi-steady circulation and vorticity respectively.
ΔC_p	Pressure discontinuity on the flat plate aerofoil surface (z = 0).
Δn, Δn_e	Bandwidth, effective filter bandwidth (Appendix B).
δ	Boundary layer thickness.
δ_m	Boundary layer thickness of mean U profile.
ε, ε_b, etc.	Blockage correction factors (Chapter 4), or normalized errors (Appendix B).
Θ_o	Oscillating aerofoil peak amplitude in pitch.
$\Theta(t)$	Phase angle (Appendix E).
λ	Wavelength, see Eqn. (3.1); see also Eqn. (E-5).
Λ	Pressure factor for blockage corrections (Table 4).
ν	Kinematic viscosity of fluid.
ξ	Distance in the streamwise direction.
ρ	Fluid density.
τ_w	Wall shear stress.
u_i	Component of velocity in the i^{th} direction.
φ, ϕ	Phase angle.
ω (= $2\pi n$)	Circular frequency (rad/sec).

Superscripts

$\bar{}$	As overbar denotes time mean.
$\hat{}$	Denotes amplitude, or estimate (in Appendix B).
*	In Section 3.4, quantities non-dimensionalized by the half chord.

Subscripts

EXP	Refers to experimental values.
max	Denotes maximum.
MED. ECC.	For medium eccentricity (Section 3.3.1, Table 2).
PEAK	Peak amplitude.
RMS	Root mean square ($x_{RMS} = \sqrt{\overline{x^2}}$).
s, sep	Denotes conditions at separation.
t	Refers to theoretical values.
vs	Refers to vortex shedding.
∞	Denotes conditions at infinity.

CHAPTER 1. INTRODUCTION

One of the most important aspects of industrial aerodynamics over the last few years, has been the understanding and prediction of bluff body flows. Of great interest is the assessment of lift, drag, moment and pressure induced on bluff structures such as buildings, bridges, smoke stacks, transmission lines, periscopes, radio telescopes, antennas, oil rigs, boiler tubes, etc. by unsteady flows.

A full solution of the Navier-Stokes equations is not yet known and, therefore, less difficult methods have to be followed, in order to analyze a particular flow. Up to the present, a general treatment of bluff body flows is prevented by the lack of an adequate flow model, especially if the oncoming free stream is turbulent.

It is usual when analyzing aerodynamic loading, to consider as input to the problem the factor responsible for the generation of load; this may be a velocity or pressure field or the motion of the body itself. The output would be the quantity wanted: unsteady lift, drag, etc. For a linear system a quantity very useful to the designer is the frequency response function (ratio of the power spectral density of the output, to that of the input at the same frequency), which is commonly known as the aerodynamic admittance. Its knowledge permits the calculation of unsteady forces at any frequency, if the input (usually the flow) is given and the response is assumed to be linear. The aerodynamic admittance has been calculated successfully in linearized aerodynamic theories about the unsteady lift of two-dimensional thin aerofoils as in Liepmann(1952), Jackson, Graham and Maull (1973) and McKeough (1976) but it has been extended to deal with strictly non-linear problems (dealt with as if linear), such as bluff body loading, e.g. Davenport (1961),(1962) and Vickery (1965). The non-linear character

of bluff body flows is due to:-

- Flow separation. The separating shear layers (of which the origin and position generally change with time), interact in a non-linear manner. As a result, loads at frequencies not existing in the original input, appear in the output at, for example, the frequencies of vortex shedding.
- Interaction of the rotational or turbulent oncoming flow with the body. Significant perturbations are introduced in the mean flow approaching the body with a subsequent distortion of the flow vortex lines. This latter process is non-linear because the rates of strain near a bluff body are large.

The degree of success of the existing theories for the flow round bluff bodies depends on the kind of simplifying assumptions made. Up to the present the most complete analysis for the distortion of an external turbulent flow round bluff bodies, is due to Hunt (1973) and is based on the "rapid distortion" theory of Batchelor and Proudman (1954). Vortex shedding (i.e. the separation problem) was not examined. Hunt's method is however extremely expensive, from the computational point of view, and for that reason he was only able to calculate some asymptotic results, in the case of a circular cylinder in turbulent flow.

It is this difficulty in developing accurate, but easy to use theoretical models for the prediction of loads in unsteady flows, that has established the experiment as the main source of information. There are lots of experimental data available to-day on the response of certain bluff body shapes to atmospheric and duct turbulence and on aeroelastic problems such as galloping and buffeting. Besides their value for immediate industrial applications and direct comparison with the theory, these data are often used as inputs to semi-empirical models. For example, these inputs may be the position of boundary layer separation

on the surface of the body, the base pressure, the drag coefficient, the Strouhal number, etc. A relatively greater proportion of work concerns unsteady drag and pressures than unsteady lift, despite the fact that the later kind of loading is equally interesting. Perhaps this is because the simplifying assumptions usually made for theoretical models about drag, lead to satisfactory results, sometimes sufficient for the present needs.

At the present, therefore, there is not very much known about the unsteady lift on bluff bodies in unsteady flows and it was this lack of information, which urged the author to investigate the aforementioned subject.

The experimental work in this study was planned as an investigation of the unsteady lift experienced by two-dimensional rigid bluff bodies, when placed in unsteady incompressible flows. Rigid bodies were chosen, i.e. for which the structural response introduces negligible flow disturbances compared to those of the unsteady flow, since they represent a large number of practical situations; in addition, it is usually easier to measure unsteady forces on rigid models.

Two kinds of input flows were employed:-

- A two-dimensional sinusoidal upwash gust convected, "frozen", with the mean free stream speed.
- Isotropic grid turbulence also convected at the free stream speed.

The importance of the former flow lies in the fact, that many complex flows can be Fourier analyzed into sinusoidal gusts of random velocity amplitude components. Thus the knowledge of the response of a bluff body to this very simple unsteady flow would help in elucidating its behaviour in more general flows in any linearized analysis of the response.

It was intended to examine the applicability of linearized

thin aerofoil theories (e.g. Sears (1941), Jackson, Graham and Maull (1973), also Chapter 2) to the present problem. The unsteady thin aerofoil theories were considered to be useful, because they can be applied directly to turbulence, in contrast to numerical models (e.g. Giesing (1968), Basu and Hancock, 1977) for which this is extremely difficult. On account of this reason, the test bodies to be used would have to be similar to thin aerofoils in the following respects:-

(i) The thickness to chord ratio should be kept fairly small, in the range of 30%, but still sufficiently large, so that the bodies could still be considered bluff.

(ii) Flow separation was to take place at or near to the rear of the models, as with unstalled aerofoils. A large unseparated surface would result in a relatively greater importance of the "direct" lift caused by the unsteady flow, over the natural vortex shedding, "indirect", lift which was examined in less detail in the present work. The bluff sections should, therefore, have a well rounded leading edge, to avoid premature separation.

(iii) The effects of camber, incidence and thickness on unsteady lift, were not to be systematically investigated. In steady flow, aerofoil camber and incidence have small effect on the theoretical lift curve slope (for moderate incidences), while thickness tends to increase it. On the other hand, aerofoil thickness was found to decrease slightly the unsteady lift curve slope in unsteady two-dimensional flow (e.g. Maeda and Kobayakawa, 1970). If the distortion of vorticity is taken into account Goldstein and Atassi (1976) indicated, that although the effects of aerofoil camber, incidence and thickness could not be explicitly separated, the last would not be as important as the first two. Taking into account these points it was realised that the applicability of aerofoil theories for lift on bluff bodies, would be

more rigorously tested if the number of pertinent variables (camber, incidence, thickness, vorticity of oncoming flow) was kept to a minimum. Since it was not possible to discard thickness when examining bluff bodies (with properties as in (ii)), it was decided to consider only symmetrical profiles (i.e. no camber), at zero mean incidence with respect to the mean free stream direction. In the case of the sinusoidal flow, it was also thought advantageous to employ an irrotational upwash gust, in order to minimize the effects of vorticity distortion.

The loading of an aerofoil is made determinate by imposing a zero loading condition (known as the Kutta-Joukowski condition) at its single trailing edge, which is the position where the flow leaves the surface. A corresponding condition would be needed to calculate the loading on a bluff body, with the difference that here there is more than one point, at which the flow leaves the surface. As the nearest to an aerofoil bluff section, one could first consider an elongated aerofoil with two fixed separation points, but of which the thickness and the distance between the separation points gradually increase. However, since not all bluff bodies have fixed separation, it would also be useful to consider a similar body with two free separation points. Applying thin aerofoil theory, the assumption is made that the zero loading condition holds across the two separation points - in effect that it holds at a mean position between the separation points, "equivalent" to the aerofoil trailing edge. In the present work, it is intended to test how reasonable this assumption is.

The aforementioned reasons led to the choice of the following test model profile sections:-

- A D shape section with the nose in the upstream direction (sometimes called C shape), consisting of a half ellipse with its major axis aligned

with the free stream, attached to a rectangular afterbody. The elliptic nose was employed in order to prevent separation ahead of the body's trailing edge (for a suitable choice of Reynolds number range), see sketch below.

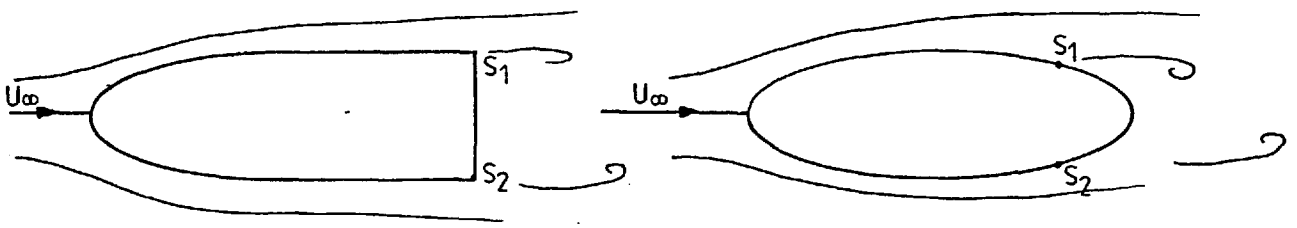

S_1, S_2 are separation points

SKETCH

- An elliptic section, of the same geometry as the nose of the D section and of the same thickness. At sufficiently high Re numbers, the two separation points lie downstream of the maximum thickness position.

Further, to be able to check how accurately linearized thin aerofoil theories apply to a moderately thick aerofoil and uncover any phenomena, which might not be related to the differences of bluff bodies and aerofoils, but to particular features of the experimental apparatus (response of force transducers, anisotropy of flow, etc.), a third model was used, this being a symmetric aerofoil at zero incidence.

In the experiments with the sinusoidal flow, an aerofoil of similar profile placed at a high incidence to the mean stream was also used. When the aerofoil was near the stall, it had two separation points, one free on the upper (suction) surface and another fixed at the trailing edge. The purpose of this was to study the behaviour of separation points in unsteady flow.

Only two-dimensional models were examined in this work, i.e. completely spanning the working section.

In the following chapter, a literature review is given, which contains data and formulae needed in the main work and which marks the areas of inadequate knowledge on the subject.

CHAPTER 2. PREVIOUS THEORETICAL AND EXPERIMENTAL WORK ON THE LOADING OF TWO-DIMENSIONAL RIGID BLUFF BODIES

2.1 FLOW SEPARATION ON TWO-DIMENSIONAL BLUFF BODIES

The striking characteristic which distinguishes a streamlined from a bluff body, is that the latter causes a significant perturbation on the flow, in which it is immersed. Separation refers to the departure from the neighbourhood of the surface of those streamlines which lay within the boundary layer upstream; for a two-dimensional bluff obstacle, with a closed boundary, separation occurs at two or more points. At these separation points, it is usually assumed, in steady flow, that the flow near the surface is reversed and the wall shear stress, τ_w, becomes zero. In the flow over a curved surface, τ_w is gradually diminishing as the separation point is approached. However, in the case of a surface with a sharp edge, the flow as a whole adjusts itself so that separation takes place at the sharp edge (or in practical terms very near to it), without any sign of decrease in the wall shear stress, as the separation point is approached. Flows, with separation points of the former type (free separation points), are much more strongly influenced by pressure gradients and changes in the oncoming stream conditions (Re number, turbulence) or wall conditions (roughness, boundary layer control by suction, etc.), than those with separation points fixed at a salient edge. Examples of both type of flows can be found in Goldstein (1965) and Schlichting (1968).

In steady flow over a body with two separation points, it is experimentally evident (e.g. Fage and Johansen, 1927) that the average rate at which vorticity is transported downstream from the one separation point is equal and opposite to the rate at which vorticity is transported

at the other separation point. The word "average" is used here because, instantaneously, these rates are not equal and opposite to each other. For small surface curvature, this means that the average velocities and pressures at the two separation points should be equal. The same applies to an unstalled aerofoil, with the difference that the two separation points lie both at the sharp trailing edge, where (but in the wake as well) the vortex strength is now zero. In aerofoil theory, this fact is expressed by the Kutta-Joukowski condition, an alternative formulation of which is that the flow leaves smoothly at the trailing edge. By means of this condition the mean lift $\overline{L}$ and the mean circulation $\overline{\Gamma}$ round an aerofoil in inviscid flow are related by the equation:-

$$\overline{L} = \rho U_\infty \overline{\Gamma} \qquad (2.1)$$

where U_∞ is the free stream speed. In the case of bluff bodies, Eqn. (2.1) would only be valid if a circulation $\overline{\Gamma}$ could be found, such that the inviscid and experimental pressure distributions were in agreement. However, flow separation cannot in general be taken into account with inviscid theories only. Therefore, Eqn. (2.1) will tend to be more correct, the closer the flow conditions round a bluff section are to those round an aerofoil.

When the oncoming flow is unsteady, there is experimental evidence, e.g. Despard and Miller (1971), that transient flow reversal occurs at all points on the surface in an adverse pressure gradient regime. It may also be that a transient reversal occurs even in a zero mean pressure gradient. Therefore, unless separation is fixed at a salient edge, there would be an ambiguity as to what is meant by separation in unsteady flow according to the conventional definition. Despard and Miller (1971) proposed a new definition (for a laminar boundary layer), i.e. that the separation position can be signalled by

the occurrence, for the first time as the surface is traversed downstream, of a continuous (i.e. at all times) reversed flow. This definition results in a unique point in the flow field and it is still valid for steady flow. On the other hand, Sears and Telionis (1971) constructed a theoretical model for separation, based on the conviction that, at least locally, the separated wake is a distinct body of fluid that bifurcates the boundary layer flow and pushes it away from the wall. Thus, they defined a "centre" of separation, not generally on the wall, which moves in the u direction with the speed of the separation phenomenon and is characterized by a zero shear stress. In the present work, when mention is made about experimental separation points in unsteady flow, it will be assumed that they are those that would have been found by applying Despard and Miller's (1971) definition.

The flux of vorticity at the two separation points A, B in unsteady flow is no longer constant nor is the total flux into the wake equal to zero. Instead, the total flux is instantaneously equal and opposite to the rate of change of circulation, Γ, about the body (constancy of circulation theorem). This is expressed mathematically as:-

$$\int_0^{\delta} j(u - u_{sep})\, dy \Bigg|_B^A = \left(\frac{1}{2} U_e'^2 - u_{sep} U_e'\right) \Bigg|_B^A = -\frac{d\Gamma}{dt} \qquad (2.2)$$

(see Sears, 1976)

where:-

δ = boundary layer thickness

j = vorticity in the boundary layer

u = velocity component parallel to the wall

u_{sep} = velocity of motion of the separation phenomenon

U_e' = value of u at the outside edge of the boundary layer

$\Big|_B^A$ stands for the difference between the flux of vorticity at the separation

points A and B.

When the vorticity is shed from a sharp edge, like the trailing edge of an aerofoil, then the points A and B both lie on the sharp edge and u_{sep} is zero. In this case, it is argued (e.g. Basu and Hancock, 1977) that the flow must leave the edge parallel to the one or the other of its surfaces, depending on the sign of the shed vorticity as shown in the sketch below.

sharp edge flows (frictionless fluid)

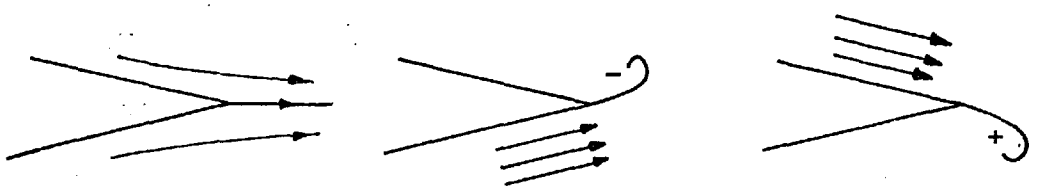

steady flow unsteady flow

SKETCH

In the case of an aerofoil, Eqn. (2.2) expresses the relation between the vortex strength at the trailing edge and the rate of change of circulation. But the same relation could have been obtained from the inviscid aerofoil theory (see Bisplinghoff et al, 1958) by appealing to the Kutta-Joukowski hypothesis, of no loading on the trailing edge. Thus, in the words of Sears (1976), there is a rather surprising identity between the vorticity production in the boundary layers and the Kutta-Joukowski condition. Eqn. (2.2) may, therefore, be termed as an equivalent Kutta-Joukowski condition for unsteady flow. Its importance lies in the fact, that in a particular flow model, it can be used to determine the value of the instantaneous circulation round the body and, depending on the accuracy of this model, to estimate the unsteady lift.

2.2 LOADING OF BLUFF BODIES IN STEADY UNIFORM FLOW

2.2.1 METHODS OF CALCULATING THE MEAN LOADS

The problem of calculating time-averaged pressures and forces round a bluff body, placed in a steady stream at relatively high Re numbers, can be approached, sometimes successfully enough, using potential flow methods combined with certain experimental results.

In Roshko (1954a) it is reported that Kirchhoff developed a "free streamline" theory in which the shear layers springing out of the body were replaced by streamlines of velocity discontinuity. The flow was divided into the wake (which did not play any role in the analysis, being a "dead air" region), and an outer potential flow region. For simple symmetric geometrical shapes, (circular cylinders, flat plates, etc.) the complex velocity potential could be found, after applying suitable conformal transformations, relating the physical and the transformed (hodograph) planes. An unrealistic assumption by Kirchoff was that the pressure in the wake was constant and equal to that in the undisturbed stream, while it is known that a lower pressure exists there. Thus, the theoretical value of the drag coefficient for a flat plate normal to the stream was 0.88, as compared with the value 2.0 found experimentally.

Roshko (1954b) refined Kirchoff's method by equating the velocity along the free stream lines leaving the body with U_s, where:-

$$U_s = k_b U_\infty \quad , \quad k_b = (1 + \overline{C}_{pb})^{\frac{1}{2}} \quad , \quad \overline{C}_{pb} = (p_{base} - p_\infty)/(\tfrac{1}{2} \rho U_\infty^2) \qquad (2.3)$$

The base pressure coefficient $\overline{C}_{pb}$ was determined experimentally and it was the only empirical input to the theoretical analysis for bodies with fixed separation points (flat plates, short rectangle, 90^o wedge). The situation is more complicated for non-fixed separation points. Assuming that in principle the transformation can be accomplished, a

second empirical input is necessary, specifying either the exact position of separation, or the curvature of the free streamline at the position of separation. Care should be taken, so that the predicted streamline does not cut into the body just downstream of separation.

Another free streamline theory employing a different approach, but containing the same degree of empiricism, was the wake source model of Parkinson and Jandali (1970). Here, the wetted surface of the bluff body was conformally mapped (usually via a Joukowski transformation) onto a circular cylinder in another plane t. The two separation points S_1 and S_2 were made critical points of the transformation. Sources and sinks of suitable strength and position were placed in the t plane so that S_1, S_2 became stagnation points of the corresponding (known) flow round the circular cylinder. For fixed separation points, again the only empirical input was $\bar{C}_{pb}$, which was used in the Bernoulli equation to specify the separation velocity. For non-fixed separation points the extra information was the same as with Roshko's method.

A more general extension of this technique was the numerical method developed by Bearman and Fackrell (1974), which combined the basic ideas of the Parkinson-Jandali model and vortex lattice theory. Using this method they replaced the wetted surface of the body by a distribution of discrete vortices. The effect of the wake was taken into account by placing sources on the rear of the wetted surface. The boundary condition of zero normal flow together with the positions of the separation points and the base pressure, sufficed to determined the vorticity distribution and the position and strength of the sources. Non-symmetric bodies with respect to the direction of the mean flow could be treated with this method. A problem would arise due to the development of a lift force, which was not predicted by the theory,

since the circulation round the surface was assumed zero. This requires an extra assumption about the flow, which may be for example that the circulation is equal to that experimentally found in the wind tunnel.

An approach involving more directly the effects of viscosity was undertaken by Howarth (1935) in order to calculate the steady load on a body with separated boundary layers. Howarth employed the inviscid flow pressure distribution round the body to start boundary layer calculations and obtain a first estimate of the position and conditions at the final separation; an arbitrary value of the circulation was initially assumed. If the calculated conditions at separation did not conform to the (equivalent for bluff bodies) Kutta-Joukowski condition in steady flow (see Section 2.1), $\overline{\Gamma}$ was varied until this could be achieved. Then, the mean lift was calculated from Eqn. (2.1). Howarth refined his method by considering the cases of fully laminar and fully turbulent boundary layers (therefore, no scale effect), as well as the case where transition was allowed to occur. There are two main disadvantages of the method described: First, Eqn. (2.1) is not valid for a bluff body, so that the analysis will tend to be more accurate for the better streamlined bodies. Second, the assumptions leading to the boundary layer equations break down at separation and consequently the conditions at separation cannot be accurately determined. On account of the first reason Howarth applied his method to a two-dimensional thin elliptic cylinder (fineness ratio 6.0). The calculated mean lift curve slopes, $\overline{\partial C_L}/\partial\alpha$, at zero incidence are given in Fig. 2.1 for fully laminar and fully turbulent boundary layers. The $\overline{\partial C_L}/\partial\alpha$ corresponding to the latter case was the greatest, while for the mixed type boundary layer calculations (partly laminar, partly turbulent) intermediate values of $\overline{\partial C_L}/\partial\alpha$ were to be expected.

2.2.2 EXPERIMENTAL WORK ON THE MEAN LOADING OF BLUFF BODIES

There is a great deal of experimental work available for the loading of bluff bodies with particular emphasis given to the circular and square cross-sections and the flat plate held normal to the free stream. Valuable information can be found in Roshko (1961) and Goldstein (1965) for circular cylinders, Vickery (1966), Pocha (1971) and Lee (1975) for square cylinders, Polhamus (1959) and Polhamus et al (1959) for rectangles and square cylinders with rounded edges, Fage and Johansen (1927) and Roshko (1954a) for flat plates. The important characteristics which were observed in the behaviour of these sections, but nevertheless are common to all other bluff sections, will now be briefly described.

The mean drag coefficient of a bluff body is much greater than that of a streamlined one; while in the latter the drag consists mainly of viscous friction, in the former it consists mainly of the difference between the normal pressures of the front and rear surfaces. Generally, the lower the pressure in the back (base) region, the greater is the drag and the curvature of the streamlines leaving the surface.

The wake is a region, where the fluid loses momentum, so that a narrow wake indicates a low mean drag while a broad wake, high drag. Especially for the bodies with non-fixed separation points the wake width and consequently the drag are strongly influenced by the Re number of the flow. This happens because the position where a laminar shear layer becomes turbulent depends on the Re number. At low Re numbers the separated shear layer is laminar and becomes turbulent at a certain distance downstream. The flow is then said to be subcritical. Free streamline theories (Section 2.2.1) are in reasonably good agreement with experiments in this flow range, especially for bodies with fixed separation points. An increase in the Re number brings the transition

upstream, until at a specific Re number (critical Re number), laminar separation and transition occur at the same point on the surface. By a further increase in the Re number the developed turbulent boundary layer, being able to sustain more effectively adverse pressure gradients, separates further downstream. As a result of the downstream movement of the separation point there is a significant narrowing of the wake with corresponding fall in the mean drag. The magnitude of this drop for elliptic cylinders of various fineness ratios can be seen in Fig. 2.2. It appears that the critical range of Re numbers occurs earlier, the less bluff is the section.

The space between laminar separation and the position where the newly formed turbulent shear layer reattaches on the surface, is occupied by a separation bubble. This is a region of recirculating fluid of nearly constant pressure (see for example Crabtree (1957) and Tani, 1964) and, therefore, it could manifest itself by a flattened portion in a mean surface pressure distribution. Fig. 2.3 displays clearly the changes that take place in the positions of laminar and turbulent boundary layer separation for an elliptic cylinder, (a geometric shape studied in the present work), when the Re number is varied. The measurements are due to Schubauer (1939). Besides the effects mentioned previously, Schubauer found that a very incomplete transition took place in the region which marked the end of the accelerating pressure gradients (near the maximum thickness of the cylinder). On account of this reason the boundary layer separation which he observed for $9 \times 10^4 \leq Re \leq 3.2 \times 10^5$, was neither purely laminar nor turbulent, but, in his words, of a "nearly laminar" type.

Several other authors, e.g. Roshko (1961), Bearman (1969), Bruun and Davies (1975), have experimented in the critical flow range

and their results confirmed not only the strong dependence on the Re number, but also the dependence on disturbances in the free stream, surface roughness and even wind tunnel installation. The agreement of the experimental results with free streamline theories is deteriorating in the critical range, due to the existence of the separation bubbles.

Generally, the bluff cylinders are found to behave differently to changes in the mean incidence than the aerofoils. For example the drag coefficient of a square cross-section cylinder (flat side facing the stream at zero incidence) decreases with increasing incidence, while a negative lift develops, see for example Lee (1975). This is caused by the reattachment of the shear layer, separating from the lower front corner, to the side of the cylinder and the subsequent narrowing of the wake. In another case, it is found that the mean lift curve slopes of certain elliptic cylinders are exceedingly high at zero incidence, e.g. Zahm et al (1928), Williams et al (1937) and Polhamus et al (1959), while the mean lift v. incidence curves are no longer straight lines for moderate incidences. Fig. 2.1 shows that even for constant fineness ratio, $\overline{\partial C_L}/\partial\alpha$ does not remain constant, when the Re number is changed. The lift curve slopes obtained theoretically by Howarth (1935) are compared in this figure with the experimental results of Williams et al (1937). It can be seen that in the critical range the experimental slopes are much greater than those predicted, but as Re increases there is a tendency towards a better agreement.

2.2.3 THE UNSTEADY LOADING OF BLUFF BODIES IN A STEADY FREE STREAM

Unsteady loads in this case may arise on bluff bodies for two reasons: Either due to vortex shedding or due to instabilities, provoked by a particular behaviour of their mean loading characteristics

with changing incidence. In the latter case, the induced oscillations either transverse to the direction of the free stream, or in torsion about the longitudinal elastic axis, are known as "galloping".

(i) Vortex shedding: The sheets of vorticity leaving the bluff body roll up alternatively further downstream to form a vortex street. The dimensionless group $S = n_{VS}b/U_\infty$, where n_{VS} is the shedding frequency (i.e. the frequency at which the vortices appear in the wake) and b the body thickness or diameter, is the Strouhal number. Experiments, e.g. Roshko (1954a), Bearman (1969), have shown that S remains sensibly constant in the subcritical range, but it is raised to higher levels in the critical range. Gerrard (1966) postulated that the main factors determining the frequency of vortex shedding are the size of the region where the vortices are initially formed and the thickness of the shear layers at the end of that region; he could then explain the relative constancy of the Strouhal number when the Re number was changed.

The unsteady pressure field round the body, induced by the wake vortices, results in fluctuating lift and drag forces, of which the frequency contents are maximum at the shedding frequency and twice the shedding frequency respectively. An elastic body may be forced to oscillate because of these loads, especially in the transverse direction, where the lift forces are greater. Stronger excitation will develop if vortex shedding is well correlated in the spanwise direction. When the vortex shedding and body natural frequencies approach coincidence, as would happen for example when the wind speed is varied, an aerodynamic resonance known as the "capture" or "lock in" effect takes place, provided that the amplitude of transverse oscillations is sufficient. What happens is that the shedding frequency occurs at the oscillation frequency for a certain range of speeds. In a circular cylinder, for

example, "lock in" appears for oscillation amplitudes exceeding 2% of the diameter approximately and could persist even if U_∞ is about 1.5 times greater, than the speed at which the shedding and natural frequencies were equal, see Owen (1973). During "lock in", the amplitude of oscillation and fluctuating pressures is increased as well as the spanwise correlation of the shed vortices and the pressures. There are also great changes in the phase between the fluctuating lift and displacement. Hysteresis effects (i.e. dependence of the "lock in" extent, force amplitude, etc. on the direction through which the natural frequency is approached by n_{vs}) are also observed, see for example the review of Mair and Maull (1971).

The fact that the vortex induced oscillations are in some cases undesirable or, even worse, cause structural damage, has led to a considerable amount of experimental investigation and some theoretical formulations. In one of them, the wake is represented by two infinite rows of staggered vortices of opposite sign. The von Karman vortex street (see Goldstein (1965) and Lamb[+], 1974) is only a special case of a stable vortex street, with spacing ratio 0.281. Sallet (1972) used this flow model to calculate the unsteady lift due to vortex shedding. Certainly, the values obtained are not likely to be very accurate, because the region where the vortices are formed and the lack of spanwise correlation were ignored. A more sophisticated method was developed by Clements and Maull[*] (1975). The wake was represented by discrete vortices shed behind a semi-infinite constant thickness square-ended body at specified time intervals. The nature of the self excited vortex shedding has also led some authors to assume that the fluid behaviour could be modelled by a simple non-linear oscillator. In one approach the fluctuating lift coefficient satisfied a van der Pol equation. A description of the various models developed can be found in Blevins (1977).

[+] Lamb, H. "Hydrodynamics" C.U.P Sixth edition, 1974.

[*] Clements P.R and Maull D.J., Progress in Aerospace Sci, 1975, 16, pp 129-146, Pergamon Press.

(ii) "Galloping": This instability is not connected with vortex shedding and the oscillation proceeds with a frequency close to the natural structural frequency. Parkinson and Brooks (1961) formulated a quasi-steady theory for bluff bodies in order to predict the characteristics of transverse galloping (amplitude, build-up time). Their theory predicted the behaviour of the oscillating body with reasonable accuracy away from the "lock in" range; it also agreed with den Hartog's criterion which states that "a section is dynamically unstable if the negative slope of the lift is greater than the ordinate of the drag curve". Experiments by the same authors suggested that the instability could be associated with the length of the afterbody. Thus, a circular cylinder, a D section and an upright rectangle vibrated under vortex excitation (because their short length of the afterbody apparently did not interfere with vortex shedding), while the square cross section and the long rectangle vibrated (for suitable values of structural damping) in a manner similar to that predicted by the theory.

The approach described above, is one of the many dealing with the prediction of the aeroelastic behaviour of bluff bodies. In several proposed models, elements from unsteady aerofoil theory are included. More information about galloping and flutter (i.e. two degrees of freedom instability) can be found in conferences on wind induced vibrations, e.g. Naudascher (1972).

2.3 LOADING OF BLUFF BODIES IN OSCILLATORY FLOWS

A general sinusoidal flow disturbance has three velocity components along the x, y, z axes of the coordinate system of the form:-

$$u_i = \hat{u}_i \, e^{i(\omega t - k_1 x - k_2 y - k_3 z)} \qquad (2.4)$$

$(i = x, y, z)$

where:

$\hat{u}_i$ is the amplitude of the fluctuating velocity;

ω is the frequency of the sinusoidal variations sensed by a point which is fixed in the coordinate system;

k_1, k_2, k_3 are wavenumbers in the x (streamwise), y (spanwise) and z (transverse) directions respectively.

The unsteady loading of aerofoils in oscillatory flows has been treated successfully by using linearised theories. In the present work, it will be attempted to use these theories in order to predict the loading of bluff bodies. Therefore, it was thought useful to describe them briefly.

2.3.1 UNSTEADY AEROFOIL THEORIES

For sufficiently small gust velocities and aerofoil thickness incidence and camber the component of the gust in the spanwise direction may be neglected. Then two unsteady components of lift loading can be identified: One is a first order component due to the transverse (upwash) component of the gust $u_z = w$, and the other is a second order component dependent on the combination of the streamwise component $u_x = u$ and the mean incidence $\bar{\alpha}$, i.e. on $u\bar{\alpha}$. There are theories for the loading due to both of these components.

If the changes in the upwash pattern occur over distances much greater than the chord of the aerofoil, then the gust is said to convect as a frozen pattern. If it is convected at the free stream speed of the flow, the wave number k_1 will be then equal to ω/U_∞, or if all wave numbers are non-dimensionalized by the half of the aerofoil chord (c/2):-

$$k_1 = k = \frac{\omega c}{2U_\infty} = \frac{\pi n c}{U_\infty} \qquad (2.5)$$

k is also called the reduced frequency and gives a measure of the gust wavelength with respect to the aerofoil chord length.

Sears (1941) determined the response of a zero thickness aerofoil and at zero mean incidence, to an upwash of the form:-

$$\alpha_g(t) = \frac{\hat{w}}{U_\infty} e^{i(\omega t - kx)} = \hat{\alpha}_g e^{i(\omega t - kx)} \tag{2.6}$$

where $\alpha_g(t)$ and $\hat{\alpha}_g$ are the fluctuating and peak gust amplitudes respectively. The coordinate x was zero at the model mid-chord point. In Sears's model the aerofoil surface and the wake were represented by a distribution of vortex singularities. Free stream vorticity was neglected in this analysis. The Kutta-Joukowski condition of no loading at the trailing edge, was assumed to apply at all times. The unsteady lift coefficient was found to be:-

$$C_L(t) = 2\pi \hat{\alpha}_g e^{i\omega t} S(k) \tag{2.7}$$

where S(k) is the Sears's response function given by:-

$$S(k) = \left(C(k)\left[J_0(k) - iJ_1(k) \right] + iJ_1(k) \right) \tag{2.8}$$

where $C(k) = H_1^{(2)}(k)/\{H_1^{(2)}(k) + iH_0^{(2)}(k)\}$ is Theodorsen's (1935) function, associated with the response of an oscillating aerofoil. J_0, J_1 are Bessel functions of the first kind. $H_1^{(2)}$, $H_0^{(2)}$ are Hänkel functions of the second kind. The squared modulus and the argument of S(k) are plotted in Figs. 2.4 and 2.5 respectively.

In later years Kemp (1952), extended Sears's theory to include the case of an upwash gust propagating at a speed $U_c \neq U_\infty$. Then the streamwise reduced frequency k_1 is equal to k', so that:-

$$k_1 = k' = \frac{\omega c}{2U_c} = \frac{\pi n c}{U_c} \tag{2.9}$$

and Sears's function is replaced by Kemp's function $S(k, k')$ such that:-

$$S(k, k') = \left[J_0(k') - iJ_1(k')\right] C(k) + i \frac{k}{k'} J_1(k') \qquad (2.10)$$

This complex function is plotted in Figs. 2.4 and 2.5, for various ratios U_c/U_∞. It is observed that the differences between $S(k)$ and $S(k, k')$ become more apparent for greater k (if k/k' = const.).

Maeda and Kobayakawa (1970) examined the problem of a thick aerofoil exposed to an upwash gust of the Sears type. The boundary conditions were exactly satisfied on the aerofoil surface by an additional distribution of sources on the mean chord line. No distortion of vorticity was taken into account and the wake vorticity was assumed to be shed as in Sears's analysis (found after employing the Kutta-Joukowski condition). The calculated response function had a magnitude lower than Sears's function.

The response of a thin aerofoil to a yawed sinusoidal upwash of the type $\hat{w}\, e^{i(\omega t - k_1 x - k_2 y)}$ and convected at the free stream speed was calculated by Graham (1970a) using an exact lifting surface theory. For a chordwise section the unsteady lift coefficient was given by:-

$$C_L(t, y) = 2\pi\, G(k_1, k_2) \frac{\hat{w}}{U_\infty} e^{i(\omega t - k_2 y)} \qquad (2.11)$$

where the response function $G(k_1, k_2)$ was calculated by Graham numerically. In Fig. 2.6 the magnitude and the argument of Graham's function are plotted against the modulus of the reduced frequency $k_g = \sqrt{k_1^2 + k_2^2}$. The various combinations between k_1 and k_2 result in the "front" of the yawed gust (i.e. the set of points with the same velocity and phase) being inclined to different angles with respect to the aerofoil leading edge. It is seen that the smaller is this angle, the closer is Graham's function to Sears's function. A perturbation expansion of $G(k_1, k_2)$ to

second order in k_2 is given in Graham and Kullar (1977). For a two-dimensional wing element of aspect ratio AR = span/chord = s/c, the unsteady lift is equal to:-

$$C_L(t) = 2\pi\, G(k_1, k_2)\, \frac{\sin(k_2 AR)}{(k_2 AR)} \cdot \frac{\hat{w}}{U_\infty} e^{i\omega t} \qquad (2.12)$$

As stated previously, for an aerofoil at incidence, there is an extra lift loading (i.e. in addition to that given by Eqn. 2.7) depending on $u\bar{\alpha}$. Horlock (1968) examined the response to a streamwise gust convected at U_∞, of the form $u = \hat{u}\, e^{i(\omega t - kx)}$. The result is:-

$$C_L(t) = 2\pi\bar{\alpha}\, \hat{u}\, e^{i\omega t}\, T(k) \qquad (2.13)$$

$$\text{with } T(k) = S(k) + J_0(k) + iJ_1(k) \qquad (2.14)$$

For a gust convected at a speed $U_c \neq U_\infty$, i.e. $u = \hat{u}\, e^{i(\omega t - k'x)}$, $k' = \frac{\pi n c}{U_c}$, the response function was calculated by Holmes (1970) as:-

$$T(k, k') = S(k, k') + J_0(k') + iJ_1(k') \qquad (2.15)$$

This function is plotted in Fig. 2.7 for several values of the ratio U_c/U_∞. It should be noted, however, that the load response can be affected, if the gusts have a dependence on the reduced frequency k_3, in the upwash direction, or if they are rotational. The last effect would be due to the distortion of vorticity, which is discussed below.

The distortion of vorticity in the free stream is a result of the interaction between the flow and the body placed in that stream. The induced velocity fields due to this interaction are as follows:-

(a) The mean perturbation of the flow, cancelling the normal component on the surface of the body.

(b) The unsteady field induced by the body, which cancels the gust on the surface.

(c) The unsteady field resulting from the distortion of the vortices by the mean flow perturbation in (a). Vortices in the free stream can be distorted by skewing, stretching and convection at different rates. The induced velocities can be found from the Biot Savart law.

(d) The unsteady field which cancels the field (c) on the surface of the body.

The mathematical approach for the calculation of the distortion effects is by solving the vorticity transport equations. These equations can be made simpler, if the inertial and viscous effects can be neglected. In the case of a random turbulent gust this results in the "rapid distortion theory", in which it is assumed that each spectral component of the gust is distorted so quickly that it has no time to exchange energy with other spectral components or be affected by viscosity. Several authors applied this method for turbulent flows round bodies like a circular cylinder (Hunt, 1973), a porous plate normal to the stream (Graham, 1972) and an aerofoil at high mean incidence (McKeough, 1976). For the aerofoil at incidence considered previously, it is reported in Graham (1970b) that the vorticity in the free stream may be neglected if the variations in the mean pressure field of the aerofoil are small compared to the total pressure of the free stream and if the displacement of the streamlines is also small.

2.3.2 THEORIES FOR THE UNSTEADY LOADING OF BODIES WITH FLOW SEPARATION

In the inviscid aerofoil theories described previously, the downstream stagnation point was located on the sharp trailing edge. The results derived can be applied to the real flow situation, where the aerofoil and its boundary layers are thin and all the way attached to

the surface. However, these results would be less representative for aerofoils with a rounded trailing edge and bluff bodies, where separation occurs at two points. With regard to this problem, there is very limited work done on the aerofoils with a rounded trailing edge and almost no work, as far as the author is aware, on bluff bodies. The main points of the existing work will now be reported. It should be emphasized that the (natural) vortex shedding phenomenon will be examined in a separate section later.

Moore (1955) calculated the unsteady lift on a thin elliptic cylinder (fineness ratio 6.0) placed in a stream of varying direction (i.e. a gust of the type $\hat{w}e^{i\omega t}$). His method was similar to that of Howarth (1935) for a laminar boundary layer (see Section 2.2.1) but was extended to include some unsteady effects. The complexity of the problem was simplified by Moore in two ways: First, he assumed that the fluctuations in the incidence $\alpha_g(t)$ of the free stream were of low frequency, that is $d\alpha_g(t)/dt$ was assumed small. This permitted the terms proportional to $d^2\alpha_g(t)/dt^2$ and all higher derivatives to be neglected. Second, he considered only the case of maximum mean lift. Then, not only the quasi-steady rate of change of circulation would be zero, but, in view of the first assumption, that to order $d\alpha_g(t)/dt$. Therefore, although the circulation about the body is perturbed, the total vorticity flux into the wake is negligible and, consequently, there would be no unsteady lift due to the wake. Still, the complication due to the unsteady movement of the separation points remained and it was calculated by using Eqn. (2.2) and the von Karman momentum equations. (The separation points were defined from the vanishing of wall shear). The choice of a thin cylinder was again based on the requirement of thin boundary layers, thus making less objective the use of potential flow methods for determining the external flow. Finally, the total lift was

found from Eqn. (2.1) and the contribution of the impulsive pressures due to the unsteady potential flow. In the case of sinusoidal variations in $\alpha_g(t)$ the unsteady lift increment is found to be also sinusoidal and to lag behind $\alpha_g(t)$ by 90 degrees. Apart from its weak points common with Howarth's method (Section 2.2.1), the theory described suffers, according to Sears (1956), from the ambiguity in defining separation in unsteady flow.

A more general approach was suggested by Sears (1976), making full use of Eqn. (2.2). He stated that in order to calculate the loading on a thin cylinder with a rounded trailing edge, a dual model was needed: A vortex sheet model, representing the cylinder and its two-layered wake by single bound and free vortex sheets (as in thin aerofoil theory) and a boundary layer model, requiring a more accurate picture of the body's contour, for the determination of the circulation. The total lift would then be calculated from the thin aerofoil formulae (in terms of vortex strength distributions) which were derived from the conservation of momentum considerations. However, there would be a questionable point about using the thin aerofoil result for the detailed pressure distribution if separation occurs upstream of the trailing edge and the separated layers are very thick; in that case the pressure calculated from the bound vortex sheet may differ from that at the body's surface. For this reason, Sears's propositions are intended for thin cylinders.

Woods (1961), presented an unsteady wake flow theory for the calculation of unsteady loads on oscillating cylinders of arbitrary thickness and shape, but with fixed separation points. The strength in the vortex sheets was determined by solving two simultaneous integral equations under two main assumptions: First, that the pressure at any point in the wake is constant and equal to its mean steady value and second that the boundary conditions of the unsteady flow can be applied

to the boundaries of the basic steady flow (which is assumed to be known). Two examples of the general theory were given, one dealing with a flat plate placed normal to a steady stream and executing oscillations in this direction and another dealing with an oscillating aerofoil fitted with a spoiler.

In a fluctuating free stream, the drag exerted on a body is given by the semi-empirical equation:-

$$D(t) = \frac{1}{2} C_D(k)\, d \cdot \rho\, U_1|U_1| + C_m(k)\, \rho \cdot S_a \frac{dU_1}{dt} \qquad (2.16)$$

where $C_D(k)$ and $C_m(k)$ are the drag and virtual mass coefficients respectively, which are functions of the reduced frequency k (see for example Davenport, 1961). d is the diameter of the body; S_a is the reference area to which C_m is based and U_1 is the stream speed far from the body.

The frequency dependent drag and virtual mass coefficients tend to their steady flow values when the reduced frequency tends to zero. Davenport (1961), was the first to introduce the concept of the aerodynamic admittance when he examined, by means of Eqn. (2.16), the unsteady drag exerted on a body placed in a stream with sinusoidal streamwise fluctuations.

2.3.3 EXPERIMENTAL WORK ON THE LOADING OF BLUFF BODIES IN AN OSCILLATORY FREE STREAM

The material available for the direct loading in sinusoidal flows is of surprisingly limited extent, since most investigations concentrate on the effects of the oscillatory flow upon vortex shedding, e.g. Pocha (1971), Hancock (as reviewed in Mair and Maull, 1971). In this sense, the present work is probably among the few dealing with the direct response of bluff bodies in sinusoidal flows.

2.3.4 EFFECTS OF OSCILLATORY FLOWS ON BOUNDARY LAYERS

Of interest are the effects, which can be caused by oscillatory flows on the boundary layer transition and separation as well as on the skin friction coefficient. This has been the subject of theoretical and experimental investigations mainly for unidirectional flows, in which the streamwise velocity oscillates sinusoidally about the mean.

Lighthill (1954) worked out, in a theoretical analysis, the fluctuations in the laminar skin friction of a cylindrical body exposed to a sinusoidally streaming flow. He found that the maxima of skin friction anticipated the maxima of the stream velocity and that if the oscillation frequency was greater than a critical value, (depending on the point on the surface) then this phase advance was 45^{o} and the skin friction behaved as if there was zero mean velocity. Unfortunately, he could not draw definite conclusions about boundary layer separation. The phase lead inside the boundary layer and the amplification of the velocity waveform, which were predicted by Lighthill, were confirmed by Despard and Miller (1971), who conducted experiments on a flat plate in a streamwise sinusoidal flow with an adverse pressure gradient. They also found the separation point to move upstream of its steady flow position; this displacement appeared to decrease with increasing dimensionless frequency $\frac{2\pi n\nu}{U_\infty^2}$, while to be almost unaffected by the amplitude of the velocity fluctuation $\frac{\Delta U}{U_\infty}$. For the type of flow mentioned above, Morkovin et al (1971) pointed out that transition to turbulence may occur much earlier than in a steady flow of the same speed U_∞.

The turbulent boundary layer is less amenable to theoretical and experimental investigation and work is still in progress. Relevant information can be found in conference proceedings, see for example

Eichelbrenner (1971). A remarkable result by Karlsson (1959), who carried out experiments with a flat plate in zero pressure gradient, was that the mean velocity profile was not significantly affected by streamwise fluctuations of amplitude as much as 30% of the free stream speed.

2.3.5 EFFECTS OF OSCILLATORY FLOWS ON VORTEX SHEDDING

An oscillatory field may affect the phenomenon of vortex shedding in many respects. In the first place, there could be a coupling between the fluctuating wake and the applied field, leading to a suppression or enhancement of the energy at vortex shedding. Which of the two will occur depends on the symmetry of the two fields and their relative frequencies. Pocha (1971) conducted experiments with a square cross section cylinder in a sinusoidal upwash gust. He found that for gust frequencies not very close to the shedding frequency, the vortex shedding lift C_{Lvs} was lower with respect to its steady flow value. As the gust frequency neared the shedding frequency (within ± 0.5 Hz) the latter was "locked in" by the former and C_{Lvs} became greater than its steady flow value, see Fig. 2.8. Pocha pointed out that the shedding of vortices was strong and very regular during "lock in", in contrast to the weak and irregular shedding away from "lock in". The role of the field symmetry on the coupling between the wake and the externally applied flow was examined by Hatfield and Morkovin (1973). When a circular cylinder was placed in a streamwise sinusoidal flow, which, in the undisturbed state, had a symmetry in pressure with respect to the cylinder chordline, no significant change in the fluctuating pressure at the separation points was found, even when the oscillation and shedding frequencies coincided. This was due to the antisymmetry of the vortex shedding pressures with respect to the cylinder chordline (in the streamwise direction - see for example Gerrard, 1961). On the other hand, a

strong excitation at "lock in" was found when an antisymmetric acoustic field in the tunnel was employed.

If the vortex shedding characteristics are sensitive to changes in the mean incidence, then the application of a sinusoidal upwash gust is expected to have an analogous effect. Pocha (1971), observed that the vortex shedding lift coefficient of a square cross section cylinder decreased, when the gust amplitude, for constant reduced frequency, was increased (see Fig. 2.8). This, he claimed, was partly a result of a quasi-steady effect, because C_{Lvs} was found to decrease with increasing mean incidence (zero incidence is counted with the flat face of the cylinder placed normal to the stream). However, the fact that the drop in C_{Lvs} was different at equal distances above and below the shedding frequency (see Fig. 2.8), may suggest that the stream fluctuations should not be counted in quasi-steady terms if $n > n_{vs}$.

2.3.6 METHODS OF PRODUCING OSCILLATORY FLOWS

The common characteristic of all the designs intended to produce two-dimensional sinusoidal gusts, is the existence of a sinusoidally fluctuating vorticity somewhere in the flow field. This vorticity, being either in the form of continuous sheets or individual clouds of vorticity, induces an unsteady velocity field, which generally has components both in the streamwise and transverse directions.

A simple example of a two-dimensional oscillatory flow is the wake of a two-dimensional bluff body. With suitable choice of the cross section and the Re number, it is possible to obtain an unsteady field with reasonably sinusoidal transverse and streamwise velocities. Graham (1969) had experimentally demonstrated, that with careful design of the end plates confining the bluff body, the spanwise coherence of the shed vortices could be considerably improved and as a result, a well correlated

gust could be obtained. This type of unsteady field was employed by Lamson (1957), Jackson (1970) and Edwards (1972) for studying the lift response of thin aerofoils. The vortex street should be of sufficient strength to ensure a measurable load on the test model, but unless the model is placed well outside the wake, an amount of background turbulence will be present as well. Further complications include the existence of a shear flow in the wake and a certain modification of the vortex street due to the presence of the model (especially if it is also a bluff body). However, the merit of the wake flow lies in the simplicity of its generation.

In a different class of gust tunnels, the unsteady flow is produced in the region behind one or more aerofoils or flaps, oscillating in a steady oncoming stream. The source of the unsteady flow is here the vorticity, which is shed continuously from the trailing edge of the oscillating bodies. A number of workers adopted this design, e.g. Hakkinen and Richardson (1957), Maeda and Kobayakawa (1970), Pocha (1971), Sawyer (1972), Newton (1973) and the present author. The advantage of this arrangement is that it allows handling a range of reduced frequencies and gust amplitudes by only adjusting the frequency and amplitude of the oscillating aerofoils or flaps. In addition, if the oscillations are controlled by a function generator, e.g. a magnetic tape input, then a gust velocity of a desired waveform may be obtained (see Sawyer, 1972). Care should be taken, so that during oscillation no stall of the aerofoils or flaps would occur, for then additional frequencies, besides the fundamental oscillation frequency, may be introduced into the flow. Pocha (1971) was faced with this problem, when the flow past the two long oscillating flaps he employed, suffered from premature separation; as a remedy, he supplied the top and bottom of the flaps with vortex generators, which induced a strong upwash at the basic frequency of oscillation. A situation which can be objectionable with the oscillating body gust

tunnels, is that of excessive mechanical vibration.

Holmes (1970) worked in a rather unique type of gust tunnel, in which the upper and lower walls, being constructed from flexible metal sheets, were allowed to move. To achieve sinusoidal flow oscillations, these walls were maintained in the form of a sine wave by a system of cams. By adjusting the phase of the upper and lower waves, it was possible to generate streamwise and transverse gusts and their combination as well as "oblique" or "yawed" gusts (see Section 2.3.1), with propagation speed equal to that of the sine waves on the moving walls. A shortcoming of this design is the inability to create gusts propagating at the free stream speed. Horlock (1974) described theoretically the properties of the unsteady flow produced in this tunnel.

Sinusoidal fluctuations in the free stream direction can be also generated by placing rotating shutters either in the working section of the tunnel, e.g. Hatfield and Morkovin (1973), or before the settling chamber, e.g. Chen and Ballengee (1971). In this way, oscillation amplitudes as big as 50% of the mean stream speed can be effected.

2.4 LOADING OF BLUFF BODIES IN TURBULENT FLOWS

A turbulent gust consists of three-dimensional gusts of all orientations and of all wavelengths between a "minimum" determined by viscous forces, and a maximum determined by the boundary conditions of the flow. The randomness is a characteristic of turbulence and dictates a statistical approach to the phenomena associated with it. In this respect, the analysis is best carried out in terms of correlations and spectra. Turbulence can be described by its three-dimensional wave number spectrum which, however, is difficult to measure experimentally. In certain problems it is realised that a full description of turbulence is not necessary, the one-dimensional and two-dimensional velocity spectra

being adequate. The former is defined as:-

$$S_{v_i}(n) = \lim_{\Delta n \to 0} \frac{1}{\Delta n} \left[\lim_{T \to \infty} \frac{1}{T} \int_0^T v_i^2 \ (t, n, \Delta n) \ dt \right] \qquad (2.17)$$

where $i = x, y, z$ and $v_i(t, n, \Delta n)$ is the velocity component in the i direction filtered at frequency n over a bandwidth Δn.

The two-dimensional spectrum is a function of two wave numbers and although it is not simply directly measurable, its Fourier transform, the cross spectrum of turbulence, is. A relationship between the two spectra will be given in the next section.

The study of turbulence becomes less complex, if it is assumed that it is homogeneous (i.e. the averaged properties are independent of position) or isotropic (averaged properties independent of direction). Another simplification occurs, if it is assumed that the turbulent gust is convected as a "frozen" pattern with the mean stream speed, U_∞. This is reasonable, if the velocity fluctuations are small compared with U_∞; space (over a distance r) correlations may then be replaced by time $\left(\tau = \frac{r}{U_\infty}\right)$ autocorrelations, which are sometimes easier to obtain in practice. An example is in the measurement of the longitudinal turbulent length scale L_x:-

$$L_x \equiv \frac{1}{\overline{u^2}} \int_0^\infty \overline{u(x) \ . \ u(x + r)} \ dr = \frac{U_\infty}{\overline{u^2}} \int_0^\infty \overline{u(t) \ . \ u(t + \tau)} \ d\tau \qquad (2.18)$$

The prediction of the unsteady lift forces, induced by an oncoming turbulent stream, appears to be limited only to streamlined bodies. For this reason, the relevant thin aerofoil theory is described next. Unless otherwise stated, the assumptions of isotropy and frozen convection (at U_∞) are meant to apply throughout.

2.4.1 UNSTEADY AEROFOIL THEORIES FOR TURBULENT FLOW

As mentioned in Section 2.3.1, the relevant component of the gust is that in the normal direction to the aerofoil surface. Due to the statistical approach to the problem, the analysis is best carried out in terms of the frequency response function, termed here as the aerodynamic admittance, $A(k_1)$. The aerodynamic admittance is defined from:-

$$|A(k_1)|^2 \equiv \frac{S_{C_L}(k_1)}{S_{\alpha_g}(k_1)} \cdot (2\pi)^{-2} \qquad (2.19)$$

S_{C_L} and S_{α_g} are the one-dimensional spectra of the lift coefficient and the upwash respectively and 2π is the theoretical mean lift curve slope of the aerofoil. Note that, when there is no case of confusion, the square of the magnitude of the aerodynamic admittance will be also called aerodynamic admittance for brevity.

The first attempt to calculate the aerodynamic admittance was made by Liepmann (1952), under two assumptions: First, that turbulence was perfectly correlated in the spanwise direction and second, that each chordwise section or "strip" responded according to Sears's theory (see Section 2.3.1). As a result, the aerodynamic admittance was simply equal to the squared modulus of Sears's function, i.e. $|S(k_1)|^2$. Ribner (1956) formulated the problem in a general way, by considering the total load response as the superposition of the individual loads induced by all the upwash spectral components of turbulence. If it is assumed that the wing does not feel any other flow disturbances, except those on its own plane (reasonable for small thickness and incidence and no vorticity distortion), then the wavenumber (or reduced frequency) in the upwash direction, k_3, would have no effect upon the load response. Then the analysis (to order $\alpha_g = w/U_\infty$) can be carried out in terms of the two wave number response function developed by Graham (1970a) for the unsteady lift due to a yawed

sinusoidal gust (see Eqn. 2.12). The theoretical aerodynamic admittance as given by Jackson, Graham and Maull (1973) is equal to:-

$$|A(k_1)_t|^2 = \frac{4}{c}\int_0^\infty |G(k_1, k_2)|^2 \frac{\sin^2(k_2 AR)}{(k_2 AR)^2} S_{ww}(k_1, k_2)\, dk_2 \qquad (2.20)$$

where $S_{ww}(k_1, k_2)$ is the two-dimensional upwash spectrum of turbulence (all the other quantities appearing are defined in Eqn. 2.12). $S_{ww}(k_1, k_2)$ is related to the normalized (with respect to the one-dimensional spectrum) upwash cross spectrum of turbulence, $R_{ww}(k_1, y)$, by the equation:-

$$S_{ww}(k_1, k_2) = \frac{1}{\pi}\int_0^\infty R_{ww}(k_1, y) \cos\left(k_2 \frac{2y}{c}\right) dy \qquad (2.21)$$

The cross spectrum provides information about the space correlation of two velocity components fluctuating with frequency k_1 and is a real quantity for homogeneous turbulence. The experimental admittances found by Jackson, Graham and Maull (1973) and also by McKeough (1976), are in good agreement with the theoretical admittances given by Eqn. (2.20). Eqn. (2.20) becomes less accurate, but easier to calculate, under the assumption of one-dimensional response of each "strip" of the aerofoil, according to Sears's theory (Section 2.3.1). Such calculations were first performed by Hakkinen and Richardson (1957) who also found the experimental lift to be generally overestimated.

In the theories described, the unsteady lift depended, to first order, on the upwash α_g. A theory, accurate to order $\bar{\alpha}\alpha_g$ for a flat plate aerofoil at mean incidence $\bar{\alpha}$, was developed by McKeough (1976), which also incorporated the effects of turbulence distortion. Using the three-dimensional spectrum of isotropic turbulence, McKeough found that the theoretical admittance increased with increasing absolute magnitude

of the mean incidence, but only moderately, because this theoretical increment did not depend on $\bar{\alpha}$, but on $(\bar{\alpha})^2$ and higher order terms. This was in agreement with his experimental results. Distortion was found to dominate over the other higher order effects only at higher frequencies. At low frequencies, the effect of vorticity distortion was to slightly decrease the theoretical admittance increment. The length scale of the approaching turbulence was found to affect the degree by which distortion contributed to the admittance: For large values of the ratio L_x/c, the distortion effect was only a small part of the theoretical increment. For L_x/c much less than 1.0, the distortion effect becomes significant, but the theory fails to predict it (unless $\alpha_g \ll L_x/c$ and the Re number is sufficiently large), because the "rapid distortion" theory (see Section 2.3.1) conditions break down. Indeed, as determined by Hunt (1973), these conditions are:-

$$\frac{1}{Re} \ll \frac{\sqrt{\overline{u^2}}}{U_\infty} \ll \min\left[\frac{L_x}{c}, 1\right] \qquad (2.22)$$

$$\text{and } \sqrt{Re} \gg \max\left[\frac{c}{L_x}, 1\right]$$

2.4.2 THEORETICAL AND EXPERIMENTAL WORK ON THE LOADING OF BLUFF BODIES IN TURBULENT FLOW

2.4.2.1 MEAN LOADING

The sensitivity of mean surface pressures to changes in the structure of the external flow, is mainly a result of the changes in the boundary layers and the separating free shear layers. Free stream turbulence, or changes in the Re number do not much influence the development of a purely laminar boundary layer. The effect on a purely turbulent boundary layer depends on the size of the boundary layer thickness δ, relative to the turbulence length scale L_x. Relevant

information can be found in Bradshaw (1974). It should be noted, that in this case the introduction of free stream turbulence is not entirely equivalent to an increase in the Re number of the (steady) flow: as an example, the boundary layer displacement thickness at a fixed position will increase due to the former effect and decrease due to the latter. On the other hand, boundary layer transition is promoted by turbulence as it is when the Re number is increased. Fig. 2.9 demonstrates this effect for an elliptic cylinder of fineness ratio 3.0. The experimental results are due to Schubauer (1939). It is seen that the data for various turbulent flows collapse into a single curve, if plotted against the dimensionless parameter $\frac{\sqrt{\overline{u^2}}}{U_\infty}\left(\frac{c}{L_x}\right)^{1/5}$, which was employed by Taylor (1936) in examining the onset of critical flow for spheres. Fig. 2.9 also shows that a turbulent flow of fixed intensity appears to be more effective as far as transition is concerned, the smaller is its length scale.

The mean pressures and forces have been experimentally investigated by a number of workers, e.g. Vickery (1966) and Lee (1975) for square cross section cylinders, Nakamura and Tomonari (1976) for rectangular cylinders, Bearman (1969) for flat plates normal to the stream, Goldstein (1965), Surry (1969), Bruun and Davies (1975) for circular cylinders and Schubauer (1939) for an elliptic cylinder (fineness ratio 3.0). Turbulence was found to cause a variety of effects depending, as stated previously, on the response of the shear layers. For example the drag coefficient, $\overline{C}_D$ of a square cylinder at zero incidence (flat side normal to the stream) decreases in turbulent flow, because of the turbulence induced thickening of the separated shear layers; the possibility of a reattachment on the parallel sides and narrowing of the wake increase, resulting in rise of the base pressure coefficient, $\overline{C}_{pb}$, and decrease in $\overline{C}_D$. In flat plates the effect is opposite, due to the increased entrainment (enhanced by turbulence) in

the base region and the sustenance of a low $\overline{C}_{pb}$. If separation is not fixed, as in the circular cylinder, then for very low Re numbers where separation is and remains laminar, the introduction of turbulence increases $\overline{C}_D$ slightly for the same reasons as with the flat plates (see Goldstein, 1965). If, however, turbulence is going to lead to an eventual turbulent separation (by promoting transition), then the drop in $\overline{C}_D$ is dramatic, on account of the downstream displacement of the separation points.

There appear to be no special methods for predicting the mean pressures in turbulent flows. However, there is no reason why the free streamline methods (Section 2.2.1) should not be applicable: Parkinson and Jandali (1970), by using their "wake source model", predicted successfully the mean pressures on a circular cylinder exposed to a turbulent stream.

2.4.2.2 UNSTEADY LOADING

(a) Unsteady Pressures: There is only a limited number of theoretical works for the calculation of unsteady pressures on a bluff body and the present situation indicates that experiment is well ahead of the theory. Vickery (1965), related linearly the local pressure on a point of a lattice structure to the streamwise velocity component of turbulence, incident on the same point, by making two assumptions: First, that the oncoming turbulence was of low intensity, and second that the individual members of the structure were small compared with the smallest wavelengths of the velocity fluctuations. It was then reasonable to treat the turbulence as unaltered by the presence of the lattice. The pressure, P(t), at a particular point was assumed to be a function of the upstream velocity U_1 and the rate of change of the velocity far upstream, so that:-

$$P(t) = \frac{1}{2} \rho U_1(t)^2 \overline{C}_D + \rho \frac{\partial U_1(t)}{\partial t} \cdot \overline{C}_m \cdot D \qquad (2.23)$$

where D is the diameter of the lattice and for $L_x >> D$, $\overline{C}_D$ and $\overline{C}_m$ were constants determined from the geometry of the structure. The fluctuating pressure p(t) would then be (if $U_1 = U_\infty + u(t)$):-

$$p(t) = \rho U_\infty \, u(t) \, \overline{C}_D + \rho \frac{\partial u(t)}{\partial t} \overline{C}_m D \qquad (2.24)$$

This approach will be increasingly inaccurate if the porosity of the plate decreases and L_x/D becomes of order 1.0 or less. Bearman (1972) had shown, that the pressure fluctuations at the stagnation point of a solid flat plate held normal to the stream, can be predicted by simply applying quasi-steady potential flow theory only if $L_x >> D$. For $L_x = O(D)$, the measured pressure spectra were in reasonable agreement with those predicted from potential flow theory (using the unsteady Bernoulli's equation $\frac{1}{2} U_1^2 + \frac{p}{\rho} + \frac{\partial \phi}{\partial t} = \text{const}\ (t)$) only at the lower reduced frequencies, $2\pi n \, L_x/U_\infty$. For higher frequencies, the effect of distortion caused the experimental spectra to drop faster. Bruun and Davies (1975), measured similar spectra for a circular cylinder and observed the same trend for fall off at high frequencies. The rate of power fall off was in reasonable agreement with that predicted theoretically by Hunt (1972). As a result, the RMS pressure fluctuations at the stagnation point of the flat plate and the cylinder, were lower when $L_x = O(D)$ than when $L_x >> D$. These effects, theoretically, continue in the same direction as L_x becomes much less than D.

(b) Unsteady Lift: Theoretical as well as experimental work about unsteady lift forces is very scarce. A step forward was made, when Davenport (1961), (1962) proposed the examination of bluff body loading in terms of aerodynamic admittances. He suggested that the instantaneous lift, L(t), acting on a "strip" of a long thin cylinder or lattice structure, induced by a streamwise and transverse spectral components of low intensity turbulence, could be expressed as follows:-

$$L(t) = \bar{L} + 2\bar{L}\frac{u}{U_\infty}\sin(2\pi nt + \phi_1)\,A_1(n) + \frac{\partial\bar{L}}{\partial\alpha}\frac{w}{U_\infty}\sin(2\pi nt + \phi_2)\,A_2(n) \quad (2.25)$$

where: A_1, A_2 are the aerodynamic admittances to be determined;

ϕ_1, ϕ_2 are phase angles;

$\bar{L}$ = mean lift.

Expressing Eqn. (2.25) in terms of corresponding spectral quantities:-

$$S_L(n) = 4\bar{L}^2\frac{S_u(n)}{U_\infty^2}|A_1(n)|^2 + \left(\frac{\partial\bar{L}}{\partial\alpha}\right)^2\cdot\frac{S_w(n)}{U_\infty^2}|A_2(n)|^2 +$$

$$+ 4\bar{L}\frac{\partial\bar{L}}{\partial\alpha}|A_1(n)\,.\,A_2(n)|\frac{S_{wu}(n)}{U_\infty^2} \quad (2.26)$$

where $S_{wu}(n)$ is the cross correlation spectrum of turbulence at the position of the "strip".

Graham (1973), took this suggestion further and applied the thin aerofoil theory of Jackson, Graham and Maull (1973) to this problem, thus taking into account, for the calculation of the theoretical admittance, the effects of spanwise incoherence of turbulence. He considered the case of symmetrical bodies at zero indicence, so that $\bar{L} = 0$. Then, $|A_2(n)|^2$ in the notation of Eqn. (2.26), would be equal to the theoretical admittance of Eqn. (2.20), for a thin aerofoil and $\partial\bar{L}/\partial\alpha$ would be the mean lift curve slope (determined experimentally in steady flow or, if possible, predicted). In this approach, the bluff body was idealized as a flat plate with two fixed separation points obeying the Kutta-Joukowski condition (i.e. of zero loading across the trailing edge) and for which the only effects of thickness was that on $\partial\bar{L}/\partial\alpha$. A correction due to turbulence distortion was also applied, following a method analogous to that presented by Graham (1972) for the distortion of turbulence by a porous plate.

To test how accurately this modified aerofoil theory applied to bluff sections, Graham carried out some experiments in nearly isotropic

turbulence and selected as his two-dimensional models D sections (flat side downstream), elliptic sections, a circular section, a rectangular section and a NACA 0015 aerofoil for comparison purposes. A comparison between the theoretical and experimental results appears in Fig. 2.10. The effect of turbulence distortion, which theoretically appears to increase the measured lift, especially at the lower frequencies, is also shown for one of the bluff sections. The agreement between theory and experiment is seen to be only reasonable for the thinnest sections (D cylinder aerofoil), for which distortion would be small. A great discrepancy (lift under-estimation) was observed for the circular and elliptic sections. This should be partly due to the fact, that the measurement of $\overline{\partial L}/\partial\alpha$ in steady flow had allowed time for the (free) separation points to adjust their positions, thus giving unrepresentative lift in unsteady flow (an obvious example being the circular cylinder, which has $\overline{\partial L}/\partial\alpha = 0$).

With reference to the circular cylinder, Surry (1969) suggested that the fluctuating lift might be considered as a component of the fluctuating drag, if it is assumed that the turbulent velocity w changes only the direction of the free stream and not its magnitude. The lift response, which was just one quarter of the (strip theory) drag response at low frequencies (see next paragraph c) was in fair agreement with the experiment for low frequencies.

(c) Unsteady Drag: Vickery (1965) used Eqn. (2.24) in order to calculate the unsteady drag on a lattice plate of overall dimensions D x D, the only body for which Eqn. (2.24) accurately applied. The spectrum of the unsteady drag $S_D(n)$ could then be determined as a double integral over the surface of the plate (note that the lateral correlation of forces was assumed identical to the lateral correlation of the upstream velocities). The result is (see also Eqn. 2.24):-

$$S_D(n) = \overline{C}_D^2 \rho^2 U_\infty^2 \left[1 + 4\pi^2 \frac{\overline{C}_m^2}{\overline{C}_D^2} \left(\frac{nD}{U_\infty}\right)^2\right] R_u'(n) \cdot S_u(n) \qquad (2.27)$$

where $R_u'(n)$ is the integral of the normalized cross spectral density of the streamwise turbulent fluctuations (see for example Appendix A of Vickery, 1969) over the surface of the plate. In analogy with the lift admittances, Eqn. (2.27) suggests the definition of an aerodynamic drag admittance, as:-

$$|X(n)|^2 \equiv \frac{S_D(n)}{S_u(n)} \cdot \frac{1}{\overline{C}_D^2 \cdot \rho^2 U_\infty^2} \qquad (2.28)$$

so that the theoretical drag admittance $|X(n)_t|^2$ for the lattice plate would be:-

$$|X(n)_t|^2 = \left[1 + \frac{4\pi^2 \overline{C}_m^2}{\overline{C}_D^2} \left(\frac{nD}{U_\infty}\right)^2\right] R_u'(n) \qquad (2.29)$$

Eqn. (2.29) has been used for the prediction of the unsteady drag on a number of bluff cross sections. The degree of success depends on how accurately the original assumptions (Section 2.4.2.2a) are maintained. For example, the presence of the bluff body changes the flow pattern of the oncoming flow so that the relationship between velocity correlations in the stream and pressures on the body become complicated. The force coefficients $\overline{C}_D$ and $\overline{C}_m$ cannot be regarded as constants and an added difficulty is that the virtual mass coefficient is in most cases unknown.

Vickery (1965) and Bearman (1969) tested some square solid plates held normal to a turbulent stream and compared the experimental drag admittances with the theoretical ones, from Eqn. (2.29), under the assumption $\overline{C}_m = 0$ and use of an empirical turbulence cross spectrum. At low values of the reduced frequency nD/U_∞ (D = size of the plate) the agreement between the theoretical and experimental results was fairly good, if L_x/D was roughly 1.5 or higher; for lower values of L_x/D,

Vickery's theory progressively underestimated the experimental drag. This effect was due to the distortion of turbulence and it was also demonstrated theoretically and experimentally by Graham (1972), who developed a theory for porous plates, including the effects of vorticity distortion. At higher reduced frequencies Vickery's theory systematically underestimated the drag and possible reasons for this could be the neglect of the virtual mass terms, as well as some wake-induced pressure fluctuations on the rear of the body, which were found by Bearman (1969) to be uncorrelated with the upstream fluctuations.

Surry (1969) had employed Eqn. (2.23) in order to obtain the spanwise cross spectrum of drag for a circular cylinder. He used a value of $\overline{C}_m$ given by potential flow theory. Comparison with his experimental results indicated a reasonable agreement only at the lower frequencies and small spanwise separations.

Unsteady drag spectra for rectangular prisms can be found in Vickery (1969).

2.4.3 EFFECTS OF TURBULENCE ON VORTEX SHEDDING

It is an experimentally evident fact, e.g. Vickery (1966), Surry (1969), Graham (1973), that the introduction of turbulence in the free stream tends to reduce the strength of vortex shedding. The induced effects depend on both the turbulence intensity and length scale. Intense turbulence of length scale large compared to the body dimensions, is likely to modulate the effective stream speed (by means of its strong, low frequency streamwise velocity fluctuations) thus causing a spread of energy away from the Strouhal peak. Graham (1973) analyzed theoretically the modulation of vortex shedding lift by the streamwise component of turbulence, assuming a constant Strouhal number and a Gaussian turbulence spectrum. The calculated spreading of energy did not contradict his

experimental results.

The effect of turbulence on the final separation and the subsequent development of the shear layers can also influence the frequency and strength of vortex shedding. For example Vickery (1966) reported that a nearly isotropic turbulence of intensity 10% and $L_x/D \simeq 1.34$, reduced the RMS vortex shedding lift of a square cross section cylinder by about 50%. This was not only a result of the increase in the base pressure (see Section 2.4.2.1), but also of the spanwise incoherence of the shed vortices effected by the turbulence. In addition turbulence decreased the circumferential coherence of the unsteady pressures partly due to the intermittent reattachment of the separated shear layers on the two parallel sides of the cylinder. The broadening of the Strouhal peak, observed by Vickery (1965), Surry (1969) and others, could have its cause (besides the previously mentioned modulation effect) to the increased randomness imposed by turbulence on the separated shear layers.

2.4.4 SCALE CONSIDERATIONS IN WIND TUNNEL EXPERIMENTS

A complete description of the forces on bluff bodies in turbulent flow, would generally require a full scale test, because wind tunnel experiments may not simulate exactly the conditions of the original flow pattern. The problem is complicated since, on one hand a full scale test is in most cases unrealistic and costly and on the other hand the real flow may not be amenable to a precise description (such as atmospheric turbulence), so that exact wind tunnel simulations would be impossible. If it could be ascertained, however, that some changes in the flow conditions, do not affect (to the degree of accuracy required), the pressures, or b.ℓs*, etc. on the body, then exact similarity of conditions between real and wind tunnel flows would

---

* boundary layers

not be necessary and this could ease considerably the experimental work. Davenport (1961), interpreting the experiments of M. Jensen, stated that, to the order of importance given, the rules for similarity between the pressures on the model and the prototype should be:-

(i) Similarity in the kinetic properties of the incident flow.

(ii) Similarity in Re number.

(iii) Similarity in shape of the body and its environment.

For example, when the model of a tall structure is to be tested in a tunnel, not only the b.ℓ of the earth should be reproduced as accurately as possible, but according to (i) any surface roughness round it must be taken into account. The roughness parameters (see Shih-Pai, 1957) r_p and r_p' should be similar:-

$$\frac{r_p}{r_p'} = \frac{\text{linear dimension of model}}{\text{linear dimension of prototype}} = \frac{D}{D'} \qquad (2.30)$$

Upon comparing two homogeneous isotropic turbulent flows, (i) is well satisfied, if the turbulence intensities are equal, and if:-

$$\frac{L_x}{L_x'} = \frac{D}{D'} \qquad (2.31)$$

where L_x, L_x' are the longitudinal turbulence length scales in the two flows.

CHAPTER 3. DESCRIPTION OF THE EXPERIMENTAL APPARATUS AND THE UNSTEADY FLOWS

The basic tools of the experimental program were:-

- The test models
- The input flows
- The apparatus for the generation of unsteady flows
- The apparatus for measuring loads and flows
- The statistical methods and apparatus for eliciting the fluctuating quantities

3.1 APPARATUS FOR THE UNSTEADY LOAD EXPERIMENT

3.1.1 FUNDAMENTAL DESIGN DECISIONS

A working and tested unsteady lift measuring system (employing piezoelectric transducers) was inherited from previous experiments, and this considerably biased the decision to continue using this system. In addition, a single pitching aerofoil gust system had been previously built by Newton (1973), and the final system used for the present project was an improved version of this, using two aerofoils.

General Decisions

(i) The turbulent flow was to be generated by grids placed at a distance x_t upstream of the test models in the wind tunnel. The mesh size M, the bar width b_t and the distance x_t, were the parameters to be determined.

(ii) The sinusoidal flow was to be produced between the vortex wakes of two aerofoils, oscillating with the same phase in pitch at zero

mean incidence (see Figs. 3.4 and 3.7). They were to be installed so as to span completely the tunnel between vertical walls (i.e. with their mean planform horizontal). A system of connecting rods attached to an eccentric rotating shaft would impose the oscillations, which if sinusoidal, would produce (theoretically) vortex wakes with sinusoidal distribution of vorticity. These in turn, would induce sinusoidal flow perturbations further downstream which, for in-phase oscillating aerofoils, would mainly consist of an upwash in the central region between the wakes. This region was expected to be practically irrotational and it was intended to select the centre plane, hereafter called the centre line, of the oscillating aerofoils, as the approximate position of the models to be tested for the measurement of unsteady lift. It should be remembered that the idealized sinusoidal upwash gust used first by Sears (1941) for the analysis of unsteady lift on a zero thickness aerofoil, at zero incidence, was rotational but distortion of vorticity was not involved in his theory to order α_g (α_g being the RMS gust amplitude, i.e. $\sqrt{\overline{w^2}}/U_\infty$). Since there would be no vorticity to be distorted in the present gust, apart from that of the relatively distant vortex wakes, it was expected that the comparison of experimental lift results with the theory of Sears would be more rigorous.

The parameters to be determined here were the aerofoil shape and dimensions, i.e. chord c', thickness b', span s', the relative position of the rotation axis (assumed on the mean chord line) $\ell'/\frac{c'}{2}$, the distance z_o of the aerofoils (vertical, since one aerofoil would be above the other), and finally their distance x_g, (in the streamwise direction) from the test models placed downstream, see sketch on the next page.

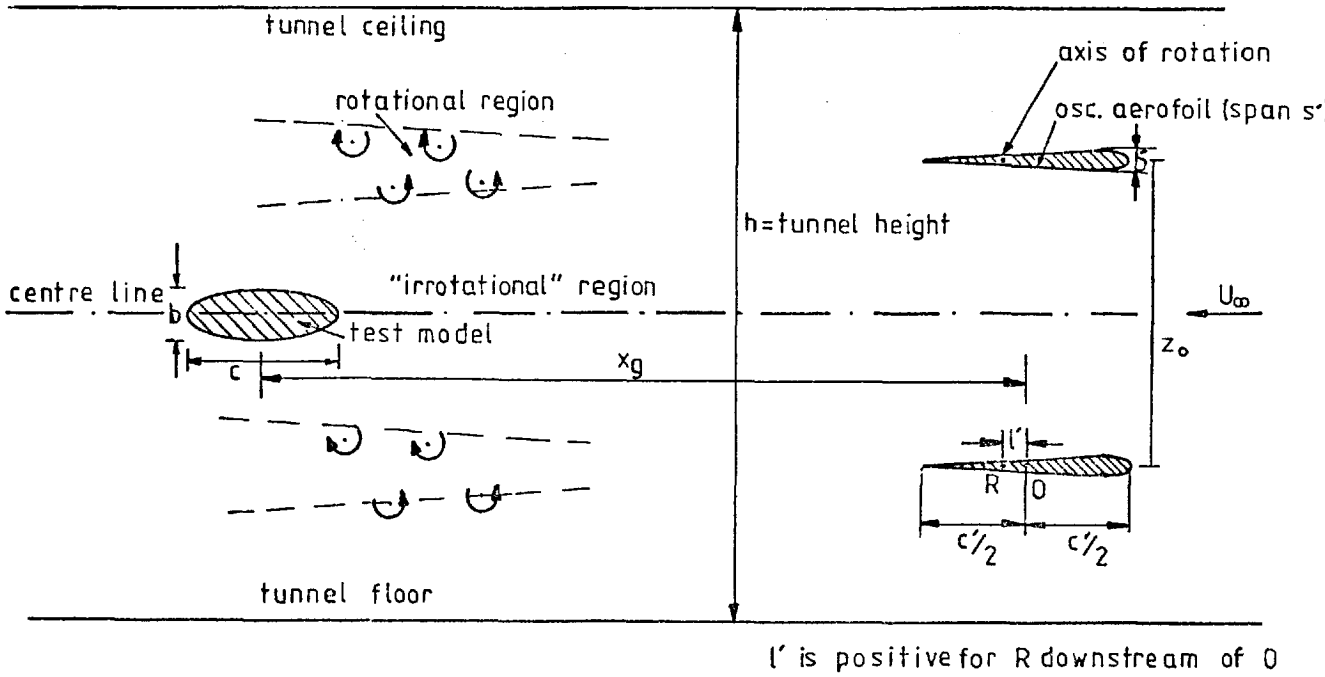

SKETCH

(iii) The unsteady lift was to be measured over a finite span "live" element of each model for the following reasons:-

- To be possible to have a model span of such dimensions, as to ensure structural rigidity.
- To be possible to include the model in the region where the flow has uniform characteristics (for example, isotropy in the case of turbulence). This would result in a more rigorous test of the existing theories.
- To minimize the effect of trailing vorticity shed by the oscillating aerofoils and the test models themselves: The spanwise bound vorticity on these bodies cannot terminate on the walls but must turn and lie on them, inducing an image vorticity of opposite strength on the other side of the wall (to maintain the boundary conditions), see sketch p. 57. There is always a small amount of vorticity, which is not cancelled in this way and which has a measurable effect on the lift. McKeough (1976) found that reducing the aspect ratio, AR, of a two-dimensional wing from 5.0 to 4.0, brought about a reduction of $\overline{\partial C_L}/\partial\alpha$ from 5.8

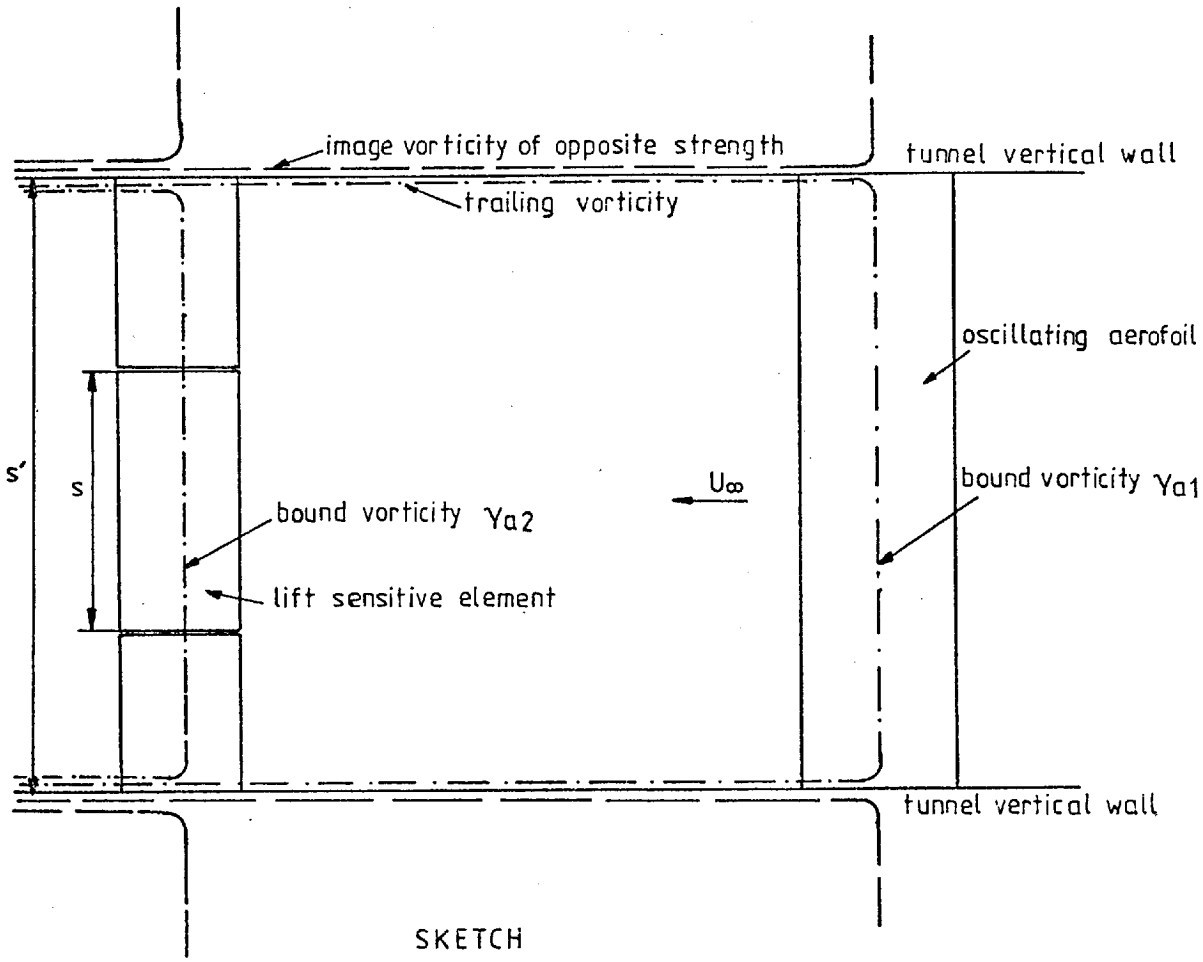

SKETCH

to 5.4, i.e. the effect of trailing vorticity becomes more important as the overall aspect ratio s′/c decreases. For the same reason, the effect of trailing vorticity will become less important as s/s′ decreases, but it will be always present for finite s′ (see Lamson, 1957). It is therefore desirable to have s′ >> s.

The parameters to be determined are the chord c, the thickness b and the span s of the test models.

(iv) For the choice of unsteady load transducers, the author favoured the piezoelectric crystals (of quartz type), because they are inherently very stiff, they have very high resonant frequencies, they are sensitive to fluctuating loads and do not drift with temperature changes. The requirement of stiffness and high mechanical resonance is important, since the test bodies are assumed to be almost rigid in the present work (i.e. perform motions which induce extremely small effective incidencies compared to those of the unsteady flow). A problem

with these crystals is their size, which could be overcome by the use of strain gauges, but these do not have the aforementioned advantages, unless suitably compensated.

Three piezoelectric transducers were available from previous experiments. Thus the decision was taken to use them, mounted externally to the test models, in conjunction with the already existing support system.

3.1.2 DESIGN OF TEST MODELS AND BASIC DIMENSIONS OF THE UNSTEADY FLOW RIGS

The problem was to find the optimum values of the variables c, b, s, c´, b´, s´, ℓ´, z_0, x_t, x_g, M, b_t under the constraints described below:-

1. In order to be able to draw more general conclusions from the tests, a wide range of flow wavelengths, compared with a linear dimension of the models, should be covered. The wavelength of a sinusoidal gust convected with the mean flow speed U_∞, is equal to $\lambda = \frac{U_\infty}{n}$, n being the frequency (Hz) of the velocity fluctuations at a point (x, y, z). A representative length in the case of turbulence is the longitudinal integral length scale L_x. If the wavelengths mentioned above are very large compared with the chord, say, of the body, then the latter would feel the very slow variations of an unsteady velocity field, and its response would be quasi-steady, a case of little interest here. On the other hand, very small length scales might invalidate thin aerofoil theory assumptions (such as the fulfillment of the Kutta-Joukowski hypothesis), result in a relatively big change of the gust intensity over the chord and lead to a significant distortion and viscous dissipation of the vortices. A rigorous comparison of experiment with theories uncorrected for distortion effects would, therefore, be precluded. The

scales of interest in the present problem should satisfy the relations:-

$$\frac{c}{L_x} = O(1) \quad \text{or} \quad \frac{c}{\lambda} = \frac{nc}{U_\infty} = O(1) \tag{3.1}$$

where O(x) stands for the "order of x".

2. The thickness to chord ratio b/c of the models should be sufficiently high to justify their classification as bluff bodies, but small enough to make a comparison with thin aerofoil theory possible. It is felt that the higher limit for b/c should be set at about 30%. As a rough idea of how the flat plate theory (Theodorsen, 1935), applies to a thick aerofoil, it is indicated that Giesing's (1968) theory for a 25% thick oscillating Joukowski aerofoil, predicts an approximate 20% drop of the circulatory lift, from the corresponding flat plate result for $c/\lambda \simeq 0.3$ (note that this depends also on the amplitude of oscillation).

The ratio b/c should be kept small, so that the mean flow is not significantly perturbed. Then the effects of turbulent vorticity distortion would be smaller and the comparison with existing theories easier.

Another reason why b/c should be low is that, in order to isolate the effects of vortex shedding, the corresponding frequency n_{vs} should be much higher than the frequency n of the sinusoidal flow (which would appear as quasi-steady):-

$n_{vs} >> n$ or:-

$$\frac{U_\infty}{\lambda} << \frac{U_\infty . S}{b} \quad , \quad S = \text{Strouhal number, say, } \simeq 0.3$$

For $\lambda/c = O(1)$, $\frac{b}{c} << 1$, therefore:-

$$\frac{b}{c} < 0.3 \qquad (3.2)$$

3. It was desirable to carry out the experiments at as high chord Reynolds numbers as possible, representative of the real flow situations. The neglect of the effects of viscosity would thus be more justifiable. To achieve this for a medium of constant kinematic viscosity ν, the highest c and U_∞ should be used, taking into account, however, that an increase in U_∞ limits the upper values of reduced frequencies $\pi nc/U_\infty$ to be attained.

The effects of varying the Re number were of interest, especially for the elliptic cross-section. It was estimated, see Schubauer (1939) and Goldstein (1965), that for an elliptic cylinder of thickness about 30%, a Re $\simeq 10^5$ would just be in the upper end of the subcritical region in smooth flow (the upper end of the critical region would lie near 4×10^5, see also Chapter 2). Hence:-

$$10^5 \lesssim \text{Re} = \frac{U_\infty \cdot c}{\nu} \qquad (3.3)$$

The maximum tunnel speed available in the Department's subsonic wind tunnels was about 45 m/sec, so that:-

$$U_\infty < 45 \text{ m/sec} \qquad (3.4)$$

4. The piezoelectric transducers available could measure unsteady axial forces with an accuracy 10^{-3} N (Newtons), up to $\pm$ 500 N maximum force. It was, therefore, decided that the lowest unsteady load that could be accurately measured, should be of the order of 0.5 N, i.e.:-

$$0.5\ \text{N} \lesssim \text{total unsteady lift} = L_t < 500\ \text{N} \tag{3.5}$$

L_t is roughly equal to $\frac{1}{2}\rho U_\infty^2\, \alpha_g \frac{\partial C_L}{\partial \alpha} S_a$, where α_g = relative gust amplitude or unsteady incidence, radians; $\partial C_L/\partial\alpha$ = corresponding lift curve slope in unsteady flow; S_a = minimum $(L_x^2,\ s\ .\ c)$. In turbulence, this area takes into account the lack of correlation of turbulent vortices in space.

α_g should not be too large, otherwise thin aerofoil theories would cease to apply, due to significant non-linear effects, and an upper limit could be set at about 0.1 rad:-

$$\alpha_g \lesssim 0.1\ \text{rad} \tag{3.6}$$

A simplified result for $\partial C_L/\partial\alpha$ was given by Liepmann (1952) for the case of perfectly correlated turbulence in the spanwise direction:-

$$\frac{\partial C_L}{\partial \alpha} = \overline{\left(\frac{\partial C_L}{\partial \alpha}\right)}\ .\ f(n)$$

where $n = \pi c/L_x$, $\overline{\partial C_L/\partial\alpha}$ = mean lift curve slope at zero incidence. If $(\overline{\partial C_L/\partial\alpha})$ is taken roughly equal to 2π (for all the models) and $\frac{c}{L_x} = O(1)$, then $f(n) \simeq 0.6$ and for the lowest Re number, Re_{min}, see Eqn. (3.3):-

$$L_t = \frac{1}{2}\ .\ \rho\ .\ (Re_{min}.\nu)^2\ .\ \frac{1}{c^2}\ .\ 2\pi\ .\ (0.6)\ .\ \min(L_x^2,\ s\ .\ c)\ .\ \alpha_g \gtrsim 0.5\ \text{N}$$

$$\text{or,}\quad \min(c^2,\ s\ .\ c)\ .\ \frac{1}{c^2}\,\alpha_g \gtrsim 0.098$$

Taking into account Eqn. (3.6), it follows that for the lowest Re number to be used, s should be of O(c). The same result would have been

obtained for the sinusoidal flow: $S_a = s \cdot c$, f = Sears's function. Therefore, if:-

$$\alpha_g = 0 \ (0.1 \text{ rad}) \tag{3.7}$$

a measurable load can be ensured, provided that:-

$$s = 0 \ (c) \tag{3.8}$$

5. To obtain a nearly isotropic and homogeneous turbulent field the test models should be placed at least 10 mesh lengths downstream of the grid. If M/b_t is between 4 and 6, then $L_x \simeq 0.4$ M and the longitudinal turbulence intensity about 5%. Since the longest working section available was 3 m approximately, x_t should satisfy the relation:-

$$10 \text{ M} \lesssim x_t < 3 \text{ metres} \tag{3.9}$$

6. Basic dimensions of the oscillating rig in relation to α_g: Later in the text (Section 3.4), a potential flow model has been constructed, to describe the flow produced by the two oscillating aerofoils. There, it is shown that the RMS gust amplitude, α_g, generated between the wakes, depends on the following factors:-

- The oscillation mode; for low reduced frequencies $k' = \pi nc'/U_\infty$, pitching oscillations result in a comparatively stronger gust, than translatory ones, and for this reason the former kind of aerofoil motion was chosen.
- The reduced frequency k'; α_g increases monotonically with k' only along the two vortical wakes, while along the centre line (see sketch

on page 56), it increases with k' starting from zero, reaches a maximum $\alpha_{g_{max}}$ at a particular $k' = k'_0$ and then decreases rapidly, see Fig. 3.1.

- On z_0/c' and z_0/h (see sketch on page 56), α_g generally increases as these ratios decrease, see Fig. 3.1.
- The position of rotation axis, α_g increasing as $\left|\frac{1}{2} - \frac{\ell'}{c'/2}\right|$ increases, i.e. the farther from the 3/4 chord point (from the leading edge) being the rotation axis.
- The amplitude Θ_0 (rad) of the pitching oscillations, α_g increasing proportionally to Θ_0.

The last parameter, Θ_0, is considered first. Θ_0 is

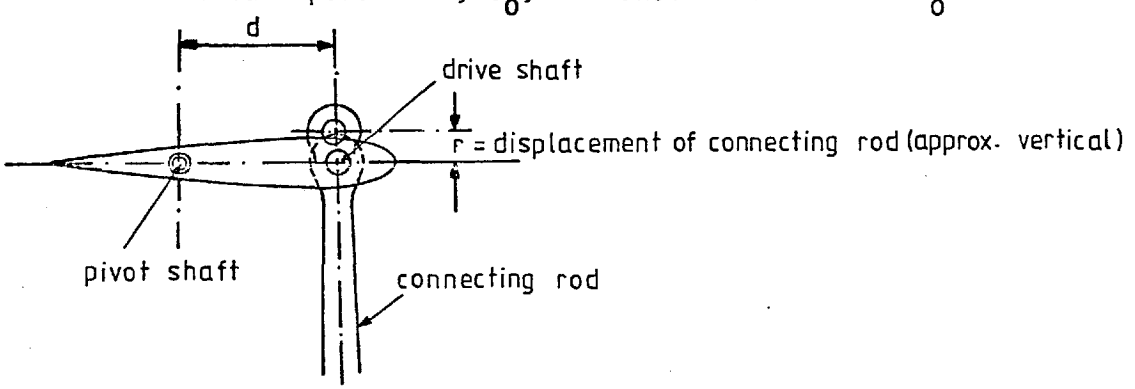

SKETCH

equal to $\tan^{-1}(r/d)$, where d is the distance between the rotation (or pivot) shaft and the shaft driving the aerofoil, and r the displacement of the connecting rod (see sketch).

To obtain a strong α_g, Θ_0 should be high. However, there are certain limitations on the maximum value of Θ_0, which are listed below.

Θ_0 should not be too high, otherwise the large wake deformations would lead to a thick vortical wake and distorted gust waveform on account of higher than the fundamental harmonics. If the reduced frequency is not large, the thickness of the fully-developed vortical wake (including the rolled up vortices) would be of the order

of the maximum aerofoil displacement, see Bratt (1950), Giesing (1968) and Wood and Kirmani (1970). It is desirable to have a thin vortical wake and a wide "irrotational" gust region (see Section 3.1.1), hence r should be small, i.e. Θ_0 should be small.

Θ_0 should be less than the stalling angle of the oscillating wings, the static value of the latter being in the range 10^0 to 18^0, depending on Re and aerofoil shape. Stall develops less readily in unsteady flow (see McKeough, 1976 and Farren, 1935), but to avoid irregular behaviour, such as sudden peaks in the $C_L(t) - \alpha(t)$ curve, it is better to keep Θ_0 below the steady stalling angle.

Θ_0 should not be large, because then either r should be large, resulting in non-sinusoidal variation of Θ (instantaneous aerofoil geometric incidence) and large connecting rod inertial forces, or d should be small requiring high values of starting torques, besides being non-practical (housing of shaft, bearings, etc.).

It was decided that Θ_0 should not be greater than 10^0, i.e.:-

$$\Theta_0 \lesssim 10^0 \ (= 0.174 \text{ rad}) \qquad (3.10)$$

As far as the rotation axis lies between the aerofoil leading and trailing edges and k′ is not large, its exact position does not affect significantly α_g. Strength considerations require that it should be close to the aerofoil cross-section gravity centre, for inertial forces to remain low, and in positions of sufficient aerofoil thickness. The same should hold for the drive shaft, which should be close to the elastic axis (or twist axis) of the wing (usually lying near the 1/4 chord point from the leading edge).

$\frac{z_0}{c}$ should not be very small, so that an adequate potential

flow region could exist between the vortex wakes. Also, to obtain an irrotational region significantly larger than the model thickness b, z_o/b should be large:-

$$\frac{z_o}{b} \gg 1 \tag{3.11}$$

$\frac{z_o}{h}$ should be kept low, if interference from the tunnel floor and ceiling is to be kept low. This kind of interference causes a reduction in the gust intensity along the centre line, which is more pronounced for low $k' = \frac{\pi n c'}{U_\infty}$ and high $\frac{z_o}{h}$. Using the results of Section 3.4, it was estimated that a reduction of 50% in gust intensity can be caused if $\frac{z_o}{h} = 0.5$, $k \simeq 0.2$ and $\frac{z_o}{c'} \simeq 2$. Therefore:-

$$\frac{z_o}{h} \lesssim 0.5 \tag{3.12}$$

7. The distance x_g (see sketch p.56) should not be too small, for then the vorticity distributions round the oscillating aerofoils and the test models may affect each other in a complicated manner and consequently introduce spurious effects on the unsteady lift measurements. The test model should also lie in the convected velocity field, far behind the oscillating aerofoil trailing edge. Five chord lengths are considered enough for the effects of bound vorticity to die out (see for example Karman and Sears, 1938,and Hakkinen and Richardson, 1956). Hence:-

$$5 \times \max (c, c') \lesssim x_g \tag{3.13}$$

On the other hand, since the effective potential flow gap

between the wakes decreases with distance downstream, due to the thickening of the shear layers and the interaction of individual vortices, x_g/c' should not be too large. As far as the widening of a single vortical wake is concerned, there is experimental evidence, Pocha (1971), Newton (1973), indicating that the angle of expansion above and below the mean chord line is very roughly 5^0 (i.e. total angle 10^0). Taking into account these considerations, the following restriction was imposed on x_g:-

$$x_g/c' \lesssim 10 \qquad (3.14)$$

8. Strength and mechanical resonance considerations: The construction of the oscillating aerofoils should be such as to prevent structural damage during operation and of sufficient rigidity, as to ensure that the wing elastic deformations would be much less than the actual amplitudes of the unsteady motions. For example, excessive bending would cause the vorticity to be shed with varying strength across the span, while twist would cause varying phase across the span.

The equilibrium of the generally out-of-phase, inertial, elastic and externally applied forces (including the aerodynamic ones), is given by a set of simultaneous partial differential equations with respect to time and wing deformations and is difficult to solve (Bisplinghoff et al, 1958). In the present case, a simplified analysis will be followed: It is required that the natural frequencies of the wing in bending n_b, and torsion n_t, are well above the frequencies of interest, to avoid mechanical resonances. The wing will be assumed to have the shape of a rectangular beam ($c' \times b' \times s'$), of isotropic material, pivoted on an axis through its gravity centre, which lies on

the elastic axis. All the loads will be assumed to act on the mid-span and on this axis. It is true that these simplifications would only give an order of magnitude of the required quantities, but a complete calculation, besides being very difficult, would need a preconception of the design. The frequencies n_b and n_t are given by the formulae (Den Hartog, 1956):-

$$n_b = \frac{11}{\pi s'^2}\sqrt{\frac{EI}{\rho_w A}} = \frac{11}{\pi}\frac{b'}{s'^2\sqrt{12}}\sqrt{\frac{E}{\rho}} \text{ (Hz)}$$

$$n_t = \frac{1}{s'}\sqrt{\frac{GJ}{I_o}} = \frac{b'}{s'}\sqrt{\frac{G(1 - 0.63\frac{b'}{c'})}{\rho_w (b'^2 + c'^2)}} \text{ (Hz)}$$

(the last expressions refer to a rectangular beam), where E = modulus of elasticity; ρ_w = density of wing material; A = cross sectional surface area; I = moment of inertia of cross section about chord; G = shear modulus of elasticity; J = torsion constant of the beam (Bisplinghoff et al, 1958) and I_o = moment of inertia of beam per unit span. Therefore:-

$$n_b >> n \tag{3.15}$$

$$n_t >> n \tag{3.16}$$

The role of the span length and the need for a lightweight material is evident from the above relations. The same considerations as before apply for the design of test models. In the highest frequencies of interest should be included those from turbulence, which are of the order U_∞/L_x, since turbulent eddies of size much less than L_x have low energy.

9. The overall aspect ratio of the models, s'/c, should be kept

high enough to maintain a two-dimensional flow, as discussed in Section 3.1.1 (iii). The span s should be sufficiently big, so that the interference caused by the support system lying below the model is small. A suggested value (see McKeough, 1976) for s'/c is 4.0, i.e.:-

$$s'/c \gtrsim 4.0 \tag{3.17}$$

It should be noted that a high aspect ratio may have the opposite effect on the stall development of a wing, see for example Moss and Murdin (1968).

10. To avoid excessive blockage of the flow, the tunnel cross sectional area should be large compared with the bluff body frontal area or the aerofoil plan area. Complete tunnel constraint corrections are not available for unsteady flows (see Reissner, 1947), but it is not thought that they would be significant if the corresponding steady flow corrections are small. Using the results of Maskell (1963) and Allen and Vicenti (1944), the following limitations were imposed on b, c and c':-

$$\frac{b}{h} \lesssim 0.05 \qquad \max \frac{(c,\ c')}{h} \lesssim 0.15 \tag{3.18}$$

As an indication, if b/h = 0.05 for a circular cylinder, it results in a correction of the measured drag of roughly - 3.5%.

Solution to the Design Problem

The difficulty in satisfying equally well all the aforestated conditions was realised when optimizing the problem.

It was apparent that because of the requirement of high Reynolds numbers, Eqn. (3.3), and low blockage, Eqn. (3.18), the biggest and/or the fastest wind tunnel should be employed (but with Mach number

less than 0.1, say).

It was decided to use the Department's largest low speed wind tunnel of octagonal cross section and dimensions: height = h = 1.22 m (4'), width = ℓ_w = 1.52 m (5') and length of working section = $x_w \simeq 2.9$ m. The level of free stream turbulence intensity (without grids) was approximately equal to 0.15%. During the course of the research, the cross section was replaced by a rectangular one measuring h = 1.22 m, ℓ_w = 1.37 m (4.5'). That alteration did not affect in any significant respect the original experimental arrangements, as well as the consistency of the results. The laboratory floor had a resonant frequency of about 15 Hz, and the author was advised that the fluctuating forces on it should not exceed 5000 N.

From Eqn. (3.9) it follows $10\,M < x_t < x_w \simeq 2.9$ m so that $M \lesssim 0.29$ m and (roughly from restriction 5) $L_x \lesssim 0.11$ m, and from Eqn. (3.1), it follows $L_x = O(c) = O(0.11\text{ m})$. The blockage restriction, from Eqn. (3.18) results in $c \lesssim 0.18$ m, $b \lesssim 0.06$ m. Finally, the chord length for all the models was taken as c = 0.1524 m (6") and from Eqn. (3.2), the thickness of the bluff bodies b = 0.0508 m (2"), resulting in a fineness ratio $\frac{c}{b} = 3.0$.

The aerofoil models for the zero and high incidence experiments were chosen to have the standard NACA 0015 profile, because for such moderately thick sections, thin aerofoil theories are expected to apply satisfactorily, see McKeough (1976), Jackson (1970), they stall at relatively high incidencies ($\simeq 15^0$) and provide thickness for rigidity requirements.

From Eqn. (3.13), $x_g \gtrsim 5c \simeq 0.75$ m, for which if the "irrotational" region behind the oscillating aerofoils, at the position of measurement, is required to have a thickness of at least 4b, ∴.

$z_o > 0.75$ m x tan 5^o x 2 + 4b $\simeq$ 0.25 m, i.e. minimum $z_o \simeq 0.25$ m. From Eqn. (3.9), $x_g < 3$ m, and from Eqn. (3.13) $\therefore$ maximum $c' \simeq 0.6$ m, if blockage limitations are left aside at the moment. Then, similarly from Eqn. (3.1), max. $n = 0 \left(\frac{U_\infty}{c}\right)$ Hz, hence max $\frac{k'}{\pi} = 0 \left(\frac{U_\infty}{c} \cdot \frac{c'}{U_\infty}\right) = 0 \left(\frac{c'}{c}\right)$. For $c' = c'_{max} \simeq 0.6$ m, max $k' \simeq \pi \times \frac{0.6}{0.152} \simeq 12$ and $\frac{z_o}{c'} \simeq \frac{0.73}{0.6} \simeq 1.2$. Then from Fig. 3.1, $\alpha_g/\Theta_o \simeq 0$, which is unacceptable. For $c' \simeq c \simeq 0.152$ m, max $k' \simeq \pi \times 1 = \pi$, $\frac{z_o}{c'} \simeq \frac{0.25}{0.152} \simeq 1.6$ and from Fig. 3.1, $\alpha_g/\Theta_o \simeq 0.1$ which is rather low but still acceptable. For $c' < c$, it can be similarly deduced that $\alpha_g/\Theta_o \simeq 0$, so that min $c' \simeq 0.152$ m = c. If the highest tunnel speed is used, max $n \simeq \frac{45}{0.152} \simeq 300$ Hz, hence max $n \simeq 300$ Hz. Assuming that $c' =$ min $c' \simeq 0.152$ m has been selected, then d (see sketch on page 63) $\simeq \frac{c'}{2} \simeq 0.075$ m. From Eqn. (4.10) $\rightarrow$ r $\simeq$ eccentricity of rotating shaft $\simeq$ d tan $10^o \simeq 0.013$ m. To obtain very nearly sinusoidal oscillations, the length ℓ'_c of the connecting rod should be much higher than r, i.e. $\ell'_c/r \gg 1$ hence $\ell'_c \gg 0.013$ m. For $\ell'_c \simeq 1$ m, it is estimated that the total mass m_t of the various reciprocating parts will be about 5 kg, $m_t \simeq 5$ kg; then the vertical inertial forces transmitted on to the laboratory floor will be: $(2\pi \times \text{max } n)^2 \times m_t \times r \simeq (2\pi)^2 \times 300^2 \times 5 \times 0.013 \simeq 2.3 \times 10^5$ N, which is unacceptable. The most disturbing factor is max n; it can be reduced, either by accepting longer gust wavelengths or trying lower tunnel speeds or both. The last solution was followed here. Note that there are systems to balance the inertial forces almost completely, but they are considered as very complicated and expensive for the present case. In order that the maximum forces transmitted to the floor do not exceed 5000 N, max n had to be reduced to 40 Hz. A combination with $U_\infty \simeq 10$ m/sec gives $\lambda = \frac{U_\infty}{\text{max } n} \simeq \frac{10}{40} = 0.25$ m, which is close to the assumed $c' \simeq 0.152$ m. Finally, $\underline{c' = 0.203 \text{ m}}$ (= 8"). For the same reasons as with the test models, plus the requirement of

thin emanating shear layers, the oscillating wings were chosen to have the NACA 0015 profile; therefore $b' \simeq 0.03$ m.

Assuming now that the oscillating wing is a rectangular beam constructed from solid hard wood with $\rho_w \simeq 600$ kg/m^3, $E \simeq 1.4 \times 10^{10}$ N/m^2, $G \simeq 5 \times 10^9$ N/m^2, the span s' can be determined from Eqns. (3.15) and (3.16), requiring the resonant frequencies to be at least 2 max n, i.e. about 80 Hz. Eqn. (3.15) gives $s' < 1.35$ m, and Eqn. (3.16) gives $s' < 2.2$ m.

Turning now to the test models, the highest frequency of interest in turbulent flow depends on $\frac{U_\infty}{L_x}$, which for $U_\infty = 45$ m/sec and $L_x \simeq c \simeq 0.152$, is 300 Hz. The test models, therefore, should have resonant frequencies at least twice this value, i.e. $300 \times 2 = 600$ Hz. The thinnest model (aerofoil) had $b \simeq 0.15\ c \simeq 0.022$ m, and if it is assumed to be constructed from aluminium, its span should be less than 0.44 m, i.e. $s < 0.44$ m (use was made of Eqns. (3.15) and (3.16) and $\rho_w \simeq 2700$ kg/m^3, $E = 7.1 \times 10^{10}$ N/m^2 for aluminium). The maximum expected loads on this model cause negligible deflections, as can be easily verified. The final values of the remaining quantities were as follows:-

span $s = 0.381$ m (= 15")

span $s' = 0.838$ m (= 33")

$z_0 = 0.475$ m (= 18")

The pivot (rotation) shaft was fixed at $\ell' \simeq 0.0019$ m downstream of the mid-chord point. The difference in the expected loads from those relative to the mid-chord point would be very small.

Constructional details for the test models (except for the

aerofoil at high incidence (which had a span s = 0.28, and is described in McKeough, 1976) are given in Fig. 3.2 and for the oscillating wings in Fig. 3.3. The last are constructed from fibre-glass filled in with a kind of very strong expanded polystyrene foam and reinforced with aluminium tubes and anti-twist rods. It is believed that this construction would be much more rigid than the hard wood construction assumed in the structural analysis mentioned before, but a reduction in s' from the calculated 1.35 m was thought necessary, since in any case the actual wing is not a rectangular beam.

Without touching the "live section", dummy sections, made from hard wood, were placed symmetrically on either side of the test sections and were mounted, during the experiments, on two wooden end plates, which formed the auxiliary vertical tunnel walls, see Fig. 3.4. These were placed parallel to each other at a distance $s' = 0.84$ m apart, symmetrically about the tunnel centre line. Thus, the overall aspect ratio of the models was $AR_o = 5.5$, while the aspect ratio of the models, $AR = 2.5$. These values comply with the requirements of Section 3.1.1 (iii).

Turbulence was produced with a mesh grid of size $M = 0.152$ m (= 6") and $M/b_t \simeq 5.0$, previously constructed in the Department. It was placed 12 M upstream of the test models, i.e. $x_t \simeq 1.82$ m. To study the effect of turbulent intensity on unsteady lift, another smaller grid was employed with $M' = 0.075$ m (= 3") and $M'/b_t' \simeq 5.0$. This was placed at the same upstream position, $x_t = 1.82$m the ratio x_t/M' being 24 approximately. A reduction in turbulent intensity was expected, at the position of the measurements, in comparison with the large grid, but a comparatively smaller change in L_x, due to increased x_t/M, see for example Baines and Peterson (1951).

3.1.3 LOAD MEASURING EQUIPMENT

The system employed to measure the unsteady lift was similar to the ones used by Jackson (1970), McKeough (1976) and others, and consisted of the following parts (see sketch below).

(i) Three thin cylindrical rods, connecting the model with the piezoelectric transducers (see also Fig. 3.4).

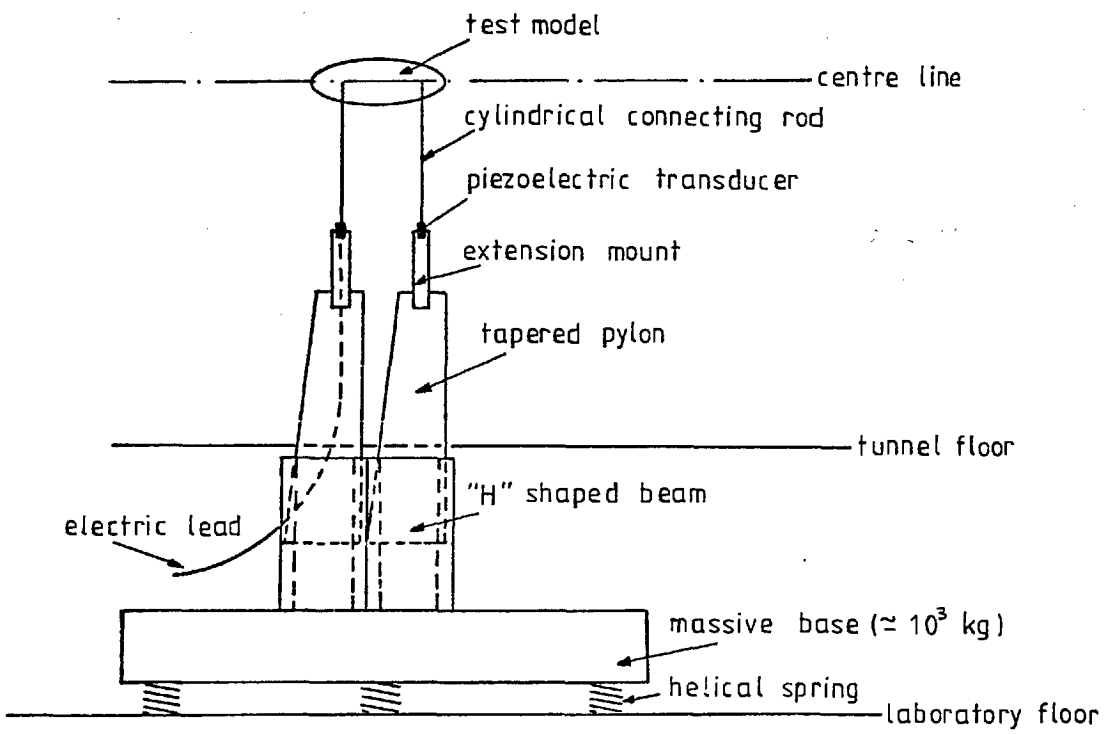

SKETCH

(ii) Three piezoelectric transducers.

(iii) Three aluminium extension mounts clamping the transducers.

(iv) Three tapered pylons attached to three "H" shaped beams.

(v) A massive base (≃ 10^3 kg) on which the beams were bolted.

(vi) Six helical springs on which the base rested.

The rods were available in two length sizes, 0.101 m (4") and 0.152 m (6"). Their diameters were 0.004 m and 0.006 m respectively. Load experiments were performed with both types, with the purpose of checking the effect of the support system of the three pylons (called also tripod

support system) and attempting to raise the support resonant frequencies even higher.

The piezoelectric transducers were of the Quartz type, and had the following characteristics:-

- Maximum measuring force ± 500 N in the axial direction.
- Resolution ≃ 1 x 10^{-3} N.
- Resonant frequency 27 KHz.
- Linearity 1%.
- Temperature range of operation - 200^{o}C to 450^{o}C.

During operation, each transducer was connected via a 5 m lead of special capacitance to a charge amplifier, the function of which was to convert the charge built up, into a proportional voltage. There was a "short time constant" switch for the measurement of fluctuating loads, and a "long time constant" switch for static loads. However, at the latter position the amplifiers tended to saturate quickly and give erroneous results, if the measurement was not taken on time. It has been suggested to the author, that the dryness of the leads could be the cure to this problem.

The role of the extension mounts was to raise the models to the centre line (see sketch on page 73). It was not possible to do this by raising the whole base or the H beams, due to limited clearance below the tunnel floor.

The massive base consisted of a double deck platform filled in with iron bars. Its great mass made the natural frequency of the balance very low, about 0.5 Hz. The helical springs were so designed as to isolate the support system from the vibrations of the floor, caused by the oscillating rig, the fan motor, footfalls, etc. Their effectiveness, as judged from the results shown in Fig. 3.5, was very good.

3.1.4 ASSEMBLING AND CALIBRATION OF THE LOAD BALANCE

First, the load balance was assembled in position without the models present, i.e. with the three cylindrical connecting rods protruding into the tunnel. Then, with the amplifiers in the "long" time setting, the response of each transducer in transverse loads was examined. This was done conveniently with a string held horizontally via a pulley and a known weight hanging at its other end. The direction of minimum response (an inherent property of the crystals) was then aligned with the mean flow direction, to ensure minimum sensitivity to drag. A detailed axial load calibration followed by placing known weights on the transducer and checking with the output voltage. Linearity was found to be 1%, as specified. The sensitivity to transverse loads was about 10% of the corresponding sensitivity to axial loads. This value was acceptable, for the zero mean incidence experiment (where $\overline{\partial C_D}/\partial\alpha$ was very small for the three models examined), but it could impose some problems in the high mean incidence experiment (discussed in Chapter 5).

Sheet metal fairings were used to cover the pylons with the purpose of improving their streamlining and preventing any aerodynamic forces acting on them (see Fig. 3.4). Care was taken to avoid any contact between the lift balance and any part of the wind tunnel, which could introduce spurious signals. Each model was bolted firmly to its position and any holes left were covered with plasticine. A 1 mm gap approximately was left between the "live" and "dummy" sections. Attempts to seal this gap with sellotape, which was then cut with a razor blade, made no difference to the lift results, and, therefore, it was decided to carry on the experiments with the unsealed gap.

A static and dynamic calibration of the assembled model

followed. For that purpose, the outputs of the three charge amplifiers were inverted and added together via an operational amplifier, the output voltage being very nearly proportional to the instantaneous vertical (here lift) force. A positive voltage corresponded to an upward force. To ensure that the response of the lift balance was linear and independent of the position of the instantaneous centre of pressure, a weight of known value was placed at various positions on the model surface. The overall linearity was in the range ± 1%. Only in the case of the aerofoil, it was found that the mounting of the back crystal affected the results. Specifically, the output voltage was lower than the expected for the values of the applied force, perhaps due to the presence of transverse components. By carefully levelling this model during mounting, the position giving the correct value of the applied force could be found.

For the dynamic calibration, use was made of an electromagnetic shaker. It was fixed as shown in the sketch below and calibrated with a single transducer (with the test model removed), assuming that the frequency response in that case was equal to 1 (as claimed by the

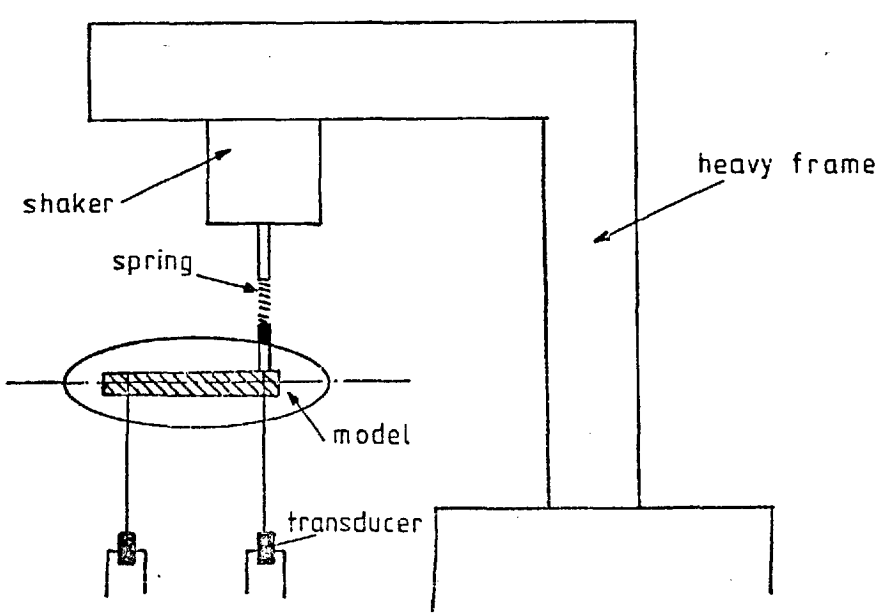

. SKETCH

manufacturers). Fig. 3.6 shows that the ratio F of the total force felt by the model, to the force exerted on a single crystal for the same frequency and amplitude of the shaker, is nearly equal to 1.0. Tests at higher frequencies than those shown in Fig. 3.6 were not attempted, because of resonances in the mounting mechanism. It is thought, however, that the transmission of forces in the actual installation would be accurate for all frequencies not close to the support's resonant frequencies. The dynamic calibration factor was assumed to be 1.0 for all the subsequent lift results.

Finally each model was tested for mechanical resonances. Excitation was achieved by tapping the body and recording the ensuing damped vibrations on a storage oscilloscope. Approximate values of the resonance frequencies could be calculated from the oscilloscope traces. It was found that the elliptic and D bodies had a first mechanical resonance at approximately 500 Hz, while the aerofoil's resonant frequency was about 300 Hz.

3.2 THE GENERATION OF TWO-DIMENSIONAL SINUSOIDAL FLOW

3.2.1 THE OSCILLATING RIG

It was decided to modify the existing grid built by Newton (1973). There were three basic components of the modified rig (see Fig. 3.7):-

- A lightweight support frame in the shape of an H (parts 6, 7).
- A motor-flywheel system (parts 5, 12), assembled to connecting rods (parts 2, 4) and support leaf springs (part 3).
- Two oscillating aerofoils (part 1) driven by the long and short connecting rods and pivoted on the end plates.

The frame, a legacy from Newton's (1973) experiment, was made from metal tube of a rectangular cross section. It consisted of two vertical supports placed one on each side of the tunnel and a horizontal

girder support, on which the platforms carrying the motor and flywheels were bolted. The DC motor had a nominal power of 0.5 HP and its speed could be controlled by means of a transistorized speed regulator. The horizontal support was clamped to the two vertical ones and could be raised or lowered or even separated from them during installation or dismantling. When the frame was screwed onto the laboratory floor, the latter received most of the vibration.

The flywheel connecting rod assembly was designed with the aim of providing:-

- Sinusoidal rotations of the aerofoils.
- Adjustability of amplitude and frequency of the oscillations.
- Smooth operation.

On account of the first requirement ℓ_c' (i.e. the length of the connecting rod defined in Section 3.1.2) should be large. Amplitude adjustment was facilitated by a movable eccentric shaft. However, this arrangement - unlike a slider-crank mechanism - could not provide equal peak displacements of the wings about their horizontal chordline; but again this asymmetry diminishes for large ℓ_c', compared with the shaft eccentricity r. It was thus decided to construct two identical connecting rods driving the lower aerofoil, of the maximum length permitted by the tunnel geometry, and connect the upper aerofoil to the lower by separate connecting rods.

With the upper frequency limit set in Section 3.1.2 (= 40 Hz), a complete calculation of the various mechanical parts could be made, which are shown in Fig. 3.7. The length of the long connecting rod ℓ_c' was taken 0.97 m and the maximum eccentricity used was r = 0.0125 m. Change of eccentricity could be achieved with a bolt fixed diametrically on the flywheel (see Fig. 3.7). The long and short connecting rods were

joined together with the aerofoil drive shaft and a rectangular leaf spring via a pin. This pin was screwed onto the spring, but it was allowed to rotate freely into the aerofoil drive shaft by means of a copper bearing insert. The steel leaf springs were clamped on the two vertical supports and provided means of stiffer wing mounting, being preferred from helical springs in that they could raise considerably the natural frequency of the system.

The installation of ball bearings in the main shaft and needle bearings in the connecting rods contributed to the smoother operation of the system.

The two end plates used by Newton (1973) were modified to account for the double aerofoil configuration. There were two wooden panels added, supplied with square openings for the leaf springs to pass through and nylon bushes to enable the pivot shafts to rotate freely.

3.2.2 PERFORMANCE OF THE OSCILLATING RIG

Before the final wind tunnel installation, the oscillating rig was tested in a false working section, made from DEXION, far from the tunnel. Tests at many frequencies and eccentric amplitudes showed that the only mechanical problem appeared to be the excessive floor and end-plate vibration, noticed at the floor resonant frequencies and also at the highest frequencies which, unfortunately, could not exceed 20 Hz, instead of the intended maximum of 40 Hz. It was hoped that the end plate vibration would be remedied in the actual stiffer tunnel installation, while the floor needed special attention. A large bin filled with gravel was placed at a suitable position near the rig and absorbed a considerable amount of floor vibration. Another effective method tried was to "mass balance" the girder support: two steel leaf

springs were bolted on it, each carrying a mass M, approximately 5 kg on the free end. The lengths of the springs were calculated so that the natural frequency of the combined body (spring-mass) corresponded to the floor natural frequency, or the horizontal girder natural frequency. At resonance, the masses vibrated strongly thus absorbing some of the energy, which otherwise would have been transmitted to the floor or the horizontal beam.

The resonances in the actual tunnel installation occurred at higher frequencies. It was possible to attain frequencies up to 25 Hz with low shaft eccentricity ($\simeq \pm 7^{o}$ aerofoil geometric incidence) and 16 Hz with the largest ($\simeq \pm 11^{o}$), without any vibration troubles. A light beam from a stroboscope was used to check that no appreciable flexing of the aerofoil took place during oscillation.

At this stage a simple mechanism was added, which enabled an accurate measurement of the aerofoil frequency (and consequently the gust frequency since the transmission ratio was equal to 1.0) and also of the phase between the aerofoil displacement and gust or lift variations. It consisted of a permanent U shaped magnet, wired with a winding and mounted on the horizontal beam of the rig and a piece of soft iron fixed onto one of the flywheels. As the iron piece passed periodically through the poles of the magnet, it induced a voltage on the winding. The electric signal generated in this way was displayed on an oscilloscope. The display showed a sharply peaked signal with period equal to the oscillation period.

Measurements of this frequency (by methods described in Appendix B) indicated that once the motor speed was set, it started drifting very slowly towards a value, which was at maximum 0.2 Hz above the preset value, after roughly 10 to 15 minutes.

This drift depended on the frequency itself, the state of lubrication and perhaps some changes in the power supply. A remedy would have been the construction of a frequency correcting device at the expense of time and money. This matter was not pursued further and this drift had to be accepted. Care, however, was taken when the actual experiment was made to allow for some "warm-up" time before each run at a particular frequency. The present design, when compared with Newton's (1973), had the following mechanical advantages:-

- Smoother operation.
- Higher running frequencies.
- Bending free motion of the oscillating aerofoils.

3.3 DESCRIPTION OF THE UNSTEADY FLOW

3.3.1 INTRODUCTION

A survey of the flow field was needed and especially of the region occupied by the test models. To localize this region along the tunnel working section, the oscillating rig was set up and some preliminary measurements were made. Due to the limited clearance between the tripod support system and the tunnel floor, and also the necessity for short supports, the chord-line of the test models was 0.051 m below the geometric tunnel centre line. For that reason the centre line of the oscillating aerofoils was also lowered by 0.051 m with respect to the tunnel centre line.

The intensity and sinusoidality of the upwash gust were measured with a cross wire (see Section 3.3.2), which was traversed along the centre line. Some traverses in the vertical direction were made as well. The frequencies tested ranged from 5 to 20 Hz and the speeds from 10 m/s to 30 m/s.

It was found that within a streamwise distance of 1 to 7.5 aerofoil chords from the oscillating aerofoil mid-chord point, the signal along the centre line was very sinusoidal and with variation in amplitude less than 15% approximately. The gust amplitude tended to drop with distance only for the lowest frequencies. Vertical traverses indicated that the irrotational region (manifested itself by a very sinusoidal signal), decreased with distance downstream, being 0.075 m in width approximately towards the end of the working section.

Taking into account the conditions imposed in Section 3.1.2 (Eqns. 3.13 and 3.14), it was decided to select the streamwise position of x_g = 1.2 m downstream of the oscillating aerofoil mid-chord point, for the subsequent unsteady flow and lift measurements. The origin of the coordinate system used in the present experiments was in the aforementioned location and in the mid-distance of the two end plates and the two oscillating aerofoils, see Fig. 3.8.

The next parameter to be determined was the actual tunnel speed. The oscillating rig was capable of producing a good sinusoidal gust over a wide range of flow speeds, but it was felt that the measurement of lift would be a problem at very low and very high speeds. After a quick set up of the lift balance, it was found that in the approximate range of speeds 10 to 30 m/sec and for all but the lowest frequencies, the output lift signal was sinusoidal (with some noise superimposed on it) and accurately measurable. As the air speed decreased below the lower limit stated above, the lift signal became less sinusoidal and noisy, due to the relatively increasing contribution from the model and support system vortex shedding. On the other hand, at very high flow speeds, the vibration of the support shields became apparent (a high frequency intermittent noise was displayed on the oscilloscope) and a

low frequency streamwise swinging motion of the models was noticed (which tended to amplitude modulate the lift signals). Therefore, it was decided to carry out the unsteady flow and load experiments in the range of speeds 10 to 30 m/sec. The corresponding Re numbers (based on the model chord) are given in Table 1.

Finally, it was the range of the oscillating aerofoils' amplitudes which had to be selected. Three amplitudes were chosen, termed "LARGE", "MEDIUM" and "SMALL" eccentricities. Details are given in Table 2.

As the variation of the aerofoil angle with time was very nearly sinusoidal, the RMS oscillating aerofoil amplitudes could be obtained from the half peak to peak $\left(\frac{P.T.P}{2}\right)$ amplitudes, after dividing by $\sqrt{2}$.

3.3.2 HOT-WIRE EQUIPMENT

During the course of the work, it was necessary to measure the streamwise as well as the transverse velocity components. This was done by using a normal U wire and a cross wire respectively. The details of the calibration methods and the accuracy of these measurements can be found in Appendix A.

3.3.3 MEASUREMENT AND PROCESSING OF SIGNALS

The output of the transducers used in the experiments was in most of the cases an electric signal, which was immediately measured and occasionally stored in analogue form on magnetic tapes or paper tapes for further processing. The properties of the signals measured included the mean and root mean square values, spectral density, frequency, correlation coefficient, number of maxima per unit time and

instantaneous or conditionally averaged amplitude. Appendix B describes the techniques employed and their relevant accuracy.

3.3.4 FLOW MEASUREMENTS

These were made in the "empty" tunnel (no support system), unless otherwise stated. It was expected that the effect of the support system would be small, causing perhaps only a change in the velocity upwash intensity and in the mean flow incidence. Since some measurements were also planned to be carried out on models not supported on the tripod but on the false walls (mean pressures and boundary layer experiments), the decision was taken to study the oscillatory flow alone and exclude any special conditions. However, quantitative results were also available with the support system installed in the tunnel, which are cited in the appropriate sections.

3.3.4.1 DYNAMIC HEAD MEASUREMENTS

A Pitot static tube was fixed permanently at the point (- 0.5 m, 0.21 m, 0.10 m). Another tube was placed near the point (0, 0, 0) and indicated an increase of dynamic head of 2.5 - 3.5% approximately, in smooth and oscillatory flow, with the support system in position. Moving the second tube away from the centre, across the span, this value increased, but by no more than 1.5%, just above one of the pylons of the support system. No noticeable change in the dynamic head was realised in the empty tunnel. Since the end plates were installed parallel to each other, this shows that the wall boundary layer displacement effects were small. A correction due to change in the mean flow speed, U_∞, was applied on the reduced frequency $k = \pi nc/U_\infty$, in cases where the support system was in the tunnel during

velocity measurements. Vertical traverses in oscillatory flow, had shown that the dynamic head increased by 2% as the point (0, 0, 0.07 m) was approached (tripod in).

Detailed flow angle measurements were not made. McKeough (1976) conducted experiments with a similar tripod system in turbulent flow and reported an increase in the mean flow incidence from 1^{o} to 2.5^{o}. The author used an X-wire to estimate the change in mean incidence due to the presence of the support system. The probe was calibrated in yaw as well as each wire individually, in the empty tunnel. Then the tripod was put in place. If this had as effect an increase in the local speed, the squared outputs from the two anemometers would have the same difference as before. Since this did not happen, it was assumed that a change in the flow incidence took place, which was estimated to be less than 1^{o}. In addition, the change in the pressure distribution over an elliptic model placed at the same position at zero incidence, indicated that the presence of the support system did not cause deviations of the flow direction by more than 1 degree. It may be that since McKeough's support system was bulkier than the author's, it caused greater changes in the mean flow direction.

3.3.4.2 VELOCITY UPWASH MEASUREMENTS IN THE X, Y, Z DIRECTIONS

The purpose of these measurements was to examine whether the sinusoidal gust was of uniform structure, at least over that part of the working section occupied by the test models.

First, a set of measurements was made with an X-wire supported on a tube spanning the tunnel. Only the unfiltered peak voltage output was measured, as depicted from a storage oscilloscope. Starting from the point (0, 0, 0) the traverses covered the line (0, 0, - 0.3 m), (0, 0,

0.3 m), z being made dimensionless with b/2 (half the bluff body thickness, which was equal to 0.025 m). The results are presented in Fig. 3.9. The peak gust angle is non-dimensionalized with the peak oscillating aerofoil angle. It was observed that only for $\left|z/\frac{b}{2}\right| \lesssim 2$ the signal had a sinusoidal form. Outside this region the signal was gradually distorted resembling a square wave with spikes superimposed on it. This was more pronouced at higher frequencies and distances $\left|z/\frac{b}{2}\right|$. A case where that spike just appears is shown in Fig. 3.10, obtained directly from a BRUSH pen recorder. The small amount of noise superimposed on the signal was discovered to be more related to hum and interference from the coil signal (see Section 3.2.2), than to turbulence. It appears that the presence of the spike at a certain point during the cycle is related to the hot-wire encountering part of the vortex, formed after a rolling-up of the continuous vorticity shed by the oscillating aerofoil (see Hanson, Kozak and Richardson, 1966). The enhanced unsteadiness as $\left|z/\frac{b}{2}\right|$ increases, indicates that the vortical part of the flow is approached, but owing to the crudeness of the measurement, the centres of the individual vortices are hard to define.

Referring to the central part of the curves in Fig. 3.9, it is observed that the distribution of gust intensity is not symmetric with respect to the x-y plane, the minimum occurring for negative z (towards the wall closer to the centre line). More detailed traverses of the central region for three oscillating aerofoil amplitudes and several frequencies are shown in Figs. 3.11, 3.12 and 3.13. The gust intensity is seen to increase with increasing dimensionless frequency k, but to drop after a certain value in k is reached. The asymmetry mentioned before is apparent especially at high frequencies. Over one body width the variation is at most 5%. Therefore, it was decided to keep the

point (0, 0, 0) as the origin of the coordinate system and to put the models in the tunnel in such a way, such that their mid-chord point would coincide with the point (0, 0, 0). The asymmetry could be due to the fact that the oscillating aerofoils were not placed symmetrically with respect to the centre line of the tunnel.

Some further experiments were conducted with regard to the effect of the tripod support system on the gust intensity. The X-wire probe was traversed along the verticals, through the point (0, 0, 0) and the centres of the two front piezoelectric transducers. The results, presented in Fig. 3.14, are made dimensionless with the (filtered) RMS gust intensity at the point (0, 0, 0) but with the support system removed. Its effect is seen to reduce the gust intensity, mainly at the lower frequencies and at the spanwise positions just above the two front pylons.

To find out whether that behaviour was due to the presence of the support system itself or due to an inherent property of the gust, i.e. to diminish away from the centre, some measurements in the spanwise direction were made, in the empty tunnel. In the plane z = 0, the gust was found to be effectively constant (within 2%) over the region occupied by the model. Near the end plates there was a tendency for the gust intensity to drop, probably because of the effect of trailing vortices shed by the oscillating aerofoil (see Section 3.1.1 (iii)). Closer to the end plates, boundary layer effects and plate vibration would also become important.

The two-dimensionality of the flow in the spanwise direction was checked by two methods:-

- First, two X-wires were employed, one fixed at the point (0, 0, 0) and the other free to move along the y axis in the spanwise direction. The

signal from the two wires (with the support system included), were recorded at a low speed and then played back at a higher speed; then the outputs were filtered using two identical band pass filters centred at the gust frequency (multiplied by the speed-up ratio of the tape recorder) and fed into a DISA 55A06 Random Signal Correlator. The correlation coefficient R_{ww} (n_g, y) between those two signals was displayed on the instrument. (The tape recorder simply helped to raise the frequencies of interest into the range of flat frequency response of the DISA correlator, 10 Hz to 2 x 10^4 Hz, while maintaining their phase). The results are shown in Fig. 3.15. They indicate that the flow is well correlated in the spanwise direction, especially at the higher reduced frequencies, the quality of two-dimensionality decreasing as the reduced frequency decreases. The reduction in R_{ww} (n_g, y) at lower k could result from:-

(i) A slightly oblique gust, which does not encounter the two X-wires simultaneously.

(ii) A random variation of gust phase angle across the span, due to the dependence on a spanwise wave number k_2.

(iii) Relatively increased levels of turbulence, with respect to gust intensity originating from break-up of the oscillating aerofoil shed vortices. Turbulence is known to be poorly correlated in space.

- In the second method, two small aluminium aerofoils (chord = 42 mm, span ≐ 60 mm) were fixed on the two front piezoelectric transducers (their spanwise distance being about 88% of the model span). The same procedure was followed in getting the correlation coefficient for the two lift signals, when the tunnel was running. The correlation coefficients obtained were even higher than those from the X-wires, possibly because the wings responded less to the small amount of

streamwise fluctuations than the hot-wire. An instantaneous plot of lift signals is presented in Fig. 3.16, where it can be seen that for the specific value of k, the sinusoidal wave fronts appear to "hit" the model leading edge almost simultaneously.

A conclusion may be drawn at this point that the tripod support system is mainly responsible for the small reduction in gust intensity and spanwise gust correlation at the lowest reduced frequencies.

As the gust intensity was found to be approximately unchanged over one chord length of the models, it was decided to carry out the detailed measurements at the point (0, 0, 0) with no support system. This was done for two reasons:-

(i) To gain a more general view of the unsteady flow produced, independent of the details of the current programme.

(ii) To avoid blockage effects due to the simultaneous existence of the support system and the hot-wire traverse gear.

The choice of a single point for taking velocity readings is certainly not the ideal solution, because the real flow is never exactly two-dimensional, but it saves quite a lot of experimental time. This matter will be discussed again in the explanation of lift results.

3.3.4.3 DETAILED UPWASH MEASUREMENTS AT THE POINT (0, 0, 0)

In Section 3.1.1 the mechanism of production of the sinusoidal flow was suggested. Experimental evidence (e.g. Bratt, 1950; Wood and Kirmani, 1970) shows that each of the vortex wakes shed by the oscillating aerofoils starts to roll-up at a distance downstream (closer to the aerofoil trailing edge as $k' = \pi nc'/U_\infty$ increases), and form discrete vortices of alternate sign. The resulting "vortex streets" have the opposite sense of rotation to that of a Karman vortex street

and their transverse distance increases as they travel downstream (see sketch on page 56, Section 3.1.1). The result of this vortex motion is the sinusoidal flow, which is expected to be free from any streamwise component along the centre line.

The measured values of the upwash gust along the centre line are now presented. The results appear in three different ways as:-

(i) Root mean square (RMS) filtered gust amplitudes (degrees) plotted against k.

(ii) Power spectra (sec) normalized with the total mean square value of the signal against frequency n (Hz).

(iii) Variation of the dimensionless upwash (degrees) over a complete sinusoidal cycle (the upwash signal was conditionally averaged over a large number of cycles, as described in Appendix B).

Fig. 3.17 contains the results for case (i) for three different oscillating aerofoil amplitudes. The points shown at regular intervals of k, are selected from a smooth curve drawn through the original experimental points. Generally, the tendency is for the gust amplitude first to increase with $k = \pi nc/U_\infty$, reach a maximum in the region $k \simeq 0.35$ and then decrease. The reason for such a trend is that on one hand the gust intensity increases for increasing k, because stronger vorticity is shed in the wake, but on the other hand, for a point far away from the wake the gust is diminished due to counteracting vortices at higher frequencies. It is also noted that for fixed oscillating aerofoil eccentricity, a change in Re number does not significantly affect the relative gust intensity at a particular k. The collapse of the results is in the same order for all eccentricities, and this suggests that there might be a very small dependence on Re number, although the calibration constant of the cross hot-wire (different for

each speed) and the change in the effective wind speed could contribute as well.

Another conclusion emerging from Fig. 3.17 is that the gust intensity is larger for larger oscillating aerofoil amplitudes at a certain frequency k. This is expected since a higher angle of attack produces higher unsteady lift on the oscillating aerofoils and stronger wake vorticity (see Karman and Sears, 1938), which consequently induces a stronger gust.

The streamwise component u at the gust frequency was almost non-existent, but a u component at twice that frequency was about 20% of the corresponding upwash component, see Fig. 3.17. The disappearance of the primary u component is the result of the symmetry in the motion of the aerofoils. It is believed that the existence of higher harmonics in the upwash and streamwise gust components is caused by non-linear effects such as the deformation of the wake from the (assumed) state of a straight line (see for example Giesing, 1968), and the subsequent rolling-up process, pronounced for higher frequencies.

The spanwise component v was found to be at least one order of magnitude less than the corresponding w component, see Fig. 3.17.

Plots of upwash spectra (normalized with the full signal mean square value) for some selected frequencies are presented in Fig. 3.18.

It is observed that the main power is concentrated under a peak at the oscillating aerofoil frequency. At high frequencies, this peak is more sharp than at lower frequencies. For example, in the case with n_g = 18 Hz, the spectral power drops by almost four orders of magnitude in a bandwidth 0.55 n_g, while for n_g = 4.6 Hz, it drops by three orders of magnitude in a bandwidth 1.25 n_g. This spread of energy could be due to: The random change of the oscillating rig frequency about its

mean value, small random changes in the position of shed vorticity, free stream turbulence, finite filter bandwidth and electronic noise. The amount of energy enclosed under the sharp peaks was found to be in good agreement with the square of the filtered values (measured with an RMS meter). Small differences are attributed to some attenuation caused by the filter (see Appendix B). The signal to noise ratio was comparatively poor at the lowest frequencies, because the gust intensity itself was small.

The response at the second and third harmonics is marked on the plots of Fig. 3.18. Note, that the third harmonic is always stronger than the second. This may be due to a cancelling effect in the shed vorticity. The calculations of Giesing (1968), for an 8.4% thick von Mises aerofoil starting translational sinusoidal oscillations at t = 0, showed that the circulatory lift was characterized by higher harmonics, of which the third was greater than the second. As can be seen from Fig. 3.18c, the increase in the oscillating aerofoil amplitude of motion (marked as large eccentricity) does not affect the shape and spectral density of the main spectral peak, but it increases the level of higher harmonics. The relative increase in power lies between 6.5 and 8.0, meaning that the amplitudes of the corresponding oscillating components would be increased by a factor 2.5 to 2.8. If these values are compared with the increase in the oscillating aerofoil amplitude, approximately equal to 1.53 (see Table 2), the greater, non-linear contribution of the wake deformations can be realised.

The regularly spaced spikes at 50, 100, 150, 200 Hz, etc. are due to interference from the mains. Later it was discovered that the instrument responsible was the low pass filter. After it has been suitably earthed, the plots were almost free of that kind of noise, as in Fig. 3.18d. The spectrum of background noise appears lower, the

higher the gust frequency.

The conditionally averaged gust angle $\alpha_g(t)$ is plotted against the cycle phase angle ϕ in Fig. 3.19. Only one eccentricity and speed were considered, but various frequencies. For convergence of the conditional sampling program, it was required that the difference between the running averages, formed while more data points were processed, to be less than 0.01 volts (the digitized signals usually had a peak amplitude of two orders of magnitude higher, ± 1 volt p.t.p*). At the last two plots (oscillating aerofoil frequencies 4 and 3 Hz) the execution had to be stopped before convergence, since no more data records were available. It is felt, however, that the effect on the final result would be small because the calculations were very near convergence. As a comparison, a sine wave of peak amplitude equal to $\sqrt{2}\ \alpha_g$ has been plotted in phase with the averaged waves. The zero phase angle, $\phi = 0$, was taken as the position of the spike in the coil signal. The same instruments were used for the measurement of lift and velocity upwash levels, so that their phase (in fact the phase between each signal and the reference coil signal) was maintained.

It can be seen that the maxima, or minima, in the various plots do not occur at the same phase angle ϕ, this being due to different wave-lengths of each gust. Some small deviations from sinusoidality are noticed, especially near the peaks (negative and positive) and at low frequencies. One could attribute these deviations to the following reasons:-

(i) The motion of the oscillating aerofoils. As stated in Section 3.2.1, they perform a nearly sinusoidal oscillation.

(ii) Some small amount of reversed flow at the highest oscillating aerofoil angle position.

---

* peak to peak

(iii) Turbulence in the signal, especially its lowest components, coming from the aerofoil's turbulent shear layers and possibly from some partial break-up into a turbulent vortex.

(iv) Higher harmonics. The input to the conditional averaging computer program was low-passed at a high frequency, so that the averaged output might well contain some components of the second and third harmonics of the gust.

(v) The fact that the absolute values of the peaks are not exactly the same, could be due to a small amount of DC voltage in the electronics.

These results show that the gust can be assumed to be satisfactorily sinusoidal. The plots in Fig. 3.19 will find another application later in this work, when the phase between fluctuating lift and velocity is presented.

3.4 A SIMPLIFIED MATHEMATICAL MODEL FOR THE SINUSOIDAL FLOW

3.4.1 FORMULATION OF THE PROBLEM

In this section, an attempt has been made to construct a simple potential flow model with the aim of predicting the velocity field of the flow generated by two aerofoils, performing pitching oscillations about points on their chordline in a smooth free stream. A schematic representation of this model flow is shown in Fig. 3.20

3.4.2 ASSUMPTIONS

The following assumptions are made:-

(i) The oscillating aerofoils are simulated by flat plates of zero thickness.

(ii) Sinusoidal pitching oscillations of small amplitude, Θ_0,

are assumed, for the unsteady thin aerofoil theory (see Karman and Sears, 1938) to apply.

(iii) The two-dimensional vorticity shed continuously downstream and convected with the free stream velocity U_∞, is concentrated on the extension of the mean aerofoil chord lines.

(iv) The two vortical wakes (which in fact are the only rotational regions of the field), extend infinitely in both ($-\infty$, $+\infty$) directions and do not interact with each other (for the calculation of the upwash only).

(v) The Kutta-Joukowski condition for the oscillating aerofoils is fulfilled at all times.

Assumption (iii) makes the problem a linear one and (iv) simplifies the problem in that the calculation of the unsteady flow induced by two isolated oscillating aerofoils will suffice for the calculation of the combined flow field.

3.4.3 METHOD OF SOLUTION

The vorticity in the wake is determined from unsteady thin aerofoil theory and then the induced velocities are obtained from an application of Biot-Savart's law.

Any point on the aerofoil chord line is described by the equation (see Fig. 3.20):-

$$z_a(x, t) = \bar{z}_a(x)\, e^{i\omega t} = (x - \ell')\, \Theta_o\, e^{i\omega t} \qquad (3.19)$$

$\omega = 2\pi n$, n = oscillation frequency (Hz). The actual oscillation is given by the real part of Eqn. (3.19). The boundary condition of zero normal velocity gives at the aerofoil surface:-

$$w_a\ (x,\ t) = \frac{\partial z_a\ (x,\ t)}{\partial t} + U_\infty \frac{\partial z_a\ (x,\ t)}{\partial x} \tag{3.20}$$

w_a is the normal (in the z direction) velocity on the aerofoil surface. With Eqn. (3.19), Eqn. (3.20) is rewritten as:-

$$w_a\ (x,\ t) = i\omega\ (x - \ell')\ \Theta_o\ e^{i\omega t} + U_\infty\ \Theta_o\ e^{i\omega t} \tag{3.21}$$

or, after introducing the dimensionless quantities:-

$$k' = \frac{\omega c'}{2U_\infty} \quad , \quad x^* = \frac{2x}{c'} \quad , \quad \xi^* = \frac{2\xi}{c'} \tag{3.22}$$

c' being the aerofoil chord length. Rearranging:-

$$w_a\ (\xi^*,\ t) = \frac{c'}{2}\left[i\omega\Theta_o\xi^* + \Theta_o\left(2\frac{U_\infty}{c'} - \frac{2\ell'}{c'}\ i\omega\right)\right] e^{i\omega t} \tag{3.23}$$

Define:- $\bar{w}_a\ (\xi^*,\ t) = w_a\ (\xi^*,\ t)/e^{i\omega t}$ (3.24)

and Eqn. (3.23) becomes:-

$$\bar{w}_a\ (\xi^*,\ t) = \frac{c'}{2}\left[i\omega\Theta_o\xi^* + \Theta_o\left(2\frac{U_\infty}{c'} - \frac{2\ell}{c'}\ i\omega\right)\right] \tag{3.25}$$

For small oscillations, the problem becomes linear and all the quantities varying with time may be assumed proportional to $e^{i\omega t}$:-

$$\gamma_a\ (\xi,\ t) = \bar{\gamma}_a\ (\xi)\ e^{i\omega t} \tag{3.26a}$$

$$\Gamma\ (t) = \bar{\Gamma}\ e^{i\omega t} \tag{3.26b}$$

$$\gamma_w\ (\xi,\ t) = \bar{\gamma}_w\ (\xi)\ e^{i\omega t} \tag{3.26c}$$

where γ_a is the aerofoil bound vorticity, γ_w is the wake vorticity and Γ the circulation round the aerofoil. Then, using standard thin aerofoil theory (e.g. Bisplinghoff et al, 1958), the wake vorticity is found to be:-

$$\bar{\gamma}_w\ (k') = \frac{-4}{\pi\left[H_1^{(2)}\ (k') + iH_0^{(2)}\ (k')\right]}\left[\int_{-1}^{1}\sqrt{\frac{1+\xi^*}{1-\xi^*}}\ \bar{w}_a\ (\xi^*)\ d\xi^*\right] e^{-i\omega\xi/U_\infty} \qquad (3.27)$$

where the second kind Hänkel functions of order n can be computed from $H_n^{(2)} = J_n - i\ Y_n$, with J_n, Y_n standing for the Bessel functions of the first and second kind and order n.

Using Eqn. (3.25), one has to evaluate the integral:-

$$\int_{-1}^{1}\sqrt{\frac{1+\xi^*}{1-\xi^*}}\ (A\xi^* + B)\ d\xi^* = \int_{-1}^{1}\sqrt{\frac{1+\xi^*}{1-\xi^*}}\ A\xi^*\ d\xi^* + \int_{-1}^{1}\sqrt{\frac{1+\xi^*}{1-\xi^*}}\ Bd\xi^* \qquad (3.28)$$

where $A = i\omega\Theta_0\ \frac{c'}{2}$ and $B = \Theta_0\ (U_\infty - \ell' i\omega)$.

The first integral on the RHS* of Eqn. (3.28) is equal to $A\ .\ \frac{\pi}{2} = \frac{i\omega\Theta_0\pi c'}{4}$ and the second is equal to $B\pi = \Theta_0\pi\ (U_\infty - \ell' i\omega)$. Therefore Eqn. (3.27) becomes:-

$$\bar{\gamma}_w\ (\xi) = F\ (k')\ .\ e^{-i\frac{2k'}{c'}\xi} \qquad (3.29)$$

$$\text{where } F\ (k') \equiv \frac{-4\ \Theta_0\ U_\infty\left[1 + \left(\frac{1}{2} - \frac{2\ell'}{c'}\right) k'i\right]}{H_1^{(2)} + i\ H_0^{(2)}} \qquad (3.30)$$

This analysis has assumed non-interfering aerofoils. Each vortex wake

---

* right hand side

induces a velocity field at the test point. The vortex wake has been assumed to extend infinitely up and downstream unchanged. Therefore, the total velocity field is equal to the sum of two contributions.

The upwash component (w) of a single vortex street is given by Biot Savart's law:-

$$w\ (x,\ z,\ t) = \frac{1}{2\pi} \int_{-\infty}^{\infty} \frac{(x - \xi)\ \overline{\gamma}_w\ (\xi)\ e^{i\omega t}\ d\xi}{(x - \xi)^2 + z^2} =$$

$$= \frac{e^{i\omega t}}{2\pi} F\ (k') \int_{-\infty}^{\infty} \frac{e^{-i \frac{2k'}{c'} \xi}\ (x - \xi)\ d\xi}{(x - \xi)^2 + z^2} \qquad (3.31)$$

The $-\infty$ lower limit is justified from assumption (iv). Hence:-

$$w\ (x,\ z,\ t) = \frac{i}{2} F\ (k')\ e^{i\omega t} \cdot e^{-i \frac{2k'}{c'} x} \cdot e^{-\frac{2k'}{c'} |z|} \qquad (3.32)$$

so that w is an even function of z. The combined field has a resultant upwash velocity at some point B (see Fig. 3.20):-

$$w\ (x,\ z,\ t) = \frac{i}{2} F\ (k')\ e^{i\ (\omega t - \frac{2k'}{c'} x)} \left[e^{-\frac{2k'}{c'} z_1} + e^{-\frac{2k'}{c'} z_2} \right] \qquad (3.33)$$

where z_1 and z_2 are always counted positive.

The dimensionless gust amplitude is equal to:-

$$\frac{w}{U_\infty} \cdot \frac{1}{\Theta_0} = \alpha_g\ (t) =$$

$$= \frac{-2i \left[1 + \left(\frac{1}{2} - \frac{2\ell'}{c'} \right) k'i \right] \left[e^{-\frac{2k'}{c'} z_1} + e^{-\frac{2k'}{c'} z_2} \right]}{\left[H_1^{(2)}\ (k') + iH_0^{(2)}\ (k') \right]} e^{i(\omega t - \frac{2k'}{c'} x)} \qquad (3.34)$$

The absolute value of Eqn. (3.34) gives the peak amplitude of the dimensionless gust comparable to the one measured by a X hot-wire.

For the streamwise component (u) of a single sheet one can find similarly:-

$$u\,(x,\,z,\,t) = -\frac{z}{2\pi}\int_{-\infty}^{\infty}\frac{\bar{\gamma}_w\,(\xi)\,e^{i\omega t}\,d\xi}{(x-\xi)^2+z^2} = -\frac{z}{2\pi}\int_{-\infty}^{\infty}\frac{F\,(k')\,e^{-i\frac{2k'}{c'}\xi}\,e^{i\omega t}\,d\xi}{(x-\xi)^2+z^2} =$$

$$= \pm\frac{F\,(k')}{2}\,e^{i\omega t}\,e^{-i\frac{2k'}{c'}x}\,e^{-\frac{2k'}{c'}|z|} \qquad (3.35)$$

$\frac{2k'}{c'} > 0$

The sign + for $z < 0$

The sign - for $z > 0$

so that u is an odd function of z (for a single aerofoil). The combined field is found to be:-

$$u\,(x,\,z,\,t) = \frac{1}{2}F\,(k')\,e^{i(\omega t-\frac{2k'}{c'}x)}\left[e^{-\frac{2k'}{c'}z_1} - e^{-\frac{2k'}{c'}z_2}\right] \qquad (3.36a)$$

Between the wakes
Region II, (see Fig. 3.20)

$$u\,(x,\,z,\,t) = \pm\frac{1}{2}F\,(k')\,e^{i(\omega t-\frac{2k'}{c'}x)}\left[e^{-\frac{2k'}{c'}z_1} + e^{-\frac{2k'}{c'}z_2}\right] \qquad (3.36b)$$

Outside the wakes
Regions III and I

3.4.4 DISCUSSION OF RESULTS AND COMPARISON WITH THE EXPERIMENT

The solutions for u and w concern only the oscillating aerofoils in an infinite free stream. The tunnel walls, roof and floor require that the actual velocities should fall to zero there. This boundary condition may be accounted for by introducing suitable distributions of image vorticity in planes parallel to those of the vortex wakes, and of such sign and distance from the centre line so as to maintain the boundary conditions. Figs. 3.21a, b, c and d show the effect that this correction has on the unconstrained results for two cases:-

(i) When an infinite number of images are considered.

(ii) When only the two closest to the centre line image distributions are considered.

It is seen that the effect of the walls is to decrease the dimensionless gust amplitude at all frequencies (without introducing any phase changes), but their effect to become increasingly less important as $k' \to \infty$. This correction suggests that assumption (iv) is expected to get worse at low k' because of the interference from one sheet on the opposite aerofoil.

The corresponding function $F'(k')$ for a system of two aerofoils performing heaving oscillations of amplitude $\Theta_0 b \left[1 + \frac{2\ell'}{c'}\right]$, i.e. equal to the greatest deviation of the trailing edge or the leading edge of the rotationally oscillating aerofoils, is equal to:-

$$\left[-4i\omega\Theta_0 \frac{c'}{2}\left[1 + \frac{2\ell'}{c'}\right]\right] \Big/ \left[H_1^{(2)}(k') + iH_0^{(2)}(k')\right] \qquad (3.37)$$

The ratio of the two functions (see Eqn. 3.30) is:-

$$J = \frac{|F(k')|}{|F'(k')|} = \frac{\left|1 + \left(\frac{1}{2} - \frac{2\ell'}{c'}\right) ik'\right|}{\left|ik' \left(1 + \frac{2\ell'}{c'}\right)\right|} \qquad (3.38)$$

which indicates that for $0 \lesssim k' \lesssim 1.0$ the pitching oscillations produce a much stronger gust than the translational oscillations. For example, in the author's case $\frac{2\ell'}{c'}$ was equal to 0.1875 and J = 8.425 for $k' = 0.1$ and J = 1.100 for $k' = 0.8$.

As expected, the vorticity $\frac{\partial u}{\partial z} - \frac{\partial w}{\partial x}$ is everywhere zero except on the two vortex wakes. The u component is zero on the centre line (see Eqn. (3.36a), for $z_1 = z_2$) and this is in agreement with the experimental results. It can also be shown that all the pressure gradients are zero.

The gust amplitude $\alpha_g(t)$ is seen to be proportional to the oscillating aerofoil amplitude Θ_0. Therefore, the choice of Θ_0 to non-dimensionalize the gust amplitude is justified.

Eqn. (3.34), for the gust amplitude $\alpha_g(t)$, was fed with suitable values from the author's experiment ($z_1 = z_2 = 0.228$ m, $c' = 0.203$ m, $2\ell'/c' = 0.1875$), and the results (corrected and uncorrected for wall interference), are plotted in Figs. 3.21a, b, c and d, against the model reduced frequency $k = \pi nc/U_\infty$. The experimental results are in good agreement with those predicted and corrected for wall interference, for k up to about 0.35. Above this value, the experimental values are higher than the predicted, the deviation increasing as k further increases. Taking into account the experimental errors, there is no clear evidence whether a particular aerofoil amplitude Θ_0 exhibits better agreement than any other.

For low reduced frequencies k, discrepancies may arise due

to the uncertainty in measuring the gust and the aerofoil vorticity γ_a affecting the (assumed) infinite vortex sheets.

In the range of large k, the vorticity shed is much stronger and a rolling-up process, as opposed to the continuous distribution assumed, is more likely to happen at an earlier stage (this introduces higher harmonics in the upwash and streamwise gusts).

The proposed theoretical model does not account for these phenomena. In any case, the maximum near $k \simeq 0.35$ is realised theoretically.

A different approach in normalizing the gust amplitude results is presented in Fig. 3.22. The oscillating aerofoil angle, the fluctuating lift obtained from two miniature wings fixed on the two front piezoelectric crystals and the gust angle, are correspondingly normalized with the similar quantities at medium eccentricity. If the theory was in absolute agreement with the experiment, then all these ratios should have collapsed on two straight lines. There is a reasonable scatter in the points, except for the large eccentricity below $k = 0.1$, where the experimental values fall below the theoretical ones. A premature corner separation (see McKeough, 1976) at the maximum aerofoil incidence ($\simeq 10^0$) could be responsible for this, at such low values of k. It may also be possible that this is an effect of roll-up of the wake, which will be more pronounced for stronger wake vorticity (due to high pitch amplitude Θ_0).

The variation of dimensionless gust amplitude in the vertical (z) direction, for various k, is plotted in Fig. 3.23 and in more detail in Figs. 3.11 to 3.13 (note, $\frac{b}{2}$ is the half bluff body height). It is observed that while the gust intensity for $z = 0$ (centre line) reaches a maximum value (for $k \simeq 0.35$) and then decreases, along the two vortex cores, $\left|z/\left(\frac{b}{2}\right)\right| = 9$, it increases monotonically with reduced frequency k, because $|F(k)| \to \infty$ as $k \to \infty$ (see Eqn. 3.30). In the experiments, an

increase in the velocity amplitude does indeed occur at some distance from the centre line, see Fig. 3.9, though for $|z/\frac{b}{2}| < 9$. However, the data of Fig. 3.9 refers to measured peak, unfiltered fluctuations (obtained by means of an oscilloscope), which do not represent the real power of the first harmonic meant by the $\alpha_g(t)$ of Eqn. (3.34). It is also observed that the effective centre line of the unsteady flow is shifted towards the nearest wall (here the tunnel floor), as was found experimentally, though to a greater extent.

Finally, an attempt was made to examine whether the sinusoidal gust was convected at the free stream speed U_∞ (assumption (iii)). For this purpose, a U wire was placed alternately at the points (0.06 m, 0, 0.12 m) and (- 0.305 m, 0, 0.12 m) in the empty tunnel. The anemometer outputs were recorded simultaneously with the reference spiky signal, thus enabling their phase difference to be calculated fairly accurately (within ± 3%). Four speeds were tried at medium eccentricity. In Fig. 3.24, the straight line which corresponds to a genuine frozen gust convected with the free stream speed lies above the experimental points. Although the accuracy of the measurements is not very good, this tends to indicate that the convection velocity of the shed vortices is slightly higher than the free stream velocity, which agrees with the findings of Wood and Kirmani (1970). The presence of the tripod support system did not cause any noticeable effect on the results.

3.5 CONCLUSIONS REGARDING THE SINUSOIDAL FLOW

The flow generated in the region between the oscillating aerofoils appears to meet satisfactorily the requirements imposed in Section 3.1.2. In particular, for tunnel speeds 10 to 30 m/sec, it was possible to obtain RMS upwash gust amplitudes from 0.5^o to 5^o approximately

and reduced frequencies $k = \pi nc/U_\infty$ ($c = 0.152$ m) from 0.05 to 0.8 approximately.

The flow is well correlated in the spanwise direction and the convection speed nearly that of the free stream. None of its qualities, at least in the region occupied by the test models, is significantly affected by that part of the unsteady load balance protruding into the tunnel (tripod support system).

Compared with some previous designs for producing oscillatory flows (see Section 2.3.6), the present oscillating rig has the following advantages:-

(i) Over the designs, which use the wake of a bluff body as oscillatory flow (Jackson, 1970; Edwards, 1972), it has the advantage that there is no need to resort to changes in the body dimensions in order to get a change in the reduced frequency. The gusts produced can be either in the streamwise or the normal to the mean stream directions, and convect at approximately the free stream speed; this is less true in the wake of a bluff body. In addition, the spanwise correlation of the present gust is superior to that of the shed vortices behind a body. A considerable degree of shear flow, which exists in the wake of a bluff section, was found to be very small in the region between the oscillating aerofoils of the present case.

(ii) Over the "moving wall" tunnel used by Holmes (1970), it has the advantage of producing gusts convected at the free stream speed; this also holds for the open jet gust tunnel employed by Pocha (1971). An extra advantage over those two designs is that the present oscillating rig is less complicated and bulky.

(iii) Over the "oscillating cascade" rig of Maeda and Kobayakawa (1970) and Sawyer (1972), it has the advantage of producing an extended

region of sinusoidal flow which contains no vorticity. Thus complications due to distortion of vorticity in a particular experiment can be avoided.

As discussed in Section 2.3.6, the main disadvantage of the present oscillating rig is that of mechanical vibration.

The simplified theoretical model for the prediction of the sinusoidal flow was in reasonable agreement with the experiment for reduced frequencies between 0.07 and 0.3 and in fair agreement for the other frequencies. It is thought that the representation of the vortex wakes by plane sheets (i.e. without any rolling-up of vorticity) and the effects of wall interference, should be among the main reasons for the observed discrepancies at the highest and lowest reduced frequencies. More elaborate, numerical models, such as those of Basu and Hancock (1977) or Giesing (1968) would be expected to give better results.

3.6 GENERATION AND MEASUREMENT OF TURBULENT FLOW

The dimensions of the grids for the generation of turbulence and their upstream distance relative to the models were given in Section 3.1.2. For the computation of the experimental aerodynamic admittance one needs the spectrum of the vertical velocity S_w (Eqn. 2.19), while for the calculation of the theoretical admittance of a thin aerofoil (Eqn. 2.20), the normalized cross spectrum in the spanwise direction, of the same component, is needed as well. Here, only the one-dimensional spectra were measured. The normalized (with respect to the signal mean square) u, v, w spectra are displayed in Figs. 3.25a, b, c, d and e. These digital analysis results were obtained from measurements at the point (0, 0, 0) in the (empty) 1.22 x 1.52 m working section of the tunnel. The tunnel speed corresponded to a Re number, based on the model chord (= 0.152 m), equal to 2.3×10^5. It was found that the turbulent

fields were not exactly isotropic, since for the large (M = 0.152 m) grid $u_{RMS}/U_\infty \simeq 0.067$, $v_{RMS}/U_\infty \simeq 0.059$, $w_{RMS}/U_\infty \simeq 0.06$ and for the small (M′= 0.076 m) grid, $u_{RMS}/U_\infty \simeq 0.044$, $w_{RMS}/U_\infty \simeq 0.037$.

The experimental results of Figs. 3.25a, b, c, d and e are compared with the "von Karman" spectra for isotropic turbulence (for their derivation, see for example Houbolt et al, 1964). The pertinent formulae are:-

$$\frac{S_u(n)}{\overline{u^2}} = \frac{4L_x}{U_\infty} \cdot \frac{1}{\left[1 + \left(1.3392 \left(\frac{2\pi n L_x}{U_\infty}\right)\right)^2\right]^{5/6}} \tag{3.39}$$

for the streamwise component, and:-

$$\frac{S_w(n)}{\overline{w^2}} = \frac{2L_x}{U_\infty} \cdot \frac{1 + \frac{8}{3}\left(1.3392 \cdot \frac{2\pi n L_x}{U_\infty}\right)^2}{\left[1 + \left(1.3392 \left(\frac{2\pi n L_x}{U_\infty}\right)\right)^2\right]^{11/6}} \tag{3.40}$$

for the upwash and v components. L_x is the longitudinal length scale of turbulence; its value for each of the two flows was estimated by calculating the asymptote of the experimental S_u spectrum as $n \to 0$. Then from Eqn. (3.39), L_x should be $S_u(o)\, U_\infty/(4\overline{u^2})$. The von Karman spectra (Eqns. 3.39 and 3.40) were computed for this value of L_x and the results were directly compared to the experimental spectra of Figs. 3.25a, b, c, d and e. It is observed that the agreement is good for the u spectra only, and at low to moderate frequencies. At the moderately high frequencies all the spectra are underestimated, while at the lowest the

v, w spectra are overestimated. Some analogue measurements, included in Figs. 3.25a, b, c, d and e differ to a variable degree from the digital ones. This might be due to averaging over a too short time and use of a different normalizing quantity (note that the wave analyzer measures the Mean Square Value over the range 2 to 20000 Hz, while the digital analysis program calculates the Mean Square Value from the data with frequencies up to the Nyquist frequency). Possible reasons for the discrepancies between the experimental and the (semi-empirical) von Karman spectra are:-

(i) Proper choice of L_x. Spectral power is difficult to measure accurately at very low frequencies (see Appendix B), so the estimates of L_x given above are rough.

(ii) Anisotropy. For this reason the v and w spectra are also not identical with each other.

(iii) Viscous dissipation. The high frequency vortices are affected (therefore, losing energy). This effect is not represented in the von Karman spectra.

The values of the length scales which were thought as the more appropriate for the M = 0.152 m and M′ = 0.076 m grids, were L_x = 0.0673 m ($L_x/c \simeq 0.44$) and L_x = 0.0553 m ($L_x/c \simeq 0.36$). These results and also the measured intensities and spectra are in good agreement with the corresponding results of McKeough (1976), who conducted similar measurements in the same wind tunnel, but with the load balance in it. Thus, there is an indirect indication that the tripod support system does not significantly affect the qualities of the turbulent flow at least in the region occupied by the test models.

The upwash velocity spectra are plotted in a dimensionless form in Fig. 3.26, which is useful in the computation of the aerodynamic

admittance (see Chapter 6). If the dimensionless experimental spectra could be fitted exactly to the von Karman formula, then for the same value of the reduced frequency $k' = \frac{2\pi n L_x}{U_\infty}$, the ratio of their spectral power would be equal to the ratio of their total mean squares. From Fig. 3.26 it is seen that this is not true, for the reasons (i) and (iii) mentioned previously.

During the course of the work it was necessary to determine the mean lift and drag on the bluff bodies in turbulent flow. Unfortunately, the mean load balance of the 1.52 x 1.22 m working section of the wind tunnel was closer to the grids, than the unsteady load balance, and consequently exact similarity (see Section 2.4.4) between the two flows could not be maintained. Therefore, some mean pressure measurements were also carried out in a 0.61 x 0.91 low speed wind tunnel with similar grids (0.152 m and 0.076 m mesh size) and similar models. But since it was realised, that the mean load characteristics for the two bodies and especially the lift, were not drastically altered by interchanging the two grids, the length scales of turbulence were not measured in this case. It was believed, however, that the length scales would not differ significantly from those that would be obtained in the 1.52 x 1.22 m tunnel when using the same grids and approximately the same downstream distance/mesh length ratios. Bearman (1969a) carried out detailed measurements of $\sqrt{\overline{u^2}}/U_\infty$ and L_x in a wind tunnel with grids of size comparable to the author's and the trends of his results helped to determine some unknown values of intensities and length scales by interpolation. Also the findings of Baines and Peterson (1951) were applied in certain cases. Table 3 summarizes the results of the turbulent flow measurements. It should be noted that the actually measured data agree quite well with the trends indicated in Baines and Peterson (1951).

3.7 APPARATUS FOR THE MEAN LOAD EXPERIMENT

Two wooden models were constructed for the measurement of mean lift and drag of the elliptic and D cylinders, using the weight balance of the 1.52 x 1.22 m wind tunnel. These were geometrically similar to those for the unsteady load experiment (Section 3.1.2). They had a chord length of 0.170 m and a span of 1.52 m (so that AR ≃ 9). Specially made brass holders were fitted on them to enable mounting on the balance. The mean forces on the aerofoil were measured on the same wing used by McKeough (1976), which had c = 0.31 m, AR = 5. Since the boundary layers of the 1.52 x 1.22 m tunnel cross section were quite thin and the turbulence producing grids were placed far upstream of the models, no end plates were used. The models spanned the tunnel walls completely, with a small gap of about 3 mm being left on either side.

After the mean load experiment was over, these same models were cut down in length (new span 0.765 m) for use in the 0.61 x 0.91 m wind tunnel. The mid span cross section was fitted with pressure tappings which were connected to a manometer via copper tubes glued under the surface. A layout of the pressure tappings is presented in Fig. 3.27. The pressure holes are more densely distributed in the regions where steep pressure changes were expected to arise. The model trailing edge was supplied with five holes, evenly distributed across the span. Thus, the variation of base pressure could be determined. The boundary layers of the 0.61 x 0.91 m cross section were thicker than those of the 1.52 x 1.22 m cross section and since the same models were used for both tunnels, it was decided here to use two end plates. These were made from perspex and had a cross section similar, but double in size, to that of the models. The effective span was limited to 0.45 m, implying an aspect ratio AR ≃ 2.66.

Finally, a small wooden elliptic model, of fineness ratio 3, chord length c ≃ 0.101 m and span equal to 0.457 m, was used at a later stage to check some of the lift measurements at various Re numbers. It was mounted without end plates in the 0.56 m octagonal section wind tunnel of the Department. This model also served for an elementary flow visualization.

CHAPTER 4. THE MEAN LOADING EXPERIMENT

4.1 INTRODUCTION

This chapter deals with the effects of both smooth and unsteady flows on the mean lift, drag and surface pressures of the bodies examined, since it was considered important to ascertain the mean effects of unsteady flows before proceeding to the unsteady effects. The assessment of mean lift forces would also be helpful in checking whether a quasi-steady approach can be followed in trying to predict the unsteady lift forces. Drag and surface pressures would be useful in providing a measure of the tunnel interference effects, indicating the regions of the flow regime (subcritical, critical, super-critical) and ordering the bluffness of the models and the strength of the natural vortex shedding.

Flow visualization tests are included in cases, where marked changes in the boundary layer behaviour for the various flows is noticed.

Details of the models used as well as their position in the wind tunnels are given in Section 3.7.

The free stream speed in smooth flow was recorded by means of a Pitot tube placed far upstream of the models. In turbulent flow, however, this could not be done, since the indication of the tube depends on its position if too close to the grids. A calibration of the tunnel was necessary. With the grids removed, another tube was mounted downstream of the models and its indication, for various tunnel speeds and model angles of incidence, was plotted against the reading of the front tube. Then in turbulent flow, only the back tube was used and the effective free stream speed was found by reference to the calibration curve (nearly a straight line), neglecting any effects due to change in the wake geometry (strictly valid only for bodies with

fixed separation points) and the increased dynamic head sensed by the Pitot tube, due to the extra term $\frac{1}{2}\rho U_\infty^2 \ (\overline{u^2}/U_\infty^2 + \overline{v^2}/U_\infty^2 + \overline{w^2}/U_\infty^2)$, which was very small for the turbulent intensities used.

The sensitivity of the three component load balance of the 1.52 x 1.22 m working section of the tunnel was within 0.1% of the maximum lift or drag encountered in the measurements. Incidence could be varied by an electrically controlled mechanism in steps of 0.1^o. On the other hand, the pressure measurements obtained in the 0.61 x 0.91 m and 1.52 x 1.22 m wind tunnels (for the D and elliptic cylinders only) by means of an inclined alcohol manometer were accurate to within about 1%. Incidence was changed with rotating discs attached at the ends of the models to an accuracy of 0.5^o. The pressure readings were then integrated numerically (using Simpson's rule for unequally spaced points), to give the dimensionless force coefficients with respect to body axes ($\overline{C}_{Fx}$ in the chordwise direction, $\overline{C}_{Fy}$ in the normal direction) and the chordwise position of the centre of pressure $\overline{x}_{cp}$. The lift coefficient $\overline{C}_L$ and the form drag coefficient $\overline{C}_{Df}$ are then easily obtained from a transformation of the system of axes. The errors introduced in this method are expected to account for 5% maximum of the final $\overline{C}_L$, $\overline{C}_D$ values.

Corrections due to wind tunnel interference were only applied to the free stream speed, steady forces and pressures according to Allen and Vincenti (1944) and Maskell (1963). The geometric angle of incidence $\overline{\alpha}$ was not corrected for tunnel blockage (although it would be necessary if a fully corrected lift curve slope $\overline{\partial C_L}/\partial\alpha$ was sought), because the correction would involve the measurement of pitching moment for which there were no accurate measurements at low $\overline{\alpha}$. For an aerofoil it is estimated that the percentage correction of $\overline{\alpha}$ is less than half of the lift coefficient correction. The extra three-dimensional blocking effect

of the support system in the load balance was estimated to be very small and thus it was neglected. Blockage has the effect of increasing the free stream speed U_∞ to $U_{\infty c}$ (c means corrected or effective) according to the formula:-

$$U_{\infty c} = U_\infty(1 + \varepsilon_{sb} + \varepsilon_{wb}) \tag{4.1}$$

ε_{sb} is a term due to solid blockage (from wall image effect) and ε_{wb} a corresponding term due to wake blockage (from the increased speed behind the body and outside its wake). Using (4.1) the lift coefficient can be corrected according to:-

$$\overline{C}_{Lc} = \overline{C}_L(1 - 2\varepsilon_{sb} - 2\varepsilon_{wb} - \varepsilon_{curv}) \tag{4.2}$$

the extra term ε_{curv} originating from the change of curvature of the flow, on account of the walls.

For the drag coefficient similarly:-

$$\overline{C}_{Dc} = \overline{C}_D(1 - 2\varepsilon_{sb} - 2\varepsilon_{wb} - \varepsilon_{wg}) \tag{4.3}$$

ε_{wg} appearing because of the pressure gradient in the accelerated flow behind the body. If it is assumed that the tunnel constraint does not disturb the geometry of the wake and the form of the pressure distribution round the body, then the mean pressure coefficients can be simply corrected according to:-

$$\frac{1 - \overline{C}_p}{1 - \overline{C}_{pc}} = \frac{U_{\infty c}^2}{U_\infty^2} = \frac{1 - \overline{C}_{pb}}{1 - \overline{C}_{pbc}} \tag{4.4}$$

where $\overline{C}_{pb}$ = base pressure coefficient.

The various factors appearing in these equations are functions of $\frac{S_a}{C}$ (ratio of area on which $\overline{C}_D$, $\overline{C}_L$ are based, to the cross sectional area of the tunnel, which is equal to chord length/tunnel height in our

case), Λ, which is a pressure factor depending on the shape of the base profile (given in Allen and Vincenti (1944) for various profiles), $\overline{C}_D$ and $\overline{C}_{pb}$. In Table 4 it is shown how each term is taken into account according to the shape of the test model.

Maskell's (1963) correction for ε_{wb} did not apply to the elliptic model because the roots of the equation for ε (see Table 4) were imaginary. Therefore, ε was taken equal to 1.0, as suggested by Maskell (1963). The application of Maskell's theory for bodies with non-fixed separation points is questionable, because of the change of the wake shape with constraint. As an example, for incidence $\overline{\alpha} = 5^o$ in smooth flow, the correction to $\overline{C}_L$ for the aerofoil (c/h = 0.25) was - 2.5% approximately, for the D cylinder (c/h = 0.185) - 7.5% approximately and for the elliptic cylinder (c/h = 0.185) - 3.5% approximately.

Note, that in the following, the subscript c (denoting quantities corrected for blockage) has been dropped for convenience.

4.2 MEAN LOADING OF THE NACA 0015 AEROFOIL

The mean lift and drag coefficients $\overline{C}_L$ and $\overline{C}_D$ of the NACA 0015 aerofoil were measured on the load balance and the results are plotted in Figs. 4.1 and 4.2. In one set of measurements the smooth and turbulent flow speeds employed corresponded to Re = 2.2×10^5 and 2.3×10^5 respectively, and these are essentially repeats of the measurements of McKeough (1976), who tested the same aerofoil (AR = 5.0, completely spanning the walls), but at a slightly higher Re number equal to 2.6×10^5. In another set of tests the Re number was equal to 1.2×10^5. In most cases the incidences covered ranged from zero up to a few degrees beyond the stall.

(a) Mean Lift Results: The higher Re number measurements are in very good agreement with those of McKeough (1976) for both smooth and

turbulent flows, except near the stall, since the author's measurements are corrected for blockage. It is observed that $\overline{C}_L$ varies almost linearly with incidence $\overline{\alpha}$, if the latter is well below the stalling angle. The lift curve slope at zero incidence, $\overline{\partial C_L}/\partial\alpha$, was computed using the method of least squares for points with $|\overline{\alpha}| \leq 5^0$. For both types of flow, smooth and turbulent, $\overline{\partial C_L}/\partial\alpha$ was found to be approximately equal to 5.7. It is known that thin aerofoil theory predicts a $\overline{\partial C_L}/\partial\alpha = 2\pi$ in steady flow, while thick aerofoil theory, (see for example Batchelor, 1970), gives a mean lift coefficient, for a Joukowski aerofoil, according to:-

$$\overline{C}_L \simeq 2\pi \sin\overline{\alpha} \left[1 + 0.77 \frac{\text{thickness}}{\text{chord}}\right] \qquad (4.5)$$

For a 15% thick Joukowski aerofoil then, Eqn. (4.5) gives $\overline{\partial C_L}/\partial\alpha \simeq 7.0$.

There are two main reasons for the reduction in $\overline{\partial C_L}/\partial\alpha$ from this value: viscosity and deviation from two-dimensional conditions. Due to the former, there exists a relatively thicker boundary layer on the suction side of the aerofoil, which reduces its effective angle of incidence and hence the lift. The existence of a separation point on the suction surface, which progressively departs from its position (at the trailing edge) when incidence increases, gives a picture different from that assumed by thin aerofoil theory. Brown and Stewartson (1975) discuss this matter in detail. The other reason is an experimental one, i.e. the wing is not of infinite spanwise extent, so that the downwash induced by the remaining trailing vorticity affects the lift (see also Section 3.1.1 (iii)).

In the low Re number (= 1.2×10^5) test the $\overline{C}_L$ v. $\overline{\alpha}$ curve for smooth flow is convex upwards, resulting in a $\overline{\partial C_L}/\partial\alpha \simeq 7.2$. A similar trend was noticed by Jacobs and Sherman (1934), although $\overline{\partial C_L}/\partial\alpha$ in their case was equal to 7.4 approximately. The reason for this

abnormal behaviour is that for such low Re numbers, and even for zero incidence, there exist two separation points on either side of the surface near the trailing edge. For a small change in the angle of incidence there is an unequal displacement of the separation points, leading to high initial lift values (see Pope and Harper, 1966). In turbulent flow, this phenomenon disappears and $\overline{\partial C_L}/\partial\alpha$ is again equal to 5.7 approximately.

Fig. 4.1 shows that the maximum lift coefficient, $\overline{C}_{Lmax}$, increases either by an increase in the Re number or in the level of free stream turbulence. In smooth flow and Re = 1.2×10^5 the stall of the aerofoil has the characteristics of leading edge stall, i.e. a sudden loss of lift. For the higher Re number test, the stall is a combination of leading edge-trailing edge stall as found by McKeough (1976). He states that there should be a functional relationship between the Taylor's parameter $\frac{\sqrt{\overline{u^2}}}{U_\infty} \cdot \left(\frac{c}{L_x}\right)^{1/5}$, and the Re number at which the separation bubble, in the front of the aerofoil, bursts at a particular incidence. $\overline{C}_{Lmax}$ is not necessarily a function of Taylor's parameter, but it is related to the incidence at which the bubble bursts.

(b) Flow Visualization in Sinusoidal Flow: At a later stage in this thesis, the unsteady lift on an aerofoil at high incidence in sinusoidal flow was measured, but unfortunately, it was not possible to find out quantitatively what was the effect of such a flow upon the $\overline{C}_L$ v. $\overline{\alpha}$ curve and $\overline{C}_{Lmax}$, because the load balance was situated too close to the oscillating aerofoils. To obtain a picture of the mean flow when the sinusoidal gust was applied, a simple tuft flow visualization experiment was carried out, using the load model mounted on the unsteady lift balance. Tufts were fitted on the surface of the aerofoil from the leading edge up to the trailing edge. Since there was no remote control mechanism for the change of incidence, the aerofoil was mounted

on the transducers at a high incidence (from 10.5^{o} - 13.5^{o}) and the wind tunnel was switched on at its maximum speed, to avoid stalling. When the flow was attached, the speed was lowered to the desired value of Re number and the oscillating rig was put into action. The reduced frequencies covered the range 0.05 - 0.8 and the Re numbers 1.2×10^5 - 3×10^5. The gust frequency was increased in steps from zero up to the maximum frequency and then lowered to zero again. Stall was signalled by the complete reversal of all the tufts on the aerofoil surface and the very irregular unsteady lift signal felt by the piezoelectric transducers. The results of this flow visualization test are as follows:-

- Over the lower surface of the aerofoil the flow always appeared to be attached.
- For a fixed gust frequency, n_o, the mean flow conditions on the surface depend on whether n_o is approached from lower or higher values. If the gust frequency is decreasing, the phenomena noticed at n_o for increasing frequency, take place at a lower frequency than n_o. This is more pronounced the higher the mean incidence (with respect to stalling angle) and gust amplitude, and the lower the Re number.
- There was no long term stall, even for incidences very close to the stalling angle, when the gust was applied. "Long term" is in connection with an intermittent stall noticed at very low reduced frequencies and high mean incidences: The wing remained stalled for a period ranging from a few cycles up to as many as 150 and then returned to attached flow again. This phenomenon was random in character. The only exception to this occurred, when the mean incidence was very near to the stalling angle and the gust was applied starting from zero frequency. Stall most probably occurred because the initial change of flow incidence was so slow as to act quasi-steadily. It required a significant rise in reduced frequency, i.e. k = 0.6, to bring the wing into fully attached

condition (note, however, that an inherent property of the oscillating rig is to result in higher gust amplitudes for higher frequencies). As the frequency decreased, the fully attached state was maintained, even for very low frequencies, except for the intermittent stall just mentioned. With an increase in frequency, an upstream displacement (towards the leading edge) of the (turbulent) separation position was noticed, partly due to a probable earlier transition. Immediately upstream of separation, a region of increased unsteadiness appeared, with the discernible gust frequency and sometimes an intermittent tuft reversal of short duration. This region had an extent of a few per cent of the chord and increased in length for higher gust amplitudes (at a fixed frequency). An oscillation of the separation point should have taken place there. Further upstream,all the tufts were attached on the surface, but an increased unsteadiness (containing the characteristic gust frequency) was discernible, indicating the presence of a separation bubble.

Summarizing the observations of the flow visualization and taking into account: (i) the particular gust employed (strong gust amplitude at high reduced frequencies, weak gust amplitude at low frequencies) and (ii) any hysteresis effects, it can be said that the wing at least does not stall in sinusoidal flow, as long as it does not stall in smooth flow. This is not surprising. The mean flow near the stall is very sensitive to changes in incidence. At low frequencies, the gust amplitude applied is necessarily small, so that stall is avoided. At high frequencies the gust amplitude is large and if applied statically, it would have surely caused stall. In fact the change of incidence is applied so quickly,that the mean flow has not enough time to change significantly. Hence the unstalled condition is maintained. It is anticipated that the mean flow situation in sinusoidal flow would

be something between the smooth and turbulent flow situations.

(c) Selection of the Mean Lift Curve Slope: As far as the lift curve slope $\overline{\partial C_L}/\partial\alpha$ is concerned, there is no reason to believe that it would be different from the one found in smooth or turbulent flow, equal in both cases to 5.7 approximately, except for the lowest Re number (= 1.2×10^5) case. There, $\overline{\partial C_L}/\partial\alpha$ in sinusoidal flow is expected to lie between 7.2 (measured in smooth flow) and 5.7 (in turbulent flow). The model for the unsteady lift experiment had an effective span of 2.5 and an overall span (including the dummy wings) equal to 5.5. Since the model employed for the mean load measurements had AR = 5.0, the mean lift curve slopes measured would be the lowest values to be assigned to the lift sensitive model for the unsteady lift experiment.

(d) Mean Drag and Centre of Pressure: The mean drag results are plotted in Fig. 4.2. It can be seen that the slope $\overline{\partial C_D}/\partial\alpha$ is about two orders of magnitude lower than $\overline{\partial C_L}/\partial\alpha$ for incidences up to 7^o approximately. The relevance of this to the unsteady lift experiment will be discussed in Chapter 5. The chordwise position of the centre of pressure was not measured, but from the pitching moment measurements of McKeough (1976), it is inferred that it is close to the quarter chord point in both smooth and turbulent flows, moving towards the rear when the aerofoil stalls.

4.3 MEAN LOADING OF THE D SHAPE CYLINDER

For the determination of forces on the D cylinder the load balance and pressure models were used. Both smooth and turbulent flows were considered, the latter of two different length scales and intensities. The Re number range was 1.2×10^5 to 3.85×10^5.

(a) Boundary Layer Separation: Tuft flow visualization and boundary layer measurements, indicated that separation took place at the two sharp trailing edges. The boundary layer results plotted in Fig. 4.7

(for $\bar{\alpha} = 0^o$), give a boundary layer thickness (defined as the distance from the surface at which the velocity is maximum) of about 0.04 b (b = body thickness) for smooth flow and 0.065 b for turbulent flow. In both cases a turbulent boundary layer was observed at separation, which manifested itself by the presence of high frequencies in the hot-wire signal and the shape of the mean velocity profile (close to the power law $(y/\delta)^{1/7} = U/U_e$). Simmons (1974) reported a (turbulent) boundary layer thickness δ_s at separation of 0.13 b ($Re = 2.25 \times 10^4$) for a D cylinder, twice as thick as the author's. Bearman (1965) working with a 16.6% thick D cylinder, found $\delta_s \simeq 0.5$ b ($Re = 1.4 \times 10^5 - 2.56 \times 10^5$) but his model had trip wires at 20% c.

(b) Mean Surface Pressure Distributions: Figs. 4.3 to 4.5 show the variation of the mean pressure distribution $\bar{C}_p$ ($\bar{C}_p = \{p - p_\infty\}/\frac{1}{2}\rho U_\infty^2$), round the centre section of the cylinder at incidences 0^o, 5^o and 10^o (the coordinates of the pressure tappings are given in Fig. 3.27). In Fig. 4.6 the variation of base pressure, $\bar{C}_{pb}$ along the span (z = 0) is presented for zero indicence, the distance of end plates being equal to 8.30 b.

The shape of the $\bar{C}_p$ distribution in smooth flow is seen to be similar to that in turbulent flow, but of lower magnitude. A rise in $\bar{C}_p$ is noticed for increasing levels of free stream turbulence. It is thought that the rather uniform shift of $\bar{C}_p$ towards higher values in turbulent flow, could be partly due to possible calibration errors of the tunnel (especially for the large grid which introduces a greater blockage in the free stream). Note also, that at the front stagnation point $\bar{C}_p$ appears to be greater than 1.0. When turbulence is introduced, there are also two effects which might change the base pressure: One is due to the increased entrainment, caused by turbulence (which tends to drag fluid out of the base region); this leads to a decrease in $\bar{C}_{pb}$. The other is due to the increased thickness of the shear layers, leaving

the surface, on account of the diffusion by turbulence. These thick shear layers interact less readily to start the vortex formation, which is suspended until later downstream. Since the strength of the vortex shedding phenomenon decreases, a rise of the base pressure follows. The rise of $\overline{C}_{pb}$ found by introducing turbulence, suggests that the latter trend would dominate. (Note that the opposite happens for a flat plate normal to the turbulent stream, because the separating shear layers are thin).

An increase in the Re number from 2.2×10^5 to 3×10^5 does not affect $\overline{C}_p$ to a significant extent.

Over the rear flat surface of the model, $\overline{C}_p$ is distributed almost symmetrically with respect to the z = 0 plane, being always higher than $\overline{C}_{pb}$. There, turbulence tends to smooth out the pressure distribution.

In the spanwise direction the base pressure is again distributed symmetrically about the plane y = 0 and it is increased by about 10% at a distance 4 b on either side of the central region for both flows, one reason being the boundary layer effect of the end plates. A similar value, about 8% (for smooth flow, $Re = 1.7 \times 10^5$), is given by Maull and Young (1972) for a D cylinder, 16.6% thick, placed between end plates at distance 20 b apart.

Over the front of the model ($x/c \simeq 0.1 - 0.3$), it is observed that for all incidences (negative incidences were also looked at), there is a region where $\overline{C}_p$ remains almost constant and then is followed by a pressure recovery. Although this suggests the presence of a laminar separation bubble (e.g. Crabtree, 1957), the effect of possible irregularities on the surface cannot be dismissed, particularly because incidence, Re number and turbulence do not bring any drastic change in the position and shape of this pressure anomaly. A broad symmetric "hump" in $\overline{C}_p$ centred about the chordwise position x/c = 0.5 should be a potential

flow result, since it appears in the pressure distributions of several other bodies which consist of a simple geometric shape followed by an afterbody, such as a long rectangular cylinder with well rounded edges, see for example Polhamus et al (1959).

Next, by means of the pressure distributions the sectional lift and form drag coefficients were computed and the chordwise position of the centre of pressure, given as a percentage of chord from the leading edge (see Figs. 4.8 to 4.10). In the first two figures, the results from the mean load balance measurements, which give the overall lift and drag coefficients, are also included.

(c) Lift Measurements: The sectional and overall lift coefficients were close within experimental error (5%), so they are plotted with one symbol in Fig. 4.8. For the same aspect ratio, the sectional lift coefficient in the middle of the span would be greater than the overall lift coefficient. The fact that the two lift coefficients measured were roughly equal, reflects the lower value of aspect ratio (= 2.76) in the pressure measurements. It also counterbalances for the gap between the load model and the tunnel walls which lowers the overall lift measured. The lift coefficient obtained from the pressure measurements, does not include the contribution of the skin friction force (in the chordwise direction). A rough estimate of this force may be obtained from the formula for $\bar{C}_{F_x}$ for a flat plate of length ℓ_p parallel to a stream of speed U_∞. If the boundary layer is turbulent, then:-

$$\bar{C}_{F_x} = 2 \times 0.072 \times Re^{-1/5} \quad \text{and} \quad Re = U_\infty \cdot \ell_p/\nu \tag{4.6}$$

(see Schlichting, 1968). The effect of thickness can be roughly taken into account by replacing U_∞ by U_{max}, the maximum speed outside the boundary layer. Then:-

$$\overline{C}_D \simeq 2 \times 0.072 \times \left(\frac{U_{max} \cdot \ell_p}{\nu}\right)^{-1/5} \cdot \left(\frac{U_{max}}{U_\infty}\right)^2 \qquad (4.7)$$

For $\overline{\alpha} = 10^o$, U_{max} is at most $2U_\infty$ (see Fig. 4.5) so that the upper value of $\overline{C}_D$ would be equal to 0.043, at a Re = 2.2×10^5. This is very small compared with the normal force $\overline{C}_{Fy} = 1.15$ (computed from Fig. 4.5) and makes a maximum contribution to $\overline{C}_L$ equal to 0.043 sin 10^o which is less than 1% of the lift coefficient measured in the lift balance.

Fig. 4.8 shows that the $\overline{C}_L$ v. $\overline{\alpha}$ curve is nearly a straight line up to a few degrees before the stall. Its slope at $\overline{\alpha} = 0$ lies between 6.0 and 6.5, which is higher than the value of 5.7 found for the aerofoil. If it is assumed that the D section behaves like a fat aerofoil, then this difference in the mean lift curve slopes could be partly explained in terms of the greater thickness of the bluff body. The idealization of the D cylinder with an aerofoil is not unreasonable if it is taken into account that the flow over the former was found to be attached all the way up to the sharp edges and the pressure in the base region uniform (see Figs. 4.5 to 4.8). Therefore, instead of the Kutta- Joukowski condition of zero loading at the trailing edge, an "equivalent" Kutta-Joukowski condition of zero loading across the two sharp edges is now assumed (though satisfied only in a "mean" sense, as discussed in Sections 2.1 and 2.2.1). For a 33.3% thick Joukowski aerofoil, i.e. of maximum thickness equal to that of the D cylinder, potential flow theory (e.g. Batchelor, 1970) gives $\overline{\partial C_L}/\partial\alpha = 7.9$. This value is about 25% greater from the average of the experimental lift curve slopes given previously. Note that the experimental lift of the NACA 0015 aerofoil is also overestimated by roughly the same percentage (see Section 4.2a). In turbulent flow $\overline{\partial C_L}/\partial\alpha$ is lowered by approximately 7%, while almost no change was observed for the aerofoil. It is considered that a comparatively increased asymmetric thickening of the

boundary layers could be the reason, although, as stated previously, calibration errors could also account for this.

The maximum lift coefficient is seen to rise to values considerably greater than those of the NACA 0015 aerofoil, at the same Re number. It is also greater than the $\overline{C}_{Lmax}$ encountered for aerofoils of thickness 6 to 24% at much higher Re numbers ($\simeq 6 \times 10^6$, see for example Abbot and Doenhoff, 1959). Turbulence has the effect of increasing $\overline{C}_{Lmax}$ and delaying the stall development.

(d) Mean Drag and Centre of Pressure Results: The mean drag coefficient, obtained from the load balance and the integration of normal pressures, is plotted in Fig. 4.9. The slope $\overline{\partial C_D}/\partial\alpha$ is very small, except when stall is approached. The chordwise position of the centre of pressure (computed from the detailed pressure distribution) is shown in Fig. 4.10. Both figures indicate that changes in the Re number or introduction of turbulence do not cause appreciable effects, provided the mean incidence is low.

(e) Loading in Sinusoidal Flow: So far from the two unsteady flows only turbulence was considered. Systematic measurements in sinusoidal flow were not performed. It was, however, qualitatively observed that over the useful range of incidences, the pressure distribution in sinusoidal flow differed only very slightly from the corresponding distribution in smooth flow, even when the highest gust amplitudes at the highest reduced frequencies were tried. Since experimental errors could lead to greater deviations, it is assumed that the lift curve slopes in the smooth and sinusoidal flows are the same.

(f) Selection of the Mean Life Curve Slope: The question remains as to what values of $\overline{\partial C_L}/\partial\alpha$ to ascribe to the model in unsteady flow (AR = 2.5). Due to the presence of the dummy ends, it is expected that two-dimensional conditions will prevail over the central part of the arrange-

ment (see Fig. 3.4). The lift curve slopes in smooth and sinusoidal flows, therefore, can be taken equal to the measured (or assumed) cross sectional slopes (for the model with AR = 2.76). It was shown previously that these are roughly equal to the overall $\overline{\partial C_L}/\partial\alpha$ (see Fig. 4.8). The turbulent flow employed in the unsteady lift experiment had different characteristics from the one used in the mean load experiment (consult Table 3). Fig. 4.8 shows that $\overline{\partial C_L}/\partial\alpha$ in turbulent flow is only very slightly sensitive to changes in the length scale or intensity. Therefore, for the same reasons as before, the lift curve slopes of the unsteady lift sensitive model can be taken equal to those measured over the other models. Pertinent values are given in Fig. 4.8.

4.4 MEAN LOADING OF THE ELLIPTIC CYLINDER

Similar measurements to those described previously for the D shape cylinder, were performed on the elliptic cylinder, and the results appear in Figs. 4.6 and 4.10 to 4.18. In addition, a flow visualization was undertaken, in order to investigate how the unsteady flow applied, had affected the mean separation of the boundary layer.

(a) Flow Visualization Results: The "oil and chalk" method was used. It consisted of applying a mixture of kerosene and powdered chalk on the surface of the model and then quickly switching on the tunnel at the desired speed, until the kerosene evaporated. If the flow is adequately two-dimensional and the surface of the body free from any irregularities, such as machining engravings, etc., then the deposition of the dried up powder will concentrate in the positions where the shear stress is minimum, i.e. along the separation lines in the spanwise direction. Laminar and/or turbulent separation can be visualized in this way.

One set of tests was carried out, while the oscillating rig was set up in the 1.52 x 1.22 m tunnel. Several runs indicated that the

application of sinusoidal gust did not alter the surface flow pattern as compared with that in smooth flow, of course within the accuracy limits of the method. It was thus decided to perform the tests in a more convenient situation,where turbulence would be included. The final tests were made in the Departmental 0.56 m octagonal section wind tunnel, on a 0.101 m chord model (see Section 3.7), and the results appear in Fig. 4.11. Some of the photographs of Fig. 4.11 are not very clear, one reason being that the mixture could not be evenly applied on the surface. Near to the walls, the flow is seen also to depart from two-dimensionality. The surface flow pattern across the span sometimes showed a kind of "eruption" of material, the position of which was not repeatable. It is thus difficult to say whether they represent a three-dimensional flow, such as "cells" of vorticity or that they are just caused by surface tension effects. In any case, the general pattern depicted from the photographs, indicates that the separation across the cylinder is not perfectly two-dimensional. This is a characteristic of the critical flow regime.

The positions of laminar and turbulent boundary layer separation for $\bar{\alpha} = 0^{o}$ ($Re = 1.3 \times 10^{5}$, smooth flow) are indicated by the two white lines in Fig. 4.11, Photo. 1 (the upper one is just visible). At $\bar{\alpha} = 4^{o}$, Photo. 2, both lines move slightly upstream (the position of these lines was measured with a flexible tape over the surface). In turbulent flow (corresponding Photos. 3 and 4) only the turbulent boundary layer separation shows up, which happens further downstream of the turbulent separation in smooth flow. Again, separation moves upstream, when the incidence is increased. Taylor's parameter is about 0.082 for the turbulent flow considered ($L_x/c = 0.2$, $\sqrt{\overline{u^2}}/U_\infty \simeq 0.06$), so that transition would have probably taken place quite early, judging from the experimental results of Fig. 2.9. Increasing the Re number to

2.2×10^5 in smooth flow at $\bar{\alpha} = 0$ has the effect of moving laminar separation downstream and turbulent separation slightly upstream, Photo. 5. When the Re number is increased to 3×10^5 ($\bar{\alpha} = 0$, smooth flow, Photo. 6) there is no clear indication where separation takes place, because in the central region there is a thick line indicating that laminar and turbulent separation move downstream, in a position close to the turbulent separation of Photo. 3 (turbulent flow).

The approximate positions of laminar and turbulent separation are plotted more clearly in Fig. 4.12, and they are also compared with Schubauer's (1939) results in Fig. 2.3, for $\bar{\alpha} = 0^0$. The author's results for laminar separation in smooth flow are varying with Re number in the same direction as Schubauer's "nearly laminar" separation. This term was attributed by Schubauer (1939) to the separation of a boundary layer which maintained the general aspects of a laminar boundary layer, but which became turbulent just before separation, probably via natural transition. He found that to happen for $9 \times 10^4 \leq Re \leq 3.2 \times 10^5$. The author found that separation took place via a laminar separation bubble at least for $Re > 1.3 \times 10^5$, so that in Fig. 2.3 the discrepancy in the laminar separation positions, increasing as Re increases, is due to the fact that, while the author's points represent true laminar separation, Schubauer's indicate the final "nearly laminar" separation. The higher levels of free stream turbulence in Schubauer's wind tunnel (0.85%) should have brought the opposite effect, but it is thought that surface roughness, to which the models are sensitive, may be responsible. The positions of turbulent boundary layer separation in the range $1.3 \times 10^5 \leq Re \lesssim 3 \times 10^5$ are upstream of those found by Schubauer for $Re \gtrsim 3.2 \times 10^5$. Note, however, that the author's results show a tendency to agree with Schubauer's at the upper range of Re numbers ($\simeq 3 \times 10^5$), see Fig. 2.3. The position of turbulent boundary layer separation in turbulent flow

found by Schubauer is close to the author's, located at about 0.92 c from the leading edge.

In order to get an idea about the position of the turbulent shear layer after separation, hot-wire traverses across the wake were made at x/c = 1.02 (see Fig. 4.12) for smooth, sinusoidal and turbulent flows. On passing the hot-wire through the free shear layer, a peak in the longitudinal RMS velocity is expected to appear, see for example Bearman (1965) and Hanson and Richardson* (1968). This indeed was the case in smooth and sinusoidal flows, the peak being located at z/b ≃ 0.24 - 0.25, while in turbulent flow only a small "hump" in the u_{RMS} v. z/b curve was observed at z/b ≃ 0.20. The peak in sinusoidal flow was somewhat broader than in smooth flow possibly due to the fluctuation of the separation point (note that the intensity of the sinusoidal flow is not uniform itself). With these data a conjectural mean position of the free shear layer was drawn up in Fig. 4.12, suggesting that the wake width is smaller than the distance of the upper and lower separation points (for zero angle of incidence).

Taking into account the above results and those of Schubauer (1939), the following remarks can be made (cylinder at zero incidence):-

- The critical regime in smooth flow extends from Re ≃ 9 x 10^4 up to about 3 x 10^5.
- The present sinusoidal flow does not alter the mean positions of separation of smooth flow.
- Towards the end of the critical regime there is some evidence that final separation is invariable with changes in Re number.
- The shear layers tend to bend inwards after separation.
- Application of free stream turbulence moves the turbulent boundary layer separation downstream and reduces the width of the wake.

(b) Mean Surface Pressure Distributions: Mean pressures on the

* Hanson, F.B and Richardson, P.D. Trans. ASME J. Basic Eng, 90, Dec. 1968.

surface of the model were measured for incidences 0^0, 5^0, 9^0, 10^0, 15^0 and the results are plotted in Figs 4.13–4.17.

The $\overline{C}_p$ plots for $\overline{\alpha} \simeq 0^0$ are shown in Fig. 4.13. The sinusoidal and smooth flow results at Re = 2.2 x 10^5 are almost identical. The present results also agree with those of Schubauer (1939), except near the base region. This could be because Schubauer's model was not put between end plates and also the aspect ratio (= 4.58) was higher than the author's (= 2.76). There is also good agreement, over the unseparated region, with the pressure coefficient calculated from potential flow.

An increase of Re number to 3.85 x 10^5 brings about an increase in $\overline{C}_p$ near the base. With free stream turbulence present, at Re = 2.2 x 10^5, $\overline{C}_p$ is not significantly changed unless the greatest turbulent intensity is employed (7.8% approximately). The increase in $\overline{C}_{pb}$ is of the same order as when Re was increased to 3.85 x 10^5. However, there is also an overall increase in $\overline{C}_p$, which was again encountered in the D cylinder results. The shape of $\overline{C}_p$ between the pressure tappings 12 and 15, indicating the presence of a bubble, agrees with the findings of the flow visualization tests.

For higher incidences, Figs. 4.14, 4.16, 4.17, the effects of free stream turbulence and increase in Re number are also evident, particularly over the lower (pressure) surface. It appears that separation is delayed there, with consequences on the mean lift, which will be discussed later.

The plots in Fig. 4.15 compare the pressure distributions at $\overline{\alpha} = 9^0$ for smooth and sinusoidal flow. It is seen that the pressure changes to a greater extent over the upper (suction) surface than on the lower surface and in the same manner as in turbulent flow, though to a lesser degree.

At zero incidence, the base pressure is much higher than for

the D shape cylinder (see Fig. 4.6) and uniform along the span even fairly close to the end plates. For the strongest turbulent flow ($\sqrt{\overline{u^2}}/U_\infty$ = 0.078) there is an increase in $\overline{C}_{pb}$ of about 40% near the end plates, with respect to the mid-span value.

(c) Lift Measurements: Fig. 4.18 contains a series of $\overline{C}_L$ v. $\overline{\alpha}$ curves for various Re numbers and types of flows. $\overline{C}_L$ was again calculated from the overall lift measurements on the load balance (AR = 9.0 in the 1.52 x 1.22 m tunnel, AR ≃ 5.5 in the 0.56 m tunnel) and integration of normal pressures (AR ≃ 2.76 between end plates). Some interesting features of Fig. 4.18 will now be discussed.

(i) Smooth Flow: It is observed that the shape of $\overline{C}_L$ v. $\overline{\alpha}$ curves depends strongly on the Re number of the flow. Starting from the lowest Re number examined, equal to 5.8 x 10^4, it is seen that $\overline{\partial C_L}/\partial\alpha$ is very low, up to an incidence of about 10^o, after which it increases sharply and then is kept constant, until stall is reached. The same trend, though not so pronounced, is noticed for Re ≃ 1.2 x 10^5. For further increase in the Re number a different sequence is observed. The lift curve slope is at first very high and then as the incidence increases, it drops off gradually. A characteristic of all these curves is that they roughly converge to a maximum lift coefficient of 1.2.

The variation of $\overline{\partial C_L}/\partial\alpha$ (at zero incidence) against Re number is plotted in Fig. 2.1, where similar slopes of elliptic cylinders of various fineness ratios have been collected from other sources. Also in Fig. 4.18, the results of Zahm et al (1928) for a geometrically similar to the author's elliptic cylinder, at Re number = 1.37 x 10^5, are plotted. These results have been corrected by the author for infinite aspect ratio, by interpolation on Zahm et al results for elliptic cylinders of fineness ratios 2.5 and 4.0. From both Figs. 2.1 and 4.18, it is observed that Zahm et al's results are lower than the

author's, coming gradually to a better agreement, as the incidence increases, actually resulting in approximately the same $\overline{C}_{Lmax}$. The reasons for these discrepancies could be due to the different levels of free stream turbulence in each tunnel and the finite aspect ratio (not very serious, because Zahm et al (1928) found it to be small for slightly geometrically different elliptic cylinders).

In the lowest Re number case (= 5.8×10^4) the flow separation should have been laminar and near the front for low incidences, resulting in a low $\overline{C}_L$. Then at a particular value of $\overline{\alpha}$ the separated layer should have reattached as a turbulent boundary layer, separating further back, producing as a result a sudden increase in the lift (shown in Fig. 4.18).

If the Re number is sufficiently high, say above 1.2×10^5, then as the flow visualization has shown, there is a final turbulent separation. The pressure coefficient plots of Figs. 4.14 to 4.17 indicate that as the Re number increases at constant $\overline{\alpha}$, there is a weaker suction on the upper surface and a delayed separation on the lower (pressure) surface, and these tendencies combined, result in a lower lift. Hence, in Fig. 2.1, the peak in the $\overline{\partial C_L}/\partial\alpha$ v. Re curve may be explained. Note that other authors as well found a strong dependence of the mean lift curve slope on the Re number, e.g. Williams et al (1937) (fineness ratio 6.0, Re between 3.1×10^5 and 7.21×10^6) and Polhamus et al (1959) (fineness ratio 2.0, Re between 3.5×10^5 and 2×10^6). Williams et al's (1937) experiments, performed in a compressed air tunnel, could not include such low Re numbers as to realise the above-mentioned peak (which must appear, since at zero speed there will be no lift), but the tendency for $\overline{\partial C_L}/\partial\alpha$ to drop rapidly with increasing Re number was evident (see Fig. 2.1). Similarly high lift curve slope appears in the results of Zahm et al (1928) for elliptic cylinders of fineness ratios 2.5, 3.5

and 4.0. It is conjectured that if all other conditions are the same and only the fineness ratio and Re number are allowed to vary, then these peaks would appear the earlier, the lower the fineness ratio (i.e. the thicker the cylinder). However, as Fig. 2.1 shows this may not be true for too low fineness ratio, say, 1.7 (see in the same figure, Modi and Wiland's (1970) results) and certainly not for a circular cylinder (fineness ratio = 1.0).

Assuming the elliptic cylinder to behave like a fat aerofoil with a Kutta-Joukowski condition holding between the two separation points, leads to a $\overline{\partial C_L}/\partial\alpha = 7.9$ (see also Section 4.3c on the D cylinder). This value is in disagreement with both the maximum and the minimum lift curve slopes (see Fig. 4.18). The reasons are that the pressure in the base region is not uniform and that the (free) separation points lie forward of the trailing edge (hence potential flow cannot be applied in the separated region). Another Kutta-Joukowski condition could be to assume a single downstream stagnation point fixed at the point of minimum radius of curvature in the trailing edge region. Then, potential flow theory (e.g. Woods, 1961) gives:-

$$\overline{C_L} \simeq \overline{\alpha} \cdot 2 \cdot \pi \cdot \left(1 + \frac{b}{c}\right) \qquad (4.8)$$

which for b/c = 1/3, results in $\overline{\partial C_L}/\partial\alpha \simeq 8.37$. Again, this value lies between the minimum and maximum experimental values.

Fig. 4.18 shows that in the range $5.8 \times 10^4 \leq Re \leq 2.2 \times 10^5$, stall occurs gradually at quite high incidences, while $\overline{C}_{Lmax}$ does not change very much. A thick aerofoil section exhibiting a similar behaviour is the Göttingen 387 (see Goldstein, 1965). As Figs. 5.14 to 5.17 indicate, the pressure distributions at high incidences tend to become equal, despite the changes in the Re number, resulting in roughly the same positions of turbulent separation. This could explain why $\overline{C}_{Lmax}$

changes only little, when the Re number is varied.

When trip wires were fitted on the upper and lower surfaces of the model, a great reduction of lift was observed, see Fig. 4.18. The trip wires consisted of two steel wires of diameter less than 0.5 mm fitted at 0.25 c from the leading edge, along the generators of the 0.101 m elliptic model (which was used in the octagonal 0.56 m tunnel). This position was selected to be ahead of the early beginning of transition reported by Schubauer (1939), at roughly 0.4 c from the leading edge. The diameter of the wire was of the magnitude suggested in Pankhurst and Holder (1952) and although the wires were fitted further upstream of the expected transition region for smooth flow at the same Re number, the final effect on $\overline{C}_L$ is seen to be large (see Goldstein, 1965).

(ii) Sinusoidal Flow: The changes on the mean lift produced by the application of sinusoidal flow are seen to be only mild (Fig. 4.18). There is an overall reduction in $\overline{C}_L$, especially for moderate incidences, with a corresponding reduction in $\overline{\partial C_L/\partial\alpha}$. (Note that the values of the lift curve slope given in Fig. 4.18 are approximate, because not many experimental points were available). It appears that $\overline{\partial C_L/\partial\alpha}$ changes less if the Re number is increased, but this fact should not be taken as general, since the gust reduced frequency (and amplitude) were not kept constant when the Re number was changed.

(iii) Turbulent Flow: When the oncoming flow is turbulent, Fig. 4.18 demonstrates that there is a dramatic fall in the lift curve slope from its corresponding value in smooth flow. However, $\overline{C}_{Lmax}$ is of the same level, though occurring at higher incidences, about 30^o (not shown in Fig. 4.18). The values of $\overline{\partial C_L/\partial\alpha}$ for Re = 2.2×10^5 and 1.2×10^5 are of the same order with those measured in smooth flow, but at a higher Re number, equal to 3.85×10^5. It appears, therefore, that as far as $\overline{\partial C_L/\partial\alpha}$ is concerned, an increase in the level of free stream turbulence

is equivalent, in the critical range, to an increase in the Re number. This holds generally in phenomena strongly dependent on boundary layer transition, as found by McKeough (1976). An increase in the free stream turbulence level or the Re number, is expected to cause an earlier transition, which on the lower (pressure) surface of the model would lead to a turbulent boundary layer separating further downstream of its smooth flow position. The result is a greater suction on this side (see Figs. 4.14, 4.16, 4.17) and a greater contribution in the reduction of lift, a fact which was confirmed experimentally.

(d) Mean Drag and Centre of Pressure Results: The profile and form drag coefficients are plotted in Fig. 4.19 and the chordwise position of the centre of pressure in Fig. 4.10. Unlike the case of the D cylinder, the Re number and free stream turbulence effects are observed to be considerable.

(e) Selection of Mean Lift Curve Slope: In smooth flow it was found that the values of $\overline{C}_L$ measured on the three elliptic models, at constant Re number, were not the same, but sometimes differed by as much as 7%. The cross sectional $\overline{C}_L$ (obtained from the pressure measurements) was not the highest of the three, as it would be expected. The comparatively higher level of free stream turbulence (to which the ellipse is very sensitive in the critical flow regime), existing in the 0.61 x 0.91 m wind tunnel where the pressure measurements were made, should mainly account for that. Yet, a representative $\overline{C}_L$ v. $\overline{\alpha}$ curve was needed for the unsteady lift sensitive model (AR = 2.5). Due to the large aspect ratio of the mean load model used in the 1.52 x 1.22 m tunnel (AR = 9.0) and the low turbulence level of the same wind tunnel, it was decided to select its $\overline{C}_L$ v. $\overline{\alpha}$ curve as the most representative. Those curves are plotted in Fig. 4.18.

In sinusoidal flow, only the cross sectional mean $\overline{C}_L$ was available and as such is plotted in Fig. 4.18. It can be assumed

roughly equal to the lift coefficient of the unsteady lift model, since the free stream disturbances are for both the same.

For turbulent flow, exact similarity of the flow conditions at constant Re number could not be facilitated in the three tunnels. However, as Fig. 4.18 indicates, the variations in $\overline{\partial C_L}/\partial\alpha$ at a particular Re number are more sensitive to changes in turbulence intensity than length scale. Accordingly, at Re $\simeq 2.2 \times 10^5$, the lift curve slope corresponding to the highest intensity (= 7.8%) in the mean load experiment, can be taken as representative for the unsteady lift model when exposed to turbulence of similarly high intensity (= 6.7%, consult Table 3, M = 0.152 m) this slope being equal to 3.85 per radian (see Fig. 4.18). The slope $\overline{\partial C_L}/\partial\alpha = 4.0$, found for intensities 4.4 - 5.9% would be suitable for the unsteady lift model when the turbulence of intensity is 4.4% (Table 3, M = 0.076 m).

4.5 CONCLUSIONS REGARDING THE MEAN LOADING EXPERIMENT

The dependence of mean loads on the Re number and free stream unsteadiness is much stronger for the bodies with free separation points (aerofoil at high incidence, ellipse), than for those with fixed separation points (D cylinder, aerofoil at moderate incidences).

Of the two unsteady flows considered only turbulence had a pronounced effect on the mean loading, tending to diminish the mean lift curve slope of the elliptic model at zero incidence and delay the aerofoil stall. The turbulent flow with the greater intensity appeared to cause the greater changes in the mean loads.

An increase in the Re number is not always "equivalent" to the introduction of free stream turbulence, but the results depend on the state of the boundary layers.

The maximum lift coefficient of the aerofoil and the $\overline{\partial C_L}/\partial\alpha$

for the ellipse (for Re $\geq$ 1.2 x 10^5) are clearly influenced by an increase in Re number, in the same way as by introducing free stream turbulence.

At low Re numbers in smooth flow, the lift curve slopes and the minimum drag coefficients of the ellipse and the aerofoil exhibit a rather unusual behaviour with change of incidence. Turbulence tends to restore the behaviour observed at higher Re numbers.

Under the assumption of an "equivalent" Kutta-Joukowski condition of zero loading across the trailing edge of the bluff sections, thick aerofoil theory predicts reasonably well the mean lift of the D cylinder but not on the elliptic cylinder.

CHAPTER 5. THE SINUSOIDAL LOADING EXPERIMENT

5.1 INTRODUCTION

The sinusoidal loading experiment was carried out with the oscillating rig assembled as in Fig. 3.4. To check the results for repeatability, two sets of experiments were made: one in the old octagonal cross-section wind tunnel (width = 1.52 m, height = 1.22 m), and another in the rectangular cross-section (1.37 m x 1.22 m) (which actually replaced the old octagonal cross-section). The differences were found to be within the range of experimental error. Therefore, the data from both sets appear in a unified form, unless otherwise stated.

Tests were undertaken at Re numbers 1.2×10^5, 1.6×10^5, 2.2×10^5 and 3×10^5, the upper and lower limits being imposed for the reasons stated in Sections 3.1.2 and 3.3.1.

In conjunction with the frequencies attained by the oscillating rig, this range of speeds enabled reduced frequencies $\left(k = \frac{\pi nc}{U_\infty}\right)$ from 0.04 up to 0.8 approximately, to be attained. Even for the highest reduced frequencies of the present case, the sinusoidal lift variation can be considered as quasi-steady when compared with the lift variations due to vortex shedding, and approximately uncorrelated with it. Therefore, the purely sinusoidal and the vortex shedding lift measurements will be presented separately.

Following the same procedure as for the upwash, the unsteady lift results appear in the form of frequency spectra, filtered RMS values and variations of lift amplitude with time (either averaged over a large number of periods, or as instantaneous raw signals from a pen recorder). The accuracy and the errors arising in these measurements are described in Appendix B.

The bulk of the experimental work was carried out with the load sensitive models described in Section 3.1.2 and Fig. 3.2, but during the course of the work, short tests were performed with four modified shapes shown in Fig. 5.1. In the first three, the trailing edge of the elliptic cylinder was modified by attaching two bent aluminium plates (as illustrated in Fig. 5.1), while the fourth model consisted of the elliptic cylinder supplied with trip wires, of diameter 0.004 c approximately, which were fitted at a distance 0.25 c from the leading edge. The mean lift characteristic of this last model is only available and it is plotted in Fig. 4.18. The purpose of doing those measurements was to examine, in a qualitative manner, the possible effect of oscillations of the separation points, on the unsteady lift.

As far as wind tunnel interference effects are concerned, there are no known theories which fully account for tunnel blockage in unsteady flow, nor a common practice exists, as to how experimental results may be approximately corrected. Holmes (1970) did not apply any correction to his unsteady lift results (obtained for a NACA 0012 aerofoil in an upwash gust), but he pointed out that the quasi-steady correction, of the order - 8%, is not likely to be sufficient in the unsteady flow. Graham (1973) working mainly with bluff bodies in turbulent flow applied quasi-steadily Maskell's (1963) correction on all the load coefficients, thus taking into account only the "wake blockage". Simmons (1976) made full (i.e. including all terms given in Table 4) quasi-steady corrections for the angle of pitch and moment of a NACA 0012 aerofoil oscillating in a steady stream. He justified this by noting that the theoretical lift blockage corrections of Jones (1950) for Theodorsen's (1935) analysis, when applied to his experiments (chord/tunnel height $\simeq$ 0.33), differed by a small amount from those for a stationary aerofoil. Recently, Kullar (1978) working in a similar way as Reissner (1947) in inviscid

flow, calculated the change in Sears's function for a flat plate aerofoil placed symmetrically with respect to the wind tunnel walls. Kullar's correction pertinent to the present work, will be given in Section 5.3.3.

If the same blockage ratios had been used in the measurement of both the mean and the fluctuating loads, then the application of a quasi-steady correction would be unnecessary for the computation of the aerodynamic admittance (see Eqn. (6.5)), since the same corrections would apply to the numerator and the denominator. However, the ratio c/h in the unsteady load experiment was 0.125, while in the mean load was between 0.14 and 0.25. In the former case, there was the extra blocking effect of the tripod support system and also the induced change in the reduced frequency, which had to be taken into account. It was, therefore, decided to apply, as a first approximation, the corrections given by Eqns. (5.1) to (5.4) quasi-steadily. Since the drag coefficient in this stage of the work was not known, it was taken equal to the corrected drag coefficient found in the mean load experiment, at the mean incidence, at which the unsteady lift experiment was performed. The blocking effect of the support system was assumed to be equivalent to an effective increase in the free stream speed, applying in addition Maskell's (1963) correction for three-dimensional bodies (i.e. the factor ϵ appearing in Table 4 was taken equal to 2.5, as Maskell suggests). The support system was assumed to consist of three rectangular Joukowski aerofoils of thickness roughly 30%, with drag coefficients estimated from Goldstein (1965). The resulting small increase in the free stream speed was added to that caused by the test models themselves. In this way the unsteady lift coefficient, the reduced frequency and the Re number were corrected. The fact that a constant drag coefficient was used for calculating the corrections (i.e. by neglecting the changes in incidence of the stream),

causes very small error, because for the zero incidence unsteady load experiment, it can be seen from Figs. 4.2, 4.9 and 4.19, that $\overline{\partial C_D}/\partial\alpha$ is very small. The calculated increase of the dynamic head due to the support system was roughly 2%, and considering the maximum lift correction for the D cylinder (about - 4.5%), it is seen that the maximum overall correction applied to unsteady lift results is approximately - 6.5%. As for the case of the aerofoil at high mean incidence, the quasi-steady correction is so small ($\simeq$ - 1.5% at $\bar{\alpha} = 17^{o}$), that the fluctuations above and below the mean angle of incidence do not need special attention.

The fluctuating vortex shedding lift coefficient has not been corrected for blockage, since no aerodynamic admittance was calculated, or comparison with previous work was sought. The values of the Strouhal number given, are also uncorrected for blockage, although in this case there is a correction, proposed by Vickery (1966) based on the constancy of the Roshko's Universal Strouhal number.

5.2 EXPERIMENTAL RESULTS

This section deals with the measurement of:-

- The sinusoidal lift (sinusoidal refers to the model response at the gust frequency and the related harmonics).
- The phase between the sinusoidal lift and upwash at the mid-chord point.
- The chord-wise position of the centre of sinusoidal pressure.
- The natural vortex shedding lift.
- The Strouhal number.

Unless otherwise indicated, it is implied in the following that the results refer to the zero mean incidence tests.

5.2.1 UNSTEADY LIFT MEASUREMENTS

5.2.1.1 SPECTRAL ANALYSIS

Selected unsteady lift spectra of the NACA 0015 aerofoil, the D cylinder and the elliptic cylinder, all at zero incidence, appear in Figs. 5.2 to 5.5. They were computed digitally by the method outlined in Appendix B. Note, that both the frequency (Hz) and spectral density (sec) scales are logarithmic, with base 10. The spectral density is normalized with the mean square (N^2) of the full signal. No correction has been applied to the digitized data for frequency response of filters, amplifiers, force transducers, etc. However, the digitized spectra of two reference sinusoidal signals, fed outside and through the system, as well as the transducer calibration given in Fig. 3.6, indicated that the errors arising were much lower than the other systematic and statistical errors. The numbers appearing on top of some of the spectral peaks show the corresponding frequency in Hz. These values are only approximate, in view of the finite spectral bandwidth, plotting inaccuracies, etc. Strictly, the statistical average frequency of a smoothly varying single spectral peak with density S_x is equal to:-

$$\left[\int_0^\infty S_x\, n^2\, dn \Big/ \int_0^\infty S_x\, dn\right]^{\frac{1}{2}}$$

see for example Crandall and Mark (1963). The symbol n_g is used exclusively to denote the first harmonic of the upwash or lift. The spectral density of this harmonic is employed as a measure of the density at other harmonics or peaks appearing on the spectra. "Linear response" is not meant in this section in a strict sense, because the normalized and not the absolute values of the spectra are presented. It tends rather to indicate that the suitably normalized frequency spectra

of the input and the output are the same, a necessary condition for strict linearity. Next, the spectra for each model are examined separately.

(a) NACA 0015 Aerofoil

The lift spectra for sinusoidal flow are displayed in Figs. 5.2a, d and 5.3a and for smooth flow in Fig. 5.5, all at a Re number of 2.2×10^5. As is inferred from the smooth flow spectrum, the strongest mechanical resonance occurs at a frequency of 289 Hz. There are also smaller intensity resonances in the low frequency range, e.g. at 5, 12, 26 and 35 Hz (see Figs. 5.2a and 5.5). The extraneous noise spectrum (i.e. with zero wind speed), measured with a wave analyzer, indicated that even at the highest oscillating rig frequency, the power at the oscillation frequency was negligible, being mainly concentrated under the strongest mechanical resonance. Thus, it is certain that the spectral peaks centred at the gust frequency are almost entirely caused by the corresponding upwash. This is also true for the other models. The relatively elevated spectral density in Fig. 5.5a for low frequencies is thought to be a result of background turbulence and electronic noise. In sinusoidal flow the lift spectra exhibit a distinct peak, centred at the gust frequency. The height of this peak is 2 to 3 orders of magnitude greater than that of the next highest peak in the spectrum, and by more than 4 orders of magnitude greater than the average spectral level of background noise. This is an indication of good sensitivity of the present experiment. The top of the peak corresponds to a value of the normalized spectral density of 0.6 approximately. For increasing gust frequency, the width of the spectral peak (defined for example as the frequency bandwidth, at which the power falls by a certain percentage) becomes narrower. This is a characteristic of the oscillating rig, since it was observed in the upwash spectra as well (see Fig. 3.18).

Comparison between the lift and gust spectral peaks, for the

same gust frequency and eccentricity, reveals that they are very similar and in fact they become almost identical at the highest frequencies. A possible change in the preset frequency, which is more likely to happen at the lower frequencies, could, however, be responsible for the lift and upwash peaks not being identical in this region.

It can be seen from Figs. 5.2a, d and 5.3a that there exist higher harmonics in the lift response. These harmonics may be thought of as the combined response of the aerofoil to the already existing higher harmonics in the gust (assuming the aerofoil to behave linearly), and the generally non-linear response of the aerofoil to the fundamental gust harmonic. The strength of the higher harmonics in the lift spectra appears to be ordered as the corresponding upwash harmonics, unless they are obscured by a minor mechanical resonance or noise from the mains. Thus, in Figs. 3.18a and 5.2d ($n_g \simeq 4.6$ Hz), the second harmonic (at $n \simeq 9.2$ Hz) is lower than the third harmonic ($n \simeq 13.8$ Hz).

It was interesting to note that, keeping the gust frequency fixed, while lowering the Re number, the main spectral peak changed only very little, but the power in the higher harmonics increased with respect to the first harmonic. Similar behaviour was observed in the upwash spectra, see Figs. 3.18c, d. This is more a result of the non-linear effects introduced by increasing the reduced frequency for roughly constant gust amplitude (see for example Giesing, 1968), than a Re number effect.

Upon increasing the gust amplitude at constant frequency, the shape of the main peak remains unchanged, for both the upwash and lift spectra, see Figs. 3.18c and 5.3a. The,relatively to the first, levels of the second and third harmonics are raised by a greater factor, (roughly 1.2 to 2.5) than the corresponding upwash harmonics (see Section 3.3.4.3), meaning that in this case the aerofoil may respond more "non-

linearly" than for lower gust amplitudes. The comparatively enhanced spectrum of background noise (see Fig. 5.3a, symbol ⊙), suggests that the flow could be more irregular at greater gust amplitudes. In connection with this last point, it may be observed from Figs. 3.18, 5.2a, d and 5.3a that the level of lift background noise, for medium eccentricity, is an order of magnitude lower than the corresponding upwash level, taking as reference the height of the main spectral peaks. This is because the wing is less sensitive to disturbances than the hot-wire, especially at high frequencies.

The interesting points which may be drawn from the examination of the lift spectra are, therefore:-

- The aerofoil responds in an essentially linear manner to the incident flow. Note that although the results presented here covered only a limited number of frequencies, gust amplitudes and Re numbers, this kind of behaviour was found to hold generally.
- It follows from the great similarity of the main lift and upwash spectral peaks, and also from their narrowness, that the values of the experimental aerodynamic admittance, formed either as the ratio of corresponding spectral powers, or as the ratio of corresponding filtered mean square values (see Appendix B), should very nearly be the same.
- The aerodynamic lift spectrum is not accurately represented as the strongest mechanical resonance (at 289 Hz), is approached. A safe upper limit can be taken as 200 Hz.

(b) D Cylinder

The lift spectra for the sinusoidal flow are shown in Figs. 5.2b, e and 5.3b, c, d and for the steady flow in Fig. 5.5b. There are two main mechanical resonances, one between 24 to 26 Hz and the other between 477 to 481 Hz (the slight differences in the resonant frequencies

are due to different experimental set-ups). At first it was thought that the low frequency resonance was associated with vortex shedding from the model or the tripod support system. However, this peak does not appear in the spectrum of u fluctuations, in the wake of the cylinder (see Fig. 5.6h) and its frequency does not change, when varying the Re number (Figs. 5.3b, c and 5.5b). Therefore, its origin is not aerodynamic, but mechanical.

As in the aerofoil case, the lift response is characterized by a very strong peak, centred at the gust frequency, which is followed by the, much smaller, peaks at higher harmonics. It is remarkable that, with the exception of very low frequencies, the main spectral peak of the D cylinder and these corresponding to the aerofoil and the upwash, have almost the same shape. Relative to the first harmonic, the second and third are greater or equal to the corresponding aerofoil harmonics (unless the latter coincide with a mechanical resonance, as it happens when $n_g \simeq 18$ Hz). Apart from the fact that the D cylinder has a large fluctuating wake as compared to that of the aerofoil, a greater contribution from unsteady drag (showing up in the lift spectra due to the "cross talk" described in Section 3.1.4), could lead to enhanced higher harmonics. It should be noted, however, that the spectral peak at the gust frequency is also clearly predominant for this bluff section. Unexpectedly, the increase in the oscillating aerofoil amplitude, at all other conditions fixed, did not bring about a change in the higher harmonic levels, similar to that for the aerofoil. For example, in Figs. 5.3c, d, the second and third harmonics are raised by a factor of 2.5 and 3 respectively, while the corresponding numbers for the aerofoil (Fig. 5.3a) are roughly 16.0 and 8.0. Thus, the values for the D cylinder lie between the increase factors of the upwash harmonics (Section 3.3.4.3) and the oscillating aerofoil factors (see Table 2). Possible reasons may be:-

- Transfer of power to other harmonics. Note for example in Fig. 5.3c, that the fourth harmonic (at 40 Hz) is considerably increased. This could be due to the sinusoidal vortical wakes shed, at the two sharp trailing edges of the cylinder, interacting in a different way than in the case of the aerofoil.
- The presence of the natural vortex shedding peak, which is of the same order of magnitude as the higher harmonic peaks. Although, it is at a relatively remote position, this peak may interfere, in terms of power, with other spectral peaks.
- Mechanical resonances, which may be excited to a different degree, depending on the external forces.

The overall greater unsteadiness of the flow round the D cylinder, is reflected in the spectral level of background noise, which is higher than the corresponding one for the aerofoil. Note, however, that the relative level of noise is suppressed, when increasing the gust amplitude, in contrast to the aerofoil.

The same general comments can be made about the response of the D cylinder in sinusoidal flow, as was done for the aerofoil. In particular, it is noteworthy, that there is no sign of strong non-linear behaviour of the lift.

(c) Elliptic Cylinder

Figs. 5.2c, f and 5.4a, b, c show the sinusoidal flow lift spectra, while Figs. 5.5c, d, e, the smooth flow ones. The main mechanical resonances occur between 440 and 480 Hz and between 22.5 and 25.5 Hz. (Note, that as with the other models the exact position of the resonant frequencies depended upon the particular experimental arrangement).

Before proceeding to the sinusoidal lift response, the origin of some rather curious peaks appearing in the spectra for all the Re numbers will be investigated; namely, those between 50 and 56 Hz for

Re = 2.2 x 10^5 (Figs. 5.2c, f, 5.4a, b and 5.5c), at approximately 76 Hz for Re = 3 x 10^5 (Fig. 5.4c), between 29 to 36 Hz for Re = 1.6 x 10^5 (Fig. 5.5d) and at approximately 16 Hz for Re = 1.2 x 10^5 (Fig. 5.5e). These peaks are observed in both steady and oscillatory flows; therefore, they cannot be caused by the latter. Their explanation in terms of natural vortex shedding, leads to unrealistically small values of Strouhal number (0.13 - 0.08). Indeed, Modi and Wiland (1970) and Schramm (1966) tested elliptic cylinders of similar fineness ratios at subcritical Re numbers and found quite higher Strouhal numbers (0.23 - 0.40). The author's experiments were undertaken at critical Re numbers, and in view of the results of Bearman (1969b) for the rise in the Strouhal frequency of a circular cylinder as the critical flow regime is approached, it is expected that the vortex shedding frequencies would be considerably higher than those mentioned previously. In fact, this is what happens, as it is realised by referring back to Figs. 5.2, 5.4 and 5.5, where rather broad peaks appear at high frequencies. The following possibilities were considered, in an attempt to explain this phenomenon:-

1. Interference due to vortex shedding from the tripod support system (shown in Fig. 3.4). Apart from the fact that the shedding frequencies related to this body are expected to be much higher, this possibility should be precluded, because similar peaks also appear in the spectra of u fluctuations, measured in the wake of a solid elliptic cylinder (chord = 0.17 m), which was mounted between the vertical walls of the 0.61 x 0.91 m wind tunnel, i.e. without any support system, see Figs. 5.6a, b, c, d, e (end plates were used, see Fig. 4.6).

2. Extraneous acoustical input. It may be that a pressure field generated by the vibrations of the tunnel walls (in particular, the two vertical end plates) could have affected the unsteady pressure on the

model (for example as found in the experimental results of Surry, 1969). If that was the case, or if another acoustic wave was responsible, the excitation frequency would have always been the same and, of course, it would have appeared on the other models as well. Therefore, this possibility is also excluded.

3. Role of the separation bubbles. Bearman (1969b), working on a circular cylinder in the subcritical and critical flow regimes and in steady flow, found that at a particular Re number, two peaks appeared in the velocity spectra in the wake (the second peak was at a frequency less than twice the first, so that it was not caused by the influence of the central wake region). He claimed that the two peaks on the spectrum indicated the Strouhal number just before and just after one separation bubble was formed on the surface of the cylinder. In the author's experiments such a Re number could not be found, nor was the flow particularly unsteady as Bearman (1969b) reported. Also, unlike Bearman's (1969b) observations, no discontinuity in the variation of base pressure against Re number, or mean lift coefficient different from zero (at zero mean incidence) was realised. In addition, if the lower peak in the author's results, corresponded to shedding in subcritical flow (as in Bearman, 1969b), the Strouhal number should have been higher (see Schramm, 1966). However, the idea of an asymmetric (in space and time) formation of the separation bubbles cannot be entirely dismissed. Fig. 2.3 also shows that the formation of the separation bubbles varies according to the particular experiment. It can be seen from Figs. 5.6a, b, c, d that when the elliptic cylinder is at an angle of incidence relative to the free stream, the frequency of the higher (vortex shedding) spectral peak changes little (note, it is uncorrected for blockage), while its intensity progressively increases in relation to the lower curious peak,

of which the frequency is also nearly constant. At an incidence of 15^{o}, the lower peak completely disappears, as it does when the free stream is turbulent (Fig. 5.6g), or the steady oncoming flow subcritical (Fig. 5.6f). These tests are only to indicate that the mechanism which controls the intensity of the lower peak depends on the state of separation (the spectra refer to one side of the wake only).

4. Three-dimensionality in vortex shedding. It may be that vorticity is shed at different phases along the model span in a form of spanwise cells, similar to the kind observed by Gaster (1969), Maull and Young (1972) and Mair and Stansby (1975). Gaster (1969) tested a slightly tapering circular cylinder in a uniform low Re number flow, and found that vortex shedding occurred in patches, which were repeated regularly at a lower frequency; the Strouhal number in each spanwise cell was constant. The other authors mentioned, tested D section cylinders in a shear flow of which the vorticity vector was normal to the cylinder axis. They found that a longitudinal vortex served as a boundary between the observed spanwise cells, allowing different frequencies in the wake. Neither of these two conditions (i.e. tapering or shear flow) occurred in the author's experiments. However, the flow in the wake was irregular, as it can be judged from the oil flow visualization (Fig. 4.11) and the spanwise correlation measurements shown in Figs. 6.6 and 6.7. Even for a D section cylinder, in uniform flow Graham (1969) found that the shed vortices were not coherent, unless the end plates were at a distance apart no greater than 4 b (b = body thickness). It is thought, that this incoherency combined with possible asymmetries due to bubble formation (see previous section), could lead to the shedding process taking place in patches, with a repetition frequency equal to the frequency of the curious peak described. The shape of the spectral peak (rather broad) could indicate the degree of

randomness of the phenomenon. By plotting this frequency in a dimensionless form, ns'/U_∞, (s' = total span) against the Re number, $U_\infty.s'/\nu$, in Fig. 5.7, it may be argued that (except for one experimental point, which is at the highest Re number), roughly, n depends only on U_∞^2/ν (since ns'/U_∞ is roughly proportional to $U_\infty s'/\nu$), a result also obtained by Gaster (1969). The closeness of the experimental points for models of different spans (see Fig. 5.7) shows that the span length is the appropriate non-dimensionalizing quantity. Another point, which is in support of the shedding in patches, is the high degree of spanwise correlation found at this frequency, even higher than the correlation measured at the Strouhal frequency. It should be emphasized, that these suggestions are only based on a few measurements. Further work would be needed to explain this phenomenon, and in particular, flow visualization by smoke (in a larger model, to reduce the wind speed), may be helpful. The spectral peak described does not affect the main spectral peak of the sinusoidal lift, because it is several orders of magnitude lower. Its shape can, however, be modified, in fact become narrower, when it coincides with a higher lift harmonic (compare Figs. 5.2c and f), implying that in this case shedding might become more coherent.

The sinusoidal lift response is now examined. From Figs. 5.2 and 5.3 it is observed that the strong peak at the gust frequency characterizes the lift response of the elliptic cylinder. Its shape is very similar to those of the gust, aerofoil and D cylinder, especially at the higher frequencies. The higher lift harmonics are generally greater (relatively to the first) compared to those of the gust and the other models (unless they interfere with a minor mechanical resonance, as in Figs. 5.4a, b). An additional reason for this non-linearity (see also section on D cylinder) is thought to be a possible movement of the separation points.

The spectral level of background noise is comparatively larger than in the D section cylinder and the aerofoil, an indication of a greater deviation from two-dimensionality. Partly, this is on account of the spread of energy away from the vortex shedding peak, which is observed to be significantly suppressed.

Increasing the gust amplitude, with all the other variables fixed, has the effect of increasing the relative strength of the higher harmonics, but not as much as for the aerofoil or the gust, perhaps for the reasons mentioned previously (see the D cylinder results). The effect on the spectral level of background noise is in the same direction as for the D cylinder, i.e. the noise is relatively suppressed.

Summarizing the results from the unsteady lift spectra, it can be said, that the sinusoidal response of the elliptic cylinder is of basically linear type, though less linear than the responses of the aerofoil and the D cylinder. The comments made for the aerofoil case hold here as well.

5.2.1.2 MEASUREMENTS OF THE RMS LIFT COEFFICIENT

In this section, the RMS lift measurements performed on a frequency band, which is centred at the gust frequency are given. The spectra presented in Section 5.2.1.1 confirm that the filtering method outlined in Appendix B is meaningful. All results refer to the zero mean incidence experiment.

(a) NACA 0015 aerofoil: Fig. 5.8 displays the variation of the filtered RMS lift coefficient, C_L, with reduced frequency $k = \pi nc/U_\infty$, for the NACA 0015 aerofoil. Four Re numbers, 1.2×10^5, 1.6×10^5, 2.2×10^5 and 3×10^5, and three oscillating aerofoil pitch amplitudes (marked as eccentricities) were tested.

The experimental results for each eccentricity are spread about a mean line, which is of similar shape to that of the RMS gust amplitude variation (Fig. 3.17). However, the observed maximum occurs here at a lower value of k. That seems to be a result of the progressively increasing influence from the aerofoil wake, which according to Sears's theory (Section 2.3.1), tends to diminish the unsteady lift as k increases. The values of the lift coefficient are ordered as the corresponding gust amplitudes, i.e. the greater the eccentricity, the greater the lift coefficient. By simply superimposing Figs. 5.8 and 3.17, it can be seen that, the proportionality is maintained. In conjunction with the spectral analysis results, this provides satisfactory evidence of a strong linear response of the aerofoil, over the range of variables examined here.

Altering the Re number, at constant k and eccentricity, has the effect of slightly changing the lift coefficient and gust amplitude in the same direction (on average) and roughly by the same percentage. Therefore, it could be claimed that the scale effect is probably more important for the flow round the oscillating aerofoils, than the aerofoil exposed to the sinusoidal gust, but errors in the hot-wire calibration and inappropriate tunnel interference corrections, may render this argument untrue. There are also some factors, which could affect the level of the experimental results at fixed Re number and introduce scatter:-

- Fixing the oscillating aerofoil amplitude. It was stated in Section 3.2.1, that the adjustment of aerofoil pitch amplitude, was accomplished by moving (mechanically) an eccentric shaft. Although it has been tried, as far as possible, to carry out all measurements at a particular Re number and then change the oscillating aerofoil amplitude, this was not always the case. The errors introduced by readjusting the shaft eccentricity to its previous position would shift the overall level of lift.

- Although the gap between the "live" section and the dummy ones, and the length of the cylindrical rods supporting the aerofoil (see Fig. 3.4) caused insignificant changes in the filtered RMS lift values, they should be remembered as possible factors introducing scatter.
- Measurement of RMS value. Comparison between the filtered RMS values and those obtained by integrating the areas under the spectral peaks and taking the square root, showed a maximum discrepancy of 5%, at the lowest frequencies. It is thought that this uncertainty in measuring the RMS values is an additional source of scatter, which in the present results (for constant k, Re and eccentricity) did not exceed 6%.

(b) D cylinder: In Fig. 5.9 the results for the D section are presented. The unsteady lift coefficient values are always higher, compared to those of the aerofoil. However, they can be made to roughly coincide over the entire frequency range, if the D section results are divided by a factor ranging from 1.16 to 1.21. In all other results (effect of Re number, reduced frequency, aerofoil amplitude) the comments made for the aerofoil also apply here. The experimental points, when shifted downwards do not correspond exactly to those for the aerofoil, partly because the blockage corrections involved, change both C_L and k.

The fact that the unsteady lifts of the aerofoil and the D cylinder are approximately connected by a proportionality relationship , shows that the corresponding unsteady flows about the two might be quite similar. If the spectral analysis results are also taken into account, there could be no doubt that, with regard to the D cylinder, the lift response is strongly linear.

The situation is somewhat different, when the unsteady lift coefficient of a modified elliptic cylinder is considered (see Figs. 5.9 and 5.1). It can be seen from Fig. 5.9, that the experimental results

for this body do not follow the general trend of the D section points, i.e. they cannot be assumed proportional to the aerofoil's results. Re number effects are not likely to be the cause, since the Re number for this model (= 2.5 x 10^5) lies between the Re numbers already examined. Although the mean load characteristic is not known, it is thought that it could not contribute to the deviation. Rather, it may be an irregular behaviour of the separation points, which makes the results for the two bodies look different. Namely, it could be that separation takes place either upstream of or at the two sharp trailing edges of the cylinder, depending partly on how rapidly the flow changes about it, i.e. depending on k. If separation takes place at the two sharp trailing edges, then only a small deviation from the D section results is to be expected. But if separation occurs upstream of the trailing edge, then the flow picture would be altered, due to possible oscillation of the separation points and interference of the two parallel plates with the wake. This test shows, therefore, that the consistent behaviour realised with the D section is associated with the two separation points being fixed at the sharp trailing edges.

(c) Elliptic cylinder: The elliptic cylinder measurements are plotted in Figs. 5.10, 5.11 and 5.12. Interesting points are:-

- The measured lift coefficients are higher compared to those of the aerofoil, with the exception of a few experimental points at very high k, which are lower. At these highest reduced frequencies the lift signal appeared less steady and less sinusoidal. The departure from sinusoidality might be due to the relatively growing extraneous noise and the features of the flow itself, but the unsteadiness indicates an irregular flow behaviour.
- The results depend very strongly on the Re number. The greatest

influence is observed for $1.2 \times 10^5 \leq Re \leq 2.2 \times 10^5$, the range over which the mean lift coefficient is also greatly affected (see Fig. 4.18).

- Unlike the D cylinder, here the C_L v. k curve cannot be made to coincide with corresponding aerofoil curve, by a simple multiplication. For example, when $1.2 \times 10^5 \leq Re \leq 2.2 \times 10^5$ and k is low, C_L is about 80% higher than the C_L of the aerofoil, while at high k, it is only 40% higher. However, when $Re = 3 \times 10^5$, C_L varies with k in approximately the same manner as in the aerofoil and the D section cases.
- Although difficult to discern from the plots, there appears to be a systematic effect of gust amplitude (Re number fixed), expressed in the relative reduction of C_L, when the eccentricity is large. This, and the strong Re number dependence, make the elliptic cylinder behave less linearly than the aerofoil and the D cylinder.

Some results for the modified elliptic shapes (see Fig. 5.1) are displayed in Fig. 5.12. The ellipse with a single, short trailing edge (marked as number 2) is tested at a Re number 2.35×10^5, and the lift coefficients obtained follow the same curve as the data for the simple ellipse, at $Re = 3 \times 10^5$. Assuming that the Re number increase from 2.2×10^5 (in which case C_L is high) to 2.35×10^5 is rather small to affect the lift coefficient, the short trailing edge could have reduced C_L in the following ways:-

(i) Reduce the mean lift.

(ii) Interfere with the wake.

(iii) Alter the position and path of the separation points.

The modified ellipse with the longer trailing edge (number 3) tested at $Re = 2.6 \times 10^5$, exhibits consistently lower values of C_L. The lift coefficient approaches, from below, that of the aerofoil ($Re = 3 \times 10^5$) as k increases. In this case, the effect of increased Re number can be added to the reasons for the reduction of C_L.

Finally, the lift coefficient of the elliptic cylinder fitted with trip wires at 0.25 c from the leading edge (number 4) is always lower from both C_L of the aerofoil and the simple elliptic cylinder, tested at the same Re number (= 2.2 x 10^5). As k increases, C_L becomes a greater percentage of the aerofoil's corresponding coefficient. At low k, the drop of unsteady lift relative to the aerofoil, corresponds approximately to the drop of the mean lift (measured on a similar model, see Fig. 4.18) below that of the aerofoil (Fig. 4.1).

The experimental results presented in this section indicate that the sinusoidal lift can be made to depend on fewer parameters, if the separation points are held fixed. The significance of this fact will also be discussed later.

5.2.1.3 VARIATION OF FLUCTUATING LIFT COEFFICIENT WITH TIME

The measurements described in this section, deal with the variation of the fluctuating lift coefficient in the time domain. The oscillating signals are shown in a full cycle, which is the average of a large number of similar cycles (see Appendix B). The time axis is expressed as phase angle ωt (degrees), the origin being the same as in the corresponding gust amplitude plots (Fig. 3.19). The fluctuating lift signal, as it comes out from the charge amplifiers, does not include any mean load. Here, both the zero and the high mean incidence experiments are described.

Fig. 5.13a to f shows a few selected C_L v. ωt curves for the D and elliptic cylinders, at Re = 2.2 x 10^5 and medium eccentricity. The variation of gust amplitude is also shown for comparison. It is observed that, at high frequencies, C_L and α_g vary in an apparently sinusoidal manner. This can be seen clearly in Fig. 5.13c, f by

reference to a pure sine wave, with the same period and peak amplitude as C_L. As the frequency decreases, the deviation from sinusoidality of both C_L and α_g is more evident. Possible reasons for this lack of sinusoidality could be:-

- The existence of higher harmonics, which are not smoothed out in the conditionally averaging method.
- Insufficient averaging time.
- The effect of the tripod support system.
- The presence of a small DC component in the signal.

The last two reasons would lead to an asymmetric type of signal, like the one in Fig. 5.13b. In general, however, the variation of lift follows fairly closely the variations of the gust for both bluff bodies and for the aerofoil as well (of which the results are not presented here). It is noteworthy, that in all tests the variation of C_L with incidence over a complete cycle forms an anticlockwise loop (see also Section 5.2.2 on phase measurements).

5.2.2 LIFT-UPWASH PHASE MEASUREMENTS

The phase between the lift and the upwash, with respect to the mid-chord point, is plotted in Figs. 5.14, 5.15 and 5.16. Both the fluctuating lift and upwash signals were processed under identical conditions to ensure uniform phase shift, relative to the fixed origin. To determine the phase, the position in the cycle of each signal (instantaneous or conditionally averaged) was measured with respect to the spiky reference signal (Section 3.2.2) and the two results were subtracted. It was estimated that the maximum error in measuring the phase of each quantity, was about 3%, so that the overall maximum error in the phase between $C_L(t)$ and $\alpha_g(t)$ would be $\pm$ 3%, implying a scatter band of about 20^o maximum. The same and certainly more accurate results

could have been effected by the cross-spectral density approach, at the expense of computer time and digital tape.

(a) NACA 0015 Aerofoil: In Fig. 5.14 the phase relating to the NACA 0015 aerofoil is shown. Only the medium eccentricity position of the oscillating aerofoils was considered, but four Re numbers ranging from 1.2×10^5 up to 3×10^5 were used. The absolute value of the phase is seen to increase from low values, at small k, and remain more or less constant for the higher reduced frequencies. Due to the considerable scatter a systematic Re number effect is not discernible. For the range of reduced frequencies considered, however, ($k < 0.6$) the experimental values are of the correct sign, according to the thin aerofoil theory, i.e. the sinusoidal lift lags behind the gust velocity. This shows that the vortical wake produces the anticipated effect. In contrast to the present results, Holmes (1970) reported a lead instead of a lag, for a NACA 0012 aerofoil, which he tested in a "moving wall" gust tunnel (Section 2.3.6). There is, however, an important difference in the gusts employed by Holmes and the author: In the former the ratio of the gust wavelength to chord length is kept constant (so that the quasi-steady interaction is maintained) and the frequency of the gust is varied (so that the unsteady interaction is varied); in the latter both interactions are allowed to change. Maeda and Kobayakawa (1970) presented the phase results for a NACA 0012 aerofoil for $k < 0.0175$. Their results exhibit an enormous degree of scatter with k and a reasonable one with mean incidence (mean incidences up to 9^o were examined). Since they do not state the method of determining the phase (note, the results are scattered about the line $\phi = 225^o$), a comparison with the author's results (which could be meaningful due to the small differences in the NACA 0015 and 0012 profiles), is not possible. In the, apparently easier to handle, case of an oscillating

aerofoil in a uniform stream, the existing data from previous workers tend to be somewhat more coherent, as it is for example realised by a glance at the papers of Silverstein et al (1939), Reid et al (1940), Halfman (1952) and Spurk (1964).

(b) D Cylinder: The D section experimental results are displayed in Fig. 5.15, with flow parameters the same as in the aerofoil. A certain amount of scatter is again evident, but the general trend indicates a greater lag of lift behind the upwash, as compared to that of the aerofoil. Otherwise the data for both models are similar.

(c) Elliptic Cylinder: The phase measurements for the elliptic cylinder, appearing in Fig. 5.16 are on average different from those presented for the aerofoil and the D section in two respects. First, the phase lag is greater and second it tends to increase rather than remain constant, at the higher frequencies. It is also noticed, that the points corresponding to the greatest Re number examined tend to have the smaller lag, while those for the lower Re numbers (1.6×10^5 and 1.2×10^5) to show on average, a tendency for bigger phase lags.

5.2.3 MEASUREMENTS OF THE CHORDWISE POSITION OF THE CENTRE OF PRESSURE

In Chapter 4, the centre of pressure was determined for the two bluff sections, with the help of the mean surface pressures and the results were plotted in Fig. 4.10. In the present experiment unsteady pressures were not measured, but instead the three individual signals from the piezoelectric transducers were processed instantaneously, to yield the instantaneous point of action of the fluctuating lift force. Indeed, if it is assumed that the transducers respond only to forces in the vertical upwash direction and the three cylindrical connecting rods (Figs. 3.2 and 3.4) exert point forces, then the centre of pressure

in the x-y plane can be found by applying the theorem of moments. The method followed consisted of recording simultaneously in the analogue tape recorder (odd or even channel positions only) the three lift signals and the coil reference signal. Then each lift signal was played back together with the reference signal and tape recorder output was filtered and recorded on paper, by means of a BRUSH two-channel pen recorder. The three pairs of plots thus obtained, corresponding to a specific model, k, Re, $\bar{\alpha}$ and rig eccentricity, were analyzed graphically to determine the chordwise position of the centre of pressure. Since only a limited number of cycles could be handled (usually 10) the statistical reliability of the results is not very good. Particularly inaccurate are the results, when the lift signals are about to become zero, due to augmented graphical errors, hence calculations in this region were not attempted. A minimum error of ± 3% was estimated. Also, due to the analogue filtering involved, the migrations in the centre of pressure due to vortex shedding and the harmonics higher than the third were eliminated.

An important result was that the forces sensed by the two (front) transducers were virtually identical in amplitude and phase. Although the detailed load distribution remains unknown, this is a significant indication of two-dimensionality of the unsteady flow about the models. Hence, at zero mean incidence, the resultant unsteady force lies essentially in the vertical plane through the mid-span.

(a) NACA 0015 Aerofoil: In the case of the aerofoil at zero incidence no quantitative results are available, but by displaying the individual lift signals in a storage oscilloscope, it was observed that the centre of pressure, being located in the mid span plane, did not on average deviate much from the quarter chord point position. Note, that the thin aerofoil theory predicts a centre of pressure located

exactly at the quarter chord point, at all times, and a pressure distribution of the same form, $\Delta C_p \sim \sqrt{(1 - x)(1 + x)}$, both in steady and frozen unsteady flows (see Graham, 1970b). Despite the fact that the overall lift response was very sinusoidal, the signal from each transducer departed slightly from the sinusoidal and symmetrical forms, especially the one in the rear of the aerofoil. Possible reasons for this behaviour could be:-

- The existence of a small reversed flow near the aerofoil trailing edge. Holmes (1970) attributed to this fact the distorted shape of the unsteady pressure coefficient near the trailing edge of a NACA 0012 aerofoil, but instead of a worsening in the load waveform with increasing frequency (observed by Holmes), an improvement was experienced in the present case.
- The sensitivity of the transducers to transverse loads (Section 3.1.4).
- The influence of the tripod support system (Figs. 3.4, 3.15).

(b) D Cylinder: In Figs. 5.13a the migration of the centre of pressure over a complete cycle is shown, pertinent to the D section. The centre of pressure position is measured in fractions of the chord from the leading edge, x_{cp}/c. Taking into account the experimental inaccuracies, it is seen that for the flow parameters considered, $k = 0.22$, $Re = 2.2 \times 10^5$, medium eccentricity, the centre of pressure performs an excursion within close limits about the 35% c position approximately. The centre of pressure of the steady lift force, plotted in Fig. 4.10, at mean incidences comparable with those of the unsteady upwash (i.e. 0 to 5^0), is observed to lie at about 28% c from the leading edge. This difference indicates that the shapes of the mean and unsteady pressure distributions are not generally the same.

The points regarding the sinusoidality of each separate lift signal (from each transducer) which were made for the aerofoil can be

also repeated here.

(c) Elliptic Cylinder: The values of x_{cp}/c for the elliptic cylinder are shown in Figs. 5.13d, f with corresponding reduced frequencies 0.12 and 0.22. The centre of pressure oscillates about the 40% c position, which is within the range covered by the centre of pressure of the mean lift force, under a quasi-steady change of incidence (see Fig. 4.10). There does not seem to be any significant change in x_{cp}/c for the two reduced frequencies examined considering the experimental errors involved.

The lack of sinusoidality of the individual transducer outputs was more evident, than in the two other models, because of the extended reversed flow on the rear of the ellipse. However, no serious worsening of the two-dimensionality occurred.

5.2.4 NATURAL VORTEX SHEDDING IN SINUSOIDAL FLOW

In this section, the effects of the sinusoidal flow upon the vortex shedding spectra of the two bluff bodies is briefly examined. In Sections 5.2.1.1b, c, it was pointed out which spectral peaks should not be confused with vortex shedding. Using this information, and assuming a universal Strouhal number $S^* = nd_w/U_w$ in the range of 0.16 to 0.18 (where d_w is the value in the wake width, see Roshko (1954a), and U_w the mean speed at separation ($= U_\infty \sqrt{1 - \bar{C}_{pb}}$), the location of the intrinsic shedding frequencies could be ascertained. The wake width was roughly estimated from hot-wire traverses in the wake and also from the mean position of boundary layer separation (see Figs. 4.7 and 4.12).

The spectra are presented in a dimensionless form, i.e. the absolute lift coefficient spectra are multiplied by U_∞/b, to eliminate time and the result is divided by the mean square of the lift coefficient due to vortex shedding $(C_{Lvs})^2$. This last quantity was determined as

follows: The numerical values of the lift spectra, as obtained from the digital analysis program (Appendix B), were smoothed over frequency, so that they could be more clearly plotted. Then a curve of the form $c_1 \exp(-c_2|n - n_{vs}|^{c_3})$ was fitted through the smoothed points, where c_1, c_2, c_3 were constants to be found and n_{vs} the vortex shedding frequency (Hz), chosen as the frequency at which the lift spectrum was maximum. For the D section this fitting required that the experimental and mathematical curves had the same maxima, S_{max} at $n = n_{vs}$, and common points at 0.5 S_{max} and 0.05 S_{max}. For the elliptic section the two curves would have common points at $n = n_{vs}$, and approximately at $n = n_{vs} \pm 0.05\ n_{vs}$ and $n = n_{vs} \pm 0.15\ n_{vs}$. The computed area under each one of these curves, from $n = 0$ to ∞, was defined as $(C_{Lvs})^2$, taking into account the calibration factors, etc. It is recognized that there will be some "cross talk" between the lift power due to the sinusoidal gust and that due to vortex shedding, so that the lift coefficient, just defined, would not include only the (natural) vortex shedding contribution. However, from Figs. 3.18, 5.3 and 5.4, it can be seen that the power due to the upwash drops significantly before the much higher shedding frequencies are reached (spectra for $Re \geq 2.2 \times 10^5$ were only analyzed to yield C_{Lvs}). Therefore, the direct contribution of the unsteady sinusoidal lift to C_{Lvs} is expected to be small. Since the levels of the vortex shedding lift spectra are generally very low compared with the first harmonic of the sinusoidal lift (especially for the elliptic model, see Fig. 5.4), the existing background noise will limit the accuracy of measuring the former and consequently of C_{Lvs}. All quantities presented are uncorrected for tunnel blockage.

(a) D Cylinder: The dimensionless vortex shedding lift spectra are plotted in Fig. 5.17 for both smooth and sinusoidal flows. On the same figure the corresponding values of C_{Lvs} obtained by numerical

integration are given. It is observed that the shape of the spectra is not appreciably affected by changes in Re number or reduced frequency. The different levelling of S_{max} could be partly attributed to the uncertainty in measuring absolute spectral power and changes in the experimental arrangement. When compared to the uniform flow RMS lift coefficients of the square cross section cylinder at zero incidence ($C_{Lvs} \simeq 1.3 - 1.4$, Re of the order 10^5, see Vickery (1966) and Pocha, 1971), or the circular cylinder ($C_{Lvs} \simeq 0.8 - 0.15$, $10^2 \lesssim Re \lesssim 10^6$, see Fung (1960) and Sallet, 1972), the D section cylinder is seen to be of a much smaller "bluffness". It should be pointed out that the present values of C_{Lvs} are in qualitative agreement with those calculated by applying a potential flow model, derived by Sallet (1972) with inputs the measured mean drag coefficient and Strouhal number and principal assumption of a von Karman vortex street with spacing ratio 0.281. Actually, the predicted C_{Lvs} are 2 to 3 times higher than those measured and this could be partly due to the fact, that the theoretical model gives the cross sectional C_{Lvs} and not the overall lift coefficient measured here, which is the sum of all the, non-perfectly correlated loads across the span (see Figs. 6.6 and 6.7).

Fig. 5.17 shows that the introduction of the sinusoidal flow reduces the vortex shedding lift coefficient, as it does an increase in the Re number from 2.2×10^5 to 3×10^5. As k increases, C_{Lvs} becomes gradually lower with respect to its value in steady flow. It is also observed that the effect of increasing the gust amplitude, at constant k, is to lower C_{Lvs}. Thus the present results are similar to those reported by Pocha (1971) (see Section 2.3.5 and Fig. 2.8). Pocha attributed the decrease in C_{Lvs}, outside the "lock in" range, to two factors: One was due to the interference of the gust periodic flow with the vortex shedding flow, leading to a progressive weakening and

irregularity of the shed vortices as the gust frequency neared the shedding frequency (but still not very close to it); the other was due to the effective incidence of the gust (which quasi-steadily would reduce C_{Lvs}, as found experimentally in steady flow). Although the author's experimental conditons are not identical to those of Pocha (for example Pocha's sinusoidal gust is convected downstream at half the free stream speed), these reasons could account for the reduction in C_{Lvs} encountered in the present experiments.

The effect of a sinusoidal cross flow upon vortex shedding for a long, square ended body, was studied theoretically by Clements and Maull (1975). During the "unlocked" type of shedding, the rate of shedding of vorticity, $d\Gamma/dt$, was found to exhibit large periodic variations in both its amplitude and period of oscillation. It is thought that this irregularity could act as to lower C_{Lvs} relative to its value in steady flow (where $d\Gamma/dt$ was settled to a steady periodic form). The present results may then be explained in terms of this argument.

The vortex shedding lift may be also modulated by the streamwise component of the sinusoidal gust. A simplified analysis, presented in Appendix E, shows that, under the assumption of a constant Strouhal number, the shedding spectrum would decrease and become broader in the presence of a uniform streamwise sinusoidal component. This effect is not likely to be important here, because u is very small in the region occupied by the test models, but more important in turbulent flow, where u is much stronger.

Fig. 5.19 displays the limits of variation of the Strouhal number with Re number for various types of flows. It can be seen that for $10^5 \lesssim Re \lesssim 3 \times 10^5$, the Strouhal number may be assumed constant, at the value of 0.265 within ± 4%. This value differs by less than 4% from the Strouhal numbers reported by other workers, who have tested D sections

of thickness to chord ratios 0.167 to 0.667, see for example Maull and Young (1972), Bearman (1965) and Graham (1969).

(b) Elliptic Cylinder: The lift spectra appear in Fig. 5.18, with flow conditions as in the D cylinder. There is very little difference between the smooth and sinusoidal flow spectra at the same value of Re number. However, in smooth flow, an increase of Re number from 2.2×10^5 to 3×10^5 results in two different types of spectra altogether. The Strouhal number is raised, the maximum spectral level is decreased and there is some evidence of some broadening of the spectrum above n_{vs} and of a narrowing below n_{vs}. These changes are too large to be attributed to measurement inaccuracies (which, it should be emphasized, are higher than for the D section, due to the very low levels of the spectra). The corresponding lift coefficients are not, however, significantly altered, because the trends of lowering and broadening the spectrum might cancel each other.

The theoretical model of Sallet (1972) mentioned earlier, gives lift coefficients as much as 5 times the experimental ones. The lack of spanwise coherence of the shed vortices (which is worse than in the D section, see Figs. 6.6 and 6.7), should be partly responsible for this discrepancy. Modi and Wiland (1970) are known to have measured RMS lift coefficients of elliptic cylinders of fineness ratios 1.25 and 1.67 in uniform flow. They found values of C_{Lvs} an order of magnitude higher than those presented here. Besides the different fineness ratio, their results are not, however, comparable with the author's, first because their models had a larger aspect ratio ($\simeq$ 11 compared with 2.5 of the author's) and second, because they had experimented at subcritical Re numbers (C_{Lvs} is expected to drop significantly as the critical regime is entered, see Sallet (1972) and Fung, 1960).

The fact that the shedding lift coefficient undergoes only a

small reduction in sinusoidal flow, compared to the corresponding reduction of the D cylinder, may be explained by observing that the Strouhal frequencies of the elliptic cylinder are almost twice those of the D cylinder. Thus, any interference between the vortex shedding and the sinusoidal flows would be weaker for the elliptic cylinder, although the "gust angle" effect might be more important due to the non-fixed positions of the separation points.

The variation of the Strouhal number against Re number, shown in Fig. 5.19, indicates a strong Re number effect. In uniform flow, the Strouhal number is seen to decrease as the critical regime is approached, stay rather constant at Re $\simeq 10^5$ and then increase rapidly to quite high values at Re $\simeq 3 \times 10^5$. It is noticed that approximately the same behaviour is followed in the sinusoidal flow. The sudden changes in the Strouhal number are associated with the corresponding changes in the positions of mean separation, reported in Chapter 4. For subcritical Re numbers (Re $\lesssim 10^5$), the Strouhal numbers found here are between those measured by Schramm (1966), for elliptic cylinders of fineness ratios 2.0 to 4.0. Finally, a comparison between the Strouhal numbers of the elliptic and D cylinders, reveals that the former is of a considerably smaller "bluffness".

5.3 COMPARISON OF THE EXPERIMENTAL RESULTS WITH THE THEORY AND DISCUSSION

5.3.1 THEORY

The unsteady thin aerofoil theory, originally developed by Sears (1941) was described in Section 2.3.1. This theory is here modified in two different ways, in an attempt to predict the linear gust loading of the models (i.e. excluding the vortex shedding loading). The corresponding Kutta-Joukowski condition employed is that the pressure at

each separation point is instantaneously equal to the base pressure, i.e. the condition of zero loading across the trailing edge is applied. The two bluff bodies are idealized as flat plates and the two vortex sheets shed from the separation points of each body are assumed to lie both at the extension of the flat plate chord. Thus the "effective" trailing edge of each bluff body is assumed to coincide with the trailing edge of the flat plate. To first order, thickness does not affect the problem in unsteady thin aerofoil theory, though the mean lift curve slope is influenced by thickness. Therefore, the modifications applied relate to the mean loading only.

Under the one type of modification, the factor 2π, which appears on the right hand side of Eqn. (2.7) and which is equal to the theoretical lift curve slope of a flat plate in steady flow, is replaced by $\overline{\partial C_L}/\partial\alpha$, this being the experimentally determined mean lift curve slope of the model at zero incidence. The steady flow values of $\overline{\partial C_L}/\partial\alpha$ are marked on Figs. 4.1, 4.8 and 4.18. Thus Eqn. (2.7) for the predicted unsteady lift becomes:-

$$C_L(t) = R\left[\frac{\overline{\partial C_L}}{\partial\alpha} \cdot \hat{\alpha}_g \cdot e^{i\omega t} \cdot S(k)\right] \qquad (5.1)$$

(R stands for the real part) where $C_L(t)$ and $\alpha_g(t) = R(\hat{\alpha}_g \cdot e^{i\omega t})$ are the sinusoidally varying lift coefficient and gust amplitude (rad) at the mid-chord point, respectively and S(k) is Sears's function, given from Eqn. (2.8). If only the variation of the lift coefficient amplitude is required (i.e. not the phase relative to the gust), then Eqn. (5.1) can be written as:-

$$\left|C_L(t)\right| = \frac{\overline{\partial C_L}}{\partial\alpha} \cdot \left|\alpha_g(t)\right| \cdot \left|S(k)\right| \qquad (5.2)$$

The replacement of 2π by $\overline{\partial C_L}/\partial\alpha$ is justified by the fact, that at very low reduced frequencies, $|C_L(t)/(\hat{\alpha}_g\, e^{i\omega t})|$ should tend to $\overline{\partial C_L}/\partial\alpha$, by definition, since $S(k) \to 1$, and the model is effectively exposed to a stream of varying direction. The assumption is then made, that the reasons responsible for the deviation of the mean lift from its theoretical value in steady flow, continue in the unsteady flow as well. Note that Eqn. (5.1) only serves to change the amplitude of the fluctuating lift, while the phase, the shape of the chordwise pressure distribution and the centre of pressure are assumed still to be given by Sears's theory.

It is realised that the proposed theoretical model cannot reveal the special features of the individual unsteady flows, because the empirical input is introduced from a quasi-steady point of view. The unsteady aerodynamics of the test models are in this way treated identically, although there are reasons to believe that their response would be different,for example,due to the conditions at separation characterizing each case. The thickness effect is only partly taken into account (i.e. incorporated in $\overline{\partial C_L}/\partial\alpha$).

In the other type of modification, the magnitude of the fluctuating lift coefficient is assumed to be given by the relationship:-

$$C_L(t) = \left[\overline{C}_{L_{\overline{\alpha} + \alpha_g(t)}} - \overline{C}_{L_{\overline{\alpha}}}\right] \cdot |S(k)| \qquad (5.3)$$

where $\overline{C}_{L_{\overline{\alpha} + \alpha_g(t)}}$ and $\overline{C}_{L_{\overline{\alpha}}}$ are the steady flow mean lift coefficients at incidences $\overline{\alpha} + \alpha_g(t)$ and $\overline{\alpha}$ respectively. If the $\overline{C}_L$ v. $\overline{\alpha}$ curve is a straight line (e.g. as in the aerofoil or D sections at low incidences, see Figs. 4.1 and 4.8), then Eqn. (5.3) gives the same result as Eqn. (5.2). If this is not the case, however, (e.g. elliptic model or aerofoil at high

incidence, see Figs. 4.18 and 4.1) the two equations give different answers. The idea underlying the above formulation is that the unsteady lift may be considered as an increment of the mean lift at the various incidences, with the wake effect represented only by a reduction in the lift amplitude (due to the $|S(k)|$ term). Again, this is correct in the limit $k \to 0$, because only then the instantaneous angle of incidence can be taken equal to $\bar{\alpha} + \alpha_g(t)$ and the wake effect can be neglected ($S(k) \to 1$).

Two refinements were applied in Eqns. (5.2) and (5.3) before making the comparison between the experimental and the predicted fluctuating lift coefficients. The one was to substitute α_g with the corresponding value at the mid-chord point, but with the tripod support system installed in the tunnel. The new gust amplitude is denoted by $\alpha_g(0, 0, 0)$ (see Fig. 3.14). This constitutes a simplified approach towards estimating the effect of the tripod support system, of which more will be said in Section 5.3.3. The other refinement was to replace $|S(k)|$ by an effective Sears function $|S_e(k)|$ which accounts for the lack of two-dimensionality of the gust (see Fig. 3.15). How $|S_e(k)|$ can be computed, will also be discussed in Section 5.3.3. With these two changes, Eqns. (5.2) and (5.3) become:-

$$C_L(t) = \overline{\frac{\partial C_L}{\partial \alpha}} \cdot \alpha_g(0, 0, 0, t) \cdot |S_e(k)| \qquad (5.2a)$$

$$C_L(t) = \left[\overline{C}_{L_{\bar{\alpha} + \alpha_g(0, 0, 0, t)}} - \overline{C}_{L_{\bar{\alpha}}} \right] \cdot |S_e(k)| \qquad (5.3a)$$

It will be seen later, that the corrections applied are negligible at higher frequencies, say $k \gtrsim 0.15$.

5.3.2 COMPARISON OF EXPERIMENTAL RESULTS WITH THE THEORY

The phase and centre of pressure results can be directly compared to Sears's theoretical results, see Section 2.3.1. For the comparison of the experimental lift results with the theory described previously, two methods were followed:-

- The first is an aerodynamic admittance approach which is defined here as:-

$$|A(k)| \equiv \sqrt{\frac{S_{C_L}(k)}{S_{\alpha_g}(k)}} \cdot \left(\frac{\overline{\partial C_L}}{\partial \alpha}\right)^{-1} \tag{5.4}$$

where S_{C_L} and S_{α_g} are the absolute spectral densities of the lift coefficient and gust amplitude respectively and $\overline{\partial C_L}/\partial\alpha$ the experimental mean lift curve slope of the particular model. Experimental values of this function can be found, if the experimentally obtained spectra of the lift and the upwash are substituted in Eqn. (5.4). The result will be the experimental aerodynamic admittance, which will be also denoted with the symbol $|A(k)|$. According to Eqn. (5.2), however, this experimental admittance is directly comparable (at the gust frequency) to the modulus of Sears's function, $|S(k)|$ which is the theoretical admittance. Such comparisons appear in Figs. 5.20 to 5.22. Another way to compute $|A(k)|$ is by dividing the corresponding RMS filtered values of the lift coefficient and the upwash, as recommended in Appendix B:-

$$|A(k)| = \frac{C_L}{\alpha_g} \cdot \left(\frac{\overline{\partial C_L}}{\partial \alpha}\right)^{-1} \tag{5.5}$$

- The second method is to compare directly the lift coefficients predicted from Eqns. (5.2), (5.3) or (5.2a), (5.3a) with those measured (either as raw or conditionally averaged over a large number of sinusoidal cycles). Since the phase was separately measured, the predicted lift coefficient was only compared in magnitude with that

measured. This was made by adjusting the position of the predicted $C_L(t)$ waveform in a cycle so as to coincide with the experimental (see Fig. 5.13). When the measured lift was obtained directly from the pen recorder, then a comparison was made only in terms of peak amplitudes.

5.3.2.1 THE NACA 0015 AEROFOIL AT ZERO INCIDENCE

(a) Unsteady Lift: The values of the experimental aerodynamic admittance computed by means of Eqn. (5.5) are plotted against reduced frequency in Figs. 5.20a, b, c and d for Re numbers 3×10^5, 2.2×10^5, 1.6×10^5 and 1.2×10^5 respectively. The value of $\overline{\partial C_L}/\partial\alpha$ corresponding to each Re number is marked on the plots. Three oscillating aerofoil amplitudes were examined. The modulus of Sears's function is plotted as a continuous line for comparison.

It is observed that $|A(k)|$ varies almost monotonically with k. At the lowest reduced frequency, $k \simeq 0.05$, $|A(k)|$ is smaller than $|S(k)|$ by a maximum 25%. For all but one Re number, as k increases there is a progressive convergence of $|A(k)|$ toward $|S(k)|$, up to about $k \simeq 0.3$, where many of the experimental results actually lie on the Sears's curve. Beyond this point, there is a tendency for the experimental admittance to slightly exceed $|S(k)|$. For Re = 1.2×10^5, however, the situation is different. All the admittance results are at least 20% lower than $|S(k)|$ and there is no sign of better agreement at high k, as occurred for the rest of the Re numbers. It will be recalled (see Fig. 4.1) that the mean loading in steady flow, at this particular Re number, was rather peculiar, in the sense that the $\overline{C}_L$ v. $\overline{\alpha}$ curve deviated from the straight line form, leading to an augmented $\overline{\partial C_L}/\partial\alpha$ equal to 7.2. This behaviour was attributed to the existence of two free separation points on the upper and lower surfaces near the trailing edge. A return to the "normal" behaviour was realised, once the oncoming

flow became turbulent. If it is assumed that the same thing happens (i.e. the $\overline{C_L}$ v. $\overline{\alpha}$ curve becomes a straight line, for low $\overline{\alpha}$, with $\overline{\partial C_L/\partial\alpha}$ $\simeq$ 5.7), soon after a low frequency sinusoidal flow is applied, then it would appear that a suitable value of $\overline{\partial C_L/\partial\alpha}$ to be used in Eqns. (5.4) or (5.5), is 5.7 instead of 7.2. If this is done, see Fig. 5.20d, then a much better agreement of $|A(k)|$ with $|S(k)|$ is obtained. Unfortunately, it is not possible to check how this new $\overline{\partial C_L/\partial\alpha}$ fits the very low k range, due to limitations in the frequency of the oscillating rig.

It was stated in Sections 3.3.4.3 and 5.2.1.2 that there appeared to be no significant effect of the Re number upon α_g or C_L. The same applies for the experimental admittance. The scatter of $|A(k)|$ for constant k and input amplitude, but different Re numbers, can, therefore, be discussed along the same lines as in the aforementioned sections, apart, of course, for the case of Re = 1.2 x 10^5, which has just been investigated.

For constant k and Re number, the scatter in $|A(k)|$, produced by varying the gust amplitude is at maximum 14%. Again, there is no clearly distinguishable effect of the gust amplitude upon $|A(k)|$, because sometimes the curves formed by the experimental points tend to cross each other. If the gust amplitude had some effect, and this is expected to vary smoothly with α_g (for small values of α_g), then the medium eccentricity results should not have tended to be the lowest (see Fig. 5.20), but lie somewhere in the middle. The results of Maeda and Kobayakawa (1970) for a NACA 0012 aerofoil in a sinusoidal upwash, do show a systematic effect of gust amplitude, in fact a drop of as much as 30% in $|A(k)|$ was realised when α_g was reduced from about 2.83° to 0.4° (k, Re constant). Although this reduction in α_g is much greater than that attainable in the present experiments (see Fig. 3.17), there is a suspicion about the accuracy of the results of Maeda and Kobayakawa

(1970) for two reasons: First, the gust variations were extremely slow, a maximum $k \simeq 0.017$ could only be reached. Under these circumstances the aerofoil behaves rather quasi-steadily and uniformly for reasonably low incidences. Second, the impression is given in the text (p. 387) that the lift and upwash measurements took place simultaneously, a fact that can seriously affect the consistency of results. The experimental admittance found by these authors for $\alpha_g \simeq 2.83^o$ is plotted in Fig. 5.20a and it is in good agreement with $|S(k)|$, if it is taken into account that a value of $\overline{\partial C_L}/\partial\alpha$ equal to 2π was used in Eqn. (5.5).

It was mentioned that the results shown were computed by means of Eqn. (5.6), i.e. the experimental values obtained by analogue filtering were used. Some of the digital analysis results are plotted in Figs. 5.20a, b. They almost coincide with the analogue filtering results at the higher reduced frequencies (note, not all points are shown), while at $k = 0.05$ approximately, they are greater by 8% maximum. This deviation expresses the difficulty in measuring spectral power at low frequencies and it was discussed in Appendix B . On the other hand, the close agreement at the higher frequencies ($k \gtrsim 0.1$) indicates that the analogue filtering method employed is meaningful for the kind of spectra encountered in this work.

Finally, an attempt was made to determine the aerodynamic admittance frequencies other than the gust frequency. For that purpose Eqn. (5.4) was applied at frequencies $2n_g$ and $3n_g$ (second and third harmonics respectively). The results (see Figs. 5.20a, b) are spread about the Sears's curve but the scatter is considerable. The strength of mechanical resonances appearing on the spectra (Figs. 5.2, 5.3) are of the same order of magnitude as the nearby harmonics and this is one of the main reasons of the noticed scatter. The fact that some of the $|A(k)|$ values are very close to the theoretical ones could well be

fortuitous, because some power in the higher lift harmonics is expected, even if no power at the corresponding frequency exists in the input (upwash gust).

(b) Phase: In Fig. 5.14 the experimentally determined phase for medium eccentricity is compared to that given by Sears' theory (see also Fig. 2.5). The results generally indicate a greater lag of sinusoidal lift behind the upwash than Sears's theory predicts. However, the variation with k has the correct trend up to k = 0.25 approximately, but beyond that point the phase appears to become rather constant, than follow the theoretical trend. The existing scatter does not permit any definite suggestion about the effect of Re number.

(c) Centre of Pressure: As reported in Section 5.2.3, from qualitative observations only, it can be said that the centre of pressure was located near the quarter chord point, being always at the mid-span plane. This agrees with Sears's theory, which predicts a centre of pressure permanently fixed at the quarter chord point.

(d) Summary: The experimental data presented for the aerofoil are in support of the proposed theoretical model. Particularly good is the agreement in the interval $k \simeq 0.15 - 0.4$. The possible sources of discrepancy between theory and experiment over the frequency range examined will be discussed in Section 5.3.3.

5.3.2.2 THE D SECTION CYLINDER

(a) Unsteady Lift: The experimental admittance results are shown in Figs. 5.21a, b, c and d. The same flow parameters and notation were used as in the aerofoil case. There are only minor differences in the admittances of these two models, except for the lowest flow speed ($Re = 1.2 \times 10^5$), where, as mentioned in the previous section, the admittance of the aerofoil was significantly lower than $|S(k)|$. No such

thing occurs for the D section, $|A(k)|$ is near $|S(k)|$ within close limits. The D section admittances, having the same degree of scatter are somewhat higher than the corresponding aerofoil ones for which there is also evidence that $|A(k)|$ is falling off slightly faster at the higher reduced frequencies. A drop in $|A(k)|$ below $|S(k)|$ at the lowest frequencies is also observed here.

There is actually little that can be added to what has been said about the aerofoil, for the effect of Re number and gust amplitude on $|A(k)|$; no systematic effect could be traced. The same applies to the agreement between the values of $|A(k)|$ obtained by analogue and digital methods (see Figs. 5.21a, b), except for one point, at $k \simeq 0.4$ and $Re \simeq 2.2 \times 10^5$ (Fig. 5.21b). There, the two methods give results differing by 7.5%, the digital one being the lowest. Since such a discrepancy was not realised at other, similarly high frequencies, the digital analysis point may be discarded, as a rather bad point, which means that indeed the D section admittances do not drop as fast as the aerofoil ones at high k.

Some of the admittance results at the higher gust harmonics are quite close to the Sears's function, while others deviate too much, more than the corresponding aerofoil values. The probable reasons were stated in Section 5.2.1.1b. The sinusoidal lift coefficient, as predicted by Eqn. (5.2a) for $k = 0.22$ is compared with the experimental in Fig. 5.13. The agreement is very good (compare also with the closeness of the admittance results). There are only small differences in the peak levels, which can be attributed to factors discussed in Section 5.2.1.3a.

(b) Phase: The comparison between the experimental and theoretical phase results leads to the same comments made previously for the aerofoil, with the difference that here the lag of the lift is on average greater for the D section.

(c) Centre of Pressure: From Fig. 5.13, it can be seen that the chordwise position of the centre of pressure deviates significantly from the predicted quarter-chord position. If the difference of sinusoidal pressures on the upper and lower surfaces of the cylinder were tuned to the same phase along the chord (as it should happen theoretically for a thin aerofoil, see Graham, 1970b), then x_{cp}/c should have been a constant. The absence of this in Fig. 5.13a suggests that the detailed loading may deviate from that predicted by thin aerofoil theory.

(d) Summary: The agreement between the experimental and theoretical unsteady lift results is as good as that observed for the aerofoil. A frequency range of particularly close agreement also exists here, i.e. $k \simeq 0.1 - 0.3$. However, although the unsteady lift is successfully predicted there is indication that the detailed unsteady load distribution might deviate significantly from the theoretical.

5.3.2.3 THE ELLIPTIC CYLINDER

(a) Unsteady Lift: The experimental aerodynamic admittance of the elliptic cylinder is displayed in Figs. 5.22a, b, c and d. For the flow parameters employed etc., see the appropriate aerofoil section. With two exceptions, $|A(k)|$ deviates seriously from $|S(k)|$ in both magnitude and rate of variation with k. The two exceptions refer to the cases, where the Re number is the highest ($= 3 \times 10^5$), or the model is fitted with trip wires (Figs. 4.18 and 5.1). Only then the agreement between the theoretical and experimental results is similar to that obtained for the aerofoil and D cylinder. It is also noteworthy that only then $\bar{C}_L$ varies linearly with $\bar{\alpha}$ for moderate incidences. At all the other cases $|A(k)|$ underestimates $|S(k)|$ by a factor ranging from 20% to 400%, the greater deviation occurring at the highest frequencies. Attempts to adjust the overall level of $|A(k)|$ by feeding a different

value of $\overline{\partial C_L}/\partial\alpha$ in Eqns. (5.4) or (5.5) did not improve the situation. For example a value of $\overline{\partial C_L}/\partial\alpha = 8.37$ was tried, which is the potential flow result for an elliptic cylinder of fineness ratio 3.0, with a stagnation point at the trailing edge (Eqn. (4.8)). A reasonable agreement between $|A(k)|$ and $|S(k)|$ is obtained only in a small range of reduced frequencies. Note that the apparently good agreement at the lowest frequencies of Fig. 5.22b ($Re = 2.2 \times 10^5$) with $\overline{\partial C_L}/\partial\alpha = 8.37$ is rather misleading: an underestimation of $|S(k)|$ is expected at these frequencies for reasons explained in Section 5.3.3. At least this is seen to be true for the aerofoil and the D cylinder (Figs. 5.20 and 5.21).

There is no clearly evident effect of the gust amplitude upon $|A(k)|$. However, although for the aerofoil and the D cylinder the medium eccentricity $|A(k)|$ results tended to be the lowest, here it is the large eccentricity values which generally are lowest at the higher frequencies. This might be of some significance if Eqn. (5.3) really holds, because the higher the mean incidence, the lower is the rate of increase of the lift coefficient of the elliptic cylinder at Re numbers between 1.6×10^5 and 2.2×10^5 (see Fig. 4.18).

The analogue and digital results for $|A(k)|$ (Figs. 5.22a, b) are in good agreement at the higher frequencies, while at the lowest frequencies ($k \simeq 0.05$) there is a discrepancy, the digital results being the greater. See also the section on the aerofoil.

The admittances computed at the higher gust harmonics are spread about Sears's function with the same degree of scatter found previously in Sections 5.3.2.1 and 5.3.2.2.

In Figs. 5.13b, c, d, e and f the experimental lift coefficient is compared to that predicted by Eqn. (5.3a) for $Re = 2.2 \times 10^5$ and medium eccentricity. Despite the corrections to α_g and $|S(k)|$ involved, the experimental lift coefficient is still overestimated at all frequencies.

The discrepancy in the peak levels progressively increases with increasing k, being approximately 30% at k ≃ 0.065, 40% at k = 0.17 and again 30% at k ≃ 0.22. This recovery at the higher k might be due to the decrease in the local $\overline{\partial C_L}/\partial\alpha$ of the elliptic cylinder as the mean incidence increases (Fig. 4.18). It is noticed that C_L is also overestimated when the value of $\overline{C}_L$ entering Eqn. (5.3a) refers to the sinusoidal flow. Indeed, the lines appearing as "LEVEL A" and "LEVEL B" in Fig. 5.13f represent the predicted peak lift amplitude from Eqn. (5.3a), according to whether the $\overline{C}_L - \overline{\alpha}$ curves in sinusoidal flow are computed from total load or surface pressure measurements respectively (extrapolated data from Fig. 4.18 are used).

(b) Phase: There is a rather fortuitous good agreement with Sears's theory up to about k = 0.1, see Fig. 5.16. At higher reduced frequencies the lag of the lift behind the upwash is large and tends to vary in the opposite direction than Sears's theory predicts. The discrepancy is certainly greater than the one realised for the aerofoil and the D section.

(c) Centre of Pressure: The deviation from Sears's theory is even worse than in the D section. From Figs. 5.13d and f it is observed that the centre of pressure is in the region of 0.4 c, compared to 0.25 c, predicted by the theory. Figs. 5.13d and f also indicate that the detailed loading is not likely to follow the thin aerofoil loading.

(d) Summary: Except when certain special conditions relating to the behaviour of the boundary layer are met, the proposed theoretical model results in a consistently greater lift than that observed. The discrepancies are greater, the higher the reduced frequency, in contrast to what has been realised for the aerofoil and the D section. The "special" conditions mentioned above refer to either the boundary layer transition being fixed (e.g. by means of trip wires), or the flow departing from

the critical regime (this happens for Re approximately greater than 3×10^5, see Fig. 2.3). In both cases, the Re number is effectively or truly increased.

5.3.3 SOURCES OF DISCREPANCY BETWEEN THEORY AND EXPERIMENT

In this section the sources of discrepancy between theory and experiment are explored and, where possible, quantitative accounts are given. Two main categories of discrepancies are distinguished: Those originating from incomplete theory and those from inaccurate measurements.

A. Incomplete theory.

1. Viscous effects and the unsteady Kutta-Joukowski condition.

Among the assumptions of the theory, one which is not actually fulfilled is that of the perfect fluid. It is partly due to this reason, that full potential lift is not achieved on an aerofoil at incidence in a uniform steady flow, as discussed in Section 4.2. Examining the effects of viscosity on the Theodorsen's function, Giesing (1968) found that the experimental unsteady lift was lower than the theoretical over the entire frequency range (though, as he points out, the lift reduction would be less severe if the reduction in the quasi-steady lift had been taken into account) while large discrepancies in the phase occurred only in the high frequency range. Spurk (1964) reported that the discrepancy between his experimental results (dealing with the unsteady loading of oscillating aerofoils of various thicknesses) and the inviscid theory of Küssner and Gorup (1960) was mainly due to viscosity, particularly for Re numbers less than 3×10^5. He observed, however, that the agreement was good if the boundary layer transition was kept fixed by using trip wires.

The author's experiments show that the effects of Re number and consequently those of viscosity depend on the particular type of test

model. In situations where the separation points are fixed, the unsteady lift results are substantially independent of the Re number. The modification applied to Sears's formula (Eqn. (5.1)), i.e. the replacement of 2π by the experimental mean lift curve slope, was made in the sense that the effect of body thickness was similar and that the boundary layers behaved quasi-steadily (for gust frequencies well below those of vortex shedding). A measure of the quasi-steadiness in a boundary layer may be obtained by examining the ratio of the time it takes for a streamwise velocity disturbance (applied at the edge of the boundary layer), to diffuse through it, to the time required for this disturbance to change. F. K. Moore* analyzed this problem in detail and derived the conditions, under which the oscillatory flow over a flat plate could be considered as quasi-steady. The ratio mentioned previously was expressed by Moore by the parameter $(\delta^2/\nu) \cdot \left|(\partial U_e'/\partial t)/U_e'\right|$, where δ is the boundary layer thickness, U_e' the total unsteady streamwise velocity at the edge of the boundary layer, and ν the coefficient of diffusion in the fluid (equal to the kinematic viscosity for the case of a laminar boundary layer). A necessary condition for quasi-steadiness is that this parameter should be much less than unity. In order to get a rough idea of how reasonable is the assumption of boundary layer quasi-steadiness made is the present case, it will be attempted to use this parameter for the elliptic cylinder. Boundary layer measurements at constant gust amplitude and not close to separation, indicated that for $Re = 2.2 \times 10^5$, $\delta = O(c/100)$ and that the amplitude of the streamwise sinusoidal fluctuations at the edge of the boundary layer were of the order 3% of the mean velocity at this position. Hence, this parameter would be of the order $6 \times 10^{-6} \times k \times Re = 1.32\ k$, which suggests that

---

* "Unsteady laminar boundary layer flow", NACA TN 2471, 1951.

for reduced frequencies of, say, greater than 0.1 (at this particular Re number) the boundary layer may not be treated as quasi-steady.

The comparison between the theoretical and experimental admittances for the aerofoil and the D section (Figs. 5.20, 5.21) indicates that the assumption of a quasi-steady behaviour of the boundary layers does not lead to conflicting results. Further, the observed good agreement suggests that an equivalent Kutta-Joukowski condition can be applied at a position mid-way between the fixed separation points of the D section. This means that the vortex sheets shed from the two sharp trailing edges can be replaced by single vortex street consisting of their superposition, but placed along the extension of the cylinder chord line.

Things are quite different for the elliptic cylinder which has two free separation points. Here, not only the unsteady lift and the experimental admittances depend on the Re number, but there is a serious disagreement between the theoretical and experimental results. Viscosity can affect not only the mean position of the separation points, but their unsteady movement as well, with corresponding consequences on the mean and instantaneous position of the shed shear layers.

It is anticipated, that if the mean separation points are located well towards the rear, the boundary layers and the free shear layers are thin and close to the extension of the chordline, then the thin aerofoil theory would apply better. The fact that the experimental admittances of the elliptic cylinder agree better with the theoretical ones, when the Re number is high or the boundary layer is disturbed by means of trip wires (hence a delay in separation), is in support of this argument.

Eqn. (2.2) in Chapter 2, shows that the rate of change of circulation round the body (and accordingly the unsteady lift) depends

on the velocity at separation and the velocity of the separation points. The latter velocity would be zero only for the models with fixed separation points (aerofoil, D cylinder). For the elliptic cylinder, the separation points are expected to perform an unsteady movement on the surface with a velocity, phase and amplitude which, if all other parameters are fixed, would depend on how rapid are the changes of incidence in the free stream. On quasi-steady terms, the difference in $d\Gamma/dt$ found from Eqn. (2.2) by assuming first a periodic movement of the separation points and second no movement at all, is not insignificant for changes of incidence of, say 4^{o} (see Fig. 4.12). It may be argued that, as the boundary layer frequency parameter gets higher, the separation points would adjust themselves less readily to their steady flow positions, until at a certain frequency parameter, their motion may even cease. A lag in the adjustment of the separation points of a circular cylinder, exposed in a stream of rapidly changing incidence, leads to the development of an unsteady lift; specifically, to an increase of the unsteady lift from its zero value, when the incidence changes are quasi-steady. By analogy, it could also be argued that an increase in the unsteady lift of the elliptic model might be expected, when, at high enough boundary layer frequency parameters, a lag in the adjustment of the separation points appears. However, the experimental admittances of the elliptic cylinder tend to become gradually lower than the predicted, as the reduced frequency increases (see Fig. 5.22); large discrepancies are also noticed for the phase, at high reduced frequencies (Fig. 5.16). The previous arguments, therefore, appear to contradict the experimental observation.

In an attempt to clarify this point two further experiments were planned: First a boundary layer experiment with the elliptic cylinder and second, an unsteady loading experiment with a NACA 0015 aerofoil

placed at high incidence.

- Boundary layer experiment: With this experiment on the elliptic cylinder, it was hoped to establish how the amplitude of the movement of the separation points could be affected when the reduced frequency (at constant gust amplitude and Re number) was changed. For this purpose the instantaneous u boundary layer velocity profiles were measured as the (experimentally determined) mean separation point was approached. The instantaneous velocity profiles were constructed by measuring the unsteady velocity at predetermined intervals in one period of the gust and always at the same phase, for several positions inside the boundary layer (see also Appendix B and Fig. B-1) and averaging over a large number of periods. If during part of the cycle the hot-wire encounters a reversed flow (manifesting itself by the rectified shape of the anemometer output, see for example Tutu et al (1975), McCroskey et al, 1976) then this would mean that the separation point has at least reached the position where the hot-wire is placed. Thus, it was hoped that the amplitude of oscillation of the separation points would be estimated, by counting the number of "reversed" profiles in one cycle and compare the results for different streamwise positions and reduced frequencies. Unfortunately, it was found that it was very difficult to judge which velocity profiles were "reversed" and which not, see Figs. C-2 to C-10. To this difficulty in distinguishing the instantaneous profiles contributed the appearance of spikes and the measurement inaccuracies (such as the effect of loss of heat from the wire to the surface), which are discussed in Appendix C. Therefore, no definite conclusion can be drawn about the unsteady movement of the separation points from this test, though it is felt that a certain lag as well as a change in the amplitude of their movement does occur with changes in the reduced frequency.

- Unsteady loading experiment: A NACA 0015 aerofoil (chord = 0.152 m, span = 0.280 m) was placed at high incidences and its fluctuating lift was measured (see also Appendix C). At incidences near stall one of the separation points is located at the trailing edge and the other is free to move on the upper (suction) surface. The purpose of this test was to examine what would be the significance of a single free separation point on the development of unsteady lift. The results, appearing in Figs. C-11 and C-12A, B, C, indicate that, unlike the case of the ellipse, the unsteady lift remains considerably greater than the predicted at high reduced frequencies. (In fact the results are presented in the time domain and consequently include the energy of other frequencies, besides that at the gust frequency, but it is clear that the unsteady lift at the main frequency is strong. In later sections, there are given reasons for which the unsteady lift on an aerofoil at incidence is expected to be augmented; these reasons partly explain the high lift values observed here). Maeda and Kobayakawa (1970), have tested a NACA 0012 aerofoil at incidences up to 9^{o}, but their results are limited to very low frequencies (see Fig. 5.20a), and cannot be compared with the present ones. However, the information available for oscillating aerofoils at high incidence (e.g. Carta (1967), Moss and Murdin (1968), McCroskey et al, 1976), or for aerofoils of which the incidence changes suddenly from the rest (e.g. Farren (1935), Kawashima et al, 1978), indicates that large values of unsteady lift are found, especially at rapid changes of incidence. Under these conditions the delays in the boundary layer separation and reattachment are important. It has been established, that the predominant feature of such flows (called dynamic stall flows), is the shedding of a strong vortex-like disturbance from the leading edge region, which, during its chordwise passage over the aerofoil surface, helps a suction to be maintained and

hence a high lift. It may be that a similar mechanism accounts for the considerably increased unsteady lift obtained in the present tests (see Fig. C-12C, $\bar{\alpha} = 13.5^{0}$, especially for Re = 1.2×10^{5}). Even if no complete temporary separation has occurred, an oscillation of the free separation point should have taken place. The fact that, at high frequencies, (Re = const.), a different kind of behaviour was found for the aerofoil at high incidence and the ellipse, is an indication, that the relative movement of the separation points (with respect to each other), might also be an important factor. This relative movement could affect the instantaneous position of the shed shear layers and their vorticity both in magnitude and relative phase. Accordingly, the contribution to the unsteady lift from the vortical wake (assumed in the proposed theory to consist of the superposition of the two vortex layers and lie on the extension of the chordline), would be different for the two bodies. This matter is again raised in the next section (see also Appendix D). The different behaviour of the phase for the ellipse (Fig. 5.16) and the aerofoil at incidence (Fig. C-11), should also be connected to the wake effect.

The experimental results for the elliptic cylinder and the discussion given previously, suggest that the application of an "equivalent" Kutta-Joukowski condition at a fixed, "effective" trailing edge (located at the position of minimum radius of curvature of the cylinder), is not the appropriate one. Perhaps a better approach would be to look for an "effective" trailing edge moving with an appropriate phase, somewhere between the separation points of the cylinder; this could take more effectively into account the regions of separated flow over the cylinder, which are neglected in the present approach. It would be necessary, however, to have first a better knowledge as to how the separation points behave, over the frequency range of interest.

A final point concerns the application of the Kutta-Joukowski condition for the aerofoil in unsteady flow. A deviation from this condition (i.e. the tangential flow departure from the aerofoil surface) may occur only at extremely low Re numbers (for example, during a start of motion) or at very high frequencies (see for example Bechert and Pfizenmaier, 1975).

2. Wake deformation and thickness effects.

According to thin aerofoil theory the vorticity shed is convected downstream with the free stream speed along the extension of the chord line. This obviously cannot happen with the bluff bodies or the aerofoil at high incidence. But even for the NACA 0015 aerofoil at zero incidence, the initially straight vortex street may roll up further downstream, leading to the formation of discrete vortices. The deformed wake is a source of non-linearities, like the appearance of higher harmonics in the lift spectra, which are not accounted for by Sears's theory. Theoretical (e.g. Giesing, 1968) and experimental (e.g. Bratt, 1950) work on oscillating aerofoils, shows that the wake deformation depends on the reduced frequency and amplitude of oscillation, getting worse as these parameters increase. Corresponding information relating to the unsteady flow about a stationary model is very scarce. The numerical calculations of Giesing (1968) indicated only a small deformation in the wake of a thick aerofoil, which entered at constant speed a relatively very strong sharp-edged upwash gust, and an even smaller effect on the unsteady lift. Since in the present work the unsteady incidences were low to moderate (see Fig. 3.18), it is not unreasonable to expect only a small contribution from the deformation of the wake. The very little power which exists in the higher harmonics of the zero incidence lift spectra supports this argument.

In the theoretical model proposed here, the effect of body shape

on unsteady lift was simply incorporated in $\overline{\partial C_L}/\partial\alpha$. Of course, in a more sophisticated approach the shape (and consequently the thickness) of the model should affect the unsteady lift in a non-linear manner if the boundary conditions on the surface are not linearized. For the symmetric models examined in this work, the effect of thickness is of interest. Maeda and Kobayakawa (1970) calculated the effect of thickness on a NACA 0012 aerofoil and the aerodynamic admittance is plotted in Fig. 5.23, where it is compared with $|S(k)|$. It is seen that thickness causes a decrease in $|A(k)|$ below $|S(k)|$, but unfortunately the analysis of Maeda et al was limited to $k < 0.02$, so that a comparison with the author's experimental results cannot be made. To obtain an approximate idea about the influence of thickness on the unsteady lift of an aerofoil for higher k, aerodynamic admittances were computed from calculated values of Küssner's function, K, existing in the literature. This function gives the dimensionless lift development on an aerofoil travelling through a sharp-edged gust and its calculated or plotted values for various aerofoil shapes can be found in Karman and Sears (1938), Drischler (1956), Arnoldi (1969), Bisplinghoff et al (1958), Giesing (1968) and Basu and Hancock (1977). If it is assumed that the gust boundary is not affected by the body and its wake and that the wake deformation does not exist (refer to the discussion above) then there is a reciprocal relationship between K and $A(k)_t$, the complex aerodynamic admittance, (see for example Drischler (1956) and Bisplinghoff et al, 1958), because the sharp edge gust can be thought of as a superposition of sinusoidal gusts. The relationship is:-

$$A(k)_t = \left[1 + ik \int_0^\infty \left(K(s_1) - 1\right) e^{-iks_1}\, ds_1\right] e^{ik} \qquad (5.6)$$

where $s_1 = 2U_\infty \cdot t/c$ is the distance in semi chords travelled by the aerofoil after its leading edge first encounters the gust. As there is no closed algebraic form for $K(s_1)$, exponential approximations had to be used. The cases tested included a flat plate, an 8.4% thick von Mises aerofoil and a 25.5% thick Joukowski aerofoil. The flat plate was employed in order to check the accuracy of the method, and the pertinent function is (see for example Drischler, 1956):-

$$K(s_1) = 1 - 0.236e^{-0.058s_1} - 0.513e^{-0.364s_1} - 0.171e^{-2.42s_1} \quad \text{(flat plate)} \tag{5.7}$$

The approximations to $K(s_1)$ for the two thick aerofoils were obtained by fitting mathematical curves to the plotted results of Giesing (1968). Since Giesing presents his results for $s_1 \leq 4.0$, there is no means of checking the asymptotic behaviour of $K(s_1)$, a fact that limits the accuracy of the method. The approximations to $K(s_1)$ are:-

$$K(s_1) = 1 - 0.24e^{-0.058s_1} - 0.55e^{-0.364s_1} - 0.17e^{-2.42s_1} \tag{5.8}$$

for the von Mises aerofoil, 8.4% thick, and:-

$$K(s_1) = 1 - 0.274e^{-0.058s_1} - 0.695e^{-0.364s_1} - 0.003^{-2.42s_1} \tag{5.9}$$

for the 25.5% thick Joukowski aerofoil. It appears from these equations that the thicker the aerofoil the longer it takes for the unsteady lift to build up. The absolute values and the arguments of the corresponding theoretical aerodynamic admittances are plotted in Figs. 5.23 and 5.24 respectively. The original Sears's function is accurately predicted from Eqns. (5.6) and (5.7) for $k \lesssim 0.4$. For higher reduced frequencies increasing discrepancies appear. This means that the aerodynamic

admittances for the thick aerofoils are also not likely to be accurate beyond that point. As was found by Maeda and Kobayakawa (1970), $|A(k)_t|$ is less than $|S(k)|$ for a thick aerofoil. If this trend is assumed to hold for the bluff sections as well (which are 33.3% thick), then even greater reductions in $|A(k)_t|$ than those plotted in Fig. 5.23, should be expected. It is true that a drop in the experimental admittance was found in the author's experiments (see Figs. 5.20 to 5.22) for low k, but it is too much to be attributed to this effect only. For high k, a further drop of $|A(k)_t|$ below $|S(k)|$ is predicted, which conflicts with the rise found experimentally (for the aerofoil and D sections). Fig. 5.24 shows that the phase lags increase with model thickness. The predicted phases are here of the order found in the experiment (Figs. 5.14, 5.15 and 5.16).

There are also many individual factors which render the lift response of a flat plate at zero incidence different from that of a thick model and of those, three will be discussed here: Pressure gradients (in the undisturbed flow), "virtual mass" and vorticity distortion effects.

(a) Due to the first effect, the existence of an unsteady pressure gradient in the undisturbed flow in the upwash direction would generally lead to an unsteady lift force for a thick model, but not for a flat plate. The oscillating rig produces a gust which, theoretically, has zero pressure gradients (Section 3.4.4) and, therefore in this respect a flat plate aerofoil and one of arbitrary thickness should behave (theoretically) in the same way.

(b) The second effect would arise from the fact that the "virtual mass" of a thick body is different from that of a flat plate. The associated forces (termed here as "acceleration" or "inertial acceleration" forces), are those that would have been encountered, if

there was no production of circulation, due to the unsteady flow round the body. (These can be better visualized for a body oscillating in an inviscid fluid, with no production of circulation, e.g. a normal flat plate oscillating in the free stream direction).

In the present problem, the contribution due to "inertial acceleration" has been calculated for a flat plate aerofoil with the help of formulae derived by Karman and Sears (1938), Bisplinghoff (1958) and Neumark (1952) (for details, see Appendix D). Sears's function was split into a quasi-steady term S_B (representing the unsteady lift, which would be produced, if the effective incidence due to the gust was permanently maintained), a wake term S_A (representing the influence of the unsteady wake) and an "acceleration" term S_C. By adding these (complex) terms together Sears's function is recovered, see Figs. 5.25 and 5.26. It is shown in Appendix D that the "acceleration" term behaves as $J_1(k)$, i.e. it starts from zero, when the aerofoil is exposed to a steady flow and, as k increases, it is oscillating about zero with diminishing amplitude. By contrast, the "acceleration" forces for an oscillating model become increasingly important as the frequency gets higher. This distinct behaviour can be explained by imagining that at certain frequencies equal parts of the sinusoidal gust are accelerating in opposite directions, so that the net effect becomes zero. The question now is how much the "acceleration" term found can be influenced by an increase in the model thickness. The only relevant existing information is about the oscillating aerofoil case, again from the numerical calculations of Giesing (1968). He found that going from a flat plate aerofoil to a 25.5% thick Joukowski aerofoil, the amplitude of the "acceleration" forces was reduced by 1% for translatory oscillation and by up to 7% approximately for pitching harmonic oscillations (this figure diminishing as the frequency

increased). Therefore, it is reasonable to assume that for the NACA 0015 aerofoil the "acceleration" term would not be much different from that of the flat plate, if both are exposed to the same sinusoidal flow. There could be an effect on the bluff bodies, which are 33.3% thick, which, it is thought, should be of the order of the figures given above. Part of the increase of $|A(k)|$ above $|S(k)|$ at the higher frequencies (aerofoil and D section, Figs. 5.20 and 5.21) may be due to this effect.

At this point, an attempt was made to see whether the experimental admittances were better predicted, if it was assumed that only the quasi-steady term S_B was affected by the body shape according to $\overline{\partial C_L}/\partial\alpha$. Eqn. (5.2) would then become:-

$$C_L(t) = \alpha_g(t) \cdot \left| 2\pi \, (S_A + S_C) + S_B \cdot \overline{\partial C_L}/\partial\alpha \right| \tag{5.10}$$

and from the definition of the admittance (Eqns. (5.4) or (5.5)):-

$$|A(k)_t| = |S_m(k)| = \left| (\overline{\partial C_L}/\partial\alpha)^{-1} \cdot 2\pi \cdot (S_A + S_C) + S_B \right| \tag{5.11}$$

where the theoretical admittance $S_m(k)$ can be termed as "modified Sears's function". $S_m(k)$ is plotted in Fig. 5.27 along with the original Sears's function. From Figs. 5.14 to 5.16, 5.20 to 5.22 and 5.27 it is observed that, at very low k, $S_m(k)$ becomes almost equal to $S(k)$. $S_m(k)$ is not a good estimate of the experimental results for the elliptic section. The increase in $|A(k)|$ of the D section at high k is reasonably predicted by $|S_m(k)|$, but not the drop at low k, while the predicted phase lags from the argument of $S_m(k)$ are too small. For the NACA 0015 aerofoil $|S_m(k)|$ predicts a drop below $|S(k)|$ at high frequencies, which is not realised. The phases are rather more accurately predicted. These

results show that it is unlikely for the quasi-steady term to be the only one affected by changes in the model shape and thickness.

(c) The third effect comes from the distortion of the vortex sheets (shed by the oscillating aerofoils), after the models are placed between them. This would not occur if the models were of zero thickness and at zero mean incidence. The displacement of the vortex sheets will modify the unsteady upwash and with it the unsteady lift and phase; if the displacements are not symmetric with respect to the central line, so will be the variation of the lift coefficient with time. An estimate of this effect can be made, if it is assumed that the flow is inviscid and no vortex rolling-up occurs. Then the, new, mean positions of the vortex sheets can be obtained from the perturbed position of the streamlines in steady flow (note that the vorticity acquired by the fluid element remains attached to it during its inviscid motion). Here, the case of the elliptic cylinder and the aerofoil at high incidence are examined. The corresponding steady potential flow streamlines, which are coincident with the two parallel vortex sheets in the undisturbed flow, are plotted in Fig. 5.28. Following a simplified approach, the observed outward expansion of the sheets could affect the unsteady flow in two ways: First, a change in the gust amplitude at the mid-chord point would occur, because as it was found in Section 3.4.3, α_g depends on $e^{-2k'z/c'}$ (see also Fig. 3.20). This effect would become more important as k increases. For example, if it is assumed that the vortex sheets are on the whole uniformly displaced by the maximum amount indicated in Fig. 5.28, while maintaining their original straight shape, then the reduction in the gust amplitude at the mid-chord point, for $k = 1.0$, would be approximately 3% for the elliptic cylinder and 25% for the aerofoil at incidence. Second, the change in the (theoretically sinusoidal) distribution of vorticity in the distorted region would

affect both the gust intensity and the phase between the lift and the upwash. An estimation of this effect can be obtained if the times taken for a fluid particle to travel along the distorted and undistorted streamlines between two fixed positions, is known. The difference of the times taken can be compared with a time scale, such as the period T_g of the sinusoidal flow. Roughly, it was estimated that the aerofoil at incidence ($\bar{\alpha} = 14^o$) would cause again a greater distortion than the elliptic cylinder. For decreasing reduced frequency this distortion effect would become less important. Concluding, it can be said that in the zero incidence experiment, none of the effects described in this paragraph is likely to cause significant discrepancies between the theoretical and the experimental results. In the high mean incidence tests, the vorticity distortion effect should be included in the main reasons for the discrepancies encountered.

3. Lack of two-dimensionality.

The type of unsteady flow assumed in Sears's theory cannot be exactly realised in the experiment. At first, there is no such thing as a perfectly spanwise correlated sinusoidal gust. Indeed, the cross spectrum of the upwash, Fig. 3.15, indicates a lack of correlation across the span, though a mild one. This is most probably caused by a random change in the inclination of the gust fronts as they travel downstream. Therefore, a slight dependence on a random spanwise reduced frequency should be expected. In that case the theoretical aerodynamic admittance for a flat plate aerofoil can be calculated from Eqn. (2.20), provided the cross spectrum of the upwash, the model aspect ratio and the response function $G(k_1, k_2)$ calculated by Graham (1970a) for the response to a yawed sinusoidal gust are known (see also Fig. 2.6). Here, since the lack in two-dimensionality is only mild, it is reasonable to assume that each chordwise station responds

according to Sears's theory, feeling only the upwash fluctuations local to it (strip theory). Jackson, Graham and Maull (1973) derived a simple expression, replacing Eqn. (2.20), which with the symbols used here is:-

$$|A(k)_t| = |S(k)| \cdot \left[\int_0^2 R_{ww}(n_g, y') - \frac{1}{2}\int_0^2 R_{ww}(n_g, y')\, y'\, dy'\right]^{\frac{1}{2}} \qquad (5.12)$$

where $y' = y/(s/2)$. This theoretical admittance is then a correction to Sears's function and is equal to the function $|S_e(k)|$ of Eqns. (5.2a) and (5.3a). The cross spectrum of the upwash fluctuations at the gust frequency (assuming that the field is homogeneous, i.e. that the cross spectrum depends on $\Delta y'$ rather than y'), was approximated by a curve of the form $e^{c_1 y'^{c_2}}$ (c_1, c_2 constants to be determined), which was fitted to the experimental results of Fig. 3.15. Note, that for such high spanwise correlations the size of reduction in $|S(k)|$ should not depend too much on the choice of the fitted function, as pointed out by Jackson (1970). The theoretical admittance obtained from Eqn. (5.12) is plotted in Fig. 5.23 along with Sears's function modulus. It is observed that $|A(k)_t|$ approaches $|S(k)|$ from below as k increases, the maximum deviation being about 5%, at $k \simeq 0.06$. The variation of $|A(k)_t|$ agrees now better with the variation of the experimental admittances, shown in Figs. 5.20 to 5.22. Although the experimental admittance still remains lower at small values of the reduced frequency, the lack of spanwise correlation is thought to be one of the main reasons for this discrepancy.

The same effect on the aerodynamic admittance, would occur for a not correctly aligned model with respect to a perfectly two-dimensional gust. Every effort was made to install the test models such that their leading edge would be parallel to the trailing edge of the oscillating

aerofoils. Assuming an error of one or two degrees, the effect on the admittance should be negligible (see for example Edwards, 1972).

4. Tunnel interference effects.

In the theory it is assumed that the unsteady flow field is of infinite extent in all directions, while in reality the tests were undertaken in a wind tunnel of finite dimensions. A deviation from the theory is expected due to a variety of effects such as the wall and tripod support system interference, the influence of the oscillating aerofoils and the finite extent of the unsteady wake shed by the test models.

Mention was made in Section 5.1 about a method of blockage correction developed by Kullar (1978) for a flat plate aerofoil in an unsteady inviscid flow. He employed the method of images, which simulate the walls parallel to the plane of the aerofoil, and required the boundary conditions on the aerofoil to be satisfied as in the classical thin aerofoil theory. The result is a correction to Sears's function involving terms of the order $(c/h)^2$, $(c/h)^4$, $(c/h)^6$, etc. In the developed formula the first term is only retained and the value suitable to the author's experimental arrangement is fitted ($c/h = 0.125$). The corrected Sears's function (denoted with the same symbol, i.e. $S(k)$) is plotted in Figs. 5.23 and 5.24. Its absolute value is greater than $|S(k)|$ in the low frequency range, while at the higher frequencies, the two functions tend to become equal. As $k \to 0$, the correction tends to the steady flow result. The maximum correction to $|S(k)|$ does not occur for $k = 0$, but for some low frequency (which is difficult to establish due to a lengthy series summation required at low frequencies). The same trend is observed in the results of Reissner (1947) relating to blockage corrections for oscillating aerofoils. The unsteady corrections indicated by Fig. 5.23, show that the quasi-steady corrections applied to the present experimental admittances, after the wake blockage

and thickness effects are excluded, tend to slightly undercorrect $|A(k)|$ at low k and slightly overcorrect $|A(k)|$ at high k. On the other hand, the corrected phases, shown in Fig. 5.24, tend to agree better with the experimental ones for low to moderate frequencies, since an increase in the phase lag due to blockage is predicted.

In Section 3.3.4.2, it was found that the effect of the tripod support system was to decrease the intensity of the upwash over almost the whole area occupied by the models, with the lower frequency being the mostly affected. The uniformity of the gust intensity was also impaired in all three directions (Fig. 3.14). This fact was not taken into account in the computation of the experimental admittances, because the "empty" tunnel values of α_g were used. A simple correction would be to employ an "effective" gust amplitude equal to the arithmetic mean of values distributed across the span. Taking for example the case for k = 0.088 in Fig. 3.14, it turns out that all experimental admittances should be increased by 3% approximately, thus moving closer to $|S(k)|$. In fact, since there is also some drop in α_g below the centre line (see Fig. 3.14), the correction involved should be somewhat greater, especially for the thicker bodies.

Effects on the unsteady lift, arising from the proximity of the test models to the oscillating aerofoils, are not thought to be significant. The relevant distance is about six oscillating aerofoil chord-lengths (see Fig. 3.8). From the work of Hakkinen and Richardson (1956), it is inferred that even at a downstream distance of five chord-lengths, the gust characteristics do not "feel", within 1 to 2%, the presence of the upstream oscillating aerofoils, especially if k is large.

The finite extent of the unsteady wake behind the models, might be a little more important for the lift results, because of the diffuser following after the working section. The beginning of the

diffuser and the model mid-chord point are at a distance 5 c apart, so that by analogy with the previous case (oscillating aerofoils), the limited wake effect should not be significant.

5. The contribution of the streamwise gust.

In Section 3.3.4.3, it was found experimentally that a streamwise u gust component at twice the oscillating rig frequency ($2n_g$) existed along the centre line. Theoretically, (Section 3.4.2) the oscillating aerofoils produce a u component of frequency n_g, which is zero only along the centre line. When an aerofoil at a non-zero mean incidence is exposed to such a streamwise gust, it experiences an unsteady lift of magnitude and phase given by Eqn. (2.13). The unsteady lift response function T(k) (Horlock's function) is plotted in Fig. 2.7. An estimate of this "extra" unsteady lift will now be given for the nominally zero and the high mean incidence experiments.

Although the geometric incidence of a model may be zero, the effective mean incidence may be different. Assume that a 2^0 (0.035 rad) error in the effective mean incidence is possible (see also Section 3.3.4.1). The u component at frequency $2n_g$ along the centre line is about 20% of w (i.e. the upwash component, see Fig. 3.17), while that at frequency n_g is negligible, even at distances from the centre line equal to the maximum thickness of the bluff sections. The ratio $|T(2k)/S(k)|$ becomes maximum for $k \simeq 0.5$, reaching a value of 2.5 approximately. It follows that the unsteady lift due to the streamwise gust cannot be more than 1.75% of the corresponding lift due to transverse gust. Although this result refers to a flat plate aerofoil, it may not be much different for the bodies examined in the present work. Anyway the experimental admittance results do not contain this small contribution because of the filtering at frequencies less than $2n_g$.

In the high mean incidence test the NACA 0015 aerofoil was set

to a maximum mean incidence of 13.5^{o} (0.365 rad). The predicted unsteady lift at frequency $2n_g$ should still be present as before but its magnitude should be greater, because the incidence had increased. If a uniform distribution of the streamwise gust is assumed then the figure of 1.75% stated previously, becomes 12% and the overall unsteady lift deviates more from the sinusoidal form. Here also the various parts of the wing are displaced from the centre line, where a u component at the main frequency n_g exists.

A rough estimate of the unsteady lift due to this component can be made, if it is assumed that the value of u is everywhere the same and equal to that prevailing in the position of the remotest part of the wing, i.e. the leading edge (this distance being about 0.23 c from the centre line). Theoretically, (Section 3.4.3) the ratios $|u/w|$ and $|T(k)/S(k)|$ are increasing functions of k, so that the ratio of the corresponding lift coefficients will also increase with k. Typical calculated values are given below:-

k	$C_{Lstr.}/C_{Lupw.}$
0.2	0.04
1.0	0.25

It is seen that a considerable amplification of the overall unsteady lift may occur at high frequencies, if the contributions from the u and w components are not much out of phase. This phase difference will also lead to a non-sinusoidal shape of the overall lift. Both effects were observed in the high incidence tests, (see Fig. C-11).

6. Convection speed of the gust.

The measurements described in Section 3.4.4 suggest that, assuming the gust to travel downstream as a frozen pattern, the convection

speed U_c is slightly higher than the free stream speed U_∞. For example at $k \simeq 0.35$, one experimental point in Fig. 3.24 indicates that $U_c \simeq 1.12\ U_\infty$. The unsteady lift response will be then determined from Kemp's function, plotted in Figs. 2.4 and 2.5. For the values of k and U_c/U_∞ given above, the lift response of a flat plate aerofoil should be about 6% higher than Sears's theory predicts. Although it is not known how well Kemp's (1952) theory applies to thick aerofoils (and even more to bluff bodies), this figure is of the same order as the rise in the experimental admittances at high k, observed for the aerofoil and the D section (Figs. 5.20 and 5.21). However, although theoretically the phase lag should decrease with respect to Sears's result, the experiment showed that an increase in the lag took place (Figs. 5.21, 5.22 and 5.23).

B. Inaccurate measurements.

The possible inaccuracies introduced in each particular experiment were stated in the appropriate sections. The topics covered included among them the hot-wire techniques, the load measuring techniques, the installation of the test models (e.g. the gap effect between the "live" and "dummy" sections, the surface irregularities, the length of the supporting rods, etc.) and the extraneous noise. Special attention was paid to the errors due to the measurement of the fluctuating signals (Appendix B). Here, two of these subjects will be discussed further: That of the load measurements and that of the aerodynamic admittance computation.

1. The experimental mean lift curve slopes used in the unsteady lift and admittance predictions (Eqns. (5.1) to (5.5)), may be partly responsible for the discrepancies at the lower reduced frequencies. There are two reasons for this. First, as stated in Chapter 4, the models employed for the measurements of the mean and fluctuating loads, were not the same. Therefore, the asymptotic behaviour of the unsteady

load model as $k \to 0$, may not result in exactly the same $\overline{\partial C_L}/\partial\alpha$, found on the mean load model. This would be a systematic effect for all the three models examined and the fact that all the admittances lie below $|S(k)|$, for small k, may be related with this matter. Second, even if the unsteady and steady load models are identical in every respect, there are the errors in measuring $\overline{C}_L$ and $\overline{\partial C_L}/\partial\alpha$. If the $\overline{C}_L$ v. $\overline{\alpha}$ curve is not a straight line near the origin, then the computation of $\overline{\partial C_L}/\partial\alpha$ for $\overline{\alpha} = 0$ is more inaccurate, because a lot of experimental points are needed.

The systematic rise of the experimental admittance above $|S(k)|$, observed for the aerofoil and the D section at high k, could have some of its cause in the presence of mechanical resonances. Although it was found, that the lift spectra for the "wind off" condition (but the oscillating rig running), contained no significant power at the rig frequency, it may be that, during the actual run "wind on", some small extra (i.e. non-aerodynamic) power did appear. The strength of this excitation could be greater at high frequencies (which are anyway close to the mechanical resonance observed).

In Section 3.1.4 it was stated that the piezoelectric transducers picked up about 10% of the transverse (here drag) load as axial load, leading to a wrong measurement of the true lift force. In unsteady flow the drag fluctuations are expected to be strong for the aerofoil at high incidence. On purely quasi-steady terms, if for example $\overline{\alpha} = 12^o$ and $\alpha_g \simeq 2^o$, the fluctuating lift should be roughly 3 times the fluctuating drag. This means that the "extra" lift due to transverse loads would be about 3% of the true lift. The large values of unsteady lift, for high k, realised in the experiment will include this contribution. Another effect,which could be associated with the drop of lift at very low frequencies, is the frequency response of the transducers. These were

calibrated with respect only to static loads (Section 3.1.4). A drift observed during these calibrations suggests that the frequency response of the transducers may not be flat at very low frequencies. This may partly account for the drop of the unsteady lift at low frequencies, when the transducers were used in the "short" or "dynamic response" mode.

2. Figs. 5.20 to 5.21 show that the low frequency experimental admittances computed from the digital analysis data, are systematically higher than those computed from the analogue filtering data. Therefore, they are closer to Sears's theoretical curve. The reasons for this disagreement were analysed in Appendix B and it is felt that at that particular frequency range, the digital analysis method leads to a better representation of the experimental aerodynamic admittance.

5.4 CONCLUSIONS REGARDING THE SINUSOIDAL LOADING EXPERIMENT

The experimental results and discussion presented in Sections 5.2 to 5.4, demonstrate that the proposed theoretical model for the prediction of lift in unsteady flow, does not apply with an equal degree of success for all bodies examined. This model is a simple modification of the unsteady thin aerofoil theory (Section 2.3.1) and consists of treating the bodies as flat plates of equal chord, thus effectively assuming instantaneously equal pressure at the separation points and neglecting the effect of thickness on the unsteady lift. The trailing edge of the flat plate is now an "equivalent" or "effective" trailing edge for the application of the Kutta-Joukowski condition. However, the fact that thickness does affect the mean lift, is taken into account by replacing the theoretical mean lift curve slope of a thin aerofoil ($= 2\pi$), by the experimentally determined mean lift curve slope in smooth flow. In the following, the main conclusions drawn from the investigation of each particular test model (at zero mean incidence) are listed.

1. NACA 0015 aerofoil.

Over the examined range of reduced frequencies (0.05 - 0.8 approximately) and RMS gust amplitudes (0.5^{o} to 5^{o} approximately), the aerofoil responds in an essentially linear manner to the incident sinusoidal upwash. This is suggested by both the great similarity between the upwash and corresponding lift spectra, which, it should be noted, are characterized by a very strong peak centred at the gust frequency and very little power in the other harmonics, and the fact that the shape of the complex aerodynamic admittance (frequency response function) is, within an experimental error of 15%, unique, i.e. it does not depend on the gust amplitude.

All the experimental results (lift, phase, etc.) are substantially independent of the Re number, except for one case (Re = 1.2×10^{5}) for which the magnitude of the aerodynamic admittance departs from the generally observed level. This discrepancy most probably appears, because the value of $\overline{\partial C_L}/\partial\alpha$ used in the computation of the admittance is not the appropriate one. The invariability of the results with Re number is associated with the existence of the sharp trailing edge, at which the single separation point is fixed.

When certain sources of discrepancy are taken into account, then the magnitude of the experimental admittance $|A(k)|$ is in good agreement with the magnitude $|S(k)|$ of Sears's function (Eqn. (2.8)). More specifically, it was found that the lack of correlation of the gust in the spanwise direction, the tripod supporting the aerofoil, and the employed analogue filtering method each tended to decrease the value of $|A(k)|$ by a small percentage at low frequencies ($k = 0.05 - 0.15$ approximately). The values of the aerodynamic admittance corrected for these additive effects are seen to be close to Sears's function within experimental error. Since the factors mentioned, accounting for the

drop of $|A(k)|$ are almost totally independent of the body considered, they will not be repeated when stating the conclusions for the rest of the models.

On the other hand, the observed tendency of $|A(k)|$ to exceed $|S(k)|$ at the highest frequencies ($k \gtrsim 0.5$) could be due to one or more of the following reasons:-

- Contribution of mechanical resonances.
- Gust convection speed higher than the free stream speed.
- Different contribution of the "inertial acceleration" terms with respect to the quasi-steady and wake terms, than thin aerofoil theory predicts.

The experimental phase lags between the sinusoidal lift and the upwash at the mid-chord point are in reasonable agreement with the theoretical (especially if k is less than 0.25 approximately) and almost always greater.

Among the reasons which cause discrepancies in the admittance results at high k, that of the gust convection speed tends to decrease the phase lag, while viscosity, thickness and wind tunnel blockage tend to increase it, so that the net effect appears as an increase in the phase lag.

There is evidence that the experimental centre of pressure in unsteady flow is close to the theoretical located at the quarter chord point.

Therefore, it is concluded that the proposed modified unsteady aerofoil theory is capable of predicting the unsteady lift on the present aerofoil and, it is believed, on two-dimensional aerofoils of similar shape, provided the structure of the incident gust and the experimental mean lift curve slope are known and the Re number of the flow is sufficiently high so that the boundary layers remain thin and attached. A suggested lower limit of the Re number is one above which

the experimental mean lift curve slope stays sensibly constant.

It should be emphasized that there are many other factors causing discrepancies between theory and experiment, which were not mentioned here, but of which the influence was estimated to be small in Section 5.3.3.

The overall significance of the good agreement between the experimental and theoretical aerofoil results, is that it proves the present experimental set-up to be adequate for testing Sears's theory.

2. D cylinder.

This model exhibits a behaviour very similar to that of the aerofoil so that many of the conclusions stated can be also repeated here. Only the differences are, therefore, pointed out.

Both the mean and the unsteady lift results of the D cylinder were found to be insensitive to changes in the Re number, so, therefore, were the experimental admittances. The lift spectral power at the higher harmonics is slightly increased in comparison with the aerofoil, suggesting only a small deterioration in the linearity of the lift response. At all Re numbers the quality of the agreement between the experimental admittances and $|S(k)|$ is as good as observed for the aerofoil for $Re > 1.2 \times 10^5$. Here $|A(k)|$ is rather uniformly greater than the aerofoil admittance and the rate of fall at high k is slightly smaller. An extra reason for this to happen (i.e. except those previously mentioned for the aerofoil) could be that of tunnel blockage on both the $\overline{\partial C_L}/\partial\alpha$ and unsteady lift values. Theoretically, the effect of thickness on the unsteady lift of a thick aerofoil as k increases should result in a progressive decrease of the admittance below $|S(k)|$. The absence of this trend in the D section admittances suggests that thickness may not be as important (for the admittance) as the factors mentioned previously.

The experimentally determined phase lags are systematically greater than the predicted values and also than the aerofoil values. It is thought that among other reasons, the additional model thickness contributes to this discrepancy.

The unsteady centre of pressure was found to lie further downstream from the quarter chord point, predicted by thin aerofoil theory. There is also some indication that the chordwise sinusoidal loading is not tuned to a single phase, as it would happen theoretically for a flat plate. These observations also apply for the elliptic cylinder.

As far as the natural vortex shedding lift coefficient is concerned, a reduction from its smooth flow value was noticed, when the sinusoidal flow was applied. The effect of the sinusoidal flow was more pronounced as the gust frequency was approaching the shedding frequency (though remaining much smaller). This agrees with the findings of other workers, e.g. Pocha (1971). Modulation effects are considered to be probable reasons for this drop in vortex shedding lift. A similar drop in the lift was found to occur for the elliptic cylinder (for which the Strouhal frequency was even more greater than the gust frequency) though relatively smaller.

These results point to the conclusion that the unsteady lift on the D cylinder can be satisfactorily predicted by the proposed modified aerofoil theory, over the range of reduced frequencies examined (i.e. well below those of the natural vortex shedding), with an additional input the experimental mean lift curve slope. Thus, the idea of having a fixed, "effective", trailing edge (for the shedding of vorticity in a single, "equivalent" sheet) mid-way between the two fixed separation points, is proved to be a reasonable one. It is believed that the unsteady lift on similar kinds of bodies (large

unseparated surface in the direction of the free stream and fixed separation points), can be predicted with a similar degree of success, when using this theory. Further, it is thought that the idea of a fixed, "effective", trailing edge for such bodies may be fruitful for more elaborate load calculation methods.

3. Elliptic cylinder.

The response of the elliptic cylinder to the incident gust is distinctly different from that of the aerofoil and the D section. It is found that the results are strongly influenced by the Re number, though this influence tends to become less important as the Re number increases. There is also some evidence, that the magnitude of the gust intensity (α_g), which for the previously examined models had no significant effect, appears to be here relatively more important.

The values of the experimental admittance appear to follow two trends:-

(a) If the Re number is high (about 3×10^5), or the boundary layer transition is fixed (e.g. by means of trip wires), $|A(k)|$ is seen to behave in a similar way to that found for the aerofoil and the D section (i.e. to approach $|S(k)|$ as k increases and to slightly exceed $|S(k)|$ above a certain reduced frequency).

(b) In the case where the above conditons are not met, then $|A(k)|$ is found to fall off faster than $|S(k)|$, remaining always lower. The rate of this drop is greater, the lower the Re number, so that for $Re = 1.2 \times 10^5$ and $k \simeq 0.7$ the experimental admittance is about 4 times lower than $|S(k)|$. The sources of discrepancy mentioned so far, including the change in the mean loading characteristics with increasing k, cannot produce deviations of this order.

One factor, which is thought to seriously affect the elliptic cylinder lift results and is not present in the aerofoil and the D section,

is that of the unsteady movement of the separation points, despite the fact that some boundary layer experiments could not provide a conclusive answer, as to how much, or how, these separation points move. Further support for the role played by the separation points is obtained from the following remarks: First from the trend (a) of the aerodynamic admittance mentioned previously, i.e. at high Re numbers or with a tripped boundary layer. It would appear that this trend is also associated with the fact, that the separation points lie further downstream in this case. Therefore, they are closer together and the separated surface of the cylinder is smaller. Second, the unsteady lift on a NACA 0015 aerofoil placed at high incidence (which, therefore, is expected to have one free separation point and one fixed at the trailing edge), exhibited the opposite behaviour, under the same conditions as the elliptic cylinder, at high frequencies. Third, it is the indication that an increase in the magnitude of the gust intensity (α_g), affected (actually slightly decreased) the aerodynamic admittance, in a different manner than in the case of the aerofoil and the D section. If, when all other conditions are fixed, the separation points respond in a different manner to relatively big changes of the stream incidence, than to small ones, a corresponding effect upon the unsteady lift behaviour is to be expected.

It should be concluded, therefore, that the existence of two free separation points, makes the idea of a fixed, "effective" trailing edge inappropriate for the calculation of the unsteady lift on the elliptic cylinder, using the proposed modified thin aerofoil theory. It is felt that the same would apply to bluff bodies with the same kind of separation. It may be, that the definition of an "effective" trailing edge for the shedding of vorticity, between the separation points, but allowed to move in a certain manner, is likely to produce

more reasonable results in a suitable theoretical model. Still, however, a knowledge of the behaviour of the separation points in unsteady flow should be necessary.

CHAPTER 6. THE TURBULENT LOADING EXPERIMENT

6.1 INTRODUCTION

This chapter describes the unsteady lift measurements and the comparison with the theory, for the NACA 0015 aerofoil, the D shape cylinder and the elliptic cylinder, placed at zero mean incidence in grid produced turbulence.

The models were those used in the sinusoidal loading experiment (chord = 0.152 m, aspect ratio = 2.5) and, in an identical manner as in that experiment, they were installed in the unsteady load balance of the 1.22 x 1.52 m wind tunnel.

The unsteady lift measurements are presented in the form of power spectra, which were obtained after analyzing digitally the recorded data (see Appendix B).

Turbulence of two different intensities and length scales was employed with characteristics given in Section 3.6 and Table 3. The experiments were carried out at a Re number of 2.3×10^5, which was slightly higher than in the sinusoidal loading case.

Corrections due to tunnel blockage were applied in the way suggested in Section 5.1.

Following Graham (1973), the broad-band and narrow-band (vortex shedding) contributions to the total lift spectrum are examined separately. This is permissible when, as it is likely in the present case, the incident (isotropic) turbulent field and vortex shedding are not correlated.

6.2 BROAD-BAND RESPONSE

6.2.1 EXPERIMENTAL RESULTS

The spectra of the lift coefficient, non-dimensionalized

with the free stream speed U_∞ and the turbulence length scale L_x, are plotted against the reduced frequency $k' = 2\pi nL_x/U_\infty$ in Figs. 6.1 and 6.2. The corresponding estimated values of L_x/c are 0.36 and 0.44. The points shown are taken from a smooth curve, which was fitted to the data obtained directly from the computer (after the calibration constants, etc. were taken into account). This resulted in some uncertainty of the spectral levels for very low frequencies.

Figs. 6.1 and 6.2 show that most of the lift energy is concentrated at reduced frequencies less than 1.0 approximately; there, the differences in the spectral levels for the three models are clearly distinguishable. Above $k' \simeq 1.0$, the spectral power drops rapidly (except when it rises locally to form the shedding peak) becoming an order of magnitude smaller at $k' = 2.0$. In the low frequency range, the D section is observed to always have the greatest spectral power. However, while for $L_x/c = 0.36$ the model next in power magnitude is the ellipse, for $L_x/c = 0.44$, it is the aerofoil which shows this trend. The differences are such that they cannot be simply attributed to the plotting uncertainty mentioned previously. Another point which needs attention is the drop in power for $k' < 0.1$ noticed for all three models with $L_x/c = 0.36$, (Fig. 6.1). If this was due to experimental inaccuracies, such as transducer and filter response, intermittent contact of the "live" with the "dummy" sections, or insufficient averaging time, then it would have appeared in the spectra with $L_x/c = 0.44$ as well. The cause should, therefore, be of an aerodynamic origin.

For frequencies $k' > 1.0$ approximately, the aerofoil and D section results are close to each other, but those of the elliptic section tend to fall off faster, while remaining always the lowest.

Examination of corresponding mean square values of the upwash intensity and the lift coefficient, indicated that both changed in the

same direction and by the same order of magnitude.

6.2.2 COMPARISON OF THE EXPERIMENTAL RESULTS WITH THE THEORY AND DISCUSSION

6.2.2.1 THE THEORETICAL AND EXPERIMENTAL ADMITTANCES

For the prediction of the unsteady loading in turbulent flow, the approach adopted in sinusoidal flow will be followed. Namely, the unsteady lift is assumed to be given by the exact theory for a flat plate (Section 2.4.1), but adjusted for the effect of mean lift curve slope. In fact, this is the method employed by Graham (1973) in his paper on bluff bodies (described in the present work in Section 2.4.2.2b). The comparison between the theoretical and experimental results is made in terms of aerodynamic admittances. In Chapter 5 the aerodynamic admittance was defined by Eqn. (5.4) and it was explained how it can be measured experimentally. Here, this definition is kept, but for compatibility with the existing formulae in the literature, the square of this admittance will be used, i.e.:-

$$|A(k)|^2 = \frac{S_{C_L}}{S_{\alpha_g}} \cdot \left(\frac{\overline{\partial C_L}}{\partial \alpha}\right)^{-2} \qquad (6.1)$$

To avoid confusion, it should be noted that this squared value is termed in this chapter simply as the aerodynamic admittance for brevity.

A question arises as to what value of $\overline{\partial C_L}/\partial\alpha$ should be used. In sinusoidal flow, it was taken equal to the corresponding smooth flow value and the justification was that for very low frequencies the body will behave quasi-steadily, since the flow is always very two-dimensional. Although turbulence is more correlated the lower the frequency, a body exposed to it will feel the velocity fluctuations at all frequencies. Also, the mean lift curve slope of the elliptic model was found to be particularly sensitive to changes in the levels of free stream turbulence

(see Chapter 4) and it is thought that even in well correlated turbulence (L_x/c large) this effect would still be present. In view of the points made, it was decided to use the values of $\overline{\partial C_L}/\partial\alpha$ measured in turbulent flow (see Figs. 4.1, 4.8 and 4.18). The experimental admittance denoted by $|A(k)|^2$ or $|A(k)_{EXP}|^2$ can then be computed, if the measured values of the upwash and lift spectra (Figs. 3.26, 6.1 and 6.2) are fed into Eqn. (6.1).

The theoretical admittance $|A(k)_t|^2$ is simply that derived by Jackson, Graham and Maull (1973) for a flat plate aerofoil in isotropic turbulence (see Eqns. (2.20), (2.21)), i.e.:-

$$|A(k_1)_t|^2 = \frac{4}{c}\int_0^\infty |G(k_1, k_2)|^2 \frac{\sin^2(k_2 AR)}{(k_2 AR)^2} S_{ww}(k_1, k_2)\, dk_2 \qquad (2.20)$$

It is noted, that in order to calculate $|A(k_1)_t|^2$, the structure of the incident turbulent field should be known. S_{ww} is related to the normalized upwash cross spectrum of turbulence, R_{ww}, by means of Eqn. (2.21). Jackson, Graham and Maull (1973) show how the measurement of R_{ww} can be accomplished in homogeneous turbulence. Then, if an empirical curve could be fitted to the measured values of R_{ww}, its Fourier transform (Eqn. (2.21)) would give S_{ww}, and $|A(k_1)_t|^2$ would be calculated from Eqn. (2.20) via a single numerical integration. In the present work, such measurements were not made. Instead, it was assumed that R_{ww} could be reasonably predicted by von Karman's cross spectrum for isotropic turbulence (see for example McKeough, 1976):-

$$R_{ww}(k_1, y) = \frac{2^{1/6}\cdot y^{*5/6}}{\Gamma(5/6)}\left[K_{5/6}(y^*) - \frac{3y^*}{3 + 8k_1^*}\cdot K_{1/6}(y^*)\right] \qquad (6.2)$$

where:

Γ is the gamma function.

K_n is the modified Bessel function of the second kind;

$$k_1^* = \frac{\Gamma(1/3) \cdot k_1 \cdot 2 \cdot L_x}{\Gamma(1/2) \cdot \Gamma(5/6) \cdot c}$$

$$y^* = \frac{\Gamma(1/2) \cdot \Gamma(5/6) \cdot (1 + k_1^{*2})^{1/2} \cdot y}{\Gamma(1/3) \cdot L_x}$$

The value of L_x entering Eqn. (6.2) was that estimated from the experimental u spectra (Section 3.6 and Fig. 3.26). In McKeough (1976) the derived two-dimensional spectrum S_{ww} is found to be:-

$$S_{ww}(k_1, k_2) = \frac{8}{2\pi} \cdot L_x \left\{ \frac{k_1^{*2} + k_2^{+2} + k_1^{*2} k_2^{+2}}{(1+k_1^{*2})^{1/2}(1+k_2^{+2})^{7/3}(3+8k_1^{*2})} \right\} \cdot \frac{\Gamma(1/3)^2}{\Gamma(5/6)^2} \qquad (6.3)$$

where: $$k_2^+ = \frac{\Gamma(1/3) \cdot 2 \cdot L_x \cdot k_2}{\Gamma(1/2) \cdot \Gamma(5/6) \cdot (1 + k_1^{*2})^{1/2} \cdot c}$$

It is realised that the calculation of the admittance would be more accurate if R_{ww} is obtained directly from the particular experimental arrangement. For example, any effects of anisotropy, (evidenced from the different intensities of the u, v, w components) are not taken into account, when assuming that R_{ww} follows exactly the von Karman formula. However, even if R_{ww} had been measured, an uncertainty in the value of $|A(k_1)_t|^2$ at low k_1 is difficult to avoid. This, as McKeough (1976) pointed out, is because the theoretical admittance result is sensitive to the $R_{ww}(k_1, y)$ data fit over the range of y, in which $R_{ww}(k_1, y)$ is appreciably non-zero. In order to have an idea of how much the theoretical admittance given above, (Eqn. (2.20)) would differ from those derived with less rigorous assumptions, two other theoretical admittances were considered: One is obtained from the "strip" theory (see Sections 2.4.1 and 5.3.3), in which $G(k_1, k_2)$ is replaced by S(k), the Sears's function. Then Eqn. (2.20) becomes:-

$$|A(k_1)_t|^2 = |S(k_1)|^2 \int_0^\infty \frac{\sin^2(k_2 AR)}{(k_2 AR)^2} \cdot S_{ww}(k_1, k_2)\, dk_2 \qquad (6.4)$$

The other theoretical admittance is simply the squared modulus of Sears's function (Liepmann, 1952), i.e. $|A(k_1)_t|^2 = |S(k_1)|^2$.

The theoretical admittances given by Eqns. (2.20) and (6.4) are plotted in Figs. 6.3 and 6.4 for three values of the ratio L_x/c, 0.44, 0.40 and 0.36. For the calculation of $|A(k_1)_t|^2$ from Eqn. (2.20), a computer program written by McKeough (1976) was used. Note that the argument has been changed from $k_1 = k = \pi nc/U_\infty$, to $k' = 2\pi nL_x/U_\infty$, so that $|A(k')_t|^2 = |A\left(k_1 \frac{2L_x}{c}\right)_t|^2$.

It can be seen from Figs. 6.3 and 6.4 that, for constant k' and L_x/c, strip theory predicts a higher lift than the exact (Graham's) theory, but much less lift than the entirely two-dimensional theory of Sears. This is because spanwise correlation effects are important in the present case, where L_x is of the order of the body dimensions. But even if L_x was much higher than c, the strip and exact theories would approach Sears's theory only for very small AR, i.e. for a very narrow strip model. The exact and strip theories (for L_x/c = constant) come closer together as the reduced frequency increases. Examination of the integrand in Eqn. (2.20), shows that its value falls rapidly to zero from its value at $k_2 = 0$ and k_1 constant, because $G(k_1, k_2)$, S_{ww} and the ratio including the sine term are all decreasing, as k_2 increases (see also Fig. 2.6). The replacement of $|G(k_1, k_2)|$ by $|S(k_1)|$ in the strip theory when k_1 is small would make a considerable difference in the integral, because $|G(k_1, k_2)| \to 0$ as $k_2 \to \infty$, while $|S(k_1)|$ does not depend on k_2. However, for very high k_1 both $|G(k_1, k_2)|$ and $|S(k_1)|$ tend to zero, irrespective of k_2 (see Graham, 1970a), and, therefore, in conjunction with the strong term $\sin^2(k_2 AR)/(k_2 AR)^2$ (which knocks out the differences between $|S(k_1)|$ and $|G(k_1, k_2)|$ at high k_2), the integral in Eqn. (2.20) would give more or less the same answer in the exact and strip theories. Similarly, it may be shown that the exact admittances

approach each other at high k_1, when plotted in terms of $k = \pi nc/U_\infty$, for various values of L_x/c. The general tendency for all admittances is to increase with increasing value of L_x/c.

6.2.2.2 THE COMPARISON

In Figs. 6.3 and 6.4 the experimental admittances are compared to the theoretical.

(a) NACA 0015 Aerofoil: Considering first the case with $L_x/c = 0.36$, it is observed that the agreement between the experimental and the exact (Eqn. (2.20)) theoretical admittances is good, particularly around $k' \simeq 0.2$. Generally the experimental admittance is overestimated. McKeough (1976) tested a similar NACA 0015 aerofoil under the same flow conditions but with AR = 1.66. When his results are adjusted for the mean lift curve slope factor (he had used $\overline{\partial C_L}/\partial\alpha = 2\pi$), then the agreement between the theory and his experimental results, is very similar to that of the present case.

The agreement is noticeably worse for $L_x/c = 0.44$, where the experimental admittance is overestimated by approximately 25% (on average), except for the lowest frequencies ($k' \lesssim 0.15$), where it is underestimated. However, if the results, after being suitably plotted, are compared with the theoretical curve with $L_x/c = 0.40$, the agreement is better, in fact quite similar to that found in the results of Jackson, Graham and Maull (1973) (for $L_x/c = 0.42$ and AR = 2.67) and Graham (1973) (for $L_x/c = 0.42$ and AR = 2.5). The theoretical admittances of Graham (1973) are corrected for turbulence distortion. This indicates that the turbulence distortion effects for the aerofoil at such values of L_x/c are not likely to be large.

Strip theory overestimates the experimental lift by roughly 250% at the lowest frequencies and 40% at the highest frequencies. There is no clear evidence of which value of L_x/c gives better agreement,

though it is expected that strip theory would give more reasonable load predictions at high values of the length scale to span ratios.

Sears's theory is by more than 500% higher than the experimental results, for all k.

(b) D Cylinder: The experimental admittances of the D section are seen to be higher than those of the aerofoil, up to about $k' \simeq 1.0$ and then become lower. It should be noted, that the sinusoidal flow admittances exhibited a similar behaviour.

Now, unlike the previous case, the agreement with the theory appears to be better for $L_x/c = 0.44$ than $L_x/c = 0.36$. For the latter value, there is a large disagreement at low frequencies, i.e. the experimental admittance is about 200% higher than the theoretical. Besides the uncertainty in measuring power at low frequencies, it is also the response of the transducers to drag (due to both u and w) and the distortion effect which may contribute to this discrepancy. Graham (1973) conducted similar measurements on a D section (see Fig. 2.10) and his theoretical admittance corrected for distortion ($L_x/c = 0.28$), is higher than the uncorrected; at low k', the difference is of the order of the discrepancy reported above.

The drop in the values of the experimental admittances below the theoretical for high k', which is observed here (even if the curve for $L_x/c = 0.40$ is used), appears also in the results of Graham (1973), see Fig. 2.10. Note that this is a systematic result, which cannot be attributed to the distortion effects, because the corrections of Graham showed the corrected and uncorrected theoretical admittances to be very close at high k'.

Strip theory again overestimates the experimental admittances at all frequencies. A tendency towards a better agreement for low k' and $L_x/c = 0.36$ is not a sign that strip theory is accurate, because the rise

in $|A(k)|$, discussed previously is most probably due to other effects.

(c) Elliptic Cylinder: This model is seen to have the greatest experimental admittance. $|A(k')|^2$ is underestimated up to about $k' = 1.5$ and then drops faster than in the other two models. The same kind of variation was found also by Graham (1973), see Fig. 2.10. The lift underestimation is greatest for the case $L_x/c = 0.36$, being of the order of 300% at low k'. This is a rather unexpected behaviour, in view of the sinusoidal flow results, where the experimental admittance was overestimated. It is also noteworthy that, while in the sinusoidal flow, the drop in $|A(k)|$ occurred for reduced frequencies less than 1.0, here it is postponed until k' is greater than 1.5 approximately.

The choice of a non-appropriate $\overline{\partial C_L}/\partial\alpha$ would result in shifting the overall levels of the experimental admittance. A value of $\overline{\partial C_L}/\partial\alpha = 8.37$ has been tried (theoretical lift curve slope of a 33.3% thick elliptic aerofoil, see Eqn. (4.8)), which gives a better agreement at low k', but an equally great disagreement (overestimation) for moderate and high k'.

6.2.2.3 SOURCES OF DISCREPANCY BETWEEN THEORY AND EXPERIMENT

Some of the discrepancies encountered in the turbulent flow experiment are common with those reported for the sinusoidal flow experiment, so they will not be repeated in detail here. In particular, the errors due to wind tunnel interference, measurement of velocity, spectral power and $\overline{\partial C_L}/\partial\alpha$, response of piezoelectric transducers and mechanical resonances, should be of the same order of magnitude as reported in Section 5.3.3.

An error in the mean effective incidence should not be of importance, because, as was shown by McKeough (1976), the influence on the theoretical admittance goes as $(\bar{\alpha})^2$ for a flat plate aerofoil. The

"inertial acceleration" effect (Section 5.3.3) could lead to discrepancies for the thick bodies at high k'. The higher harmonics, appearing in the lift response to a single spectral component (Sections 5.2.1.1 and 5.3.3), will be present here and they will tend to increase the experimental admittance. In Section 5.2.1.1, it was found that the relative strength of these harmonics was greatest for the elliptic cylinder and lowest for the aerofoil. The fact that the turbulence experimental admittances are ordered in the same way could be partly due to this effect. Sources of discrepancy which are of relatively greater importance are as follows:-

1. Use of the von Karman cross spectrum. As stated previously $|A(k')_t|^2$ is sensitive to the type of cross spectrum used and the large discrepancies at the lowest frequencies are certainly related to this. By assuming a von Karman spectrum, any effects of anisotropy are not taken into account.

2. Distortion of vorticity. It was stated in Chapter 2 that the vorticity of the approaching turbulence is distorted by the presence of the body for two reasons: First, because the body acts as a "source" of turbulence so that the boundary conditions on it are satisfied (important for large L_x/c) and second, because the perturbed mean flow distorts the vortex lines (important for small L_x/c). For the values of the ratio L_x/c and the bodies considered here, a contribution from both sources is expected.

Fig. 2.10 shows how the correction for distortion, applied by Graham (1973) for a D shape cylinder, affects the theoretical admittance: Theoretically the lift should appear higher due to distortion, especially at the lower frequencies. Consequently, this effect could account for the high experimental admittances observed for the two bluff bodies at low k' (Figs. 6.3 and 6.4), but it is thought to be small for the NACA 0015 aerofoil. The fact that the elliptic

cylinder has the highest experimental admittance is hard to attribute to the distortion effect alone, because, intuitively, it should not distort the vorticity more than the D section. Graham (1973) suggested that the distortion effect could be associated with the mean drag of the body, so that the D section would cause a greater distortion.

3. Viscous effects and the unsteady Kutta-Joukowski condition.

Viscous effects are expected to become more important at high frequencies. In particular, a discrepancy between the theoretical and experimental admittances is expected because the dissipation of turbulence spectra is not taken into account in the theoretical admittances (using the von Karman spectra).

A common feature of the elliptic cylinder experimental admittances in the sinusoidal and turbulent flows, is that of a (relatively to the other bodies) rapid fall below the theoretical admittances, noticed at high frequencies, see Figs. 5.22, 6.3, 6.4 and the results of Graham (1973) in Fig. 2.10. It was said in Section 5.3.3 that this effect should be associated with the unsteady movement of the separation points (due to the sinusoidal changes of incidence) and it could be that this is also the cause in turbulent flow. However, this rapid fall occurs at considerably greater reduced frequencies in turbulent flow compared to those in sinusoidal flow with the same Re number. Since the separation points are located further downstream and are closer together in turbulent flow than in the sinusoidal or smooth flows, see Fig. 4.12, it could be that the effect of their unsteady movement on the unsteady lift, is delayed until higher frequencies are reached. In addition, by simulating the cylinder with a flat plate, the separated regions are neglected; the vorticity carried by the shear layers passing over the rear of the body depends, among other parameters, on the reduced frequency. Therefore, this effect, which will be present

in both the sinusoidal and turbulent flows, may account for the characteristic lift behaviour noticed at high frequencies. Support to these arguments is also given from the high Re number (3×10^5) results in sinusoidal flow (Fig. 5.22a), where no drop in the admittance is observed and the separation points are also located further downstream.

Therefore, like the case of the sinusoidal flow, it appears that the application of the Kutta-Joukowski condition on a fixed, "effective", trailing edge is not appropriate for the elliptic cylinder, which has two free separation points. It would also be rather difficult to comment on this matter with regard to the D section, because the deviations of the experimental from the theoretical admittances are generally greater in the turbulent than in the sinusoidal flow (see also the aerofoil theoretical and experimental results). It is clear, however, that the D section,which has two fixed separation points, behaves more consistently than the elliptic cylinder and in a manner more similar to that of the aerofoil.

4. Thickness.

The thin aerofoil theory given in Jackson, Graham and Maull (1973) is strictly valid for a flat plate. For a thick aerofoil, and, of course, for the even thicker bluff bodies, a deviation from the theory is expected partly because the variation of turbulence in the normal (upwash) direction is not taken into account. In particular, the increased rate of fall off of the experimental admittances below the theoretical, noticed for all the models at high k', could be related to the lack of turbulence correlation in the upwash direction (which is more pronounced the higher the k', see Eqn. (6.2).

6.3 NARROW BAND RESPONSE

The non-dimensionalized vortex shedding lift spectra of the D

shape and the elliptic cylinders are plotted in Figs. 6.5 and 5.18 respectively, for both smooth and turbulent flows (see Section 5.2.4 for method of non-dimensionalization).

(a) D cylinder.

Referring to the lift spectra of the D cylinder (Fig. 6.5), it is observed that the effect of turbulence is to reduce the peak spectral power from its corresponding value in smooth flow by 2.2 times approximately. Such reduction was not encountered in the sinusoidal flow experiment (see Fig. 5.17). The drop in the spectral power is the same for both turbulent flows considered here (of u intensities 6.7% and 4.4%). However, the turbulent flow spectra are broader than the smooth flow ones. These trends also appear in the results of Graham (1973) who tested D shape cylinders in smooth and turbulent flows.

The root mean square vortex shedding lift coefficients, C_{Lvs}, computed from the spectra (see Fig. 6.5) are seen to be lower in turbulent flow by a factor of 1.7 approximately, with respect to their smooth flow value.

Turbulence appears to reduce slightly the Strouhal number, and this also agrees with the findings of Graham (1973).

The results reported above, can be discussed as follows:-

- The slight decrease in the Strouhal number is thought to be a consequence of the thickening of the separating boundary layers due to the action of turbulence diffusion. When the shear layers are thick, a concentration of vorticity sufficient to initiate vortex shedding is delayed, so that the shedding frequency decreases. This suspension in the formation of a vortex (and so the relative reduction in the strength of vortex shedding) would tend to increase slightly the base pressure, when turbulence is added, a fact which was realised in the mean pressure measurements (see Section 4.3 and Fig. 4.3).

- The reason mentioned above is partly responsible for the lowering in the spectral levels and C_{Lvs}. An additional reason for this lowering is thought to be the modulation of the vortex shedding lift by the randomly fluctuating u component (see Section 5.2.4 and Appendix E). The effect of modulation is here more important than in the sinusoidal flow, because the modulating streamwise (u) component is much stronger. Note that the increased amount of turbulence carried by the two thickened shear layers also contributes to the randomness of vortex shedding and the broadening of the lift spectra.
- Turbulence can also lead to a decrease in the vortex shedding lift coefficient, by affecting the spanwise correlation of the shed vortices and consequently the spanwise correlation of the sectional lift. Fig. 6.6 shows how the spanwise correlation of the u component, in the wake of the cylinder, falls after turbulence is introduced. The decrease in the spanwise correlation occurs for the total (broad-band) fluctuations and the narrow-band (at the shedding frequency) fluctuations. The result is that the spanwise correlation length ℓ_c $\left[\ell_c = \int_{span} R_{uu}(y, n_{vs})\, dy\right]$ of the u fluctuations at the shedding frequency is about 2.2 b for smooth flow and 1.65 b for turbulent flow. A corresponding change in the correlation of pressures on the surface of the body is expected, so that on average C_{Lvs} decreases in turbulent flow. It should be noted that the direct contribution of turbulence to the total C_{Lvs} is expected to be small, first because the height of the vortex shedding spectral peak is much greater than the power of turbulence at the same (i.e. the Strouhal) frequency, and second because at such high frequencies turbulence is relatively poorly correlated: see for example Fig. 6.6, where the "Townsend" or "Vickery" (1965) normalized cross spectrum of isotropic turbulence is plotted for Strouhal frequency $S \simeq 0.26$. The formula is:-

$$R_{uu}(y, n) = \theta K_1(\theta) - \frac{\theta^2}{2} K_0(\theta) \qquad (6.5)$$

where $\theta = \frac{y}{L_x} \sqrt{1 + \left(\frac{2\pi L_x n}{U_\infty}\right)^2}$

K_n are modified Bessel functions of the second kind

and here $n = n_{vs}$.

- The effect of the rapid changes in the angle of incidence, caused by the w component of turbulence, could have an effect on C_{Lvs} (see also Section 5.2.4), but it is not certain in what direction, because the shedding behaviour of the D section at various angles of incidence, in steady flow, is not known. However, the random nature of these changes could partly account for the observed broadening of the vortex shedding spectra.

(b) Elliptic cylinder.

The dimensionless vortex shedding lift spectra for smooth and turbulent flows are plotted in Fig. 5.18. As in the D section, the maximum spectral power is found to decrease when turbulence is applied. The flow with the greater turbulent intensity causes the greatest drop, - 17% approximately. But unlike case (a), the vortex shedding lift coefficients appear to be greater in turbulent than in smooth flow (note, however, that C_{Lvs} is defined in a different manner than for the D cylinder, see Section 5.2.4).

It is believed that the increase in the Strouhal number with increasing levels of free stream turbulence is mainly due to the displacement of the mean separation points further downstream, as the flow visualization tests had indicated (Figs. 4.11, 4.12). Consequently the wake is narrower and the interaction between the shed shear layers is facilitated within shorter time, thus increasing the vortex shedding frequency. The ensuing increase in the mean base pressure, shown in Fig. 4.13, is greater, the greater the turbulence intensity. Note that

similar effects are introduced by an increase in the Re number (Figs. 4.12, 4.13, 5.18, 5.19), with the only exception that the RMS lift coefficient is lowered.

- The increase in C_{Lvs} with increasing turbulence level seems to be rather curious in view of the increase in the base pressure and the decrease in the narrow-band spanwise correlation (see Fig. 6.7). The following factors could account for this behaviour.

(i) Broadening of the vortex shedding peak. (For the reasons leading to this broadening see case (a); an additional reason is thought to be the random excursion of the separation points away from their mean position). If the peak spectral levels were the same, then the broader spectrum would give the greater C_{Lvs}, according to the way C_{Lvs} is defined for the ellipse (Section 5.2.4).

(ii) Direct contribution from turbulence. Although turbulence energy falls rapidly at such high frequencies as the vortex shedding ($S \simeq 0.44$), there could be a contribution to the shedding peak, which is not very much higher than the turbulence power at the same frequency.

(iii) It may be that turbulence causes a different degree of excitation of mechanical resonances than the smooth flow, which could contribute to the power at high frequencies.

6.4 CONCLUSIONS REGARDING THE TURBULENT LOADING EXPERIMENT

- The linearized thin aerofoil theory of Jackson, Graham and Maull (1973) and the modified thin aerofoil theory of Graham (1973) (i.e. taking account only of the mean lift curve slope effect, see also Section 2.4.2.2b), predict reasonably well the unsteady lift of the NACA 0015 aerofoil and the D cylinder, when placed in grid produced turbulence of length scale of the order of the body dimensions. For the aerofoil, the agreement between the theoretical and experimental results shows

also the adequacy of the present experimental set-up for testing these theories. For the case of the D cylinder, which has two fixed separation points, this agreement means that the application of the Kutta-Joukowski condition at an "equivalent", fixed trailing edge, mid-way between the separation points, is suitable for turbulent flow as well as for sinusoidal flow. The modified aerofoil theory should, therefore, be capable of predicting the unsteady lift on similar bluff bodies (with large unseparated surface in the free stream direction and two fixed separation points) in turbulent flow. This theory would be helpful in practical situations, where the application of other methods, such as numerical models, would be difficult and, from the computational point of view, extremely expensive. However, this theory underestimates the unsteady lift on the elliptic cylinder over most of the frequency range, as was also found experimentally by Graham (1973).

- Of the sources of discrepancy between theory and experiment, arising at the lower frequencies, those of vorticity distortion and inappropriate turbulence representation, are the more important. Due to the former, the lift is expected to be more underestimated, the greater the thickness to chord ratio. The response of the transducers could also partly account for the discrepancies at low frequencies.

- At the highest frequencies, the distortion effects would become less severe, while those of thickness and viscosity may be responsible for the increased rate of fall of the experimental lift below the theoretical.

- Especially for the elliptic cylinder, the systematic lift underestimation up to about $k' = \frac{2\pi n L_x}{U_\infty} = 1.5$ should be partly attributed to the use of an unsuitable $\overline{\partial C_L}/\partial\alpha$. At higher frequencies, it is thought that the increased rate of fall of the experimental lift relative to the theoretical should be associated with the unsteady movement of the separation points. A similar behaviour was observed in the sinusoidal

flow, though at lower frequencies. The results of the experiments in these two flows, point to the conclusion that thin aerofoil theories will not give generally a reasonable prediction of the loading, when the separation points of the body are free. If calculation method is sought, then an input providing information about the behaviour of the separation points should be included.

The influence of turbulence on the vortex shedding of the bluff bodies, is to decrease the peak spectral power at the Strouhal frequency, broaden the vortex shedding spectra and impair the narrow-band spanwise correlation of the shed vortices. These effects are like an effective increase in the Re number for the elliptic model, which has free separation points. The broadening and reduction of spectral power are also results of a modulation of the vortex shedding signal by the fluctuating streamwise component. When turbulence is applied, the vortex shedding lift coefficient of the D section is observed to decrease, while that of the elliptic section (which is much smaller than the vortex shedding lift of the D section), appears to increase.

CHAPTER 7. OVERALL CONCLUSIONS AND SUGGESTIONS FOR FURTHER WORK

The NACA 0015 aerofoil (placed at zero mean incidence), which was used in the present work as a measure of the adequacy of the employed sinusoidal and turbulent flows, confirmed the validity of thin aerofoil theories. The effect of thickness was satisfactorily taken into account by substituting, in the theoretical thin aerofoil result, the theoretical mean lift curve slope ($= 2\pi$) with the experimentally found.

In order to predict the unsteady lift on the D and elliptic cylinders, the assumptions were made that they had zero thickness, that the Kutta-Joukowski condition for the shedding of vorticity could be applied at a fixed trailing edge (located at the end of the chordline) and that the thickness effect could be taken into account as mentioned above, for the aerofoil.

Using this modified thin aerofoil theory the unsteady lift on the D cylinder was reasonably well predicted in both sinusoidal and turbulent flows. Due to the large unseparated surface of this body in the streamwise direction and the location of the two fixed separation points right at the end, the unsteady flow is realistically simulated by that round a flat plate. The assumption that the two shear layers, leaving tangentially the two parallel surfaces of the cylinder, can be replaced by a single vortex sheet lying along the extension of the chordline and of equivalent vorticity, equal to the sum of the two shear layer vorticities, was found to lead to realistic results.

On the other hand, the application of this modified theory to the calculation of the unsteady lift on the elliptic cylinder, has not generally produced satisfactory results. This occurred especially at high reduced frequencies where, depending on the Re number, a variable

degree of discrepancy from the theory was found. Here the separation points lie upstream of the assumed "effective" trailing edge, and their mean position depends on the Re number. Thus, there is a separated region on the cylinder, which cannot be accurately represented by the potential flow of the flat plate, and to a greater extent the more upstream the separation points are located. Generally, there would be an unsteady movement of the separation points, due to the unsteady changes of incidence and, therefore, the instantaneous position, vorticity strength and form of vorticity distribution of the shed shear layers will also be affected, and accordingly the unsteady lift. It had not been possible, however, to establish how the separation points actually moved with changing frequency. A more elaborate experimental investigation on this subject would be helpful. If, for example, the behaviour of the separation points in unsteady flow is known, it may be that the construction of a theoretical model, similar to that given here, but with the adoption of an "equivalent" moving trailing edge between the separation points, could lead to more satisfactory results.

The present experiments were not planned to investigate the vortex shedding phenomenon in detail. The reduction of the vortex shedding power in both the sinusoidal and turbulent flows, which is partly due to modulation effects,can be studied experimentally in a streamwise sinusoidal flow. The present oscillating rig is capable of producing such a flow, if the oscillating aerofoils are forced to move out of phase.

LIST OF REFERENCES

Abbot, I. H. and Doenhoff, von A. E.	1959	"Theory of wing sections", Dover Publications.
Allen, H. J. and Vincenti, W. G.	1944	"Wall interference in a two-dimensional flow wind tunnel, with consideration of the effect of compressibility", NACA Report 782, 155-184.
Arnoldi, R. A.	1969	"Unsteady aerfoil response", Conference on basic aerodynamic noise research, NASA SP-207.
Baines, W. D. and Peterson, E. G.	1951	"An investigation of flow through screens", Trans. ASME, 73, 467-480.
Basu, B. C. and Hancock, G. J.	1977	"The unsteady motion of a two-dimensional aerofoil in incompressible inviscid flow", University of London, Queen Mary College, QMC-EP 1018/R.
Batchelor, G. K.	1970	"An introduction to fluid dynamics". Cambridge University Press.
Batchelor; G. K. and Proudman, I.	1954	"The effect of rapid distortion of a fluid in a turbulent motion", Quart. J. Mech. App. Math., 7, 83.
Bearman, P. W.	1965	"Investigation of the flow behind a two-dimensional model with a blunt trailing edge and fitted with splitter plates", J. Fluid Mech., 21, 241-255.
Bearman, P. W.	1969a	"An investigation of the forces on flat plates in turbulent flow", NPL Aero. Report 1296.
Bearman, P. W.	1969b	"On vortex shedding from a circular cylinder in the critical Reynolds number regime", J. Fluid Mech., 37, 577-585.
Bearman, P. W.	1972	"Some measurements of the distortion of turbulence approaching a two-dimensional bluff body", J. Fluid Mech., 53, 451-467.

Bearman, P. W. and Fackrell, J. E.	1974	"Calculation of two-dimensional and axisymmetric bluff body potential flow", I.C. Aero. Report No. 74-07.
Bechert, D. and Pfizenmaier, E.	1975	"Optical compensation measurements on the unsteady exit condition at a nozzle discharge edge", J. Fluid Mech. 71, 123-144.
Bellhouse, B. J. and Schultz, D. L.	1969	"The measurement of fluctuating skin friction in air with heated thin-film gauges", J. Fluid Mech., 32, 675-680.
Bendat, J. S. and Piersol, A. G.	1971	"Random data: Analysis and measurement procedures", Wiley - Interscience.
Bisplinghoff, R. L. et al	1958	"Aeroelasticity", McGraw-Hill.
Blevins, D. B.	1977	"Flow induced vibration", Van Nostrand Reinhold.
Bradbury, L. J. S.	1969	"A pulsed wire technique for velocity measurements in highly turbulent flows", N.P.L. Aero. Report 1284.
Bradshaw, P.	1971	"An introduction to turbulence and its measurement ", Pergamon Press.
Bradshaw, P.	1974	"Effect of free stream turbulence on turbulent shear layers", I.C. Aero. Report 74-10.
Bratt, J. B.	1950	"Flow patterns in the wake of an oscillating aerofoil", ARC Reports and Memoranda 2773.
Brown, S. N. and Stewartson, K.	1975	"Wake curvature and the KUTTA condition in laminar flow", Aero. Quart., 26, 275.
Brunn, H. H. and Davies, P. O. A. L.	1975	"An experimental investigation of the unsteady pressure forces on a circular cylinder in a turbulent cross flow", J. Sound and Vibration, 40.
Carta, F. O.	1967	"The unsteady normal force response of an aerofoil in a periodically distorted inlet flow including stalling effects", AIAA Paper No. 67-18.

Chen, C. F. and Ballengee, D. B.	1971	"Vortex shedding from circular cylinder in an oscillating free stream", AIAA J. 9, 340.
Crabtree, L. F.	1957	"Effects of leading-edge separation on thin wings in two-dimensional incompressible flow", J. Aero. Sci., 24, 597-604.
Crandall, S. H.	1963	"Random vibrations in mechanical systems", Academic Press.
Davenport, A. G.	1961	"An application of statistical concepts to the wind loading of structures", Proc. Inst. Civil Eng. No. 6480, 19.
Davenport, A. G.	1962	"The response of slender, line-like structures to a gusty wind", Proc. Inst. Civil Eng., No. 6610, 23.
Davies, M. E.	1974	"Spectral analysis programs POWSPEC and COPHASE", I.C. Aero. TN 74-103.
Den Hartog, J. P.	1956	"Mechanical vibrations", McGraw-Hill.
Despard, R. A. and Miller, J. A.	1971	"Separation in oscillating laminar boundary-layer flows", J. Fluid Mech., 47, 21-31.
Drischler, J.	1956	"Calculation and compilation of unsteady lift functions for a rigid wing subjected to sinusoidal gusts and sinusoidal oscillations", NACA TN 3748
Dubbel	1970	"Taschenbuch für den Machinenbau", Springer Verlag.
Edwards, P. E.	1972	"The aerodynamic loading on a yawed wing in a sinusoidal gust", I.C., M.Sc. project.
Eichelbrenner, E. A. (Ed.)	1971	"Recent research on unsteady boundary layers", IUTAM Symposium, Quebec, Canada.
Fage, A.	1926	"The flow of air and of an inviscid fluid around an elliptic cylinder and an aerofoil of infinite span, especially in the region of the forward stagnation point", ARC R & M, No. 1097.

Fage, A. and Johansen, F. C.	1927	"On the flow of air behind an inclined flat plate of infinite span", ARC R & M, No. 1104.
Farren, W. S.	1935	"The reaction on a wing whose angle of incidence is changing rapidly. Wind tunnel experiments with a short period recording balance", ARC R & M, No. 1648.
Fung, Y. C.	1960	"Fluctuating lift and drag acting on a cylinder in a flow at supercritical Reynolds numbers", J. Aero. Sci., 27.
Gaster, M.	1969	"Vortex shedding from slender cones at low Reynolds numbers", J. Fluid Mech., 38, 565-576.
Gerrard, J. H.	1961	"An experimental investigation of the oscillating lift and drag of a circular cylinder shedding turbulent vortices", J. Fluid. Mech., 11, 244.
Gerrard, J. H.	1966	"The mechanics of formation region of vortices behind bluff bodies", J. Fluid Mech., 25, 401-413.
Giesing, J. P.	1968	"Non-linear two-dimensional unsteady potential flow with lift ", J. of Aircraft, 5, No. 2, 135-143.
Goldstein, M.	1965	"Modern developments in fluid dynamics", Vol. I & II, Dover Publications.
Goldstein, M. and Atassi, H.	1976	"A complete second-order theory for the unsteady flow about an airfoil due to a periodic gust", J. Fluid Mech., 74, 741-765.
Graham, J. M. R.	1969	"The effect of end-plates on the two-dimensionality of a vortex wake", Aero. Quart., XX.
Graham, J. M. R.	1970a	"Lifting surface theory for the problem of an arbitrarily yawed sinusoidal gust incident on a thin aerofoil in incompressible flow", Aero. Quart., XXI.

Graham, J. M. R.	1970b	"Similarity rules for thin aerofoils in non-stationary subsonic flows", J. Fluid Mech., 43, 753-766.
Graham, J. M. R.	1972	"The drag of porous plates in a turbulent stream", I.C. Aero. Report, No. 72-20.
Graham, J. M. R.	1973	"Lift forces on cylinders in a turbulent flow", International Symposium: Vibration problems in industry, Keswick, UK.
Graham, J. M. R. and Kullar, I.	1977	"Small perturbation expansions in unsteady aerofoil theory", J. Fluid Mech., 83, 209-224.
Hakkinen, R. J. and Richardson, A. S.	1957	"Theoretical and experimental investigation of random gust loads, I: Aerodynamic transfer function of a simple wing configuration in incompressible flow", NACA TN 3878.
Halfman, R. L.	1952	"Experimental aerodynamic derivatives of a sinusoidally oscillating aerofoil in a two-dimensional flow", NACA Report 1108.
Hanson, F. B.; Kozak, S. H. and Richardson, P. D.	1966	"Velocity spikes in separated flows", J. Fluid Mech., 25, 43-50.
Hatfield, H. M. and Morkovin, M. V.	1973	"Effect on oscillating free stream on the unsteady pressure on a circular cylinder", ASME J. Fluids Eng., 95.
Holmes, D. W.	1970	"Experimental pressure distributions on aerofoils in transverse and streamwise gusts", CUED/A-Turbo/TR 21, Cambridge.
Horlock, J. H.	1968	"Fluctuating lift forces on aerofoils moving through transverse and chordwise gusts", Trans. ASME J. Basic Eng., 90, 494-500.
Houbolt, J. C. et al	1964	"Dynamic response of airplanes to atmospheric turbulence including flight data on input and response", NASA TR R-199.

Howarth, L.	1935	"The theoretical determination of the lift coefficient for a thin elliptic cylinder", Proc. Roy. Soc. London, A 149, 558.
Hunt, J. C. R.	1972	"A theory for fluctuating pressures on bluff bodies in turbulent flows", IUTAM-IAHR Symposium: Flow induced vibrations, Karlsruhe.
Hunt, J. C. R.	1973	"A theory of turbulent flow round two-dimensional bluff bodies", J. Fluid Mech., 61.
Jackson, R.	1970	"The loading of rectangular wings in unsteady flows", Ph.D. Thesis, Cambridge University.
Jackson, R.; Graham, J. M. R. and Maull, D. J.	1973	"The lift on a wing in a turbulent flow", Aero. Quart., XXIV.
Jacobs, E. N. and Sherman, A.	1934	"Aerofoil section characteristics as affected by variations of the Reynolds number", NACA Report No. 586.
Jones, W. P.	1950	"Wind-tunnel interference effects on measurements of aerodynamic coefficients for oscillating aero-foils", ARC R & M, 2786.
Karlsson, S. K. F.	1959	"An unsteady turbulent boundary layer", J. Fluid Mech., 5, 637.
Karman, von T. and Sears, W. R.	1938	"Airfoil theory for non-uniform motion", J. Aero. Sci., 5, No. 10.
Kawashima, S. et al	1978	"Aerodynamic response for the aero-foil experiencing sudden change in angle of attack", Trans. Japan Soc. Aeron. Space Sciences, 21, No. 52, p.76.
Kemp, N. H.	1952	"On the lift and circulation of airfoils in some unsteady flow problems", J. Aero. Sci., 19, Readers' forum.
Kullar, I.	1978	Ph.D. Thesis to be published, London University, Imperial College.

Küssner, H. G. and Gorup, von G.	1960	"Instationäre linearizierte Theorie der Flügelprofile endlicher Dicke in inkompressibler Strömung", Mitteilungen des Max Plank Inst. für Strömungsforschung und der Aerod. Versuchsanstalt, No. 26.
Lamson, P.	1957	"Measurements of lift fluctuations due to turbulence", NACA TN 3880.
Lee, B. E.	1975	"The effect of turbulence on the surface pressure field of a square prism", J. Fluid Mech., 69.
Liepmann, H. W.	1952	"On the application of statistical concepts to the buffeting problem", J. Aero. Sci., 19, No. 12.
Lighthill, M. J.	1954	"The response of laminar skin friction and heat transfer to fluctuations in the stream velocity", Proc. Roy. Soc. London, Series A, 224, 1-23.
Maeda, H. and Kobayakawa, M.	1970	"Studies on the gust response of a wing. I: Response of a two-dimensional rigid wing", Memoirs Kyoto Univ. (Japan), 32, 379.
Maekawa, T. and Mizuno, S.	1966	"Flow around the separation point and in the near-wake of a circular cylinder", IUTAM Symposium on boundary layers and turbulence, Japan, Kyoto, The Physics of Fluids Supplement, PS 184.
Mair, W. A. and Maull, D. J.	1971	"Bluff bodies and vortex shedding - a report on Euromech 17", J. Fluid Mech., 45, 209-224.
Mair, W. A. and Stanby, P. K.	1975	"Vortex wakes of bluff cylinders in shear flow", SIAM J. App. Math., 28, 519.
Maskell, E. C.	1963	"A theory of the blockage effects on bluff bodies and stalled wings in a closed wind tunnel", ARC R & M, 3400.
Maull, D. J. and Young, R. A.	1972	"Vortex shedding from a bluff body in a shear flow", IUTAM-IAHR Symposium: Flow induced structural vibrations, Karlsruhe.

McCroskey, W. J. et al	1976	"Dynamic stall experiments on oscillating airfoils", AIAA J., 14, I.
McCroskey, W. J. and Philippe, J. J.	1974	"Unsteady viscous flow on oscillating aerofoils", AIAA 12th Aero. Sci. Meeting, Paper No. 74-182.
McKeough, P.	1976	"Effects of turbulence on aerofoils at high incidence", Ph.D. Thesis, London University, Imperial College.
Modi, V. J. and Wiland, E.	1970	"Unsteady aerodynamics of stationary elliptic cylinders in subcritical flow", AIAA J., No. 10.
Moore, F. K.	1955	"Lift hysteresis at stall as an unsteady boundary-layer phenomenon", NACA TN 3571.
Morkovin, M. V. et al	1971	"On the response of laminar boundary layers to periodic changes in free stream speed", IUTAM Symposium: Recent research on unsteady boundary layers, Quebec, Canada.
Moss, G. F. and Murdin, P. M.	1968	"Two-dimensional low speed tunnel tests on the NACA 0012 section including measurements made during pitching oscillations at the stall", RAE, TR68104.
Nakamura Y. and Tomonari, Y.	1976	"The effect of turbulence on the drags of rectangular prisms", Trans. Japan Soc. Aero. Space Sci., 19, No. 44.
Naudascher, E. (Ed.)	1978	"Flow induced structural vibrations", IUTAM-IAHR Symposium, Karlsruhe.
Neumark, S.	1952	"Pressure distribution on an aerofoil in non-uniform motion", J. Aero. Sci., 19, 214-215.
Newton, J. W.	1973	"The aerodynamic loading on a swept wing in a sinusoidal gust", M.Sc. Thesis, London University, I.C.
Owen, P. R.	1973	"The aerodynamics of aircraft and other things", The Aeronautical Journal, 77, No. 752.
Pankhurst, R. C. and Holder, D. W.	1952	"Wind tunnel technique", Sir Isaac Pitman.

Parkinson, G.V and Brooks N.P.H	1961	"On the aeroelastic instability of bluff cylinders" Trans. ASME, J. Appl. Mech, 28, 252-258
Parkinson, G. V. and Jandali, T.	1970	"A wake source model for bluff body potential flow", J. Fluid Mech., 40, 577.
Pocha, J. J.	1971	"On unsteady flow past cylinders of square cross section", Ph.D. Thesis, London University, Q.M.C.
Polhamus, E. C.	1959	"Effect of flow incidence and Reynolds number on low-speed aerodynamic characteristics of several non-circular cylinders with applications to directional stability and spinning", NASA TR R-29.
Polhamus, E. C. et al	1959	"Pressure and force characteristics of non-circular cylinders as affected by Reynolds number with a method included for determining the potential flow about arbitrary shapes", NASA TR R-46.
Pope, A. and Harper, J. J.	1966	"Low speed wind tunnel testing", John Wiley.
Reid, E. G. and Vincenti, W.	1940	"An experimental determination of the lift of an oscillating airfoil", J. Aero. Sci., 8, No. 1.
Reissner, E.	1947	"Wind tunnel corrections for the two-dimensional theory of oscillating aero-foils", Cornell Aero. Lab. Report No. SB-318-8-3.
Ribner, H. S.	1956	"Spectral theory of buffeting and gust response: unification and extension", J. Aero. Sci., 23.
Roshko, A.	1954a	"On the drag and shedding frequency of two-dimensional bluff bodies", NACA TN 3169.
Roshko, A.	1954b	"A new hodograph for free streamline theory", NACA TN 3168.
Roshko, A.	1961	"Experiments on the flow past a circular cylinder at very high Reynolds number", J. Fluid Mech., 10, 345.
Sallet, D. W.	1972	"On the prediction of flutter forces", IUTAM-IAHR Symposium: Flow induced structural vibrations, Karlsruhe.

Sawyer, R. A.	1972	"Torsional stability of H sections in random vertical gusts", IUTAM-IAHR Symposium: Flow induced structural vibrations, Karlsruhe.
Schlichting, H.	1968	"Boundary layer theory", McGraw-Hill.
Schramm, W.	1966	"Wirbelfrequenzmessungen an umströmten Bauteilen", Institut für Leichtbau, Dresden, Mitteilungen 5, Heft 8.
Schubauer, G. B.	1939	"Air flow in the boundary layer of an elliptic cylinder", NACA Report 652.
Sears, W. R.	1941	"Some aspects of non-stationary airfoil theory and its practical application", J. Aero. Sci., 8, No. 2.
Sears, W. R.	1956	"Some recent developments in airfoil theory", J. Aero. Sci., 23.
Sears, W. R.	1976	"Unsteady motion of airfoils with boundary layer separation", AIAA Journ., 14, 216.
Sears, W. R. and Telionis, D. P.	1971	"Unsteady boundary layer separation", IUTAM Symposium: Recent research on unsteady boundary layers, Quebec, Canada.
Shih-I-Pai	1957	"Viscous flow theory II: turbulent flow", Van Nostrand.
Silverstein, A. and Joyner, U. T.	1939	"Experimental verification of the theory of oscillating aerofoils", NACA Report 673.
Simmons, J. E. L.	1974	"The relationship between the base pressure on a bluff body and the velocity at separation", The Aeronautical Journal, 330-331.
Simmons, J. M.	1976	"Aerodynamic measurements for an oscillating two-dimensional jet-flap airfoil", AIAA J., 14, No. 6.
Spurk, J.	1963	"Messungen der aerodynamischen Beiwerte Schwingender Flügelprofile im Wind Kanal und Vergleigh mit der Theorie", Mitteilungen des Max Plank Instituts für Strömungsforchung und der AVA, Göttingen, No. 29.

Surry, D.	1969	"The effect of high intensity turbulence on the aerodynamics of a rigid circular cylinder at subcritical Reynolds numbers", UTIAS Report No. 142.
Tani, L	1964	"Low speed flows involving bubble separations", Progress in Aero. Sci., 5, 70-104.
Taylor, G. I.	1936	"Statistical theory of turbulence part 5. Effect of turbulence on boundary layer. Theoretical discussion of relationship between scale of turbulence and critical resistance of spheres", Proc. Roy. Soc. London, Series A, 156, 307-317.
Theodorsen, T.	1935	"General theory of aerodynamic instability and the mechanism of flutter", NACA Report 496.
Tutu, N. K. and Chevray, R.	1975	"Cross-wire anemometry in high intensity turbulence", J. Fluid Mech., 71, 785-800.
Vickery, B. J.	1965	"On the flow behind a coarse grid and its use as a model of atmospheric turbulence in studies related to wind loads on buildings", NPL Aero. Report 1143.
Vickery, B. J.	1966	"Fluctuating lift and drag on a long cylinder of square cross section in a smooth and in a turbulent stream", J. Fluid Mech., 25.
Williams, D. H. and Brown, A. F.	1937	"Experiments on an elliptic cylinder in the compressed air tunnel", ARC R & M, No. 1817.
Wills, J. A. B.	1962	"The correction of hot-wire readings for proximity to a solid boundary", J. Fluid Mech., 12, 338-396.
Wood, C. J. and Kirmani, S. F. A.	1970	"Visualization of heaving aerofoil wakes including the effect of a jet flap", J. Fluid Mech., 41, 627-640.
Woods, L. C.	1961	"The theory of subsonic plane flow", Cambridge University Press.
Zahm, A. F. et al	1928	"Forces on elliptic cylinder in uniform air stream", NACA Report 289, 217.

TABLE I : WIND TUNNEL SPEEDS FOR UNSTEADY LOAD EXPERIMENT

U_∞ NOMINAL TUNNEL SPEED m/sec.	Re NUMBER U_∞. c/ν
29.55	3.0×10^5
21.74	2.2×10^5
15.75	1.6×10^5
11.85	1.2×10^5

TABLE 2 : OSCILLATING AEROFOIL AMPLITUDES FOR UNSTEADY LOAD EXPERIMENT

ECCENTRICITY	RADIUS OF ECCENTRICITY (m)	OSCILLATING AEROFOIL ANGLE (PEAK TO PEAK /2) (degrees)
LARGE	0.0125	10.12
MEDIUM	0.0085	6.85
SMALL	0.0045	3.55

TABLE 3 : DETAILS OF TURBULENT FLOWS.

tunnel width (m)	tunnel height (m)	mesh size M (m)	downstream distance x/M	nominal tunnel speed (m/sec)	longitudinal length scale (m)	$\frac{\sqrt{\overline{u^2}}}{U_\infty}$	$\frac{\sqrt{\overline{w^2}}}{U_\infty}$	$\frac{\sqrt{\overline{v^2}}}{U_\infty}$
I.52	I.22	0.076	24.0	22.6	0.055	0.044	0.037	
I.52	I.22	0.I52	I2.0	22.6	0.067	0.067	0.06	0.059
I.52	I.22	0.076	I3.3	20.3	0.03I*	0.059*		
I.52	I.22	0.076	I3.3	I0.6	0.03I*	0.059*		
I.52	I.22	0.I52	6.6	20.3				
I.52	I.22	0.I52	6.6	I0.6				
I.52	I.22	0.076	I3.3	II.3	0.03I*	0.059*		
I.52	I.22	0.076	I3.3	5.9	0.03I*	0.059*		
0.6I	0.9I	0.I52	I0.0	I9.4	0.063*	0.078		
0.6I	0.9I	0.I52	I0.0	I0.6	0.063*	0.078		
0.6I	0.9I	0.076	20.0	I9.4	0.046*	0.044		
0.6I	0.9I	0.076	20.0	I0.6	0.046*	0.044		
0.5I	0.5I	0.05I	I3.0	32.5	0.02I*	0.06*		

VALUES MARKED WITH AN ASTERISK ARE NOT MEASURED BY THE AUTHOR, BUT OBTAINED FROM OTHER SOURSES: McKEOUGH[1976], BEARMAN[1969A] & BAINES AND PETERSON [1951]

TABLE 4: TERMS IN THE FORMULA FOR BLOCKAGE CORRECTIONS (MEAN LOADING)

TEST MODEL	Λ	ϵ_{sb}	ϵ_{wb}	ϵ_{curv}	ϵ_{wg}
NACA 0015 AEROFOIL	0.305	$\Lambda \cdot \frac{\pi^2}{48} \cdot (\frac{c}{h})^2$	$\frac{c}{4h} \cdot \overline{C}_D$	$\frac{\pi^2}{48} \cdot (\frac{c}{h})^2$	$\Lambda \frac{\pi^2}{48} \cdot (\frac{c}{h})^2$
D CYLINDER	~ 1.0	$\Lambda \cdot \frac{\pi^2}{48} \cdot (\frac{c}{h})^2$	$\frac{\epsilon}{2} \cdot \frac{c}{h} \cdot \overline{C}_D$	$\frac{\pi^2}{48} \cdot (\frac{c}{h})^2$	$\Lambda \cdot \frac{\pi^2}{48} \cdot (\frac{c}{h})^2$
ELLIPTIC CYLINDER	0.89	$\Lambda \frac{\pi^2}{48} \cdot (\frac{c}{h})^2$	$\frac{c}{h} \cdot \frac{1}{2} \cdot \overline{C}_D$	$\frac{\pi^2}{48} \cdot (\frac{c}{h})^2$	$\Lambda \frac{\pi^2}{48} \cdot (\frac{c}{h})^2$

ϵ is obtained from: $(1 - \overline{C}_{P_b}) \frac{\epsilon}{1+\epsilon} = 1 + \epsilon \cdot \overline{C}_D \cdot \frac{c}{h}$

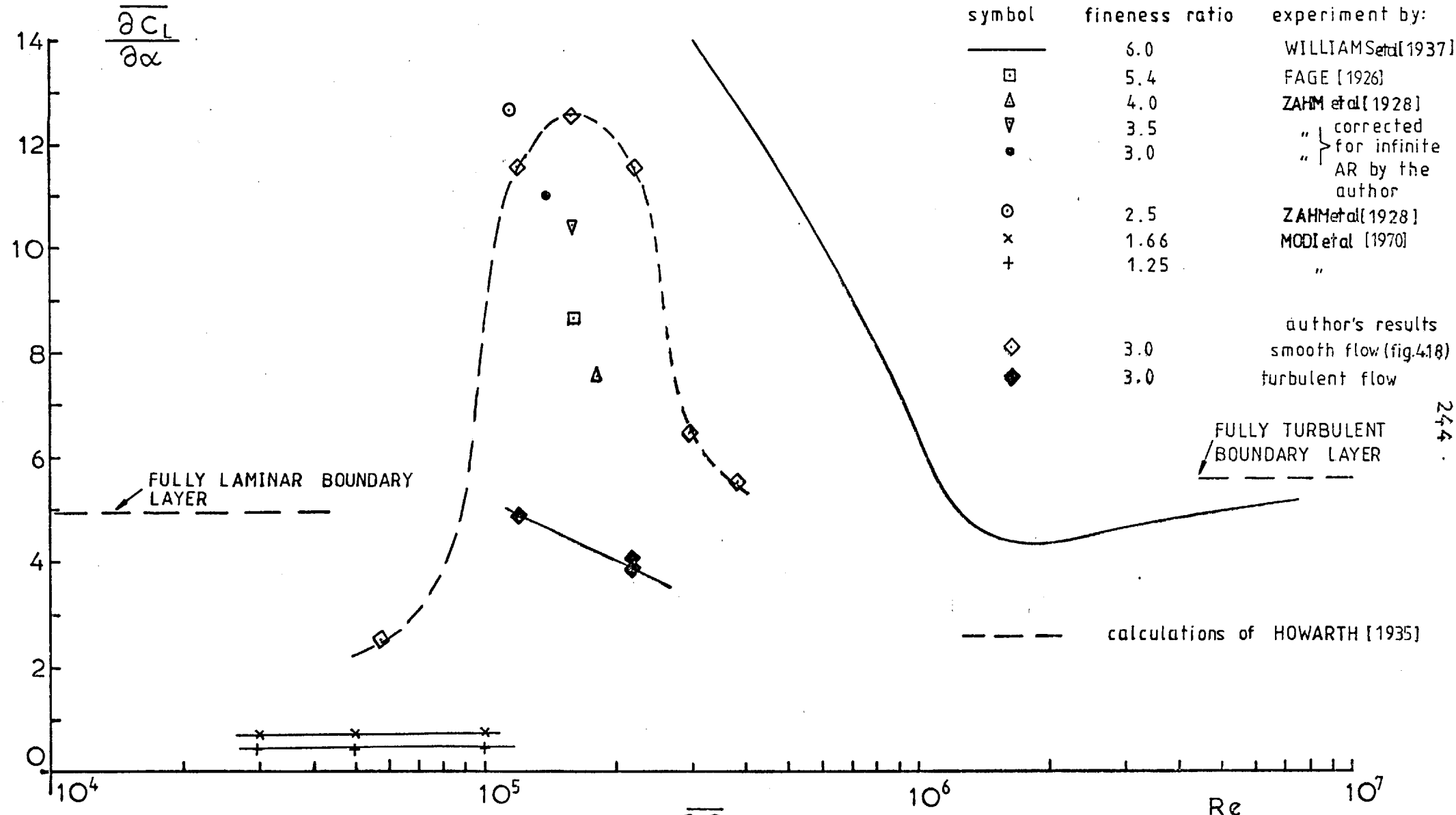

FIG. 2.1 EFFECT OF Re NUMBER ON $\frac{\partial \overline{C_L}}{\partial \alpha}$ FOR 2-D ELLIPTIC CYLINDERS OF VARIOUS FINENESS RATIOS.

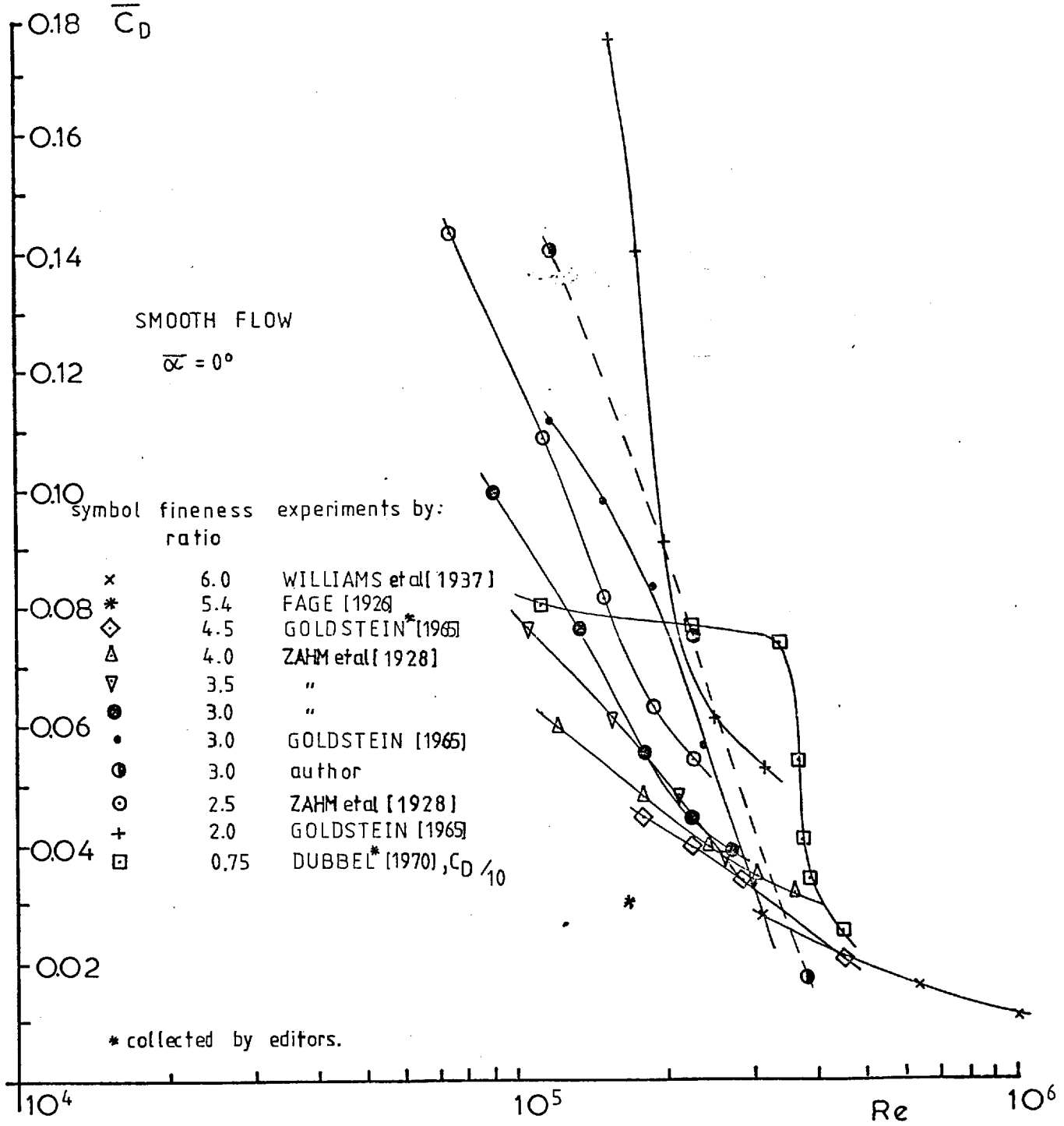

FIG. 2.2 EFFECT OF Re NUMBER ON $\overline{C_D}$ FOR 2-D ELLIPTIC CYLINDERS OF VARIOUS FINENESS RATIOS

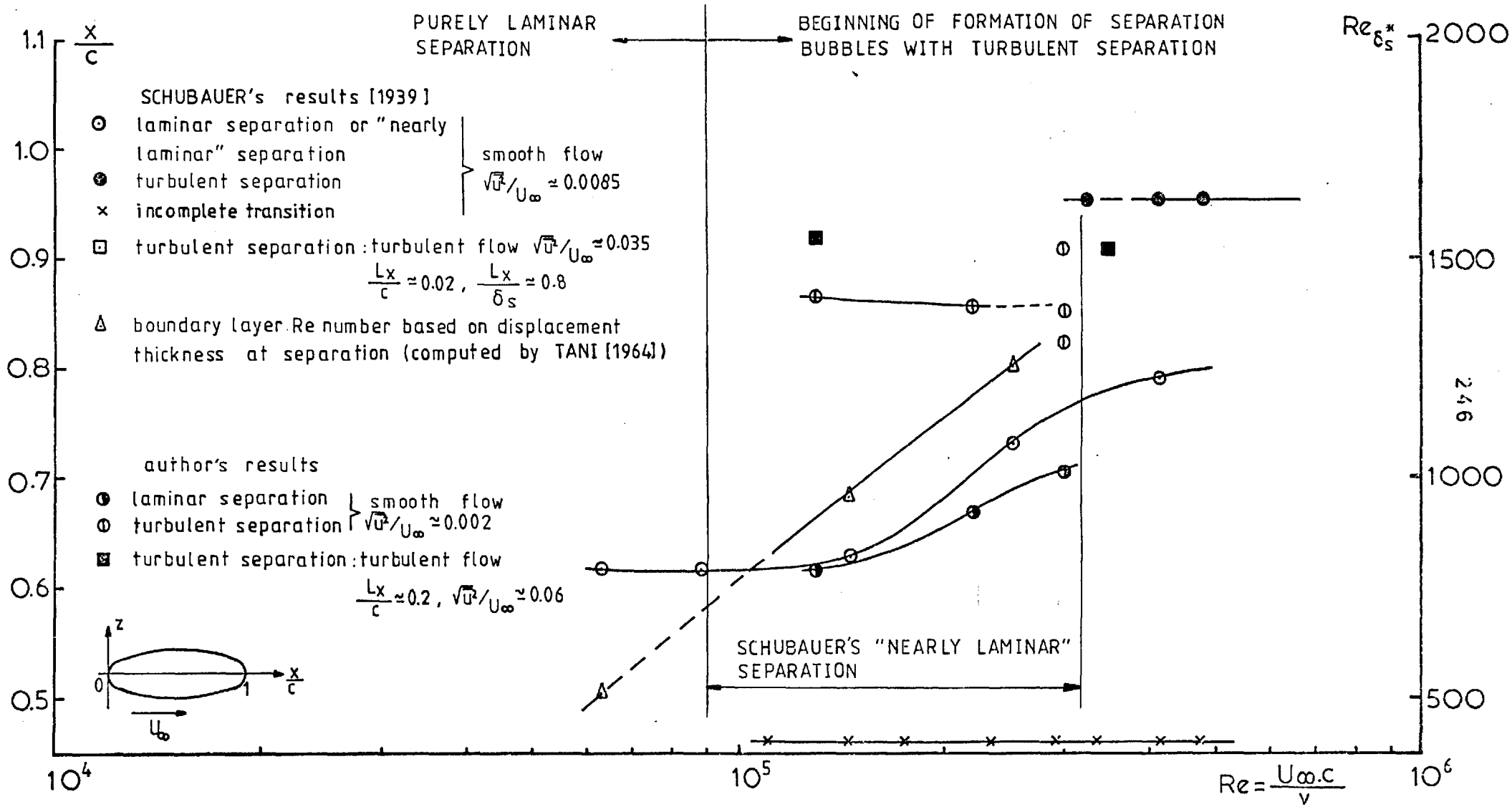

FIG. 2.3 BOUNDARY LAYER CHARACTERISTICS AS FUNCTIONS OF Re NUMBER FOR AN ELLIPTIC CYLINDER OF FINENESS RATIO 3.0, AT ZERO INCIDENCE

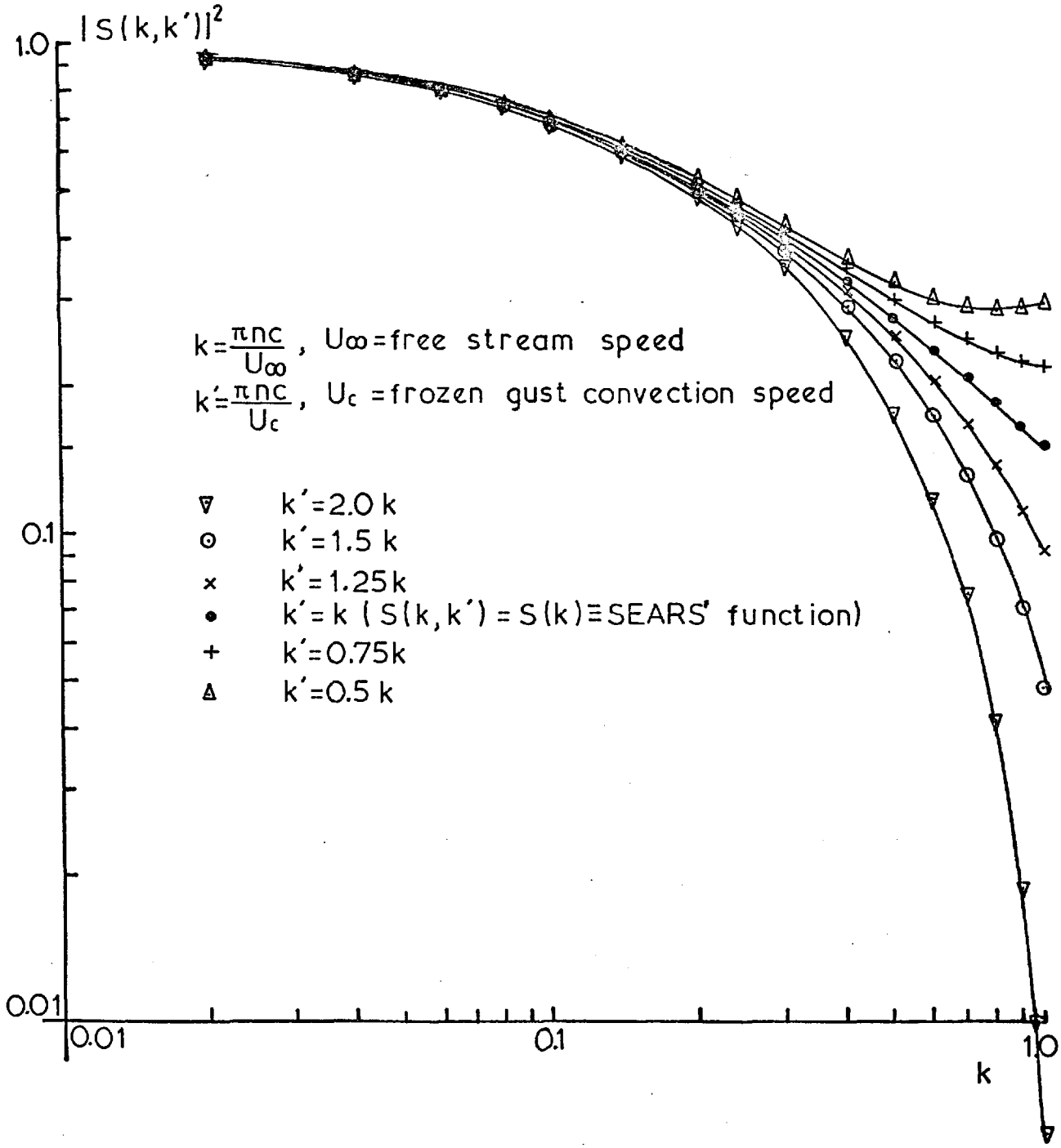

FIG. 2.4 SQUARED MODULUS OF KEMP'S FUNCTION (EQN. 2.10)

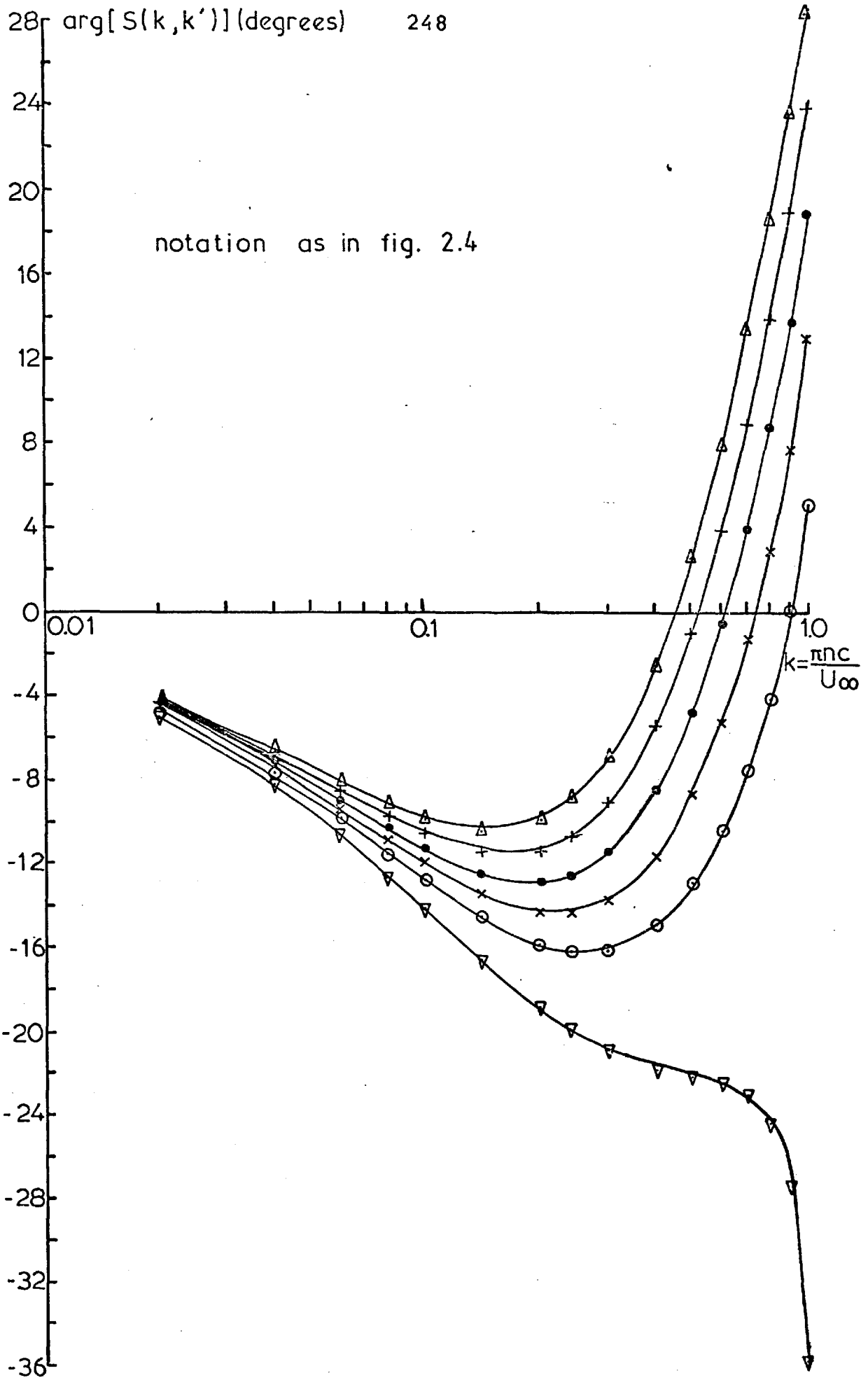

FIG. 2.5 ARGUMENT OF KEMP'S FUNCTION (SEE EQN. 2.10)

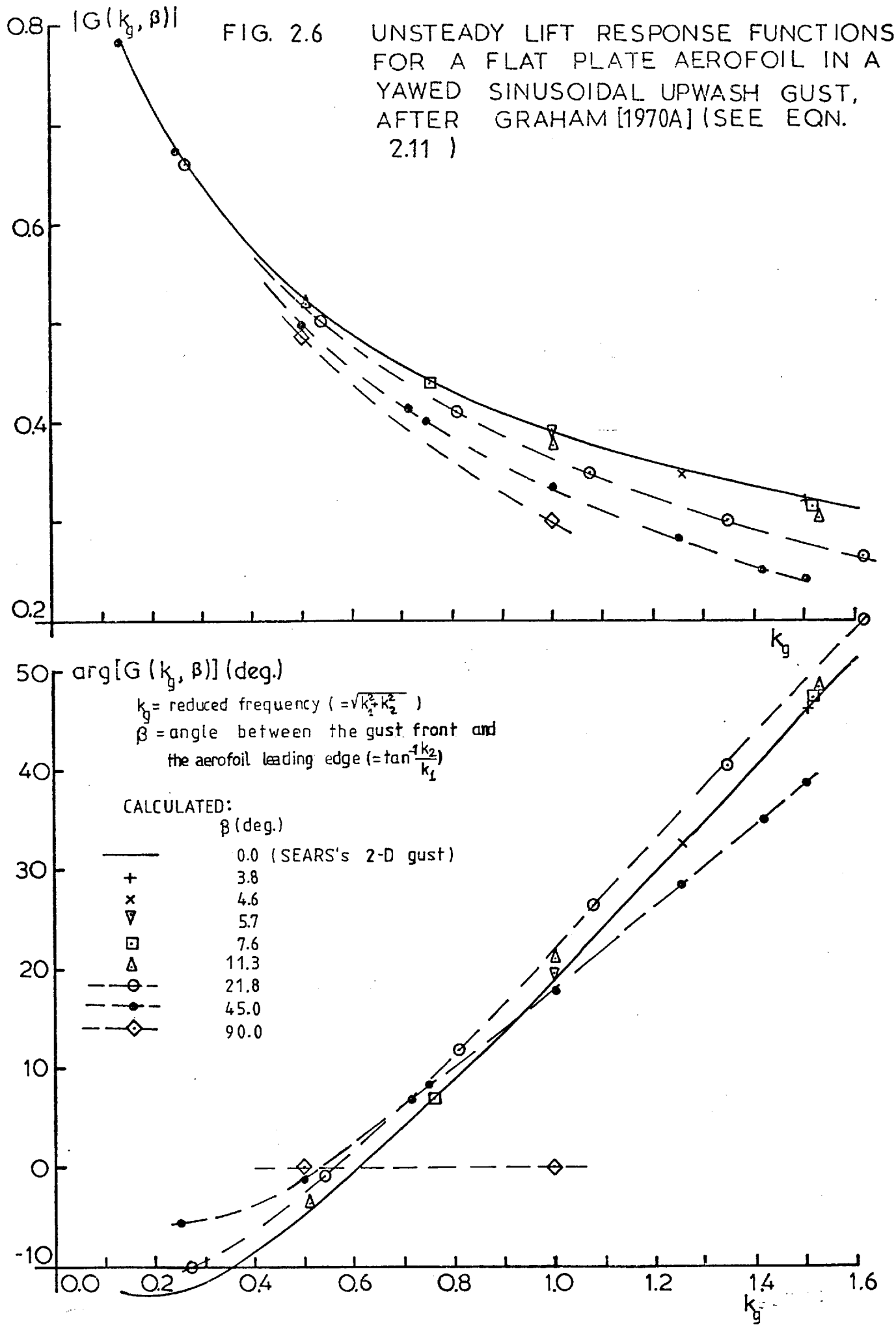

FIG. 2.6 UNSTEADY LIFT RESPONSE FUNCTIONS FOR A FLAT PLATE AEROFOIL IN A YAWED SINUSOIDAL UPWASH GUST, AFTER GRAHAM [1970A] (SEE EQN. 2.11)

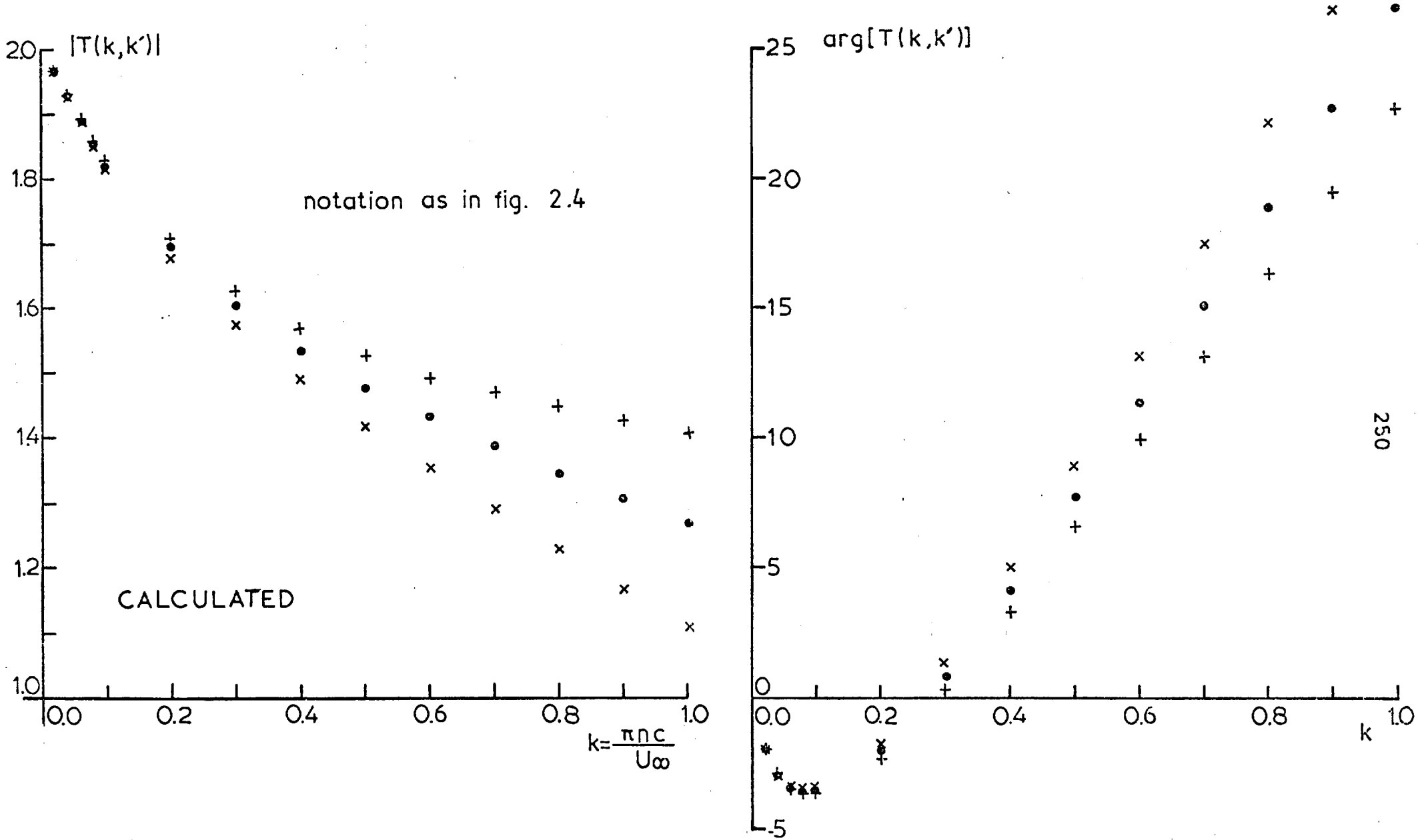

FIG. 2.7 UNSTEADY LIFT RESPONSE FUNCTIONS FOR A FLAT PLATE IN A SINUSOIDAL STREAMWISE GUST (SEE EQN. 2.15)

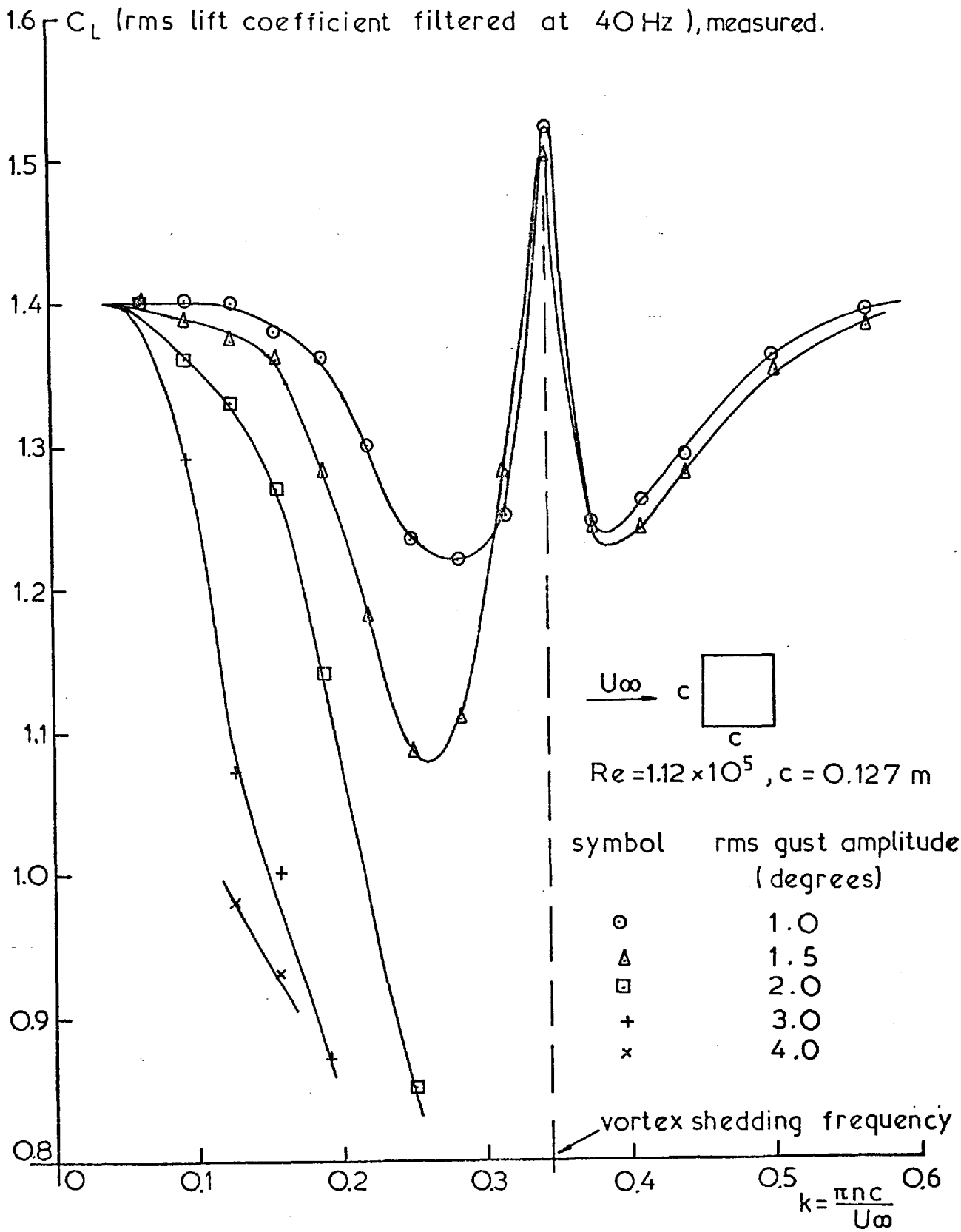

FIG. 2.8 RMS LIFT COEFFICIENT FOR A SQUARE CROSS SECTION CYLINDER IN A SINUSOIDAL UPWASH GUST, AFTER POCHA [1971]

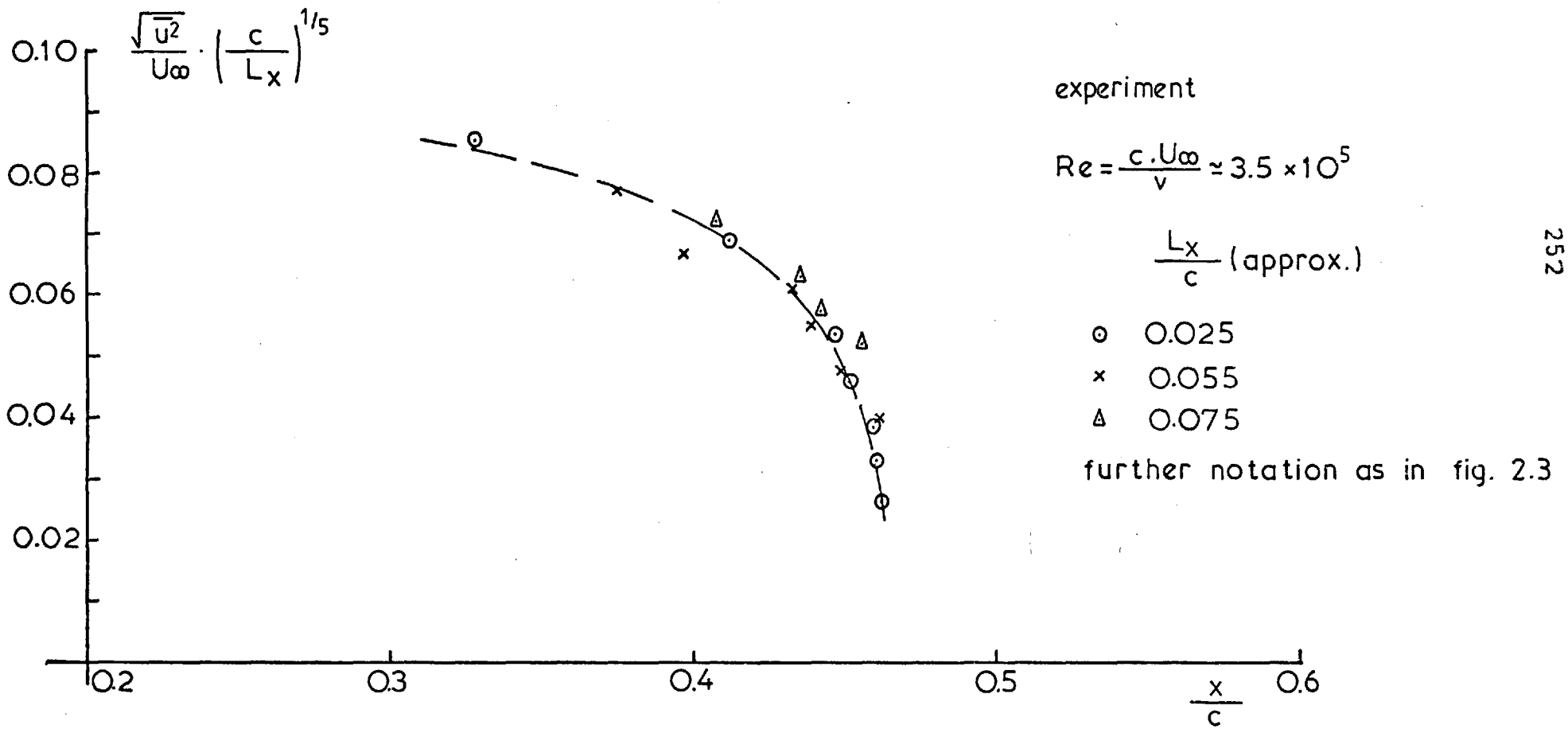

FIG. 2.9 BEGINNING OF TRANSITION FOR AN ELLIPTIC CYLINDER IN TURBULENT FLOW AFTER SCHUBAUER [1939]

$A_L = |A(k)|^2 \left(\frac{\overline{\partial c_L}}{\partial \alpha}\right)^2_{\text{theory}}$, or $\frac{S_{c_L c}}{S_{w,c}}$, (experiment).

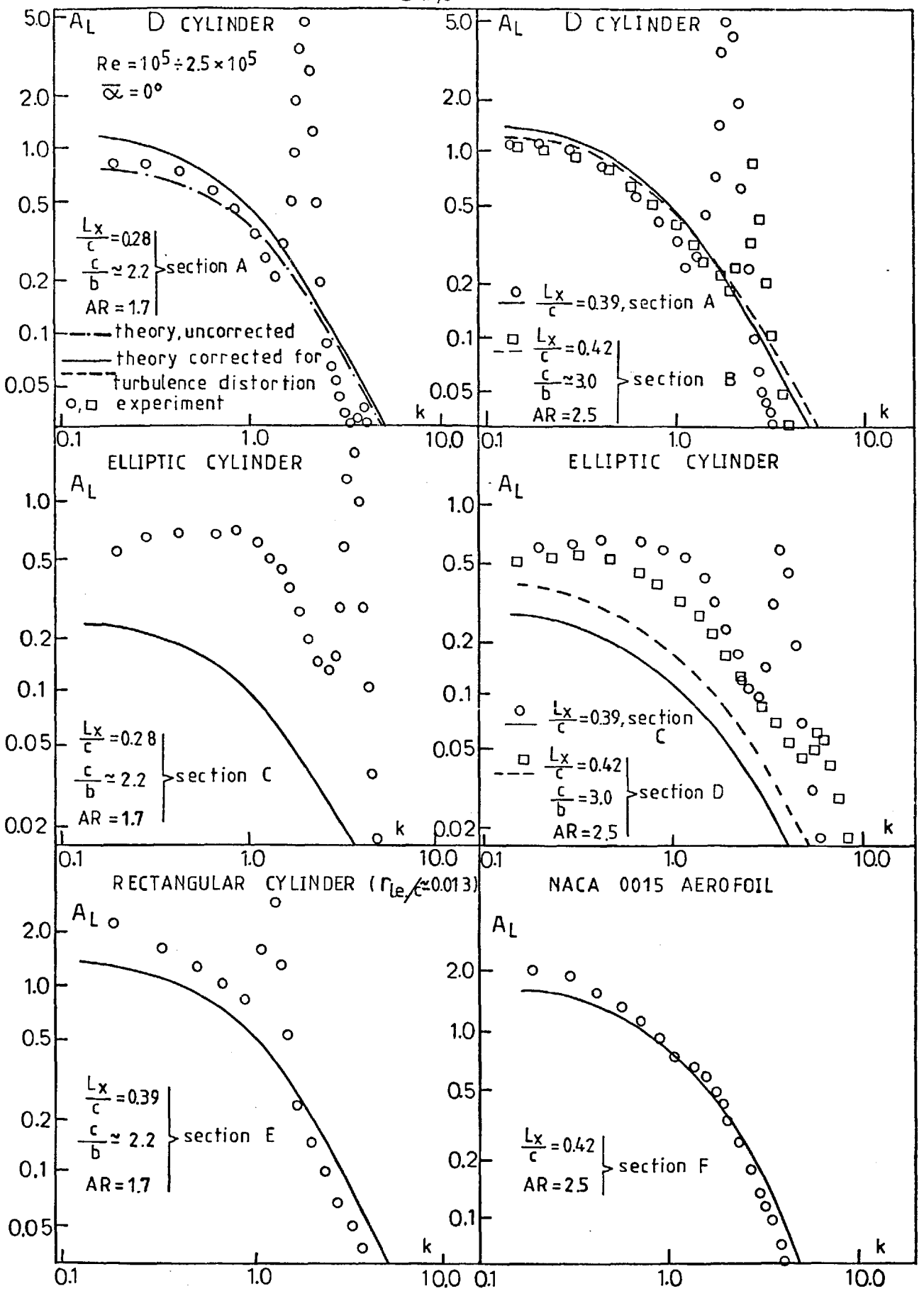

FIG. 2.10 AERODYNAMIC ADMITTANCES OF LIFT FOR TWO DIMENSIONAL CYLINDERS IN TURBULENT CROSS FLOW (BROAD BAND RESPONSE) AFTER GRAHAM [1973]

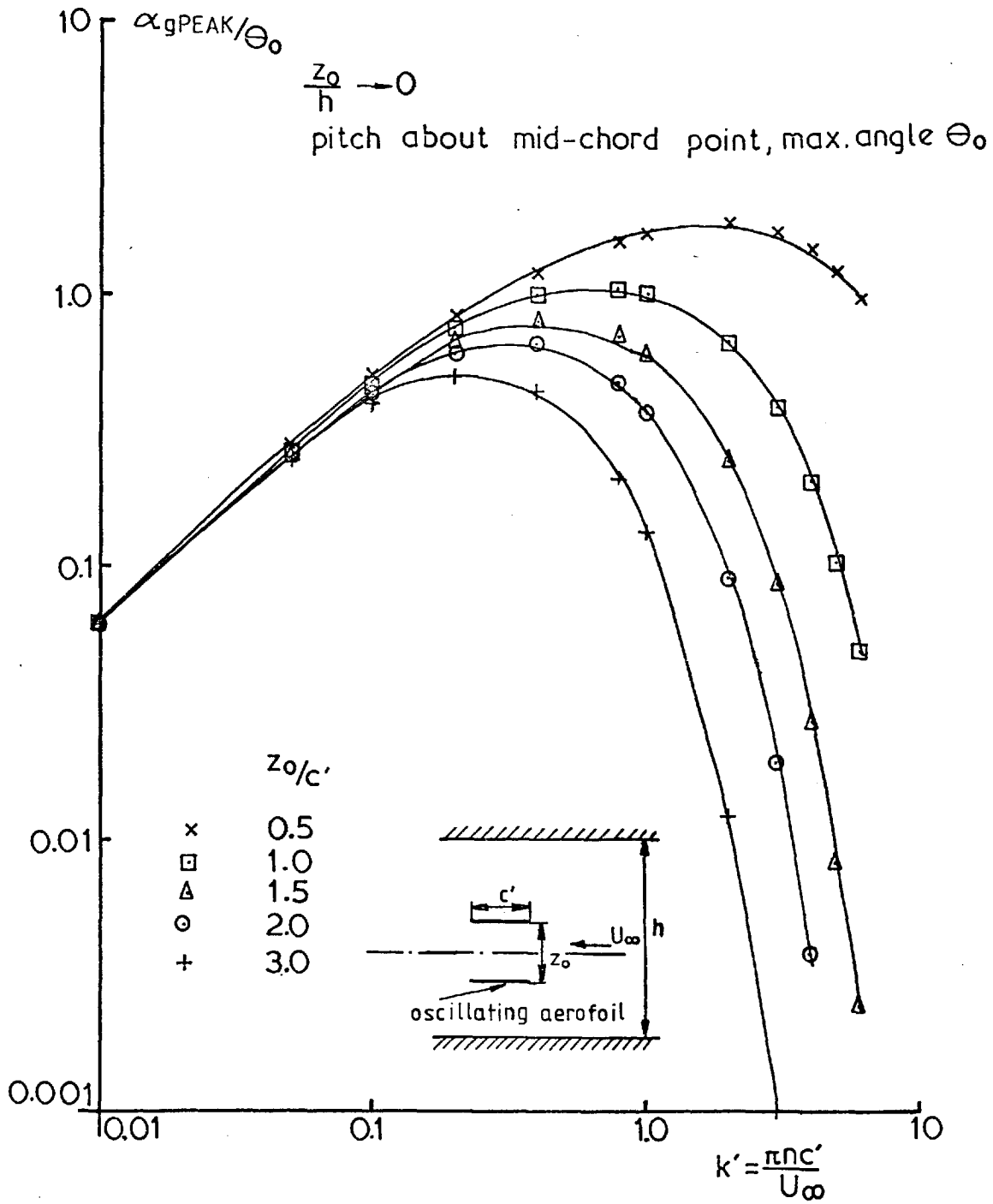

FIG. 3.1 CALCULATED DIMENSIONLESS GUST AMPLITUDE ALONG CENTRE LINE (FROM EQN. 3.34)

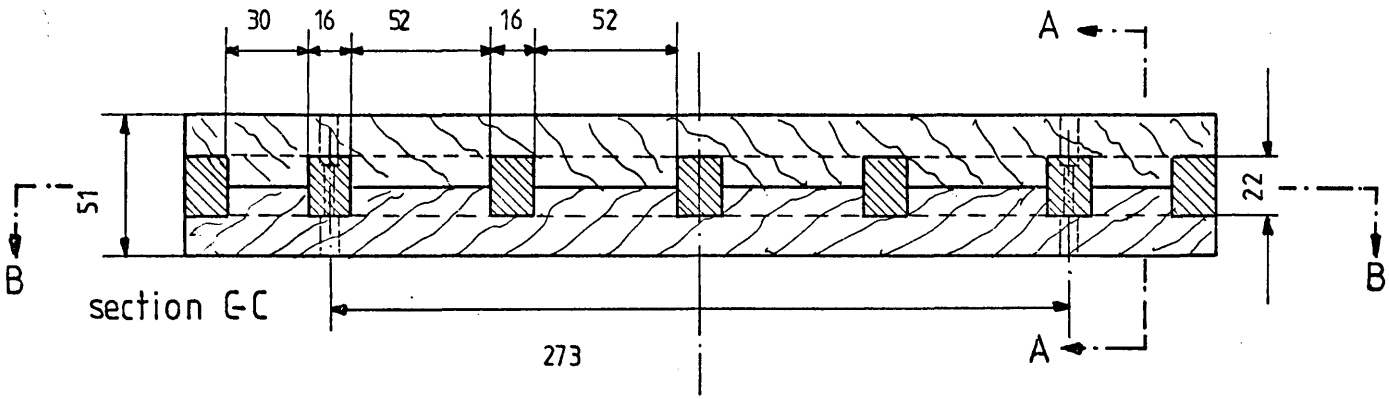

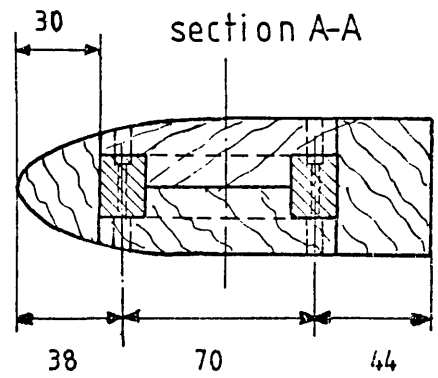

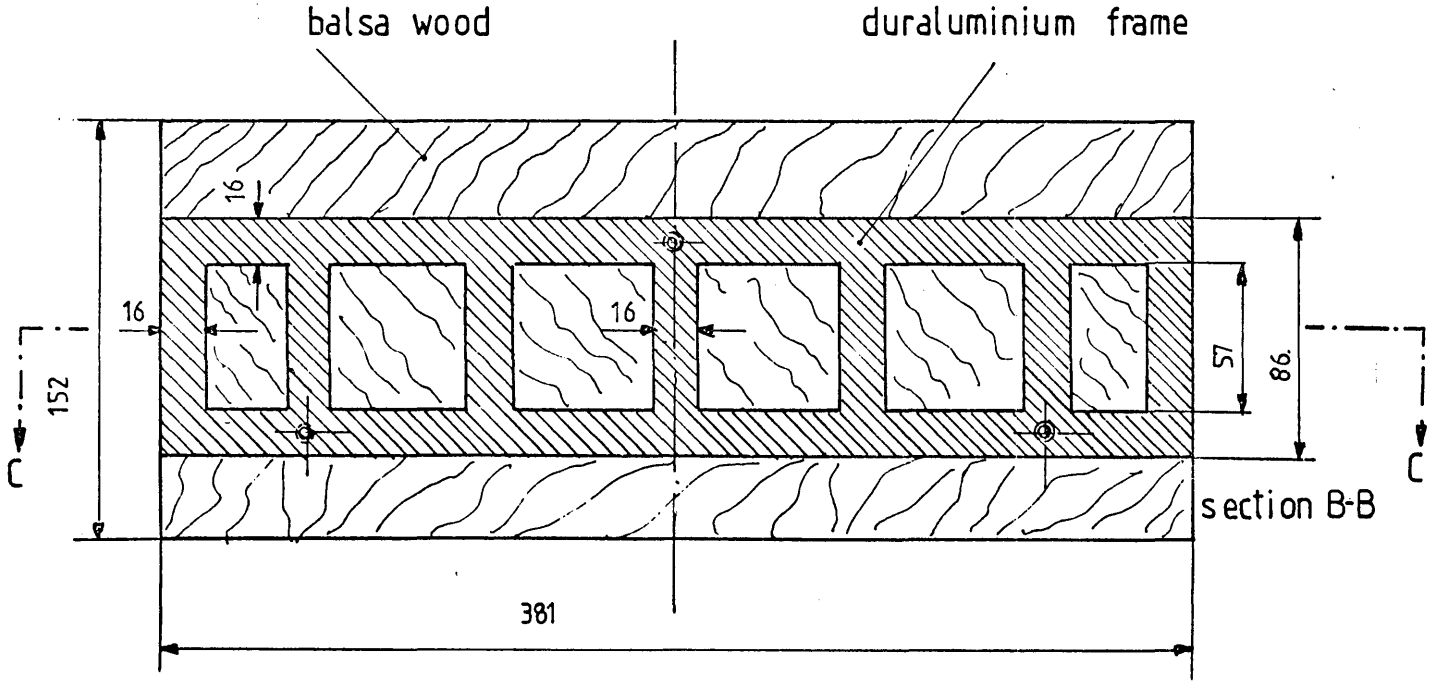

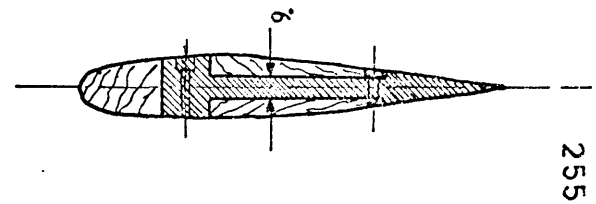

dimensions in mm

elliptic cylinder constructed as the D cylinder

FIG. 3.2 CONSTRUCTIONAL DETAILS OF THE MODELS USED IN THE UNSTEADY LIFT EXPERIMENT

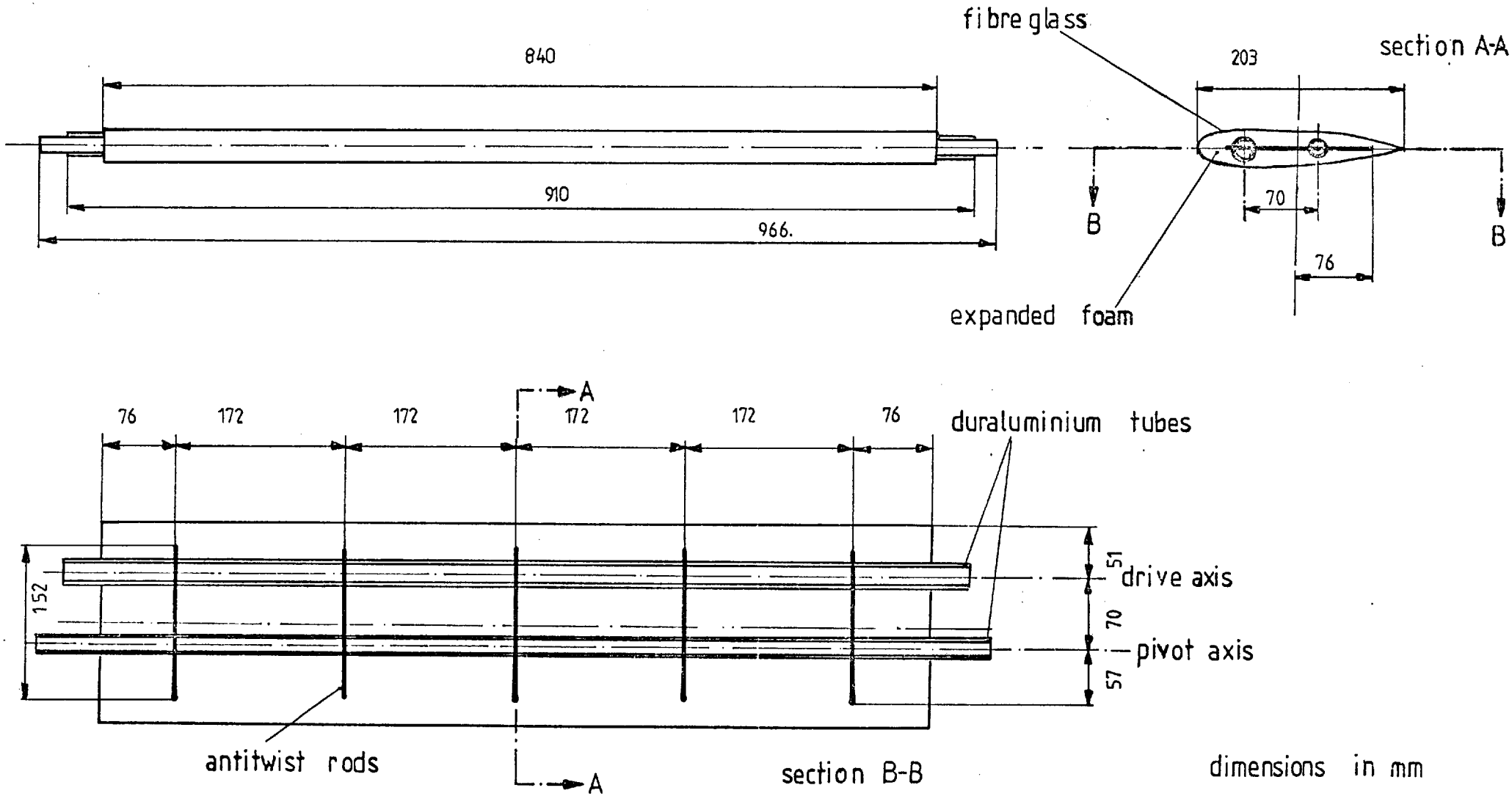

256

FIG. 3.3 CONSTRUCTIONAL DETAILS FOR OSCILLATING NACA 0015 AEROFOILS

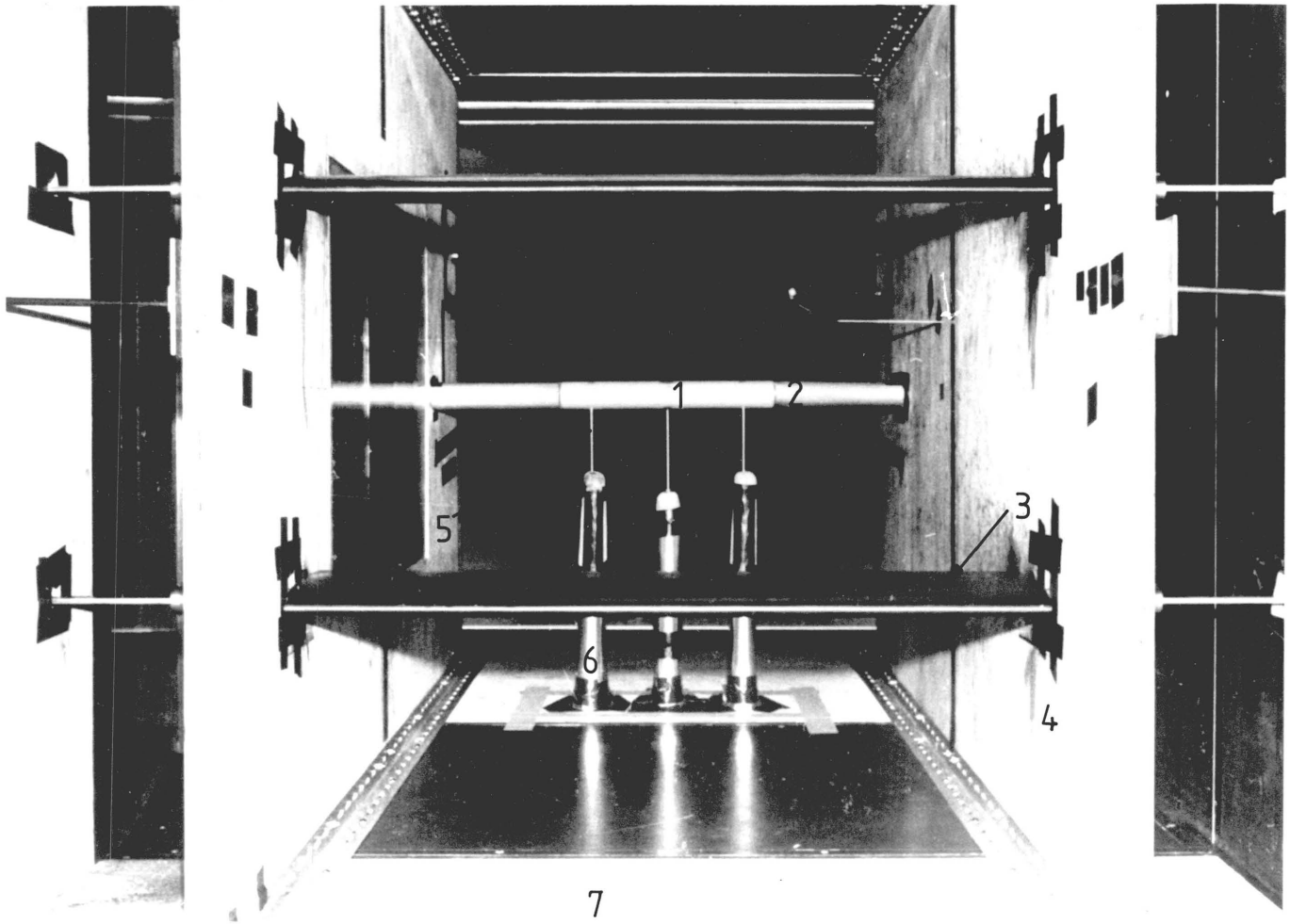

1 test model
2 dummy sections
3 oscillating wings
4 end plates
5 rods connecting model with piezoelectric transducers
6 aerodynamic shields covering the protruding pylons of the lift balance
7 tunnel floor

FIG. 3.4 WIND TUNNEL ASSEMBLY (VIEW FROM SETTLING CHAMBER)

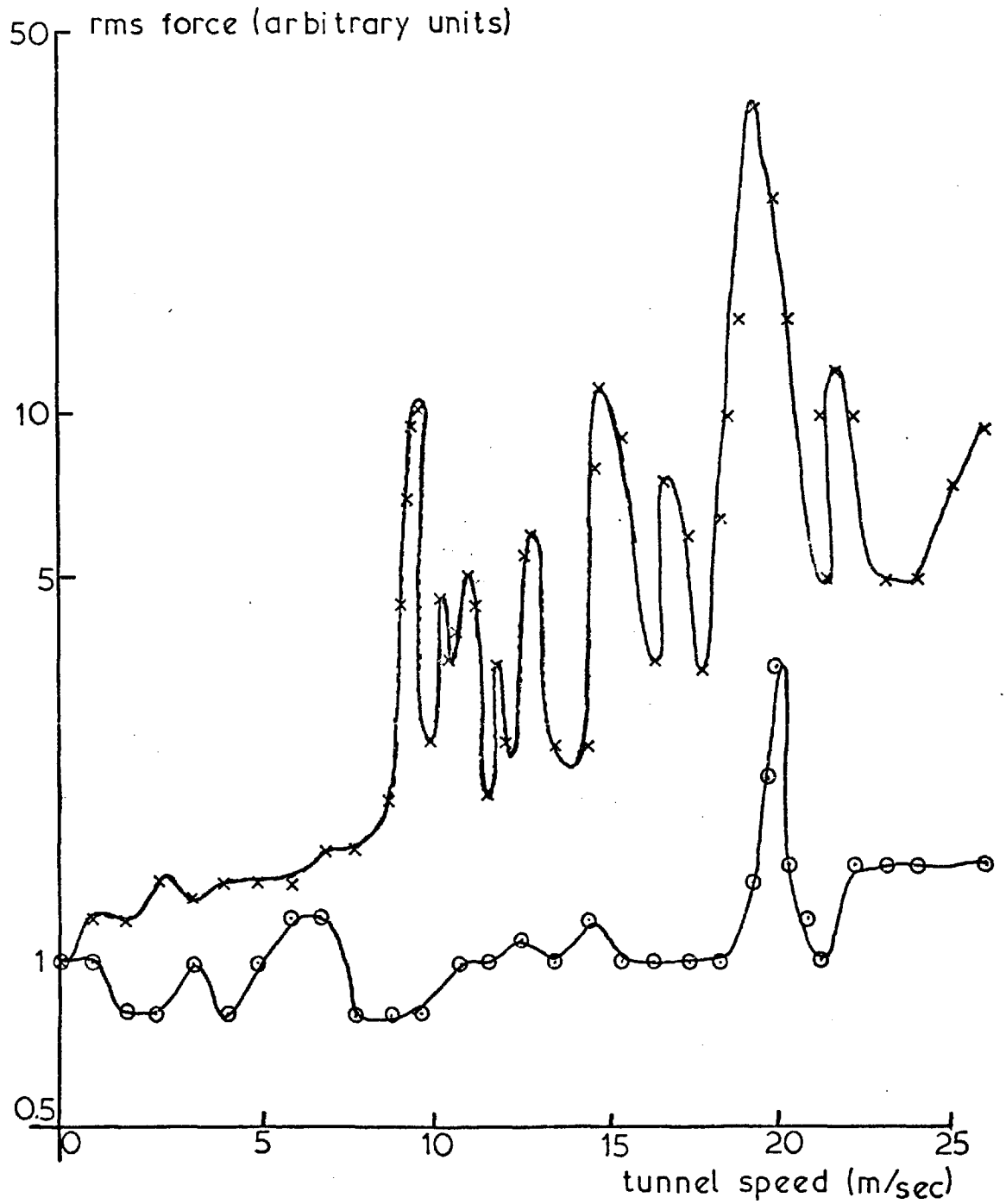

× balance installed outside the working section on the floor
⊙ " " " " " " " helical springs

FIG. 3.5 RMS FORCE TRANSMITTED THROUGH THE LOAD BALANCE TO THE AEROFOIL MODEL

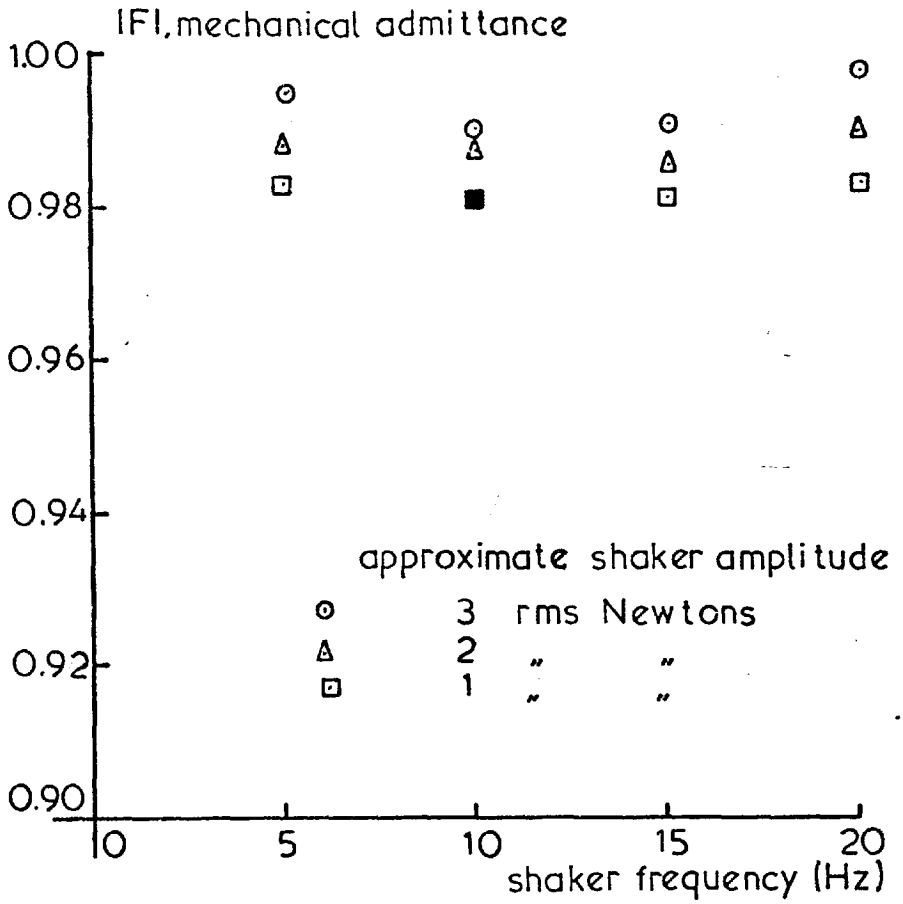

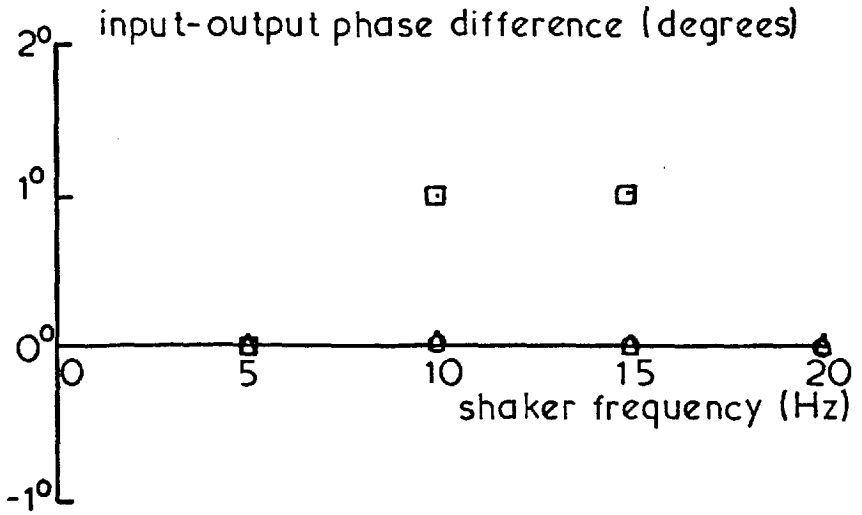

FIG. 3.6 DYNAMIC CALIBRATION OF LOAD BALANCE

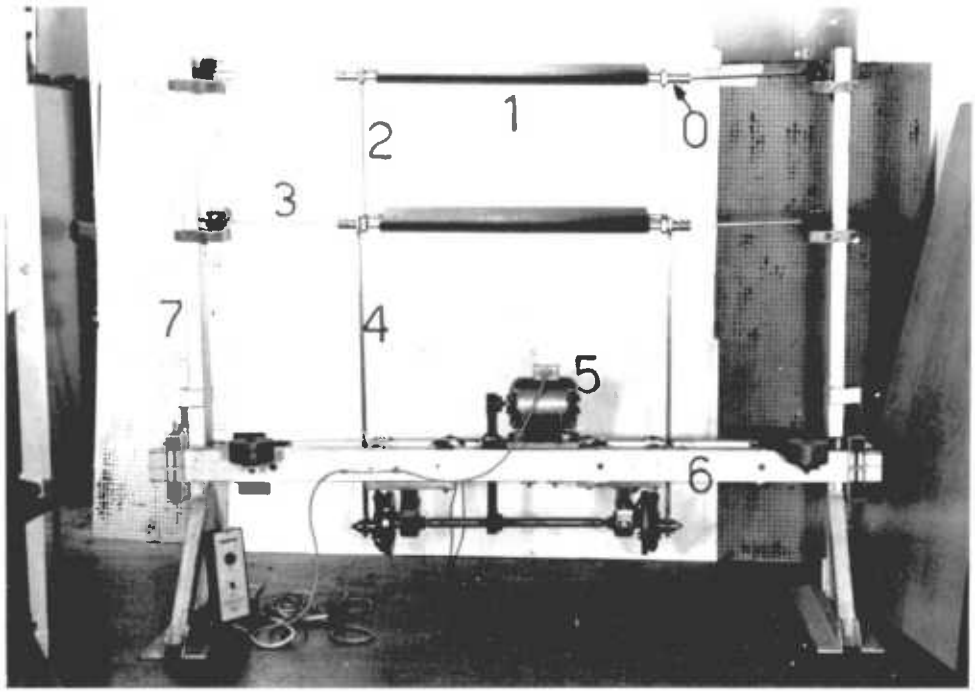

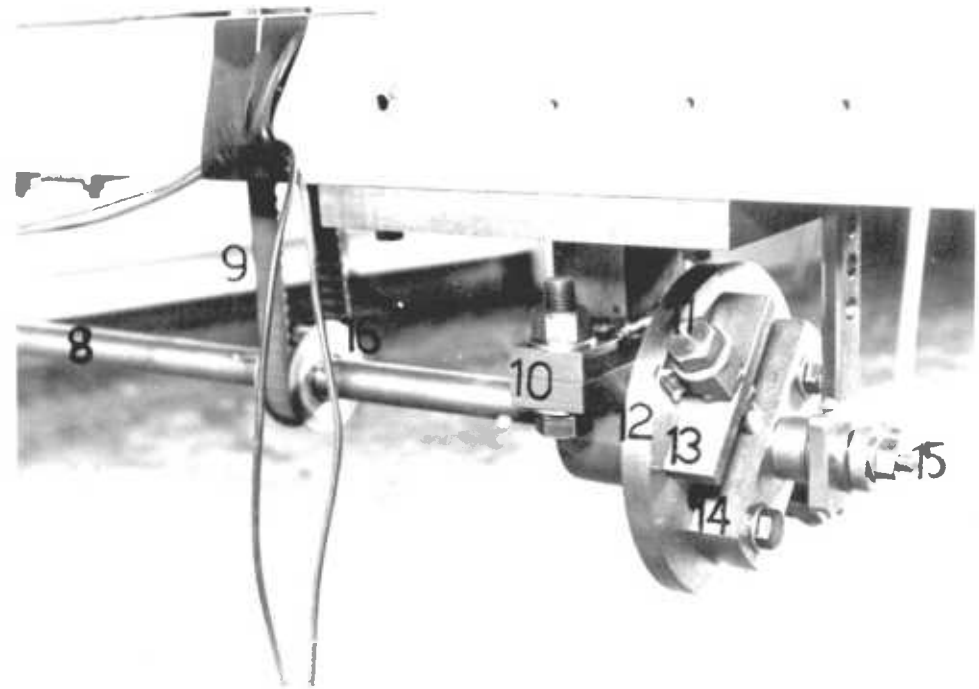

0 pin shaft
1 oscillating wing
2 short connecting rod
3 rectangular leaf spring
4 long connecting rod
5 DC motor with speed controller
6 horizontal girder support
7 vertical support
8 main shaft
9 toothed belt
10 ball bearing housing
11 bolt for changing eccentricity
12 fly-wheel
13 counter-weight
14 block carrying eccentric shaft
15 eccentric shaft
16 pulley

FIG. 3.7 THE OSCILLATING RIG.(ASSEMBLED OUTSIDE THE WIND TUNNEL)

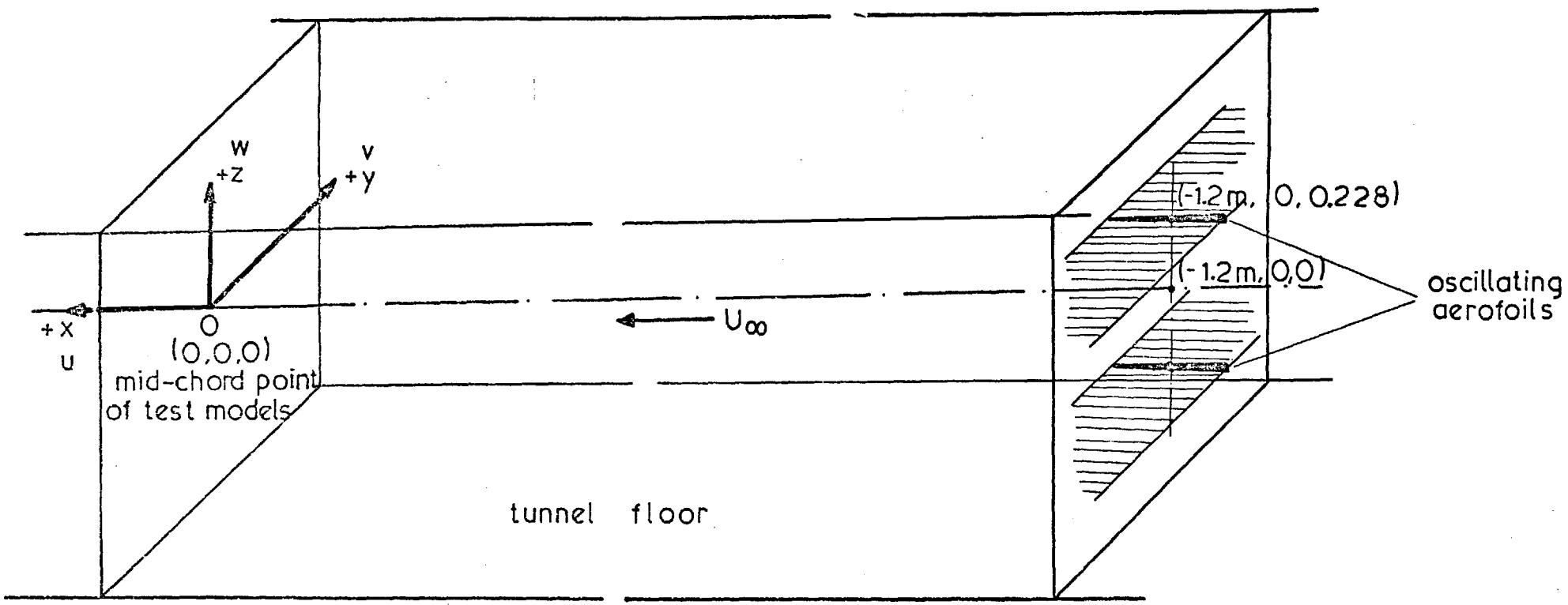

FIG. 3.8 COORDINATE SYSTEM USED IN THE EXPERIMENTS

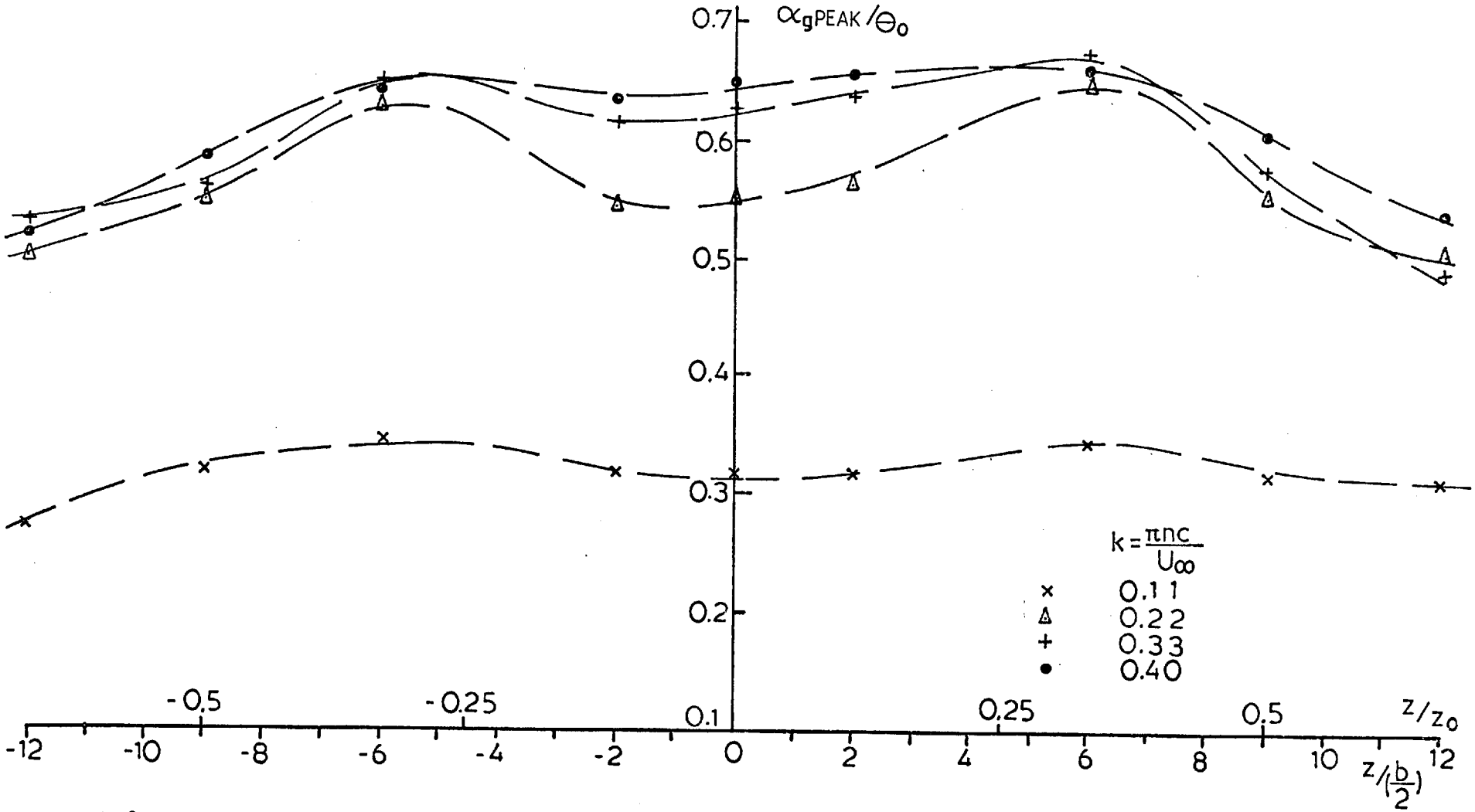

FIG. 3.9 MEASURED DIMENSIONLESS GUST AMPLITUDE (UNFILTERED) -MEDIUM ECCENTRICITY

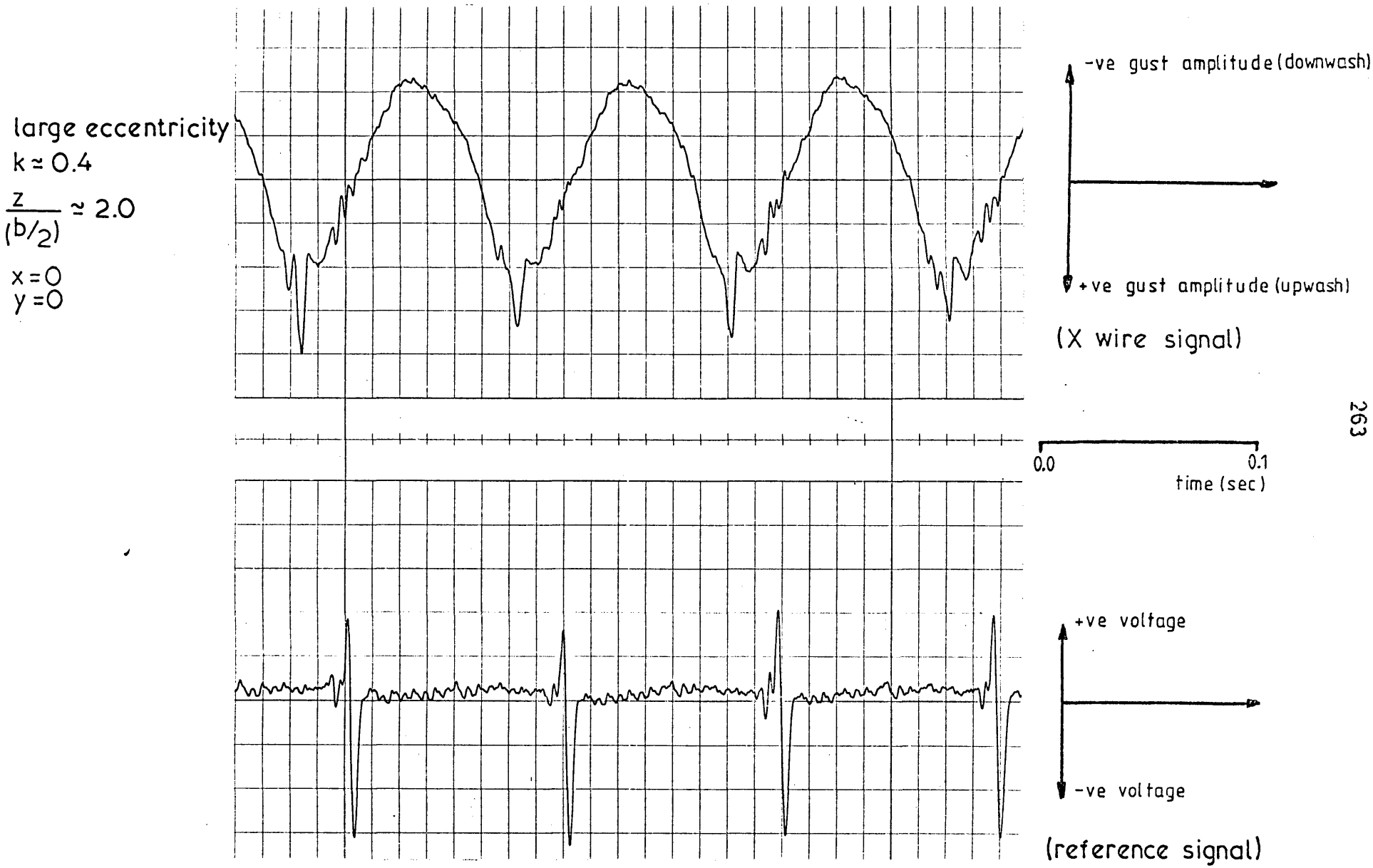

FIG. 3.10 TIME DEPENDENCE OF UPWASH (OFF CENTRE LINE)

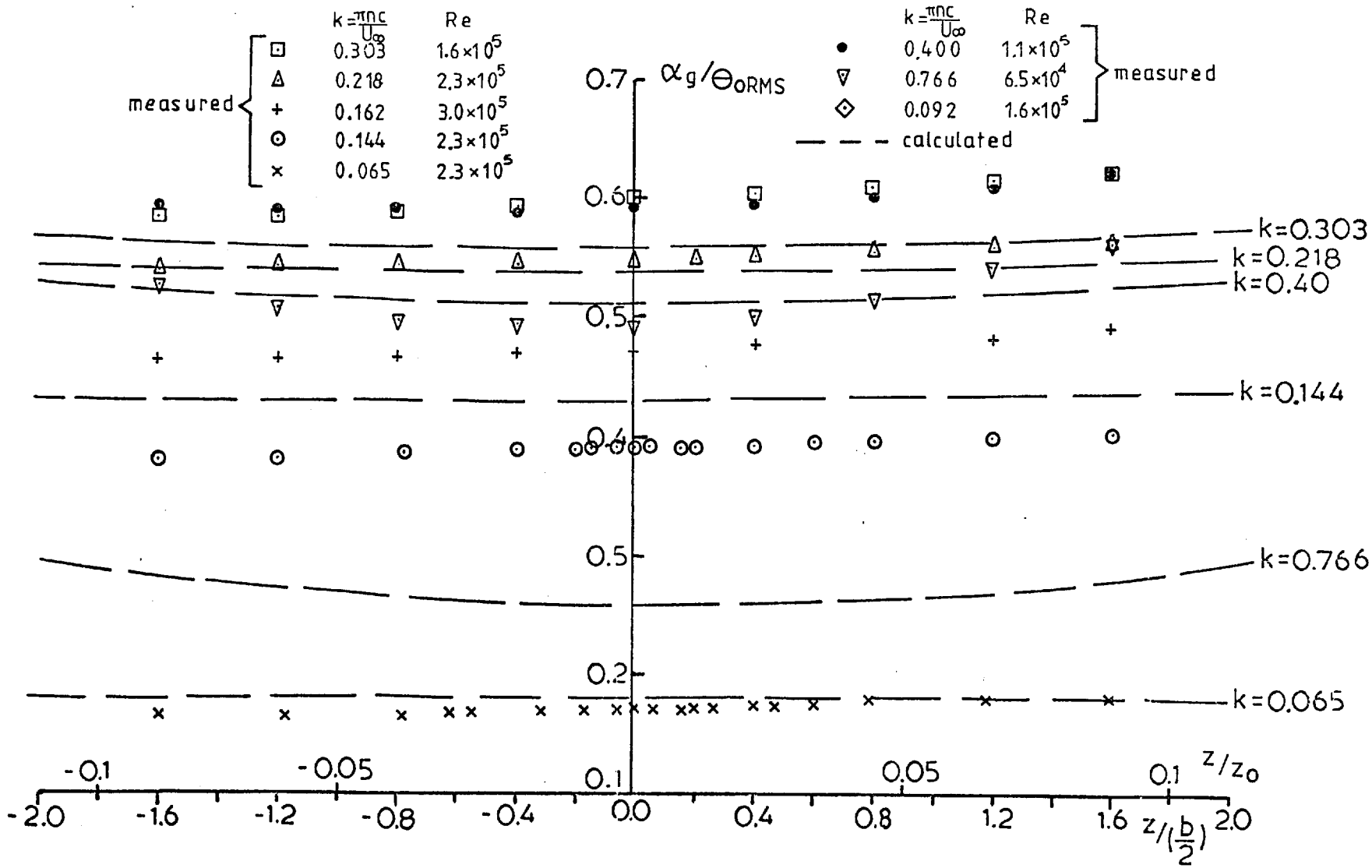

FIG. 3.11 DIMENSIONLESS GUST AMPLITUDE - LARGE ECCENTRICITY

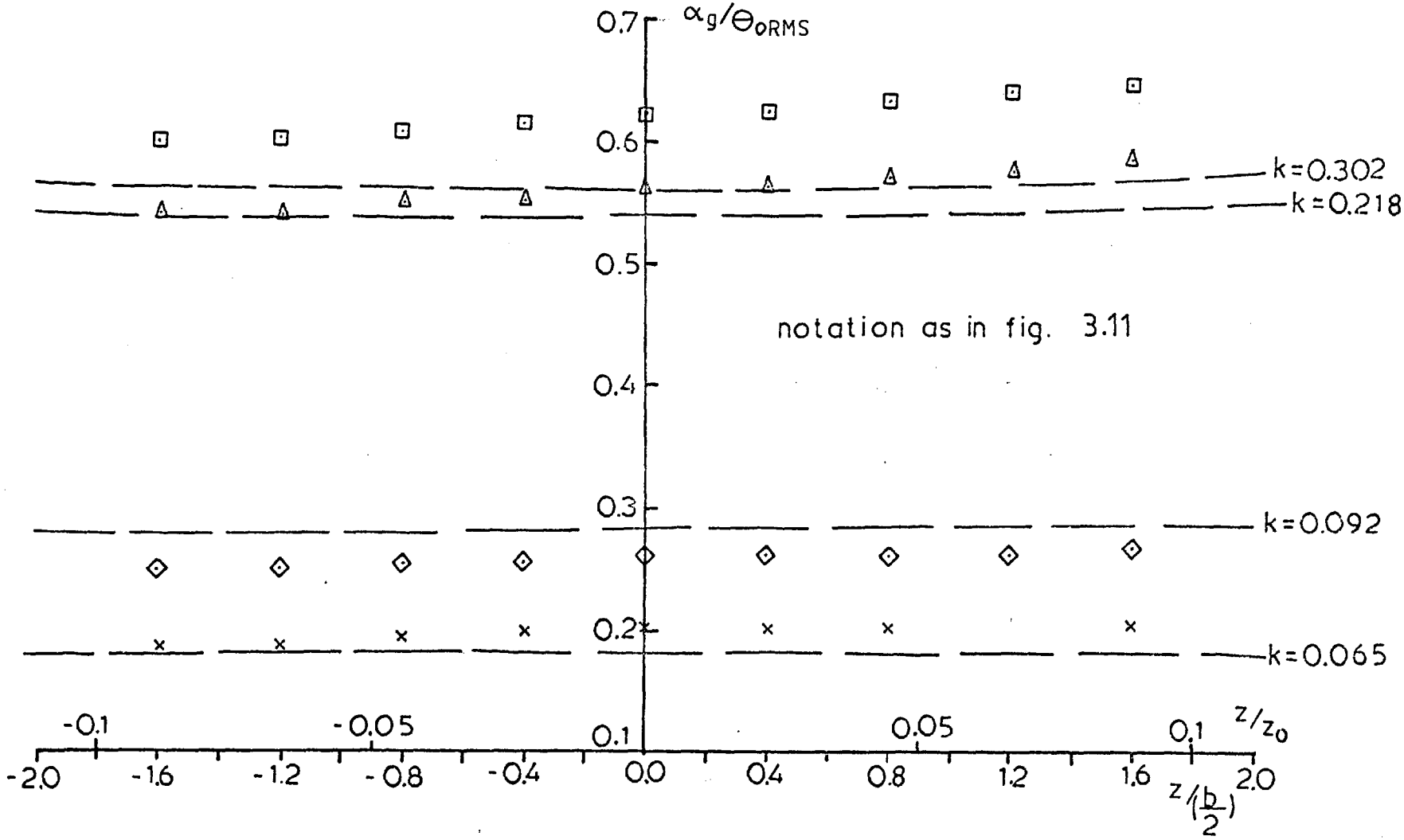

FIG. 3.12 DIMENSIONLESS GUST AMPLITUDE -MEDIUM ECCENTRICITY

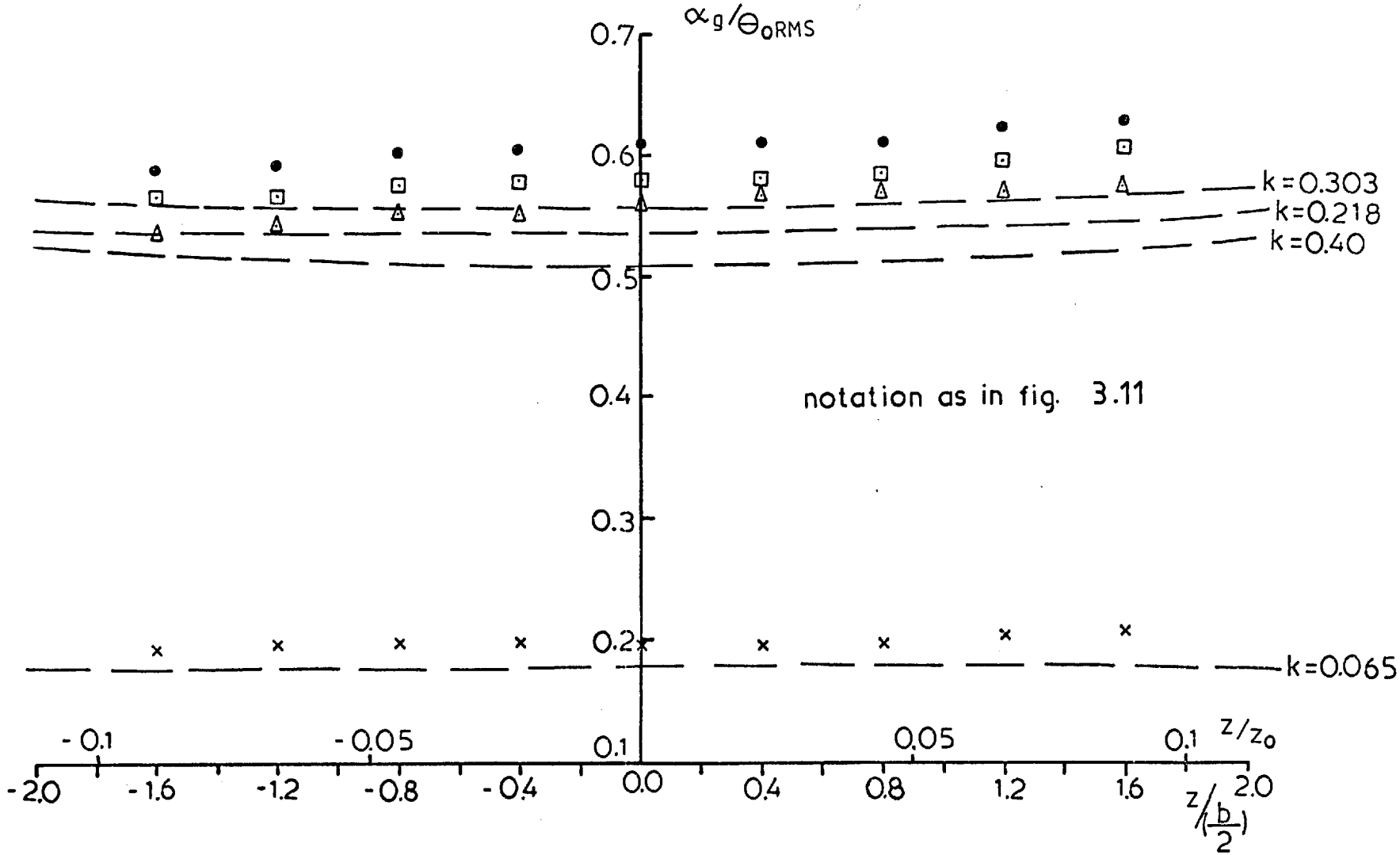

FIG. 3.13 DIMENSIONLESS GUST AMPLITUDE - SMALL ECCENTRICITY

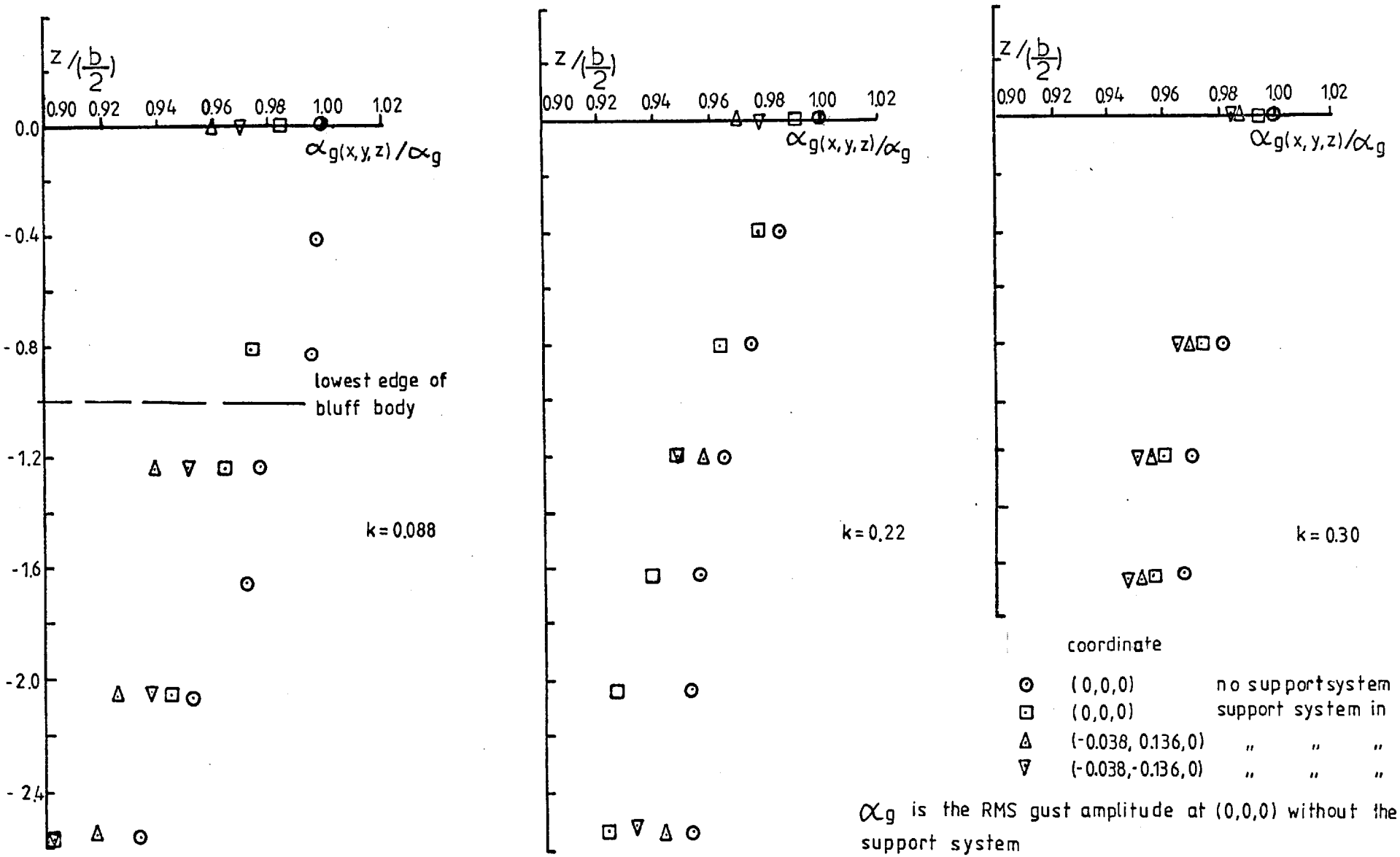

FIG. 3.14 EFFECT OF TRIPOD SUPPORT SYSTEM ON GUST INTENSITY

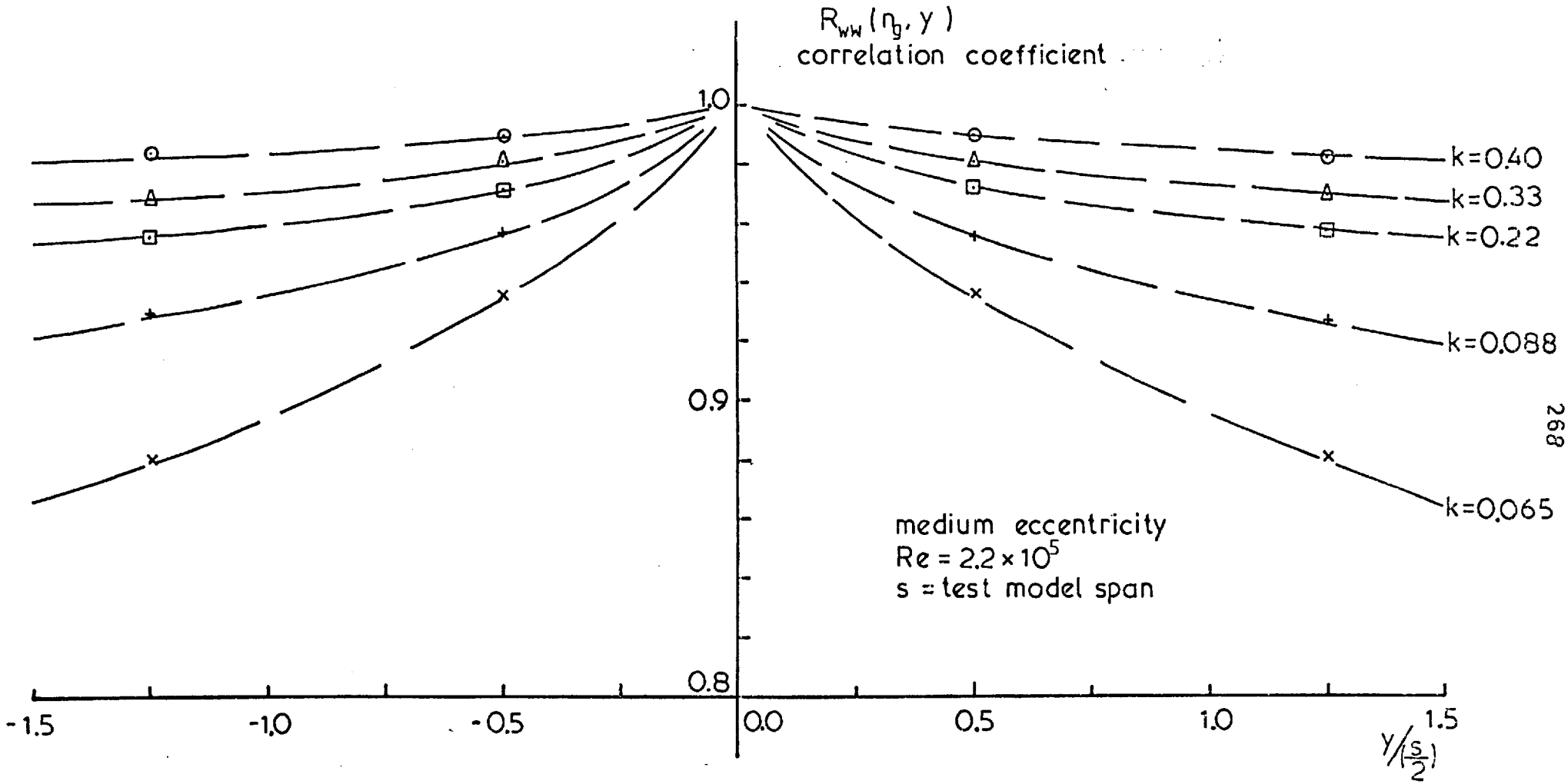

FIG. 3.15 CORRELATION COEFFICIENT OF GUST IN THE SPANWISE DIRECTION (SUPPORT TRIPOD IN), AT GUST FREQUENCY

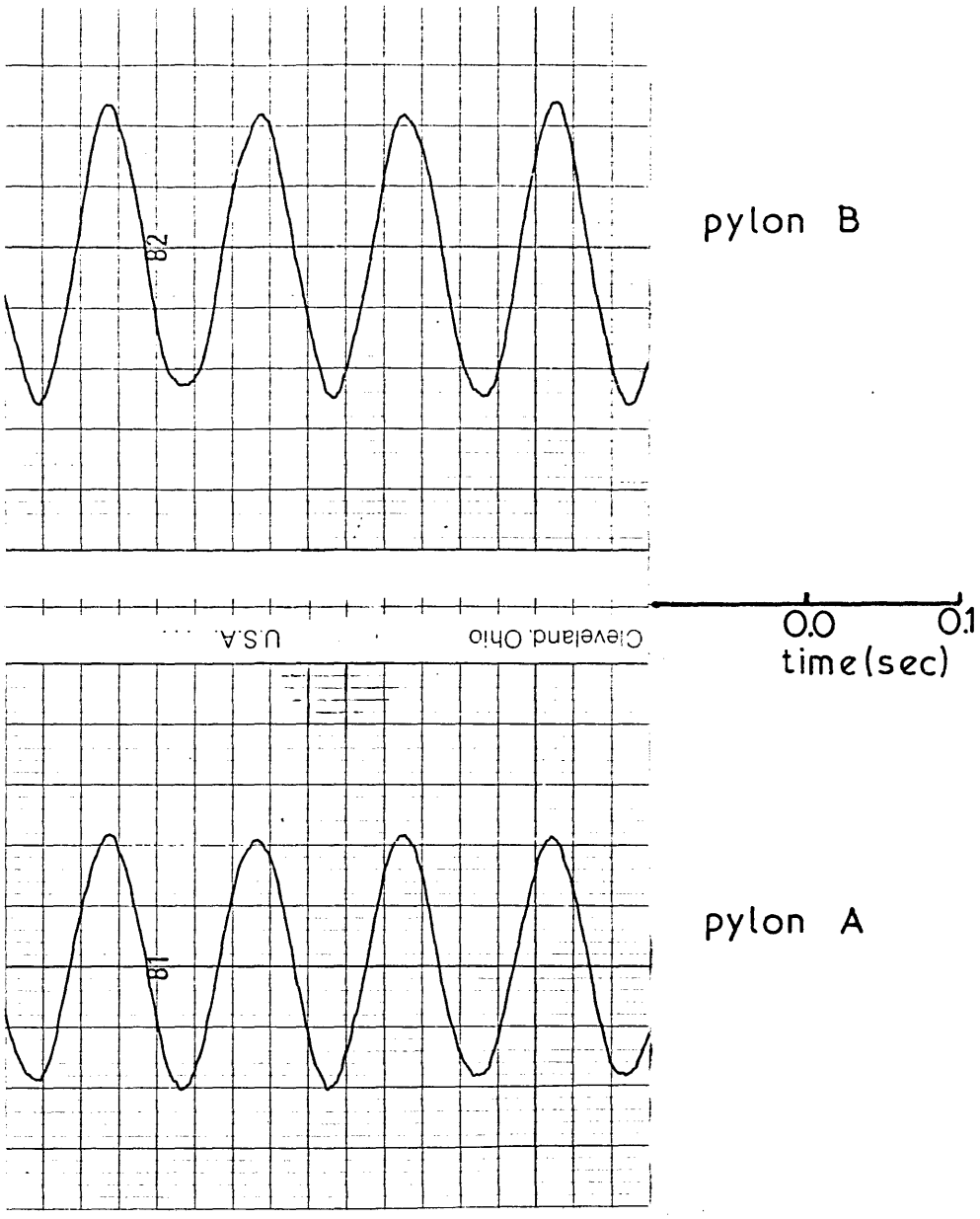

FIG. 3.16 INSTANTANEOUS PLOT OF LIFT ON TWO SMALL AEROFOILS FIXED ON FRONT PYLONS

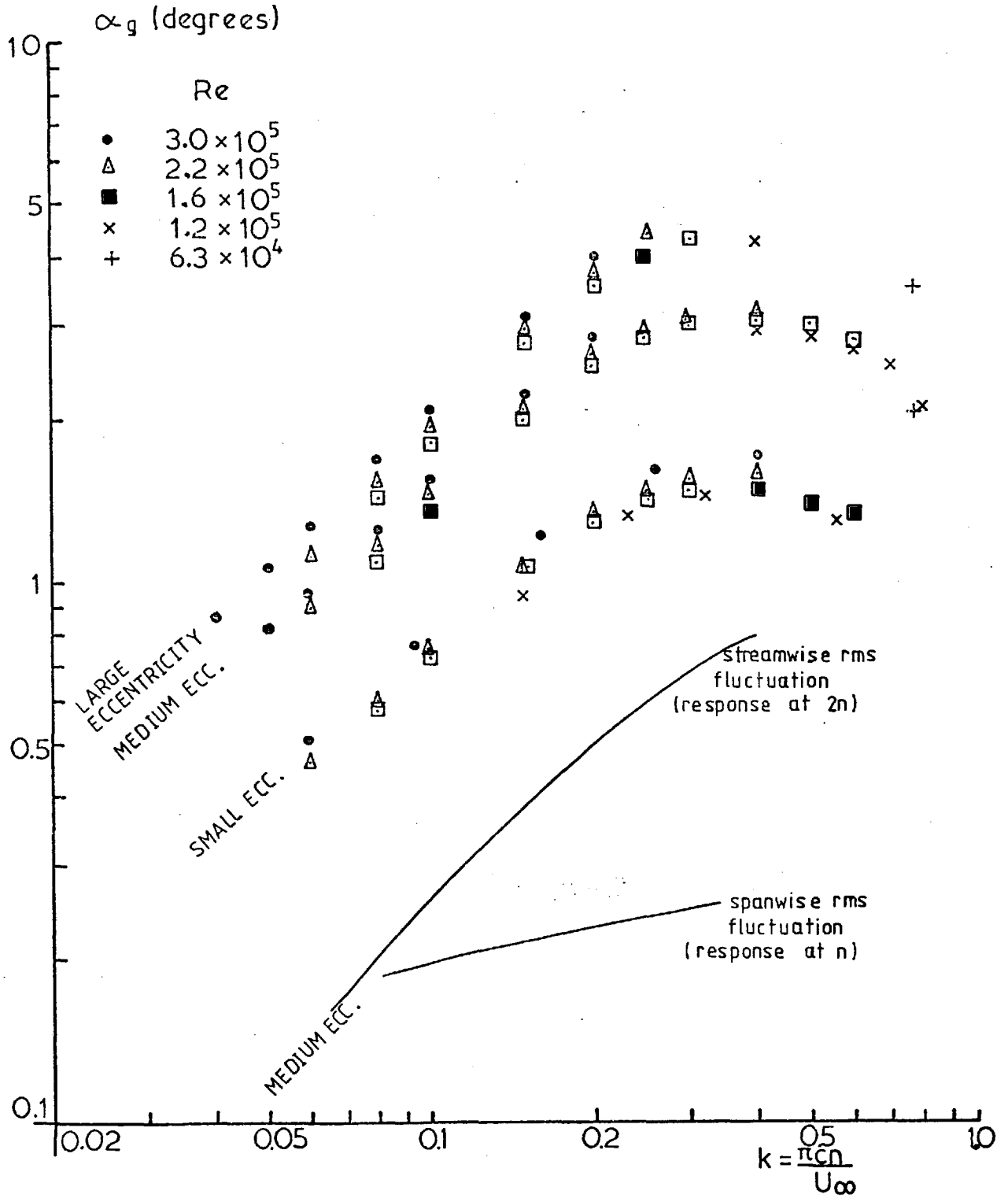

FIG. 3.17 MEASURED RMS GUST AMPLITUDE (FILTERED) IN EMPTY WIND TUNNEL (MODELS AND SUPPORT SYSTEM OUT)

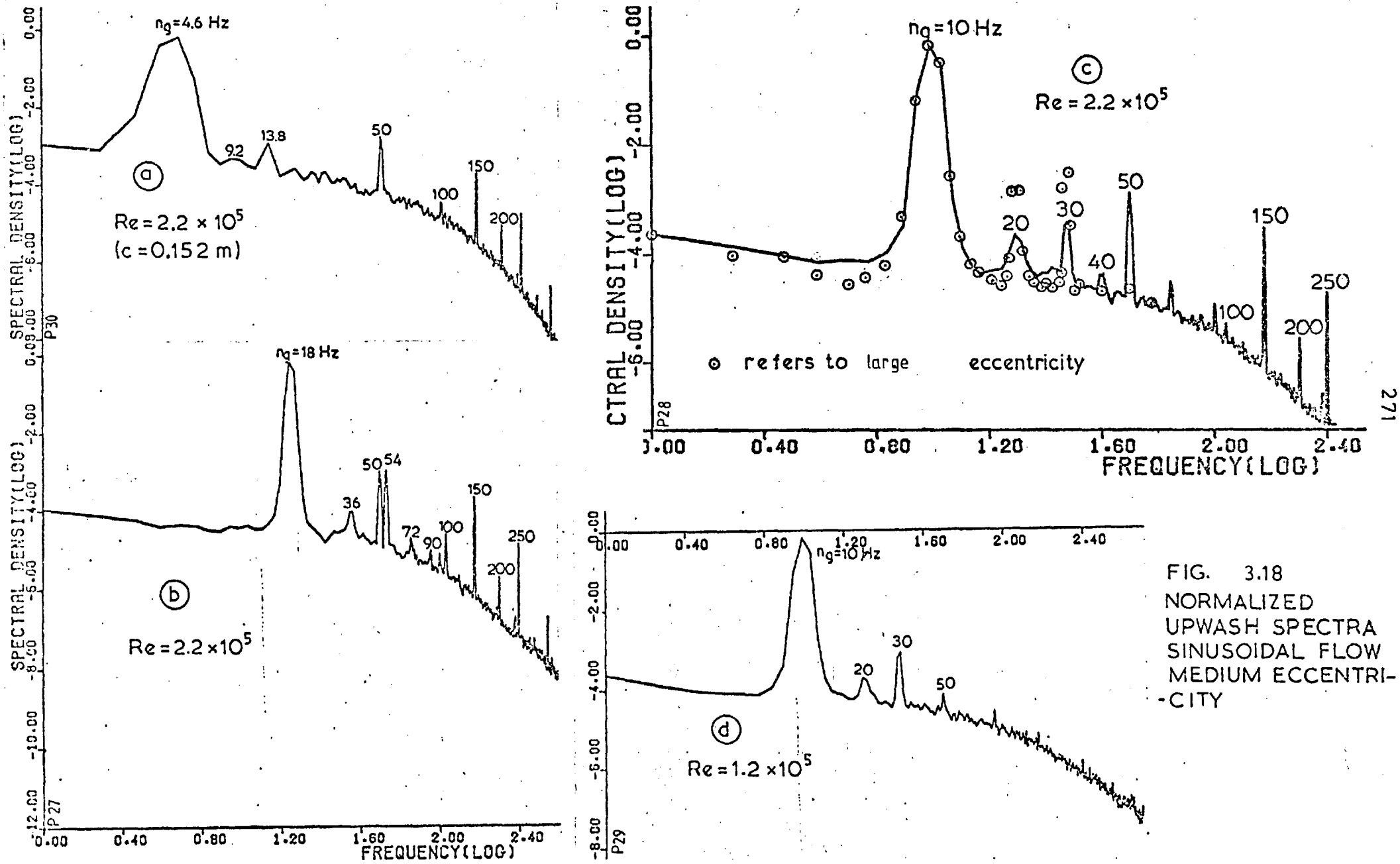

FIG. 3.18
NORMALIZED UPWASH SPECTRA SINUSOIDAL FLOW MEDIUM ECCENTRI-CITY

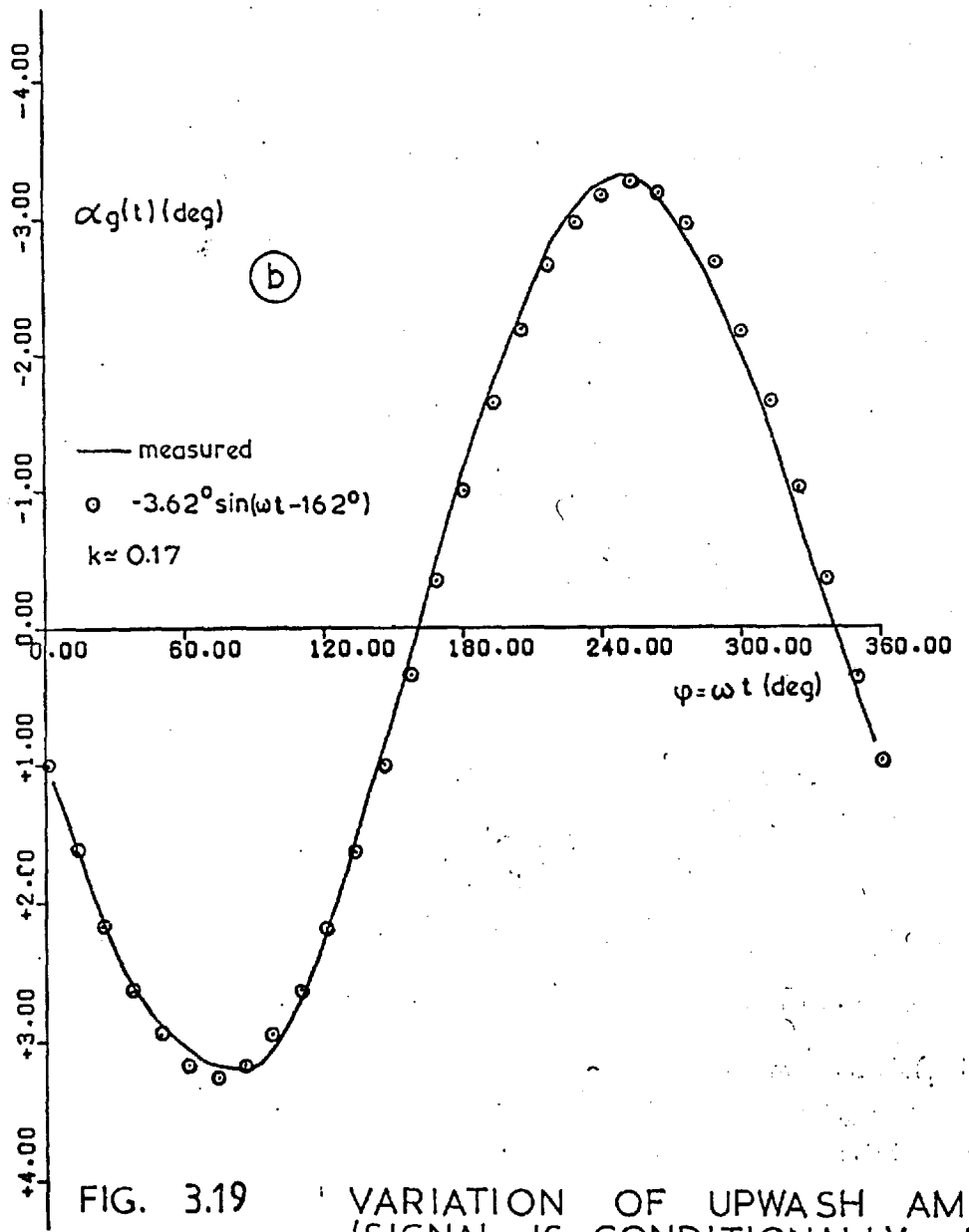

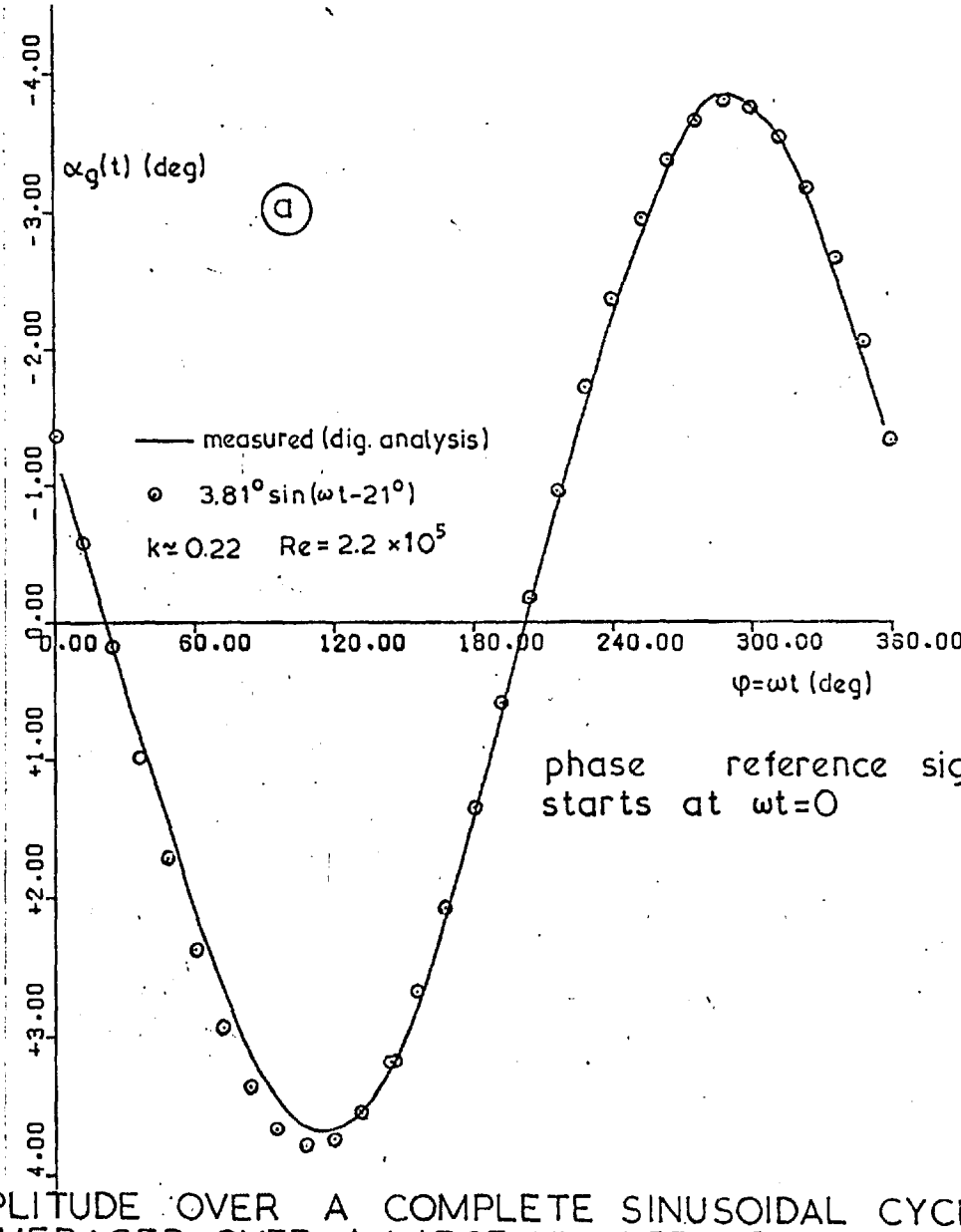

FIG. 3.19 VARIATION OF UPWASH AMPLITUDE OVER A COMPLETE SINUSOIDAL CYCLE (SIGNAL IS CONDITIONALLY AVERAGED OVER A LARGE NUMBER OF PERIODS)

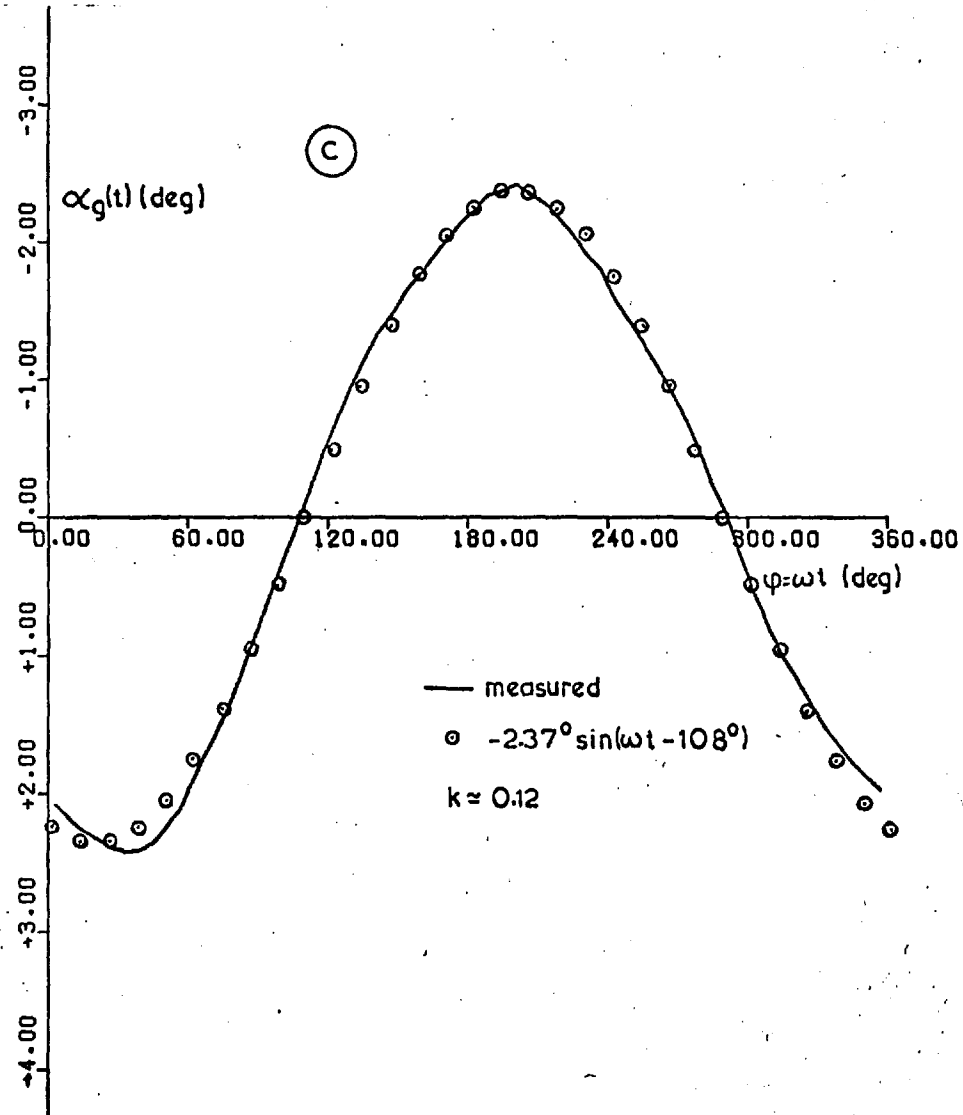

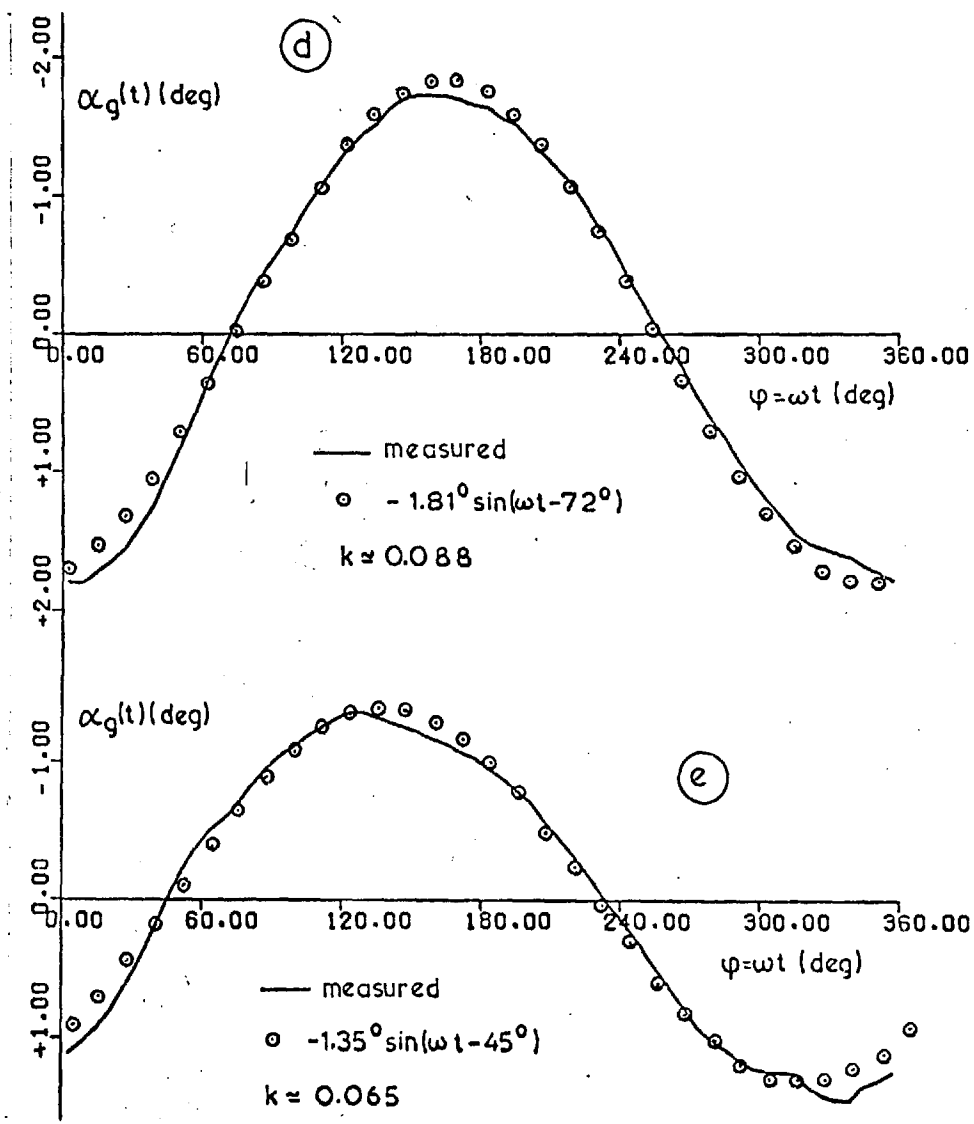

FIG. 3.19 (continued)

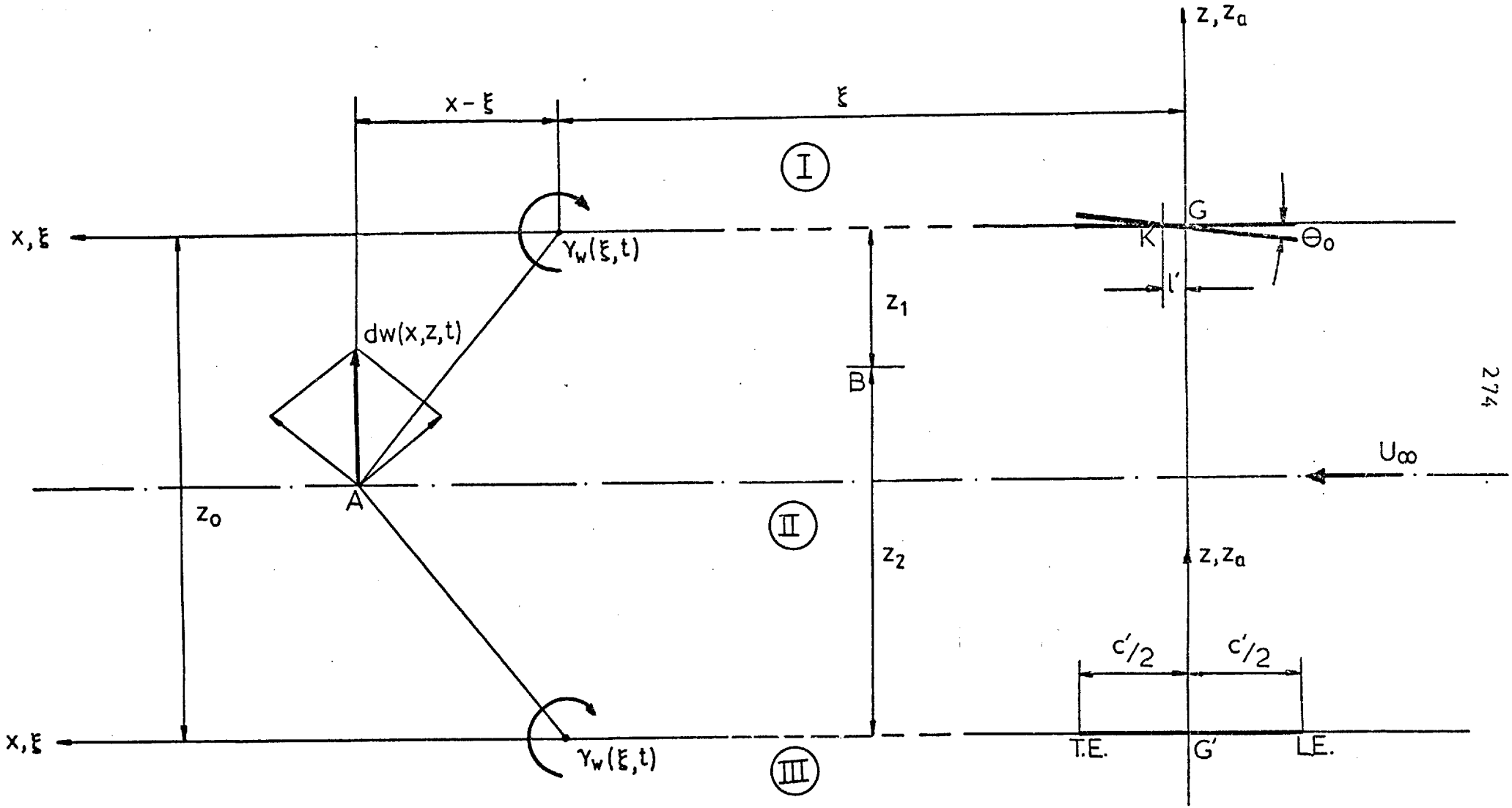

FIG. 3.20 POTENTIAL FLOW MODEL FOR OSCILLATING AEROFOILS

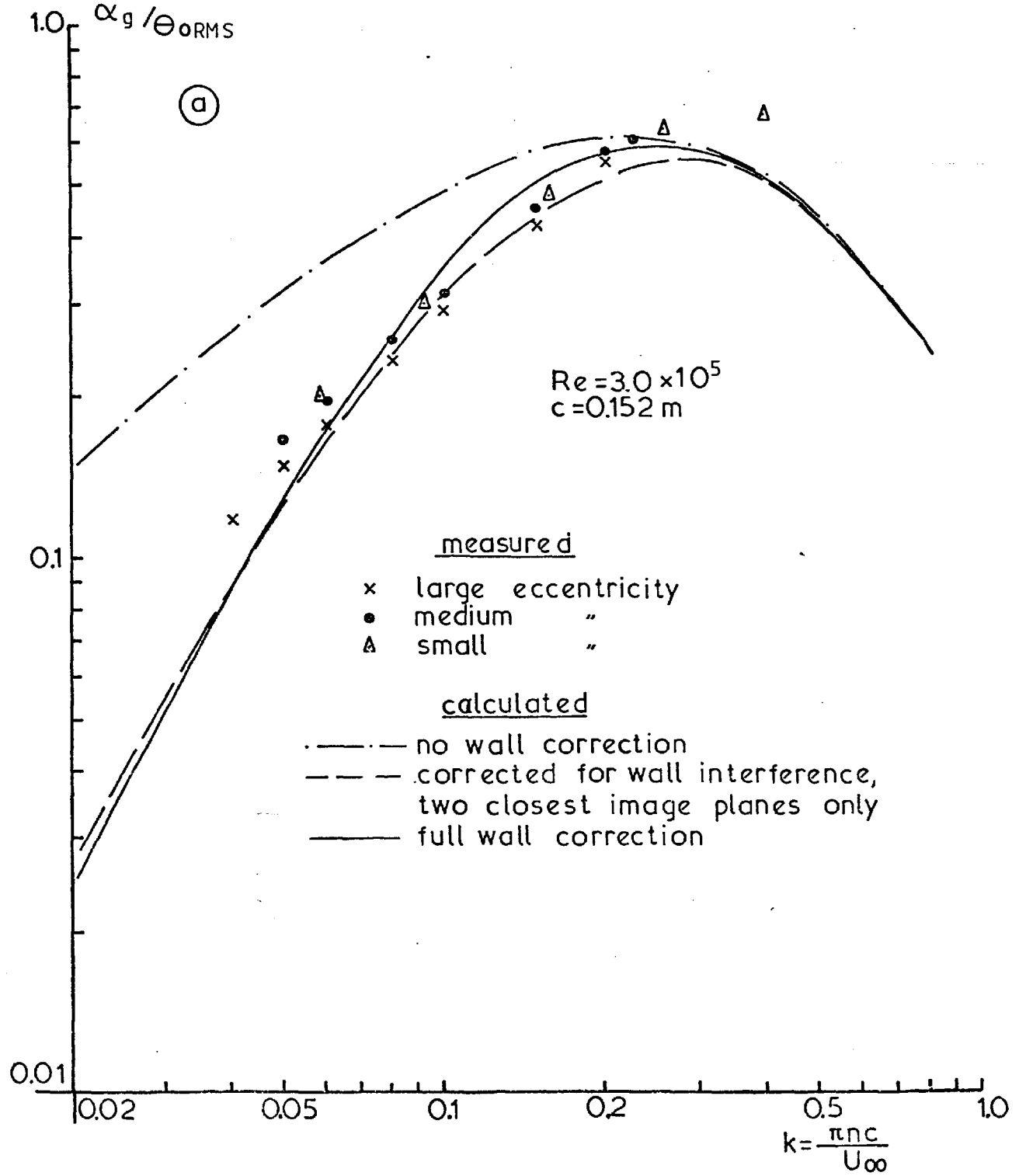

FIG. 3.21 THEORETICAL AND EXPERIMENTAL DIMENSIONLESS GUST AMPLITUDES AT CENTRE LINE

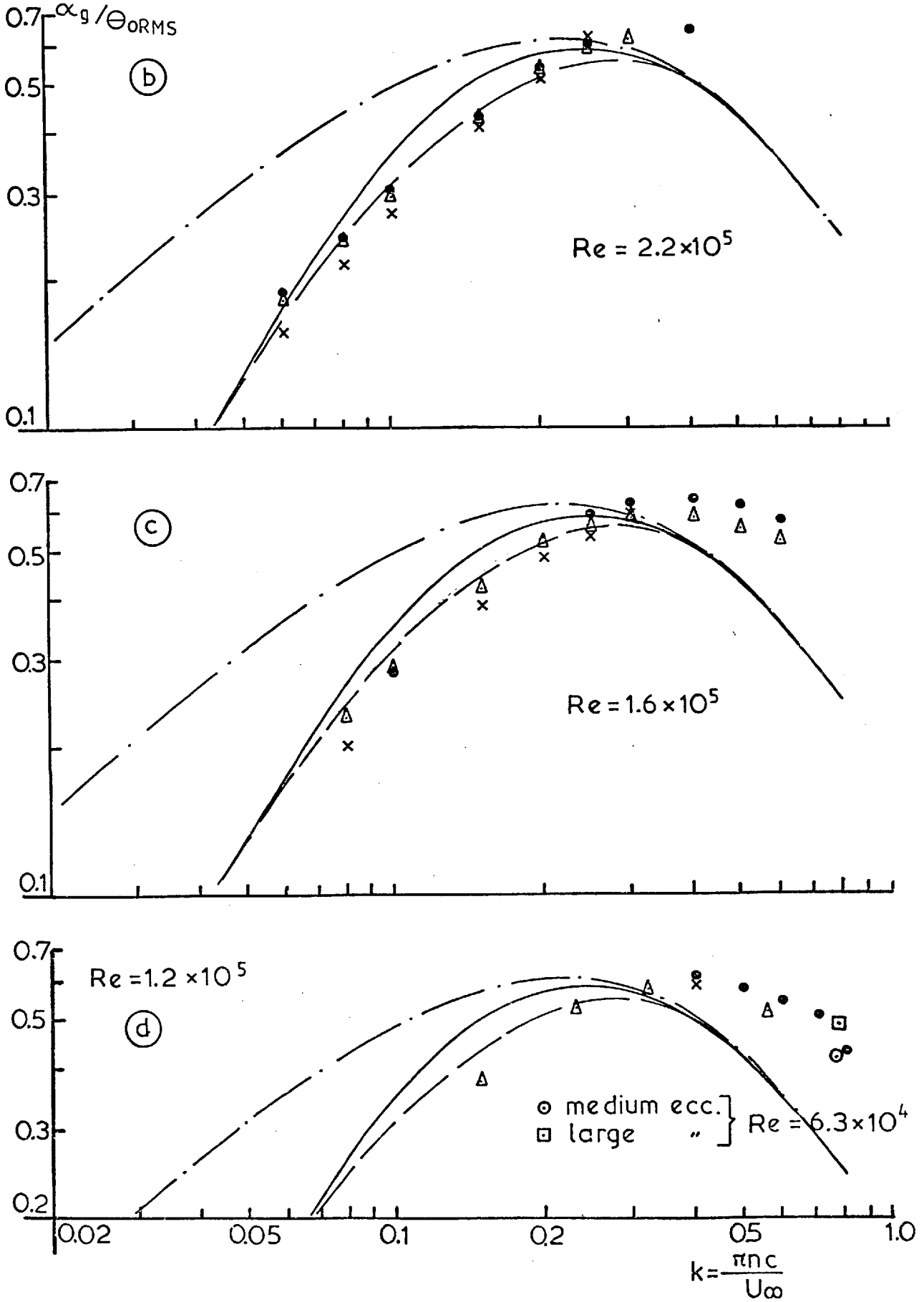

FIG. 3.21 (continued)

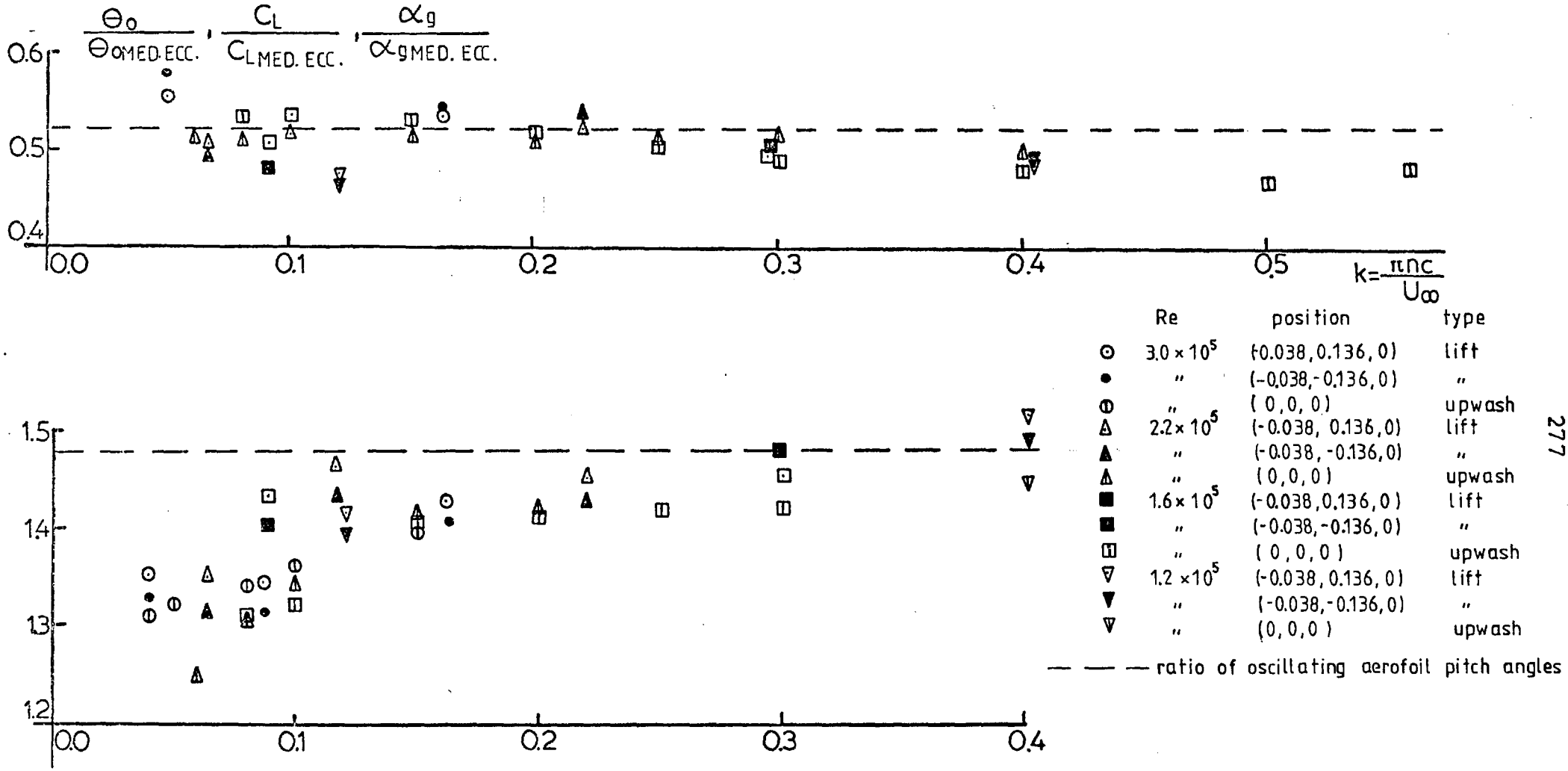

FIG. 3.22 OSCILLATING AEROFOIL PITCH ANGLE, GUST AMPLITUDE AND FLUCTUATING LIFT ON SMALL AEROFOIL NORMALIZED WITH CORRESPONDING QUANTITIES FOR MEDIUM ECCENTRICITY

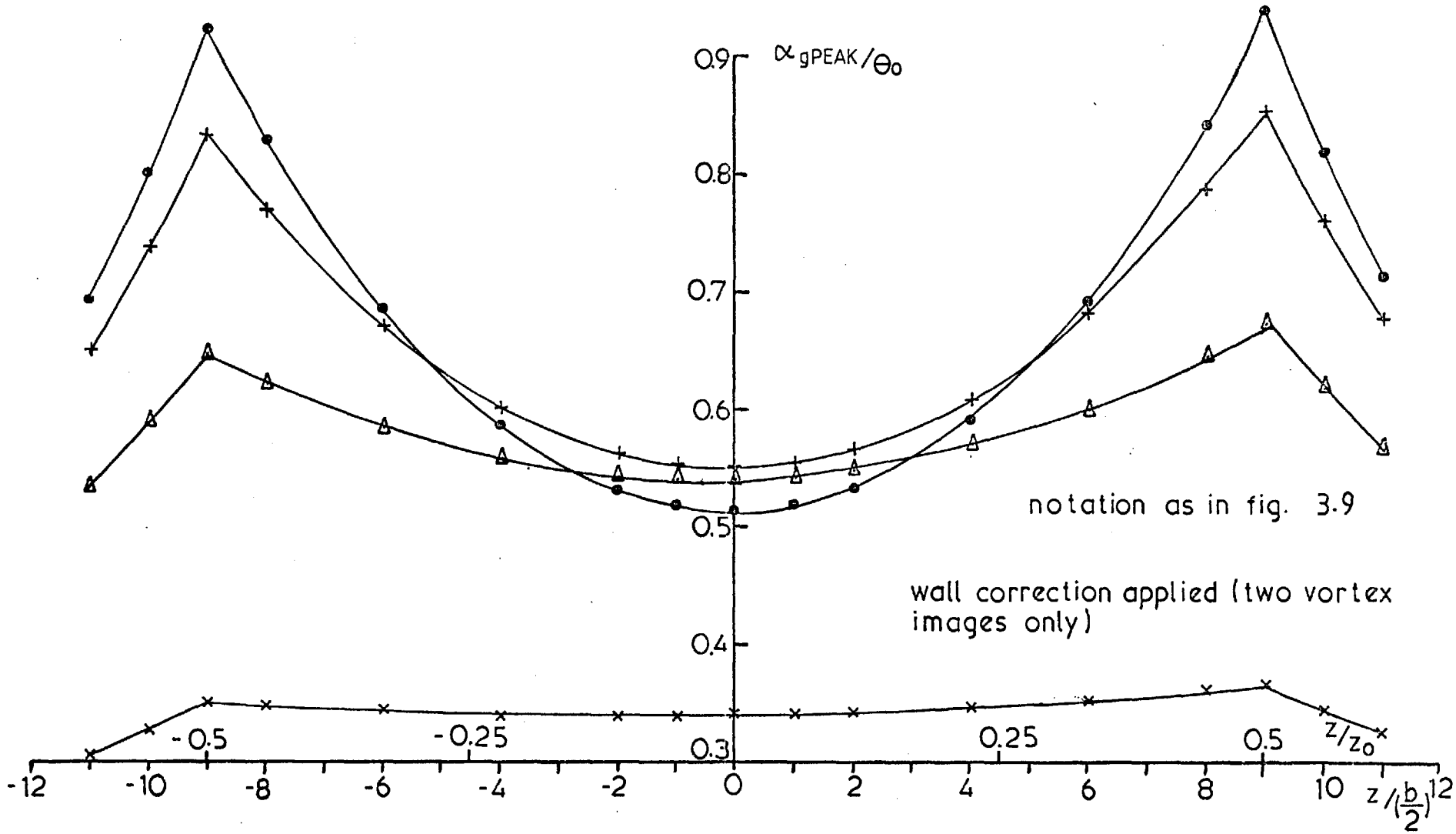

FIG. 3.23 CALCULATED DIMENSIONLESS GUST AMPLITUDE

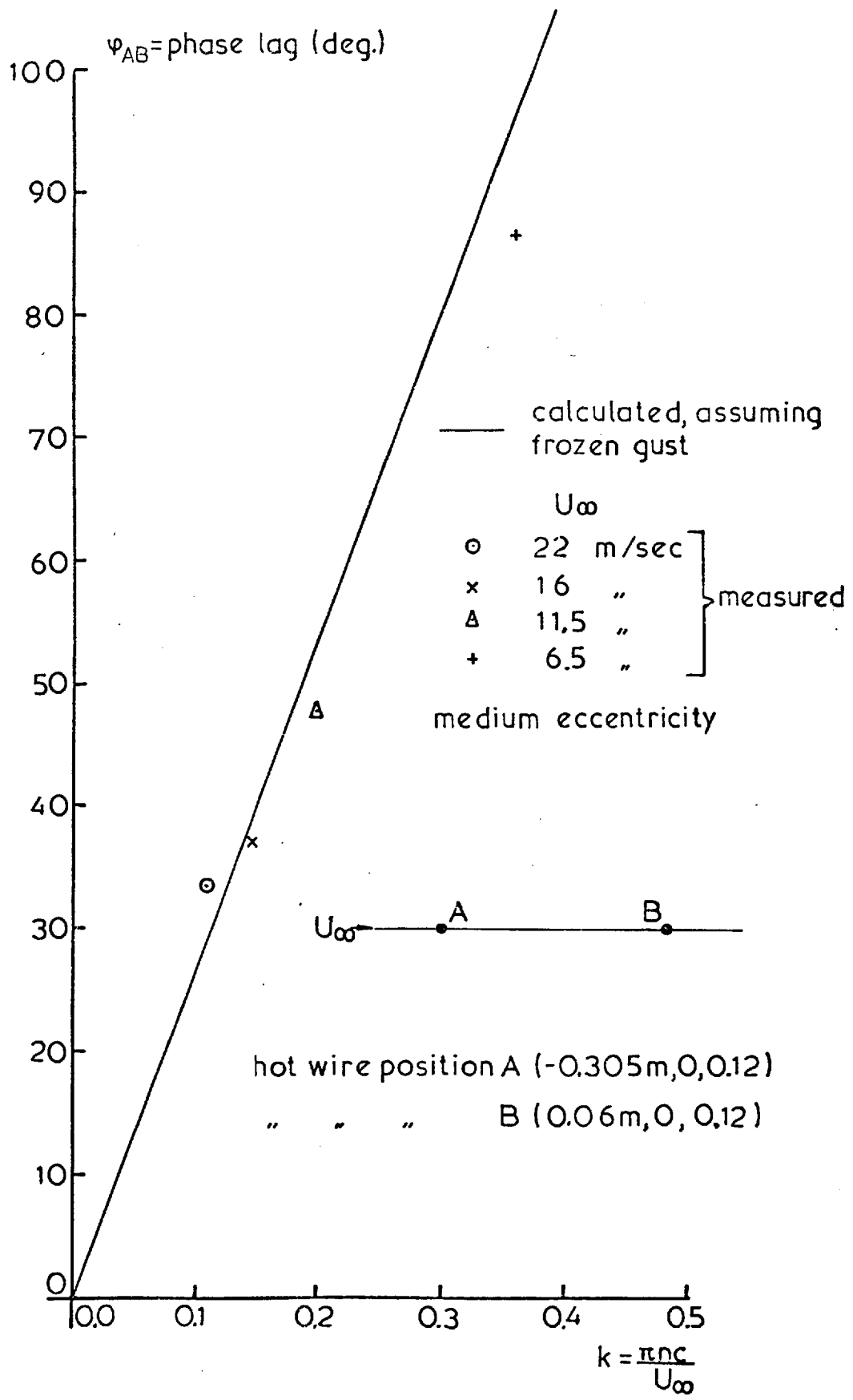

FIG. 3.24 TEST FOR FROZEN GUST ASSUMPTION

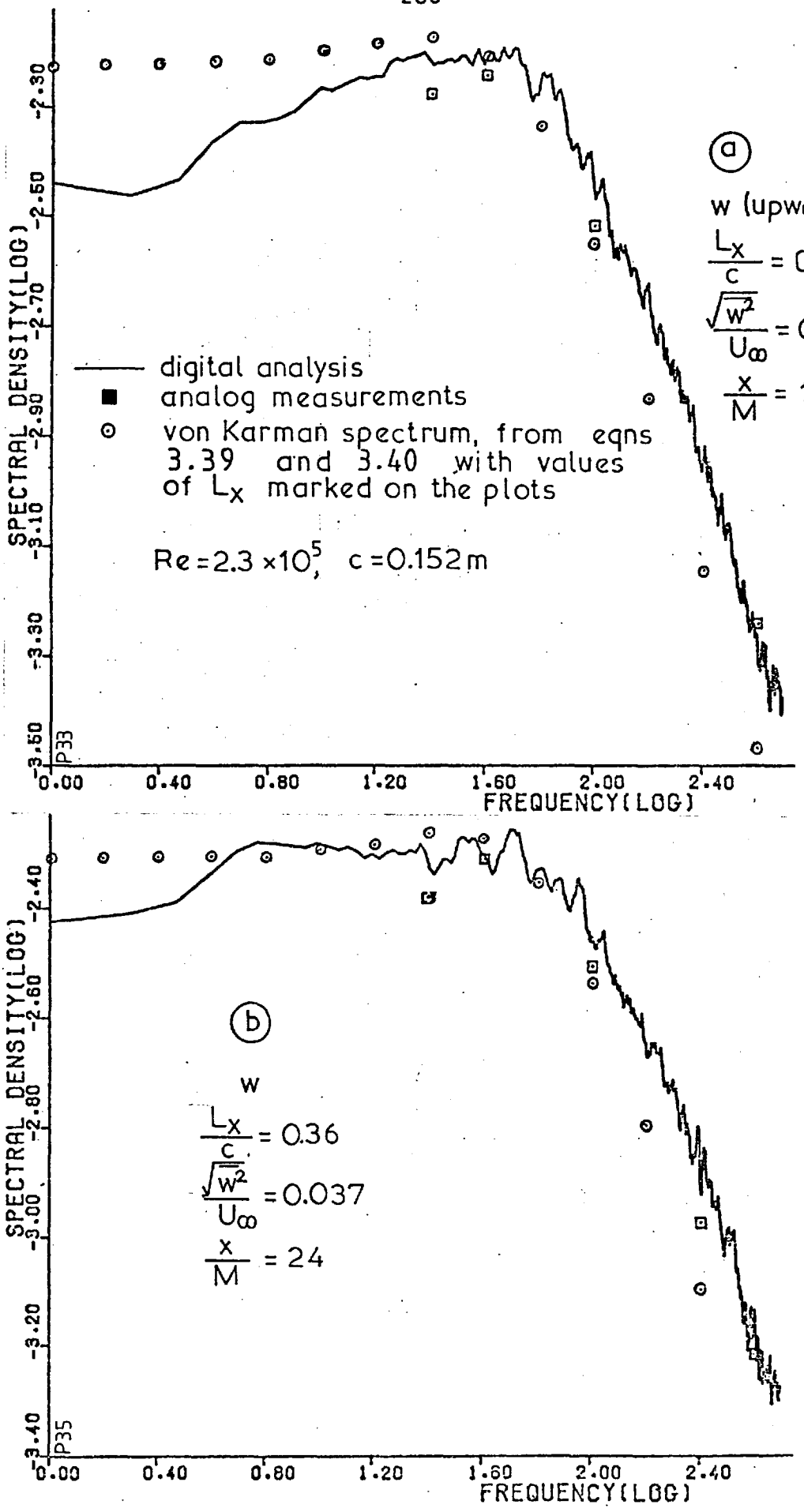

FIG. 3.25 NORMALIZED u,v,w SPECTRA OF GRID TURBULENCE AT THE POINT (0,0,0)

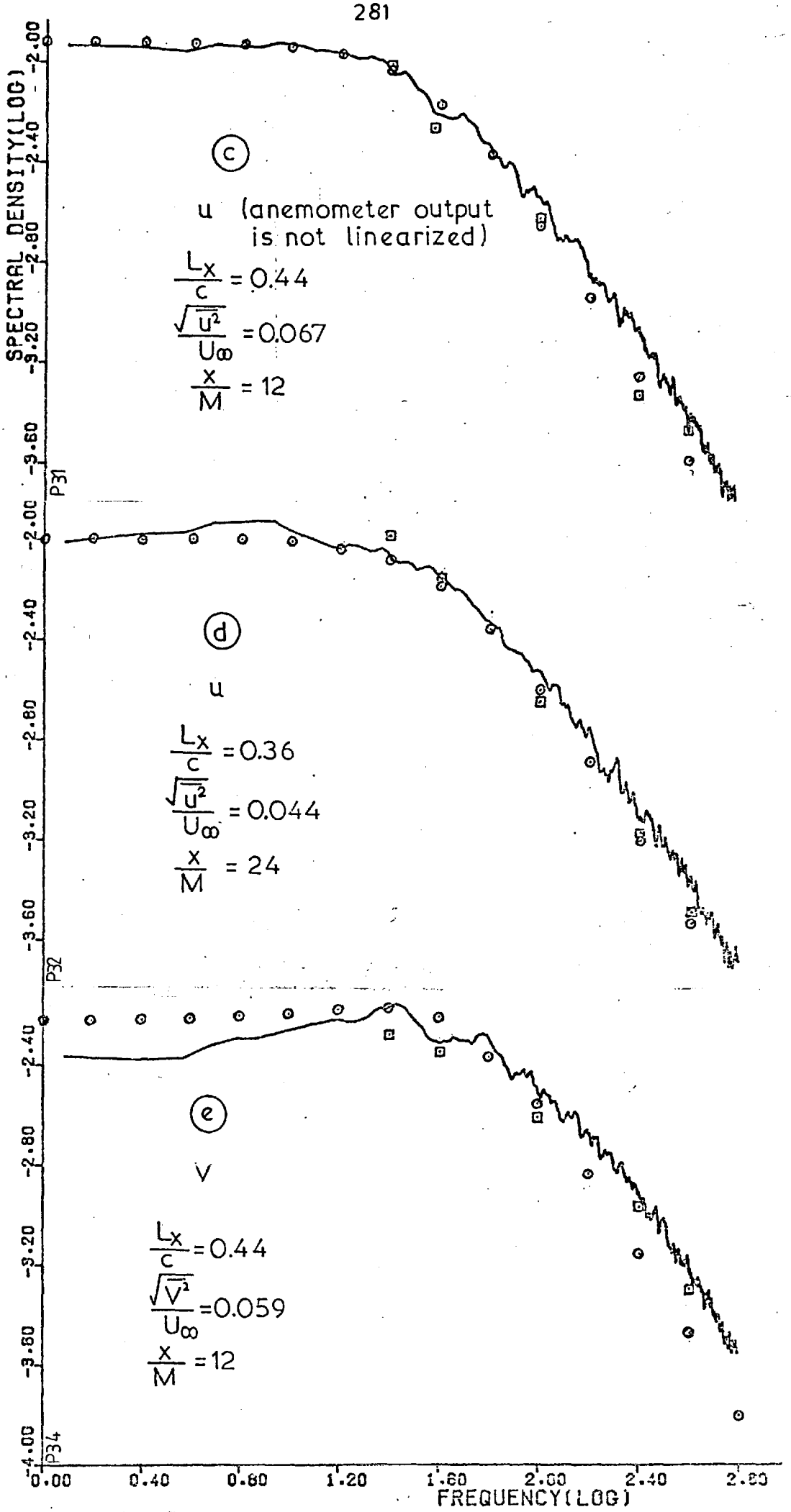

FIG. 3.25 (continued)

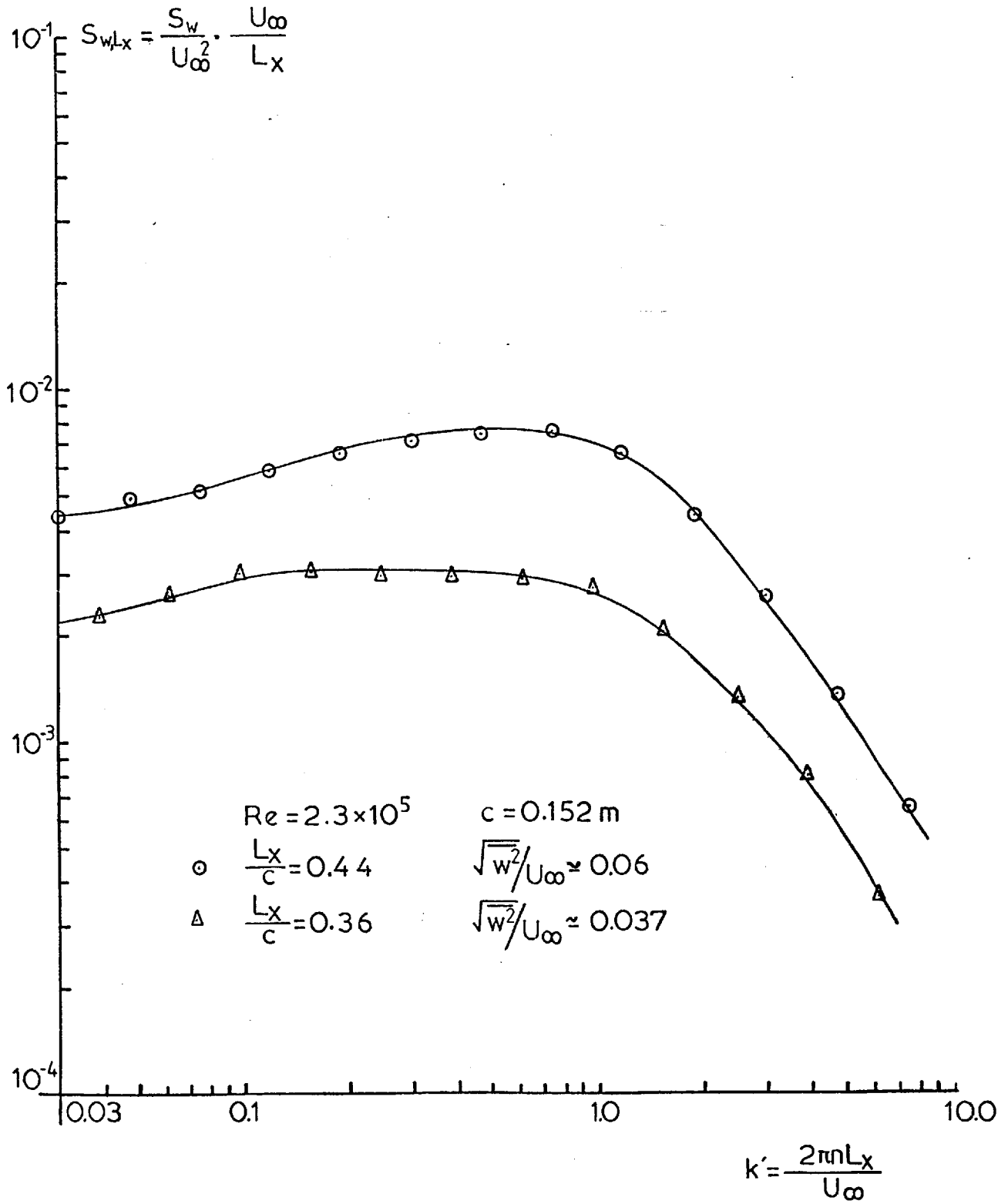

FIG. 3.26 NON DIMENSIONALIZED UPWASH SPECTRA FOR GRID TURBULENCE

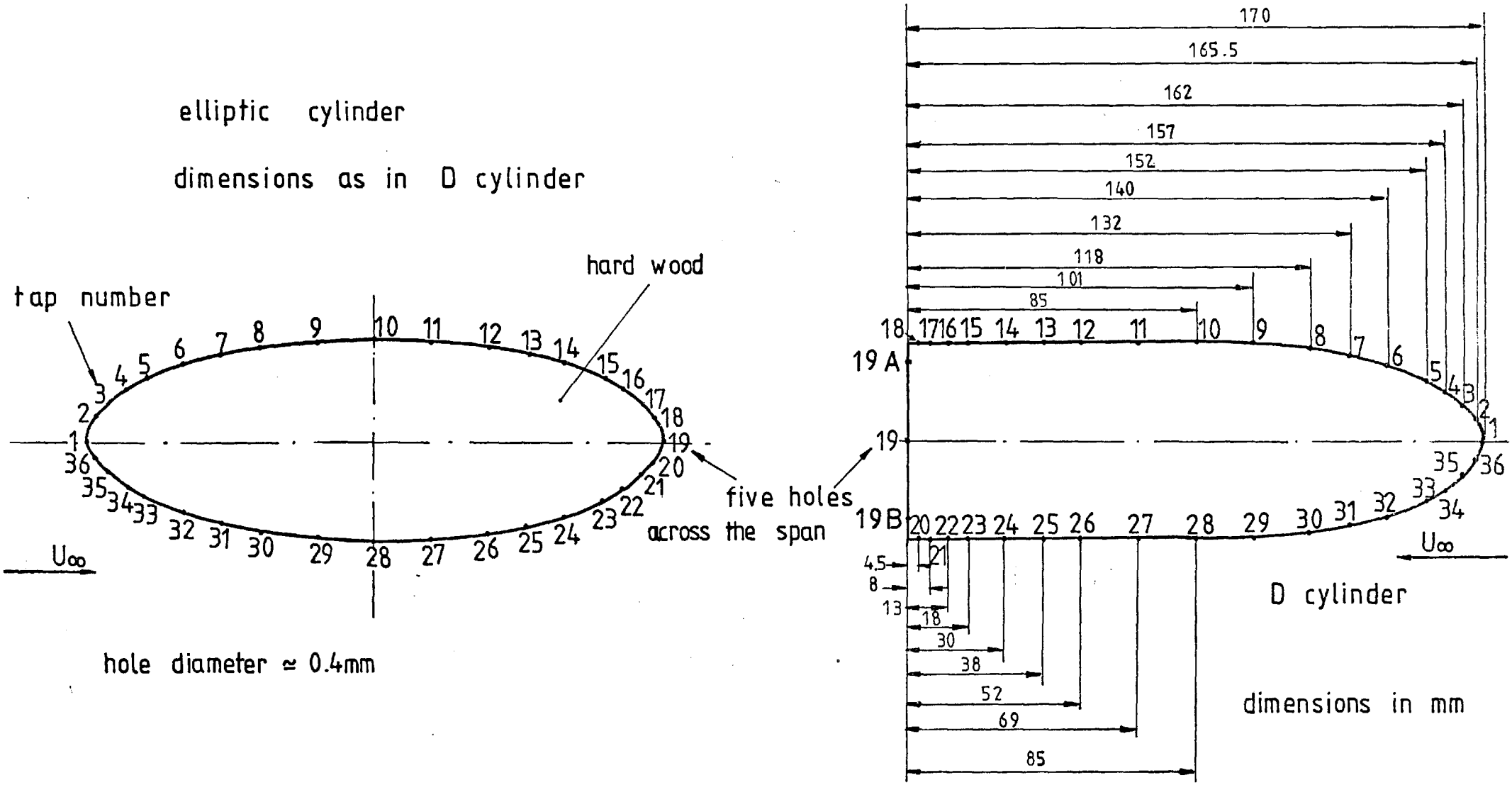

FIG. 3.27 NUMBERING SYSTEM FOR PRESSURE TAPPINGS

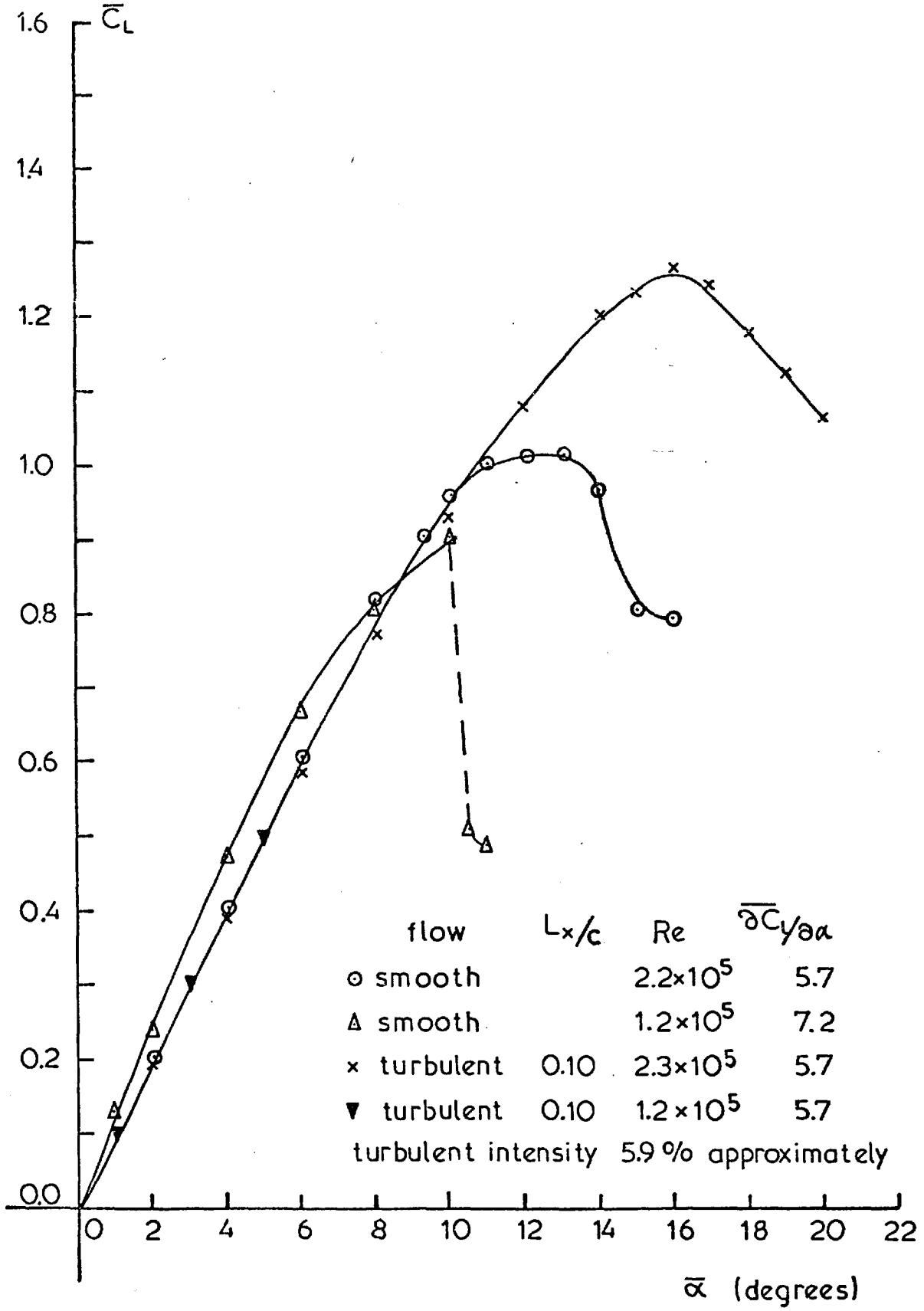

FIG. 4.1 $\bar{C}_L$ against $\bar{\alpha}$ NACA 0015, AR = 5.0

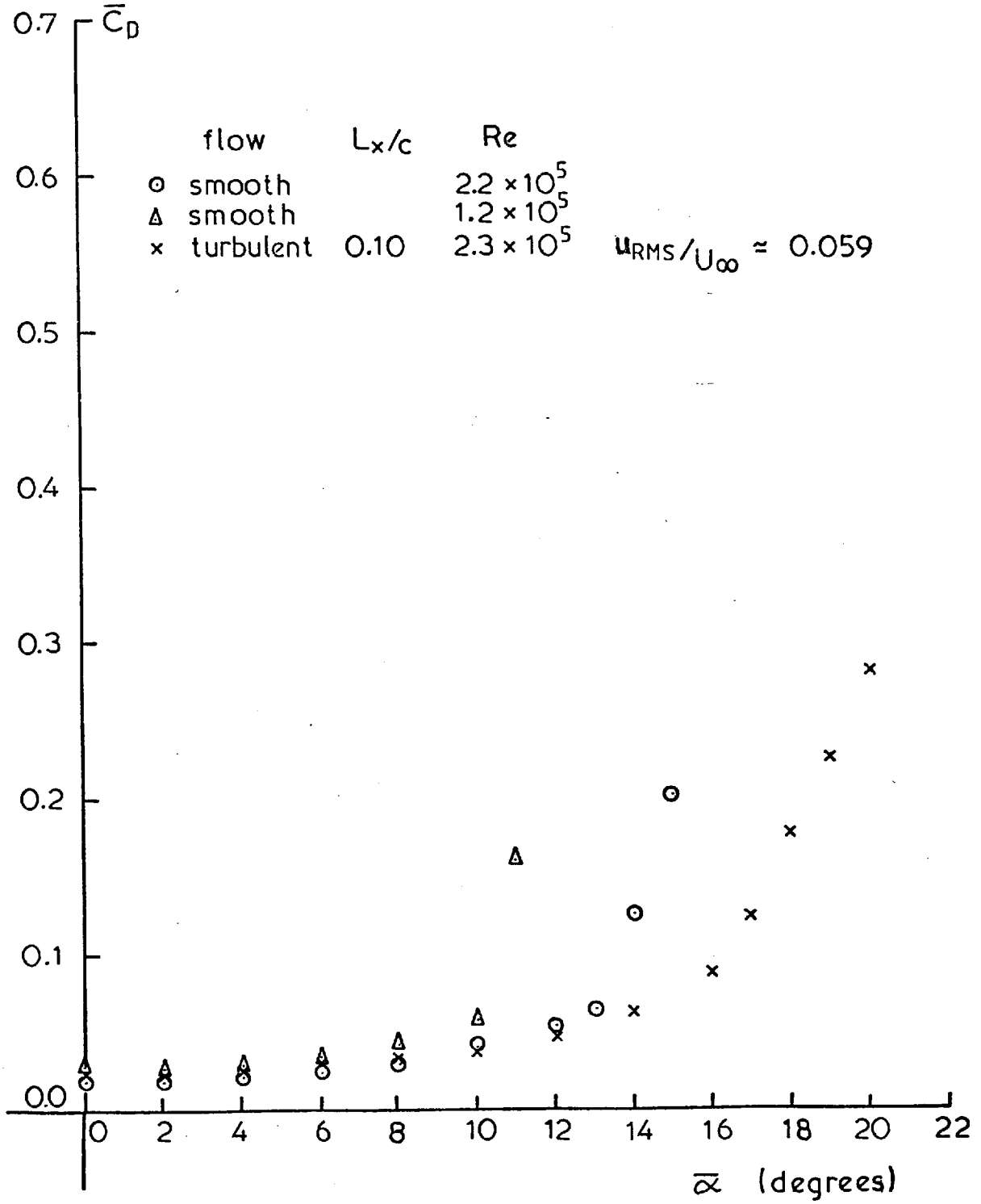

FIG. 4.2 $\bar{C}_D$ against $\bar{\alpha}$ NACA 0015, AR = 5.0

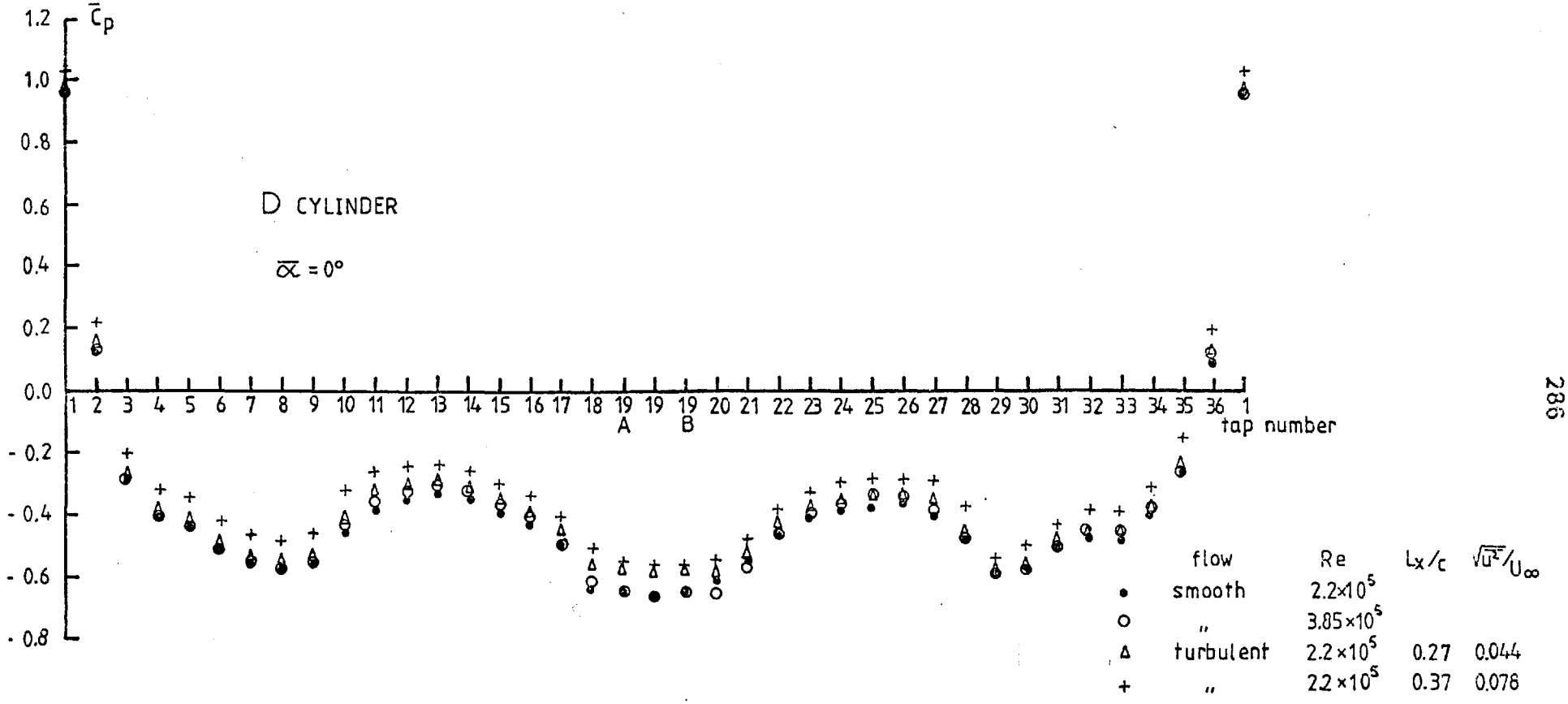

coordinates of pressure taps are given in fig. 3.27

FIG. 4.3 MEAN SURFACE PRESSURE DISTRIBUTION

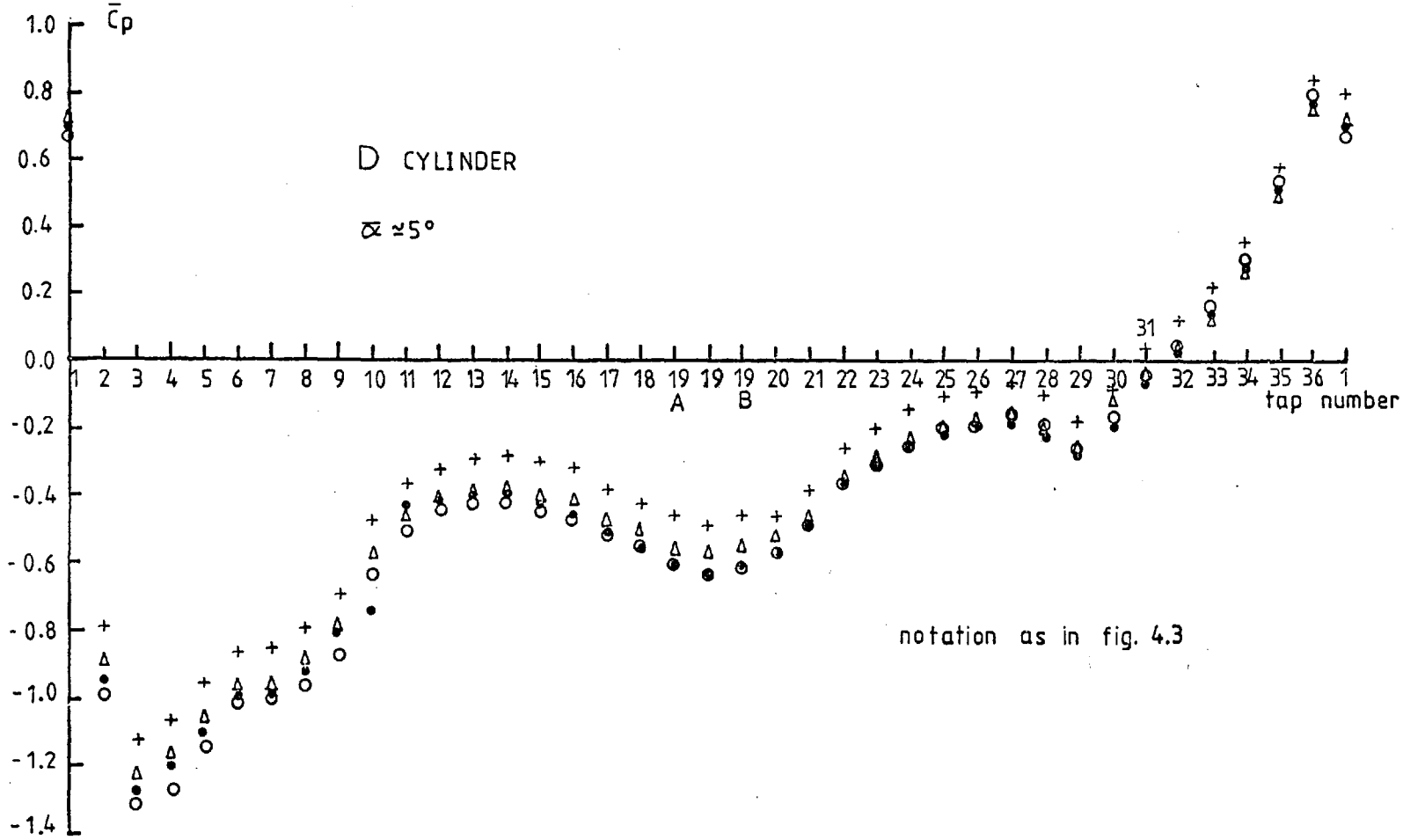

FIG. 4.4 MEAN SURFACE PRESSURE DISTRIBUTION

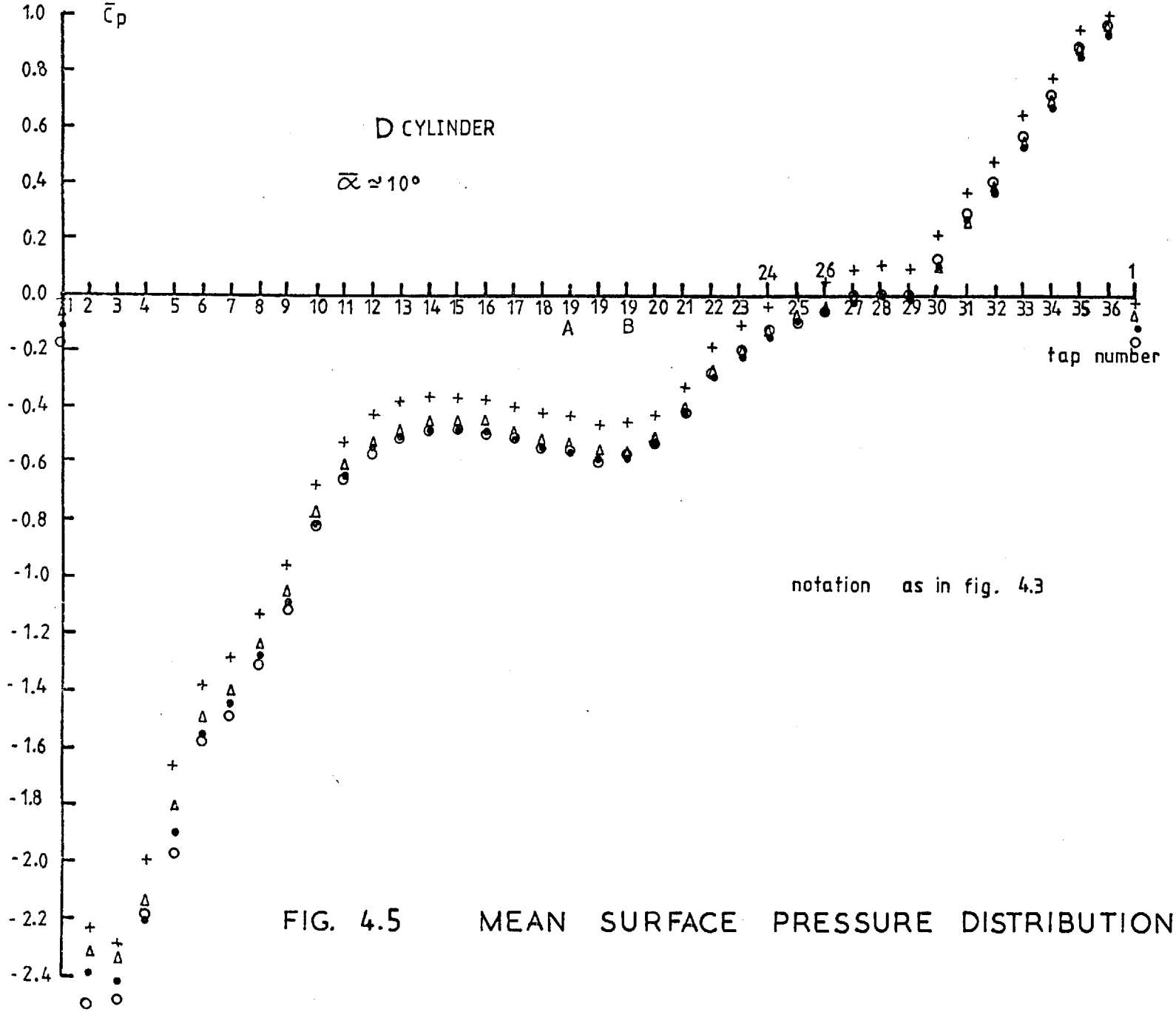

FIG. 4.5 MEAN SURFACE PRESSURE DISTRIBUTION

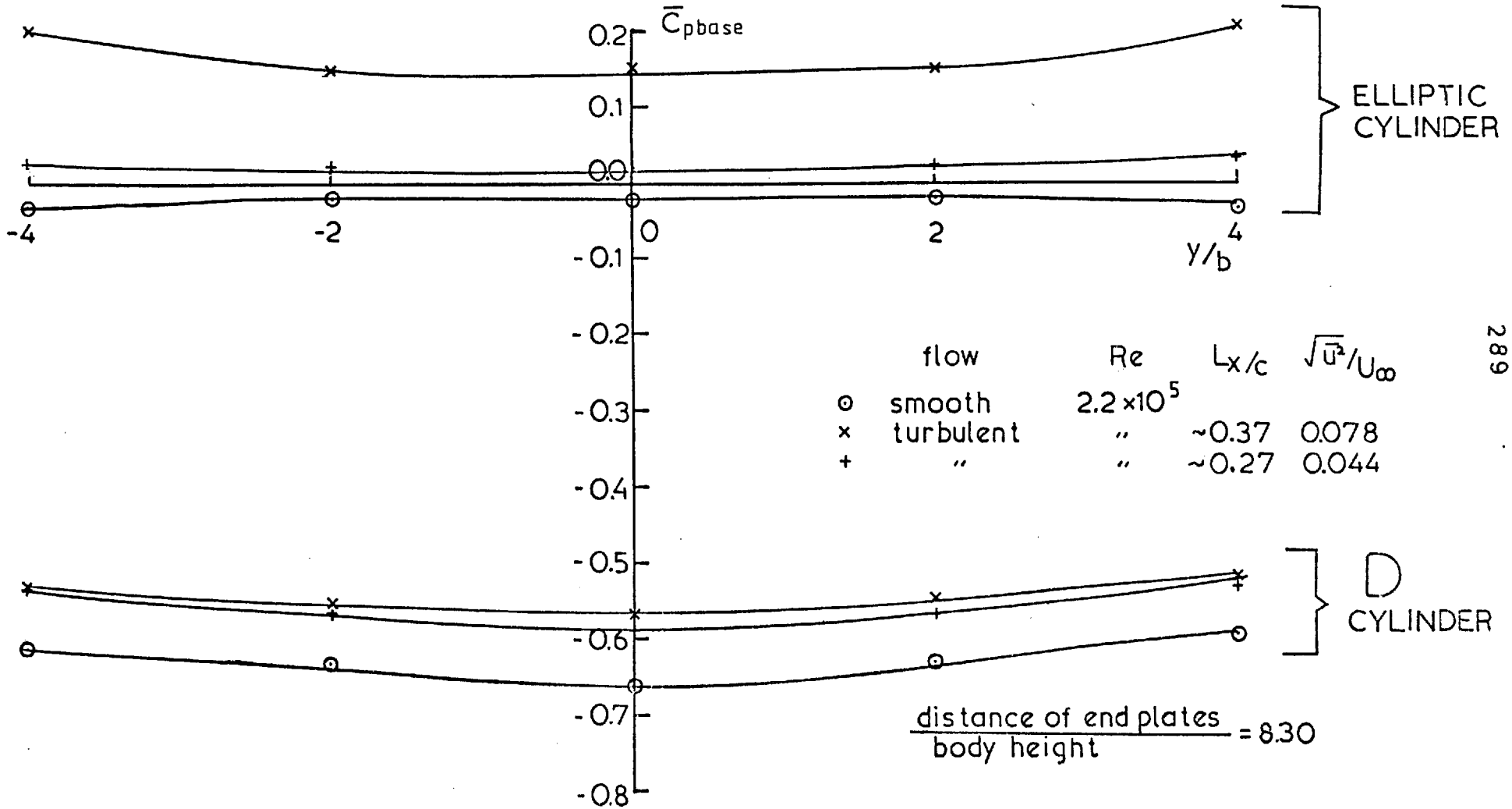

FIG. 4.6 VARIATION OF BASE PRESSURE COEFFICIENT ALONG THE SPAN OF BLUFF CYLINDERS, FOR ZERO INCIDENCE

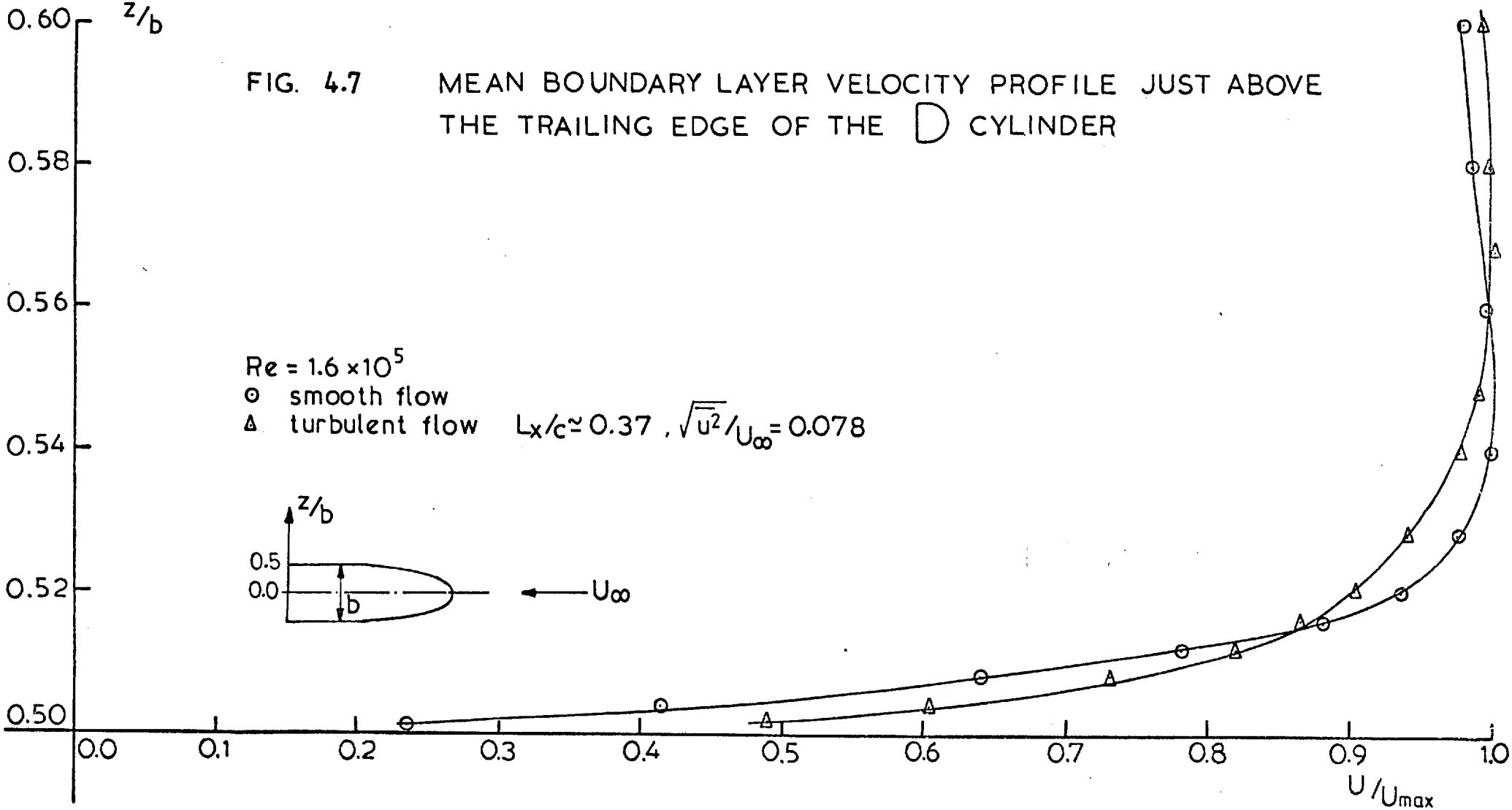

FIG. 4.7 MEAN BOUNDARY LAYER VELOCITY PROFILE JUST ABOVE THE TRAILING EDGE OF THE D CYLINDER

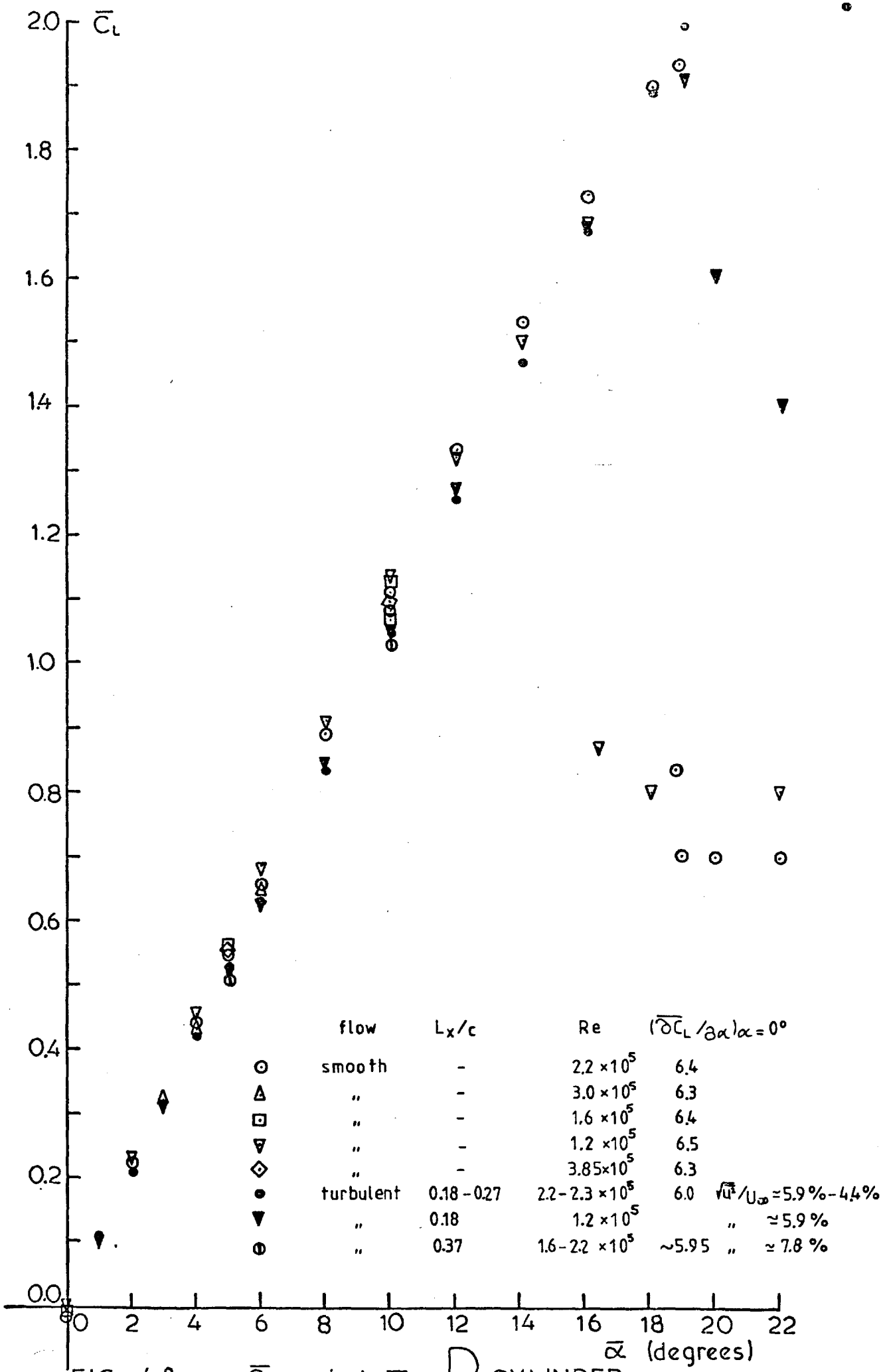

FIG. 4.8 $\overline{C_L}$ against $\overline{\alpha}$ D CYLINDER

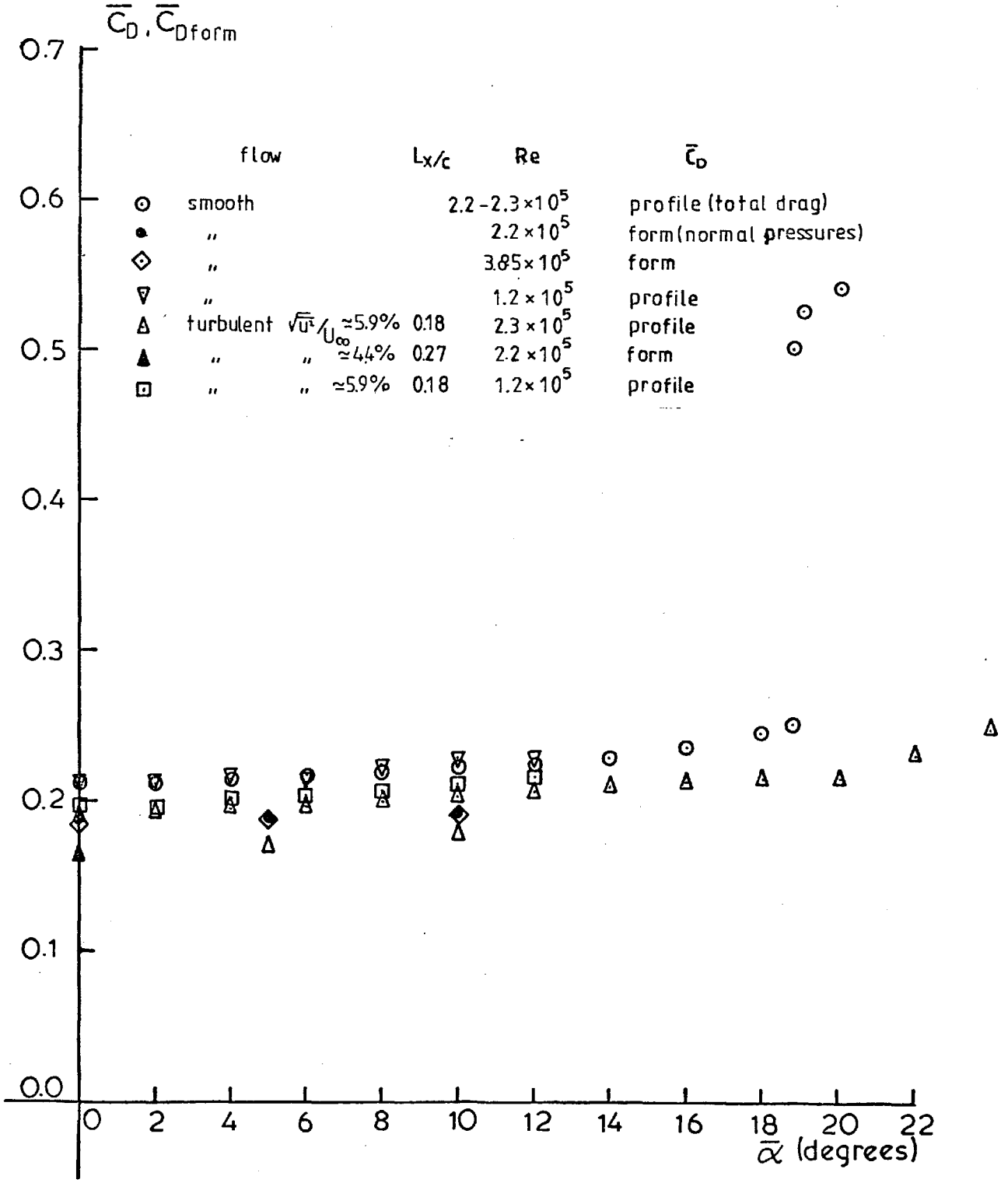

FIG. 4.9 $\overline{C}_D$, $\overline{C}_{Dform}$ against $\overline{\alpha}$ D CYLINDER

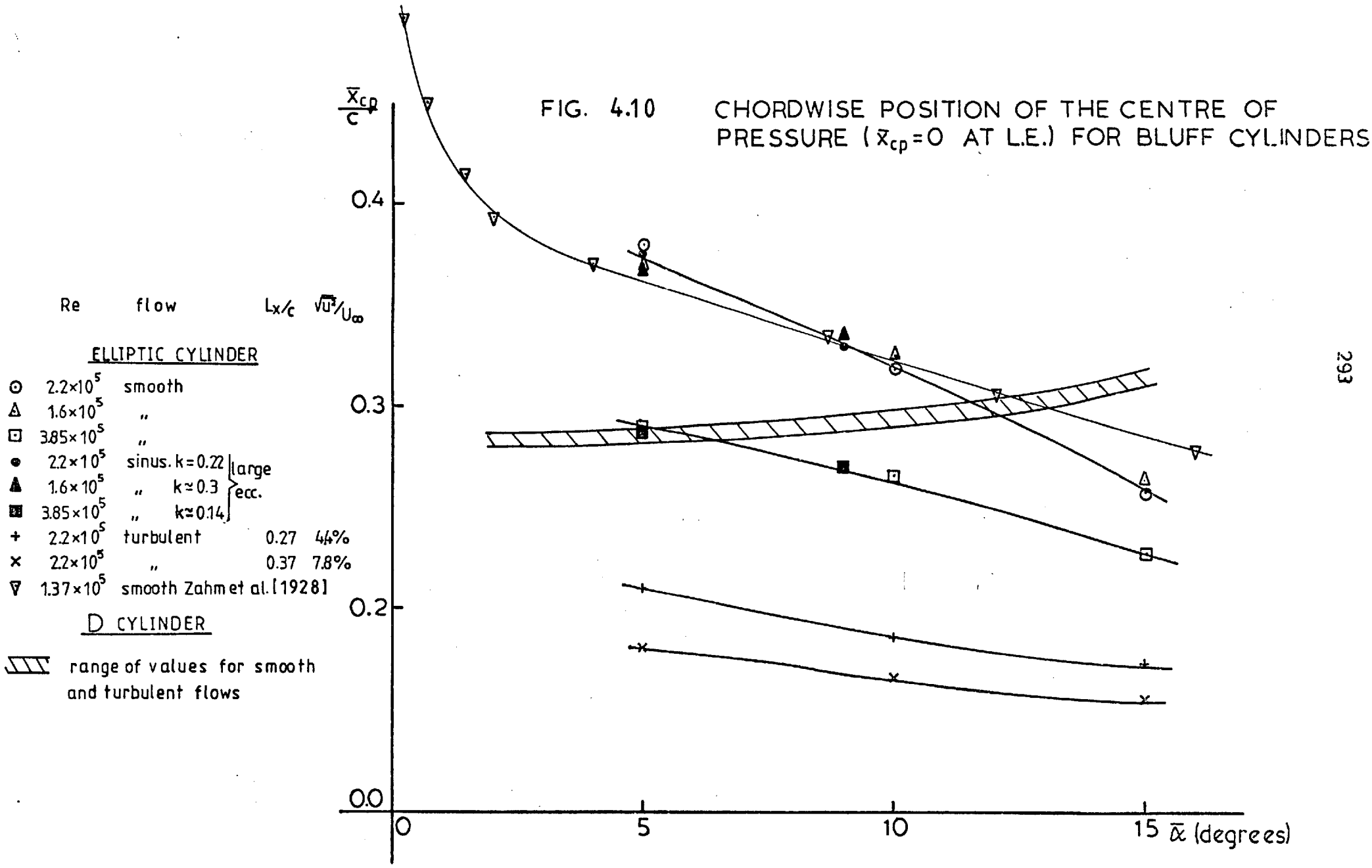

FIG. 4.10 CHORDWISE POSITION OF THE CENTRE OF PRESSURE ($\bar{x}_{cp}=0$ AT L.E.) FOR BLUFF CYLINDERS

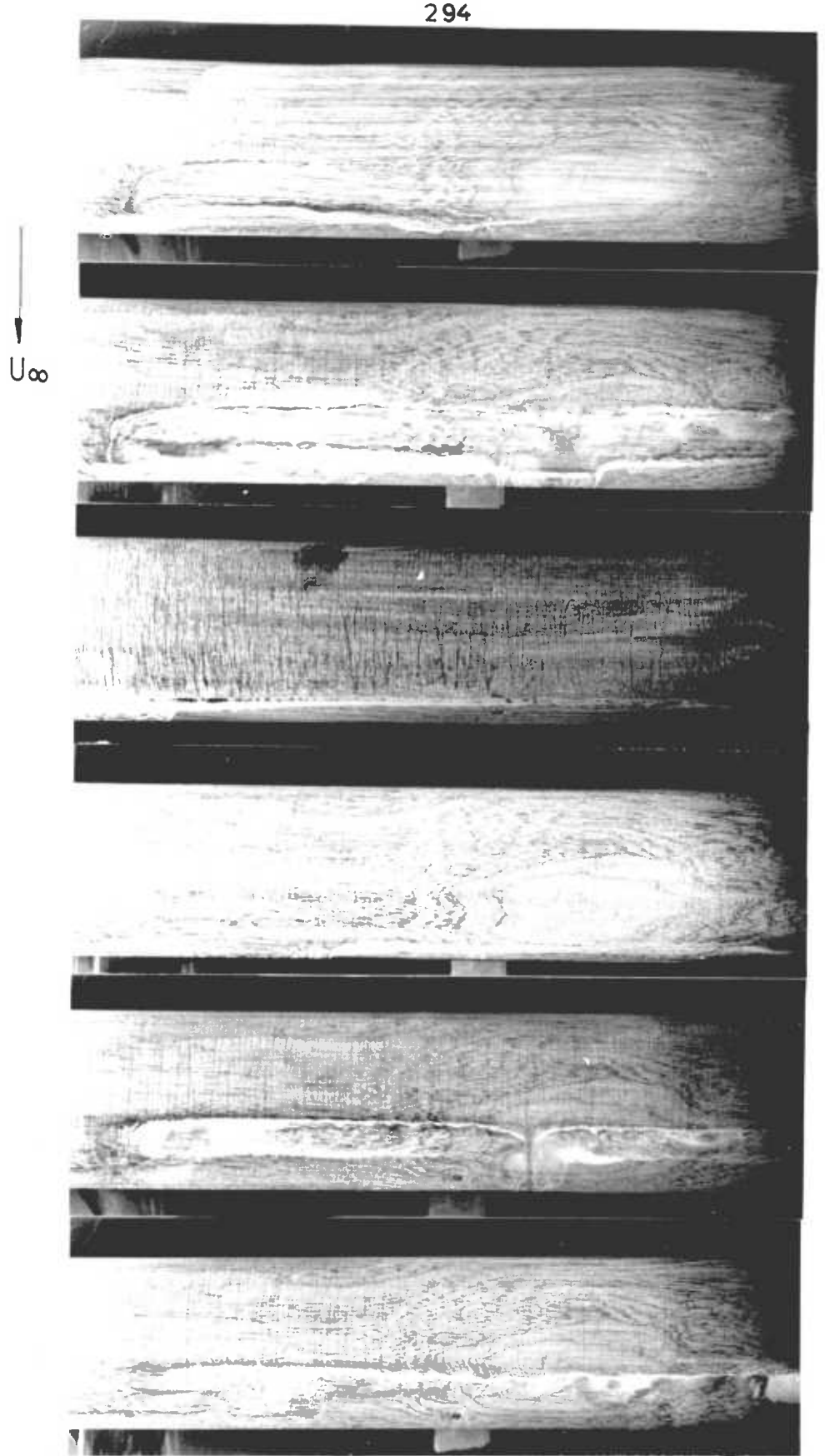

photo	Re	$\bar{\alpha}$	flow	L_x/c	$\sqrt{\overline{u^2}}/U_\infty$
1	1.3×10^5	0°	smooth	–	–
2	"	4°	"	–	–
3	"	0°	turbulent	~0.2	~0.06
4	"	4°	"	"	"
5	2.2×10^5	0°	smooth	–	–
6	3.0×10^5	0°	"	–	–

FIG. 4.11 FLOW VISUALIZATION. ELLIPTIC CYLINDER

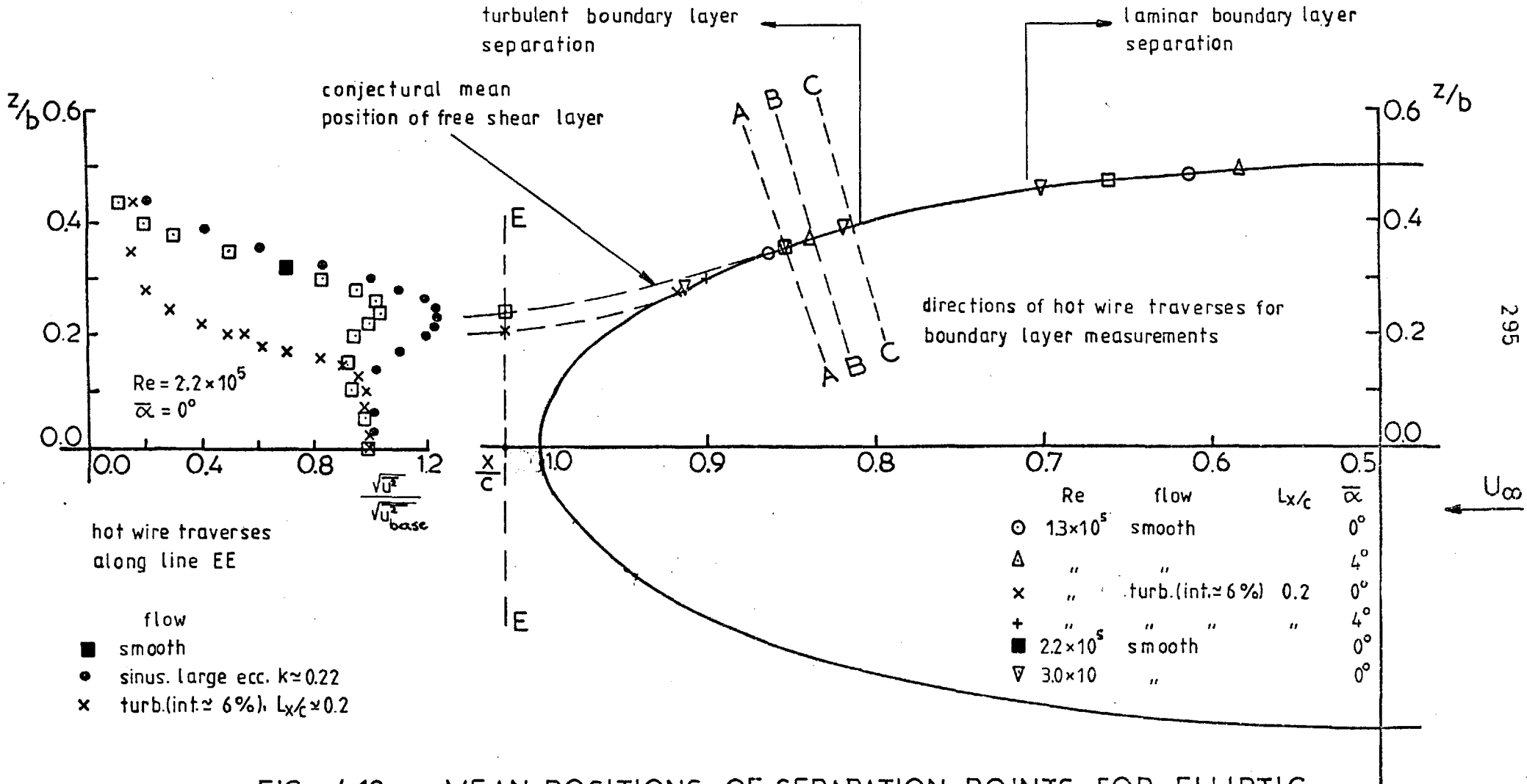

FIG. 4.12 MEAN POSITIONS OF SERAPATION POINTS FOR ELLIPTIC CYLINDER AS DEPICTED FROM FLOW VISUALIZATION

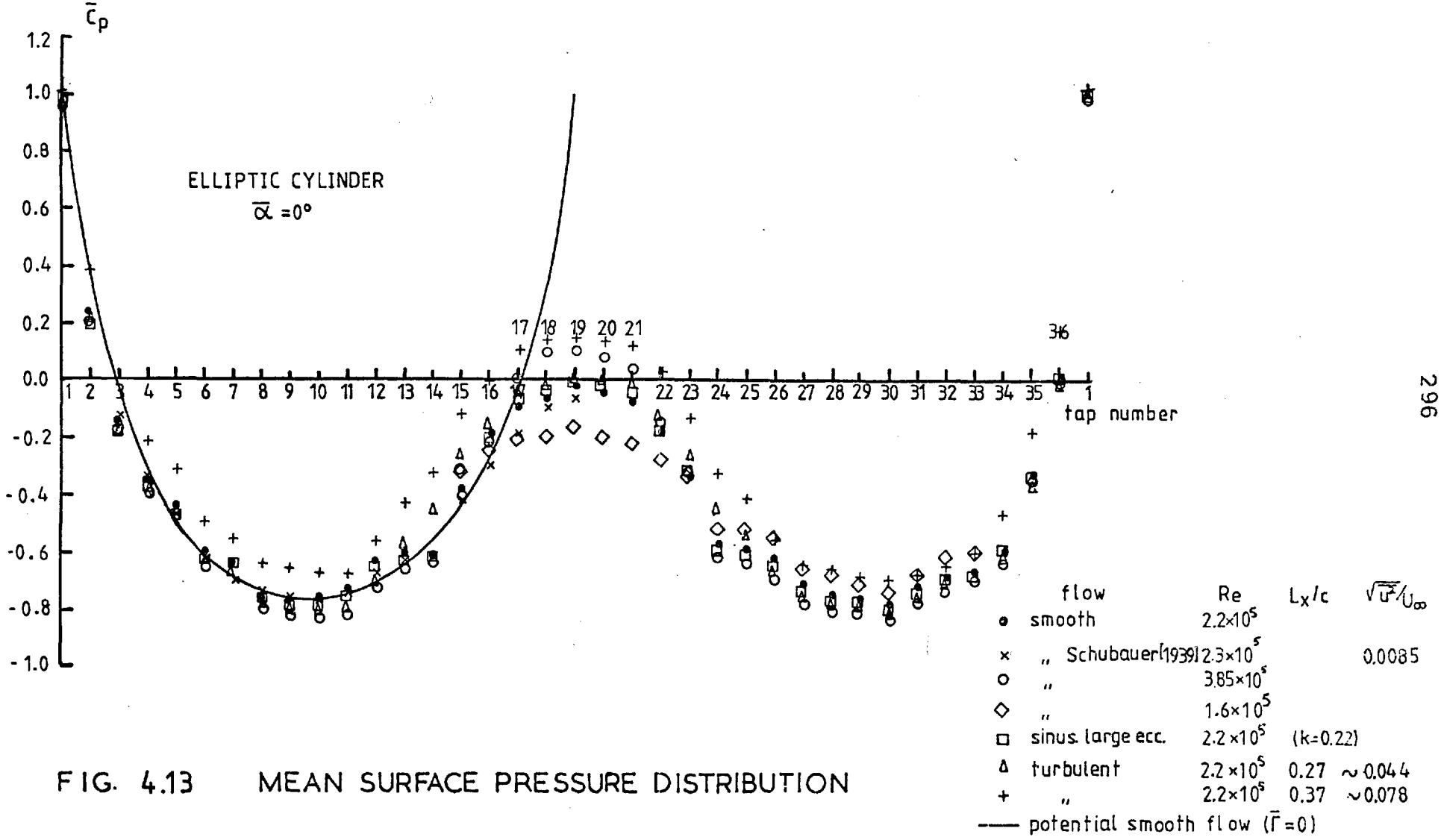

FIG. 4.13 MEAN SURFACE PRESSURE DISTRIBUTION

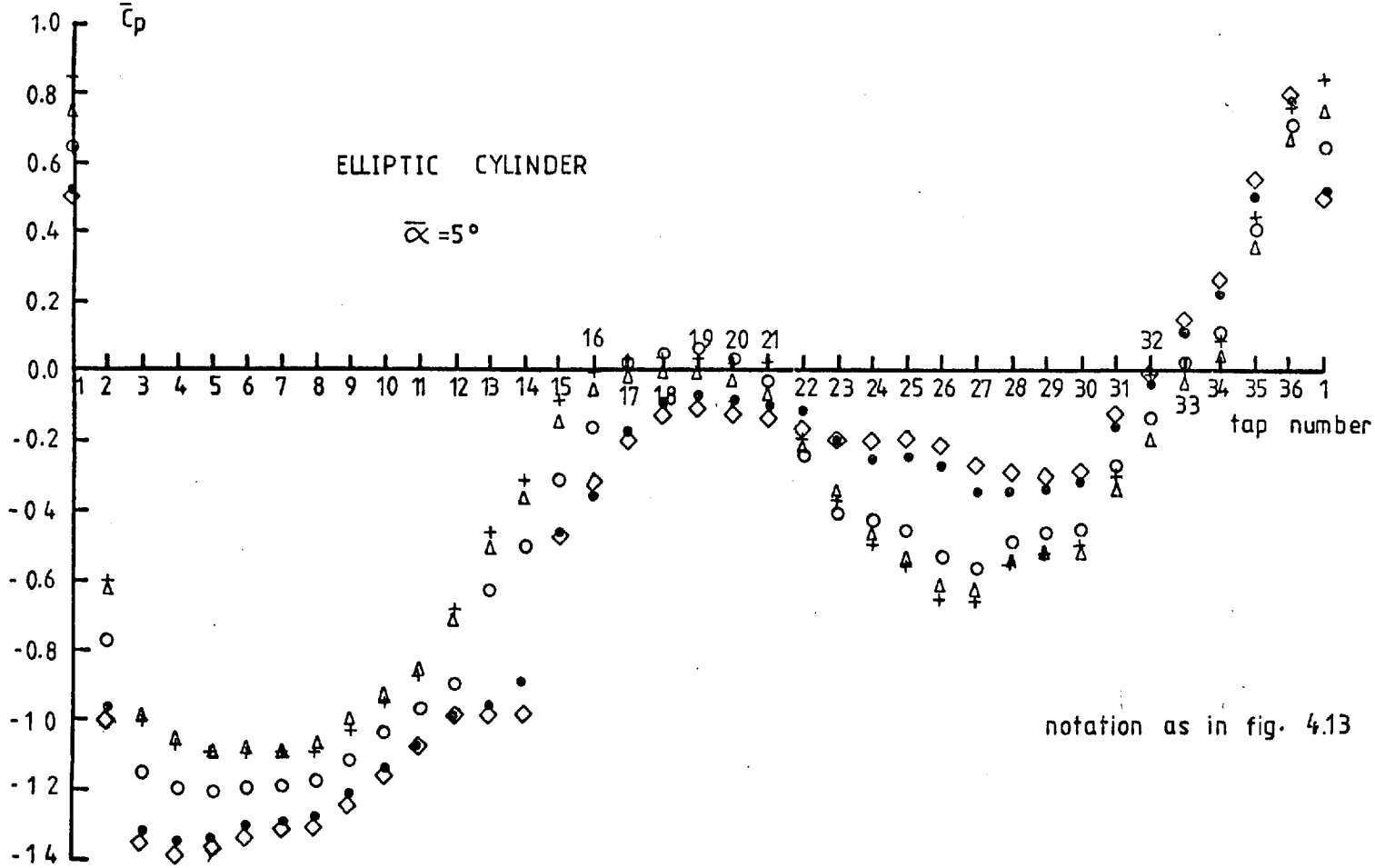

FIG. 4.14 MEAN SURFACE PRESSURE DISTRIBUTION

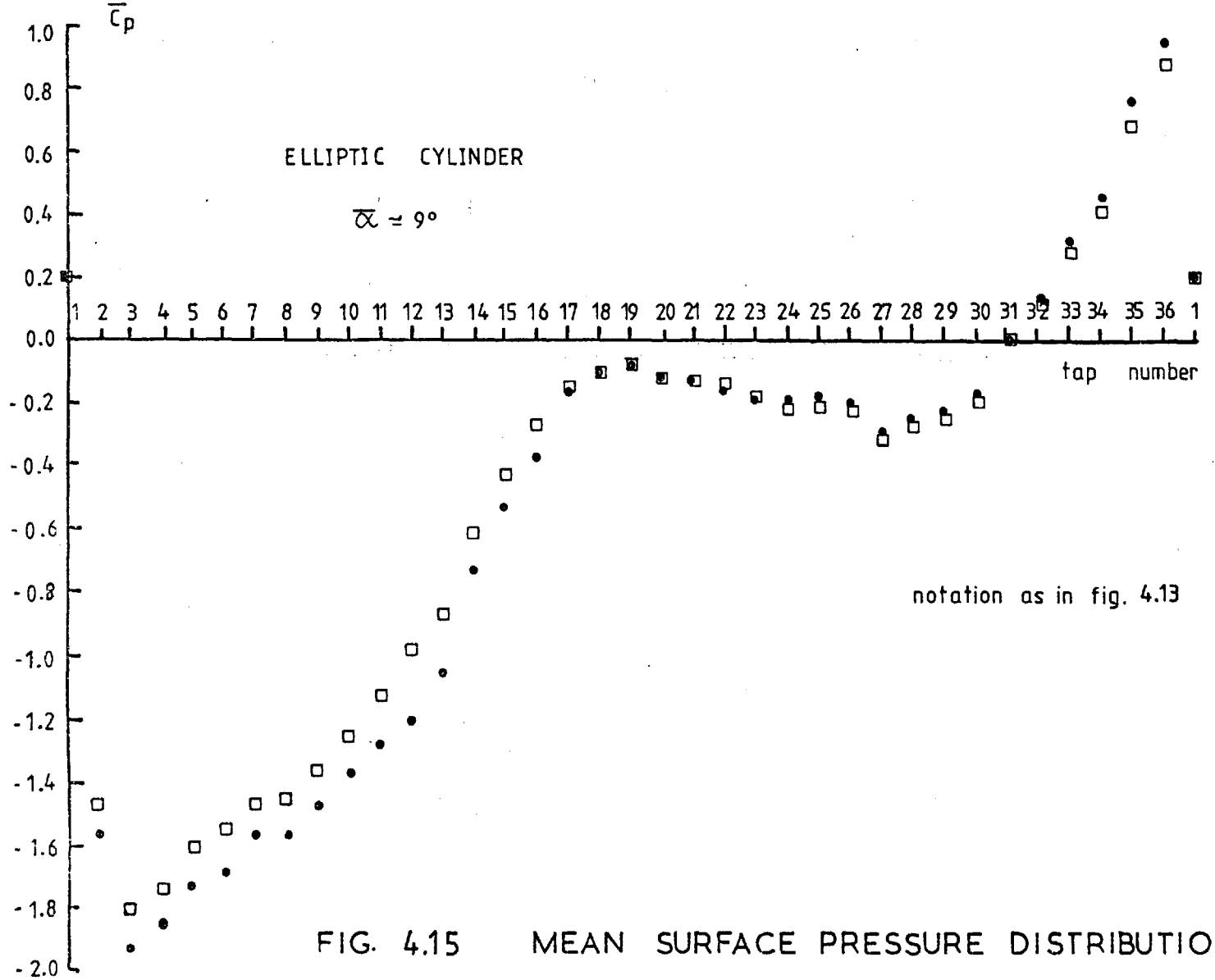

FIG. 4.15 MEAN SURFACE PRESSURE DISTRIBUTION

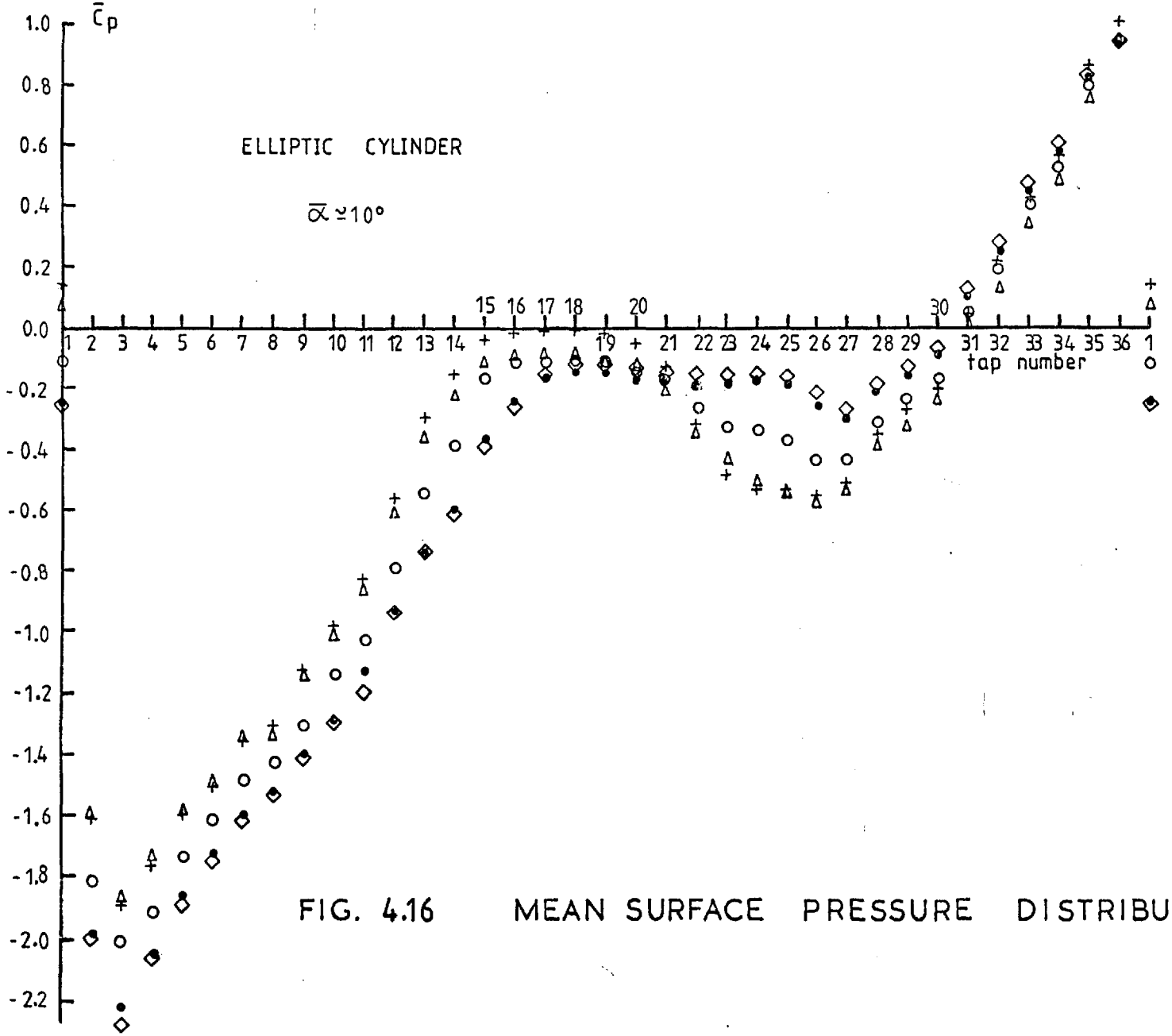

FIG. 4.16 MEAN SURFACE PRESSURE DISTRIBUTION

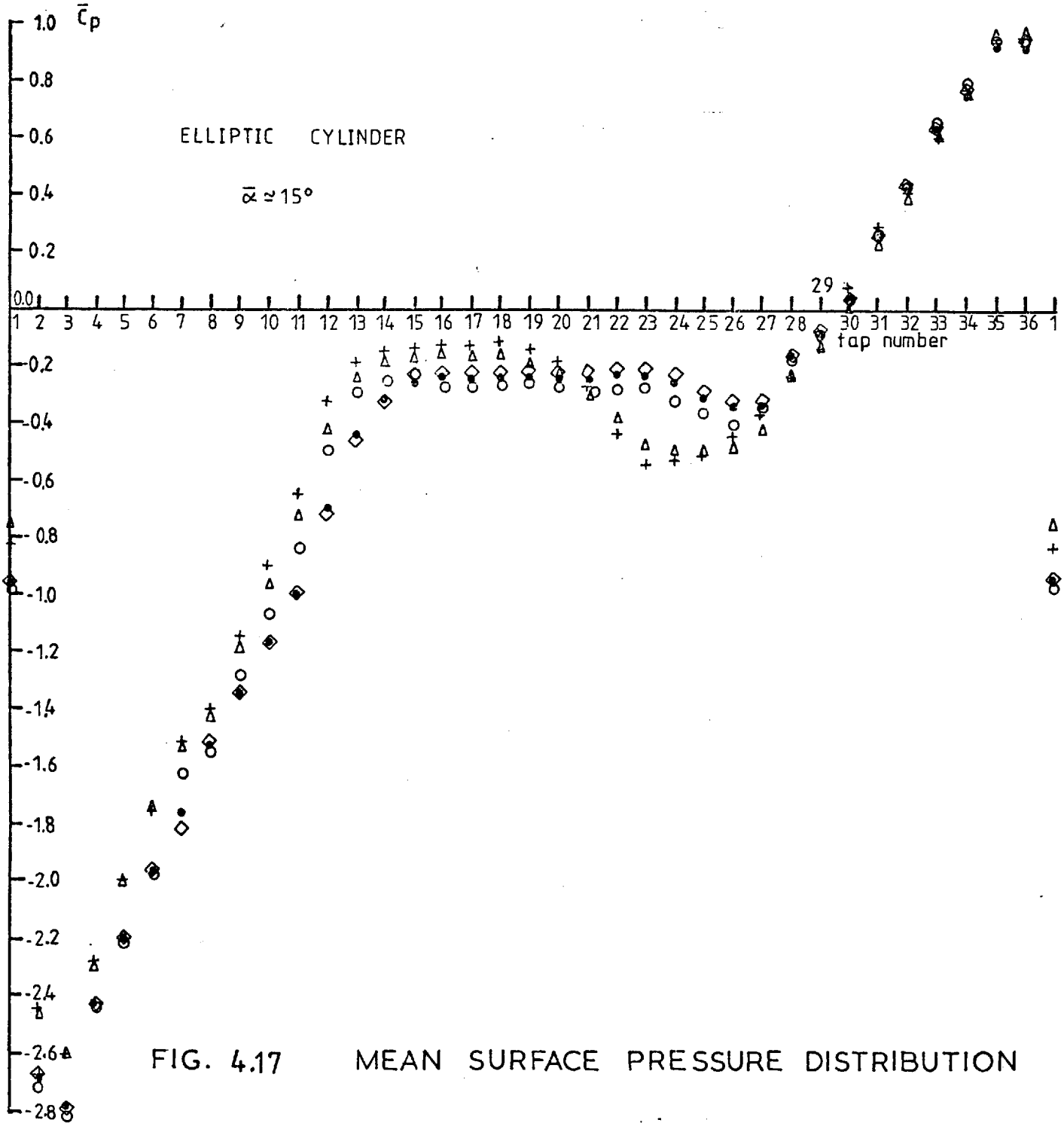

FIG. 4.17 MEAN SURFACE PRESSURE DISTRIBUTION

	flow	$L_{x/c}$	Re	$(\overline{\partial C_L/\partial\alpha})_{\alpha\simeq 0°}$	
⊙	smooth		$2.2-2.3\times10^5$	11.5	
⊡	"		1.6×10^5	12.5	
▽	"		1.2×10^5	11.5	
△	"		3.0×10^5	6.4	
◇	"		3.85×10^5	5.5	
+	" trip wires at 0.25c		2.2×10^5	4.2	
■	" Zahm et al.[1928]		1.37×10^5	10.0	, corr. inf. AR
◐	sinus. large ecc. k=0.22		2.2×10^5	~11.0	
◧	" " " k=0.30		1.6×10^5	~9.5	
◈	" " " k=0.14		3.85×10^5	~5.5	
•	turbulent	0.18	2.3×10^5	4.0	, $\sqrt{\overline{u^2}}/U_\infty \simeq 5.9\%$
◍	"	0.37	2.2×10^5	3.85	, " $\simeq 7.8\%$
×	"	~0.18	1.2×10^5	4.9	, " $\simeq 5.9\%$
◆	"	0.27	2.2×10^5	4.0	, " $\simeq 4.4\%$
▼	smooth		5.8×10^4	2.5	

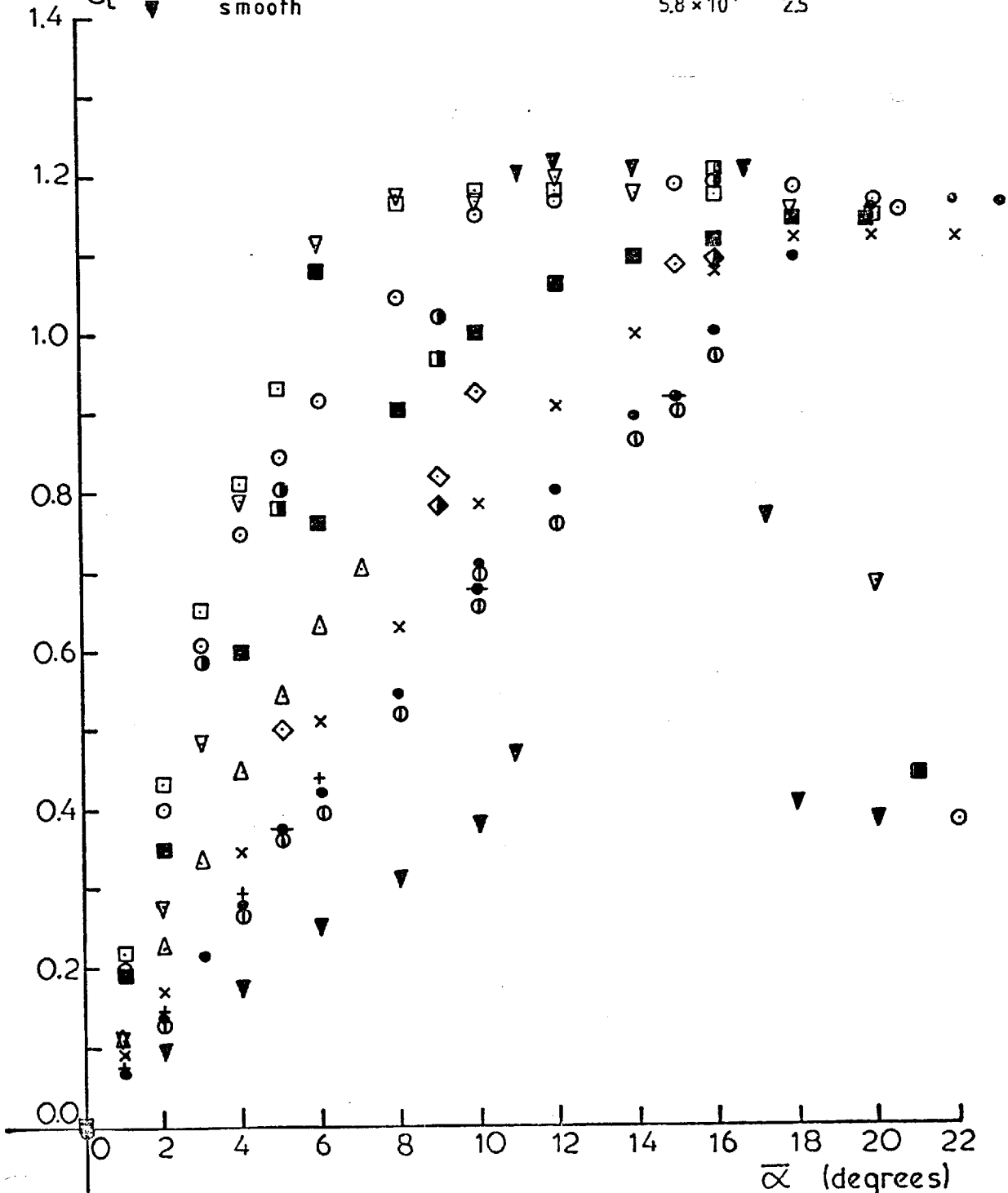

FIG. 4.18 $\overline{C_L}$ against $\overline{\alpha}$ ELLIPTIC CYLINDER

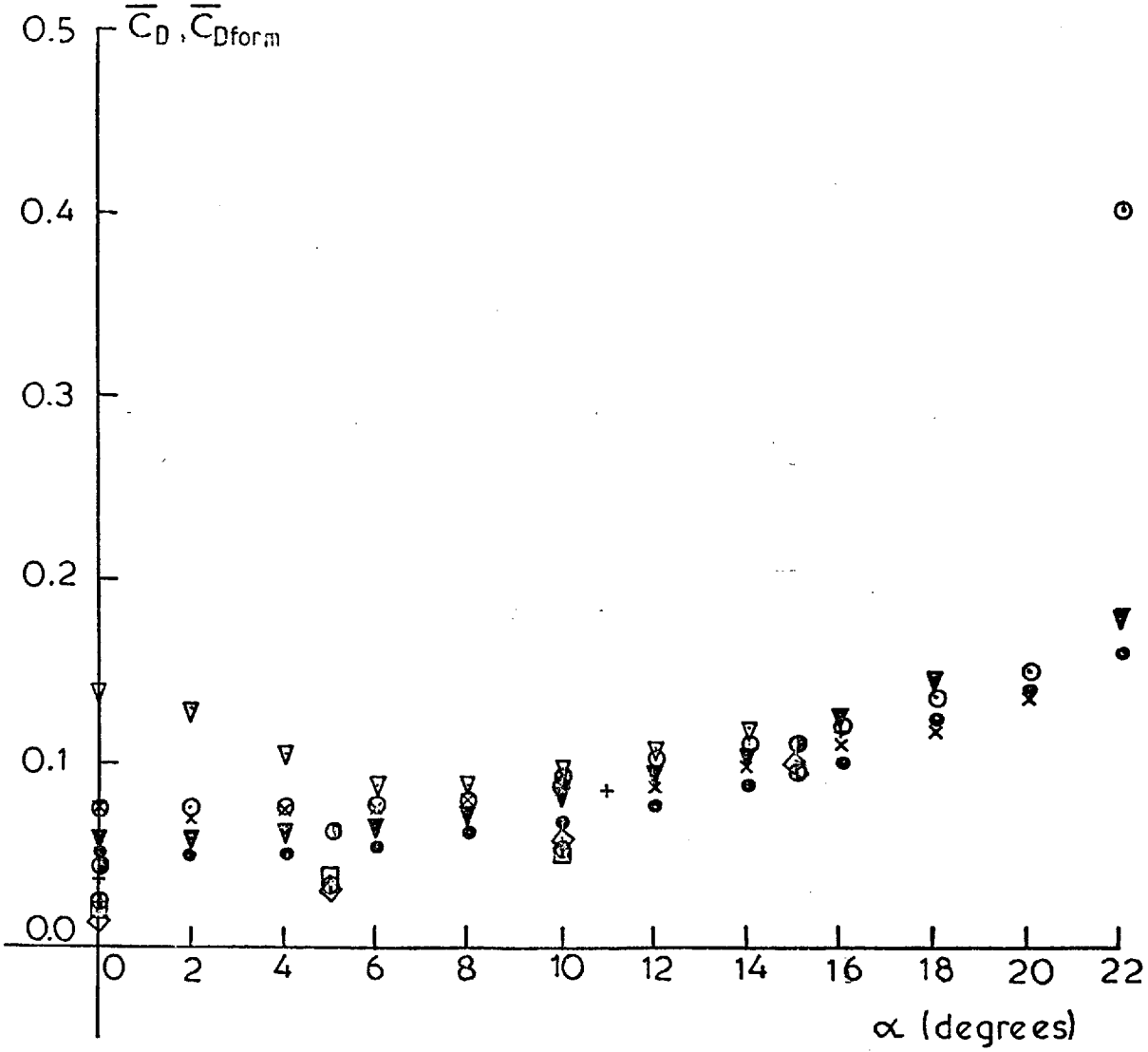

	flow	L_x/c	Re	$\overline{C}_D$
⊙	smooth		2.3×10^5	profile (total)
◑	"		2.2×10^5	form (pressure)
▽	"		1.2×10^5	profile
◇	"		3.85×10^5	form
×	" Zahm et al. [1928]		1.37×10^5	profile
+	sinusoidal large ecc. k=0.22		2.2×10^5	form
●	turbulent $\sqrt{\overline{u^2}}/U_\infty \simeq 5.9\%$	0.18	2.3×10^5	profile
◐	" " $\simeq 4.4\%$	0.27	2.2×10^5	form
▼	" " $\simeq 5.9\%$	0.18	1.2×10^5	profile
⊡	" " $\simeq 7.8\%$	0.37	2.2×10^5	form

FIG. 4.19 $\overline{C}_D$, $\overline{C}_{Dform}$ against $\overline{\alpha}$ ELLIPTIC CYLINDER

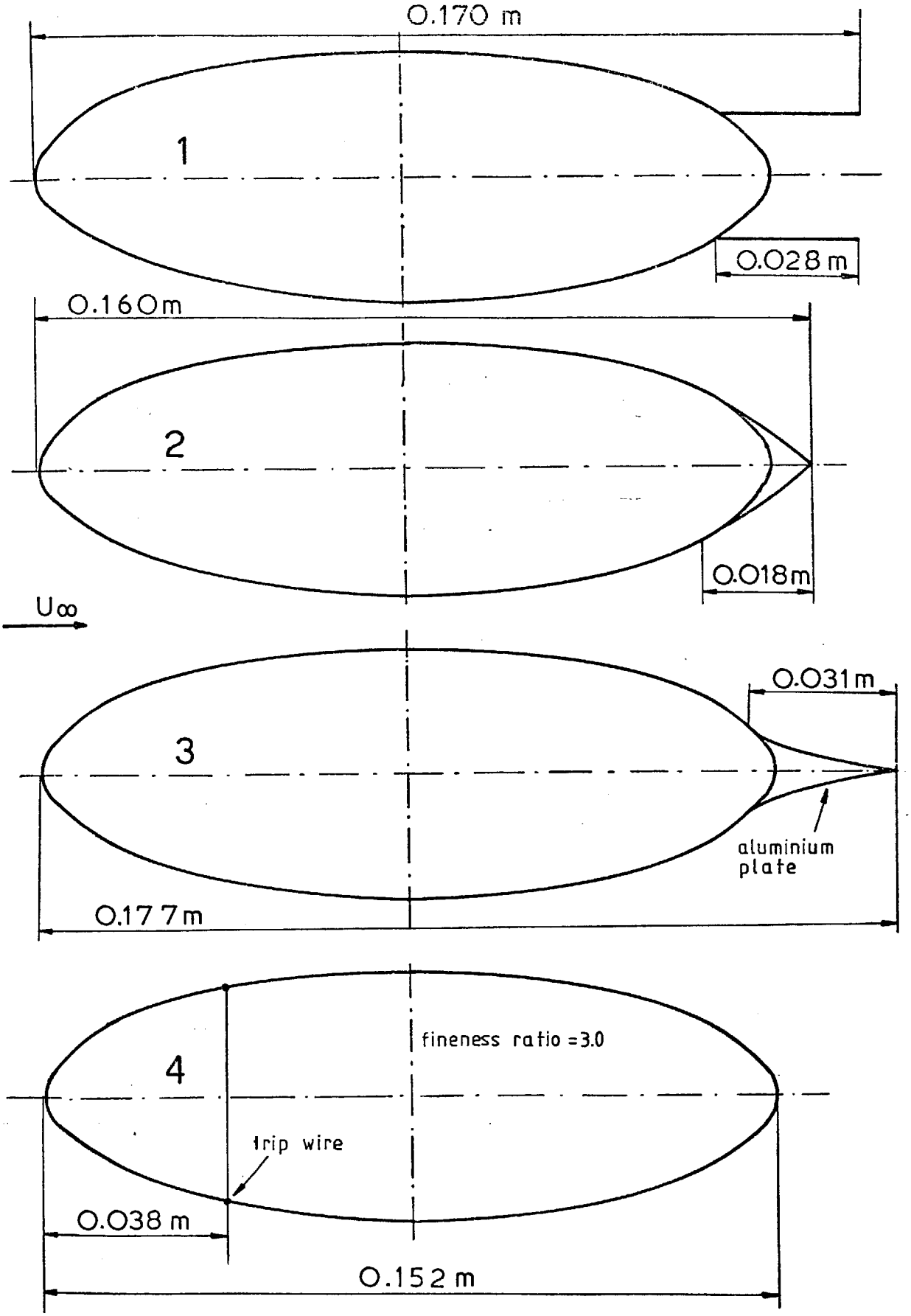

FIG. 5.1 MODIFIED TWO DIMENSIONAL ELLIPTIC CYLINDERS USED IN THE SINUSOIDAL FLOW EXPERIMENT

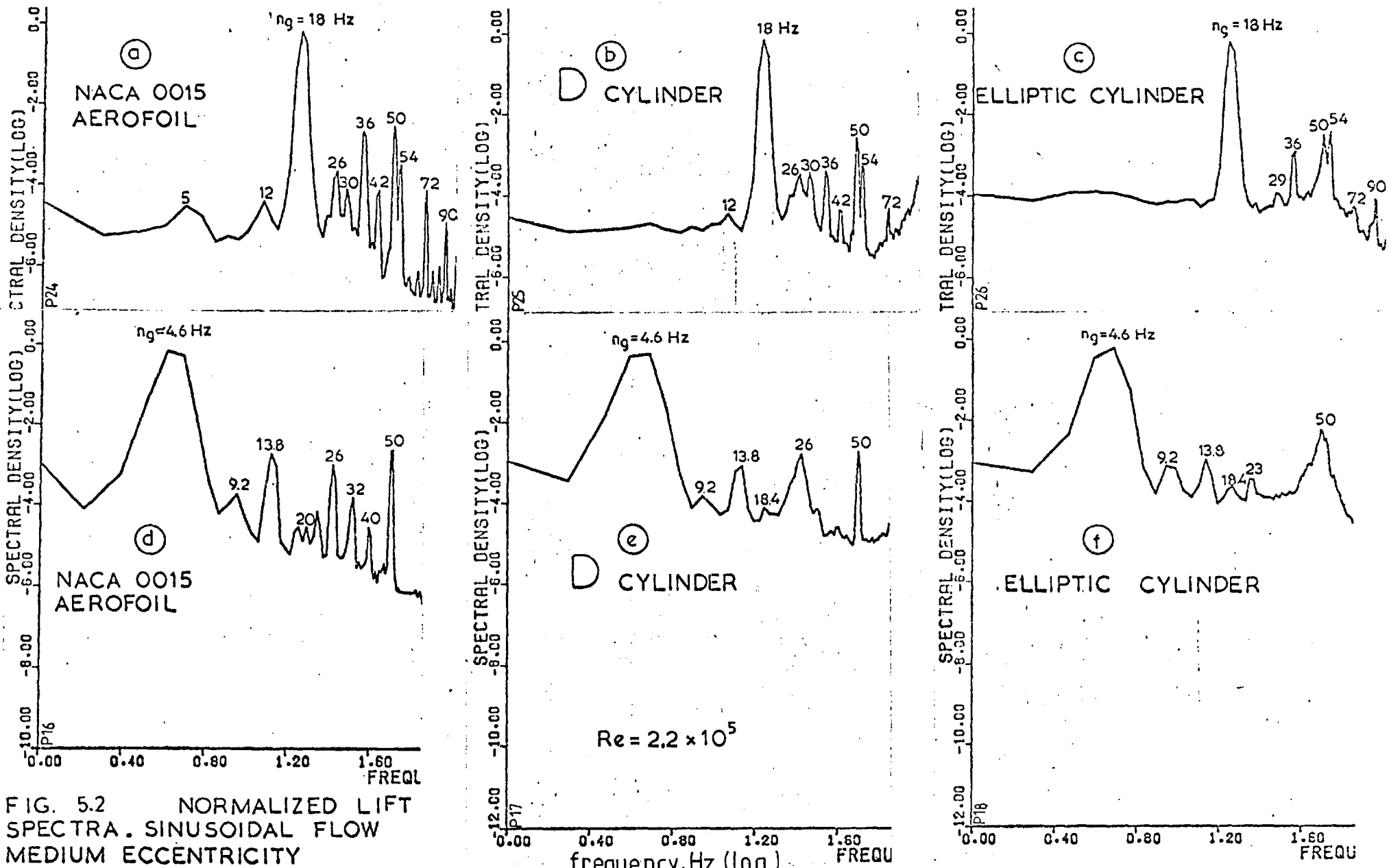

FIG. 5.2 NORMALIZED LIFT SPECTRA. SINUSOIDAL FLOW MEDIUM ECCENTRICITY

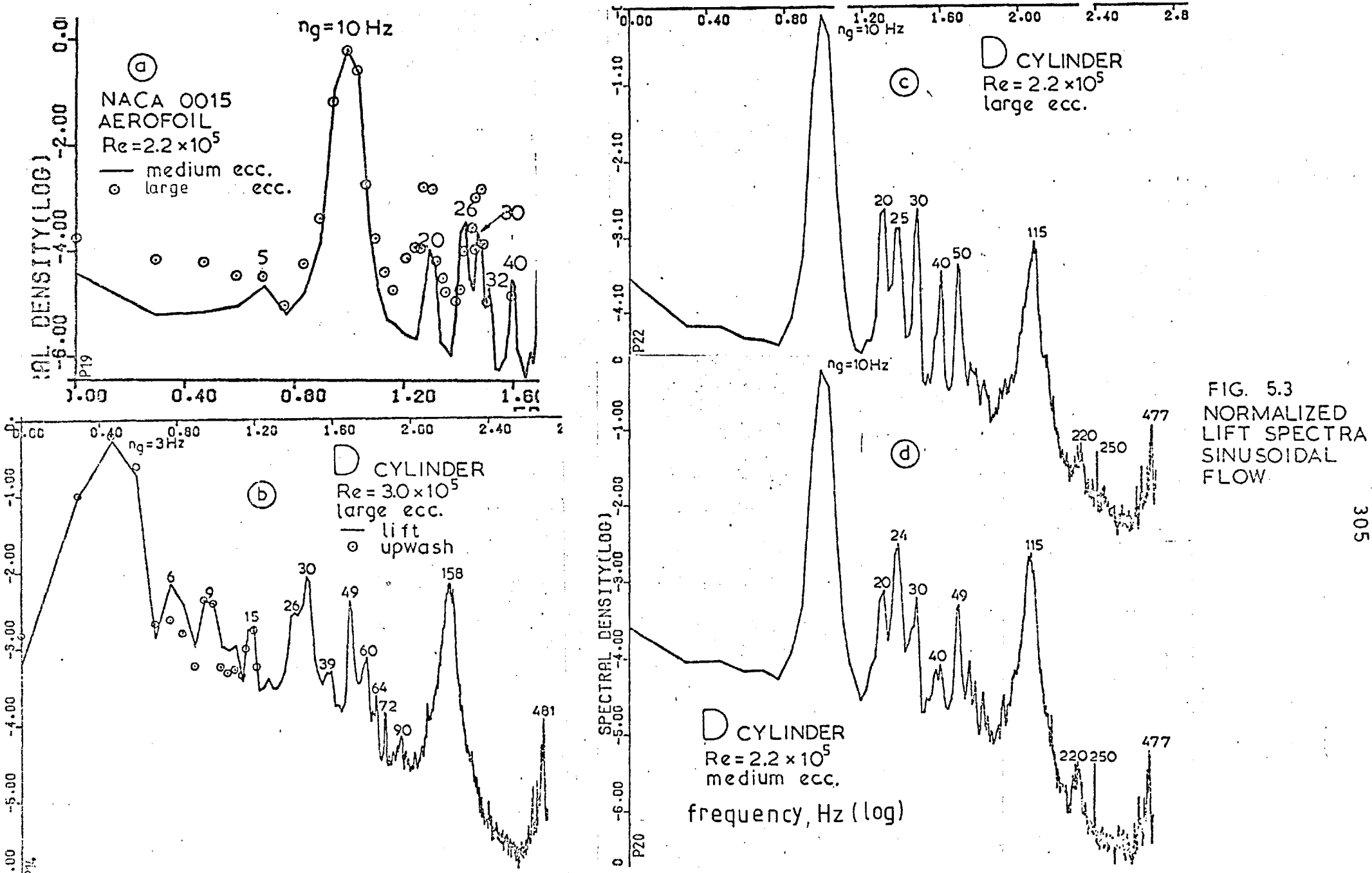

FIG. 5.3
NORMALIZED
LIFT SPECTRA
SINUSOIDAL
FLOW

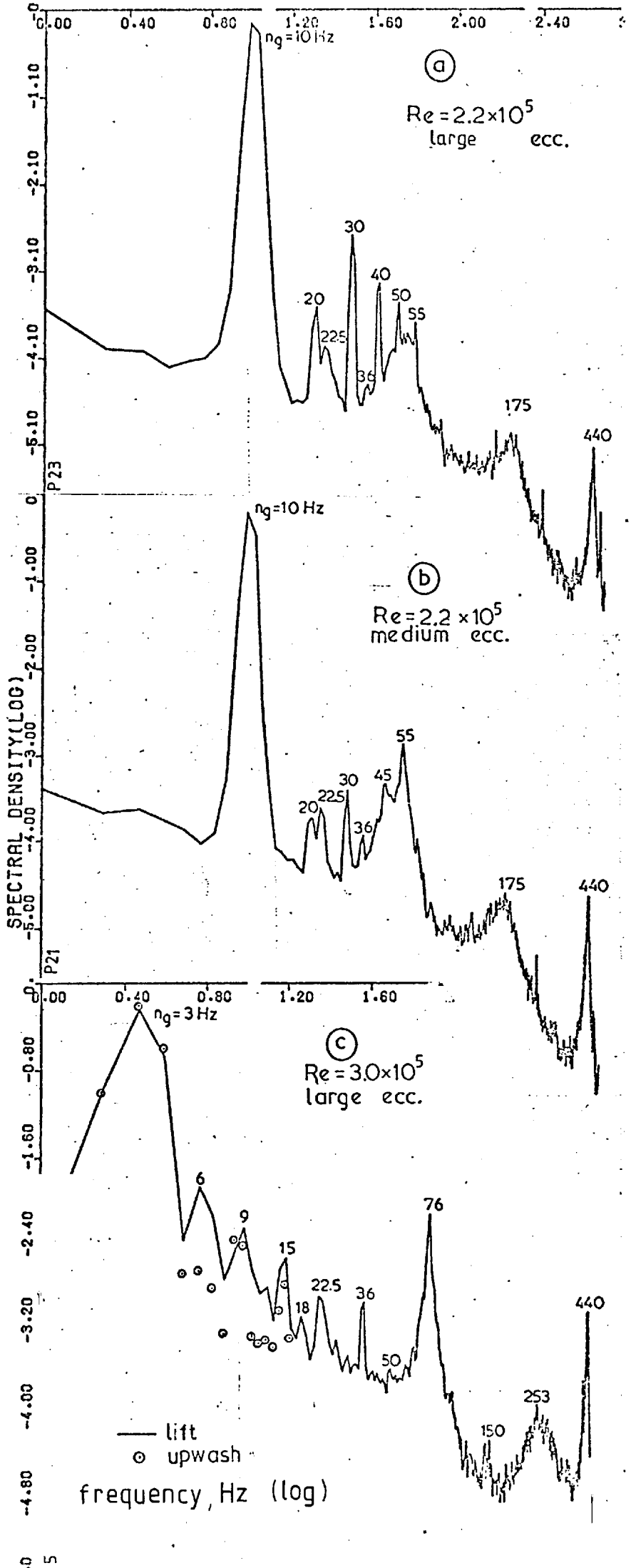

FIG. 5.4
NORMALISED
LIFT SPECTRA
SINUSOIDAL FLOW
ELLIPTIC CYLINDER

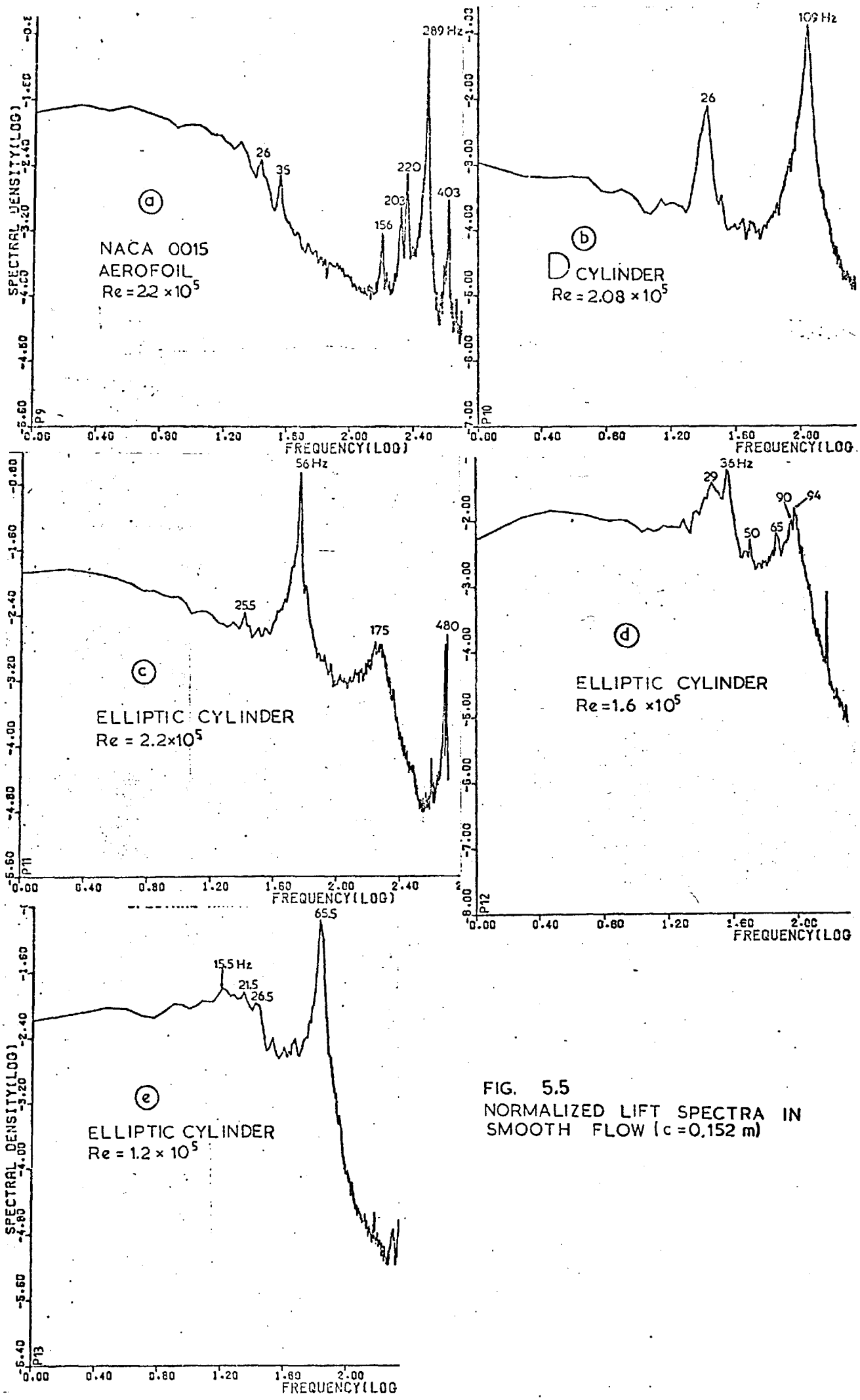

FIG. 5.5
NORMALIZED LIFT SPECTRA IN SMOOTH FLOW (c = 0.152 m)

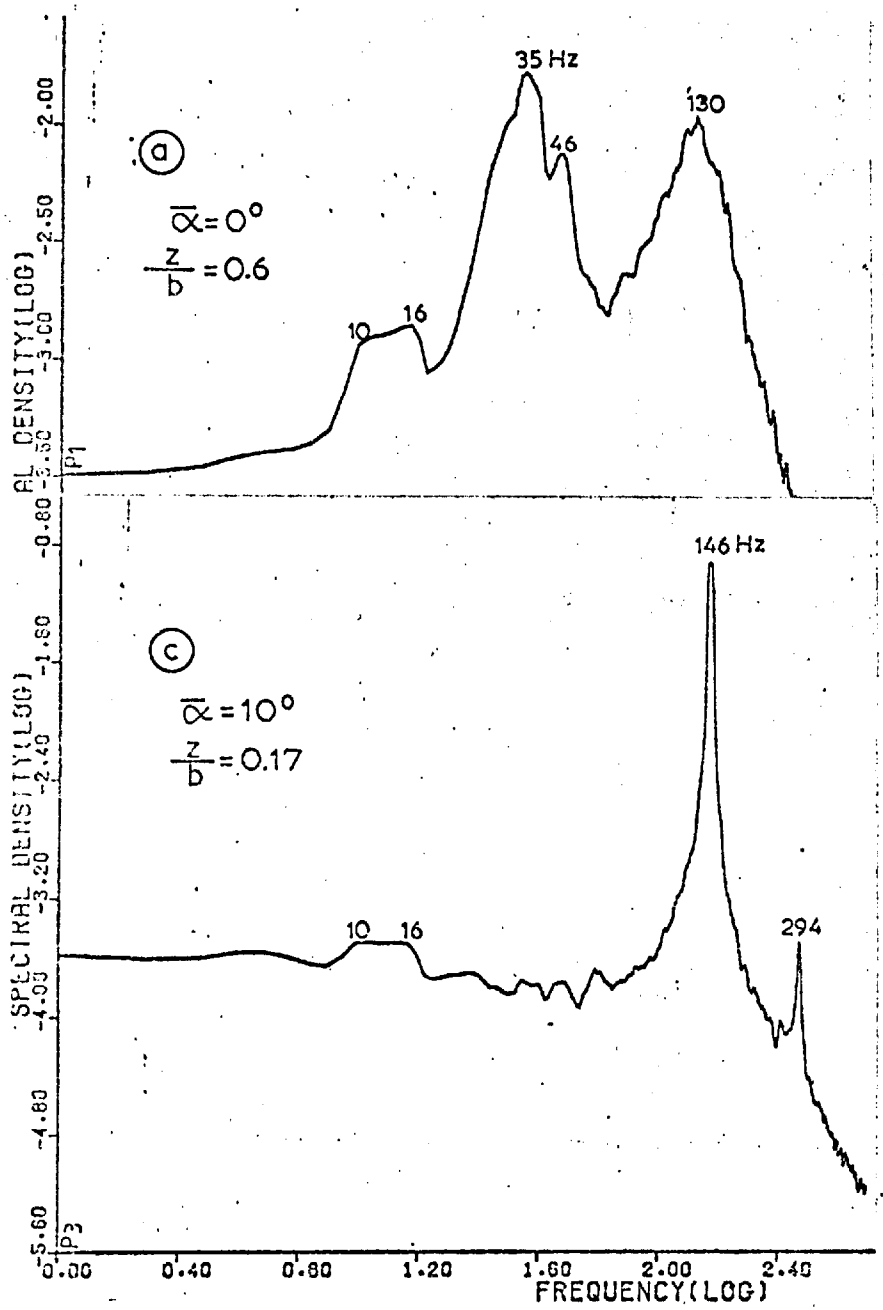

ELLIPTIC CYLINDER
$Re = 2.2 \times 10^5$
smooth flow

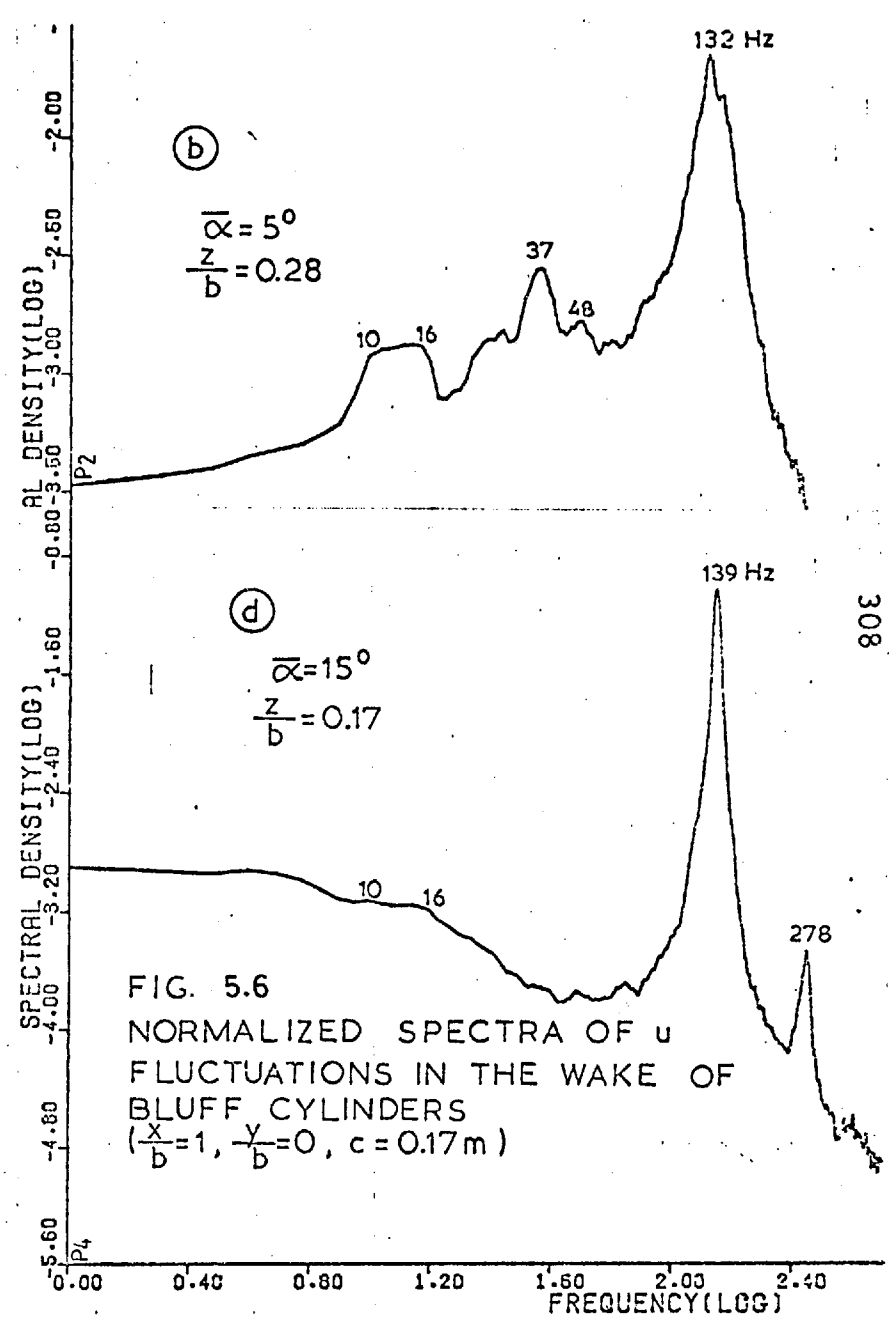

FIG. 5.6
NORMALIZED SPECTRA OF u FLUCTUATIONS IN THE WAKE OF BLUFF CYLINDERS
($\frac{x}{b}=1$, $\frac{y}{b}=0$, c = 0.17 m)

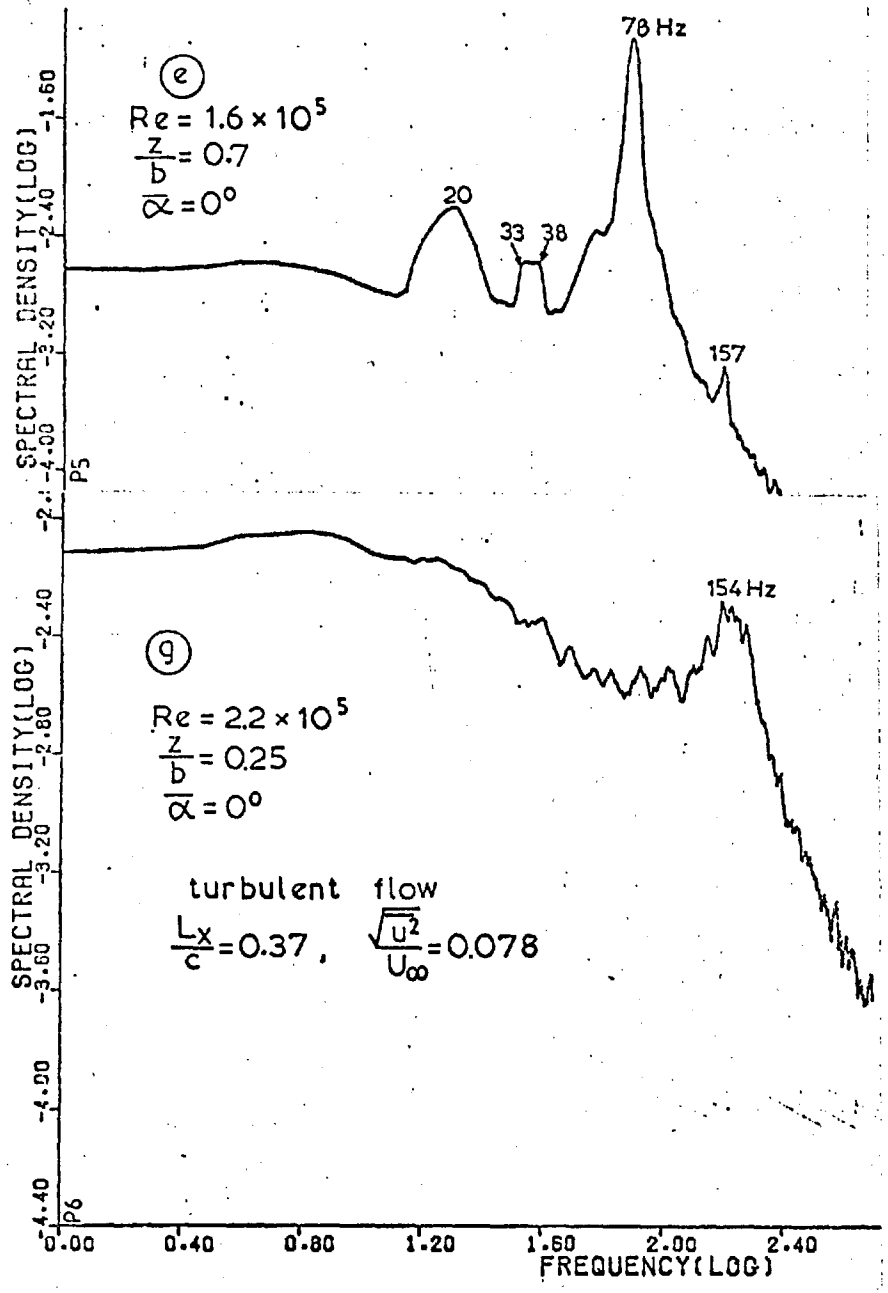

FIG. 5.6
(continued)

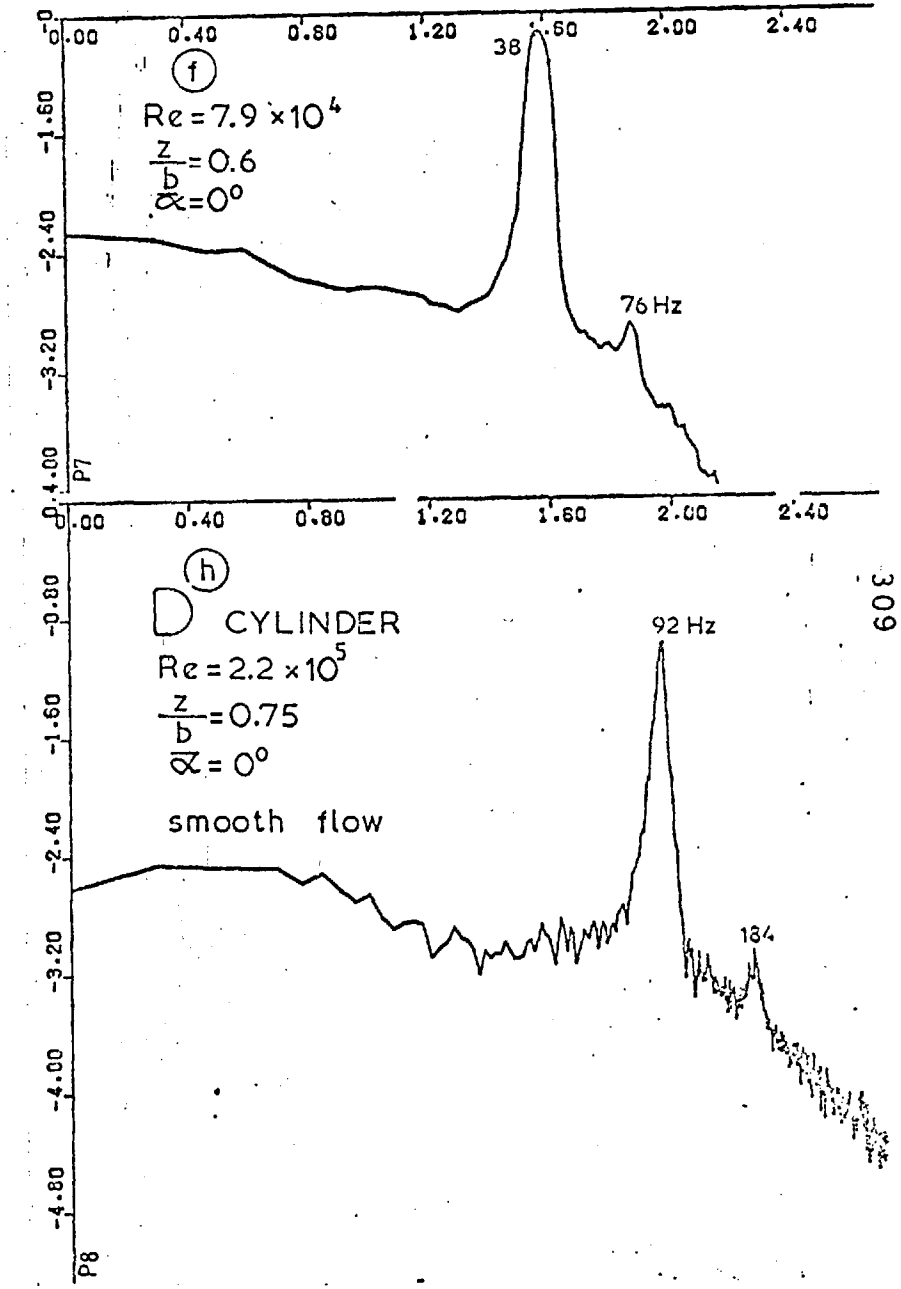

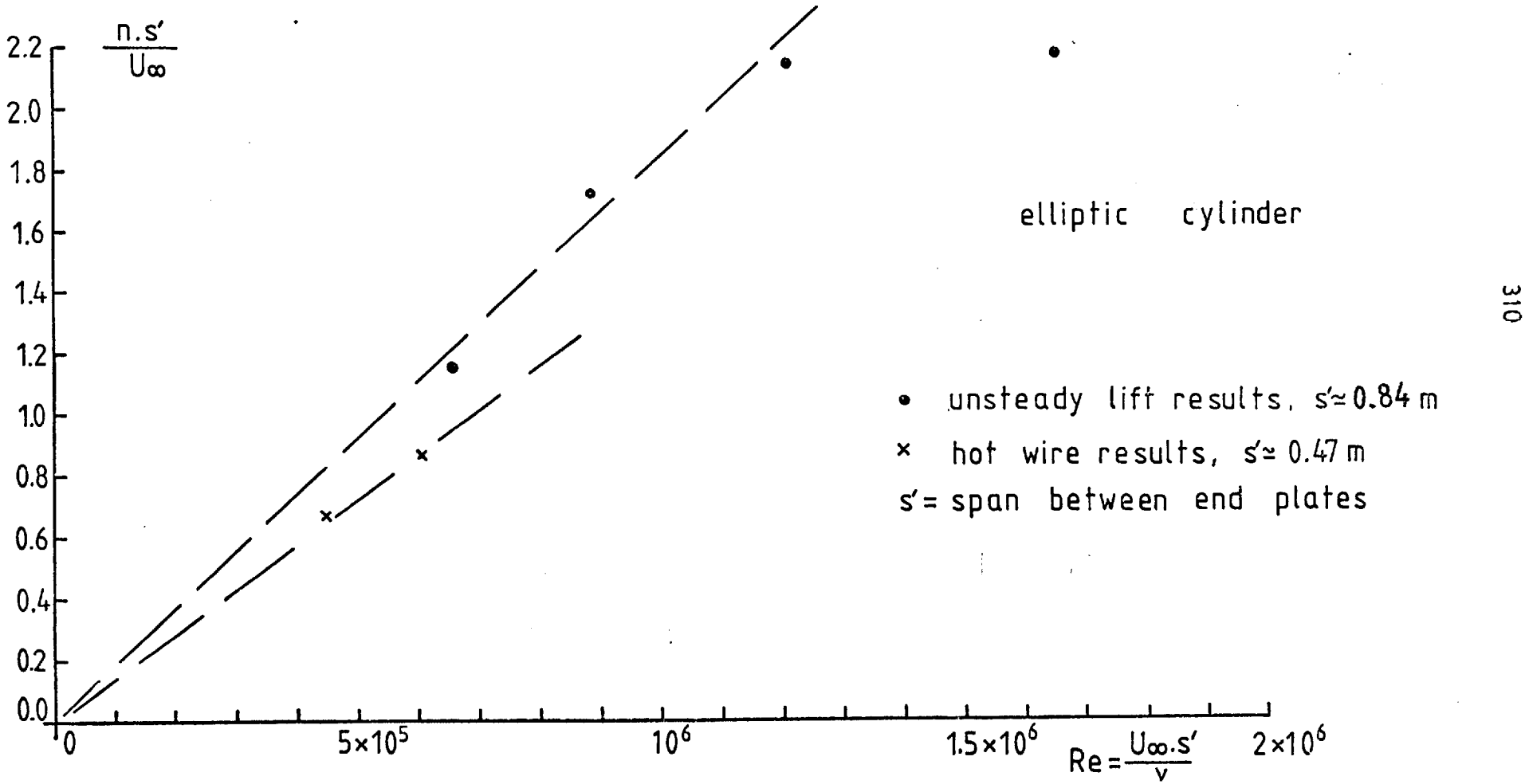

FIG. 5.7 DIMENSIONLESS FREQUENCY PARAMETER VERSUS SPAN REYNOLDS NUMBER

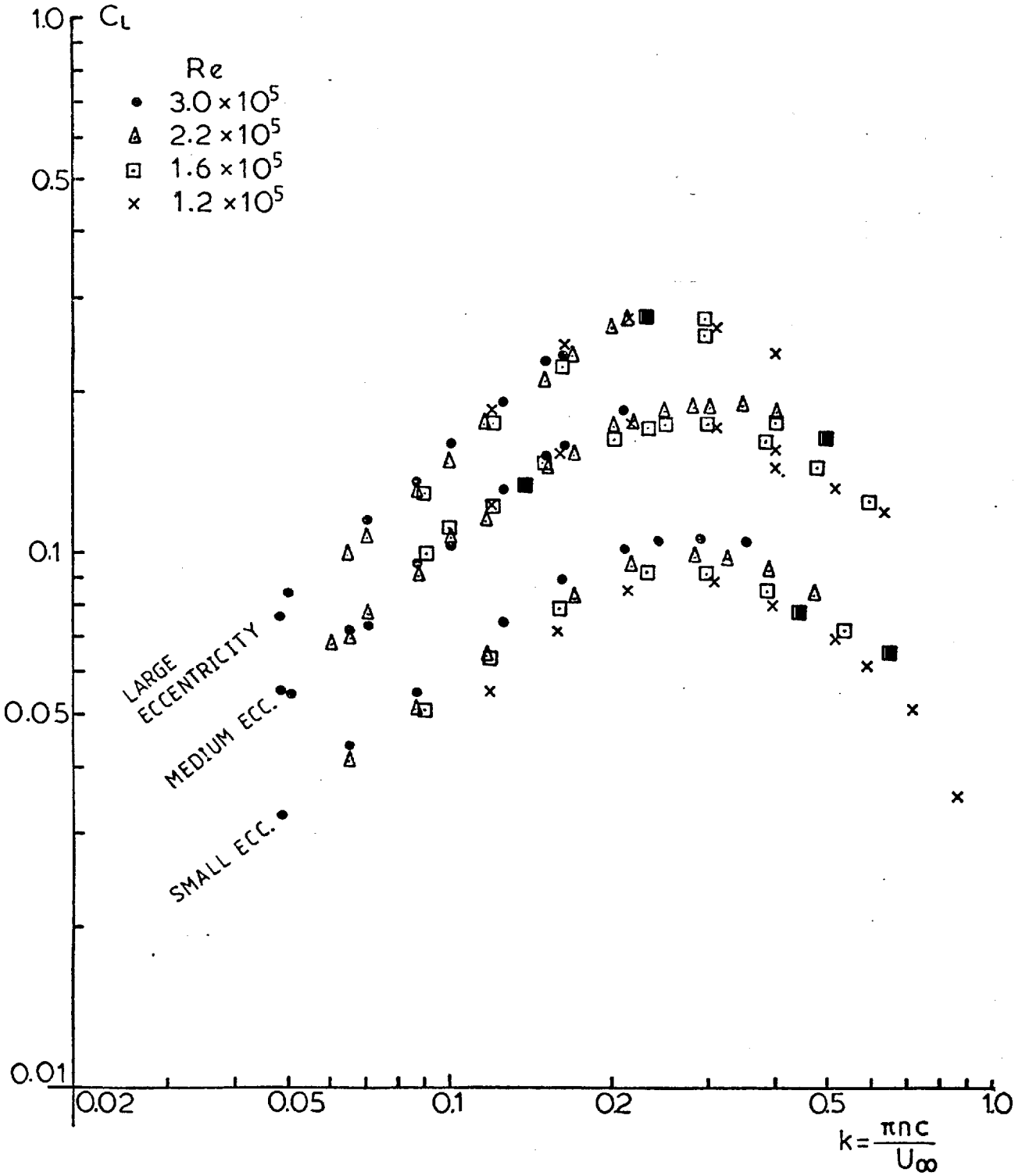

FIG. 5.8 MEASURED RMS LIFT COEFFICIENT (FILTERED) NACA 0015 AEROFOIL $\overline{\alpha} = 0^\circ$

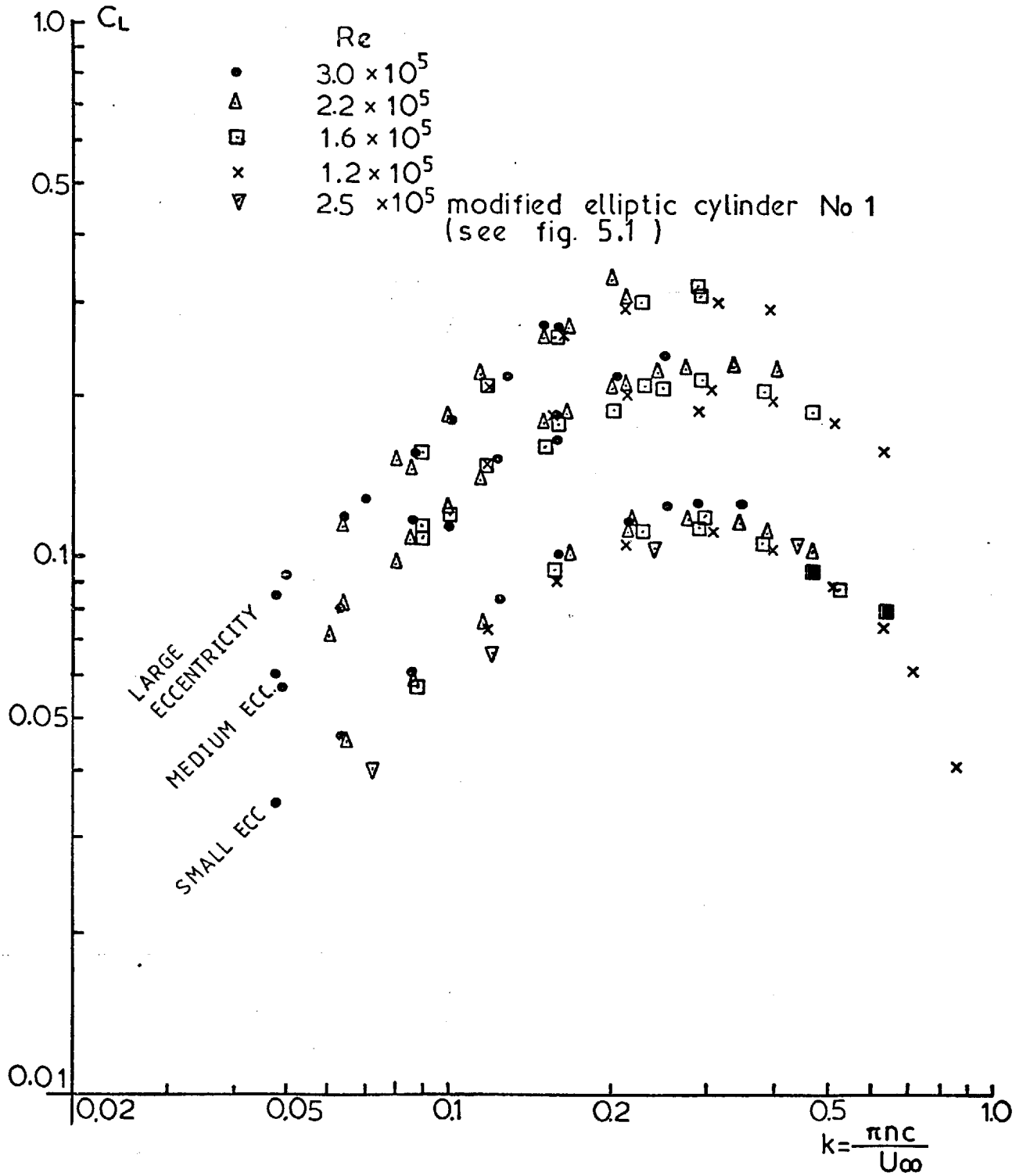

FIG. 5.9 MEASURED RMS LIFT COEFFICIENT (FILTERED) D CYLINDER

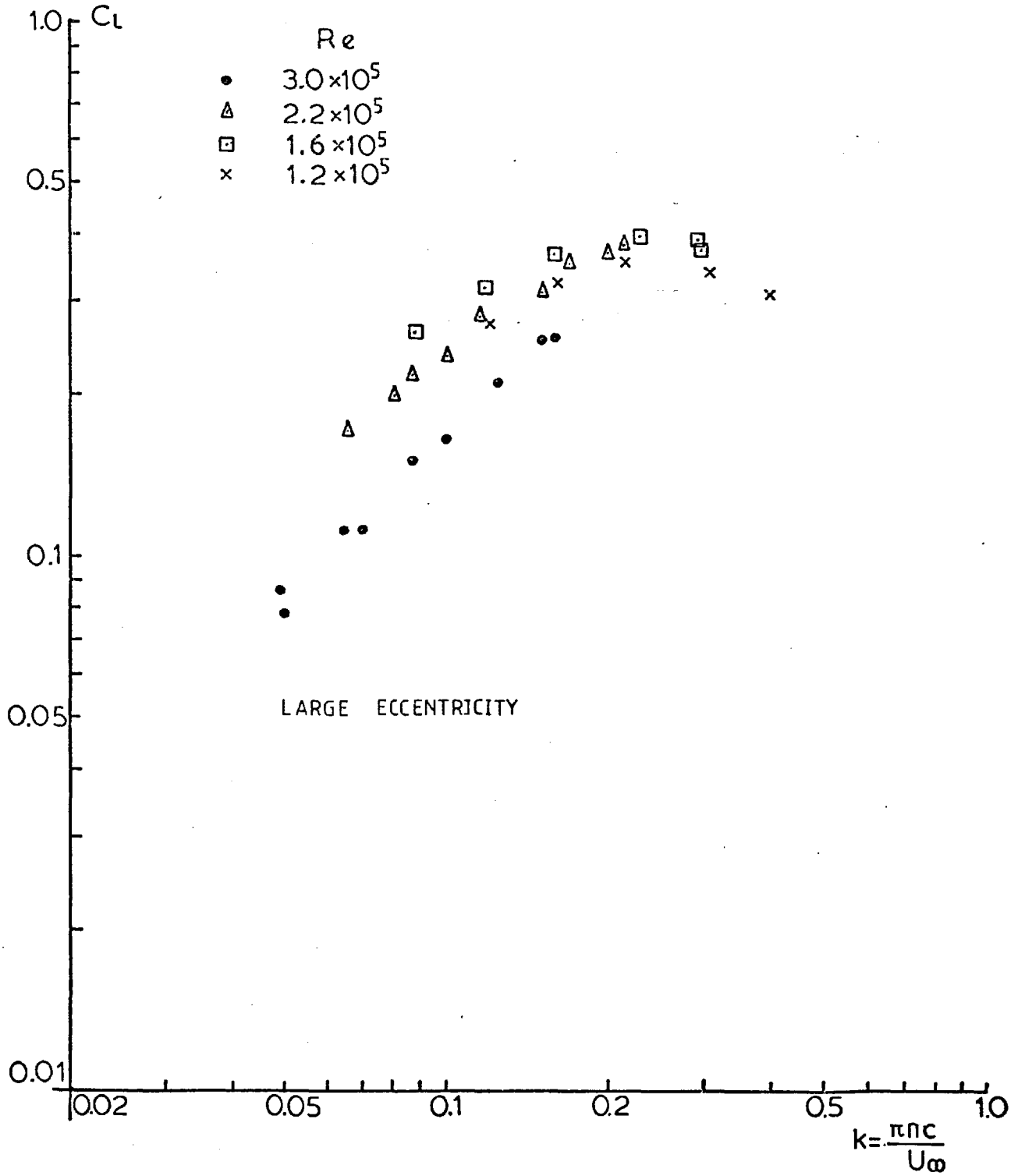

FIG. 5.10 MEASURED RMS LIFT COEFFICIENT (FILTERED) ELLIPTIC CYLINDER

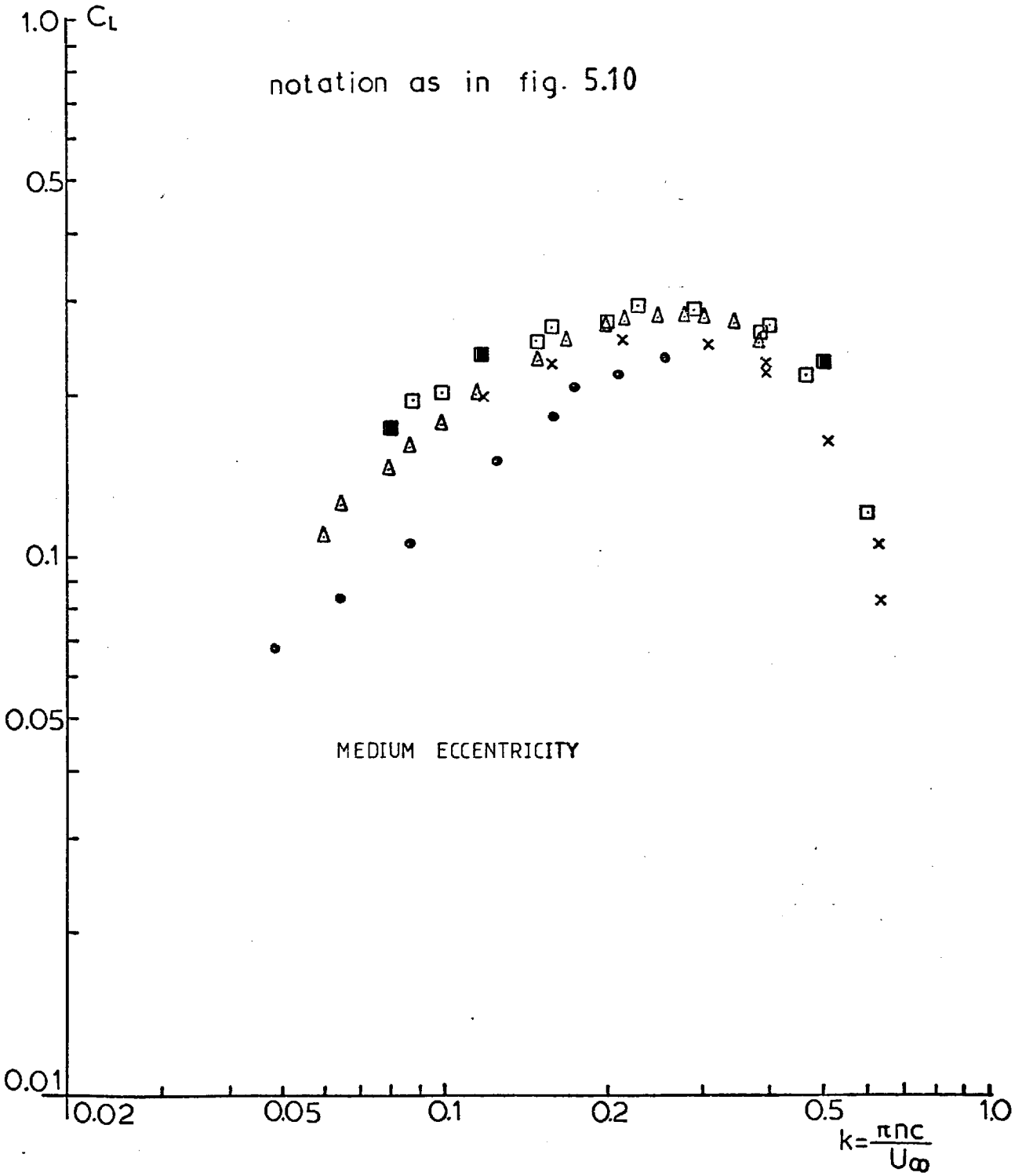

FIG. 5.11 MEASURED RMS LIFT COEFFICIENT (FILTERED) ELLIPTIC CYLINDER

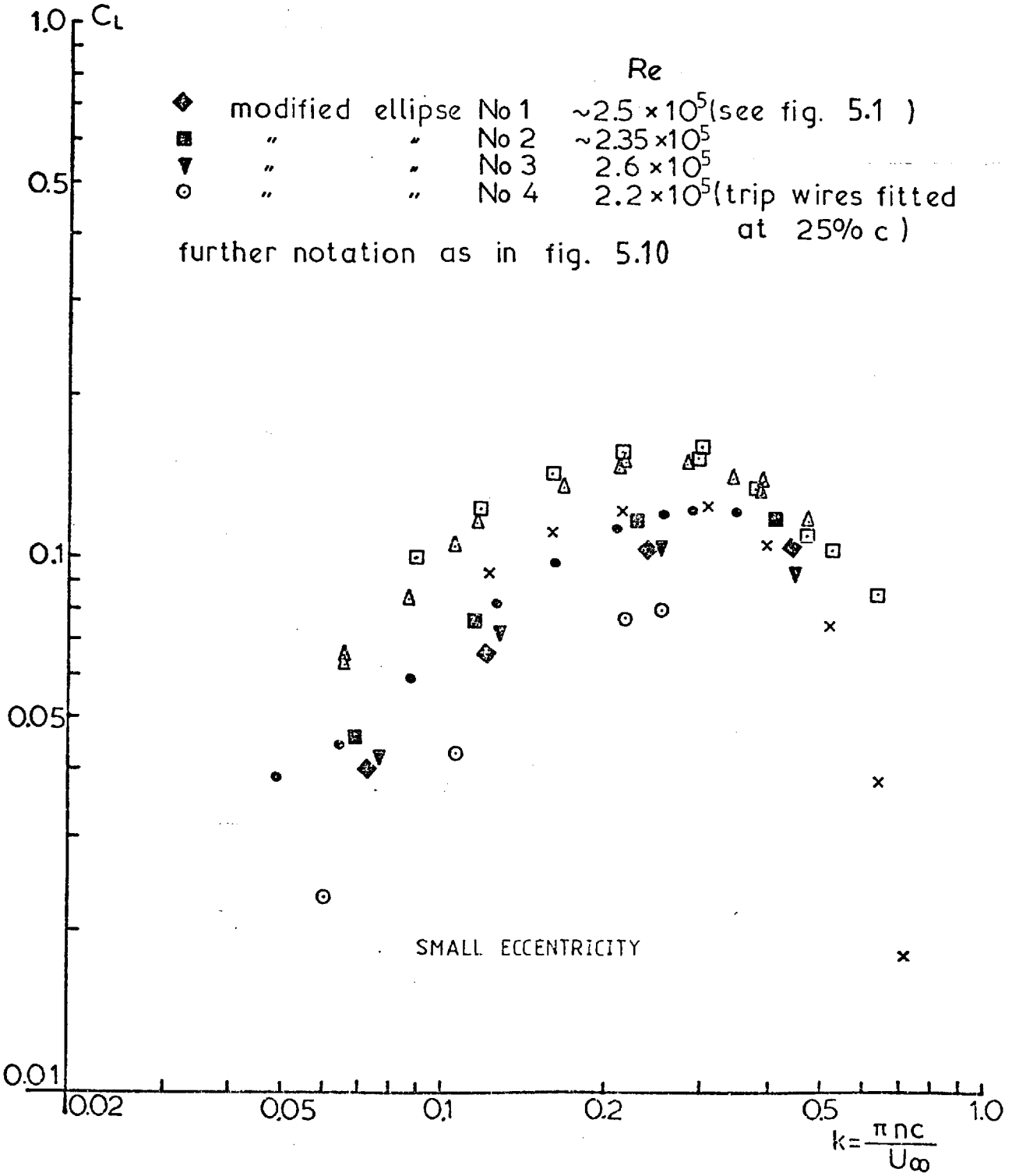

FIG. 5.12 MEASURED RMS LIFT COEFFICIENT (FILTERED) ELLIPTIC CYLINDER

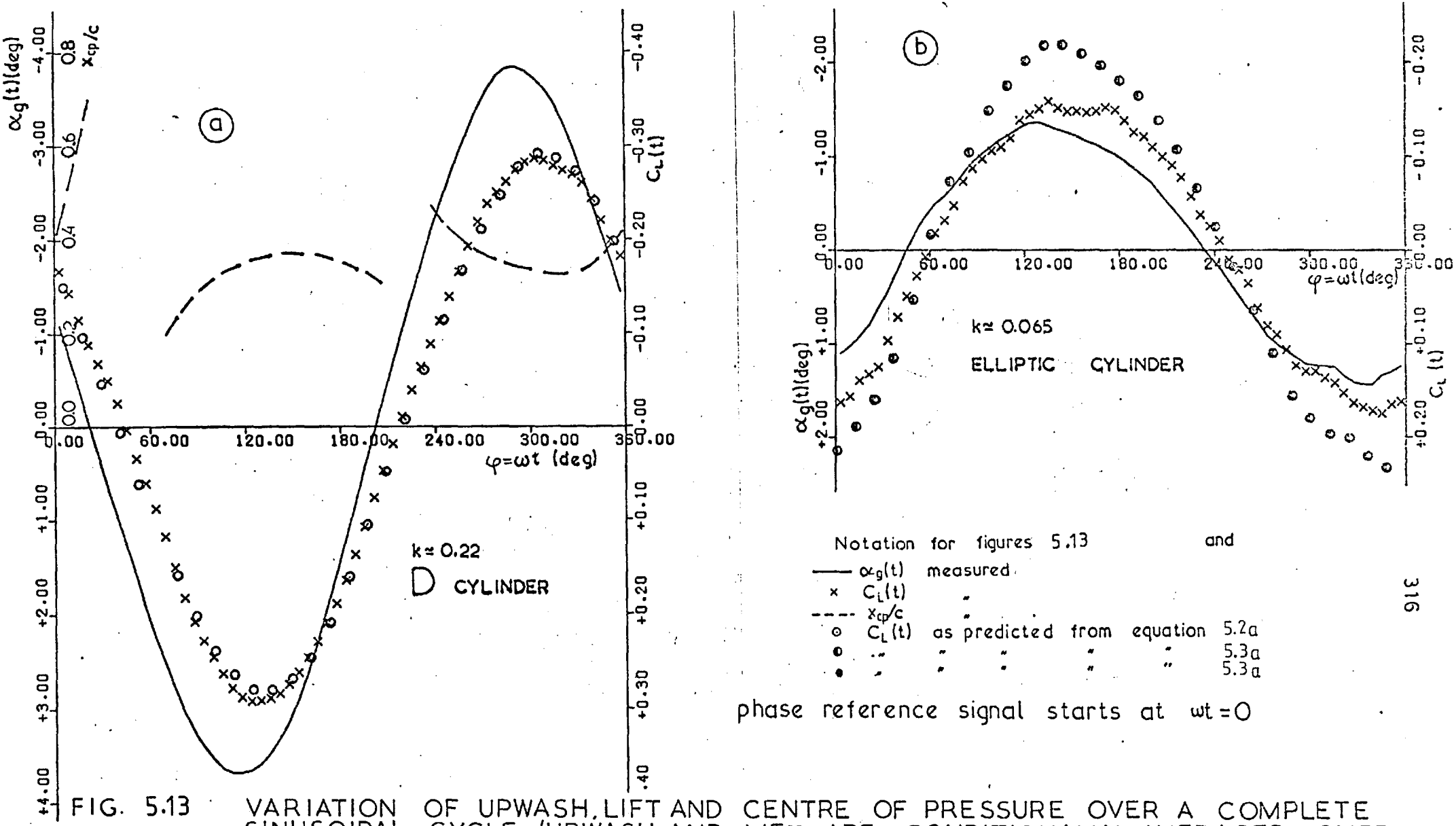

FIG. 5.13 VARIATION OF UPWASH, LIFT AND CENTRE OF PRESSURE OVER A COMPLETE SINUSOIDAL CYCLE (UPWASH AND LIFT ARE CONDITIONALLY AVERAGED OVER A LARGE NUMBER OF PERIODS)

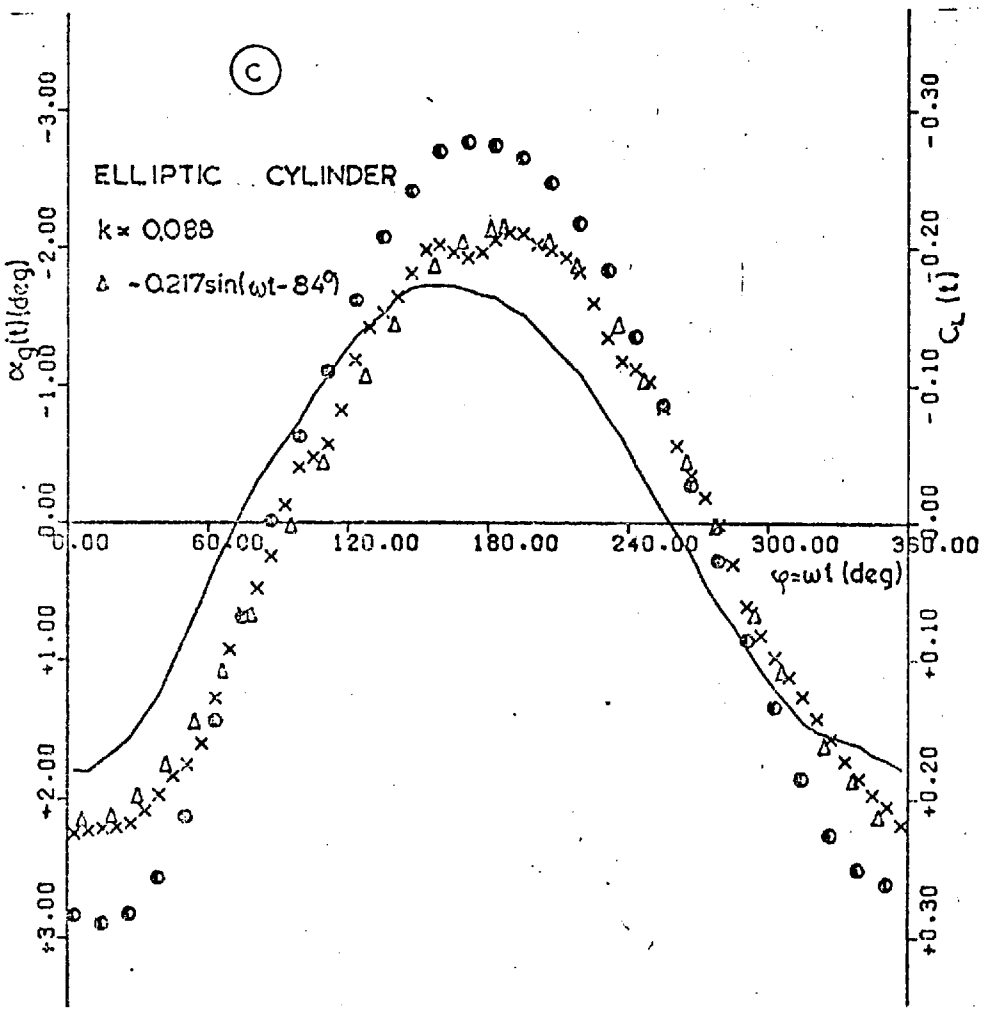

FIG. 5.13 (continued)

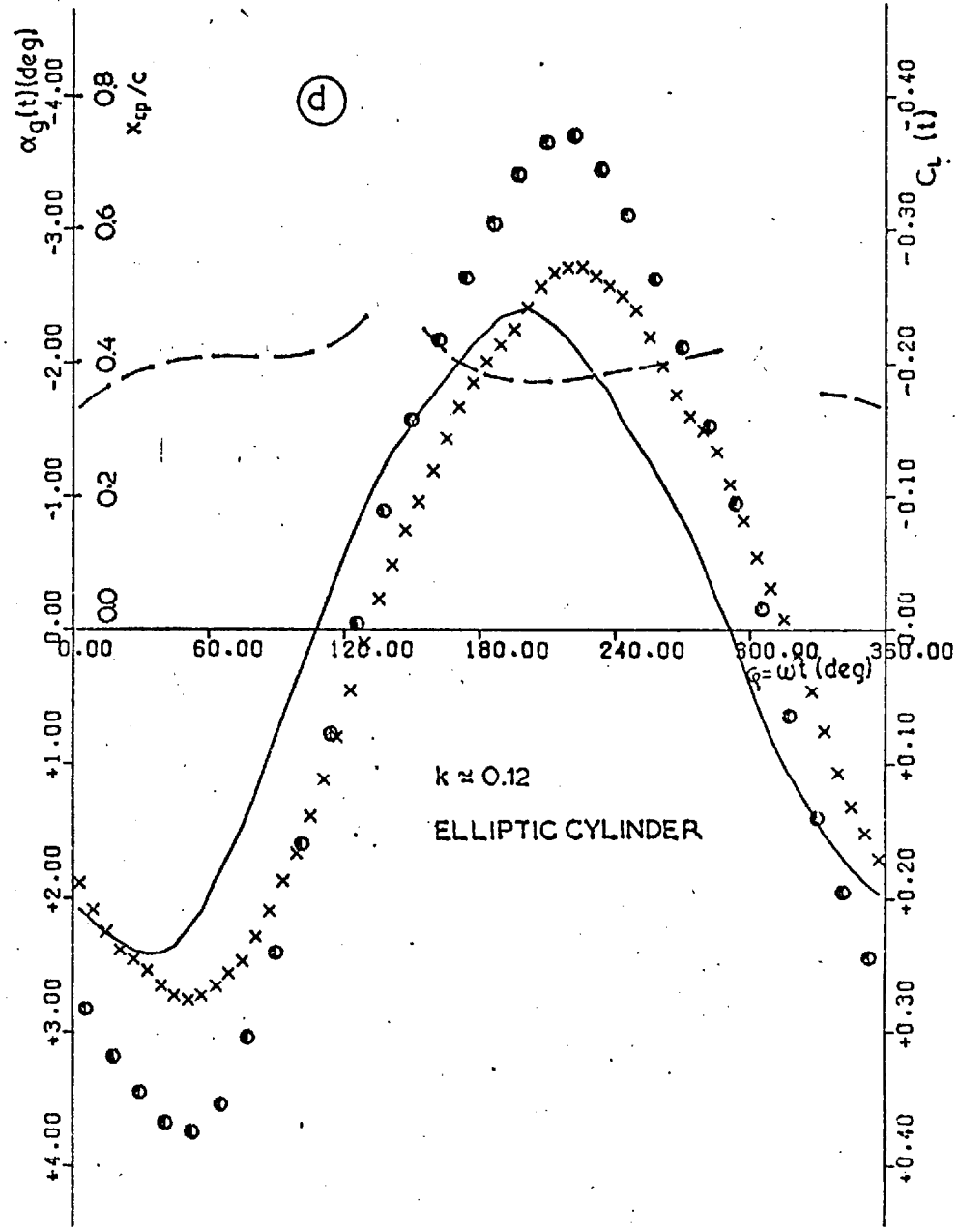

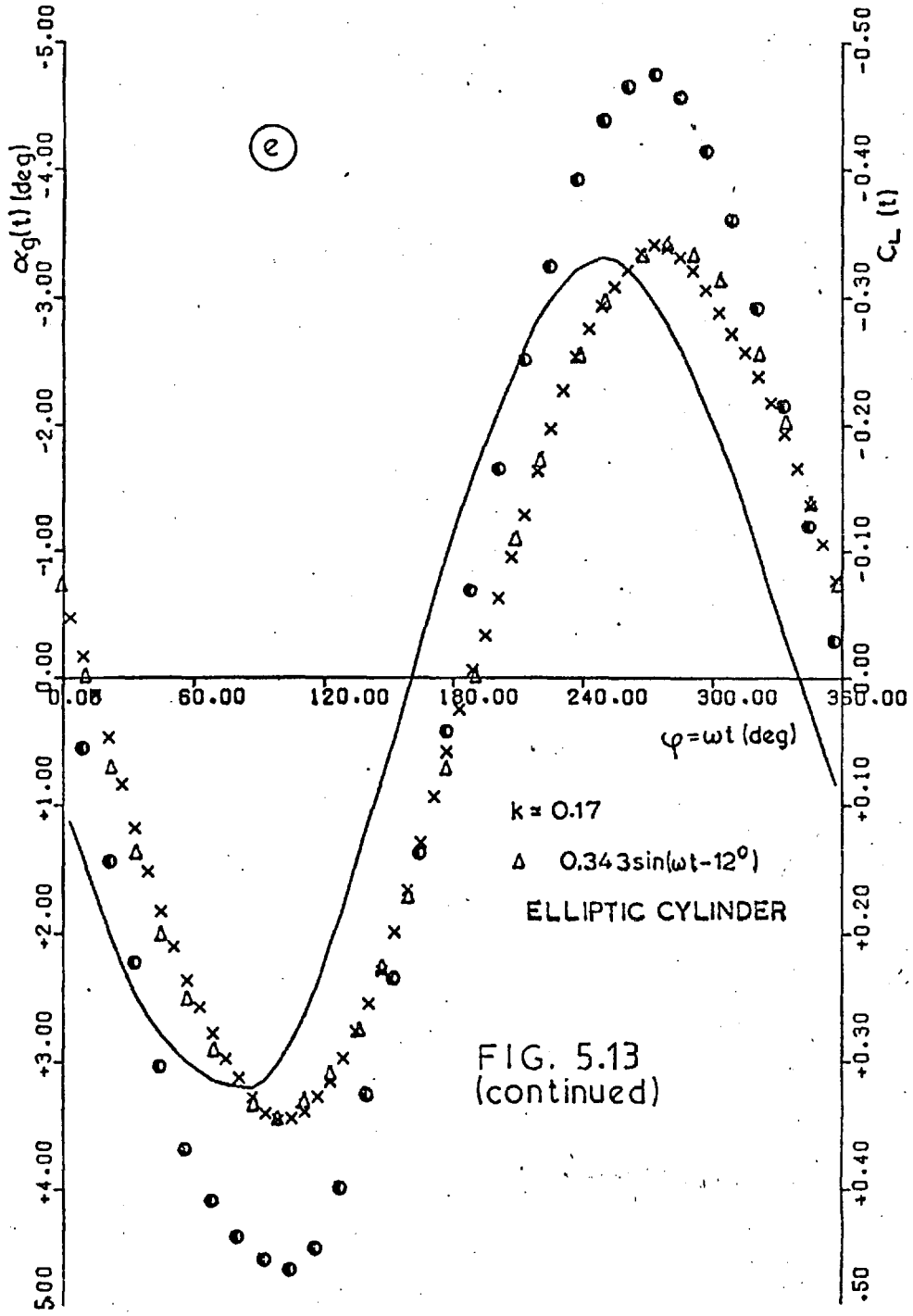

FIG. 5.13
(continued)

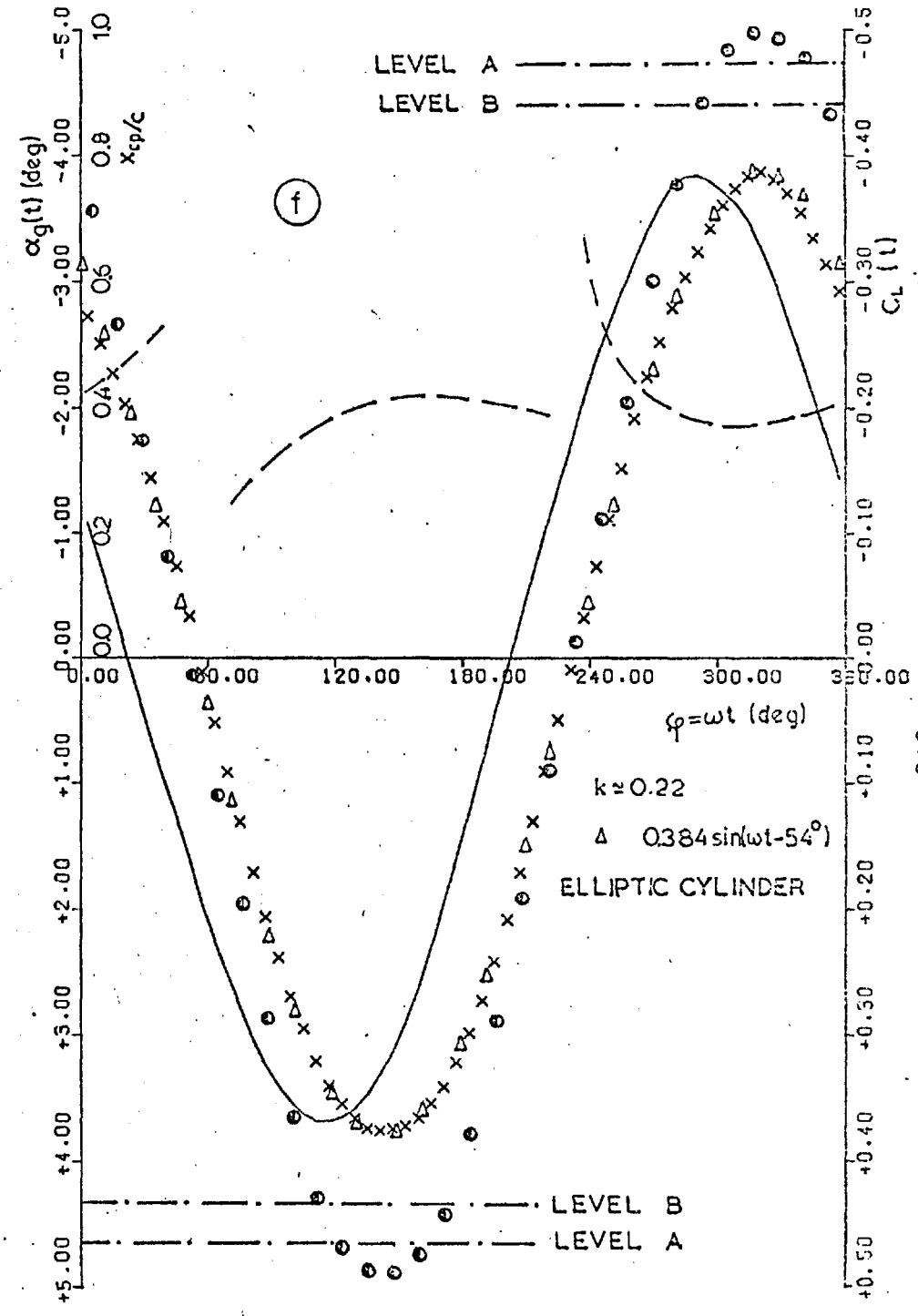

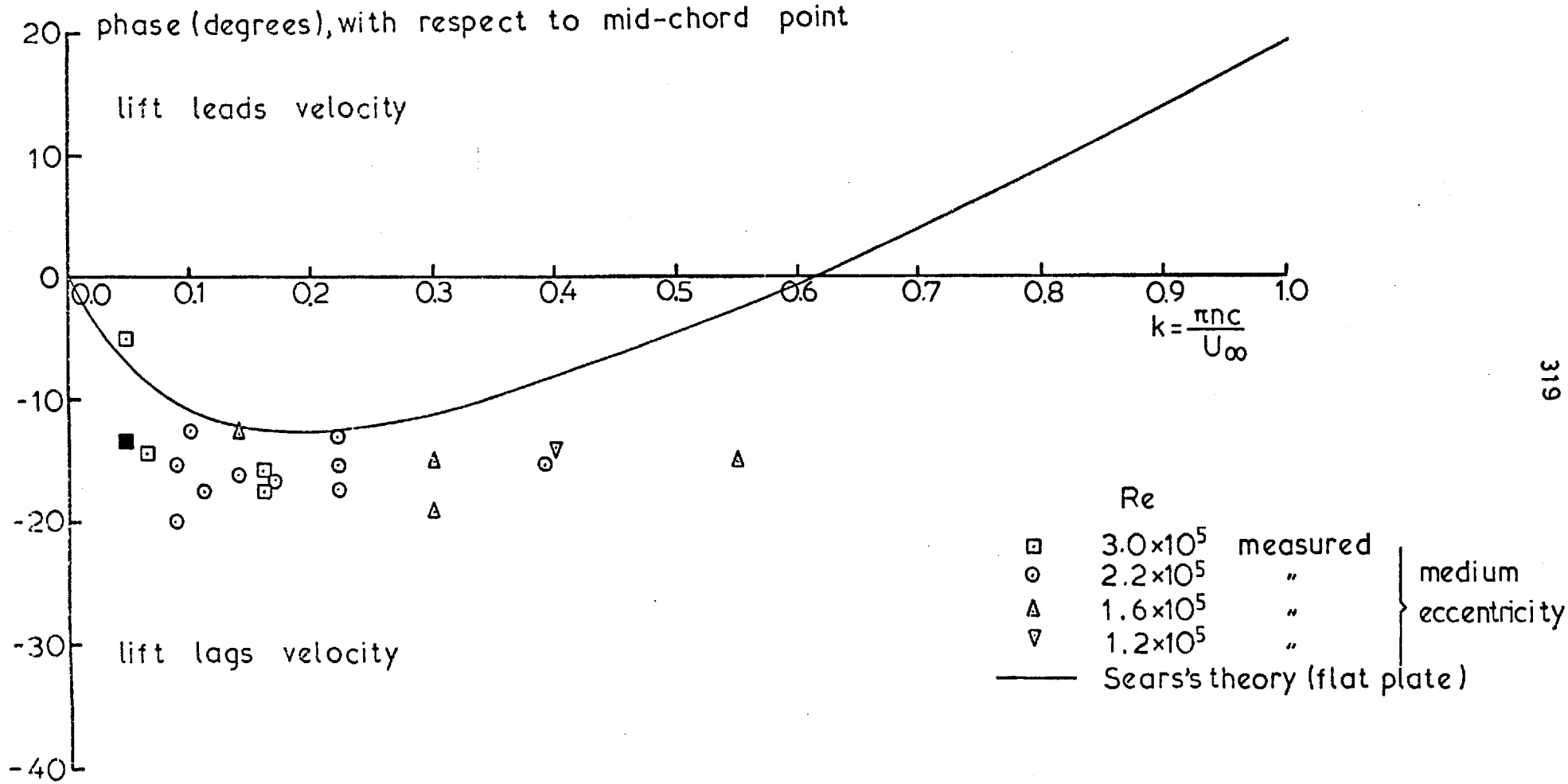

FIG. 5.14 PHASE BETWEEN LIFT AND UPWASH IN SINUSOIDAL FLOW NACA 0015 AEROFOIL

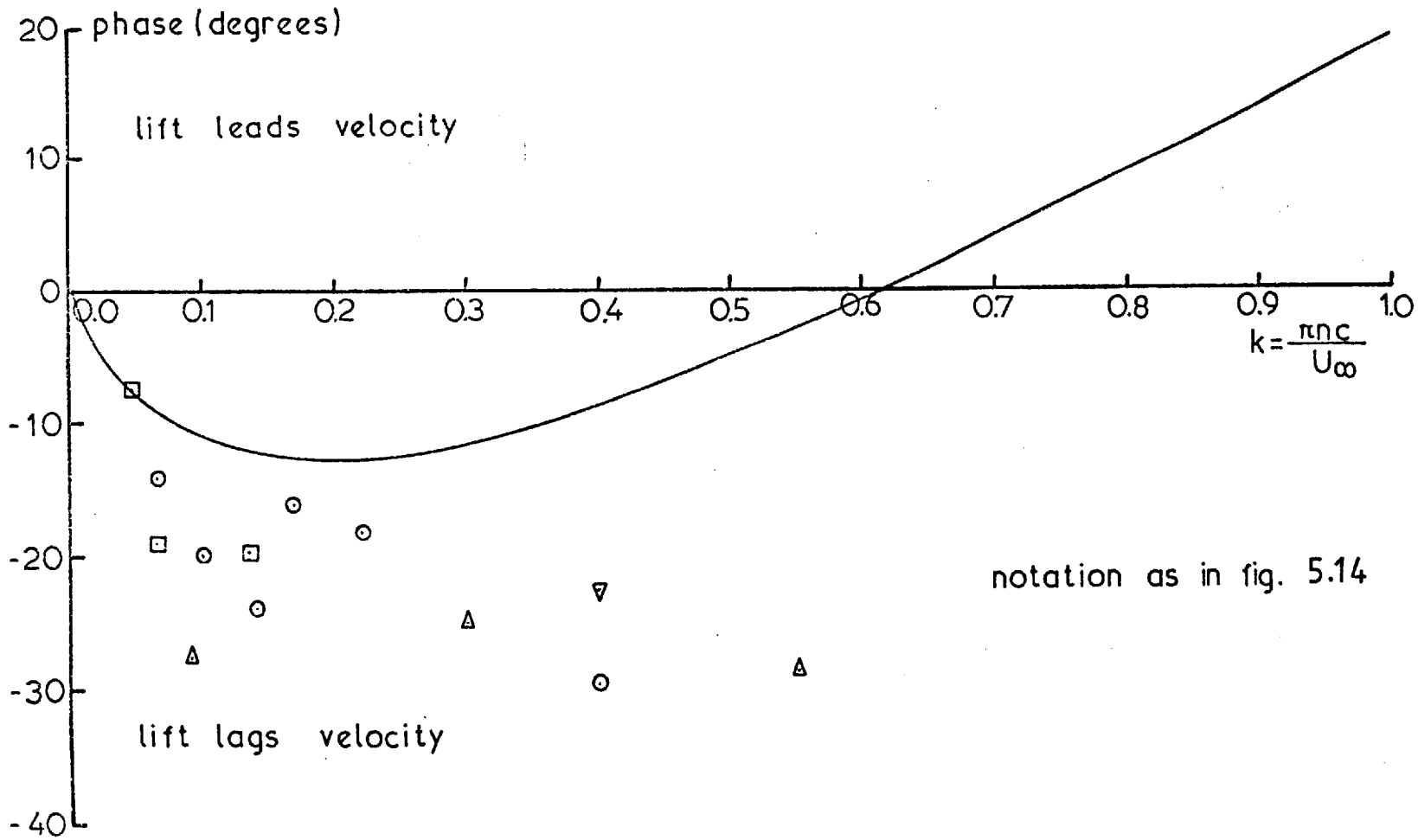

FIG. 5.15 PHASE BETWEEN LIFT AND UPWASH IN SINUSOIDAL FLOW
D CYLINDER

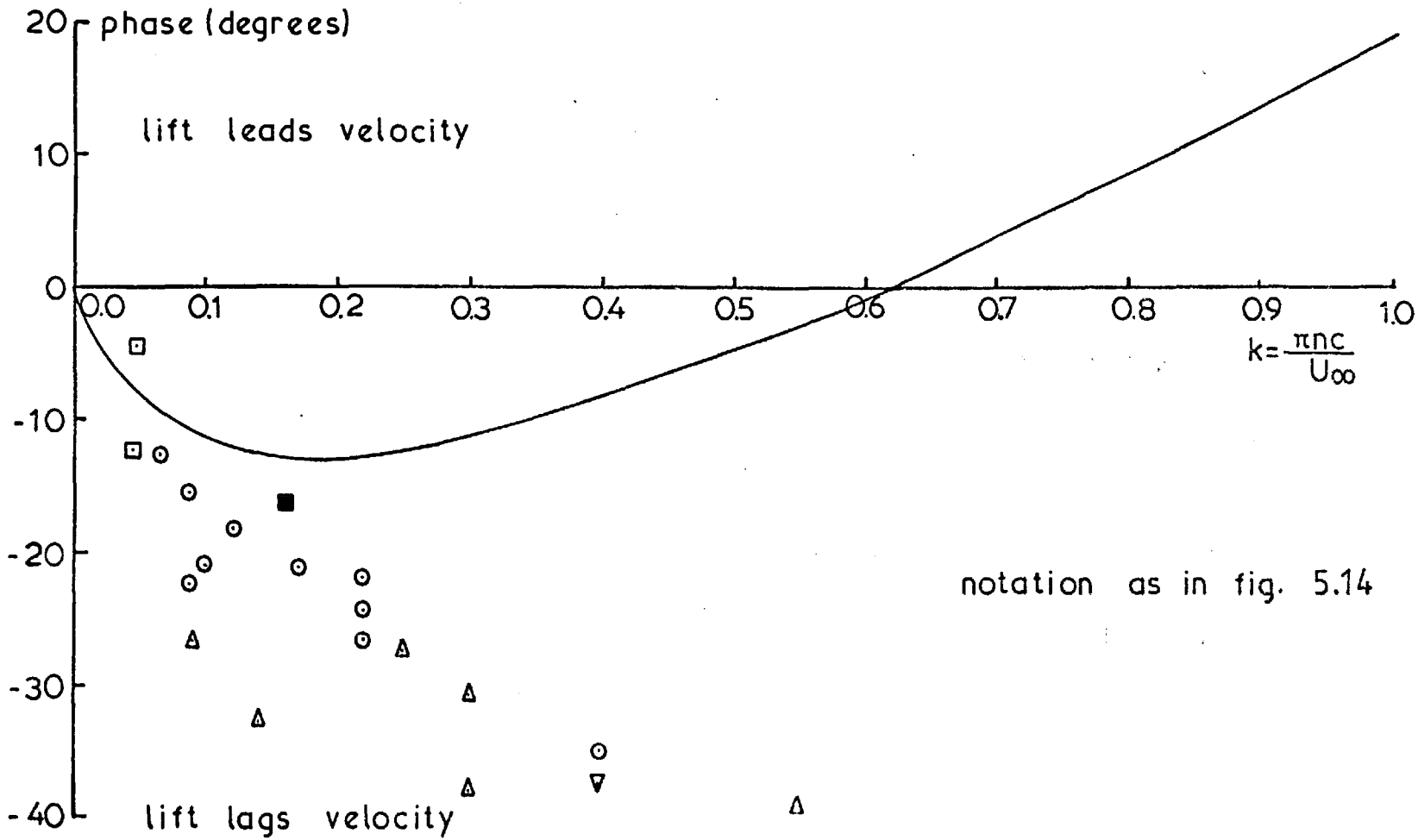

FIG. 5.16 PHASE BETWEEN LIFT AND UPWASH IN SINUSOIDAL FLOW ELLIPTIC CYLINDER

FIG. 5.17 NON DIMENSIONALIZED VORTEX SHEDDING LIFT SPECTRA IN SINUSOIDAL AND SMOOTH FLOWS

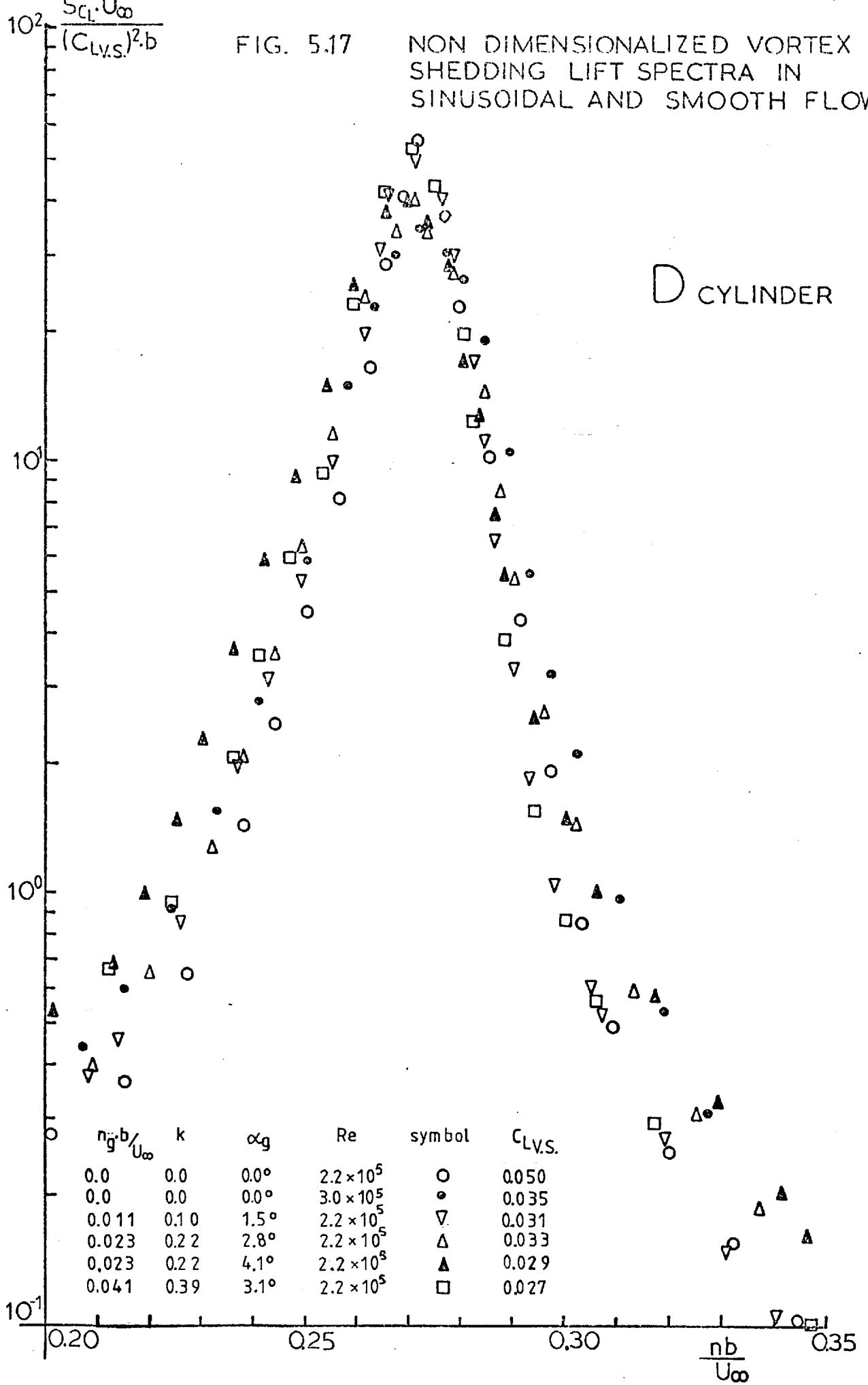

$n_g \cdot b/U_\infty$	k	α_g	Re	symbol	$C_{LV.S.}$
0.0	0.0	0.0°	2.2×10^5	○	0.050
0.0	0.0	0.0°	3.0×10^5	●	0.035
0.011	0.10	1.5°	2.2×10^5	▽	0.031
0.023	0.22	2.8°	2.2×10^5	△	0.033
0.023	0.22	4.1°	2.2×10^5	▲	0.029
0.041	0.39	3.1°	2.2×10^5	□	0.027

FIG. 5.18 NON DIMENSIONALIZED VORTEX SHEDDING LIFT SPECTRA IN STEADY AND UNSTEADY FLOWS

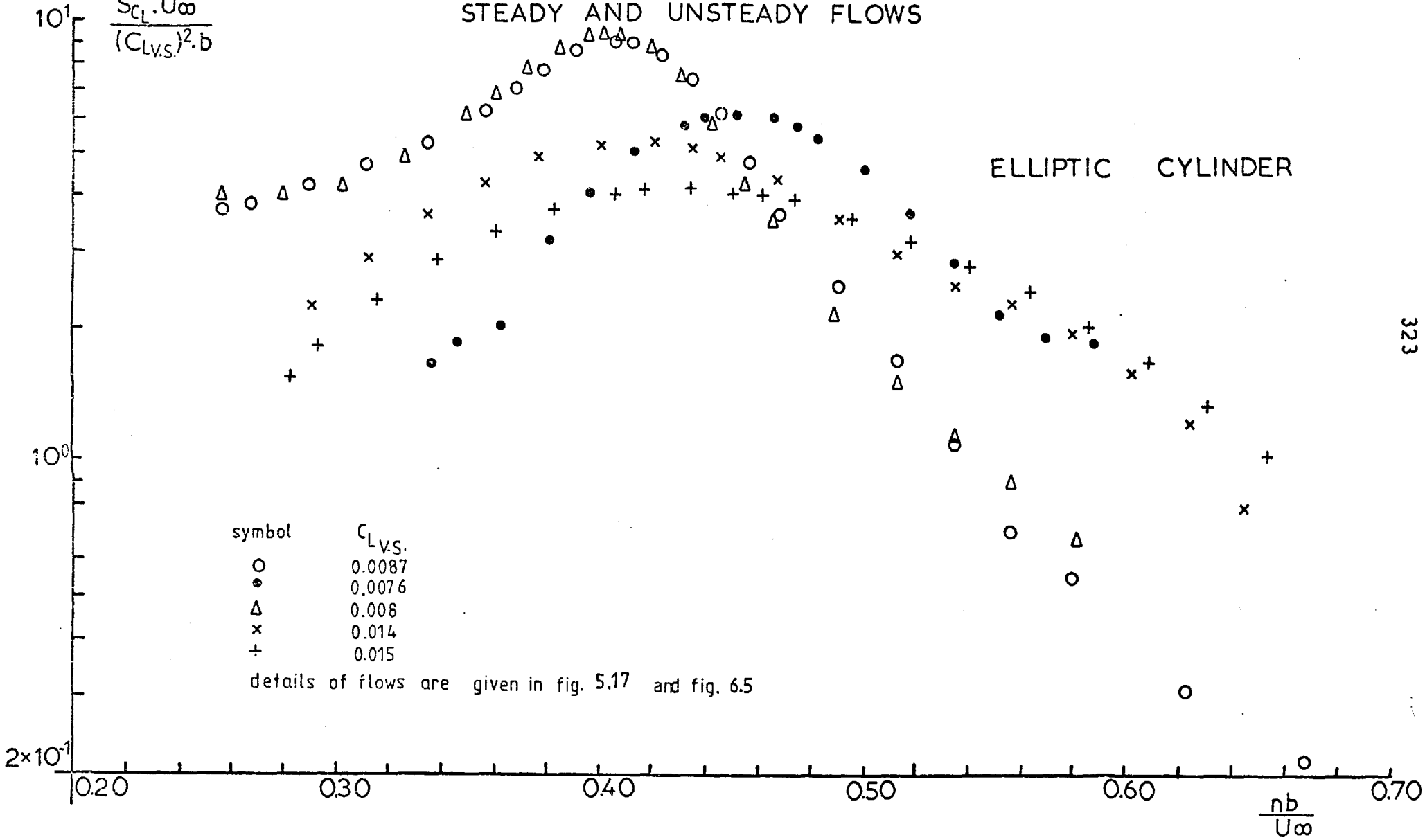

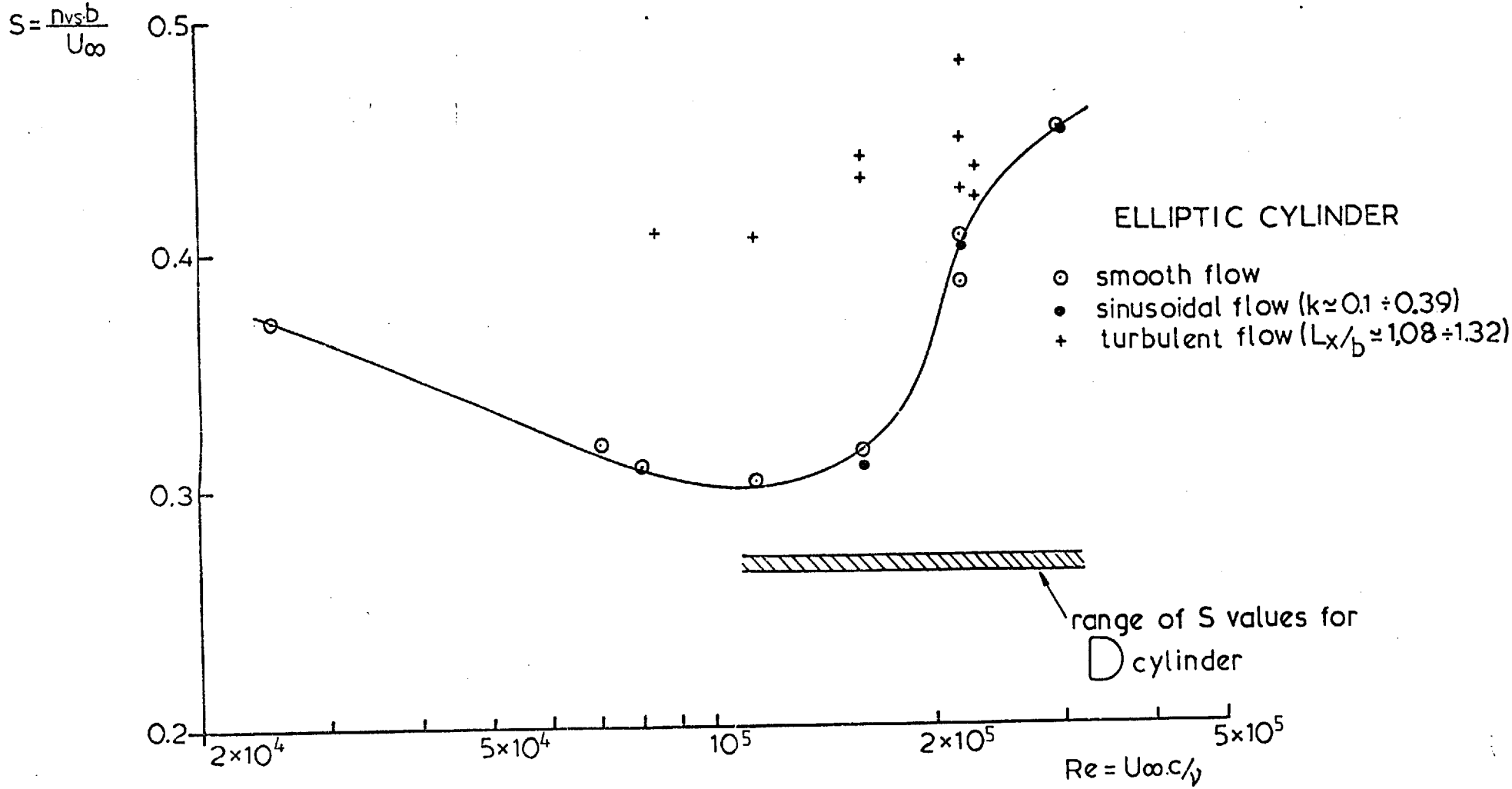

FIG. 5.19 VARIATION OF STROUHAL NUMBER WITH REYNOLDS' NUMBER $\alpha = 0°$

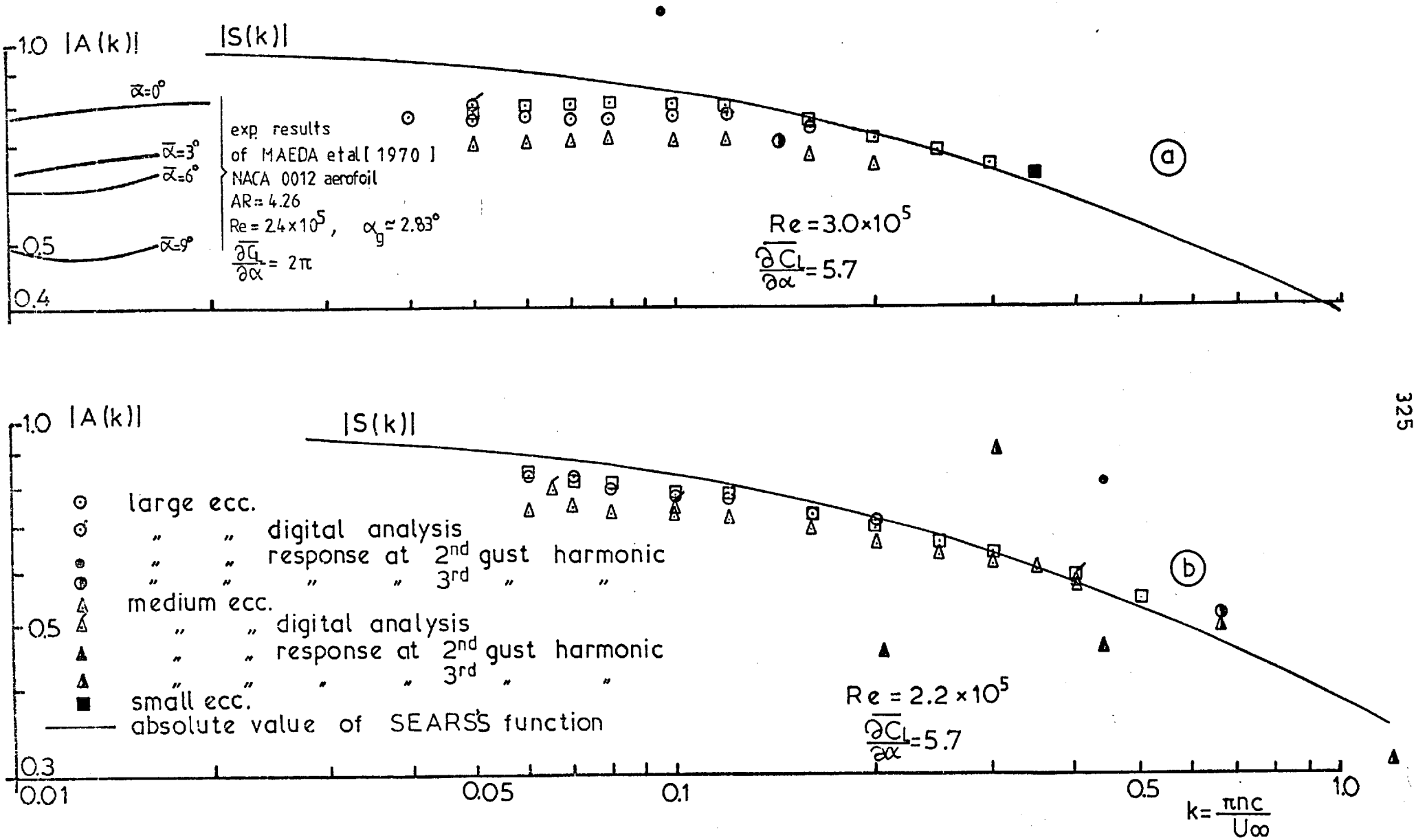

FIG. 5.20 EXPERIMENTAL AERODYNAMIC ADMITTANCE. SINUSOIDAL FLOW. NACA 0015 AEROFOIL $\bar{\alpha} = 0^{\circ}$

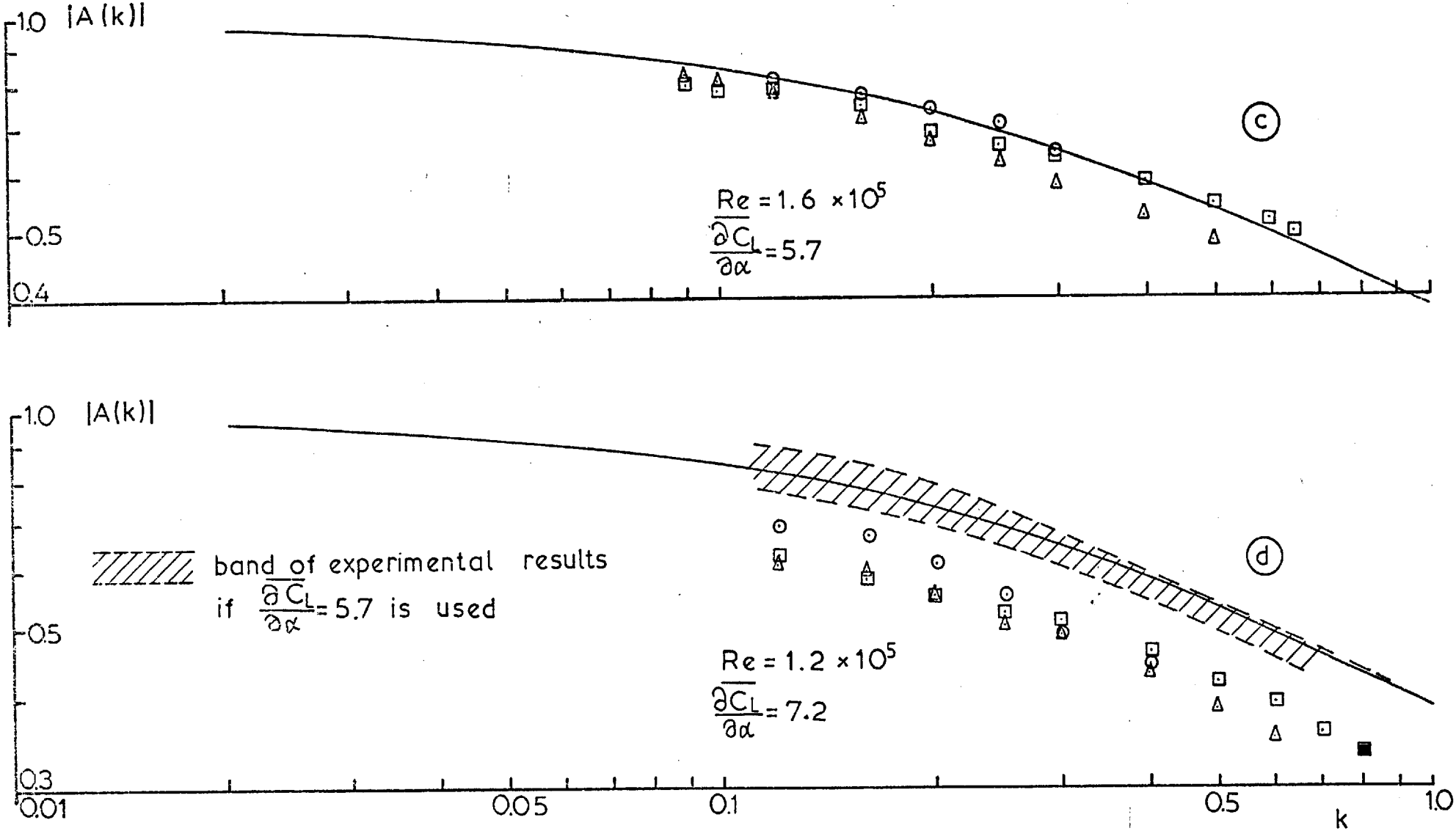

FIG. 5.20 (continued) NACA 0015 AEROFOIL $\overline{\alpha} = 0°$

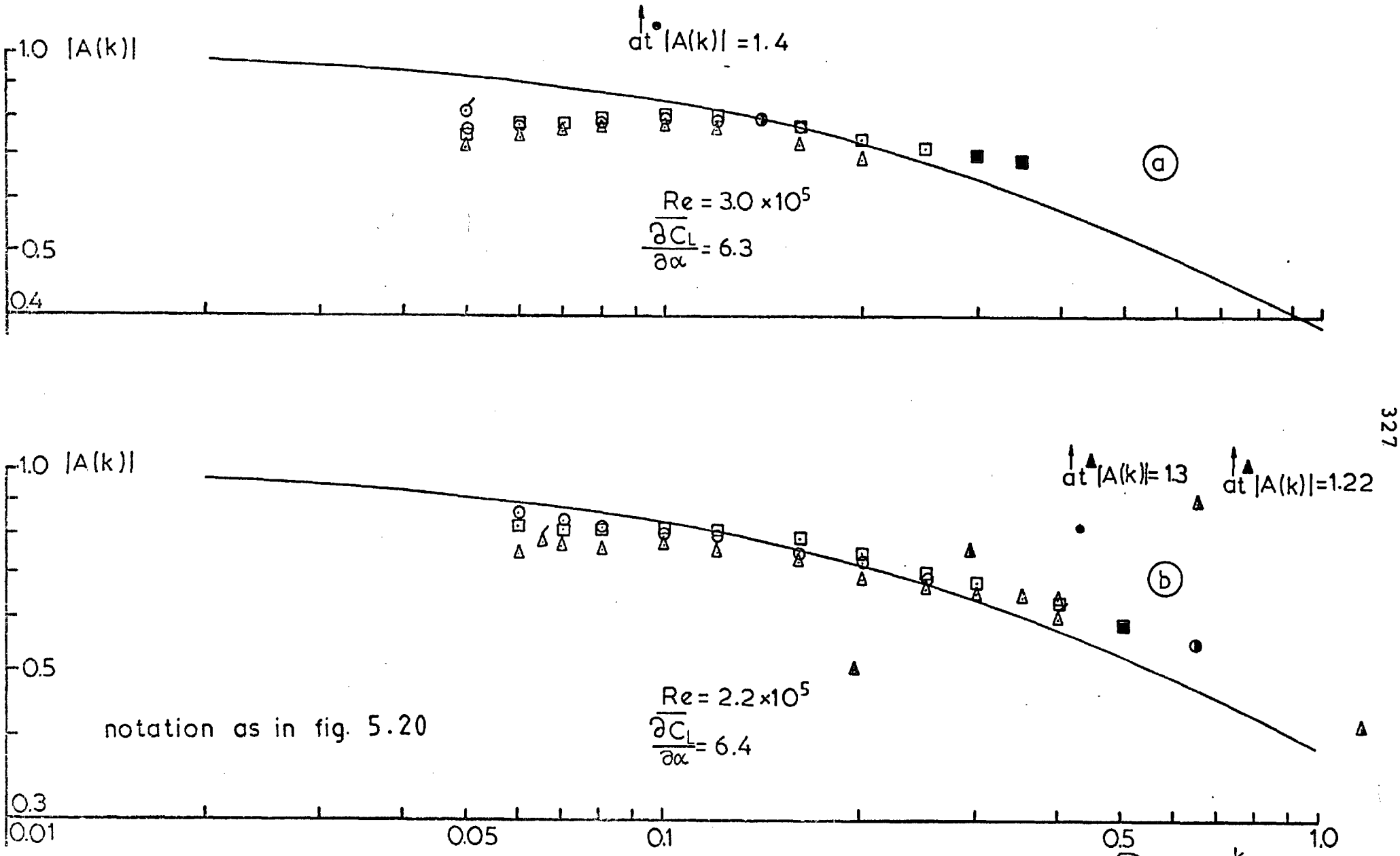

FIG. 5.21 EXPERIMENTAL AERODYNAMIC ADMITTANCE, SINUSOIDAL FLOW. D CYLINDER

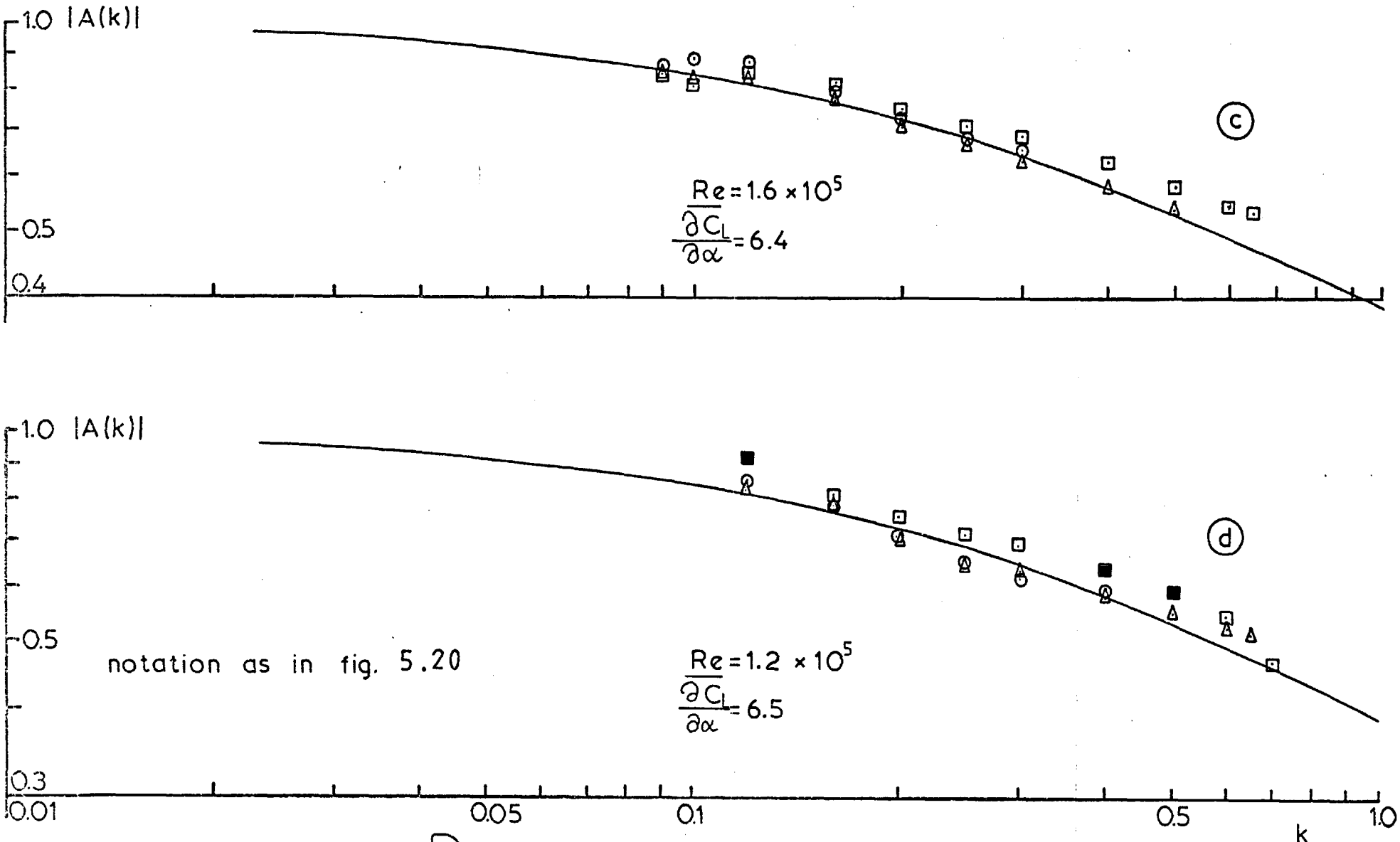

FIG. 5.21 (continued) D CYLINDER

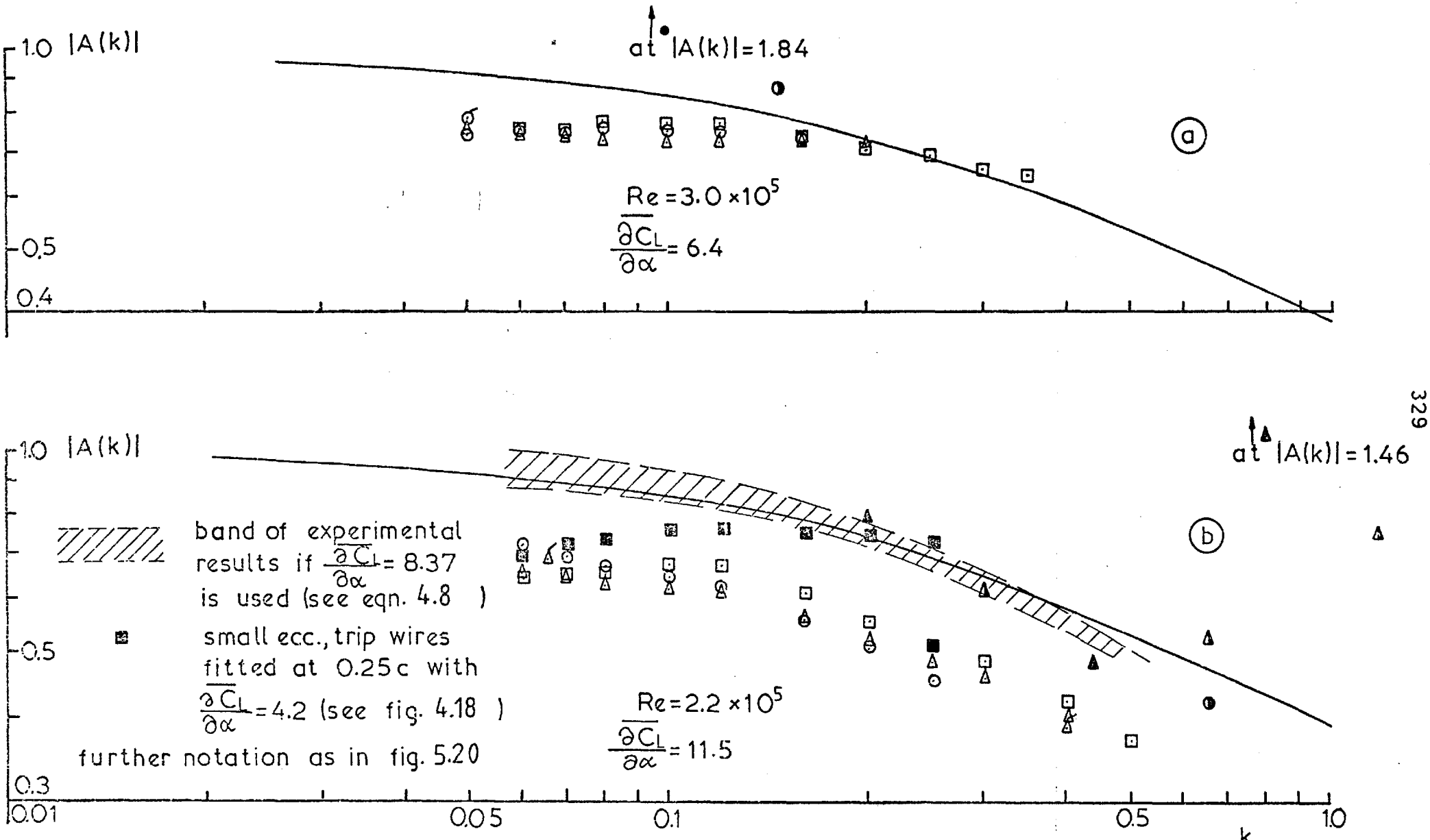

FIG. 5.22 EXPERIMENTAL AERODYNAMIC ADMITTANCE . SINUSOIDAL FLOW. ELLIPTIC CYLINDER

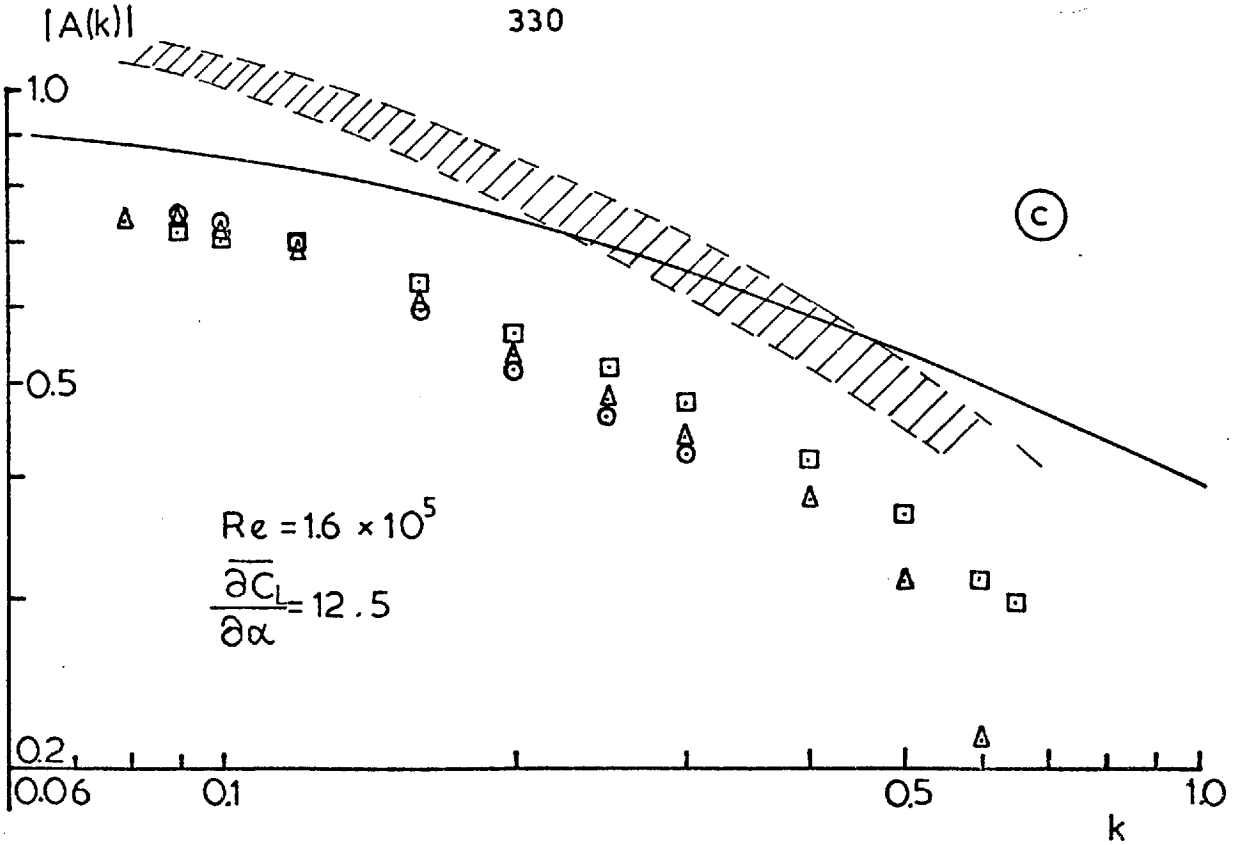

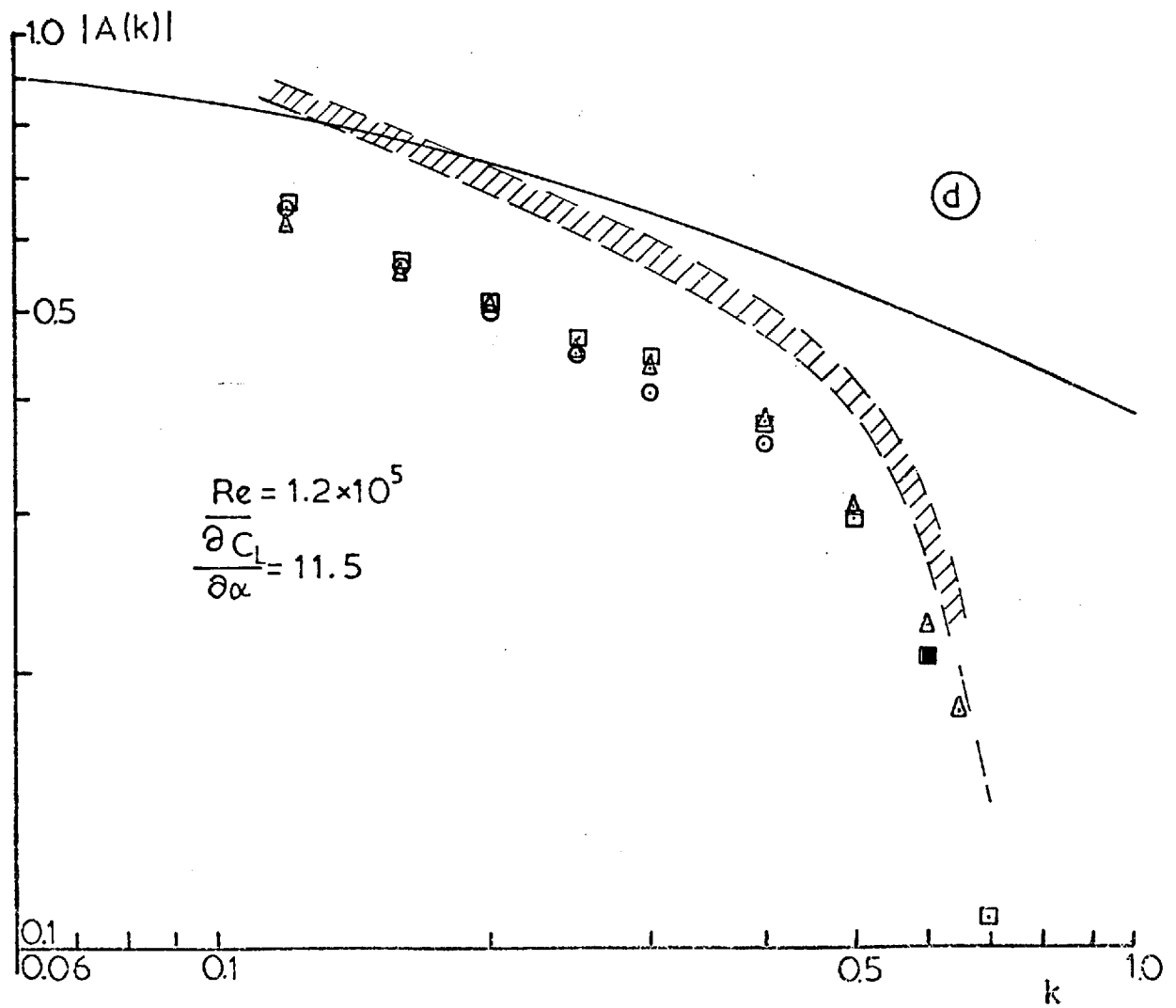

FIG. 5.22 (continued) ELLIPTIC CYLINDER

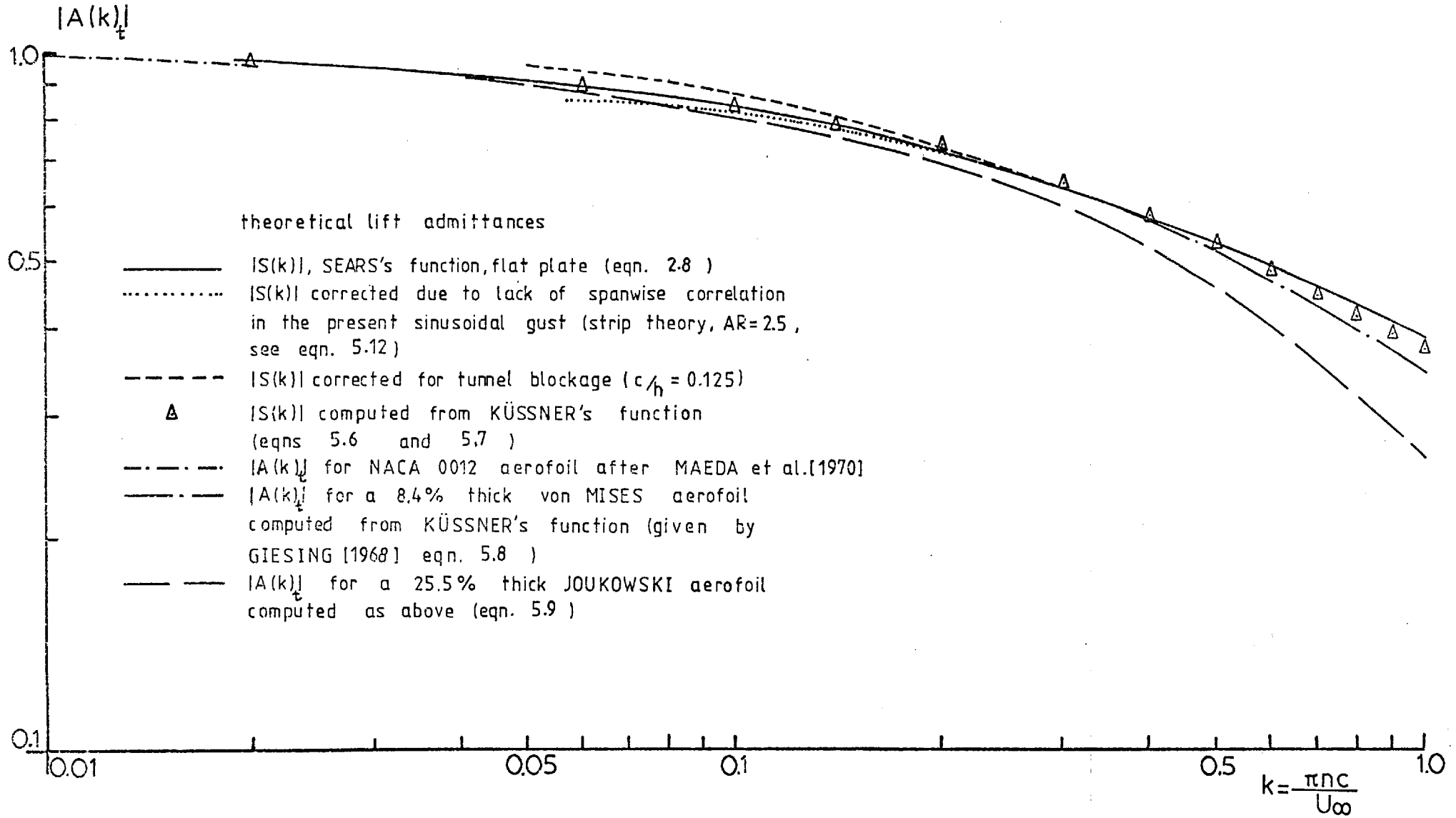

FIG. 5.23 AERODYNAMIC ADMITTANCES FOR VARIOUS AEROFOIL SHAPES AT ZERO MEAN INCIDENCE IN A TWO DIMENSIONAL SINUSOIDAL UPWASH GUST

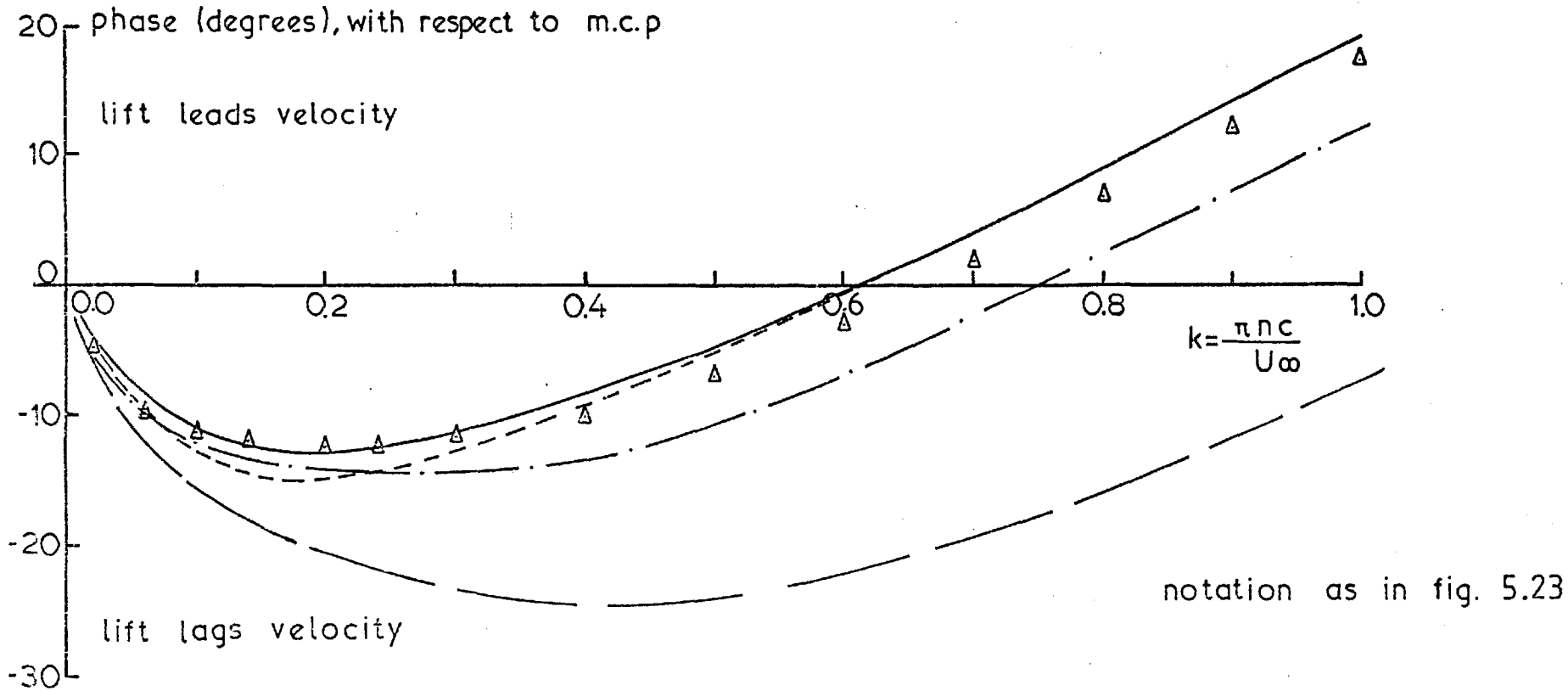

FIG. 5.24 PHASE BETWEEN UNSTEADY LIFT AND UPWASH IN SINUSOIDAL FLOW FOR VARIOUS AEROFOIL SHAPES

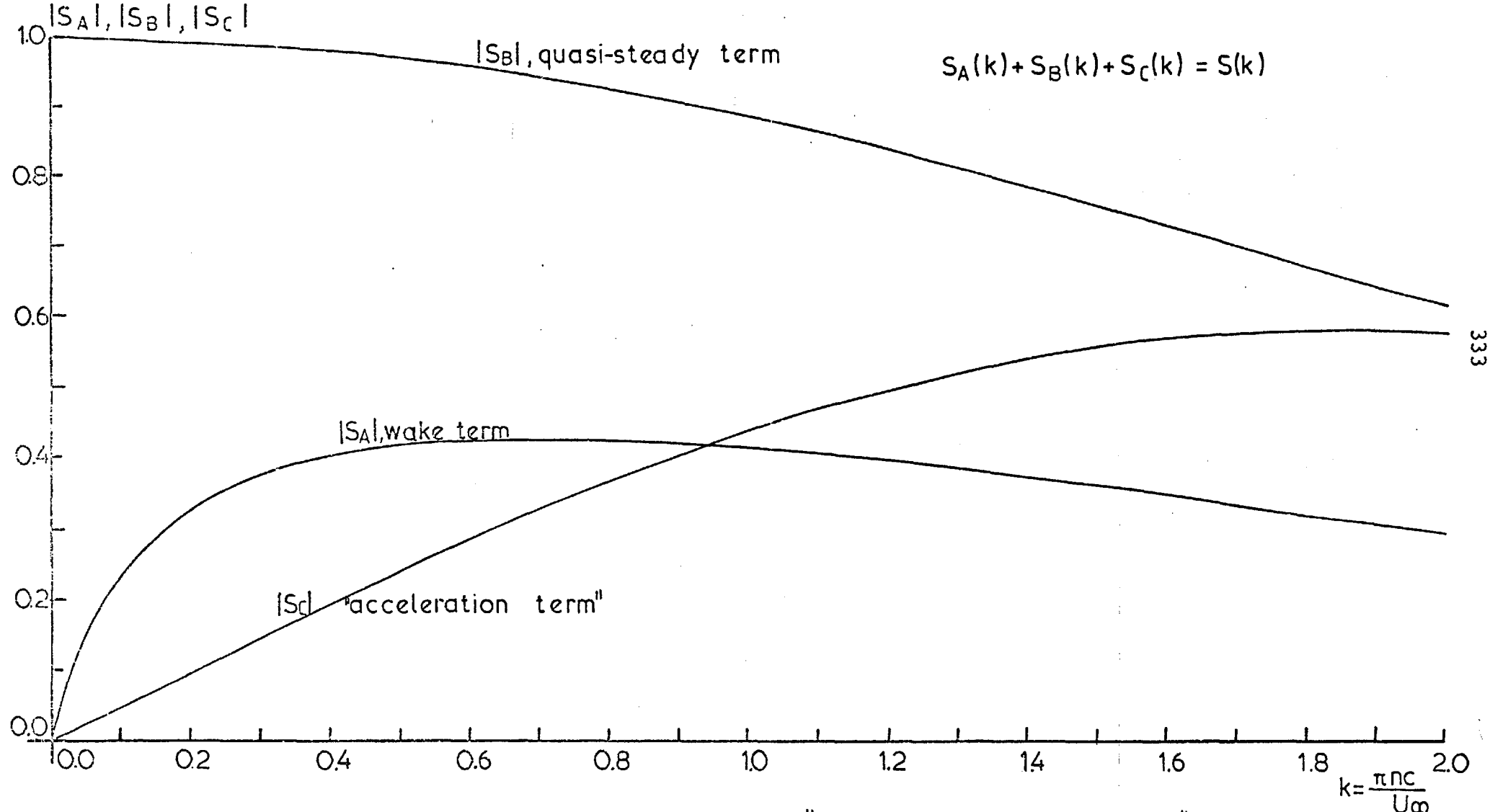

FIG. 5.25 SPLIT OF SEARS'S FUNCTION INTO "INERTIAL ACCELERATION", QUASI-STEADY AND WAKE PARTS

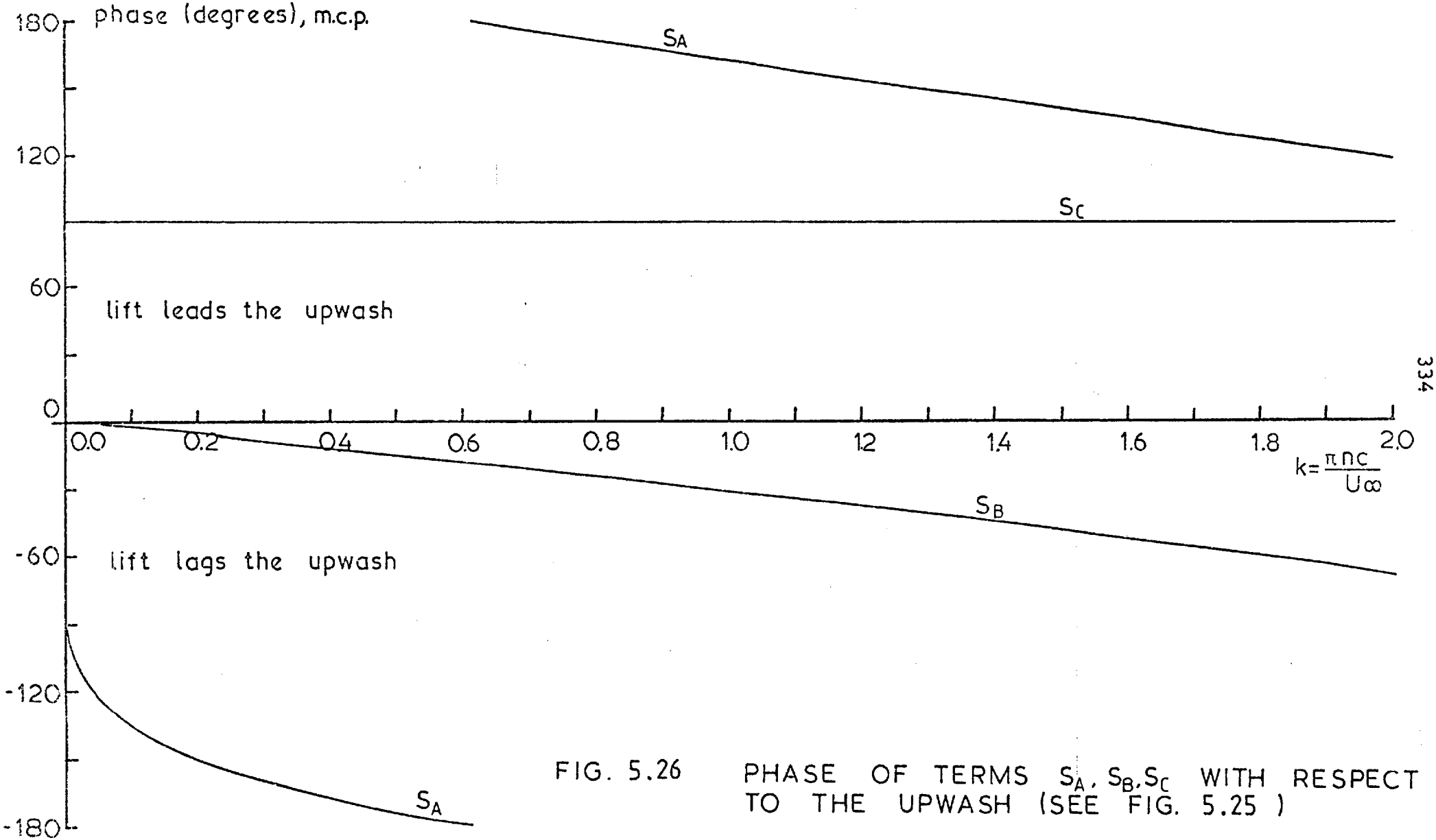

FIG. 5.26 PHASE OF TERMS S_A, S_B, S_C WITH RESPECT TO THE UPWASH (SEE FIG. 5.25)

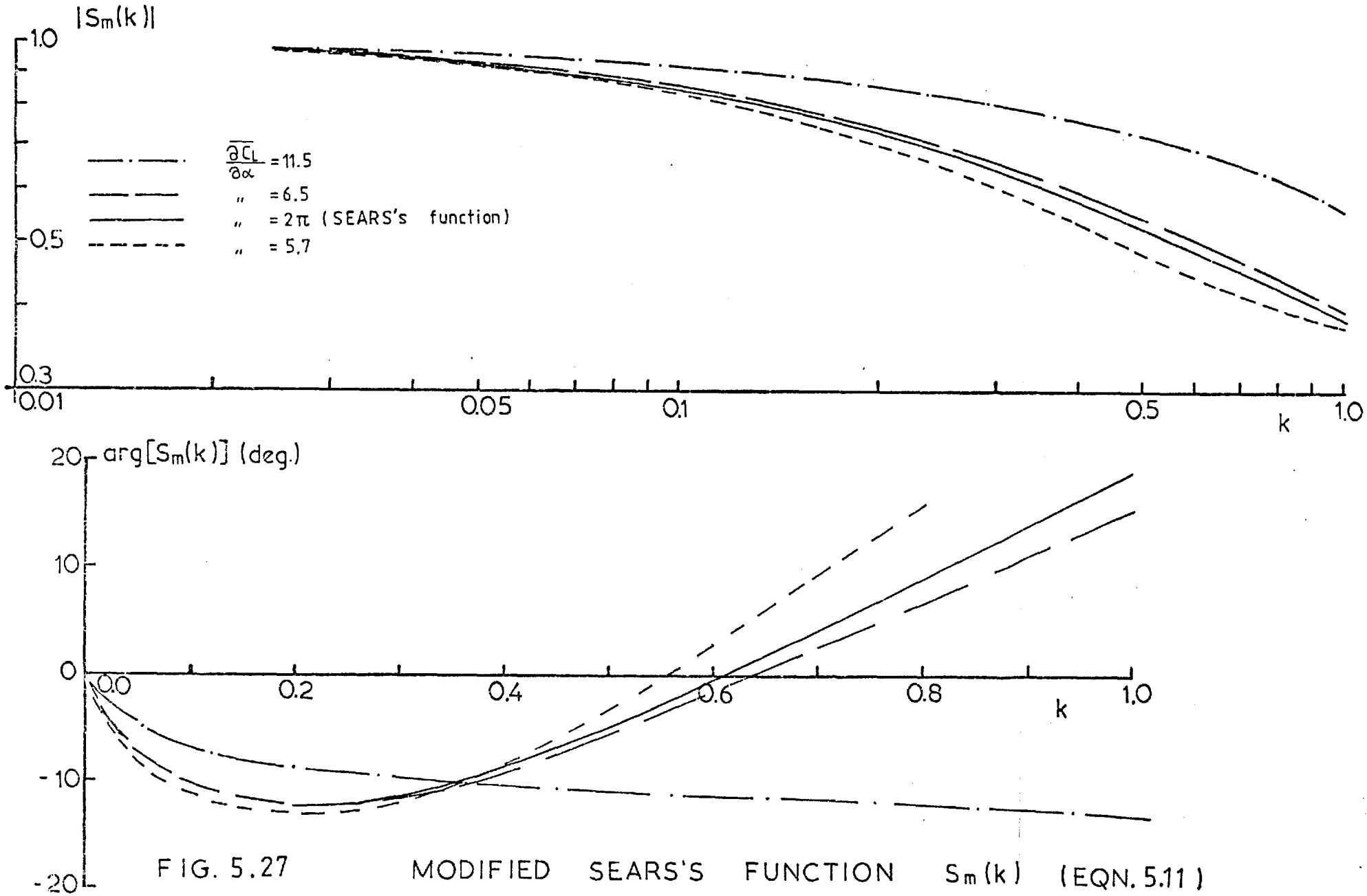

FIG. 5.27 MODIFIED SEARS'S FUNCTION $S_m(k)$ (EQN. 5.11)

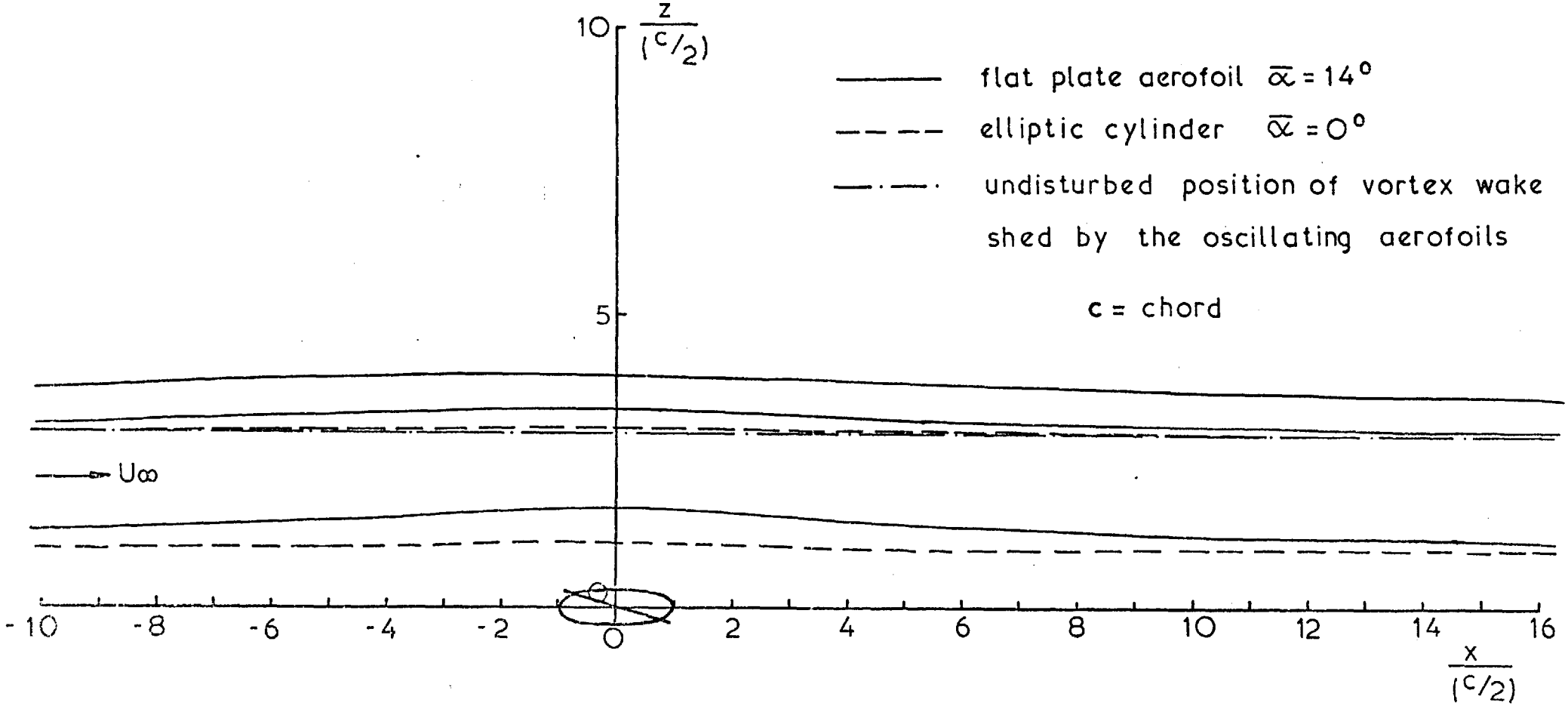

FIG. 5.28 STREAMLINE PATTERN FOR AN ELLIPSE AND AN AEROFOIL AT INCIDENCE. STEADY INVISCID FLOW

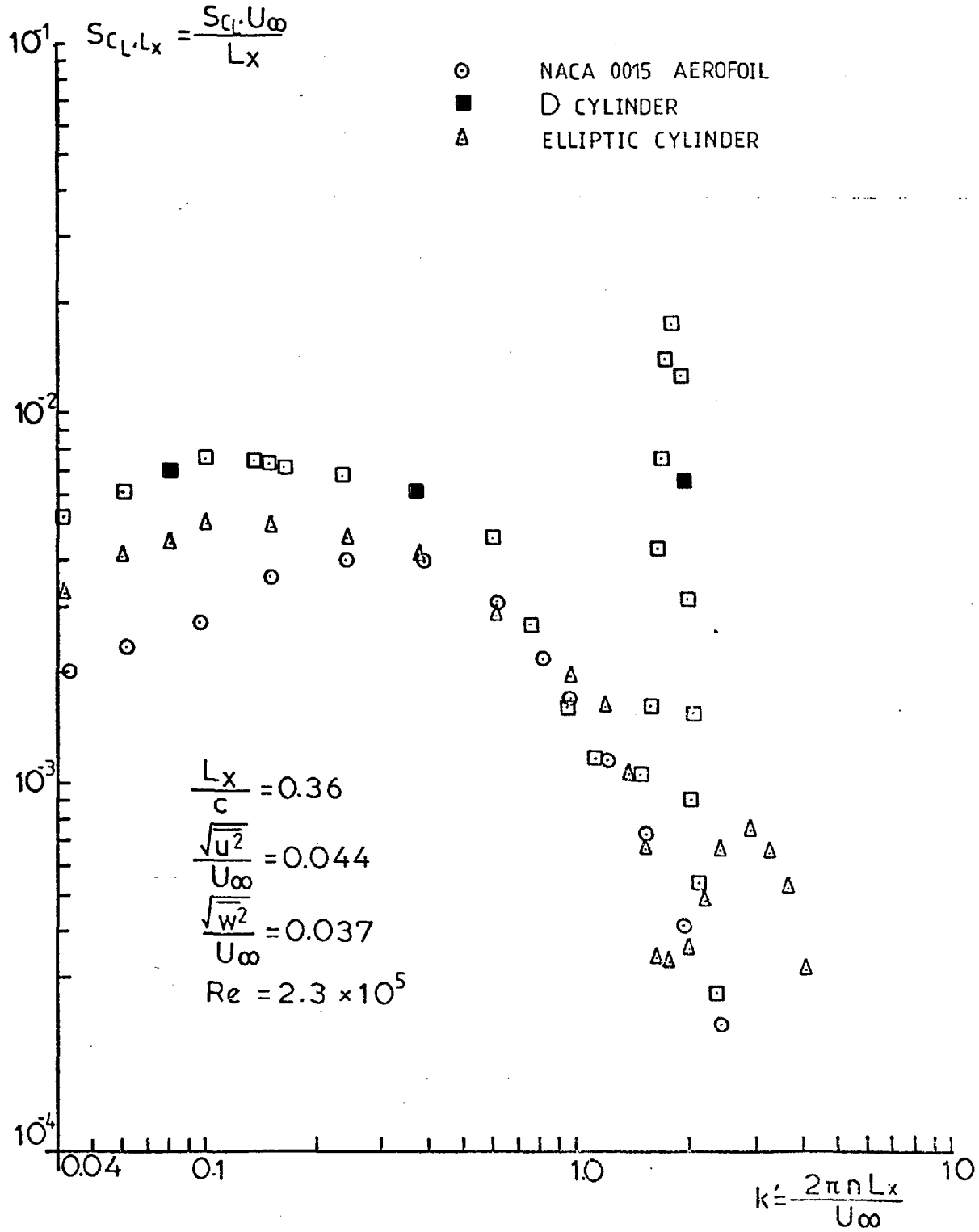

FIG. 6.1 EXPERIMENTAL NON DIMENSIONALIZED LIFT SPECTRA IN TURBULENT FLOW

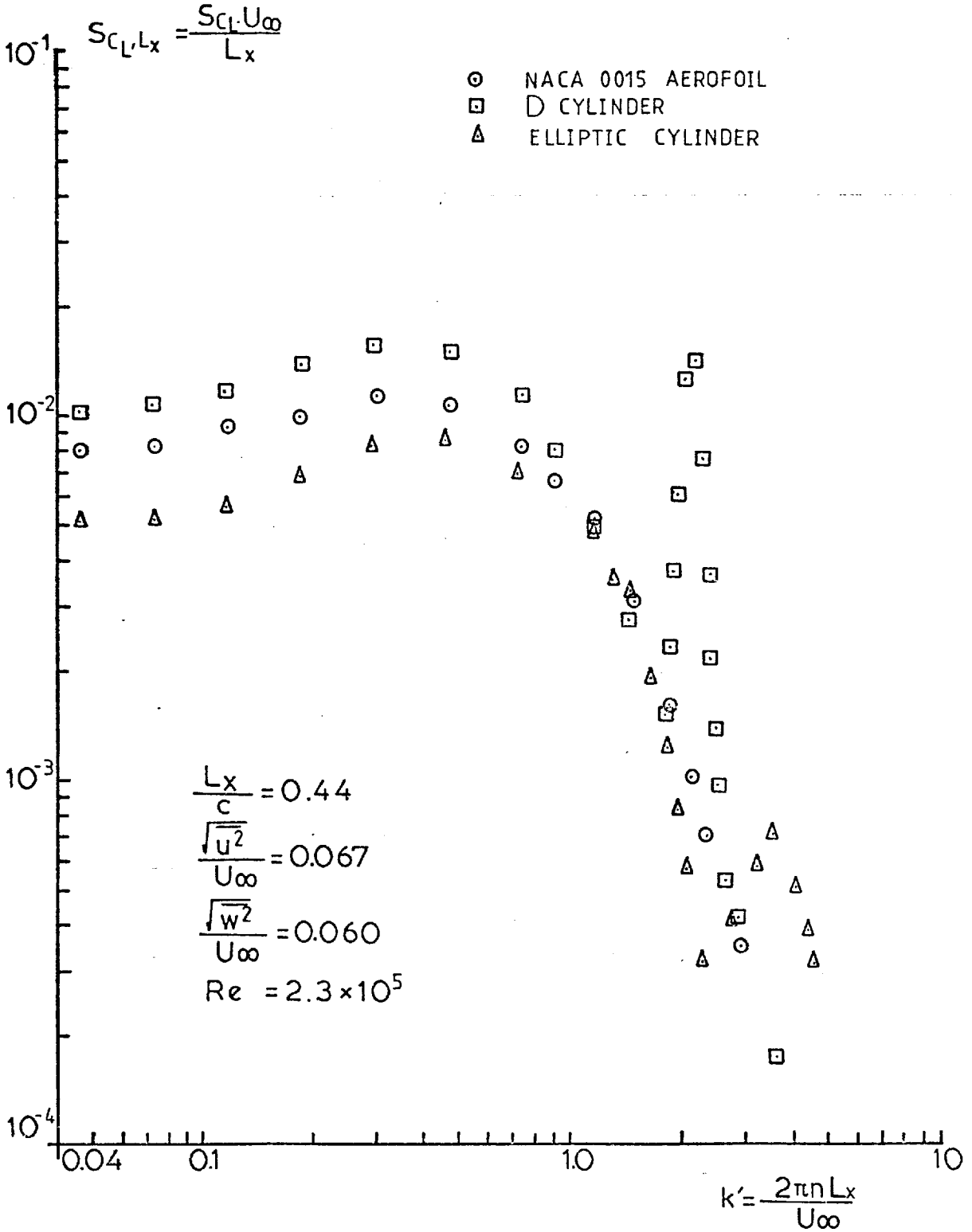

FIG. 6.2 EXPERIMENTAL NON DIMENSIONALIZED LIFT SPECTRA IN TURBULENT FLOW

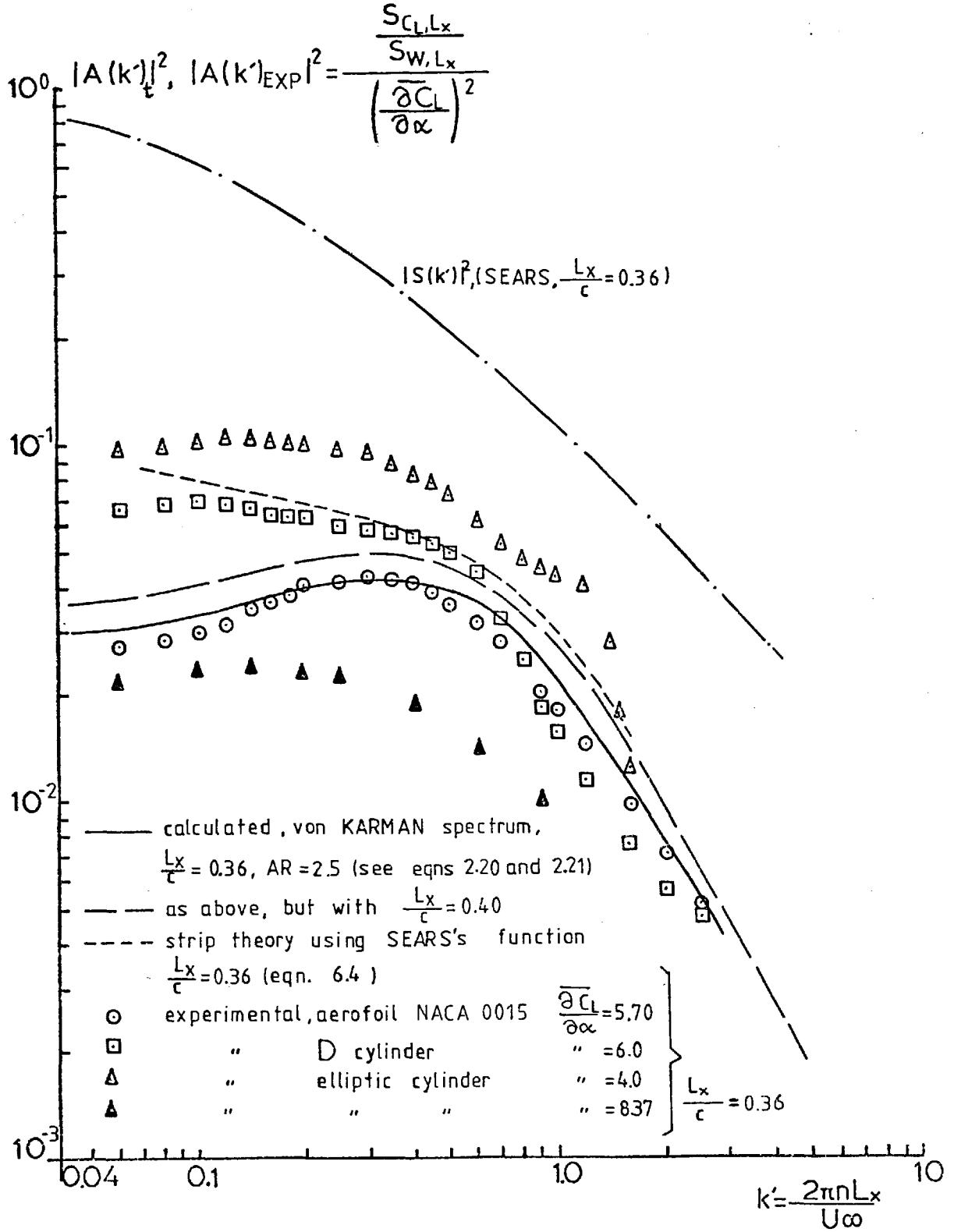

FIG. 6.3 EXPERIMENTAL AND THEORETICAL AERODYNAMIC ADMITTANCES FOR TWO DIMENSIONAL CYLINDERS IN TURBULENT FLOW (BROAD-BAND RESPONSE ONLY)

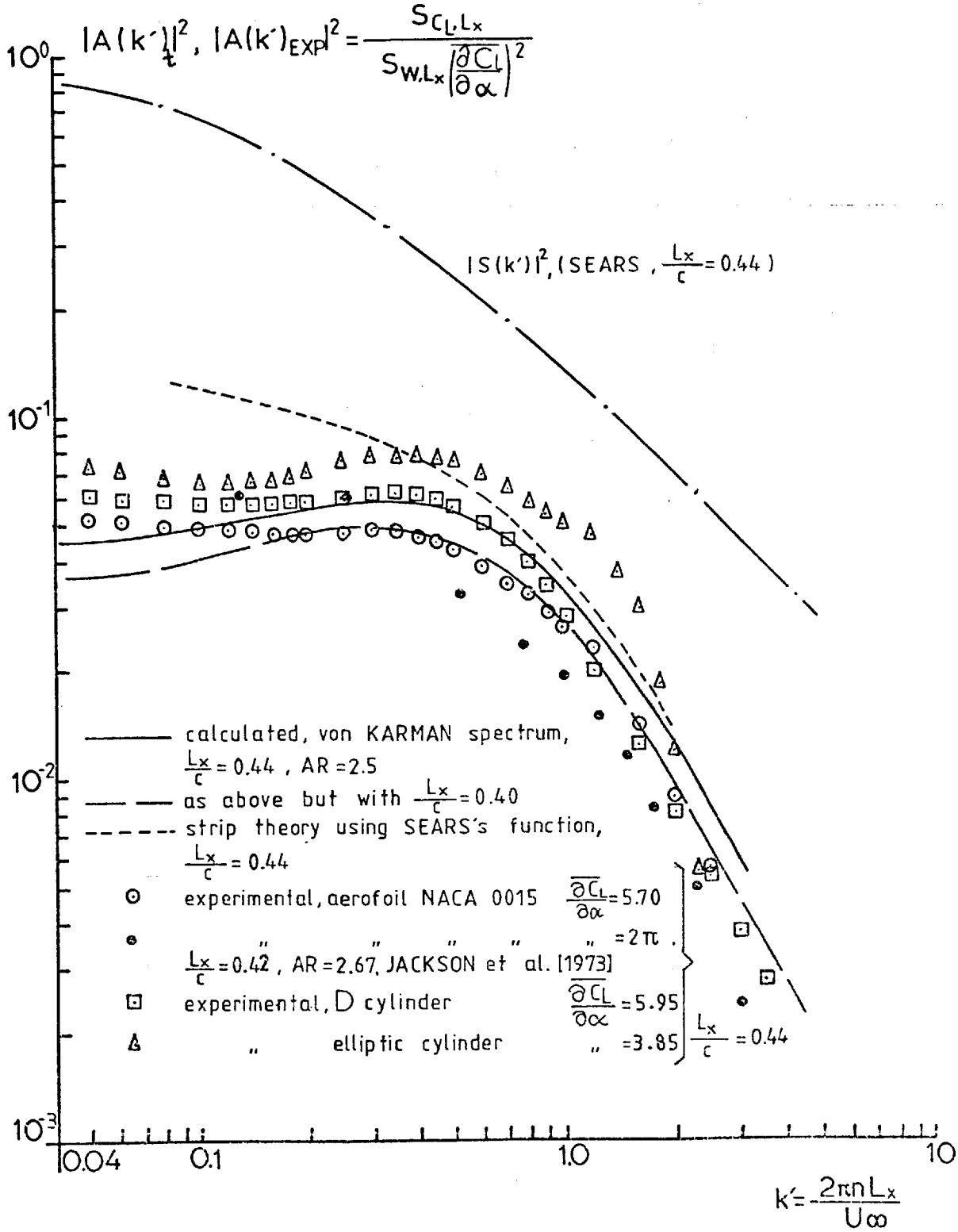

FIG. 6.4 EXPERIMENTAL AND THEORETICAL AERODYNAMIC ADMITTANCES FOR TWO DIMENSIONAL CYLINDERS IN TURBULENT FLOW (BROAD-BAND RESPONSE ONLY)

FIG. 6.5 NON DIMENSIONALIZED VORTEX SHEDDING LIFT SPECTRA IN TURBULENT AND SMOOTH FLOWS

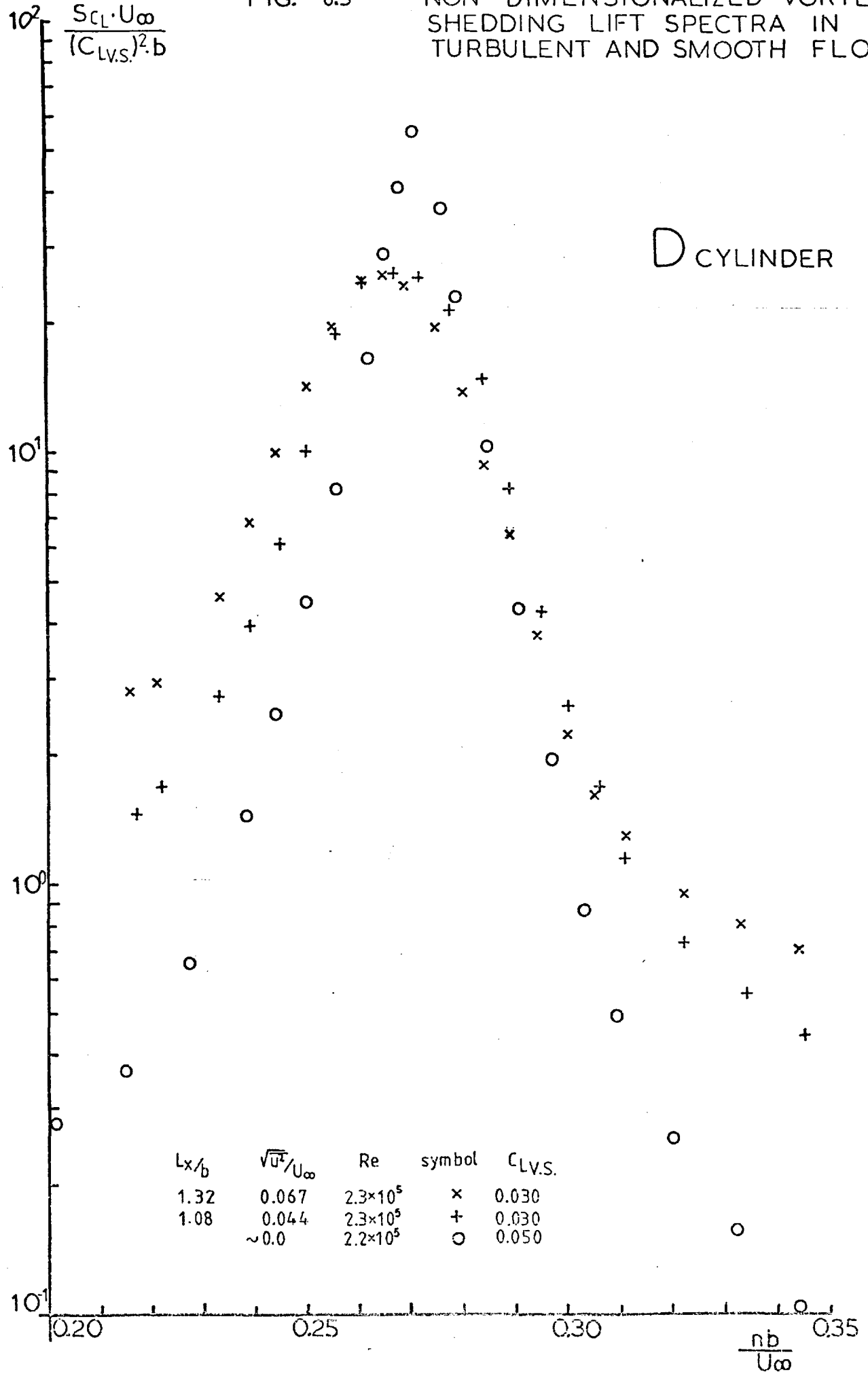

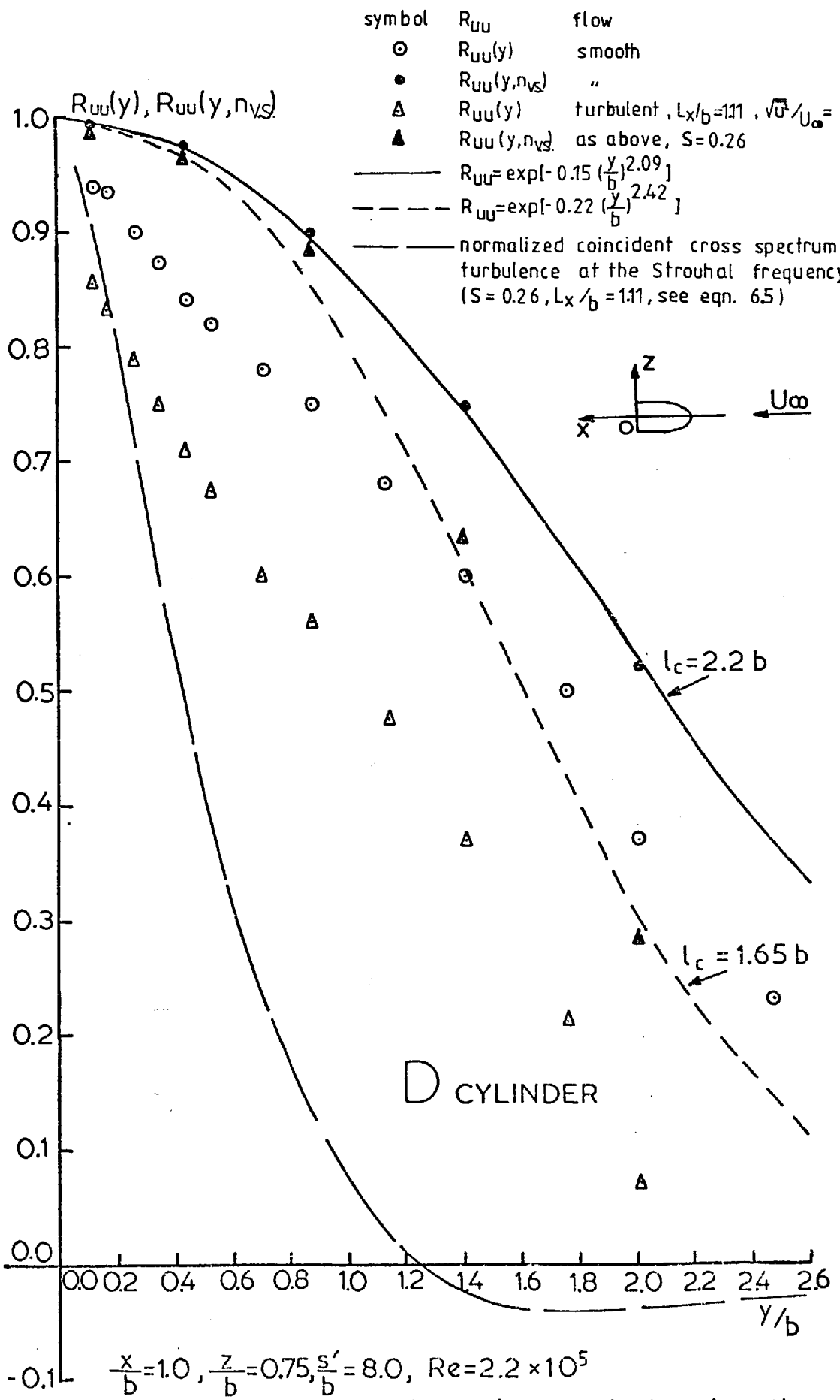

FIG. 6.6 BROAD BAND AND NARROW BAND (AT SHEDDING FREQUENCY) u VELOCITY CORRELATIONS ALONG THE MODEL SPAN

+ $R_{uu}(y, n_{v.s.})$ smooth flow , $Re = 8.5 \times 10^4$
further notation as in fig. 6.6

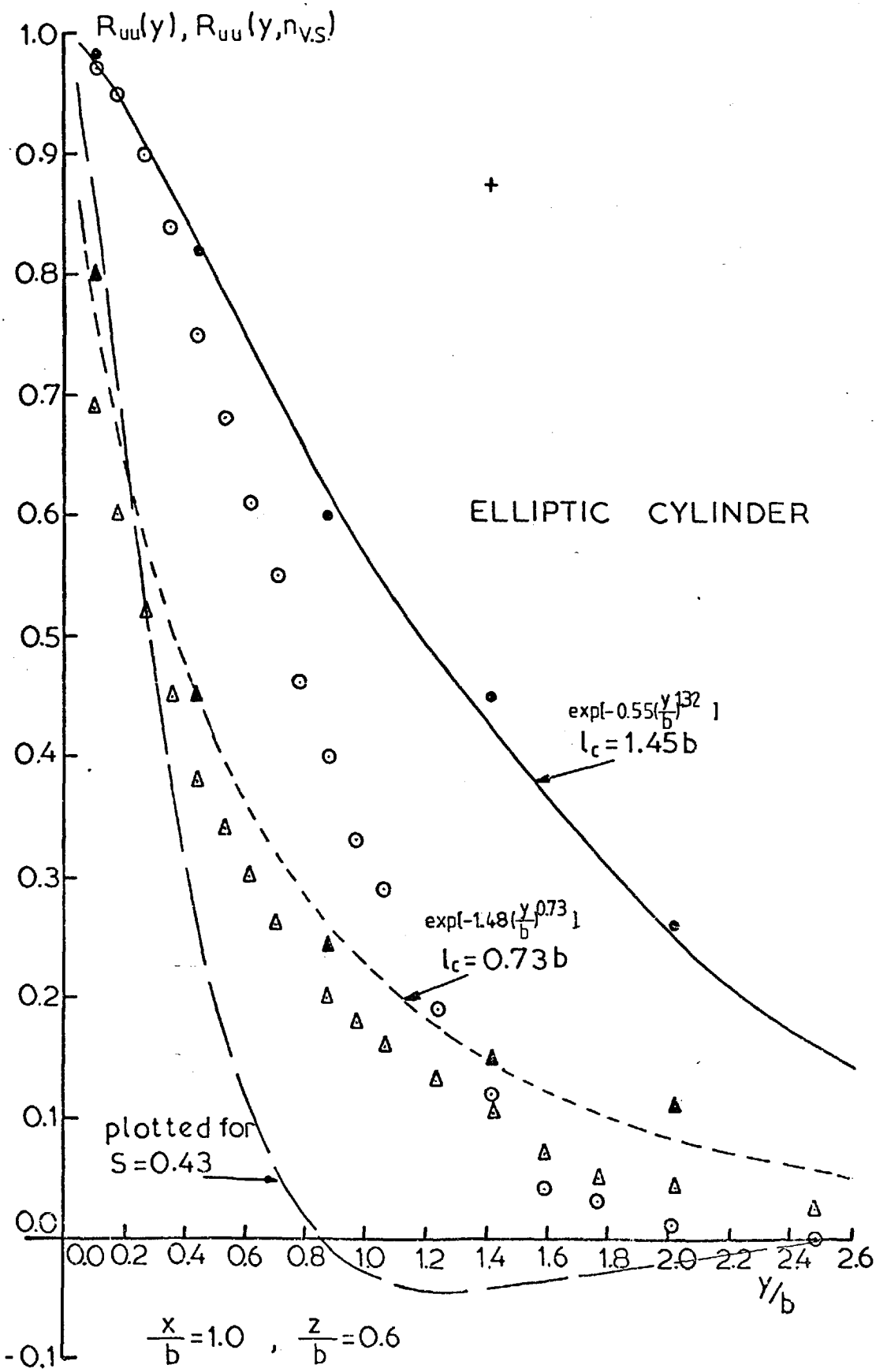

FIG. 6.7 BROAD BAND AND NARROW BAND (AT SHEDDING FREQUENCY) u VELOCITY CORRELATIONS ALONG THE MODEL SPAN

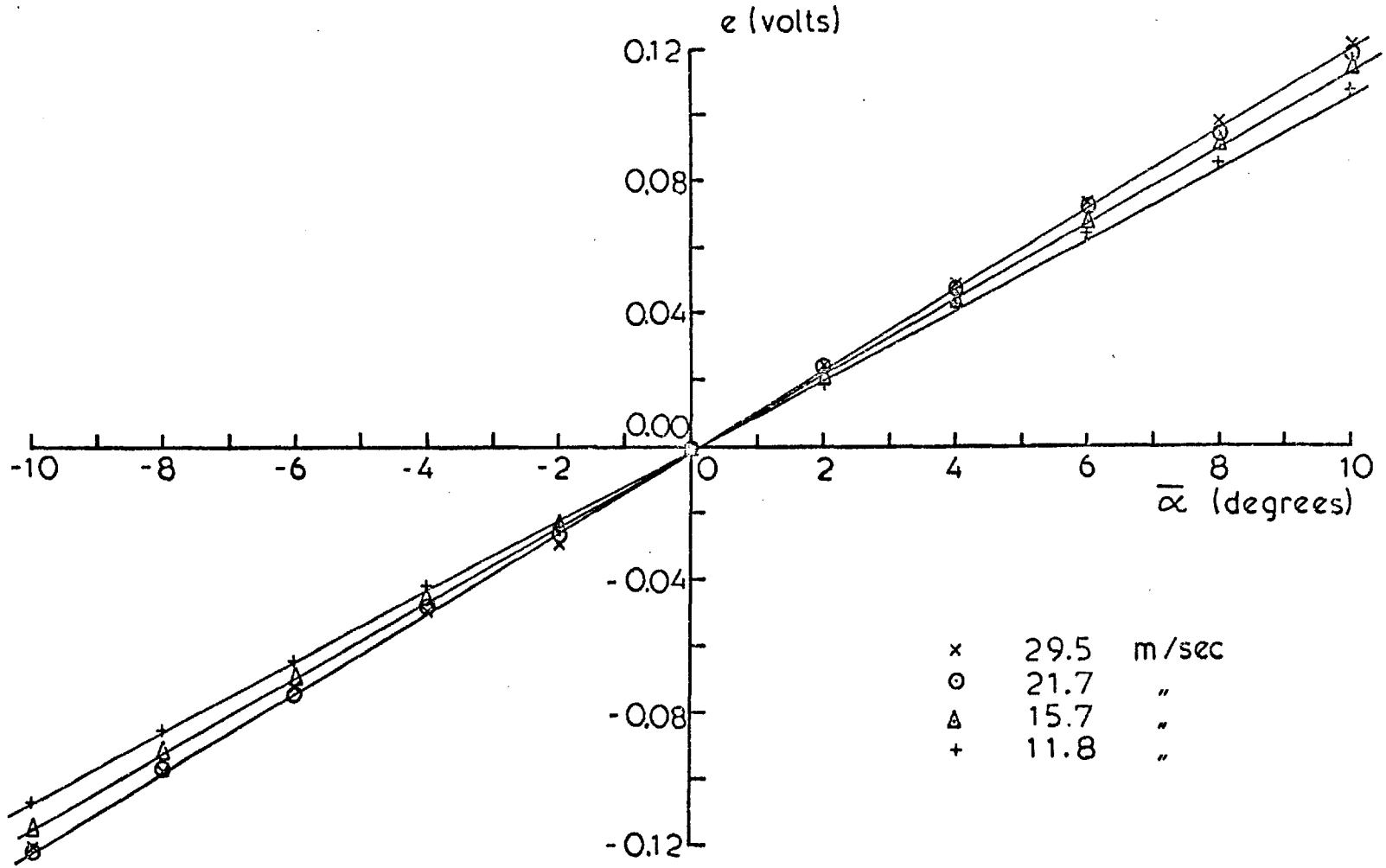

FIG. A-1 STATIC CALIBRATION OF CROSS HOT WIRE IN YAW

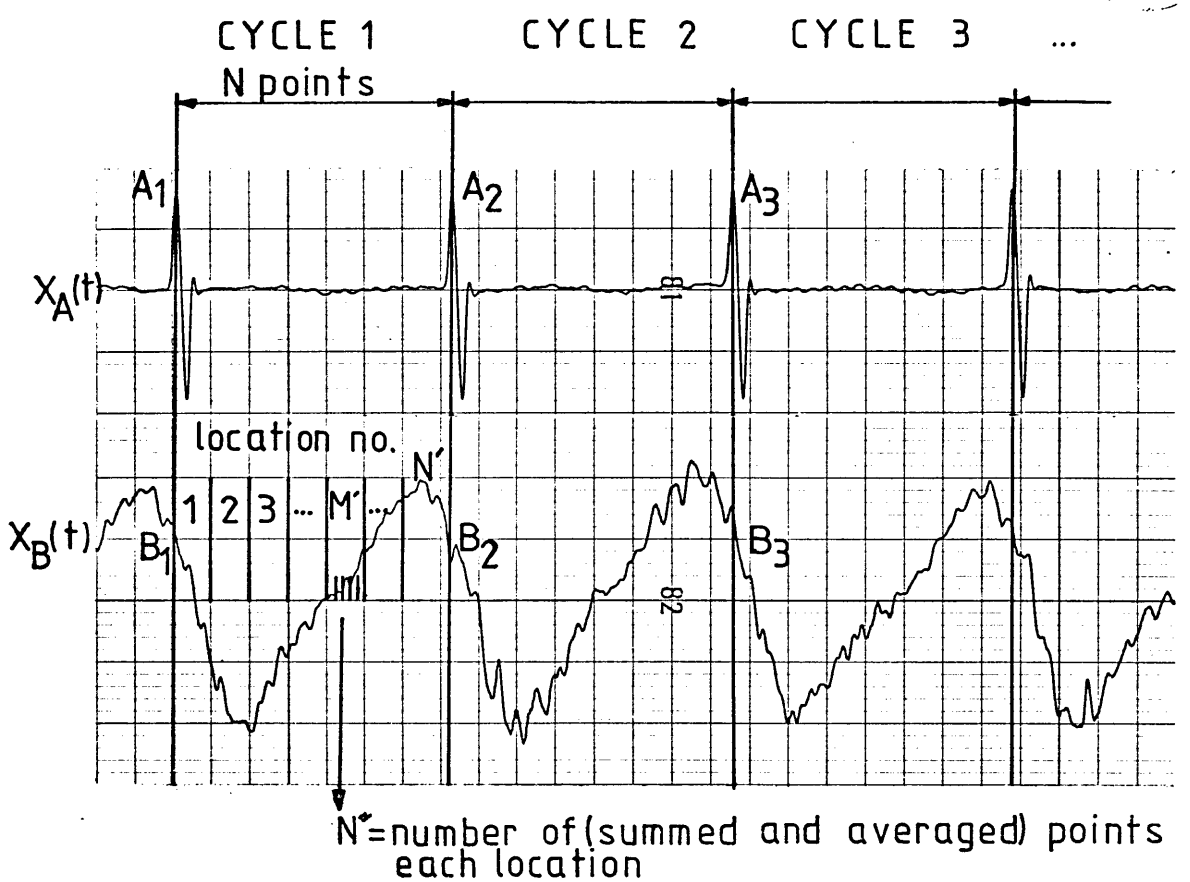

I. FIND MAXIMUM OF $X_A(t)$.
2. COUNT NUMBER OF POINTS BETWEEN THE MAXIMA A_{n-1} AND A_n, $n=1,2,3...n_a$, AVERAGE THEM OVER THE NUMBER OF CYCLES AND DENOTE THIS AVERAGE BY N, FOR ALL SUBSEQUENT CALCULATIONS.
3. DENOTE BY N′ THE NUMBER OF LOCATIONS IN EACH CYCLE.
4. FILL LOCATION I OF THE FIRST CYCLE WITH THE SUM $N''=N/N'$ OF SUCCESSIVE DIGITIZED POINTS FROM SIGNAL $X_B(t)$ AND TAKE ARITHMETIC AVERAGE, STORED IN LOCATION I. REPEAT THIS FOR NEXT LOCATION etc.
5. THE LAST LOCATION IS FILLED WITH ANY REMAINING POINTS.
6. RETURN TO 4 AND REPEAT THE SAME FOR CYCLES 2,3,4... AND STOP AFTER A PREDETERMINED NUMBER OF CYCLES.
7. DIVIDE CONTENTS OF LOCATION M′ BY THE NUMBER OF CYCLES SO FAR, $M'=2,3,4...N'-1$
8. FIND THE ARITHMETIC AVERAGE OF LOCATIONS I AND N′ AND DIVIDE BY THE NUMBER OF CYCLES SO FAR. STORE THE RESULT IN LOCATIONS I AND N′.
9. THESE RATIOS ARE THE TIME AVERAGED VALUES OF THE SIGNAL $X_B(t)$ IN THE NUMBER OF CYCLES SO FAR.
10. TEST FOR CONVERGENCE. PRINT RUNNING AVERAGES.
11. GO TO 12 IF NUMBER OF CYCLES IS GREATER THAN A GIVEN NUMBER OR IF CONVERGENCE IS SIGNALLED. OTHERWISE GO TO 6.
12. PRINT FINAL RESULTS, i.e. PHASE ANGLE OF THE CYCLE (0°- 360°) AND TIME AVERAGED SIGNAL AT CORRESPONDING PHASE.

FIG. B-1 SIMPLIFIED FLOW CHART OF CONDITIONAL AVERAGING PROGRAM.

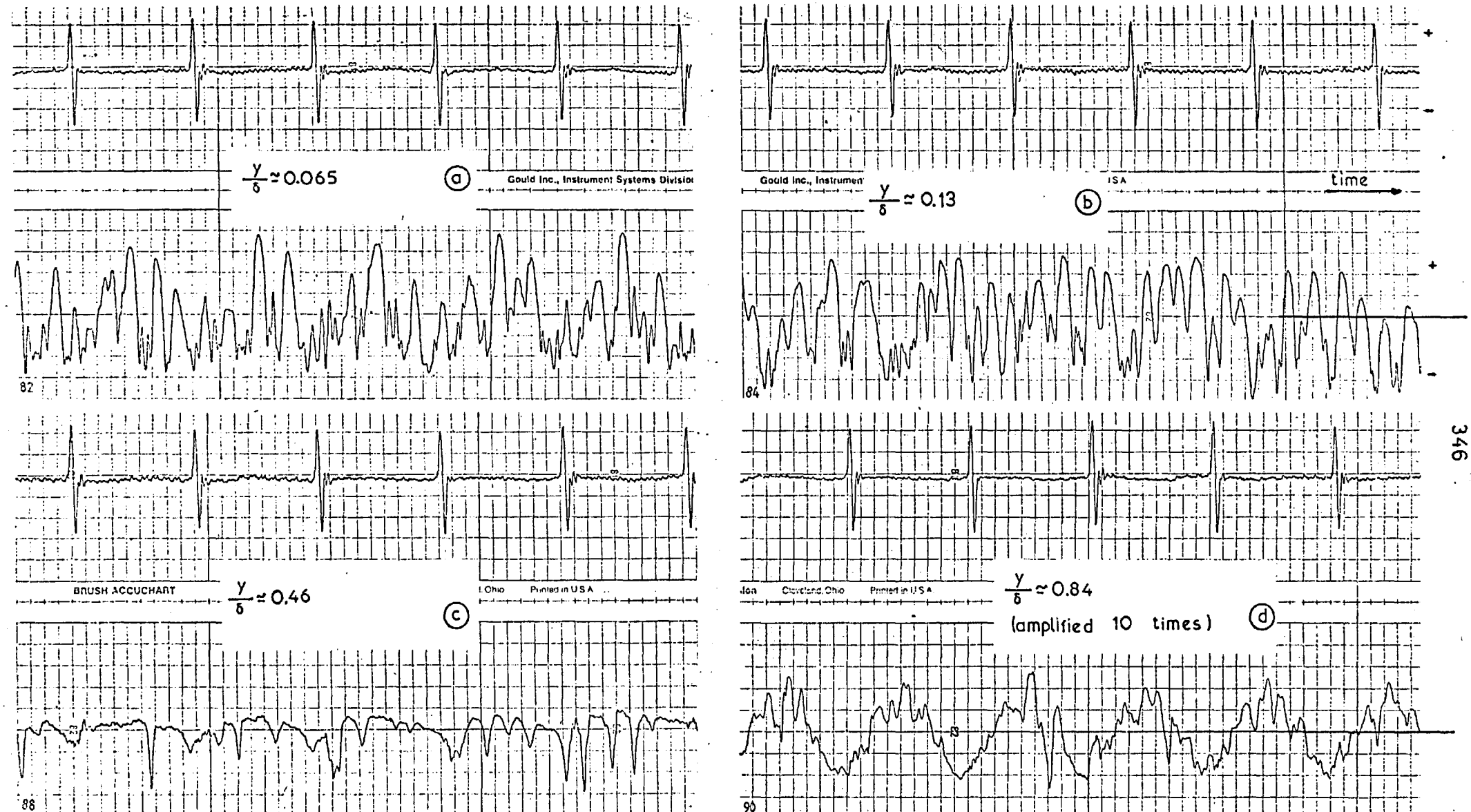

FIG. C-1 HOT WIRE TRAVERSES IN THE BOUNDARY LAYER OF THE ELLIPTIC CYLINDER NEAR SEPARATION - SINUSOIDAL FLOW
$Re = 2.2 \times 10^5$ $\frac{x}{c} \simeq 0.81$, $\frac{\pi n c}{U_\infty} \simeq 0.2$, MEDIUM ECCENTRICITY (ANEMOMETER OUTPUT IS NOT LINEARIZED)

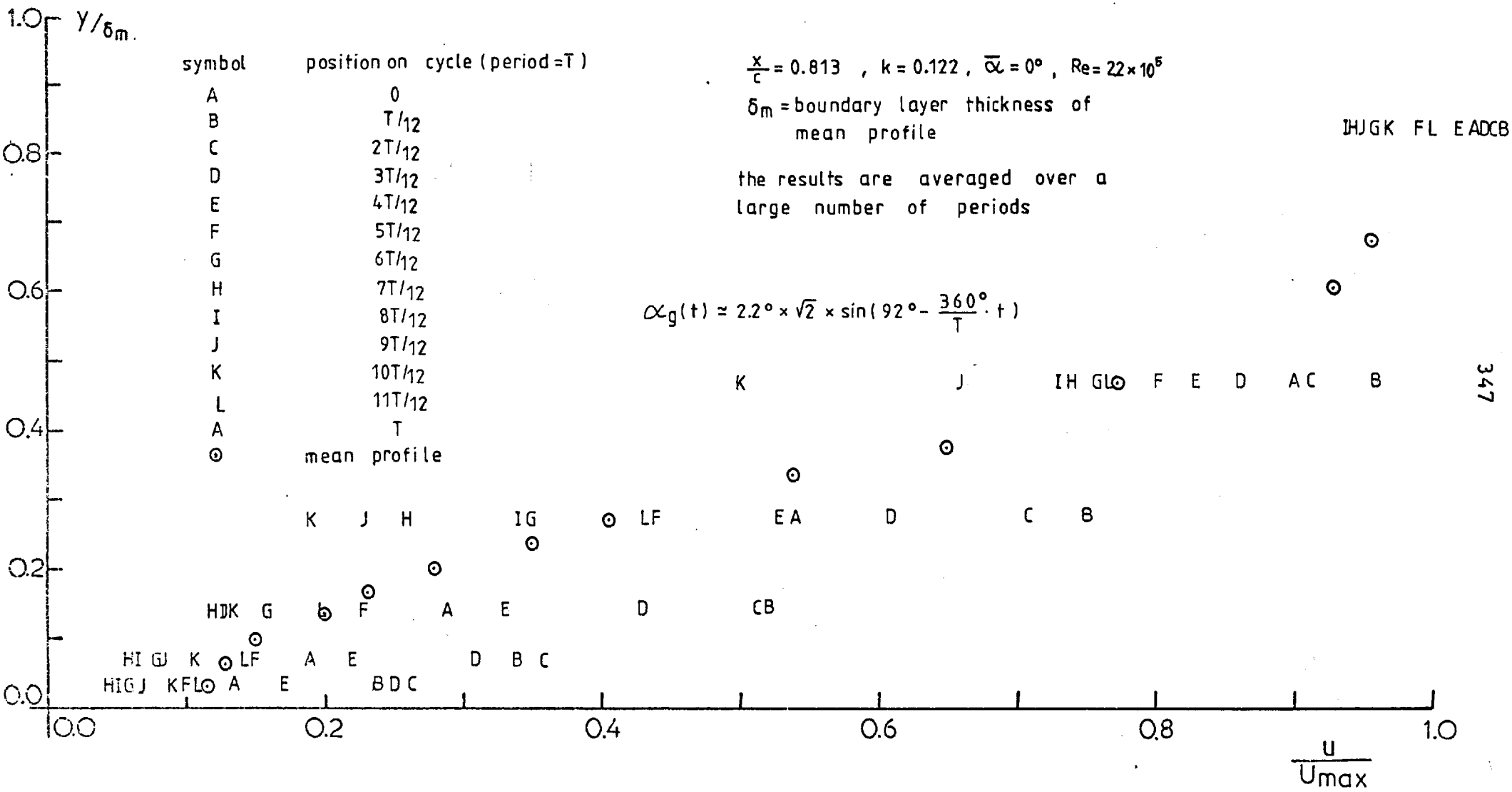

FIG. C-2 SEQUENCE OF INSTANTANEOUS VELOCITY PROFILES OVER A COMPLETE SINUSOIDAL GUST CYCLE. ELLIPTIC CYLINDER

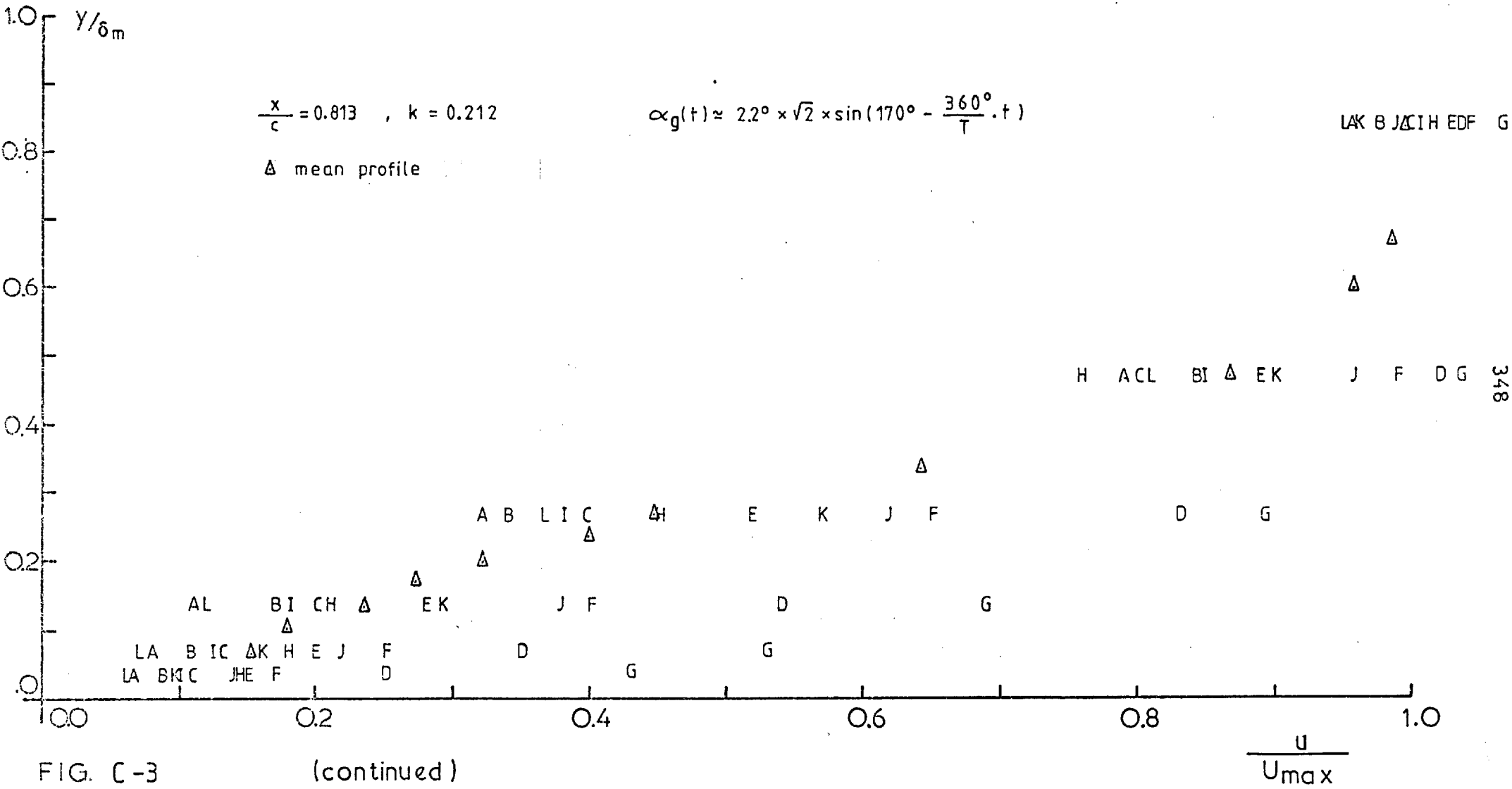

FIG. C-3 (continued)

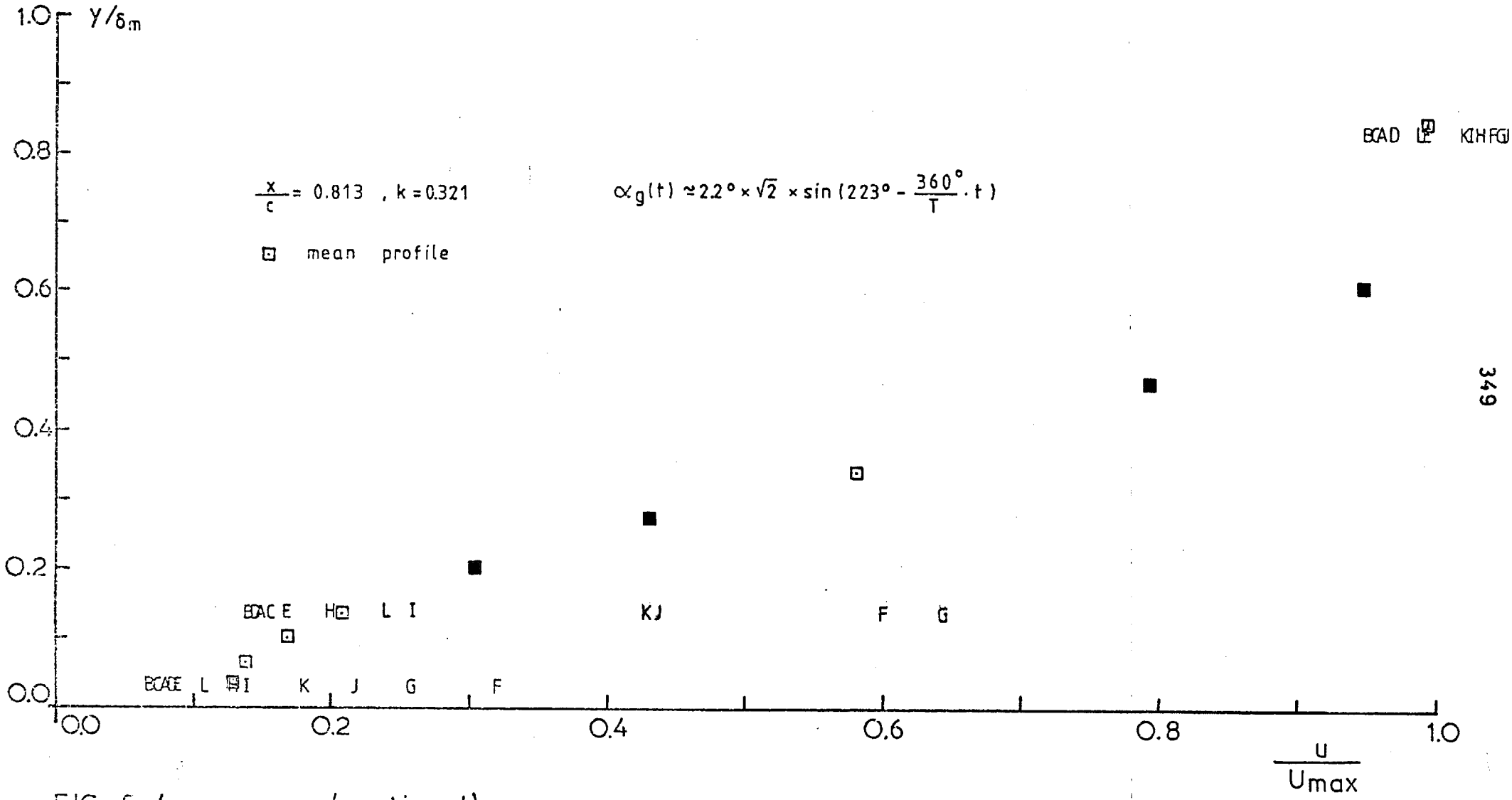

FIG. C-4 (continued)

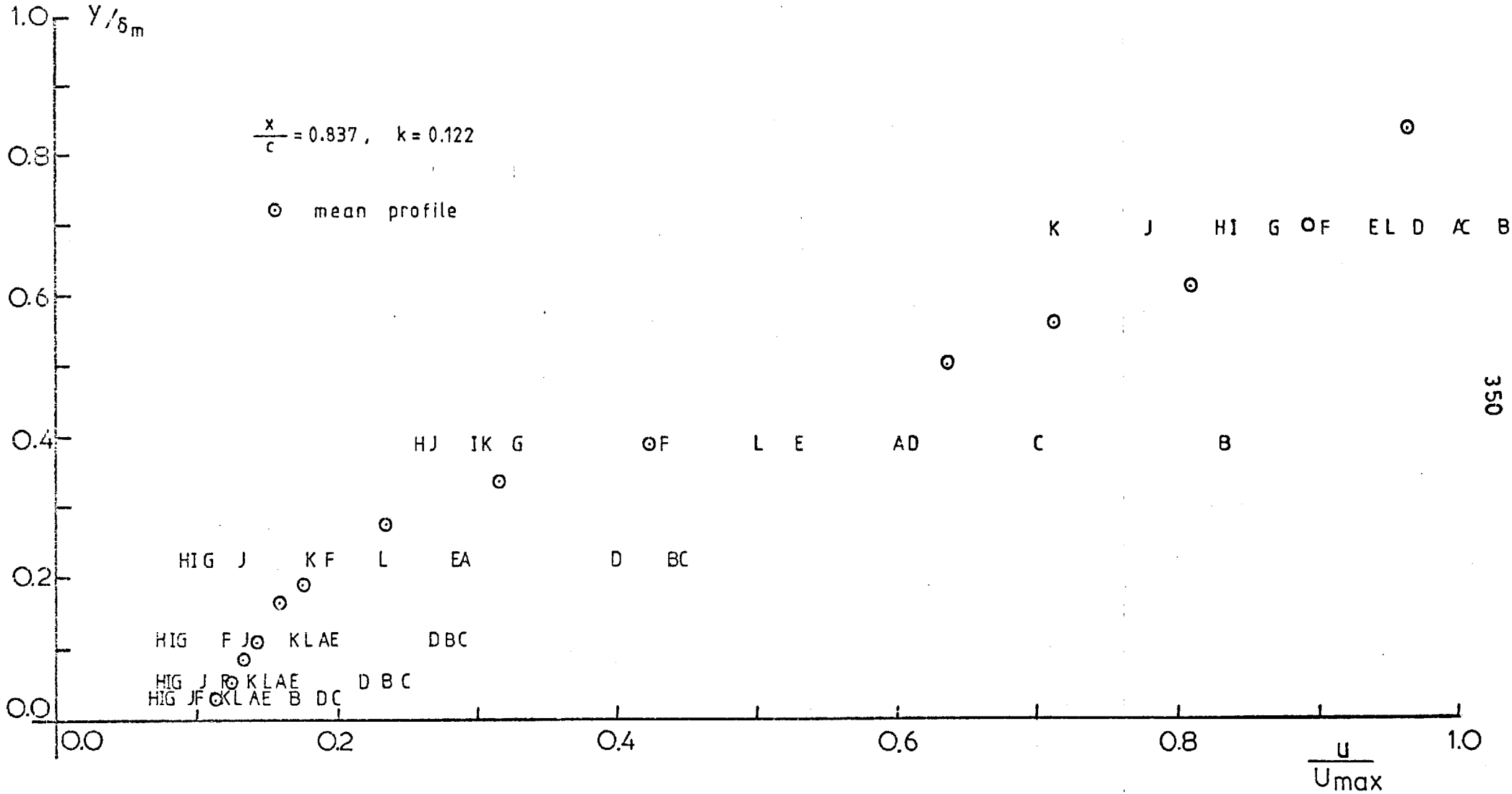

FIG. C-5 (continued)

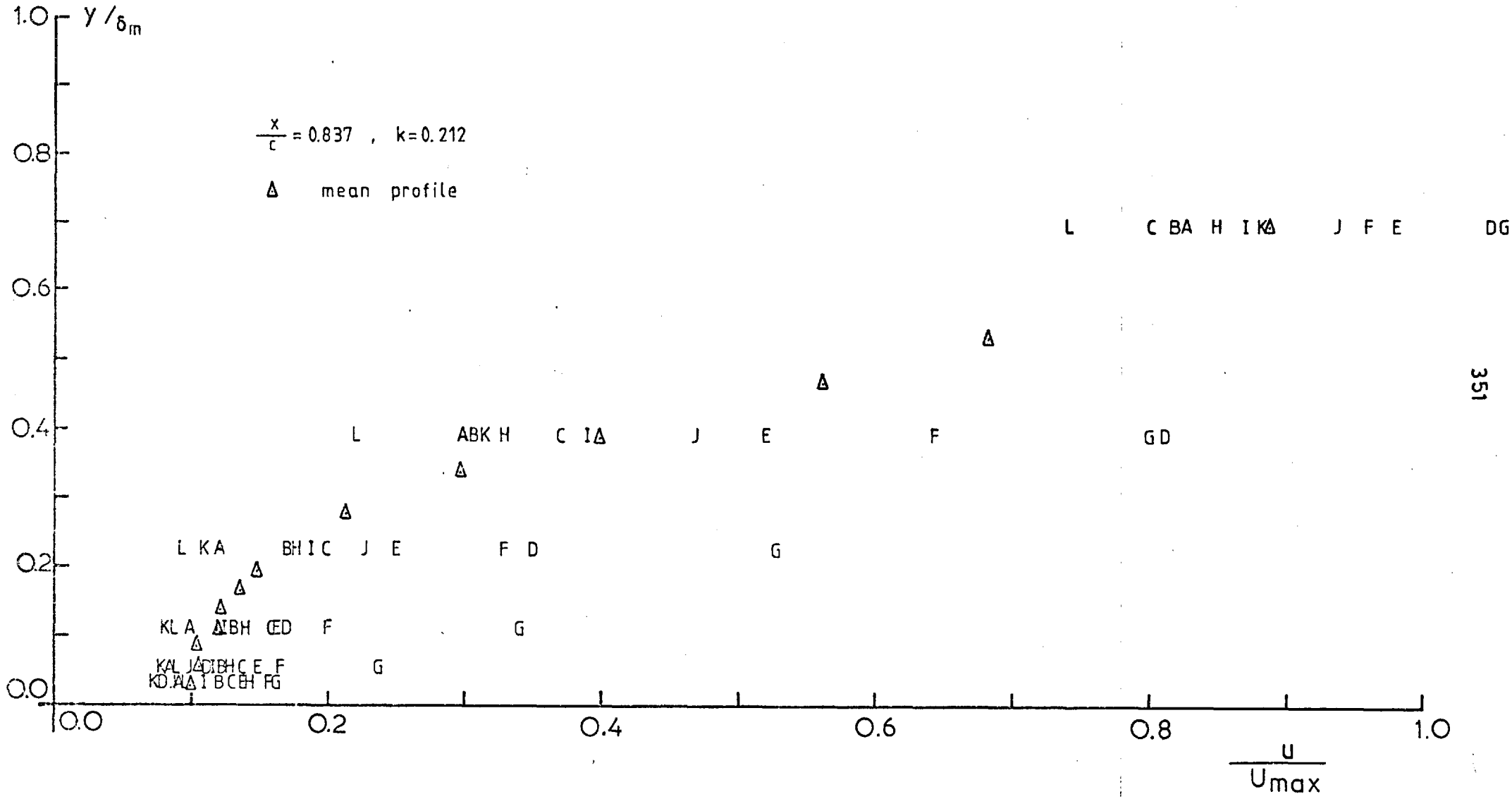

FIG. C-6 (continued)

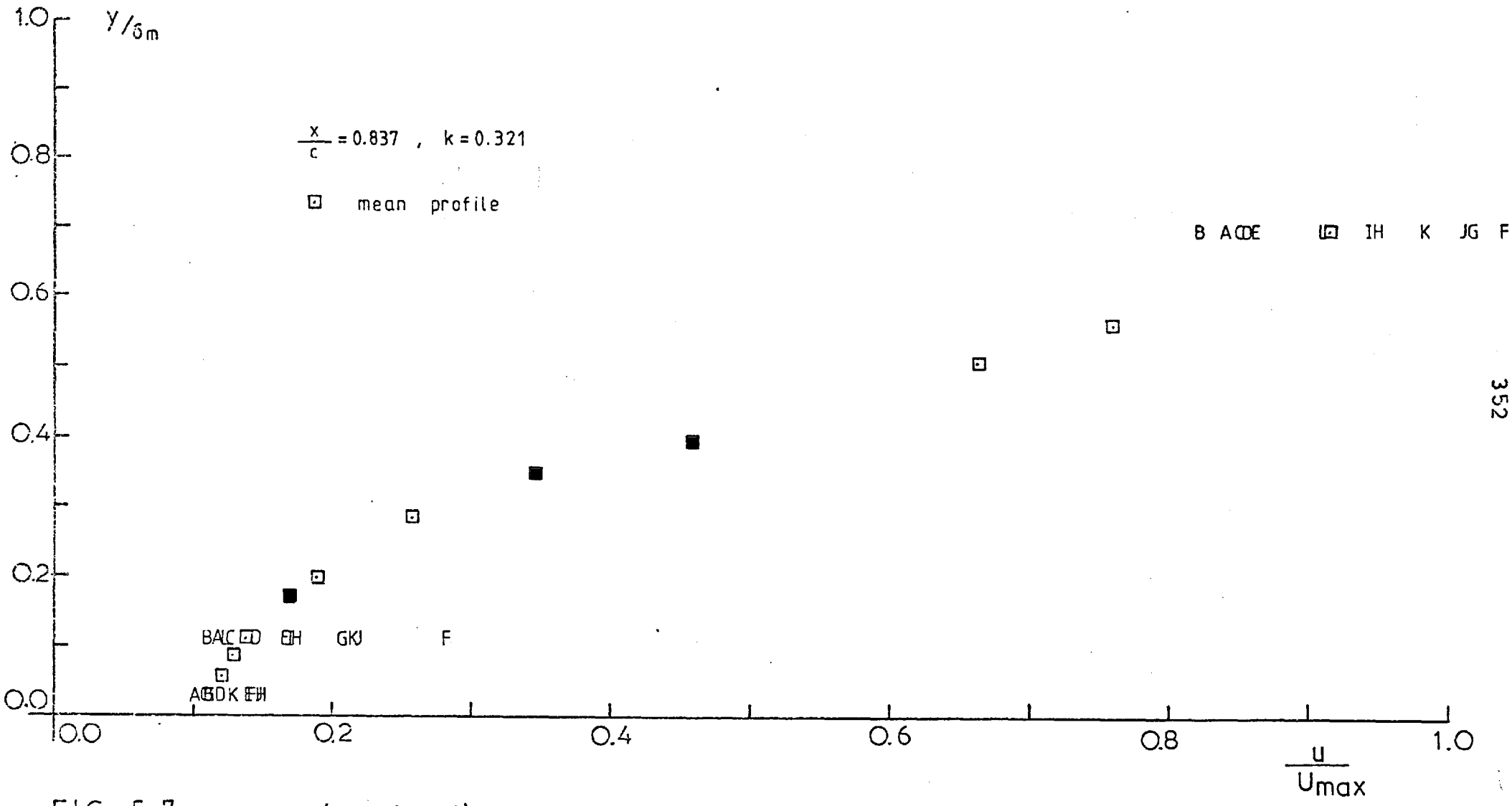

FIG. C-7 (continued)

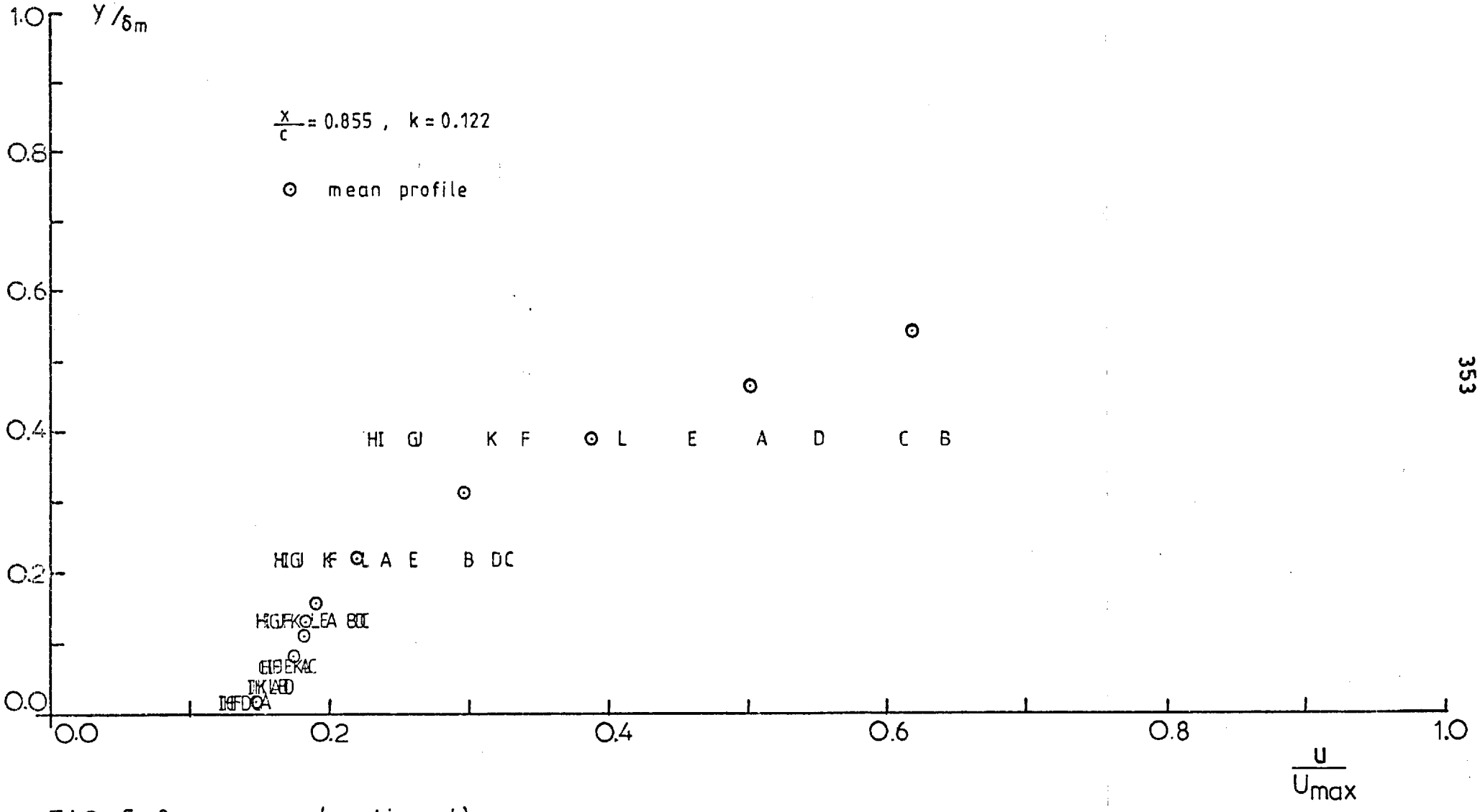

FIG. C-8 (continued)

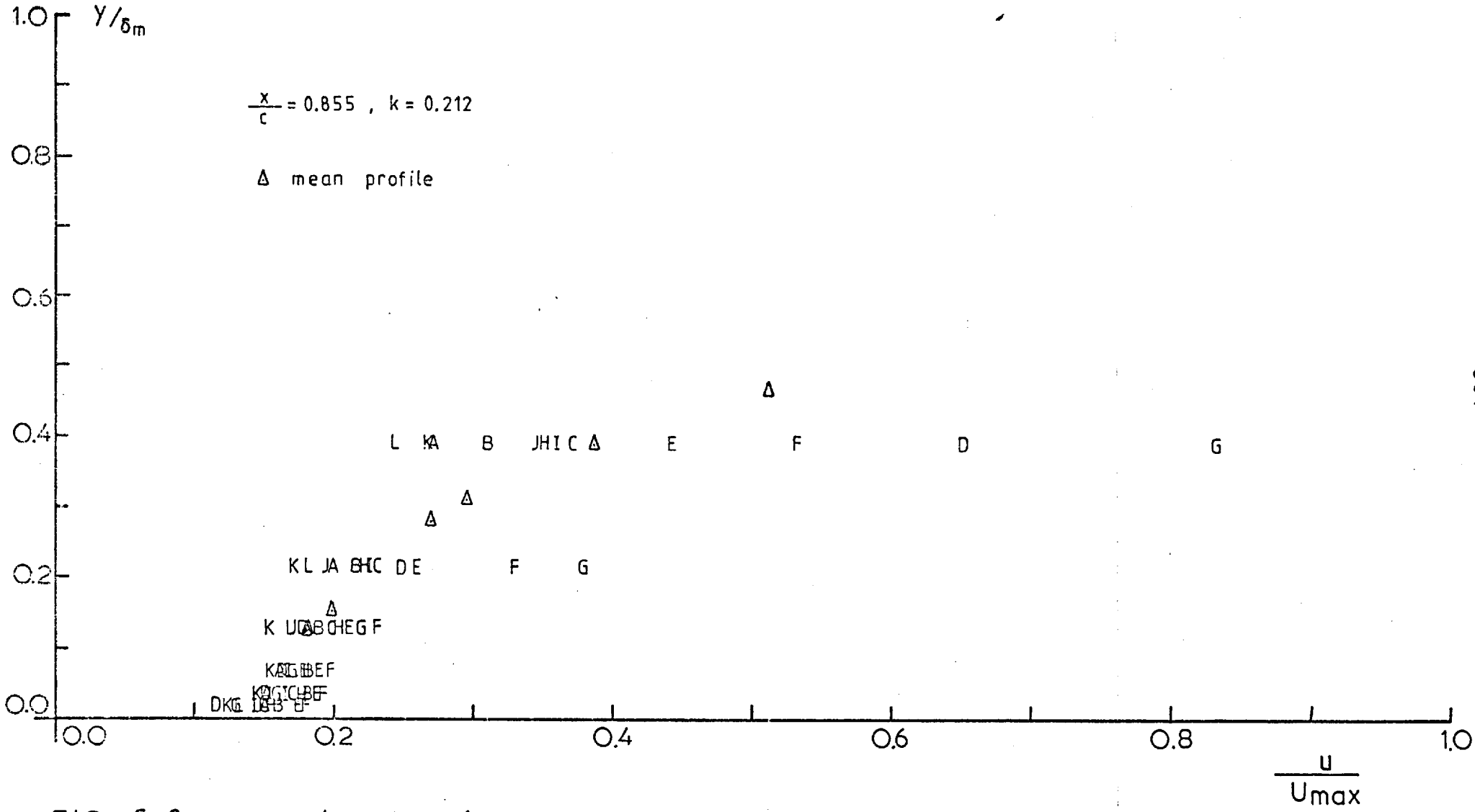

FIG. C-9 (continued)

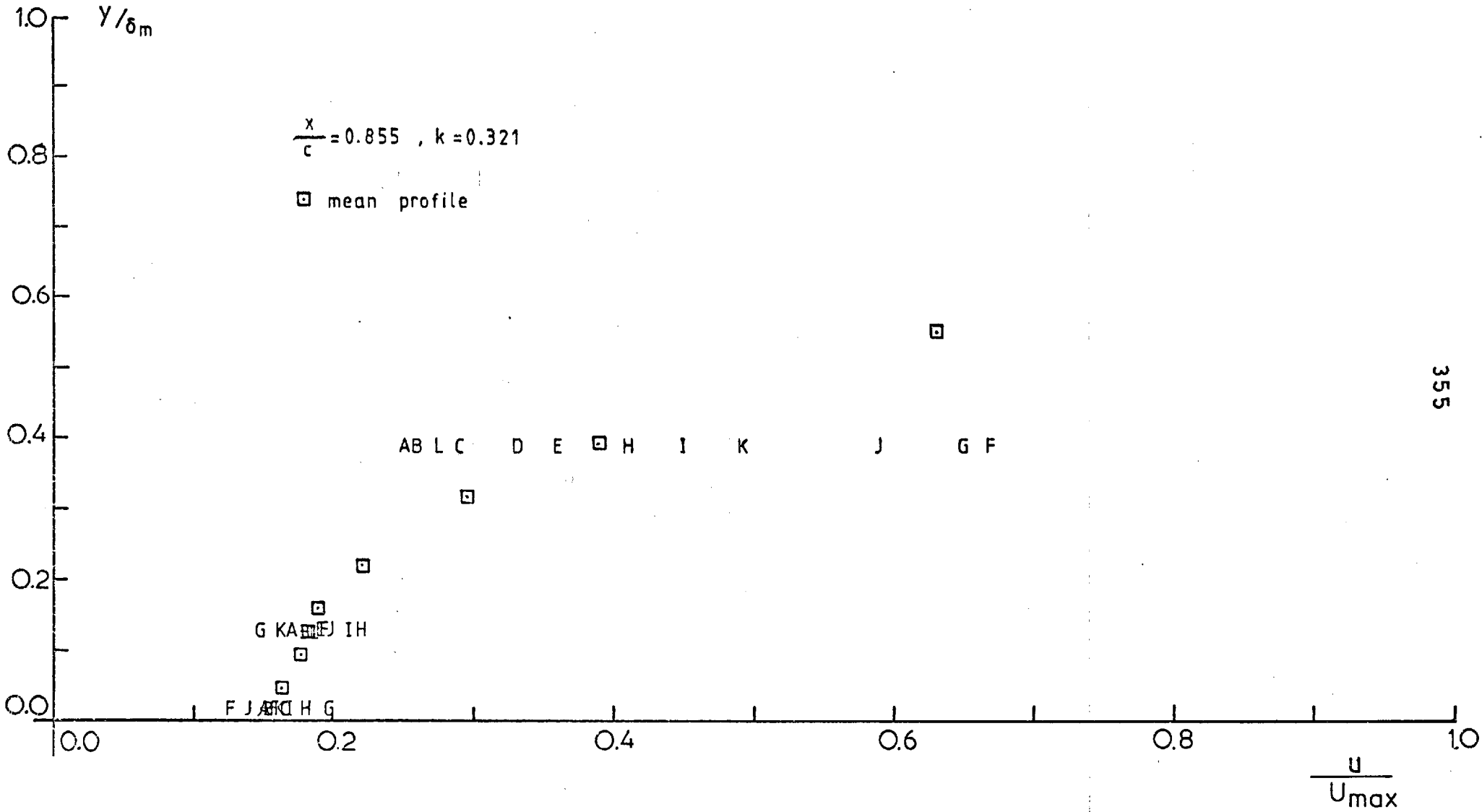

FIG. C-10 (continued)

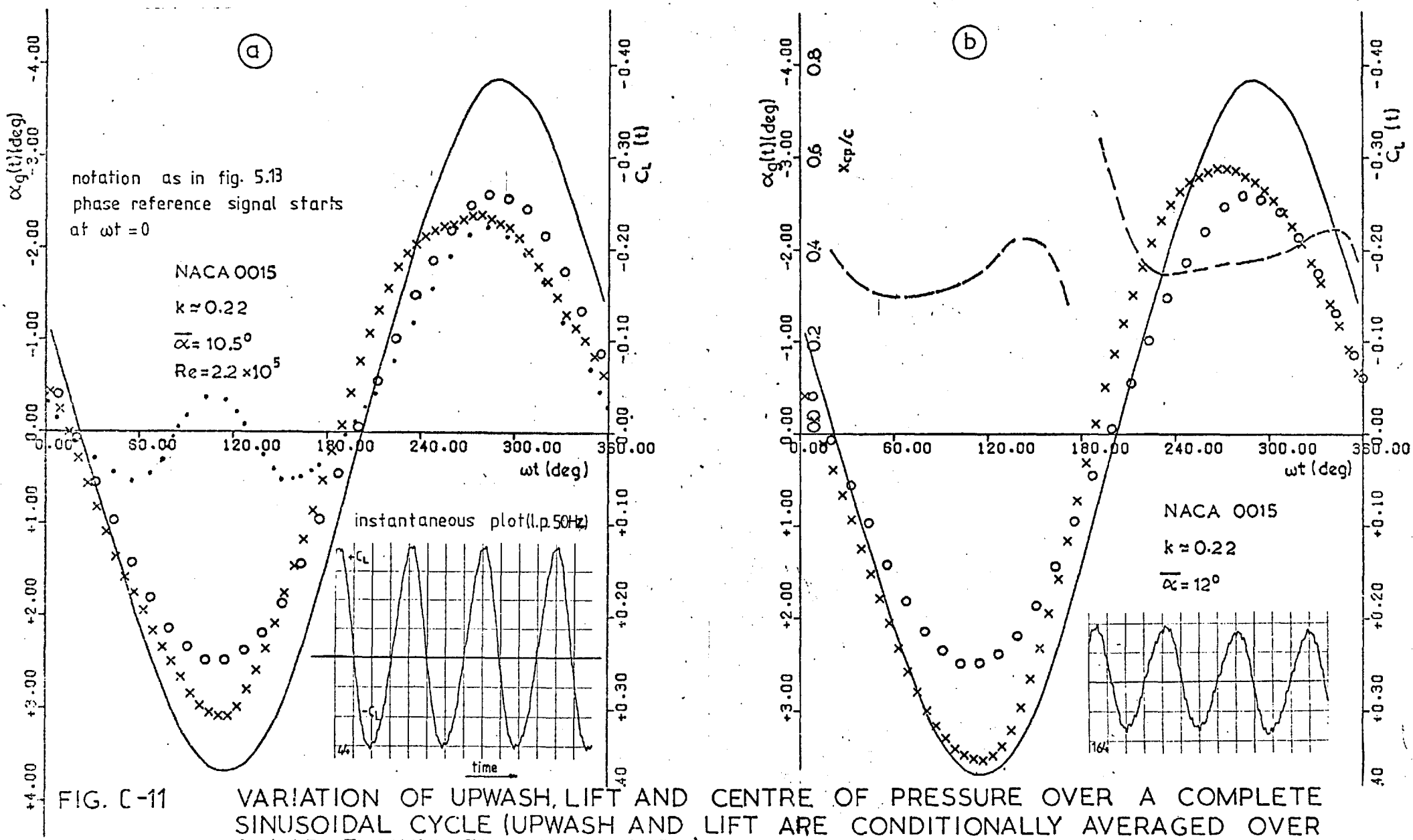

FIG. C-11 VARIATION OF UPWASH, LIFT AND CENTRE OF PRESSURE OVER A COMPLETE SINUSOIDAL CYCLE (UPWASH AND LIFT ARE CONDITIONALLY AVERAGED OVER A LARGE NUMBER OF PERIODS)

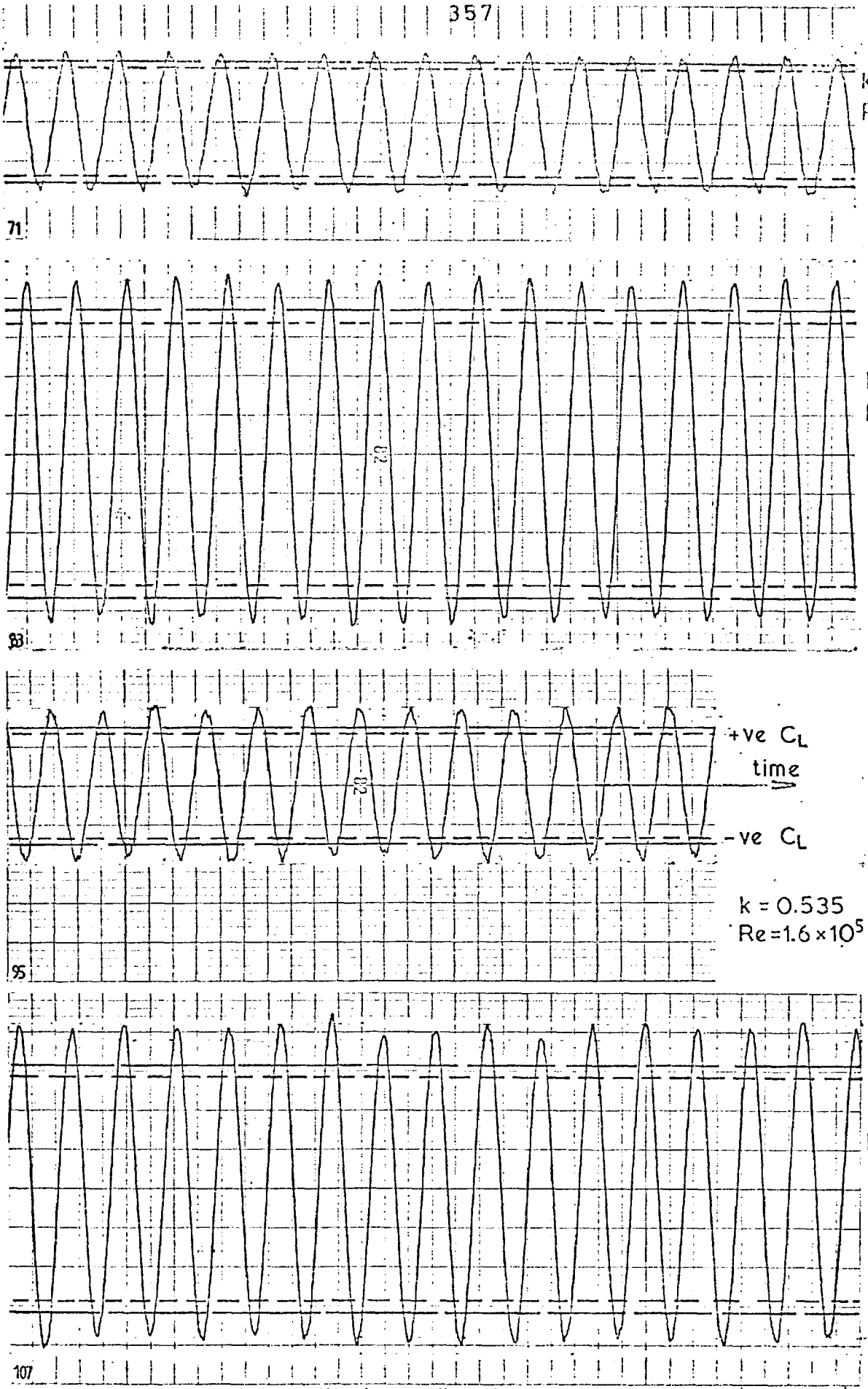

FIG. C-12A MEASURED INSTANTANEOUS LIFT AND PREDICTED PEAK LIFT AMPLITUDE FOR THE NACA 0015 AEROFOIL $\alpha = 10.5°$
($n_g \simeq 18$ Hz, LOW PASS FILTER SET AT 50Hz)
SMALL ECCENTRICITY

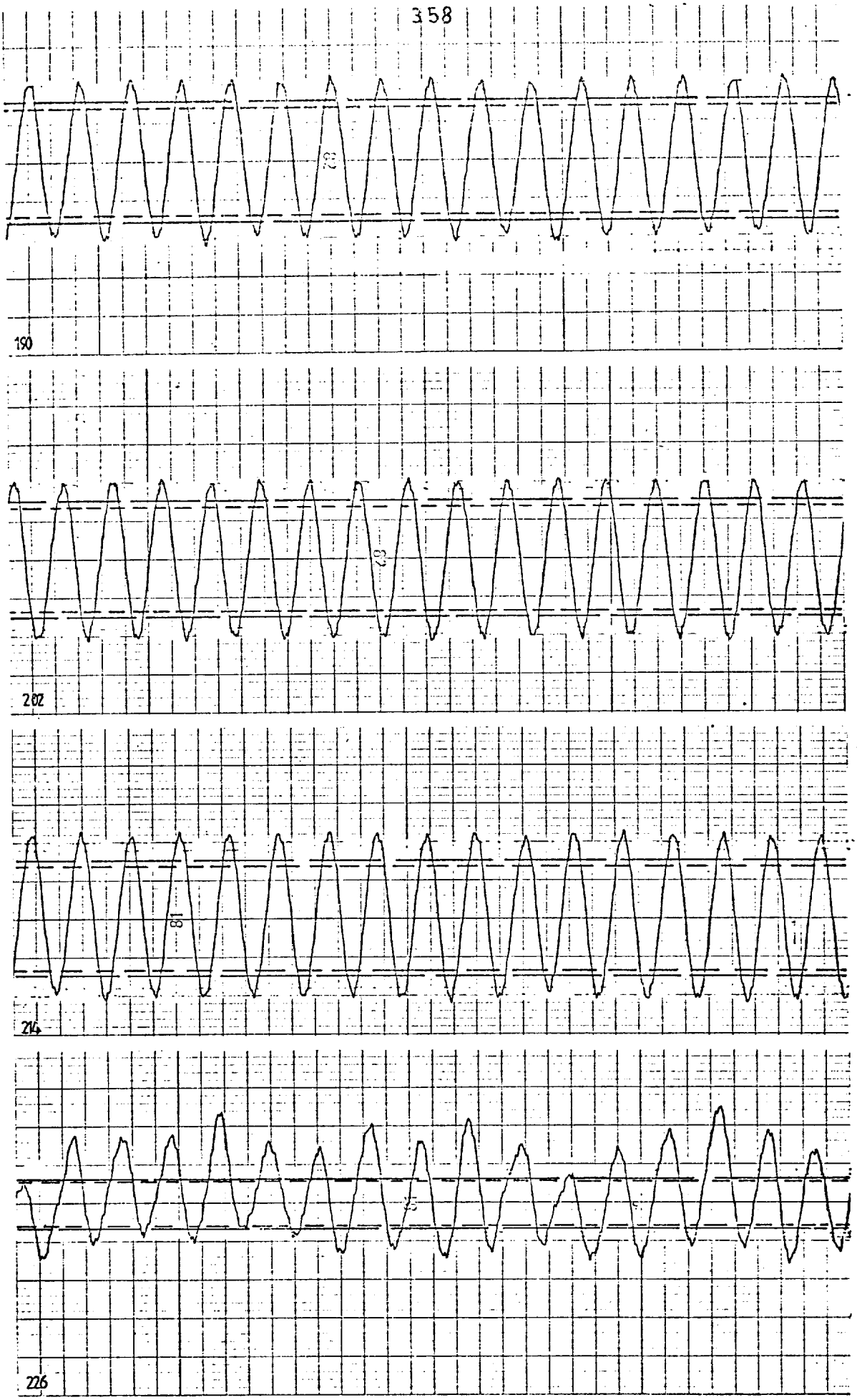

FIG. C-12 B

$\bar{\alpha}=12°$

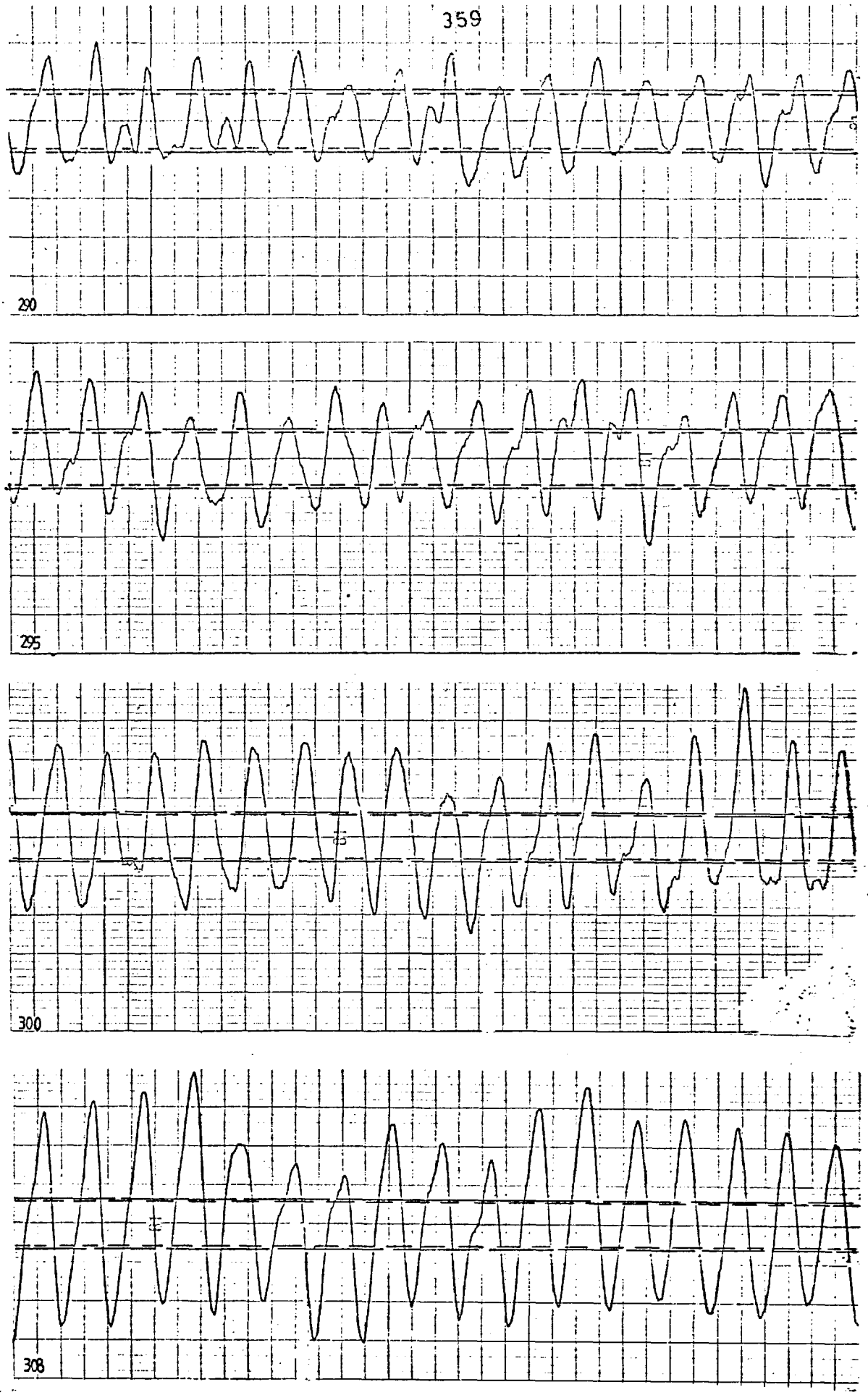

k = 0.29
Re = 3.0 × 10^5

k = 0.39
Re = 2.2 × 10^5

k = 0.535
Re = 1.6 × 10^5

k = 0.715
Re = 1.2 × 10^5

FIG. C-12C

$\bar{\alpha} = 13.5°$

APPENDIX A: HOT-WIRE TECHNIQUES

The streamwise component of the gust was measured with a normal U-wire. It is known that such a wire senses velocities only perpendicular to its axis. In the present experiments a DISA D01 constant temperature anemometer was used and the wire was calibrated with the usual methods, see for example Bradshaw (1971).

The measurement of the gust upwash w was made with an X-wire probe. The probe had first to be made insensitive to the streamwise fluctuations. This was achieved by matching the slopes of the two individual hot-wire calibration curves. The procedure followed in the (empty) tunnel was as follows. The probe was fixed at the centre line and exposed in a smooth flow of the desired speed, U_∞, at which the experiments were to be made. The signals from the two anemometers were subtracted and the result was displayed on a digital voltmeter. Then the tunnel speed was changed slowly above and below U_∞ (± 10%), while the overheat ratio of one of the wires was altered (e.g. by turning the resistance knob of the anemometer). A point was then reached where the variations in U_∞ did not affect (within 1 - 3%) the indication of the voltmeter. Accordingly, this implied that the X-probe was insensitive to (static) changes in velocity in the streamwise direction, feeling only the (static) upwash component w, i.e. the voltmeter output e would be, for $w \ll U_\infty$:-

$$e \simeq k_w w + DC \qquad k_w = \text{constant}$$

(The linear dependence follows from $w \ll U_\infty$). In unsteady flow the DC part of the fluctuating output could be removed by means of a zero suppression unit. It is assumed that the above relation would still

hold for fluctuating quantities. Next, the constant k_w was determined by calibrating the probe in yaw, see sketch below:-

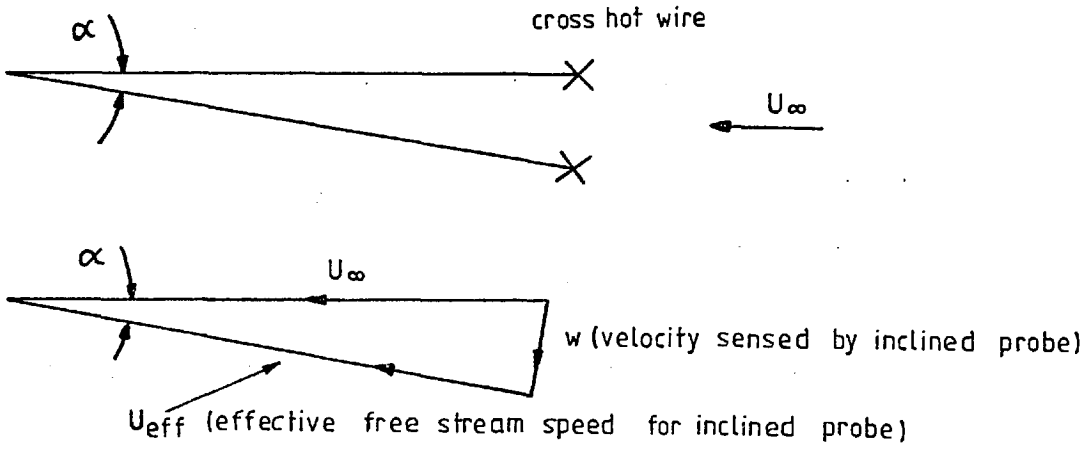

SKETCH

then $U_\infty \sin \alpha = w$ or:-

$$\alpha \simeq w/U_\infty \qquad \therefore \qquad \alpha = \frac{e}{k_w} \cdot \frac{1}{U_\infty}$$

$$\therefore \qquad e = \alpha \, k_w \, U_\infty \qquad \therefore \qquad k_w = \frac{\partial e}{\partial \alpha} \frac{1}{U_\infty}$$

It was easier to plot e against α to obtain the slope λ_w of the resulting straight line (see Fig. A-1) in volts/degree. The upwash w in m/sec could then be found from the relationships above. However, the gust amplitude $\alpha_g = w/U_\infty$ was frequently used in the representation of results. It could be computed from the relation:-

$$\alpha_g = V_{RMS}/(\mu \cdot \lambda_w) \qquad \text{(degrees)}$$

where V_{RMS} is the measured RMS voltage from the conditioner, μ is an amplification factor of the operational amplifiers and λ_w is the

calibration factor (from Fig. A-1) in volts/degree, usually in the range 0.010 to 0.012 volts/degree. It was thought that this static calibration would suffice for the needs of the present experiment, where the size of the energetic eddies was much greater than the size of the wire.

Temperature changes in the fluid could produce errors in the measured velocities (approximately a 2% error for $1^{o}C$ change) and, therefore, it had been tried to conduct the experiments at a constant fluid temperature, about $25^{o}C$. After the hot-wire measurements were completed, a second calibration followed (generally different calibration constants were obtained due to temperature effects and wire contamination). In the compilation of the results the average values were taken.

Another source of error that could be introduced in the measurement of w is the response of the wire to a small tangential (i.e. along the axis of the wire) cooling velocity. Jackson (1970) states that this effect could lead to measured values of upwash which are lower than the real ones by a factor:- $(1 + k_{\theta}^2)/(1 - k_{\theta}^2)$, where k_{θ}^2 is a constant of the order 0.04 for free stream speeds 15 to 300 m/sec. Thus the measured upwash could be as low as 92% approximately of the true upwash. This kind of correction has not been applied to the following velocity measurements, but it should be remembered as a possible source of discrepancy in the aerodynamic admittance results.

Taking into account these errors, it was estimated that the upwash measurements would be accurate within 5 to 10%.

Since it was necessary to take measurements elsewhere (besides the point (0, 0, 0)) in the flow, a simple rig had been constructed, capable of traversing the probe in all three (x, y, z) directions and also along a fixed direction. This last feature was useful for the boundary layer measurements on the elliptic model.

APPENDIX B: THE MEASUREMENT AND PROCESSING OF SIGNALS

1. Definition of Errors.

The errors which can arise when measuring a quantity, may be divided into measurement errors (associated with the condition of the instrument, experience of the user, etc.) and the statistical errors (associated with the particular measuring technique). In the latter category, the errors can be estimated if certain parameters of the system are known. Let Φ be the quantity to be measured, $\hat{\Phi}$ an estimate of Φ and $E(x)$ the symbol for the mean, or expected, value of x. Then, as suggested by Bendat and Piersol (1971), a normalized root mean square error can be defined as:-

$$\varepsilon = \sqrt{\varepsilon_r^2 + \varepsilon_b^2} \tag{B-1}$$

where:-

$$\varepsilon = \frac{\sqrt{E(\hat{\Phi}^2) - E^2(\hat{\Phi})}}{\Phi} = \frac{\text{standard deviation of } \hat{\Phi}}{\Phi}$$

is the normalized random error;

$$\varepsilon_b = \frac{E(\hat{\Phi})}{\Phi} - 1 = \frac{\text{mean value of } \hat{\Phi}}{\Phi} - 1$$

is the normalized bias error.

Generally ε will decrease when the true averaging time increases. For an instrument which has a fixed integration time constant T_c, however, little is to be gained by measuring records of length greater than about 4 to 5 T_c.

2. Measurement of Mean Value.

Digital voltmeters of the SOLARTRON and DISA types were used. For sufficiently long records (of duration greater than T_c), the bias error is negligible and the random error not more than 1%.

3. Measurement of Root Mean Square Value (RMS).

The DATRON and DISA brands of RMS meters were used. In both, there was a facility for changing T_c. The scatter of several calibration measurements indicated that a 5% maximum error in the true RMS value should be expected.

4. Measurement of Power Spectral Density.

Both, analogue methods (by using band-pass filters) and digital methods (numerical harmonic analysis) were used.

(a) Analogue Methods.

A band-pass filter of centre frequency n_o, is a device which passes frequencies only in the interval $n_o - \frac{\Delta n}{2}$ and $n_o + \frac{\Delta n}{2}$, where Δn is the real bandwidth of the filter. The frequency response function $T(n, n_o)$ of the filter, gives a measure of the output spectrum, if a white noise signal of spectral density 1.0 is fed through it. If a general signal $x(t)$ is passed through the filter, the output will be a signal $x(t, n_o, \Delta n)$ of which the true mean square value will be:-

$$\lim_{T\to\infty} \frac{1}{T} \int_0^T x^2(t, n_o, \Delta n)\, dn = \int_0^\infty |T(n, n_o)|^2 S_x(n)\, dn =$$

$$= \int_{n_o - \frac{\Delta n}{2}}^{n_o + \frac{\Delta n}{2}} |T(n, n_o)|^2 S_x(n)\, dn \qquad (B\text{-}2)$$

where $S_x(n)$ is the true spectrum of $x(t)$ and $T(n, n_o)$ is assumed to be zero outside the band $\left[n_o - \frac{\Delta n}{2}, n_o + \frac{\Delta n}{2}\right]$. Our purpose is to measure $S_x(n)$, i.e. obtain an estimate, denoted by $\hat{S}_x(n)$. In practice, the following approximations are made.

The true mean square on the left hand side of Eqn. (B-2) is replaced by its estimate, i.e. the value that would be measured with an RMS meter or integrator. Then, Eqn. (B-2) becomes:-

$$\overline{x^2(t, n_o, \Delta n)} \simeq \int_{n_o - \frac{\Delta n}{2}}^{n_o + \frac{\Delta n}{2}} |T(n, n_o)|^2 \, S_x(n) \, dn \qquad \text{(B-3)}$$

A second approximation is to assume that Δn is so small, that $S_x(n)$ may be taken as constant in the interval $\left[n_o - \frac{\Delta n}{2}, n_o + \frac{\Delta n}{2}\right]$. Eqn. (B-3) is then written as:-

$$\overline{x^2(t, n_o, \Delta n)} \simeq S_x(n_o) \int_{n_o - \frac{\Delta n}{2}}^{n_o + \frac{\Delta n}{2}} |T(n, n_o)|^2 \, dn = S_x(n_o) \cdot F(n_o, \Delta n) \qquad \text{(B-4)}$$

where $F(n_o, \Delta n)$ is a characteristic function of the filter, which can be determined once for all, if n_o and Δn are known; $F(n_o, \Delta n)$ is an effective bandwidth of the filter, Δn_e, and in the commercial wave analyzers (or "frequency spectrometers") is made proportional to n_o. Therefore, from Eqn. (B-4):-

$$S_x(n_o) \simeq \frac{\overline{x^2(t, n_o, \Delta n)}}{\text{const} \times n_o} = \frac{\overline{x^2(t, n_o, \Delta n)}}{\Delta n_e} = \hat{S}_x(n_o) \qquad \text{(B-5)}$$

Bendat and Piersol (1971) give the normalized RMS error for $\hat{S}_x$ (i.e. the estimate of the true spectrum S_x) as:-

$$\varepsilon \simeq \sqrt{\frac{1}{\Delta n_e \cdot T} + \left(\frac{\Delta n_e^2}{24} \cdot \frac{d^2 S_x(n)}{dn^2} \cdot \frac{1}{S_x(n)}\right)^2} \qquad \text{at } n = n_o \qquad \text{(B-6)}$$

where T is the averaging time.

The first term under the square root gives the square of the random error, while the second, the square of the bias error. Hence there are two conflicting requirements about the size of the bandwidth: a small bandwidth increases the random error but decreases the bias error and vice versa. However, Eqn. (B-6) also shows that the random error can be made small if the averaging time is big. The shape of the spectrum can significantly affect the accuracy of the measurement, because if $\frac{d^2 S_x}{dn^2}$ is large (e.g. when a sharp peak exists in the spectrum), then ε also becomes large, according to Eqn. (B-6). In the present work, it was a matter of importance to choose the appropriate instrument for the accurate measurement of the sharp spectral peaks, associated with the sinusoidal flow experiment. A factor which influenced the selection of the appropriate device, was the drift with time in the oscillating aerofoil frequency particularly noticed at low frequencies (see Section 3.2.2).

Two "constant percentage bandwidth" wave analyzers were available:-

- A Bruel and Kjaer 2112 analyzer with 1/3 octave bandwidth (i.e. $\Delta n_e = (2^{1/6} - 2^{-1/6})\, n_o \simeq 0.231\, n_o$) of which the lowest n_o was 25 Hz. The band-pass filters were centred at frequencies $25(2^{1/3})^m$ Hz ($m = 0, 1, 2, 3 \ldots$). These features made this instrument unsuitable for the sinusoidal flow experiment, where the frequencies of interest were below 25 Hz.
- A Muirhead K134A analyzer with option for $\Delta n_e = 0.02\, n_o$ and $\Delta n_e = 0.10\, n_o$ (corresponding filter attenuations 36 dB/octave and 25 dB/octave). The centre frequency could be changed in steps of 0.1 Hz in the range 3 Hz to 30 Hz and in steps of 1 Hz in the range

30 to 300 Hz. A disadvantage with this instrument was that the integration time constant appeared to be insufficient for the lowest frequencies and that no output facility was available, i.e. that the reading could only be taken from the front panel. The observed drift and also a random "meandering" in the frequency of the oscillating aerofoils would make the measurement of the spectral power unreliable at low frequencies. Therefore, this analyzer was also abandoned when spectral power was measured.

The solution adopted for the sinusoidal flow experiment, was to use a dual, variable frequency, filter in conjunction with an RMS meter. The filter, which had low-pass and high-pass settings, was of the Rockland 452 type. The frequency could be changed in steps of 0.01 Hz for $0 \leq n_o \leq 10$ Hz and in steps of 0.1 Hz for $10 \leq n_o \leq 100$ Hz. From the manufacturer's instruction book it was found that the input signal would be only slightly attenuated in the passband, while strongly attenuated outside this band (24 dB/octave at the cut-off frequency). The bandwidth was determined after some preliminary digital analysis spectral plots were obtained; they showed that the main response was at the fundamental gust frequency, while the lower and higher harmonics and the extraneous noise were of much lower spectral strength. Accordingly, the high-pass filter was almost invariably left in the 0.5 Hz position, while the low-pass was adjusted every time, so as to cut the power of the second and higher harmonics in the lift or upwash spectra. Roughly, the upper cut-off frequency was 1.5 to 1.6 times the gust frequency.

Computation of the Aerodynamic Admittance.

The primary use of the filtered values was to compute the experimental aerodynamic admittance, $|A(n)|$ as the ratio of the lift to

the upwash, i.e.:-

$$|A(n)|^2 = \text{const.} \frac{S_L(n)}{S_W(n)} \tag{B-7}$$

If x_L and x_W are the fluctuating voltages proportional to the fluctuating lift and upwash respectively and n_g the gust frequency, then from Eqn. (B-3):-

$$\begin{aligned} \overline{x_L^2(t, n_g, \Delta n)} &\sim \int_{n_g - \Delta n_1}^{n_g + \Delta n_2} |T(n, n_g)|^2 \cdot |A(n)|^2 \cdot S_W(n)\, dn \\ \overline{x_W^2(t, n_g, \Delta n)} &\sim \int_{n_g - \Delta n_1}^{n_g + \Delta n_2} |T(n, n_g)|^2 \cdot S_W(n)\, dn \end{aligned} \tag{B-8}$$

The integration limits were taken equal to the cut-off frequencies, at which the low-pass and high-pass filters were set by the previously described procedure. This is justified for two reasons. First, the preliminary spectra (obtained by digital analysis) indicated that, taking as centre the gust frequency, S_L can be assumed proportional to S_W, in a frequency band where both spectra are strong. Second, these spectra are sharp, so that the frequency band is small. Therefore, $|A(n)|$ can be obtained from Eqn. (B-8) as:-

$$|A(n)| \simeq \text{const.} \frac{\sqrt{\overline{x_L^2}}}{\sqrt{\overline{x_W^2}}} = \text{const.} \frac{C_L}{\alpha_g} = |\hat{A}(n)| \tag{B-9}$$

where C_L, α_g are the filtered RMS lift coefficient and upwash respectively and $|\hat{A}(n)|$ is the estimate of $|A(n)|$. Note that $|A(n)|$ was assumed to be nearly constant in the frequency band where S_L and S_W are high.

The maximum error in the estimate of the admittance (excluding

errors due to the hot-wire, transducer response, etc.) would be the sum of the maximum errors in the estimate of the root mean square values, i.e. in the region of 10%, because C_L and α_g are statistically uncorrelated in the present experiment. (If C_L and α_g were statistically correlated, e.g. if they were measured simultaneously in the laboratory, then the error would be lower).

The Bruel and Kjaer wave analyzer was suitable for the measurement of the turbulent lift and velocity spectra because these do not vary rapidly with frequency, so that Eqn. (B-4) may be assumed to hold with good accuracy.

(b) Digital Methods.

The digitization of the signals was performed by an analogue-to-digital converter, controlled by a PDP minicomputer, within an accuracy of 0.002 volts (± 1 volt was the permissible input to the converter). The data were stored in a digital tape, the contents of which could be read and processed via a spectral analysis program written by Davies (1974). As in the case of analogue filtering, the relevant parameters should be determined in such a way as to produce the minimum possible statistical error. In addition, it is the effect of aliasing, i.e. the inability to define frequencies which are higher than the "Nyquist frequency" n_N, equal to half the rate at which the data points are sampled. Thus the estimated spectral density at a frequency $n = n_x < n_N$ is equal to the sum of the spectral power existing at frequencies $2n_N + kn_x$, $k = 0, 1, 2, 3 \ldots$.

In the particular spectral analysis program used the normalized (with respect to the mean square) spectral density was given at frequencies uniformly distributed over the frequency range up to n_N; the estimates were m in number ($m \leq 513$). If SR is the sampling rate (Hz), the adjacent spectral estimates differ by:-

$$\Delta n_e = \frac{SR}{2(m-1)} = \frac{n_N}{(m-1)}$$

For good resolution the effective bandwidth should be small. The random error is again equal to $\varepsilon_r = 1/\sqrt{T\Delta n}$. To make ε_r small, say 5%, T, SR and m should be of appropriate value. If n_{max} is the maximum frequency of interest, then not only should $n_{max} < n_N$, but also it must be ensured that negligible power exists at frequencies $n > n_N$ to avoid "aliasing". A low-pass filter with cut-off frequency between n_{max} and n_N was, therefore, always used during digitizing. A high pass filter set at 0.5 Hz was also used to avoid overloading of the converter. n_{max} was roughly 25 Hz for the sinusoidal flow experiment, 400 Hz for turbulence and 250 Hz for the vortex shedding phenomenon. It is, therefore, anticipated that a single set of parameters would not give the same degree of accuracy for the frequencies of interest. For example, in the case of sinusoidal data, a fine resolution near the peak was desirable, while for the turbulence data a wide Δn_e would be acceptable. Unlike the usual analogue wave analyzers, here the bandwidth is constant, resulting in a comparatively better resolution at high frequencies. To save digital tape and to have a rather uniform picture of the results, it was decided to work with a single n_{max}, in the range of 300 to 400 Hz. To keep the true time of analogue recordings within rational limits (300 sec. maximum), Δn was kept between 0.8 and 1 Hz, and the number of estimates taken equal to 513 (= m_{max}). The sampling rate was in the range 1 to 1.2 kHz. With these parameters, the random error ε_r was estimated to be 6 to 7.5%.

The square of the aerodynamic admittance, being the ratio of the corresponding lift and velocity spectra could be estimated with a maximum normalized error of 12 to 15% (this excludes hot-wire errors, etc.).

5. Measurement of Frequency.

For the measurement of the oscillating rig frequency, the output signal from the rotating coil (Section 3.2.2) was fed into the Muirhead wave analyzer, which was preset at the desired frequency. The accuracy of the analyzer in measuring frequency was ± 0.5%. Therefore, the maximum error for the frequency measurements (taking into account the drift mentioned in Section 3.2.2) would be 6.5%.

Other methods for the measurement of frequency was by means of the spectral peaks and by counting the number of digitized points between two successive spikes from the coil reference signal. The latter method was part of a computer program performing a conditional averaging technique.

6. Measurement of Signal Amplitude via Conditional Sampling.

In the sinusoidal flow experiment, it was useful to obtain a representative picture of the signal in the time domain. Since the relevant frequency was that of the fluctuating upwash, a time averaged signal was constructed, by superimposing a large number of cycles of frequency n_g and identical phase, and then taking their arithmetic average. Random noise and frequencies uncorrelated with the main gust frequency, would thus be suppressed. A simplified flow chart of the computer program executing the averaging is shown in Fig. B-1.

APPENDIX C. EXPERIMENTS ASSOCIATED WITH THE BEHAVIOUR OF THE FREE SEPARATION POINTS

(i) Boundary layer experiment.

A conventional constant temperature U-wire was used, which was mounted on a specially designed traverse gear, enabling traverses normal to the surface of the elliptic cylinder, held at zero mean incidence. Three positions for traverses were chosen marked as AA, BB, CC in Fig. 4.12, the first being approximately the position of turbulent boundary layer separation (as depicted from the flow visualization). The measurements were conducted at a constant Re number of 2.2×10^5 (chord = 0.17 m) in both smooth and sinusoidal flows. In the latter, the RMS gust amplitude, α_g, was kept constant (= 2.2^o), while the reduced frequency $k = \pi nc/U_\infty$ was varied (values of k tried were 0.122, 0.212, 0.321). Velocities were made dimensionless with the value of the maximum mean speed encountered in the boundary layer and distances from the wall with the distance, at which this maximum was encountered.

The mean velocity profiles in smooth flow (not shown here) and in sinusoidal flow (Figs. C-2 to C-10) were close to each other, supporting the flow visualization observation, which had not indicated any displacement of the mean separation in the two flows (Section 4.4). The fact that the mean velocity does not tend to become zero as the wall is approached, is due to experimental inaccuracies. At very low speeds buoyant convection and heat radiation from the wire to the wall become important. A correction due to heat loss to the surface, proposed by Wills (1962) was tried (not shown here) and the results exhibited a more reasonable behaviour. Another source of error is the inability to reach positions very close to the wall and this is important in the present tests, where the maximum boundary layer

thickness encountered was less than 7 mm.

The instantaneous velocity was measured by applying "King's Law", with input the instantaneous voltage obtained from the hot-wire anemometer (mean plus fluctuating). As mentioned in Section 5.3.3, the picture of the instantaneous velocity profiles was confusing due to the presence of spikes in the hot-wire signals, such as those shown in Fig. C-1. These spikes had a rather regular frequency of appearance close to that reported in Section 5.2.2.1c, when the spikes in the lift and wake u velocity spectra of the elliptic cylinder were discussed. It is rather curious, however, why these spikes still appear in conditionally averaged results of the sinusoidal flow (which were processed at the gust frequency, see Fig. B-1). The strength of these spikes is greatest for the highest frequency and near the middle of the boundary layer. Maekawa et al (1966) and Hanson, Kozak and Richardson (1966) have reported spiky velocity signals in the boundary layer and the wake of a circular cylinder in smooth flow, while Morkovin et al (1971) reported the existence of spikes in the region just behind a trip wire of a flat plate, but only in sinusoidally streaming flow. The possible explanations given converge to an idea of a violent short-lived mixing of wake fluid with undisturbed, "potential flow", fluid, but the exact mechanism is not clear.

Any occurrence of mechanical vibrations in the traverse gear could affect the boundary layer measurements, because then the hot-wire would be forced to move inside the, relatively thin, boundary layer. But again this effect should be eliminated in the conditional averaging process. Anyway, no such vibrations could be traced.

There exist, of course, more elaborate ways for the detection of flow reversal such as the pulsed wire (e.g. Bradbury, 1969), or the hot film, for the measurement of the skin friction, (e.g. Bellhouse et

al, 1968) but the shape and size of the test model, as well as economic reasons prevented their use.

(ii) Unsteady loading experiment.

A NACA 0015 aerofoil was mounted on the unsteady load balance at incidences 10.5^{o}, 12^{o} and 13.5^{o}. (A complete description of this model is given in McKeough, 1976). The output of the piezoelectric transducers is the fluctuating lift (i.e. the total unsteady lift less the mean lift). No aerodynamic admittances are formed in this case, but instead the measured fluctuating lift (see Figs. C-11, C-12A, B, C) is compared in amplitude with the predicted lift from Eqns. (5.2), (5.2a) and (5.3a). The raw signals of Figs. C-12A, B, C obtained through a BRUSH pen recorder are low-pass filtered at a frequency of 50 Hz in order to remove the unwanted noise.

APPENDIX D. ANALYSIS OF THE UNSTEADY LIFT OF A THIN AEROFOIL INTO QUASI-STEADY, WAKE AND "ACCELERATION" TERMS

In Karman and Sears (1938), the lift sensed by a thin aerofoil in unsteady motion was derived. Three terms appeared in the unsteady lift response:-

The Quasi-Steady Lift Term:-

$$L_B = \rho U_\infty \Gamma_0(t) \tag{D-1}$$

The Wake Term:-

$$L_A = \rho U_\infty b_1 \int_1^\infty \frac{\gamma_w(\xi^*, t)\, d\xi^*}{\sqrt{\xi^{*2} - 1}} \tag{D-2}$$

The "Acceleration" or Apparent Mass Term:-

$$L_C = -\rho \frac{d}{dt} b_1^2 \int_{-1}^{1} \gamma_0(\xi^*, t)\, \xi^*\, d\xi^* \tag{D-3}$$

where U_∞, b_1, x, ξ are given in the sketch below:-

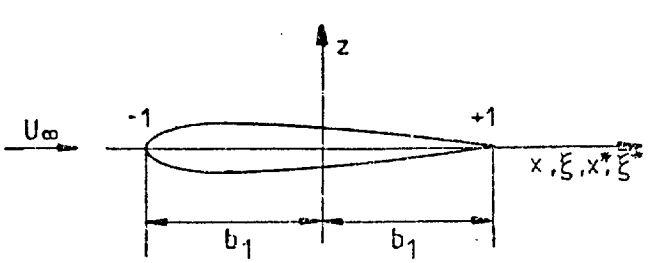

$$x^* = \frac{x}{b_1} \quad , \quad \xi^* = \frac{\xi}{b_1}$$

SKETCH

where γ_w is the wake vorticity; $\gamma_o(\xi^*, t)$ is the quasi-steady bound vorticity on the aerofoil and $\Gamma_o(t)$ is the quasi-steady circulation.

The quasi-steady bound vorticity on the aerofoil can be determined from the steady thin aerofoil theory, if the kind of unsteady motion is known, from the relationship (see Bisplinghoff et al, 1958):-

$$\gamma_o(x^*, t) = \frac{2}{\pi}\sqrt{\frac{1 - x^*}{1 + x^*}}\int_{-1}^{1}\sqrt{\frac{1 + \xi^*}{1 - \xi^*}}\,\frac{w_a(\xi^*, t)}{x^* - \xi^*}\,d\xi^* \qquad (D\text{-}4)$$

where w_a is the relative velocity upwash on any point on the aerofoil. The quasi-steady circulation can be obtained from:-

$$\Gamma_o(t) = b_1\int_{-1}^{1}\gamma_o(\xi^*, t)\,d\xi^* = -2b_1\int_{-1}^{1}\sqrt{\frac{1 + \xi^*}{1 - \xi^*}}\,w_a(\xi^*, t)\,d\xi^* \qquad (D\text{-}5)$$

because

$$\int_{-1}^{1}\sqrt{\frac{1 - x^*}{1 + x^*}}\,\frac{dx^*}{x^* - \xi^*} = -\pi$$

The terms L_A and L_B are a result of a total circulation being put round the aerofoil, while the term L_C comes from the "non-circulatory" part of γ_o, which will be denoted here by γ_{on}, i.e.:-

$$\int_{-1}^{1}\gamma_{on}\,dx^* = 0$$

The rest of γ_o is the "circulatory part" equal to:-

$$\gamma_{oc} = \frac{\Gamma_o}{\pi b_1\sqrt{1 - x^{*2}}}$$

Neumark (1952) gives the pressure distribution round the aerofoil due to the acceleration term as:-

$$\rho b_1 \frac{\partial}{\partial t} \int_{-1}^{x^*} \gamma_{on}(x^*, t)\, dx^*$$

so that:-

$$L_C = \rho b_1^2 \int_{-1}^{1} dx^* \frac{\partial}{\partial t} \left[\int_{-1}^{x^*} \gamma_{on}(x^*, t)\, dx^* \right] \qquad \text{(D-6)}$$

Neumark proves that the double integral in Eqn. (D-6) reduces to Eqn. (D-3), because γ_{oc} does not contribute to this integral.

In deriving the above relationships no restriction whatsoever was placed on the time dependence of the motion. For simple harmonic motions, Karman and Sears (1938) prove that:-

$$L_A = - L_B\{1 - C(k)\} \qquad \text{(D-7)}$$

where $k = \omega b_1/U_\infty$ and C(k) is Theodorsen's function (see Eqn. (2.8)). If the aerofoil is exposed to a sinusoidal gust of the type $\hat{w} e^{i(\omega t - kx^*)}$, then the relative velocity at any point on the aerofoil surface would be $- \hat{w} e^{i(\omega t - kx^*)}$, so that L_A, L_B, L_C can be immediately determined, by putting $w_a(\xi^*, t) = - \hat{w} e^{i(\omega t - k\xi^*)}$ in the previous equations.

(a) Quasi-Steady Lift.

$$L_B = \rho U_\infty \Gamma_o(t) = 2\rho U_\infty b_1 e^{i\omega t} \hat{w} \int_{-1}^{1} \sqrt{\frac{1 + \xi^*}{1 - \xi^*}}\, e^{-ik\xi^*}\, d\xi^* =$$

$$= 2\rho U_\infty b_1 \hat{w} e^{i\omega t} \pi \{J_o(k) - i J_1(k)\} \qquad \text{(D-8)}$$

The term S_B mentioned in Section 5.3.3 is equal to $J_0 - iJ_1$.

(b) Wake Vorticity Lift.

From (D-7):-

$$L_A = -2\pi \rho U_\infty b_1 \hat{w} e^{i\omega t} \left[1 - C(k)\right] \left[J_0(k) - iJ_1(k)\right] \qquad \text{(D-9)}$$

so that the term S_A of Section 5.3.3 is equal to $\left[C(k) - 1\right] \left[J_0(k) - iJ_1(k)\right]$.

(c) "Acceleration" or Apparent Mass Lift.

From Eqns. (D-3) and (D-4):-

$$L_C = -\frac{2}{\pi} \rho b_1^2 (-\hat{w}) \frac{d}{dt} \left[\int_{-1}^{1} \sqrt{\frac{1 - x^*}{1 + x^*}}\, x^* \left(\int_{-1}^{1} \sqrt{\frac{1 + \xi^*}{1 - \xi^*}} \frac{e^{-ik\xi^*}}{x^* - \xi^*} e^{i\omega t}\, d\xi^* \right) dx^* \right] \qquad \text{(D-10)}$$

or:-

$$L_C = \frac{2}{\pi} \rho b_1^2\, i\omega \hat{w} e^{i\omega t} \int_{-1}^{1} \sqrt{\frac{1 + \xi^*}{1 - \xi^*}}\, e^{-ik\xi^*}\, \pi(1 - \xi^*)\, d\xi^* =$$

$$= 2\rho b_1^2\, i\omega \hat{w} e^{i\omega t} \left[\pi(J_0 - iJ_1) - \frac{\pi}{2} J_0 + \frac{\pi}{2} J_2 + i\pi J_1 \right] = i\, 2\pi\rho U_\infty b_1 \hat{w} J_1(k) \qquad \text{(D-11)}$$

so that the term S_C of Section 5.3.3 is equal to $iJ_1(k)$.

From Eqn. (D-8), (D-9) and (D-11), it can be verified that:-

$$L_A + L_B + L_C = 2\pi \rho U_\infty b_1 \hat{w} e^{i\omega t} (S_A + S_B + S_C) = 2\pi\rho U_\infty b_1 \hat{w} e^{i\omega t} S(k)$$

where S(k) is Sear's function. For k = 0, the known steady flow result is obtained, with the wake and "acceleration" terms becoming zero, as expected.

APPENDIX E. THE MODULATION OF VORTEX SHEDDING BY A SINUSOIDALLY VARYING STREAMWISE VELOCITY COMPONENT

In this simplified analysis, it will be assumed that the Strouhal number is constant and that the vortex shedding lift in smooth flow is a pure sinusoidal wave, i.e.:-

$$L = \hat{L}_o e^{2\pi n_{vs} it} = \frac{1}{2} \rho U_\infty^2 \cdot c \cdot C_{Lvs} \cdot e^{2\pi n_{vs} it} \qquad (E\text{-}1)$$

where:-

$$\frac{n_{vs} \cdot b}{U_\infty} = S = \text{const.} \qquad (E\text{-}2)$$

Let a streamwise velocity component $u(t) = \hat{u} e^{2\pi n t i}$ be introduced into the smooth stream. Then the vortex shedding lift becomes:-

$$L = \frac{1}{2} \rho \left(U_\infty + u(t)\right)^2 \cdot c \cdot C_{Lvs} \cdot \exp\left[2\pi i \left(\frac{U_\infty + u(t)}{b} \cdot S\right) t\right] \qquad (E\text{-}3)$$

since S was assumed to be constant. Therefore, the lift is amplitude modulated by the term $U_\infty + u(t)$ and frequency modulated by the term:-

$$\exp\left[2\pi i \left(\frac{U_\infty + u(t)}{b} \cdot S\right) t\right]$$

(a) Frequency modulation.

The modulated lift will be given by:-

$$L = \hat{L} e^{i\theta(t)} \qquad (E\text{-}4)$$

where $\theta(t)$ is a time varying phase. From Eqn. (E-3), the radian frequency is:-

$$\omega = 2\pi n_{vs} + \frac{2\pi \hat{Su} e^{i2\pi nt}}{b} = \omega_o + \lambda e^{i\omega_1 t} \qquad \text{(E-5)}$$

where:-

$$\omega_o = 2\pi n_{vs} \quad , \quad \lambda = \frac{2\pi \hat{Su}}{b} \quad , \quad \omega_1 = 2\pi n$$

Since $\omega = \frac{d\theta(t)}{dt}$, the phase $\theta(t)$ is given by:-

$$\theta(t) = \int_{t_o}^{t} (\omega_o + \lambda e^{i\omega_1 t})\, dt = \omega_o t + \theta' + \frac{\lambda}{i\omega_1} e^{i\omega_1 t} \quad , \quad (\theta' = \text{const})$$

For simplicity it will be assumed that the initial phases between the sinusoidally varying signals is zero. Therefore, putting $\lambda' = \frac{\lambda}{\omega_1}$:-

$$\theta(t) = \omega_o t + \lambda' \sin \omega_1 t \qquad \text{(E-6)}$$

The lift, from Eqn. (E-4), becomes:-

$$L = \hat{L}\, e^{i(\omega_o t + \lambda' \sin \omega_1 t)}$$

which, due to the relation $e^{iz \sin\phi} = \sum_{m=-\infty}^{\infty} J_m(z)\, e^{im\phi}$, gives the result:-

$$\begin{aligned} L = \hat{L}\Big[& J_o(\lambda') \cos \omega_o t - J_1(\lambda') \left[\cos(\omega_o - \omega_1)\, t - \cos(\omega_o + \omega_1)\, t\right] + \\ & J_2(\lambda') \left[\cos(\omega_o - 2\omega_1)\, t + \cos(\omega_o + 2\omega_1)\, t\right] - \\ & J_3(\lambda') \left[\cos(\omega_o - 3\omega_1)\, t - \cos(\omega_o + 3\omega_1)\, t\right] + \ldots . \end{aligned} \qquad \text{(E-7)}$$

Thus, it is observed that the spectral power at the original vortex shedding frequency will decrease, while power at other frequencies will appear, if the u component is introduced.

(b) Amplitude Modulation.

The vortex shedding lift coefficient will be proportional to:-

$$1 + \frac{u(t)^2}{U_\infty^2} + \frac{2u(t)}{U_\infty} \simeq 1 + \frac{2u(t)}{U_\infty} \qquad \text{if } \hat{u} << U_\infty$$

Again, assuming for simplicity a zero phase between the fluctuating sinusoidal signals, the modulated lift coefficient will be:-

$$C_{L_m} = C_{L_{VS}} \left[\cos \omega_0 t + \cos(\omega_0 + \omega_1)\, t + \cos(\omega_0 - \omega_1)\, t\right] \qquad \text{(E-8)}$$

Therefore, two additional frequencies are introduced in the original (single frequency) spectrum.